

Appendices (original papers I–X)

Paper I

***Sanguina nivaloides* and *Sanguina aurantia* gen. et spp. nov. (Chlorophyta):
the taxonomy, phylogeny, biogeography and ecology of two newly
recognised algae causing red and orange snow**

Procházková L¹, Leya T², Křížková H¹ & Nedbalová L^{1,3}

***FEMS Microbiology Ecology* 95(6): fiz064, 2019**

¹ Charles University, Faculty of Science, Department of Ecology, Viničná 7, 128 44 Prague 2,
Czech Republic

² Fraunhofer Institute for Cell Therapy and Immunology, Branch Bioanalytics and
Bioprocesses IZI-BB, Extremophile Research & Biobank CCCryo, Am Muehlenberg 13,
14476 Potsdam-Golm, Germany

³ The Czech Academy of Sciences, Institute of Botany, Dukelská 135, Třeboň, 379 82,
Czech Republic



RESEARCH ARTICLE

Sanguina nivaloides and *Sanguina aurantia* gen. et spp. nov. (Chlorophyta): the taxonomy, phylogeny, biogeography and ecology of two newly recognised algae causing red and orange snow

Lenka Procházková^{1,*}, Thomas Leya², Heda Křížková¹ and Linda Nedbalová^{1,3}

¹Charles University, Faculty of Science, Department of Ecology, Viničná 7, 128 44 Prague 2, Czech Republic,

²Fraunhofer Institute for Cell Therapy and Immunology, Branch Bioanalytics and Bioprocesses IZI-BB, Extremophile Research & Biobank CCCryo, Am Muehlenberg 13, 14476 Potsdam-Golm, Germany

and ³The Czech Academy of Sciences, Institute of Botany, Dukelská 135, Třeboň, 379 82, Czech Republic

*Corresponding author: Charles University, Faculty of Science, Department of Ecology, Viničná 7, 128 44, Prague 2, Czech Republic. Tel: +420 221951809; E-mail: lenkacerven@gmail.com

One sentence summary: Red and orange spherical cysts causing snow colouration across several continents were investigated with regards to their geographic distribution, ecology, ultrastructure and phylogeny; the cosmopolitan distribution of a new independent lineage *Sanguina* within the Chlamydomonadales was molecularly confirmed.

[†]Lenka Procházková, <http://orcid.org/0000-0003-3995-6483>

ABSTRACT

Melting snowfields in polar and alpine regions often exhibit a red and orange colouration caused by microalgae. The diversity of these organisms is still poorly understood. We applied a polyphasic approach using three molecular markers and light and electron microscopy to investigate spherical cysts sampled from alpine mountains in Europe, North America and South America as well as from both polar regions. Molecular analyses revealed the presence of a single independent lineage within the Chlamydomonadales. The genus *Sanguina* is described, with *Sanguina nivaloides* as its type. It is distinguishable from other red cysts forming alga by the number of cell wall layers, cell size, cell surface morphology and habitat preference. *Sanguina nivaloides* is a diverse species containing a total of 18 haplotypes according to nuclear ribosomal DNA internal transcribed spacer 2, with low nucleotide divergence ($\leq 3.5\%$). Based on molecular data we demonstrate that it has a cosmopolitan distribution with an absence of geographical structuring, indicating an effective dispersal strategy with the cysts being transported all around the globe, including trans-equatorially. Additionally, *Sanguina aurantia* is described, with small spherical orange cysts often clustered by means of mucilaginous sheaths, and causing orange blooms in snow in subarctic and Arctic regions.

Keywords: snow algae; red snow; haplotype network; *Chlamydomonas nivalis*

Received: 20 December 2018; Accepted: 9 May 2019

© FEMS 2019. This is an Open Access article distributed under the terms of the Creative Commons Attribution Non-Commercial License (<http://creativecommons.org/licenses/by-nc/4.0/>), which permits non-commercial re-use, distribution, and reproduction in any medium, provided the original work is properly cited. For commercial re-use, please contact journals.permissions@oup.com

INTRODUCTION

Several algal species are reported to cause the macroscopic phenomenon of orange and red to pinkish snow, the latter often referred to as 'watermelon snow' or 'blood snow' when occurring as mass developments, including *Chlamydomonas nivalis* (Wille 1903; Kol 1968; Czygan 1970; Fjerdningstad et al. 1974; Kawecka 1981; Gradinger and Nürnberg 1996; Leya 2004), *Chloromonas nivalis* (Remias et al. 2010; Matsuzaki, Nozaki and Kawachi 2018), *Cr. brevispina* (Hoham, Roemer and Mullet 1979), *Cr. polyptera* (Remias et al. 2013), *Cr. rubroleosa* (Ling and Seppelt 1993), *Cr. nivalis* subsp. *tatrae* (Procházková et al. 2018a), *Chlorosarcina antarctica* (Ling 2002), *Smithsonimonas abbotii* (Kol 1942), *Chlainomonas kolii* (Novis 2002) and *Chlainomonas rubra* (Hoham 1974).

One of the first field samples of red snow was collected during the Northern Expedition under Captain Ross in August 1818 to Baffin Bay (75°54' N 67°15' W) between northern Greenland and Canada (Bauer 1819) and brought back to England to be investigated. Red snow has been reported from almost all polar and alpine regions (Kol 1968; Marchant 1982; Mataloni and Tesolín 1997; Thomas and Broady 1997). The first phylogenetic studies that identified a separate clade comprising solely red spherical cysts were based on 18S rRNA gene data (Leya 2004; Remias et al. 2010, 2013), but a deeper molecular identification based on nuclear ribosomal DNA internal transcribed spacer 2 (ITS2) sequence data so far has been missing for this taxon except for a recent study by Segawa et al. (2018) investigating samples from both poles. Red spherical cysts have also been the focus of a few metagenomic studies carried out in the USA (Brown, Ungerer and Jumpponen 2016), Japan (Terashima et al. 2017), the Arctic (Lutz et al. 2016; Segawa et al. 2018) and the Antarctic (Segawa et al. 2018). However, detailed investigations of red snow from mid-latitude mountain ranges like those in Europe are lacking.

Though modern microscopes are much better equipped than 200 years ago, a persistent problem is that the red spherical cysts abundantly found in melting snow simply do not reveal enough intracellular details that can be used for a deep morphological description and thus, identification. The unicellular, thick-walled cyst stages ['cysts' = unicellular life cycle stage protected from unfavourable environmental conditions with a wall, which was built exogenously or endogenously according to Ettl and Gärtner (2014)] dominate snow surfaces during summer. The characteristic dark blood-red pigment astaxanthin is accumulated in similarly large quantities only in *Haematococcus lacustris*, *Chlainomonas rubra* and some others (Remias, Lütz-Meindl and Lütz 2005). In many cases astaxanthin covers the cysts' chloroplast structure almost entirely, making light microscopy hardly illuminating. A first revision of *Chlamydomonas* by Pröschold et al. (2001) revealed how important chloroplast morphology is for consistency with the phylogeny of the Chlamydomonadaceae. Many snow algal species are held as live cultures in culture collections (e.g. CCCryo, UTEX, CCAP), but none of these 'green' species ever formed a single phylogenetic clade together with red spherical cysts from red snow. Instead, all 18S rRNA gene phylogenetic studies have revealed a single clade comprising immobile spherical red cysts (Leya 2004; Leya, Müller, Ling et al. 2004; Remias et al. 2010, 2013). This 'red snow' clade is clearly separated from other clades of *Chlamydomonas*, *Chloromonas*, *Lobochlamys*, *Oogamochlamys*, *Haematococcus*, *Carteria*, etc. Most likely, green, flagellated isolates from red snow field samples often were misinterpreted as having resulted from red spherical cysts or even vice versa; e.g. Novakovskaya et al. (2018) thought to

have observed such a phenomenon when linking green isolates of *Cr. reticulata* from snow samples to red cysts in the same sample. The lack of knowledge about other life cycle stages, whether vegetative (e.g. green actively dividing cells with a well-visible chloroplast) or sexual (e.g. gametes), and the lack of sufficient molecular data from red spherical cysts, have been the most hindering in identifying their true taxonomy.

In this study we used a polyphasic approach to study field material composed of spherical red and orange cysts sampled from alpine habitats in Europe, North America, South America and both polar regions. Our aims were (i) to reveal their molecular diversity based on ITS2 rDNA and rbcL gene sequences, (ii) to describe their morphological and ultrastructural cellular details using light, transmission and scanning electron microscopy, and (iii) to characterise their habitat conditions (pH, conductivity, elevation). Furthermore, we wanted (iv) to describe the geographic distribution of haplotypes detected by establishing a haplotype network, and (v) to test the existence of spatial patterns (Mantel test, sPCA). Based on the results, a new genus-level taxonomy of the examined species is proposed with a description of two new species: the new genus *Sanguina* Leya, Procházková et Nedbalová with *Sanguina nivaloides* Procházková, Leya et Nedbalová and *Sanguina aurantia* Leya, Procházková et Nedbalová.

MATERIALS AND METHODS

Sampling localities

Patches of clearly visible red- or orange-coloured snow caused by spherical red or orange cells were collected from 42 localities in melting seasons between the years 1999 and 2018 (Fig. 1, Supplementary Tables 1 and 2): 22 samples originated from alpine sites in continental Europe, three from sites in North America and one from South America. Moreover, 14 samples were collected at polar sites on the island of Spitsbergen (Svalbard archipelago) and two from polar sites on the Antarctic Peninsula.

To ensure the selection of 'clean' (mono-specific) bloom spots and to avoid a taxonomically diverse sample, a field microscope was used to check the sample in the field before collection. In the lab, samples were further thoroughly examined using laboratory light microscopy (see below) prior to molecular analyses. If the sample appeared to be too diverse, it was discarded. In addition, Alanagreh et al. (2017) reported that the dominant haplotype was usually evident from the Sanger sequencing, similar as in cloning approach.

Measurements of pH and conductivity and snow water equivalent (referred to as 'snow water content' in the paper cited) were carried out according to Procházková et al. (2018a).

In addition we were also able to investigate red cysts collected in 1851, namely from the desiccated sample 'MB.ES.1781c', further labelled 'Rother Schnee Crimsen [sic] Cliff Beverly 1851, 76°3'N.B. 1781c' obtained from the Ehrenberg Collection at the Museum für Naturkunde in Berlin. This historical material was collected during the Grinnel Arctic Expedition (1850–1851) under Lieut. De Haven of the U.S. American Marines from red snow on scarlet-coloured cliffs (Crimson Cliffs) in Baffin Bay on the Greenland coast (Beverly Greenland), though a bit further north of the location, from where the Ross type sample of 1818 originated (75°54' N 67°15' W; Ross 1820). Unfortunately, the latter material was not traceable and could not be included in this study.

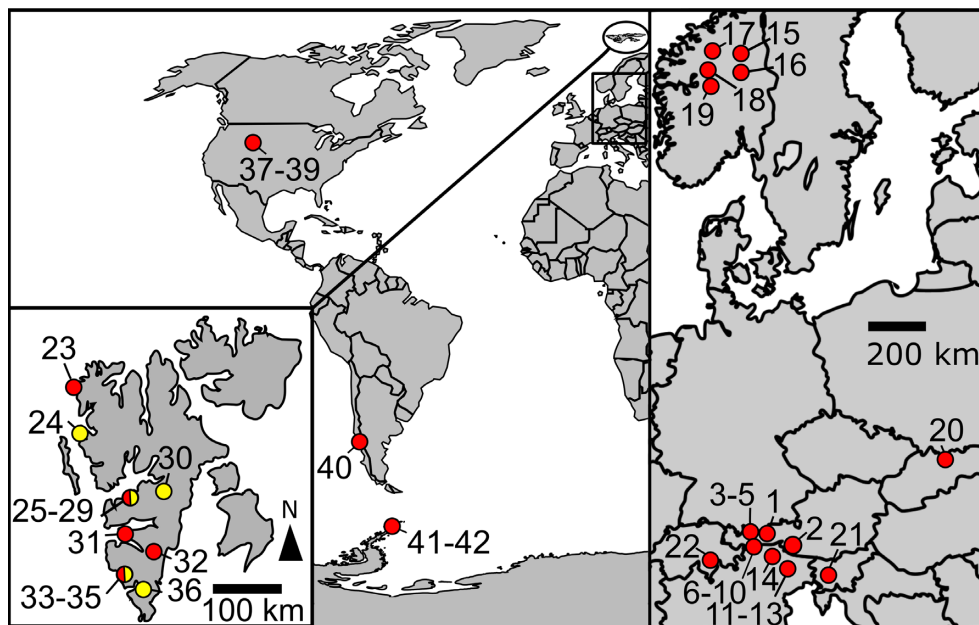


Figure 1. Sampling locations of *Sanguina nivaloides* (red circles), *Sanguina aurantia* (yellow circles) and regions where both species were sampled (red-yellow circles) in continental Europe (right), on the archipelago of Svalbard (left), in North and South America (middle) and in Antarctica (middle). Numbering corresponds to the sample origin from the following countries: Austria (1–10; 1-Haferkarlespitze, 2-High Tauern, 3–5 K uhfai, 6–10  tztal Alps), Italy (11–14; 11–13 Dolomites, 14-Sarntal Alps), Norway (15–19), Slovakia (20-High Tatra Mountains), Slovenia (21-Julien Alps), Switzerland (22-Urner Alps), Svalbard (Norway) (23–36; 23-Amsterdam ya, 24-Ny  lesund, 25–29 Longyearbyen, 30-Raggfjellet, 31-Midterhuken, 32-Doktorbreen, 33–35 Hornsund, 36-Chomjakovbreen), Colorado (USA) (37–39 Rocky Mountains), Argentina (40-Patagonia), Antarctica (41–42 Antarctic Peninsula). Habitat description of sampling localities including geographical data are shown in Supplementary Table 1.

Light and electron microscopy

Light microscopy was performed using an Olympus BX43 (Olympus Corporation, Japan) equipped with a DXM 1200F digital camera (Nikon, USA). Microphotographs were further processed using the QuickPHOTO Camera 3.0 software (Promicra, Czech Republic). The same software or cell^P software (version 3.4, Olympus Soft Imaging Solutions GmbH, Germany) was used to measure cell sizes. Preparation of samples for scanning and transmission electron microscopy (SEM and TEM) followed the protocol described in Proch azkov a et al. (2018a). The diameters of around 40 cysts were measured for each field sample. Measurements of red cysts from 1851 from the desiccated sample 'MB_ES_1781c' were also included.

DNA extraction and PCR

DNA isolation was carried out using the DNeasy Plant Mini Kit (Qiagen, Germany) as described in Proch azkov a et al. (2018a). If less than 20 mg wet biomass was available, DNA was extracted using the Instagene Matrix (Bio-Rad Laboratories, USA) according to Remias et al. (2016). The 18S small subunit ribosomal RNA gene (18S rRNA gene), internal transcribed spacer region 2 (ITS2 rDNA) and ribulose-1,5-bisphosphate carboxylase/oxygenase large subunit (rbcL) gene regions were amplified from DNA by polymerase chain reaction (PCR) using the primers listed in Supplementary Table 3. Primer pairs involved in the PCR of 18S were P2/P4, 18F2/18R2, FC/RF and FA/RD. In order to amplify ITS2 we used ITS1/ITS4, ITS5/ITS4, SSU/LSU, A11500af/LR3 and TW81/AB28. For PCR of rbcL, we used the primer pairs rbcL1F/rbcL7R, rbcL1F/rbcL4R, rbcL10F/rbcL7R, rbcL8F/rbcL7R, Snow-F3/Snow-R12 and Snow-F0/Snow-R12. The amplification reactions for these markers are described in Proch azkov a et al. (2018a). PCR products were purified and

sequenced using an Applied Biosystems automated sequencer (ABI 3730xl) at Macrogen (Netherlands). Chromatograms of all newly obtained sequences were carefully examined using the program FinchTV 1.4.0 (Geospiza, USA). Only sequences showing distinct single peaks in the electropherogram were used. The nuclear rDNA ITS2 region was identified using a web interface for the ITS2 database showing the position of the 26S motif (<http://its2.bioapps.biozentrum.uniwuerzburg.de/cgi-bin/index.pl?annotator>; Koetschan et al. 2010). The sequences obtained were submitted to the NIH genetic sequence database GenBank at NCBI (accession numbers are shown in Supplementary Tables 4–6).

Molecular analyses

Our 18S rRNA gene alignment contained 96 sequences (1544 bp) and the rbcL matrix consisted of 62 sequences (954 bp); members of *Chaetophora*-clade were selected as the outgroup. The best-fit nucleotide substitution model was estimated by jModeltest 2.0.1 (Posada 2008). Based on the Akaike Information Criterion (AIC), the TIM2+I+G model was selected for the 18S rRNA gene. Three partitions were set for rbcL gene sequences and the following substitution models were applied: GTR+I+G (1st codon position), TIM3+I (2nd codon position) and GTR+I+G (3rd codon position). The 18S rRNA gene and rbcL phylogenetic trees were inferred by Bayesian Inference (BI) and Maximum Likelihood (ML) according to Nedbalov a et al. (2017), with the minor modification that Markov Chain Monte Carlo runs were carried out for three million generations in BI. Convergence of the two cold chains was checked by the average standard deviation of split frequencies (0.000014 and 0.001613 for the 18S rRNA gene and rbcL dataset, respectively). Bootstrap analyses were performed by maximum likelihood and Bayesian posterior probabilities were calculated as described by Nedbalov a et al. (2017).

The 42 sequences of ITS2 rDNA obtained during this study were used as the main dataset which was split into a red snow dataset (35 sequences) and an orange snow dataset (seven sequences). The extended dataset additionally included selected published sequences, which were assigned to the investigated species based on a pairwise comparison using BLAST. The newly generated ITS2 sequences of our red snow sample RS.0015–2010 (accession number MK728599) and orange snow sample RS.0017–2010 (accession number MK728634) were used as a query. Samples of these additional sequences originated from Colorado and Washington states (USA) (NCBI accession codes KX063716.1–KX063729.1 and KX063743.1–KX063753.1; Brown, Ungerer and Jumpponen 2016), and from Alaska (AB902998.1), Greenland (AB902971.1), the Austrian Alps (GU117577.1; Remias et al. 2010) Japan (AB903028.1) and Tadjikistan (AB902973.1, AB903025.1). The individual sequences of specimens with ambiguous positions (one or two ambiguous bases out of 205 bp in these specimens from the main dataset: redCol, 4HT, 2SLOV, 4D, 9D; one or eight ambiguous bases out of 205 bp in specimens of the extended dataset: AL1, JP1) were resolved using the PHASE algorithm implemented in DnaSP v.6.0. (Librado and Rozas 2009). PHASE assumes Hardy-Weinberg equilibrium and uses a coalescent-based Bayesian method to infer haplotypes (Librado and Rozas 2009). This means the PHASE algorithm can successfully infer haplotypes if a sufficiently high number of homozygous sequences are used. All samples were resolved with a strong support. Haplotypes were delineated at the 100% similarity threshold (i.e. two sequences belong to the same haplotype if they are identical). Only different haplotypes were used in the ITS2 secondary structure modelling, whereas all haplotypes were used in the ITS2 haplotype network analysis. For the ITS2 haplotype network of a species causing red snow the main dataset and extended dataset consisted of 40 and 59 sequences, respectively. For the ITS2 haplotype network of a species causing orange snow the main dataset and extended dataset consisted of seven and 21 sequences, respectively.

The ITS2 rDNA sequences were folded using the Mfold server at <http://mfold.rna.albany.edu/?q5mfold> (Zuker 2003). The secondary structure model that was consistent with the following specific features of the nuclear rDNA ITS2 was selected, namely four helices and a U–U mismatch in helix II (Coleman 2007). The ITS2 sequences were aligned on the basis of the sequence-structure analysis (Schultz and Wolf 2009) using the 4SALE tool (Seibel et al. 2006, 2008). At this step a manual validation and correction of the sequence alignment and secondary structure was necessary. The alignments of the main and the extended dataset included 213 bp and both were used in the consensus secondary structure modelling and haplotype network. The secondary structure of the nuclear rDNA ITS2 of specimen RS.0015–2010 (accession number MK728599) was drawn using Visualization Applet for RNA (VARNA) version 3.9 (Darty, Denise and Ponty 2009). The consensus secondary structure was edited using Inkscape software version 0.91 (Free Software Foundation Inc., USA). The number of compensatory base changes (CBC; a double-sided base change of a nucleotide pair in a helix, retaining the secondary structure) between haplotypes was evaluated using the 4SALE tool. The nuclear network for ITS2 was constructed by TCS software version 1.21 (Clement, Posada and Crandall 2000) using statistic parsimony under a 95% connection limit. Then we ran a second analysis, reducing the connection limit to 91% in an attempt to infer connections among sub-networks. Gaps were considered the fifth phylogenetic character

(Vukić, Ulqini and Šanda 2017). The final edit of the haplotype network was again carried out in Inkscape.

Geographic relationships

To investigate the spatial genetic structure of the red snow alga studied, we summarised genotype allele frequency data of the variable ITS2 rDNA marker by performing a spatial principal component analysis (sPCA). A principal component analysis (PCA) summarises multivariate genetic information into a few linearly uncorrelated variables, the principal components (Jombart, Pontier and Dufour 2009). The PCA method was recently modified to include spatial information to investigate the part of the genetic variation that is or is not spatially structured, the sPCA (Jombart et al. 2008). The sPCA analyses a matrix of relative allele frequencies, which contains genotypes in rows and alleles in columns. Geographic coordinates of sampling points are used as input data for the creation of a list of weights derived from a connection network (function 'chooseCN'). Our sPCAs were performed with the *adegenet* package in R software (Jombart 2008), and using the function 'spca' and bar plots of the sPCA eigenvalues were produced showing the amount of genetic diversity (as measured by the multivariate method being used) represented by each principal component. To test for the existence of global and/or local structure, we performed two Monte Carlo multivariate tests (Jombart et al. 2008). The outputs are represented as figures showing two histograms (one for the global test and one for the local test) of permuted test statistics, and the reference distribution of these statistics is obtained by randomly permuting the rows of the genotype datamatrix. Spatial PCA was carried out for two versions of the datasets of the red spherical cysts: (i) Europe, America, Antarctica and Svalbard, and (ii) Europe. To assess the significance of the correlation between ITS2-based genetic and geographic distance matrices of the investigated species causing red snow, we also performed a classical Mantel test ('mantel.randtest') using the package *adegenet* in the R software. Pairwise Euclidean distances for both distance matrices were computed using the function 'dist'. Haplotype diversity of the species studied within and among mountain ranges (European Alps, Tatra Mountains, continental Norway, Svalbard, Rocky Mountains, Patagonia) and polar regions (Svalbard, Antarctica) were evaluated using the program MEGA (version 7.0.14); genetic distances between ITS2 sequences were generated using both uncorrected (p-distance) and corrected pairwise distance [Kimura two-parameter (K2P) distance]. The number of base differences, uncorrected (p-distance) and corrected pairwise distance (K2P) between 18 ITS2 haplotypes of red cysts and two ITS2 haplotypes of orange cysts were evaluated with MEGA as well.

RESULTS

Habitat conditions

The species causing red snow in this study, *Sanguina nivaloides*, occurred on temporary (alpine meadows, polar rocks, permafrost) or persistent (glaciers) snowfields in both alpine and polar regions (Supplementary Fig. 1). This species was hardly found at mountain sites below the timber line (e.g. sample 'sub-alpine'). It was observed occasionally in massive amounts on open icy glacier surfaces, though as long as there is a snow layer on the glacier, this habitat is also occupied. The species causing orange snow in this study, *Sanguina aurantia*, occurred at similar habitats on Svalbard only. At localities where these species

are found once, they appear consistently year after year, forming reddish or orange blooms in summer, producing the well-known macroscopic phenomenon of red snow or blood snow due to the dominating red pigment astaxanthin in its cysts. Colour shades can vary from orange (orange spherical cysts) and pink to dark cherry and blood red (red spherical cysts) (Supplementary Fig. 2). These localities are usually well-defined in their extent and can cover areas from a few square metres up to several hundreds of square metres. Over summer and with melting of the snow cover algal populations are slowly exposed on the snow surface, and are often washed down from snow fields in alpine regions, resulting in intensely coloured streaks on the otherwise white snow. If a snow field is not persistent over the summer months, the cysts can end up on permafrost or rocky soil, and then covered by fresh snow at the end of the summer. There they are a 'seed bank' serving as an inoculum for the next melting season when the newly encountered habitat is suitable. In addition, they may be dispersed to other locations by strong winds or storms, which are e.g. typical for autumn in the polar region around Svalbard. Snow fields with blooms of *Sanguina nivaloides* can be almost flat or be part of a steep slope, with any variation in between. Blooms have been observed at sites close to alpine pathways and on pastures, as well as at polar sites far away from any signs of civilisation, e.g. on remote inland glaciers on Spitsbergen. Also, organic nutrient input was not a decisive factor, as we found red snow both far away and also close to bird colonies. Red snowfields were located at elevations between 13 and 585 m a.s.l. in polar regions, and between 1914 and 3731 m a.s.l. in alpine regions (Supplementary Table 1). The orange snowfields were located between 10 and 500 m a.s.l. in polar regions (Supplementary Table 2). In snowfields with *S. nivaloides* or *S. aurantia*, blooms had low electrical conductivities (3–26 $\mu\text{S cm}^{-1}$, occasionally up to 84, but usually well below 100 $\mu\text{S cm}^{-1}$) and pH values between slightly acidic (pH 4.7) and neutral (pH 7.1) (Supplementary Tables 1 and 2). Snow temperatures were naturally stable near 0°C. The water equivalent of a red blooming snowfield in the Austrian Alps amounted to $51.6 \pm 1.6\%$ (sample WP123). Snow field inclination and its cardinal direction towards the sun are thought to account for decisive differences in incident solar radiation and temperature, but neither were correlated with the occurrence of red snow.

Cytological observations

Light microscopy (Fig. 2) and electron microscopy (SEM: Fig. 3, TEM: Fig. 4) showed that field samples of *Sanguina nivaloides* consisted of red spherical cells exhibiting different accumulation levels of secondary carotenoids in abundant lipid droplets, which in mature cysts fully masked the chloroplasts making any detailed structure unrecognisable by light microscopy (Fig. 2A) and thus unusable for identification. A single parietal chloroplast and one or two large, unpigmented vacuoles were observed in young cells in their early stage of development only (Fig. 2B–D and Fig. 4C and D). The typical mature red cyst was smooth-walled (Figs 2A and 3A), but in two cases the red snow also consisted of populations of cysts with nipples (Figs 2E, 3B and 4F). A few scattered cysts with short blunt nibs (Fig. 3C) or pronounced papillae (Figs 2F and 3D) or cells carrying uniformly distributed small smooth papillae (Fig. 3E) were noticed in a population of smooth-walled cells. *Sanguina aurantia* field samples (Fig. 5) consisted of smaller spherical cysts with a striking orange-coloured cell content, the cells had an outer distant cell layer or the distant layer was absent. A few scattered cells of 'ruby'-like cysts (the term 'ruby' is frequently used for this type of cyst as the

dark red pigmented cyst content and the wall structure appear like a ruby encased in mother-of-pearl) were found in two red snow samples (Supplementary Fig. 3A–F, marked with an asterisk in Supplementary Table 4). We are certain that no sequences of those ruby cysts were used in any of the analyses in this study, as they would have been greatly outnumbered by the dominating smooth-walled cysts, even assuming they were equally amenable to DNA extraction in the first place. As far as the intracellular ultrastructure of our samples is concerned, mature cysts had a naked pyrenoid in a single chloroplast, which is forced into a central position by surrounding lipid globules (Fig. 4A) and cell walls consisted of two layers (Fig. 4B). Early stages of red cysts differed in the presence of a clearly visible single parietal chloroplast (Fig. 4C and D) and a three-layered cell wall, the outermost being fuzzy (Fig. 4E). Orange-coloured cysts of *Sanguina aurantia* differed from red cysts of *Sanguina nivaloides* in the structure of the second layer of their cell wall, being multilayered and slightly undulating on the surface (Fig. 5C and E). This layer most likely reflects the maturity of the cysts, as orange-coloured cysts of the same cell diameter but with smooth surfaces also existed in this population of *Sanguina aurantia* (Fig. 5D). Cytosolic electron-dense vacuoles filled with a crystalline structure were observed in both red cysts of *Sanguina nivaloides* and in orange-coloured cysts of *Sanguina aurantia* (Fig. 5G).

Size ranges of the orange-coloured cysts and red cysts overlapped, with 6.2–15.5 μm and 7.3–39.0 μm , respectively. The variability of cell size ranges in field samples of each haplotype of both snow algal species (for description see below) is shown in Supplementary Fig. 4. The material from Baffin Bay (sample 'MB.ES.1781c' from the Ehrenberg Collection at the Museum für Naturkunde in Berlin) contained cells in the size range typical for red cysts (Fig. 6).

Molecular identification of genus *Sanguina* and its closest relatives

According to our 18S rRNA gene and rbcL phylogenies (Figs 7 and 8), the genus *Sanguina* forms a monophyletic lineage within the Chlamydomonadaceae containing samples from nearly all regions of the Earth (Greenland, North America, South America, Africa, Europe, Asia, Svalbard and Antarctica). The closest relatives to the genus *Sanguina* are organisms found on glaciers or glacier-associated environments, such as the strain CCCryo 086–99 (cf. *Ploeotila* sp.) from a glacier surface or uncultured eukaryote clones from glacial debris in Alaska and periglacial environments on the top of Mount Kilimanjaro in Tanzania. Slightly distant relatives represent strains from the Arctic permafrost in close vicinity to glaciers and snow fields, e.g. CCCryo 101–99 and CCCryo 133–01 (both cf. *Sphaerocystis* sp.) or Arctic snow fields, e.g. CCCryo 147–01 (cf. *Coenochloris* sp.), and from soil such as 'uncultured Haematococcaceae clones' isolated from an aspen rhizosphere and *Gloeocystis* sp. from desert soil in Washington State. Phylogeny based on rbcL data (Fig. 8) showed an increased molecular variability in comparison with 18S rRNA gene data among specimens of the genus *Sanguina* because of the degeneracy of the genetic code, which accounts for the existence of synonymous mutations. Interestingly, the small orange cysts of *Sanguina aurantia* formed a small subclade within the red cyst samples of *Sanguina nivaloides*. The rbcL phylogeny confirmed the positions of cf. *Sphaerocystis* and cf. *Coenochloris* as slightly distant relatives to *Sanguina nivaloides*. Additionally, it revealed that these genera form closely related lineages (Fig. 8) to *Achoma brachiatum* isolated from an alpine herbfield soil in New

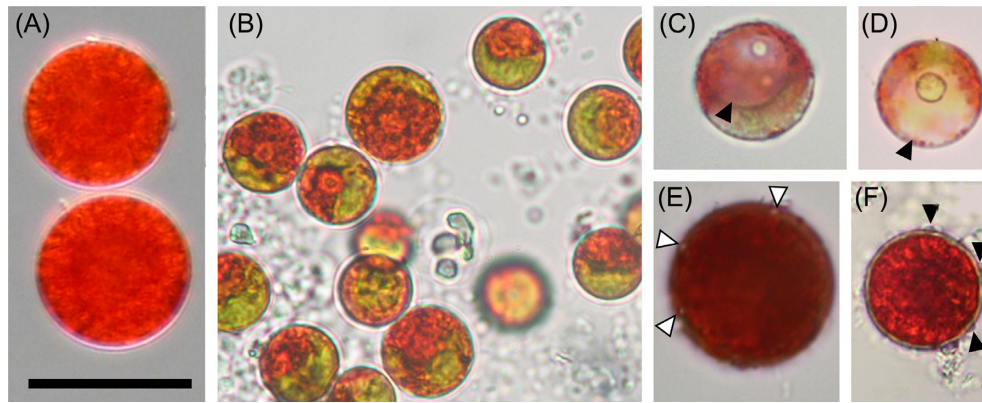


Figure 2. Light microphotographs of *Sanguina nivaloides*. (A) Typical mature red cyst with smooth cell wall (holotype specimen CCCryo RS.0015–2010), abundant lipid droplets entirely masking the cell interior and structure of the chloroplast. (B–D) Young red cysts in early stage of development, (B) showing visible parts of a single parietal chloroplast (paratype sample WP123), (C–D) depicting the large unpigmented vacuole (arrowhead) (samples: Sva4 and Saddle). (E–F) Mature red cysts of less frequent haplotypes causing red blooms, (E) visualises nipples on the cell surface (arrowheads, paratype specimen CCCryo RS.0003–2004). (F) shows pronounced papillae on cell surface (arrowheads, sample 4D). Scale bar 20 μm .

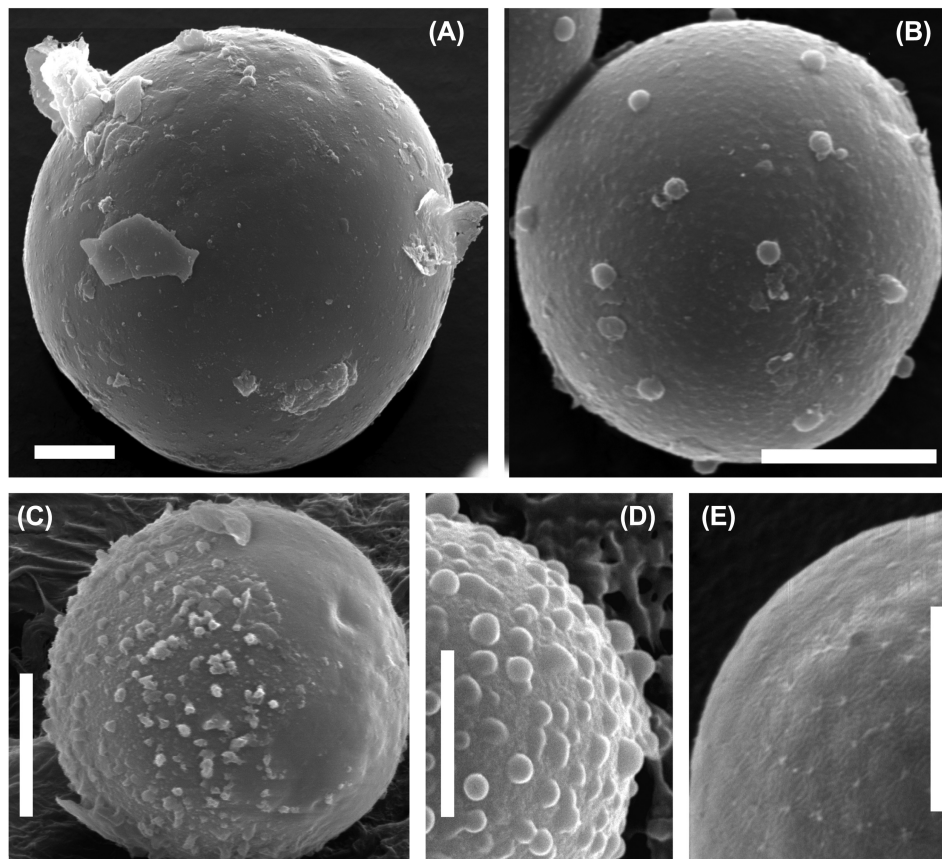


Figure 3. Scanning electron microphotographs of *Sanguina nivaloides*. (A) Typical mature red cyst with smooth cell wall (holotype specimen RS.0015–2010). (B–D) Mature red cysts of less frequent haplotypes causing blooms, (B) showing nipples on cell surface (paratype specimen RS.0003–2004), (C) depicts the smooth surface with short blunt nibs, which may represent the compressed remnants of the presumably transient primary cell wall, this cell wall layer may decompose over time (note: on the left side of the cell 'papillae' are present, on the right side they are absent, specimen RS.0011), (D) shows the pronounced papillae on the cell surface (sample 4D). (E) Scattered cells with small papillae on their cell surfaces in a population of smooth-walled cells (sample redCol). Scale bars 5 μm .

Zealand (Novis and Visnovsky 2012). Whether any of them could be assigned to the genus *Achoma* is discussed further below, but remains to be investigated. To sum up, the monophyly of the *Sanguina*-clade and the phylogenetic positions of its closest known culturable relatives were confirmed for both markers

(Supplementary Figs 5 and 6). Moreover, our phylogenetic analyses demonstrate that the positions of strains SAG 26.86 of *Cr. typhlos* (= UTEX 1969 = CCCryo 122–00), and *Cr. reticulata* SAG 29.83 (= UTEX 1970 = CCCryo 213–05) in the *Chloromonas*-clade based on 18S rRNA gene and *rbcl* phylogenetic trees clearly differed from the position of *S. nivaloides* (Supplementary Figs 5 and

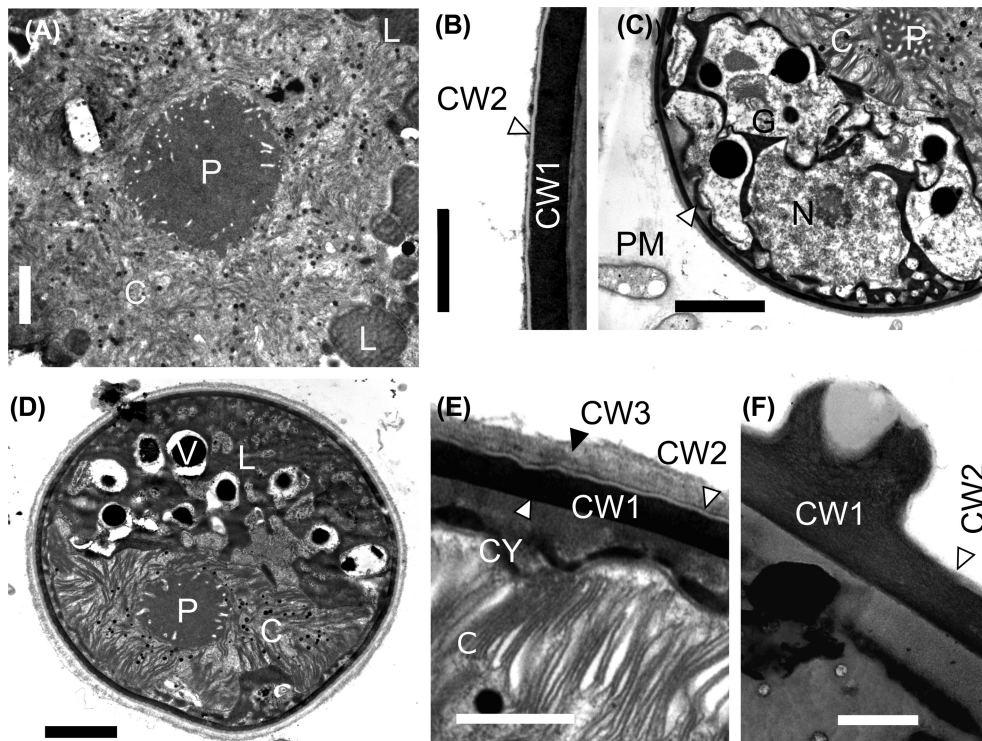


Figure 4. Transmission electron microphotographs of *Sanguina nivaloides*. (A, B) Mature red cyst (holotype specimen RS.0015–2010), (A) shows the centrally located plastid with a naked pyrenoid, surrounded by abundant lipid droplets. (B) depicts the electron-dense thick cell wall covered with a very thin transparent layer. (C–E) Young red cyst (paratype sample WP123), (C) shows the large cytoplasmic-free area (arrowhead) between the cytoplasmic membrane and the cell wall, the nucleus and the parietal plastid, as well as parts of the Golgi apparatus, no lipid bodies visible, (D) depicts the parietal plastid with a naked pyrenoid, lipid bodies and vacuoles, (E) shows a detail of the cell wall consisting of three layers: the innermost—thick electron dense (CW1), the middle one—very thin electron transparent (CW2; trilaminar sheath) and the fuzzy upper layer (CW3; presumably the primary cell wall). (F) A detail of a cell wall nipple of less frequent haplotypes (paratype specimen RS 0003–2004). C = chloroplast, CY = cytoplasm, CW1 = cell wall 1, CW2 = cell wall 2, G = Golgi stacks, L = lipid globules, N = nucleus, P = pyrenoid, PM = plasmatic membrane, V = vacuole. Scale bars = 2 μ m for (A, C, D). Scale bars = 0.5 μ m for (B, E, F).

6). These strains were isolated from snow samples and were formerly believed to cause red snow, and thus, they originally were (mis)identified as *Cd. nivalis* and *Cd. yellowstonensis* (Sutton 1970), respectively. The former is still listed under two different names, as *Cr. typhlos* (SAG) and *Cd. augustae* (UTEX), as is the latter, *Cr. reticulata* (SAG) and *Cr. clathrata* (UTEX); in both cases the designations at SAG are correct. Moreover, strain CCAP 11/128 (= UTEX 2824 = CPC 528 = CCCryo 214–05; accession number HQ404886.1) is listed as *Cd. nivalis* at UTEX (and others), but in our phylogeny proved to be *Cr. typhlos* based on the comparison of its ITS2 sequences (pairwise blast search), with 100% identity and no CBC for this marker with CCCryo 122–00 of *Cr. typhlos* (= SAG 26.86 = UTEX 1969 = CCAP 11/51B = IAM C-263 = NIES 2226 = IU 1969 [original deposition]; accession number HQ404869.1).

The CBC species concept applied to *Sanguina nivaloides* and *Sanguina aurantia*

The network analysis of field samples of *Sanguina nivaloides* from Europe, North America, South America and Antarctica (35 specimens) applying a 95% connection limit resulted in a total of 18 ITS2 haplotypes interconnected in one network (Fig. 9). Haplotypes differed by one up to seven nucleotide changes out of 205 base pairs (Table 1). The network analysis of *Sanguina aurantia* field samples from Svalbard (seven specimens) resulted in two ITS2 haplotypes differing by one nucleotide change out of 213 bp. Based on the comparison of ITS2 rDNA secondary structures, one CBC was found between *Sanguina nivaloides* (the red

cysts) and *Sanguina aurantia* (the small orange cysts) at the 13th position in helix II (Fig. 10). However, there is no consensus as to whether the CBC detected at this position can be used for a species separation within the Chlorophyceae. In other words, some authors treat this position as a variable one (e.g. Demchenko et al. 2012), others as a conservative one (e.g. Caisová, Marin and Melkonian 2013). Most recently, CBCs in the 5' end of helix III were only treated as relevant for evaluating species boundaries between closely related taxa (Segawa et al. 2018). Sequence identities between red cysts and small orange cysts were $\geq 95.1\%$, whereas sequence identities within red cysts were $\geq 96.5\%$ (Supplementary Table 7), suggesting that both types of cysts investigated in this study are very closely related. Among the red cysts of *Sanguina nivaloides* no CBC was found in the conserved parts of this marker structure, suggesting that according to the CBC species concept as proposed by Coleman (2000), all our samples of red snow from Europe, North America, South America and Antarctica were caused by one species. The presence of the one CBC and the number of base differences between ITS2 haplotypes of *Sanguina nivaloides* (red cysts) and *Sanguina aurantia* (orange cysts) are summarised in Table 1. Interestingly, two haplotypes of red cysts (H4 and H5) lack the CBC at the 13th position in helix II in their ITS2 secondary structure when compared to small orange cysts (Table 1). When comparing three molecular markers, the lowest intraspecific variability between *S. nivaloides* and *S. aurantia* haplotypes was detected in 18S ($\leq 0.2\%$), was higher in rbcL ($\leq 4.4\%$) and the highest was in ITS2 ($\leq 4.9\%$) (Supplementary Tables 7–9).

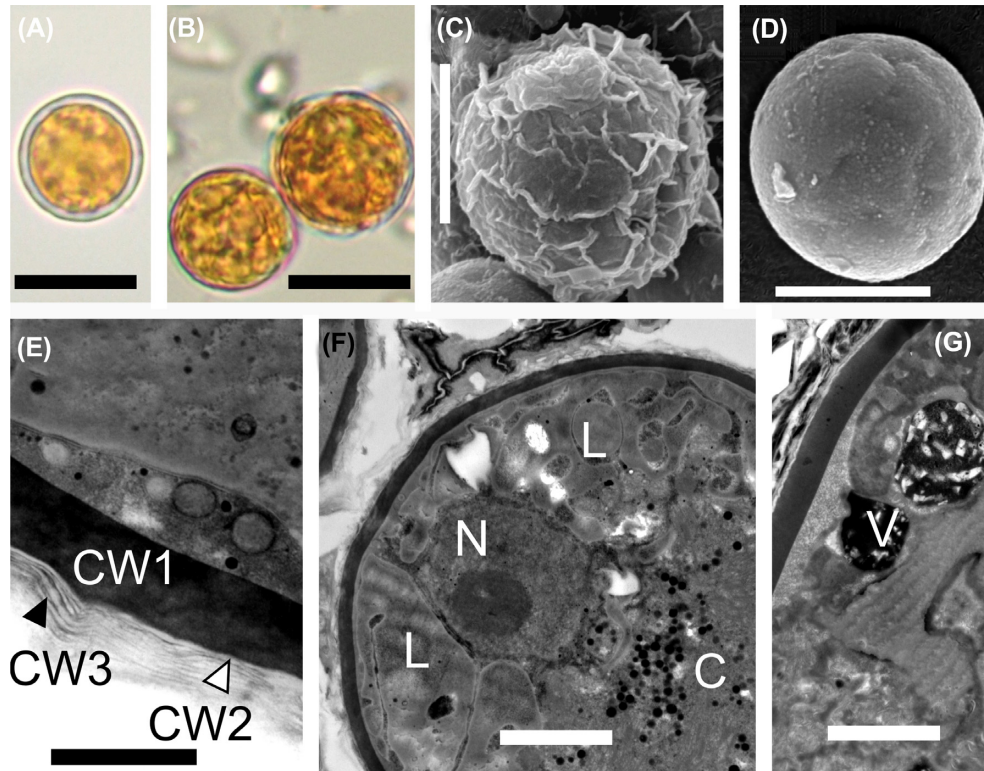


Figure 5. Light and electron micrographs of *Sanguina aurantia* (holotype specimen RS.0017–2010), (A) depicts the distant outer cell layer. (B) shows that the distant cell layer is absent. (C–D) outermost layer is wrinkled and when it is decomposed, the smooth cell wall below may appear. (E) shows details of the cell wall with the electron-dense layer (CW1) being covered by several more or less undulating thin transparent layers (CW2, CW3). (F) shows a cross-section of the cyst showing the nucleus and the centrally compressed chloroplast. (G) depicts the cytosolic electron-dense vacuoles filled with crystalline structures. C = chloroplast, CW1 = cell wall 1, CW2 = cell wall 2, CW = cell wall 3, L = lipid globules, N = nucleus, V = vacuole. Scale bars = 10 μm for (A, B), 5 μm for (C, D), 0.5 μm for (E) and 2 μm for (F, G).

Table 1. Amount of compensatory base changes in the ITS2 secondary structure (lower left) and the number of base differences/number of indels (each of two bp length) (upper right; e.g. ‘3/4’ means that 3 differences and 4 indels were found) between 18 haplotypes of *Sanguina nivaloides* (H1–H18) and two haplotypes of *Sanguina aurantia* (HA1, HA2).

	H1	H2	H3	H4	H5	H6	H7	H8	H9	H10	H11	H12	H13	H14	H15	H16	H17	H18	HA1	HA2
H1		1	2	1	5	4	2	2	3	1	2	3	2	3	3	4	3	3	3/4	4/4
H2	0		1	2	4	5	3	1	2	2	1	2	3	2	2	3	2	2	2/4	3/4
H3	0	0		3	5	6	4	2	3	3	2	3	4	3	3	4	3	3	3/4	4/4
H4	0	0	0		6	5	3	3	4	2	3	4	3	4	3	4	4	4	4/4	5/4
H5	0	0	0	0		7	5	3	6	6	5	6	7	6	6	7	3	6	4/4	5/4
H6	0	0	0	0	0		2	4	5	5	5	6	6	6	6	7	5	6	6/4	5/4
H7	0	0	0	0	0	0		2	5	3	3	4	4	4	4	5	3	4	5/4	6/4
H8	0	0	0	0	0	0	0		3	3	2	3	4	3	3	4	1	3	3/4	4/4
H9	0	0	0	0	0	0	0	0		4	3	4	5	4	4	5	4	4	4/4	3/4
H10	0	0	0	0	0	0	0	0	0		3	4	3	4	4	5	4	4	4/4	5/4
H11	0	0	0	0	0	0	0	0	0	0		1	4	1	1	2	3	1	3/4	4/4
H12	0	0	0	0	0	0	0	0	0	0	0		5	2	2	3	4	2	4/4	5/4
H13	0	0	0	0	0	0	0	0	0	0	0	0		5	5	6	5	5	5/4	6/4
H14	0	0	0	0	0	0	0	0	0	0	0	0	0		2	3	4	1	4/4	5/4
H15	0	0	0	0	0	0	0	0	0	0	0	0	0	0		1	4	2	4/4	5/4
H16	0	0	0	0	0	0	0	0	0	0	0	0	0	0	0		5	3	5/4	6/4
H17	0	0	0	0	0	0	0	0	0	0	0	0	0	0	0	0		4	4/4	5/4
H18	0	0	0	0	0	0	0	0	0	0	0	0	0	0	0	0	0		4/4	5/4
HA1	1	1	1	0	0	1	1	1	1	1	1	1	1	1	1	1	1	1		1
HA2	1	1	1	0	0	1	1	1	1	1	1	1	1	1	1	1	1	1	0	

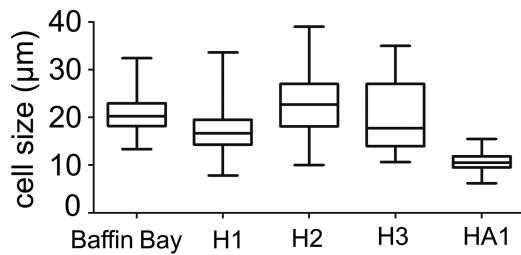


Figure 6. Cell size ranges of cysts of the most common haplotypes of *Sanguina nivaloides* (H1 and H2 = red cysts with smooth cell wall, H3 = red cysts with nipples) and *Sanguina aurantia* (HA1 = small orange cysts) in the dataset studied compared with cell sizes from the Crimson Cliffs in Baffin Bay on Greenland (specimen MB.ES.1781c) (Ehrenberg 1851; Leya 2008).

The geographic distribution of ITS2 haplotypes

For *Sanguina nivaloides* (red cysts), the most frequent haplotype of this study (H1) was found in the High Tatra Mountains (Slovakia), the Swiss Alps (Switzerland), the High Tauern (Austria), Tyrol (Austria), the Sarntal Alps (Italy), the Dolomites (Italy), the Rocky Mountains (Colorado, USA) and on Spitsbergen (Svalbard, Norway). The second most abundant haplotype (H2) occurred on several sites in continental Norway and on Spitsbergen as well as in the Rocky Mountains (Colorado, USA). A smooth cell surface was typical for most of the haplotypes of red cysts, whereas pronounced nipples were found only in a single haplotype (H3) recorded from Italy and Svalbard. Small papillae were rare and only found in scattered cells in three specimens with smooth-walled cysts (Italy—‘1D’, Switzerland—‘Furka’, Slovakia—‘Zamrzute’) belonging to the most common haplotype (H1). *Sanguina aurantia* (small orange cysts) were represented here by two haplotypes (HA1 and HA2), reported from Svalbard and phylogenetically already attributed to a clade called ‘Roter Schnee’ (Leya 2004). The Austrian Alps were shown to be rich in haplotype diversity of *Sanguina nivaloides*, with the presence of at least five (H1, H4, H9, H10 and H13). The haplotype network of this species indicates the presence of shared haplotypes among European mountain ranges, between alpine and polar habitats (e.g. Austria versus Svalbard) and between the continents investigated (Europe, North America and South America). Interestingly, the small orange cysts of *Sanguina aurantia* were not restricted only to the island of Spitsbergen in Svalbard as was implied from preliminary conclusions, but its haplotypes HA2, HA3 and HA4 were found at sampling sites in Colorado and Washington (USA), as shown in Supplementary Fig. 7. The extended version of the haplotype network of *S. nivaloides* detected four further haplotypes for this species (sequence JP1 was phased into sequences belonging to H1 and H22, the latter was connected to the ITS2 haplotype network when the TCS connection limit was lowered to 91%), which confirmed its cosmopolitan distribution e.g. in Japan, Tajikistan, Greenland and Alaska. However, for these sequences published prior to this study, no scanning electron nor light microscopy pictures of cells were available for comparison.

Spatial structuring of *Sanguina nivaloides* metapopulations

The sPCA revealed positive and negative eigenvalues for both two *S. nivaloides* datasets, indicating global (positive values) and local (negative values) patterns. However, the tests on global and local structures were not significant ($P > 0.05$, Supplementary Table 10), so *S. nivaloides* showed an absence of a distinct global

spatial genetic structure and no genetic differentiation between European regions (Supplementary Fig. 8). In other words, we did not find any phylogeographic signal in the distribution of *S. nivaloides*. Moreover, the Mantel test on pairwise geographic and genetic matrices showed no significant correlation (Supplementary Table 11). Genetic distances of *Sanguina nivaloides* ITS2 sequences within and between mountain ranges (European Alps, High Tatra Mountains, continental Norway, Rocky Mountains, Patagonia) and polar regions (Svalbard, Antarctica) were very similar (Table 2). These findings suggest a high dispersal capacity of the cysts, which could promote a continuous gene flow over long distances (on scales of different continents!). At the same time, a successful independent evolution of haplotypes in separate mountain ranges and polar regions might also be taking place as inferred from the genetic distances observed within these groups. That both scenarios are possible for *Sanguina nivaloides* is visualised by the geographical distribution of ITS2 haplotypes in its network (Fig. 9): an identical haplotype occurred in several regions, and a particular region was inhabited by a few different haplotypes.

Taxonomic treatment

Sanguina Leya, Procházková et Nedbalová, gen. nov.

Type of the name of the genus: *Sanguina nivaloides* Procházková, Leya et Nedbalová, sp. nov.

Registration: <http://phycobank.org/100627>

Initially, we attempted to reinstate one of the old genus names typified by *Uredo nivalis* F.A.Bauer 1819—*Protococcus* C.Agardh, 1824 or *Sphaerella* Sommerfeldt, 1824—but both genera names have to be rejected, in the former case versus *Chlamydomonas* Ehrenberg, 1833 (*nom. et orth. cons.*) (original publication: Ehrenberg 1834), in the latter versus *Chlorococcum* Meneghini 1842 (original publication: Meneghini 1843) (*nomen cons.*) (Farr and Zijlstra 1996+). The complicated historic synonymy and the fact that it is not possible to prove that *Uredo nivalis* F.A.Bauer 1819 is conspecific with our recent findings are the reasons why the newly established clade is described by us as a new genus and species.

Etymology: The genus name *Sanguina* refers to the striking blood-red colouration of snow caused by the bloom of its cysts.

Description: Cysts (it is unresolved whether these are of asexual or sexual origin) are spherical, contain one nucleus, a central chloroplast with one naked pyrenoid, and abundant peripheral lipid globules containing red-coloured carotenoids. According to the maturity of cysts and their astaxanthin to chlorophyll-*a* ratios, cysts can appear in different colour shades as orange-peel orange or blood red. As the secondary carotenoids are stored in lipid globules of different sizes the cytoplasm can appear speckled to homogeneous. The surface of the cysts can appear smooth, with blunt (nipples, papillae) or sharp (nibs) protrusions. In mature cysts, carotenoids mask other cell organelles beyond recognition. In young cysts a single parietal chloroplast is clearly visible. At the light microscopy level one cell wall layer can be distinguished in mature cysts and two layers in young cysts. The outermost layer in young cysts is most probably the primary cell wall, which later is shed during cyst maturation exposing the developing secondary cell wall. Vegetative stages are unknown, and no culturable strains exist. The genus is restricted in its habitat to snowfields and glacier-based snowfields in polar and alpine regions.

Diagnosis: The genus *Sanguina* differs from other genera within the Chlamydomonadaceae [i.e. the genus *Chlamydomonas* sensu Pröschold et al. (2001)] in its phylogeny, as this species

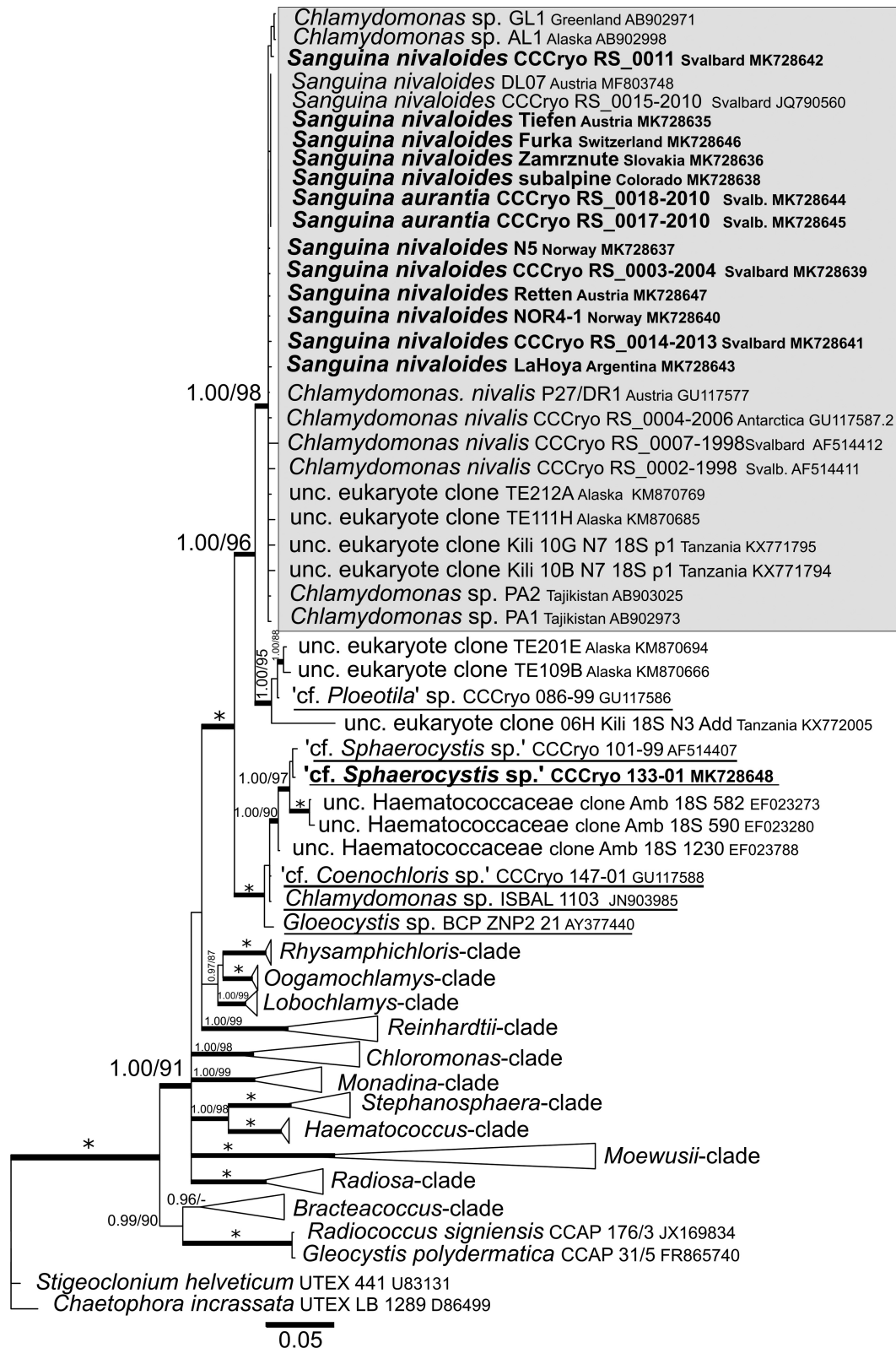


Figure 7. 18S ribosomal RNA gene-based Bayesian phylogenetic tree. The *Sanguina*-clade with *Sanguina nivalis* and *Sanguina aurantia* is highlighted in a grey box. Posterior probabilities (≥ 0.95) and bootstrap values from maximum likelihood analyses ($\geq 75\%$) are shown. Full statistical support (1.00/100) is marked with an asterisk. Thick branches represent nodes receiving the highest posterior probability support (1.00). Newly obtained sequences are in bold. Accession numbers, strain or field sample codes are indicated after each species name. Species names of the closest species that are available as laboratory cultures are underlined. Abbreviation: unc, uncultured.

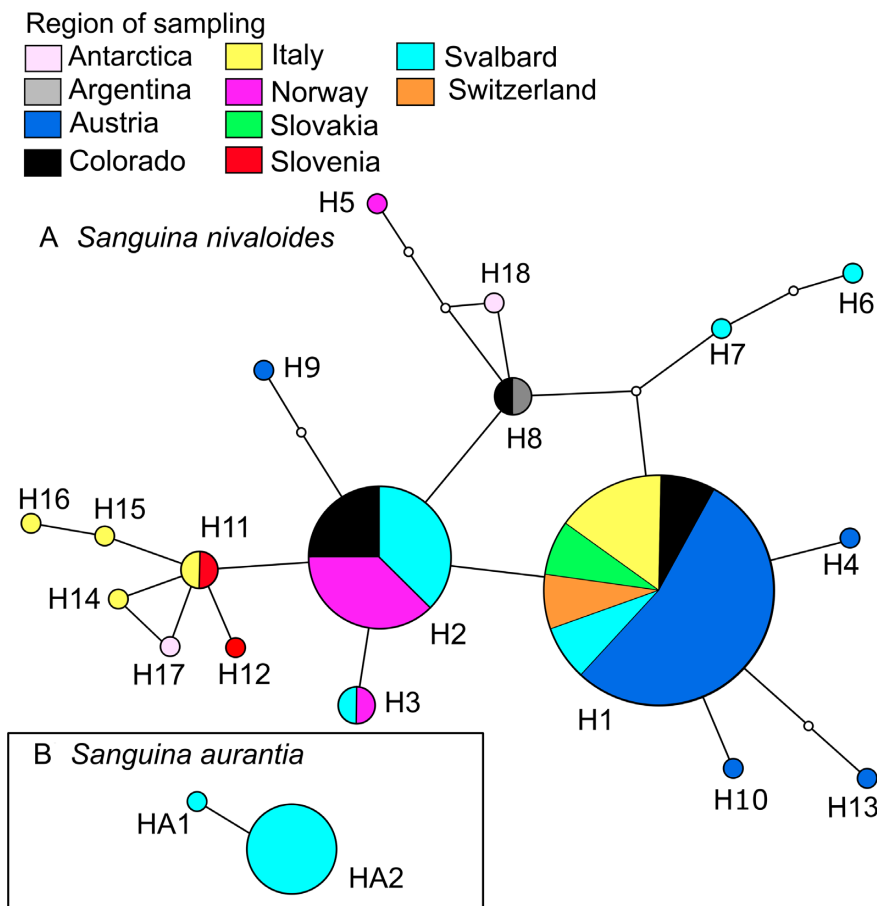


Figure 9. Geographic distribution of ITS2 rDNA haplotypes detected in this study: (A) *Sanguina nivaloides*, (B) *Sanguina aurantia*. Each haplotype network was constructed by a statistical parsimony method with a 95% connection limit. The *Sanguina nivaloides* network includes haplotypes from polar regions (Antarctica, Svalbard) and alpine regions in Europe (Austria, Italy, Norway, Slovakia, Slovenia, Switzerland), North America (Colorado) and South America (Argentina). The *Sanguina aurantia* network includes haplotypes from Svalbard. Each ball represents a haplotype (i.e. in this study's field samples, which have identical ITS2 sequences). The size of the ball is proportional to the number of specimens sampled, which belong to that specific haplotype. The colour represents a country of sampling. Lines connect each haplotype with its most similar relative. Open dots represent mutation steps between haplotypes, one dot indicates a change of one base pair.

Table 2. Mean uncorrected (p-distance; %) and corrected pairwise genetic distance (Kimura-2-parameter K2P; %) between *Sanguina nivaloides* field samples from different regions based on the ITS2 rDNA nucleotide sequence below and above the diagonal. Mean uncorrected and corrected pairwise genetic distances are shown in the first column. The presence of n.c. (not calculated) in the results denotes cases in which it was not possible to estimate evolutionary distances (single sequence from the region).

	Mean intraspecific distance	Svalbard	European Alps	Norway	Tatra Mountains	Rocky Mountains	Patagonia	Antarctica
Svalbard	1.30		1.20	1.20	0.80	0.90	1.00	1.60
European Alps	1.00	1.20		1.20	0.60	0.80	1.20	1.60
Norway	1.00	1.20	1.20		1.00	0.70	0.80	1.40
Tatra Mountains	n.c.	0.80	0.60	1.00		0.50	1.00	1.50
Rocky Mountains	0.50	0.90	0.80	0.70	0.50		0.50	1.10
Patagonia	n.c.	1.00	1.20	0.80	1.00	0.50		1.00
Antarctica	2.00	1.50	1.50	1.30	1.50	1.10	1.00	

layer, plastids are located close to the cell wall (parietal) and mean cyst sizes are larger in diameter (Procházková et al. 2018b). *Chlainomonas* sp. also differs in the blood-red, but ovoid quadri-flagellate cell stages that are quite distinct from the immobile spherical cysts of *Sanguina*. Moreover, *Chlainomonas* sp. prefers water-logged habitats, and thus usually causes the red colouration of snow-slush on frozen lakes. *Sanguina*, on the other hand, is rather found in terrestrial habitats such as snow-covered rocks

or soil and permafrost. If *Sanguina* is found close to water-logged localities, it tends to dwell on the dry parts of snow. *Smithsonimonas abbotii* (Kol 1942), a snow alga described from red snow above the timber line in Alaska, might be closely related to the genus *Chlainomonas*. It differs from *Sanguina* in its cells being surrounded by a bell-shaped cell wall, which is smooth when young and becomes progressively warty when older. Large quantities of astaxanthin are also accumulated in the resistant red cysts

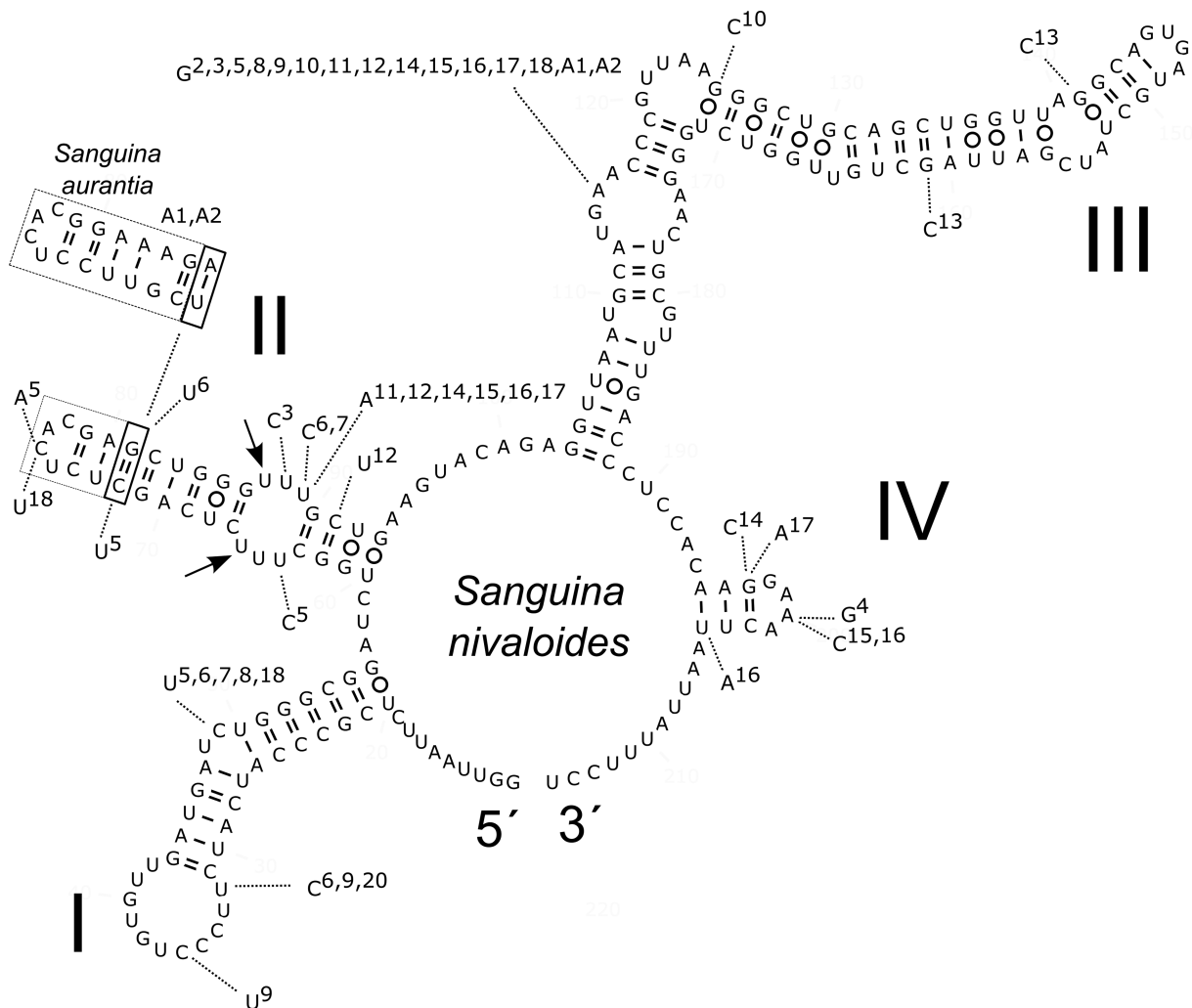


Figure 10. Comparison of the secondary structure of the ITS2 rDNA transcripts of 18 haplotypes of *Sanguina nivaloides* (H1-H18) and two haplotypes of *Sanguina aurantia* (HA1, HA2). Helices are labelled with Latin numbers (I-IV). Nucleotide differences of all haplotypes are shown outside the structure and are linked by dotted lines. Numbers 2–18, A1 and A2 indicate in which haplotype the difference was detected when compared to haplotype number 1 of *Sanguina nivaloides* (represented by the holotype specimen CCryo RS.0015–2010, accession number MK728599). One compensatory base change between *Sanguina nivaloides* and *Sanguina aurantia* is indicated by the bold rectangle. The dashed rectangle at the end of helix II is showing an expansion segment (length is not conserved). Note: the U–U mismatch in helix II (arrows). The 5' and 3' ends of the ITS2 transcript are indicated.

(aplanospores) of the genus *Haematococcus* (Allewaert et al. 2015; Mazumdar et al. 2018), which differs, however, in its 18S rRNA gene and *rbcl* sequences.

***Sanguina nivaloides* Procházková, Leya et Nedbalová, sp. nov.**

? = *Uredo nivalis* F.A.Bauer, Microscopical observation on the red snow.— *The Quarterly Journal of Literature, Science and The Arts*, London : 222–229 (incl. plate VI), Figs 1–7. 1819

? = *Chlamydomonas nivalis* (F.A.Bauer) Wille, Algologische Notizen IX–XIV. *Nyt Magazin for Naturvidenskaberne* 41: 103, 126, plate III, Figs 44, 45. 1903.

Neither of the original field samples of *Uredo nivalis* from 1818 and of *Chlamydomonas nivalis* from Wille are traceable, therefore these names are included in the synonymy with a question mark.

Nomenclatural remarks: Though we clearly do not attempt to synonymise *Cd. nivalis* with *S. nivaloides*, simply because there is no conclusive way to do so, for completeness we want to give an overview of the nomenclatural complexity relating to *Cd. nivalis*. With regard to the type of material sampled in Baffin Bay

in 1818, three homotypic synonyms are listed on the website of AlgaeBase (Guiry and Guiry 2018): *Uredo nivalis* F.A.Bauer 1819, *Protococcus nivalis* C.Agardh 1824 and *Sphaerella nivalis* (F.A.Bauer) Sommerfelt 1824. In this context *Uredo nivalis* represents the lectotype and basionym, still reflecting that the (colourless) globules were regarded as a fungus. The genus *Uredo* was typified by Persoon (1801) with its type species *U. betae* and thus is conserved against *Cd. nivalis*. Wrangel (1823) described *Lepraria kermesina*, the lectotype species of *Protococcus*, and he considered this lichen to be the organism causing the red snow. *L. kermesina* was then listed as a synonym of *Protococcus nivalis*. *Haematococcus* Flotow, 1844 was also listed as a synonym, but it was finally decided to exclude both, *Lepraria kermesina* and *Haematococcus*, from the synonymy (Andersen 2018). With regard to *Protococcus* C.Agardh, 1824 and *Sphaerella* Sommerfelt, 1824—both genus names have to be rejected, in the former case versus *Chlamydomonas* Ehrenberg, 1833 (original publication: Ehrenberg 1834) (*nom. et orth. cons.*), in the latter versus *Chlorococcum* Meneghini, 1842 (original publication: Meneghini 1843) (*nomen cons.*) (Farr and Zijlstra 1996+). In the Index Nominum Genericorum

and the literature, further synonyms for *Cd. nivalis* are listed. In her extensive and outstanding monography on the biology and limnology of snow and ice, Kol (1968) cites these synonyms, which are given here for completeness as well (some citations have been corrected, as far as possible, as wrong volume numbers or pages were cited originally): *Palmella nivalis* Hooker 1825, p. 184; *Coccolioris nivalis* Sprengel (ex parte) 1827, p. 373; *Cocophysium nivale* Link 1833, p. 342; *Gloiococcus grevillei* Shuttleworth 1840a, p. 54 and Shuttleworth 1840b, p. 405 resp.; *Discerea nivalis* Vogt 1844, p. 217 with plate 1: Figs 1-5 (as '*Discerea nivalis*'); *Hysginium nivale* Perty 1852, p. 95; *Chlamydococcus nivalis* (F.A.Bauer) A.Braun nach F.Cohn 1861, p. 54, *Haematococcus nivalis* (F.A.Bauer) C.Agardh 1828-1835, Icon. Alg., *Haematococcus nivalis* Flotow 1844. Further information on the synonymy and references on world-wide findings of *Cd. nivalis* also can be found in Kol (1968).

Holotype: Specimen CCCryo RS.0015–2010 of field sample 004/10 consisting of cysts in a desiccated (non-viable) state in the herbarium of the Botanic Garden and Botanical Museum Berlin-Dahlem (herbarium acronym: B), Freie Universität Berlin, Königin-Luise-Straße 6–8, 14 195 Berlin, Germany, no. B 40 00 43192 [<http://herbarium.bgbm.org/object/B400043192>], represented by our Figs 2A and 3A.

Isotypes: (1) desiccated, under nitrogen, in the Micropalaeo Collection, Museum für Naturkunde, Leibniz Institute for Evolution and Biodiversity, Science, Invalidenstraße 43, 10 115 Berlin, Germany, no. ECO103, (2) frozen at -80°C at DNA-bank in the herbarium of the Botanic Garden and Botanical Museum Berlin-Dahlem (herbarium acronym: B), no. B GT 00 24094 [<http://herbarium.bgbm.org/object/BGT0024094>], (3) frozen at -150°C (in triplicate) in the SAG biobank at the Department Experimental Phycology and Culture Collection of Algae at the Goettingen University (EPSAG), Nikolausberger Weg 18, 37 073 Goettingen, Germany, nos. Z000696411, Z000696414, Z000696417, (4) frozen at -150°C (in triplicate) in the CCCryo biobank at the Fraunhofer Institute for Immunology & Cell Therapy, Branch Bioanalytics and Bioprocesses IZI-BB, Am Muehlenberg 13, 144 760 Postdam, Germany, nos. 2-07-02-14, 2-07-02-15, 2-07-02-16, and (5) desiccated (in triplicate) in the CCCryo biobank, nos. D2-07-02-17, D2-07-02-18, D2-07-02-19.

Type locality: a steep snowfield surrounded by moss vegetation and rocks, stretching down northwest to sea level from Mount Midterhuken (760 m a.s.l.), southwest of Mariasundet between Bellsund and Van Mijenfjorden, Nathorst Land, Svalbard, Norway (77°39'44.298"N 14°48'58.903"E; altitude: 15 m a.s.l., specimen CCCryo RS 0015–2010, collected on 4 August 2010 by Thomas Leya & Guntram Weithoff as collectors' sample number 004/10).

Paratypes: (1) Specimen CCCryo RS.0003–2004 frozen at -150°C in the CCCryo biobank at Fraunhofer IZI-BB, no. 2-07-02-21 (Figs 2E, 3B and 4F), (2) specimen WP123 frozen at -150°C in the CCCryo biobank at Fraunhofer IZI-BB, no. 2-07-02-22 (Figs 2B and 4C-E).

Paratype localities: CCCryo RS.0003–2004: northeastern part of Doktorbreen, Nathorst Land, Svalbard, Norway (77°34'0.001"N 16°53'59.999"E; altitude: 430 m a.s.l., collected on 6 August 2004 by Thomas Leya, sample number 013-01/04); WP123: Schwarzmoos, Kühtai, Stockach, Tyrol, Austria (47°13'35.0"N 11°01'03.1"E; altitude: 2352 m a.s.l., collected on 25 May 2017 by Lenka Procházková & Daniel Remias, sample number WP123).

Registration: <http://phycobank.org/100628>

Etymology: the species epithet refers to the habitat of this species (snow).

Description: Usually smooth-walled cysts (Figs 2A and 3A), which can also be ornamented more or less regularly with nipples (Figs 2E and 3B), blunt ribs, or small or pronounced papillae. Cysts of size 7.8–39 µm in diameter, causing red snow. The astaxanthin to chlorophyll-*a* ratio of the red cysts ranges between 20:1 and 34:1 depending on the level of cyst maturity (Bidigare et al. 1993; Müller et al. 1998; Remias, Lütz-Meindl and Lütz 2005). At the light microscopy level usually only one cell wall layer is distinguishable in mature cysts (Fig. 2A) (using TEM two layers are distinguishable, Fig. 4B) and two cell wall layers for young cysts in early stages of development (Fig. 2B) (using TEM three layers are visible, Fig. 4E). The detailed structure of the cell wall is usually visible in TEM only; it contains a very thin trilaminar sheath formed below the transient primary cell wall during morphogenesis of the secondary cell wall. In early cyst stages a parietal chloroplast is clearly visible in LM, as are a large unpigmented vacuole and a naked pyrenoid (Fig. 2B). The temporary third outermost cell wall in TEM is fuzzy (Fig. 4E). Vegetative stages are unknown, as no culturable strains exist. *Sanguina nivaloides* is an extremophilic alga living in melting snowfields in polar and alpine regions.

Diagnosis: In the stage of mature cysts *S. nivaloides* has a single chloroplast located in the central position surrounding one single nucleus; (nearly) its entire cytoplasm appears dark red due to the secondary carotenoid astaxanthin. It differs from aplanospores of the genus *Haematococcus*, which have their chloroplasts localised in the interspace between oil droplets, resulting in chloroplasts with a net-like appearance (Wayama et al. 2013). It differs from *Bracteacoccus engadinensis*, which also accumulates astaxanthin in its multinuclear coenoblasts, but only in the central area, and its chloroplast is also composed of several (4–10) polygonal discs (Ettl and Gärtner 2014). It differs from *Chlainomonas rubra*, *Chlainomonas kolii* and *Chlainomonas* sp. quadriflagellates in its spherical cell shape (the latter have an ovoid cell shape) and its cell wall organisation (in *C. rubra* the protoplast is surrounded by a massive sheath of gelatinous material, *C. kolii* has a net-like outer envelope, *C. sp.* has a partially thickened cell wall) and in the absence of flagellar grooves in their cysts; persistent flagellar grooves were observed in the thick-walled cysts for *C. kolii* and *C. rubra* at least during cyst formation (Hoham 1974; Novis et al. 2008). Most importantly, *S. nivaloides* differs genetically in its 18S rRNA gene and *rbcL* sequences from red aplanospores of the genus *Haematococcus* such as *Haematococcus lacustris* (epitype, strain SAG 34-1b; 18S: AF159369.1) (Hepperle et al. 1998; Nakada and Ota 2016) and *Haematococcus alpinus* (strain: LCR-CC-261f, 18S: MF093734, *rbcL*: MF093733) (Mazumdar et al. 2018). *Sanguina nivaloides* differs from *Sanguina aurantia* in the macroscopic coloration of snowfields (the latter causes orange snow), cell size ranges (the latter is usually smaller, up to 16 µm), pigmentation (the latter has one magnitude lower level of astaxanthin to chlorophyll-*a* ratio in mature cysts), distribution (the latter was found in the Arctic and subarctic regions in North America to date) and physical association between cells (*Sanguina nivaloides* has cells that are almost always solitary, whereas *Sanguina aurantia* is often clustered by means of mucilaginous sheaths surrounding the cells). The genus *Sanguina* forms a monophyletic clade, and *S. nivaloides* is unique in its ITS2 rDNA sequence. For the holotype specimen CCCryo RS 0015–2010 the ITS2 rDNA sequence is characteristic (accession number MK728599).

Distribution: melting snow in Europe, Asia, Africa, Antarctica, the Arctic, North America, South America, New Zealand and Australia.

Sanguina aurantia Leya, Procházková et Nedbalová, sp. nov.

Holotype: specimen RS.0017–2010 of field sample 005/10–1b consisting of cysts in desiccated (non-viable) state in the herbarium of the Botanic Garden and Botanical Museum Berlin-Dahlem (herbarium acronym: B), Freie Universität Berlin, Königin-Luise-Straße 6–8, 14 195 Berlin, Germany, no. B 40 00 43197 [<http://herbarium.bgbm.org/object/B400043197>], represented by our Fig. 5B and D.

Isotype: frozen at -80°C at DNA-bank in the herbarium of the Botanic Garden and Botanical Museum Berlin-Dahlem (herbarium acronym: B), no. B GT 00 38001 [<http://herbarium.bgbm.org/object/BGT0038001>].

Type locality: snowfield at the south foot of Fugleberget, Isbjørnhamna, Hornsund, Wedel Jarlsberg Land, Svalbard, Norway (77°0'42.156"N 15°32'13.2"E; altitude: 55 m a.s.l., collected on 6 August 2010 by Thomas Leya & Guntram Weithoff, sample number 005/10–1b).

Registration: <http://phycobank.org/101398>

Etymology: the species epithet refers to the intracellular colouration of the mature cysts (orange).

Description: Usually smooth-walled cysts (Figs 5B), sometimes the outermost layer is wrinkled and when it is decomposed, the smooth cell wall below may appear. Cysts of size 6.2–15.5 µm, causing orange snow. The astaxanthin to chlorophyll ratio of the orange cysts ranges between 0.8:1 and 2.6:1 (Müller et al. 1998). At the light microscopy level usually only one cell wall layer is distinguishable in mature cysts (Fig. 5B) (using TEM two layers are distinguishable), in some cases also a distant cell wall layer is present (Fig. 5A; in TEM three layers are visible and the outermost third layer might be multilayered, Fig. 5E). The detailed structure of the cell wall is usually visible in TEM only; it contains a very thin trilaminar sheath formed below the transient primary cell wall during morphogenesis of the secondary cell wall. Vegetative stages are unknown, as no culturable strains exist.

Diagnosis: *Sanguina aurantia* differs from *Sanguina nivaloides* in the macroscopic orange colouration of snowfields (the latter causes red snow), cell size ranges (the latter is usually larger, up to 40 µm), pigmentation (the latter has a higher level of astaxanthin to chlorophyll-*a* ratio in mature cysts), distribution (the latter was shown to be cosmopolitan) and physical association between cells (*Sanguina aurantia* is often clustered by means of a mucilaginous sheath surrounding the cells, whereas *Sanguina nivaloides* has cells that are almost always solitary). For the holotype specimen CCCryo RS.0017–2010 the ITS2 rDNA sequence is characteristic (accession number MK728634).

Distribution: in melting snow in subpolar and polar regions, so far the known locations are only in the northern hemisphere (North America, the Arctic).

DISCUSSION

The first collections of red snow date back to British expeditions to the far north looking for a navigable North-West passage (N.N. 1818; Bauer 1819; Ross 1819; Bauer 1820; Ross 1820). In our study many samples of red snow cysts from around the world have yielded sequences that fell in the new clade *Sanguina*, so one is tempted to assume that the historical sample of 1818 also probably represents the red snow-causing species *S. nivaloides*; however, this cannot be proven yet. A genetic comparison was not possible as the historic sample of 1818 could not be located in museums or herbaria in either London or Berlin. Intact DNA could also not be isolated from the similar sample

collected during the Grinnell Arctic Expedition at Beverly Greenland [76°3' N in 1851 (Ehrenberg 1851; Leya 2008) a bit further north of the original location of 1818–1819 at the Crimson Cliffs (75°54' North, 67°15' West)]. Thus, we do not attempt to synonymise *S. nivaloides* with *Cd. nivalis*. In this study we have suggested that all our investigated red and orange spherical cysts belong to *Sanguina nivaloides* and *Sanguina aurantia*, respectively. We showed that the genus *Sanguina* forms one independent lineage in the Chlamydomonadaceae. The conservative nuclear marker 18S was 100% identical for these two species. Strains CCCryo 086–99, CCCryo 101–99, 133–01 and 147–01 represent the most closely related and culturable isolates/species and appear to be distributed into several lineages that are sister genera to the clade of *Sanguina*, some of them possibly representing the genus *Achoma* (Novis and Visnovsky 2012). The revised genus *Chloromonas* (Pröschold et al. 2001) so far contains the majority of other culturable snow algal species involved in coloured snow, but is robustly separated from the *Sanguina*-clade.

This study is the first record of ITS2 sequence data of spherical cysts forming red snow from Argentina and many mid-latitude alpine sites in Europe. Moreover, our data will increase the knowledge about this taxon due to several new findings on Svalbard. The ITS2 marker was previously used in this context only in studies of snow samples from the USA (Brown, Ungerer and Jumpponen 2016), Greenland, Alaska, Japan and Tajikistan (referenced in accession numbers only, see Materials and Methods) and also most recently from Antarctica and Svalbard (Segawa et al. 2018). The set of different molecular data used in this study has proved to provide valuable insights into the relationship of this taxonomically complex algal group. Haplotype networks have been used to demonstrate the intraspecific diversity (i.e. within a species) (Škaloud et al. 2015). Based on our results, *S. nivaloides* represents a diverse species containing 18 different ITS2 genotypes and *S. aurantia* has two ITS2 genotypes. According to the metagenomic study of Brown, Ungerer and Jumpponen (2016) in Colorado and Washington (USA), sequences of this locus of cysts in blooming snowfields were distributed into 30 haplotypes classified as 'Coenochloris' and 27 haplotypes termed as 'Chlamydomonas'. Further samplings in other mountain regions might reveal additional unique genotypes as shown by Segawa et al. (2018). Similarly, 15 haplotypes of ITS2 rDNA were resolved for the common 'blood rain alga' *Haematococcus lacustris* (referred to as *H. pluvialis* in the paper cited) in temperate Europe (Allewaert et al. 2015). Intraspecific diversity within the widespread lichen photobiont *Asterochloris lobophora* in Europe, America and Asia accounted for 18 haplotypes of ITS2 rDNA, while half that amount of intraspecific diversity was found for other *Asterochloris* species (Škaloud et al. 2015).

Although the overall mean distance among the ITS2 red cysts haplotypes of *S. nivaloides* was rather low [p-distance of 1.7%; this value was similarly low for *Asterochloris* lineages described by Škaloud et al. (2015)], a divergence between haplotypes can be observed with regard to the red cysts of *Sanguina nivaloides* and orange cysts of *S. aurantia* in their variable ITS2 marker (sequence differences up to 5%), which might indicate a currently ongoing genetic diversification. Such a process was described for the soil alga *Bracteacoccus bullatus* by Fučíková and Lewis (2012). Further detailed pigment studies, physiological experiments with cysts, sequencing of further highly variable molecular markers (Škaloud et al. 2015) and cultivation attempts, possibly using strategies so far unconsidered, are clearly necessary to bring a richer understanding of morphological and molecular variability within the genus *Sanguina*.

When comparing red snow samples of Baffin Bay (Greenland) from 1851 with our recent samples, this showed that cell sizes corresponded well to the cell size ranges determined in this study (Fig. 6). Spherical red globules as well as green globules 'mostly with a small stalk and fluffy attachment, being the thallus or the root and leaf layer' were reported from this sample [quotation translated into English from Ehrenberg (1851)]. While we could identify the former in the desiccated sample, the latter were not visible. However, we have also occasionally observed such stalks in recent samples [Fig. 2b in Leya (2008)]. We assume that they are fungal mycelia, which are not rare in field samples of red snow (Brown, Olson and Jumpponen 2015).

Cysts of *Sanguina nivaloides* are usually smooth-walled, and other specific variations in cell surface structure (e.g. cysts with nipples) may either reflect a level in the process of cyst maturation reached at the time of sampling or a causality between intraspecific variability and morphology (as e.g. all samples of H3 are expected to be represented by cysts with nipples, which is the case for both specimens of H3 in this study). To test this hypothesis, more specimens of the same morphologically different haplotype are needed (i.e. for H7, H14). Additionally, the observation of populations of smooth-walled cysts with the rare presence of cells with small papillae in two of our samples is in good correspondence with the findings reported from red snow in North America by Brown, Ungerer and Jumpponen (2016): they point out that very low haplotype diversity exists within the same algal bloom sampled: each algal patch was dominated by only one haplotype, with a very minor proportion of subdominant haplotypes. In the past, blooms of other snow algal taxa producing red cysts were often wrongly assigned to '*Chlamydomonas nivalis*', e.g. most often *Chlainomonas* was not recognised [see Figs 23 and 24 in Stein and Amundsen (1967), in Kawecka (1981), and in Fig. 4 in Kobayashi and Fukushima (1952)]. The first comprehensive cell ultrastructure and secondary pigment profile comparisons between cysts of *Chlainomonas* and '*Chlamydomonas nivalis*' were performed by Remias et al. (2016).

In our study, cell sizes of *S. nivaloides* red cysts correspond to the findings of Mosser et al. (1977) and Remias et al. (2005). The sizes of *S. aurantia* orange-coloured cysts from our study are in the range reported from Arctic pack ice floes (Gradinger and Nürnberg 1996) and from Spitsbergen (Müller et al. 1998; Leya 2004; Stibal et al. 2007). We assume that cell size can be highly plastic during their seasonal development, which would also explain the variable cell sizes among the haplotypes of red cysts we found, since our locations were sampled at different times during the snow melting season and were also varying in aspects related to their topographical properties (snowfield's slope angle, cardinal orientation of the site to the sun, elevation) and snow texture. Interestingly, the largest mean cell sizes were observed in samples collected either late in the season (e.g. samples '2RON', 'NOR4-1') or on glacier-based snowfields (e.g. samples '4HT', 'Foxfona', 'Retten'). Indeed, cell sizes may also reflect culture conditions as in the lichen photobiont *Asteriochloris* (Škaloud et al. 2015). An alternative hypothesis could be that cell sizes of *S. nivaloides* and *S. aurantia* haplotypes are genetically determined with some variability. Interestingly, we observed narrow cell size variations when comparing genetically very uniform small orange cysts of *S. aurantia* from the different locations on Svalbard (two haplotypes only). More observations of orange cysts of *S. aurantia* from other geographic regions are needed to test this hypothesis, e.g. a bloom in North America was genetically identical for ITS2 (accession number KX063716; Brown, Ungerer and Jumpponen 2016) to *S. aurantia* orange cysts sampled in Svalbard (this study), but for the former

no morphology data were collected. Interestingly, some haplotypes of *S. nivaloides* red cysts [i.e. H9 ('WP123'), H18 ('Esperanza-8')] were as small as *S. aurantia* orange cysts. Considering this fact, the sole parameter of cell size only should not be used for distinguishing between *S. nivaloides* and *S. aurantia* by light microscopy. Other aspects of mature cysts also should be considered such as cell wall morphology, intracellular pigmentation reflecting the astaxanthin to chlorophyll-*a* ratio and the macroscopic colour of the blooming snowfield.

Due to their small size (Wilkinson et al. 2012) and ability to resist drought and freezing stress, the cysts of *S. nivaloides* and *S. aurantia* are suitable propagules for long distance dispersal by prevailing air streams (Brown, Larson and Bold 1964; Schlichting Jr. 1969), birds (e.g. polar birds migrating between the two polar regions, such as the Arctic tern *Sterna paradisaea*) and ocean currents (Gillespie et al. 2012). Our data showed a cosmopolitan distribution of *S. nivaloides* in alpine and polar snowfields in both hemispheres, which supports the theory of a trans-equatorial dispersal of microbes (Hodač et al. 2016). No population structure was detected when analysing the ITS2 rDNA data, as there was no phylogeographic signal. Metagenomic analyses have shown red pigmented snow algae to be cosmopolitans based on the analysis of partial sequences of the 18S rRNA gene (Lutz et al. 2016) as well as of the ITS2 rDNA (Segawa et al. 2018). The latter study also detected endemic snow algal phylogenies being distributed in one of the two polar regions. Antarctica was regarded for a long time as a continent in biological isolation until large amounts of vascular plant pollen were collected on Signy Island (South Orkney Islands), and a parallel observation of the daily synoptic weather patterns revealed that roughly 1.5 times per year a corridor of strong winds develops between Tierra del Fuego (Argentina) and Antarctica (Marshall 1996). This explains our finding that the South American sample of *S. nivaloides* ('La Hoya', H8) was nearly identical in its ITS2 rDNA sequence with the haplotype from maritime Antarctica (H18) and with the most common haplotype in Europe (H1). The distribution of these small microorganisms could be controlled by selection due to local environmental factors as well as dispersal limitations. Moreover, a strong founder effect from only few propagules and intense kin competition is assumed to take place (Brown, Ungerer and Jumpponen 2016).

Concerning local environmental factors at the moment of sampling of encysted cells, the usually slightly acidic pH and low conductivity of snow patches with algal blooms resembled those of pristine, white snow presumably free of any algae. However, Brown and Jumpponen (2019) showed that snow algae are seemingly omnipresent, though in low abundances, at the surface of melting subpolar and alpine 'white snow' that are void of a visible algal bloom. Nitrate, ammonium and phosphate were not limiting nutrients for Arctic algal communities in a study by Spijkerman et al. (2012). On the other hand, atmospheric trace gases were recently recognised to play a role in supporting primary production in oligotrophic habitats in polar regions (Ji et al. 2017). None of these findings conclusively explains the patchy occurrence of red snow, which often can be observed in the same pattern year after year at the same location. Spijkerman et al. (2012) suggested that the highly patchy distribution of algal blooms in snow could be partly a result of small-scale topographical and geological characteristics influencing snowfield persistence or disappearance due to enhanced or reduced snow melt or snow accumulation. Similarly, inputs of mineral impurities can result in significantly earlier snow melt (Di Mauro et al. 2018). The slower the melting, the more prolonged is the period that is available for a snow algal population to develop. This is realised

in alpine regions at higher elevations (above 1900 m a.s.l. in this study). With regards to the availability of liquid water, the algal cells seem to thrive during the growth season in the thin but persistent aqueous reservoir that by the laws of physics remains liquid around and between snow and ice crystals (Jones et al. 2001). To find a conclusive answer about which factors on a small scale actually determine the development of snow blooms such as those of *S. nivaloides* and *S. aurantia* or whether the cysts are just randomly dispersed there, a time series sampling would be necessary to observe the development of a blooming snow field while concurrently measuring various parameters.

Red spherical cysts from the European Alps morphologically identical to *S. nivaloides* cysts were shown to tolerate short periods of elevated UV-B radiation (Remias et al. 2010) due to the massive production of secondary carotenoids, which act mainly as shading pigments, but also as very powerful radical scavengers. This is especially true of ketocarotenoid astaxanthin, which absorbs energy in the near UV-range. *Sanguina nivaloides* shows high photophysiological plasticity with a highly efficient photosystem under low irradiation and no photoinhibition up to 2000 $\mu\text{mol m}^{-2} \text{s}^{-1}$ (Procházková et al. 2018b). Additionally, inorganic rock dust particles covering mature cysts seem to provide additional shading protection (Lütz-Meindl and Lütz 2006). *Sanguina nivaloides* cysts are required to survive over summer when snow has melted, and provided they still contain chlorophyll and are not photoinhibited, the photosynthetic apparatus should continue to function (Remias, Lütz-Meindl and Lütz 2005). After total snow melt, cysts most likely ‘oversummer’ the rest of the year, generally in a dried state, on rocks, permafrost or moss-covered soil, all being subject to drastic diurnal temperature fluctuations; non-vegetated soils in particular can experience temperature changes of 30°C within 24 h (Ley, Williams and Schmidt 2004). Therefore, *S. nivaloides* cysts can be regarded as being eurythermic and desiccation-resistant. The question remains whether the vegetative stages (gametes or other green stages if they exist) are dependent on cold temperatures, which would characterise them as cryophiles.

Key triggers to a successful *S. nivaloides* cultivation have not been elucidated yet. Indeed, many green proliferating strains have been isolated from snowfields, but molecular methods and phylogeny have always shown that these isolates are taxa other than *S. nivaloides*. A well-known example of such a misinterpretation was strain UTEX 1969, which for years was listed as *Chlamydomonas nivalis* and frequently used in studies addressing cold adaptation, just as other strains erroneously were assigned to this taxon (Lu et al. 2012a,b, 2016). When, in 1990, H. Ettl and U.G. Schlösser (pers. comm.) re-identified many UTEX, CCAP and SAG strains of *Chlamydomonas*, they found that many were incorrectly named—among them also *Cd. nivalis* strains, which were first assigned to *Chlamydomonas augustae*, but later partly renamed again on the basis of the phylogenetic analyses as *Chloromonas typhlos* (Matsuzaki, Hara and Nozaki 2012) or *Cr. reticulata* (CCALA 753; CCALA 754). At present, it must be accepted that we do not have any living strain on hand to enable the studies on the life cycle of *S. nivaloides*. All diagrams describing the life cycle of this species are thus just hypothetical without any empirical proof (e.g. in terms of molecular data) (Müller, Leya and Fuhr 2001; Sattler et al. 2010; Remias 2012). Any conclusions can be made only very cautiously and indirectly based on the knowledge of life cycles of more distantly related species. The sexual life cycle of several Chlamydomonadacean species usually include the formation of zygotes into zygospores with a thick cell wall, which represents the dormant stage in the life cycle (Žárský, Kalina and Sulek 1985). After the formation and

growth of the secondary cell wall, the primary cell wall of the zygospore is shed from the surface (VanWinkle-Swift and Rickoll 2008) and the ornamented structure of the mature zygote becomes apparent (Pröschold et al. 2001). We observed a similar cell wall organisation in the ruby cysts type, which have been found so far on the Northern hemisphere in continental Norway (sample N4' and NOR4-1' in this study), in Svalbard [sample RS.0011 in this study and in Müller et al. (1998)], on Iceland (D. Remias, pers. comm.), on the western coast of Canada (L. Quarmby, pers. comm.), in Washington State in the USA (K. Thomas, pers. comm.), Oceania (P. Novis, pers. comm.), as well as in the southern hemisphere on the Antarctic King George Island (T. Leya, pers. comm.). Wille (1903) was referring to this distinctive cellular morphology in his study of *Cd. nivalis* from Djupvatshytten (Norway) (plate III, Figs 44 and 45). Their identity needs to be revealed by single cell sequencing. The first insights into their 18S rRNA gene phylogeny suggest that the ruby-type cysts might in fact be members of the *Chloromonas*-clade (Segawa et al. 2018).

The CBC species concept was successfully applied for several algal groups, e.g. snow-dwelling *Chloromonas* species (Matsuzaki et al. 2019). This concept can be used also in a metagenomic study: Segawa et al. (2018) showed that their ‘*Chlamydomonas*’ snow group B (conspecific with *S. nivaloides*) differs by one CBC in helix III only compared with the closely related ‘*Chlamydomonas*’ snow group A (see their Supplementary Figures S2 and S8). On the other hand, it was shown that the CBCs are not diagnostic in some cases at the species level and that even genera, families and orders of green algae can lack CBCs in such regions (Caisova, Marin and Melkonian 2011; Škaloud and Rindi 2013). Therefore, the presence and number of CBCs are probably direct consequences of the accumulation of mutations during the evolutionary process, simply reflecting the genetic distance among organisms. In our study, two field samples of *Sanguina nivaloides* (‘NOR4-1’ and ‘RS.0014-2013’) lack any CBC in their secondary structure when compared with *Sanguina aurantia*. Both two newly described species are closely related: they have identical 18S rRNA gene and more than 95% identical ITS2 (one CBC found). In the *rbcL* phylogeny, *S. aurantia* has been placed within *Sanguina nivaloides* field samples; this might be linked to unusual gene substitutions in *rbcL*, which was reported to result in artefacts in the phylogeny (Nozaki, Onishi and Morita 2002). Species boundaries between *S. nivaloides*, *S. aurantia* and other related species should be estimated by combination of substantial morphological, ecological and genetic difference (investigation of several molecular markers, the level of ITS2 rDNA sequence similarity should be also taken into account). *S. aurantia* has uniquely different ITS2 haplotypes to *S. nivaloides*, orange spherical cysts and red spherical cysts are clearly distinguishable, both microscopically and macroscopically, and the area of their geographic distribution is only partly overlapping. No strain for these species is available yet. According to our 18S rRNA gene and *rbcL* phylogenies, the closest known and culturable relatives of *Sanguina nivaloides* are strains CCCryo 133-01/101-99 (currently assigned to cf. *Sphaerocystis* sp.), strain CCCryo 147-01 (cf. *Coenochloris* sp.) and CCCryo 086a-99 (cf. *Ploetilla* sp.). Some of these relatives are known for their production of astaxanthin (Leya et al. 2009), though in less dominating amounts than in *S. nivaloides*, but none of them has ever been reported to cause striking snow colouring. They have been isolated from different habitats on Svalbard such as a moss and a snowfield as well as from a glacier. These strains may rather be regarded as permafrost algae than snow algae. Demchenko (2013) investigated the above strains and described them all as having coccoid cells.

When studying their life cycles he observed zooid formation in strains CCCryo 101–99 and CCCryo 086b–99. Motile stages so far have not been described for the only known species of *Plœotila* (*P. ramosa* T.Mrozinska-Webb) and since he also found slightly different characteristics in the other two strains in comparison to *Sphaerocystis* or *Coenochloris*, their attribution to these genera remains unclear (hence the ‘cf.’). Our *rbcL* phylogeny (Fig. 7) confirmed that these tentative genera form closely related lineages to *Achoma brachiatum* isolated from an alpine herbfield soil in New Zealand (Novis and Visnovsky 2012). However, as outlined above, CCCryo 101–99 and 133–01 clearly differ from strain CCCryo 147–01, the former two producing zooids and considerable amounts of secondary carotenoids and the latter lacking such cell stages and ability. Which of them actually might have to be assigned to the genus *Achoma* remains to be investigated. The three strains CCCryo 086a–99, 101–99 and 147–01 further markedly differ in the following aspects: cells are single or organised in clusters of tetrads in CCCryo 133–01, in microscopic colonies in an extracellular polymeric substance (EPS) in CCCryo 147–01, and in cells or a group of cells sitting on a mucilaginous stalk in CCCryo 086a–99. Chloroplasts are parietal (CCCryo 133–01, CCCryo 086a–99) and pot-like (CCCryo 147–01), and a pyrenoid is present. Yet *S. nivaloides* shares several features with the above mentioned three CCCryo strains: its origin from cold habitats, its parietal chloroplast with a pyrenoid (at least observable in young cysts) and its prevailing morphologic organisation as a coccoid life form.

Our study has shown that sequencing of the field-collected cysts was a suitable strategy and also the only option to decipher their phylogenetic position, as establishing actively growing isolates from them has yet to be successful. This newly described genus *Sanguina* with two closely related species *S. nivaloides* and *S. aurantia* represents a single monophyletic lineage, independent from other Chlamydomonadacean algae. Using molecular methods we showed that *S. nivaloides* has a cosmopolitan distribution in polar and alpine regions, having detected the same ITS2 haplotypes on several continents. It is possible to distinguish the cysts of *S. nivaloides* from red-coloured cysts of other algae based on the cell size, number of cell walls, plastid organisation and habitat preference. Further studies could involve single-cell sequencing methods, e.g. with a further focus on the ruby-type cysts. The genetic variability below species level might be detected using a microsatellite-based approach (Nagai et al. 2007) developed from single cell genomics (Muramoto et al. 2010). Additionally, sampling at known locations early in the season might help to discover vegetative stages of this species, enabling us to study this interesting alga in much more detail using viable cultures/isolates. The molecular identity of other red coccoid species from snow reported by Kol (1968) such as *Chlamydomonas antarcticus* (red cysts with a broad mucilage layer) or *Trochiscia* spp. (red cysts with spikes) might also yet be revealed.

SUPPLEMENTARY DATA

Supplementary data are available at [FEMSEC](https://academic.oup.com/femsec) Journal online.

ACKNOWLEDGEMENTS

We thank Petr Sklenář, Marie Bulínová, Adéla Moravcová, Eva Hejduková, Martin Pusztai (all: Charles University, Prague, Czech Republic) and Daniel Remias (University of Applied Sciences Upper Austria, Wells, Austria) for field sampling. Our sincere

thanks to Jasna Vukić (Charles University, Prague, Czech Republic) for her hints concerning haplotype network reconstruction. We are immensely grateful to Wolf-Henning Kusber (Botanischer Garten und Botanisches Museum Berlin, Germany) for his comments and great help with the taxonomic treatment. We also thank David Lazarus (Museum für Naturkunde, Berlin, Germany) for letting us have some of the historical red snow field sample of 1851. TL is specifically thankful to Günter R. Fuhr for having made numerous scientific voyages to Svalbard and the Antarctic and many invaluable experiences in the Arctic possible. We thank the reviewers, explicitly Phil Novis, for their constructive comments.

FUNDING

This work was supported by the Czech Science Foundation (GACR) project [18–02634S to LP and LN] and by the institutional long-term research plan RVO67985939 of the Institute of Botany of the Czech Academy of Sciences.

Conflicts of interest. None declared.

REFERENCES

- Agardh CA. *Systema Algarum. Lundae* 1824;XI–XXI:13–4.
- Agardh CA. *Icones Algarum Europaerum*. Leipzig: Leopold Voss, 1828–35.
- anagreh L, Pegg C, Harikumar A et al. Assessing intragenomic variation of the internal transcribed spacer two: Adapting the Illumina metagenomics protocol. *PLoS One* 2017;12:e0181491.
- Allewaert CC, Vanormelingen P, Pröschold T et al. Species diversity in European *Haematococcus pluvialis* (Chlorophyceae, Volvocales). *Phycologia* 2015;54:583–98.
- Andersen RA. Report of the nomenclature committee for algae: 19. *Taxon* 2018;67:1029–30.
- Bauer F. Microscopical observation on the red snow. *Quart J Sci Arts* 1819;7:222–9 (incl. plate VI).
- Bauer F. Red snow of Baffin's Bay. *Amer J Sci Arts* 1820;2:356.
- Bidigare RR, Ondrusek ME, Kennicutt MC, II et al. Evidence for a photoprotective function for secondary carotenoids of snow algae. *J Phycol* 1993;29:427–34.
- Brown RM, Larson DA, Bold HC. Airborne algae: Their abundance and heterogeneity. *Science* 1964;143:583–4.
- Brown SP, Jumpponen A. Microbial ecology of snow reveals taxon-specific biogeographical structure. *Microb Ecol* 2019;77:946–58.
- Brown SP, Olson BJSC, Jumpponen A. Fungi and algae co-occur in snow: An issue of shared habitat or algal facilitation of heterotrophs? *Arctic, Antarctic, and Alpine Research* 2015;47:729–49.
- Brown SP, Ungerer MC, Jumpponen A. A community of clones: Snow algae are diverse communities of spatially structured clones. *Int J Plant Sci* 2016;177:432–9.
- Caisová L, Marin B, Melkonian M. A close-up view on ITS2 evolution and speciation - a case study in the Ulvophyceae (Chlorophyta, Viridiplantae). *BMC Evol Biol* 2011;11:262.
- Caisová L, Marin B, Melkonian M. A consensus secondary structure of ITS2 in the Chlorophyta identified by phylogenetic reconstruction. *Protist* 2013;164:482–96.
- Clement M, Posada D, Crandall K. TCS: A computer program to estimate gene genealogies. *Mol Ecol* 2000;9:1657–9.
- Cohn F. *Chlamydococcus nivalis* (F.A.Bauer) A. Braun. *Rabenhorst: Algae Exsiccatae.*, 1861, 1141.

- Coleman AW. The significance of a coincidence between evolutionary landmarks found in mating affinity and a DNA sequence. *Protist* 2000;**151**:1–9.
- Coleman AW. Pan-eukaryote ITS2 homologies revealed by RNA secondary structure. *Nucleic Acids Res* 2007;**35**:3322–9.
- Czygan F-C. Blutregen und Blutschnee: Stickstoffmangel-Zellen von *Haematococcus pluvialis* und *Chlamydomonas nivalis*. *Arch Mikrobiol* 1970;**74**:69–76.
- Darty K, Denise A, Ponty Y. VARNA: Interactive drawing and editing of the RNA secondary structure. *Bioinformatics* 2009;**25**:1974–5.
- Demchenko E. Morphology, ecophysiology and molecular phylogeny of marine and psychrophilic green flagellates belonging to *Microglena* and their adaptation to changing ecological conditions. *DAAD Reports*. 2013;**322**:1–15.
- Demchenko E, Mikhailyuk T, Coleman AW et al. Generic and species concepts in *Microglena* (previously the *Chlamydomonas monadina* group) revised using an integrative approach. *Eur J Phycol* 2012;**47**:264–90.
- Di Mauro B, Garzonio R, Rossini M et al. Saharan dust events in the European Alps: Role in snowmelt and geochemical characterization. *The Cryosphere* 2019; **13**:1147–65.
- Ehrenberg CG. Dritter Beitrag zur Erkenntnis großer Organisation in der Richtung des kleinsten Raumes. *Physikalische Abhandlungen der Koeniglichen Akademie der Wissenschaften zu Berlin* 1834;**1833**:145–336.
- Ehrenberg CG, König. Preuss. Akad. Wiss. Berlin. Über eine frische Probe der die Crimson Cliffs scharlachroth färbenden Substanz aus der Baffins Bai und das sie begleitende kleinste Leben. Bericht über die zur Bekanntmachung geeigneten Verhandl. 1851:741–4.
- Ettl H, Gärtner G. *Syllabus der Boden-, Luft- und Flechtenalgen*. Springer, 2014.
- Farr ER, Zijlstra G. Index nominum genericorum (Plantarum), 1996+. <http://botany.si.edu/ing/> (18 March 2019, date last accessed).
- Fjerdingstad E, Kemp K, Fjerdingstad E et al. Chemical analyses of red “snow” from East-Greenland with remarks on *Chlamydomonas nivalis* (Bau.) Wille. *Arch Hydrobiol* 1974;**73**:70–83.
- Flotow J. Über *Haematococcus pluvialis*. *Nov Act Leop Carol* 1844;**20**:413–606.
- Fučíková K, Lewis LA. Intersection of *Chlorella*, *Muriella* and *Bracteacoccus*: Resurrecting the genus *Chromochloris* Kol et Chodat (Chlorophyceae, Chlorophyta). *Fottea* 2012;**12**:83–93.
- Gillespie RG, Baldwin BG, Waters JM et al. Long-distance dispersal: A framework for hypothesis testing. *Trends Ecol Evol* 2012;**27**:47–56.
- Gradinger R, Nürnberg D. Snow algal communities on arctic pack ice floes dominated by *Chlamydomonas nivalis* (Bauer) Wille. *Proc NIPR Symp Polar Biol* 1996;**9**:35–43.
- Guiry MD, Guiry GM. *AlgaeBase*. World-wide electronic publication, National University of Ireland, Galway, 2018. <http://www.algaebase.org> (14 June 2018, date last accessed).
- Hepperle D, Nozaki H, Hohenberger S et al. Phylogenetic position of the Phacotaceae within the Chlamydomonadales as revealed by analysis of 18S rDNA and *rbcl* sequences. *J Mol Evol* 1998;**47**:420–30.
- Hodač L, Hallmann C, Spitzer K et al. Widespread green algae *Chlorella* and *Stichococcus* exhibit polar-temperate and tropical-temperate biogeography. *FEMS Microbiol Ecol* 2016;**92**:fiw122.
- Hoham RW. New findings in the life history of the snow alga, *Chlamydomonas rubra* (Stein et Brooke) comb. nov. (Chlorophyta, Volvocales). *Syesis* 1974;**7**:239–47.
- Hoham RW, Roemer SC, Mullett JE. The life history and ecology of the snow alga *Chlamydomonas brevispina* comb. nov. (Chlorophyta, Volvocales). *Phycologia* 1979;**18**:55–70.
- Hooker JD. 36. Red snow. *Edinb J Sci* 1825;**2**:184.
- Ji M, Greening C, Vanwonderghem I et al. Atmospheric trace gases support primary production in Antarctic desert surface soil. *Nature* 2017;**552**:400–3.
- Jombart T. *adeigenet*: A R package for the multivariate analysis of genetic markers. *Bioinformatics* 2008;**24**:1403–5.
- Jombart T, Pontier D, Dufour AB. Genetic markers in the playground of multivariate analysis. *Heredity* 2009;**102**:330–41.
- Jombart T, Devillard S, Dufour AB et al. Revealing cryptic spatial patterns in genetic variability by a new multivariate method. *Heredity* 2008;**101**:92–103.
- Jones HG, Pomeroy JW, Walker DA et al. (eds.) *Snow ecology. An interdisciplinary examination of snow-covered ecosystems*. Cambridge: Cambridge University Press, 2001; 378.
- Kawecka B. Biology and ecology of snow algae 2. Formation of aplanospores in *Chlamydomonas nivalis* (Bauer) Wille (Chlorophyta, Volvocales). *Acta Hydrobiol* 1981;**23**:211–5.
- Kobayashi Y, Fukushima H. On the red and green snow newly found in Japan II. *Bot Mag Tokyo* 1952;**65**:128–36.
- Koetschan C, Förster F, Keller A et al. The ITS2 Database III—sequences and structures for phylogeny. *Nucleic Acids Res* 2010;**38**:D275–9.
- Kol E. The snow and ice algae of Alaska. *Smithsonian Miscellaneous Collection* 1942;**101**:1–36.
- Kol E. *Kryobiologie: Biologie und Limnologie des Schnees und Eises, I. Kryovegetation. Die Binnengewässer Einzeldarstellungen aus der Limnologie und ihren Nachbargebieten* Volume XXIV volume 24. Stuttgart: E. Schweizerbart'sche Verlagsbuchhandlung (Nägele u. Obermiller), 1968.
- Ley R, Williams MW, Schmidt SK. Microbial population dynamics in an extreme environment: controlling factors in talus soils at 3750 m in the Colorado Rocky Mountains. *Biogeochemistry* 2004;**68**:313–35.
- Leya T. Feldstudien und genetische Untersuchungen zur Kryophilie der Schneeealgen Nordwestspitzbergens. *Berichte aus der Biologie*. Aachen: Shaker, 2004.
- Leya T. Die „Ross-Proben“ von den Crimson Cliffs: Probe „MB_ES.1781c“ aus der Ehrenberg Sammlung des Naturkundemuseums Berlin. Berlin: Fraunhofer IBMT, 2008, 6.
- Leya T, Müller T, Ling HU et al. Snow algae from north-western Spitsbergen (Svalbard). *Reports on Polar and Marine Research* 2004;**492**:46–54.
- Leya T, Rahn A, Lütz C et al. Response of arctic snow and permafrost algae to high light and nitrogen stress by changes in pigment composition and applied aspects for biotechnology. *FEMS Microbiol Ecol* 2009;**67**:432–43.
- Librado P, Rozas J. DnaSP v5: a software for comprehensive analysis of DNA polymorphism data. *Bioinformatics* 2009;**25**:1451–2.
- Ling HU. Snow algae of the Windmill Islands, continental Antarctica: *Chlorosarcina antarctica* comb. nov. (Chlorophyceae, Chlorophyta) from pink snow, with discussion of *Chlorosarcina* and allied genera. *Phycologia* 2002;**41**:1–9.
- Ling HU, Seppelt RD. Snow algae of the Windmill Islands, continental Antarctica. 2. *Chloromonas rubroleosa* sp. nov. (Volvocales, Chlorophyta), an alga of red snow. *Eur J Phycol* 1993;**28**:77–84.
- Link DHF. 45./2. *Coccophysium nivale*. *Handbuch zur Erkennung der nutzbarsten und am häufigsten vorkommenden Gewächse Drittel Teil*. Berlin: Haude und Spenersche Buchhandlung(S.J. Josephy), 1833, 341–2.

- Lu N, Wei D, Chen F et al. Lipidomic profiling reveals lipid regulation in the snow alga *Chlamydomonas nivalis* in response to nitrate or phosphate deprivation. *Process Biochem* 2012a;48:605–13.
- Lu N, Wei D, Jiang X-L et al. Regulation of lipid metabolism in the snow alga *Chlamydomonas nivalis* in response to NaCl stress: An integrated analysis by cytomic and lipidomic approaches. *Process Biochem* 2012b;47:1163–70.
- Lu N, Chen JH, Wei D et al. Global metabolic regulation of the snow alga *Chlamydomonas nivalis* in response to nitrate or phosphate deprivation by a metabolome profile analysis. *Int J Mol Sci* 2016;17:19.
- Lutz S, Anesio AM, Raiswell R et al. The biogeography of red snow microbiomes and their role in melting arctic glaciers. *Nat Commun* 2016;7:11968.
- Lütz-Meindl U, Lütz C. Analysis of element accumulation in cell wall attached and intracellular particles of snow algae by EELS and ESI. *Micron* 2006;37:452–8.
- Marchant HJ. Snow algae from the Australian Snowy Mountains. *Phycologia* 1982;21:178–84.
- Marshall WA. Biological particles over Antarctica. *Nature* 1996;383:680.
- Mataloni G, Tesolín G. A preliminary survey of cryobiontic algal communities from Cierva Point (Antarctic Peninsula). *Antarct Sci* 1997;9:250–8.
- Matsuzaki R, Hara Y, Nozaki H. A taxonomic revision of *Chloromonas reticulata* (Volvocales, Chlorophyceae), the type species of the genus *Chloromonas*, based on multigene phylogeny and comparative light and electron microscopy. *Phycologia* 2012;51:74–85.
- Matsuzaki R, Nozaki H, Kawachi M. Taxonomic revision of *Chloromonas nivalis* (Volvocales, Chlorophyceae) strains, with the new description of two snow-inhabiting *Chloromonas* species. *PLoS One* 2018;13:e0193603.
- Matsuzaki R, Nozaki H, Takeuchi N et al. Taxonomic re-examination of “*Chloromonas nivalis* (Volvocales, Chlorophyceae) zygotes” from Japan and description of *C. muramotoi* sp. nov. *PLoS One* 2019;14:e0210986.
- Mazumdar N, Gopalakrishnan KK, Visnovsky G et al. A novel alpine species of *Haematococcus* (Chlamydomonadales: Chlorophyta) from New Zealand. *N Z J Bot* 2018;56:216–26.
- Muramoto K, Nakada T, Shitara T et al. Re-examination of the snow algal species *Chloromonas miwae* (Fukushima) Muramoto et al., comb. nov. (Volvocales, Chlorophyceae) from Japan, based on molecular phylogeny and cultured material. *Eur J Phycol* 2010;45:27–37.
- Meneghini G. Monographia Nostochinearum italicarum addito specimine de Rivulariis. *Memorie della Reale Accademia delle Scienze di Torino, ser 2* 1843;5:1–143 pls I–XVII.
- Mosser JL, Mosser AG, Brock TD. Photosynthesis in the snow: The alga *Chlamydomonas nivalis* (Chlorophyceae). *J Phycol* 1977;13:22–7.
- Müller T, Leya T, Fuhr G. Persistent snow algal fields in Spitsbergen: Field observations and a hypothesis about the annual cell circulation. *Arct Antarct Alp Res* 2001;33:42–51.
- Müller T, Bleiß W, Martin C-D et al. Snow algae from north-west Svalbard: their identification, distribution, pigment and nutrient content. *Polar Biol* 1998;20:14–32.
- Nagai S, Lian C, Yamaguchi S et al. Microsatellite markers reveal population genetic structure of the toxic dinoflagellate *Alexandrium tamarense* (Dinophyceae) in Japanese coastal waters. *J Phycol* 2007;43:43–54.
- N.N. Captain Sir John Ross has brought from Baffin's Bay a Quantity of Red Snow. London: London Times, 1818.
- Nakada T, Ota S. What is the correct name for the type of *Haematococcus* Flot. (Volvocales, Chlorophyceae)? *Taxon* 2016;65:343–8.
- Nedbalová L, Mihál M, Kviderová J et al. Identity, ecology and eco-physiology of planktic green algae dominating in ice-covered lakes on James Ross Island (northeastern Antarctic Peninsula). *Extremophiles* 2017;21:187–200.
- Novakovskaya IV, Patova EN, Boldina ON et al. Molecular phylogenetic analyses, ecology and morphological characteristics of *Chloromonas reticulata* (Goroschankin) Gobi which causes red blooming of snow in the subpolar Urals. *Cryptogam, Algal* 2018;39:199–213.
- Novis PM. Ecology of the snow alga *Chlamydomonas kolii* (Chlamydomonadales, Chlorophyta) in New Zealand. *Phycologia* 2002;41:280–92.
- Novis PM, Visnovsky G. Novel alpine algae from New Zealand: Chlorophyta. *Phytotaxa* 2012;39:1–30.
- Novis PM, Hoham RW, Beer T et al. Two snow species of the quadriflagellate green alga *Chlamydomonas* (Chlorophyta, Volvocales): Ultrastructure and phylogenetic position within the *Chloromonas* clade. *J Phycol* 2008;44:1001–12.
- Nozaki H, Onishi K, Morita E. Differences in pyrenoid morphology are correlated with differences in the rbcL genes of members of the *Chloromonas* lineage (Volvocales, Chlorophyceae). *J Mol Evol* 2002;55:414–30.
- Persoon CH, Göttingen. *Synopsis Methodica Fungorum*. 1801;1:214.
- Perty M. Zur Kenntnis kleinster Lebensformen. *Bern* 1852:1–228.
- Posada D. jModelTest: phylogenetic model averaging. *Mol Biol Evol* 2008;25:1253–6.
- Procházková L, Remias D, Řezanka T et al. *Chloromonas nivalis* subsp. *tatrae*, subsp. nov. (Chlamydomonadales, Chlorophyta): re-examination of a snow alga from the High Tatras Mountains (Slovakia). *Fottea* 2018a;18:1–18.
- Procházková L, Remias D, Holzinger A et al. Ecophysiological and morphological comparison of two populations of *Chlamydomonas* sp. (Chlorophyta) causing red snow on ice-covered lakes in the High Tatras and Austrian Alps. *Eur J Phycol* 2018b;53:230–43.
- Pröschold T, Marin B, Schlösser UG et al. Molecular phylogeny and taxonomic revision of *Chlamydomonas* (Chlorophyta). I. Emendation of *Chlamydomonas* Ehrenberg and *Chloromonas* Gobi, and description of *Oogamochlamys* gen. nov. and *Lobochlamys* gen. nov. *Protist* 2001;152:265–300.
- Remias D. Cell Structure and Physiology of Alpine Snow and Ice Algae. In: Lütz C (ed.) *Plants in Alpine Regions: Cell Physiology of Adaptation and Survival Strategies*. Wien: Springer, 2012, 175–85.
- Remias D, Lütz-Meindl U, Lütz C. Photosynthesis, pigments and ultrastructure of the alpine snow alga *Chlamydomonas nivalis*. *Eur J Phycol* 2005;40:259–68.
- Remias D, Karsten U, Lütz C et al. Physiological and morphological processes in the Alpine snow alga *Chloromonas nivalis* (Chlorophyceae) during cyst formation. *Protoplasma* 2010;243:73–86.
- Remias D, Wastian H, Lütz C et al. Insights into the biology and phylogeny of *Chloromonas polyptera* (Chlorophyta), an alga causing orange snow in Maritime Antarctica. *Antarct Sci* 2013;25:648–56.
- Remias D, Pichtová M, Pangratz M et al. Ecophysiology, secondary pigments and ultrastructure of *Chlamydomonas* sp. (Chlorophyta) from the European Alps compared with *Chlamydomonas nivalis* forming red snow. *FEMS Microbiol Ecol* 2016;92:fw030.

- Ross J. *A Voyage of Discovery, Made Under the order of the Admiralty, in His Majesty's Ships Isabella and Alexander for the Purpose of Exploring Baffin's Bay, and Inquiring into the Probability of a North-West Passage*. London: John Murray, 1819.
- Ross J (ed.) *Entdeckungsreise unter den Befehlen der Britischen Admiralität mit den Königlichen Schiffen Isabella und Alexander um Baffins-Bay auszuforschen und die Möglichkeit einer nordwestlichen Durchfahrt zu Untersuchen*. Leipzig: Friedrich Fleischer, 1820.
- Sattler B, Remias D, Lütz C et al. Leben auf Schnee und Eis. In: Erschbamer B Koch EM (eds.) *Glaziale und periglaziale Lebensräume im Raum Obergurgl*. Innsbruck: Innsbruck University Press iup, 2010.
- Schlichting HE, Jr. The importance of airborne algae and Protozoa. *J Air Pollut Control Assoc* 1969;19:946–51.
- Schultz J, Wolf M. ITS2 sequence-structure analysis in phylogenetics: A how-to manual for molecular systematics. *Mol Phylogen Evol* 2009;52:520–3.
- Segawa T, Matsuzaki R, Takeuchi N et al. Bipolar dispersal of red-snow algae. *Nat Commun* 2018;9:3094.
- Seibel PN, Müller T, Dandekar T et al. Synchronous visual analysis and editing of RNA sequence and secondary structure alignments using 4SALE. *BMC Res Notes* 2008;1:91.
- Seibel PN, Müller T, Dandekar T et al. 4SALE - A tool for synchronous RNA sequence and secondary structure alignment and editing. *BMC Bioinformatics* 2006;7:498.
- Shuttleworth RJ. Upon the colouring matter of red snow. *The Edinburgh New Philosophical Journal* 1840a;29:54–64 (with 1 coloured plate).
- Shuttleworth RJ. Nouvelles observations sur la matière colorant de la neige rouge. 1840b;25, Geneva.
- Škaloud P, Rindi F. Ecological differentiation of cryptic species within an asexual protist morphospecies: a case study of filamentous green alga *Klebsormidium* (Streptophyta). *J Eukaryot Microbiol* 2013;60:350–62.
- Škaloud P, Steinová J, Řídká T et al. Assembling the challenging puzzle of algal biodiversity: species delimitation within the genus *Asterochloris* (Trebouxiophyceae, Chlorophyta). *J Phycol* 2015;51:507–27.
- Sommerfelt SC. Om den røde Sne, eller *Sphærella nivalis* Sommerf., *Uredo nivalis* Auct. *Mag Nat videnskab* 1824;4:249–53.
- Spijkerman E, Wacker A, Weithoff G et al. Elemental and fatty acid composition of snow algae in Arctic habitats. *Front Microbiol* 2012;3:380.
- Sprengel C. *Coccolchloris nivalis* Spreng. *Syst Veg* 1827;4:373.
- Stein JR, Amundsen CC. Studies on snow algae and fungi from the front range of Colorado. *Can J Bot* 1967;45:2033–45.
- Stibal M, Elster J, Šabacká M et al. Seasonal and diel changes in photosynthetic activity of the snow alga *Chlamydomonas nivalis* (Chlorophyceae) from Svalbard determined by pulse amplitude modulation fluorometry. *FEMS Microbiol Ecol* 2007;59:265–73.
- Sutton EA. The physiology and life histories of selected cryophytes of the Pacific Northwest *Department of Oceanography* volume PhD. Corvallis, OR: Oregon State University, 1970, 98.
- Terashima M, Umezawa K, Mori S et al. Microbial community analysis of colored snow from an alpine snowfield in northern Japan reveals the prevalence of betaproteobacteria with snow algae. *Front Microbiol* 2017;8:1481.
- Thomas WH, Broady PA. Distribution of coloured snow and associated algal genera in New Zealand. *N Z J Bot* 1997;35:113–7.
- VanWinkle-Swift KP, Rickoll WL. The zygospore wall of *Chlamydomonas monoica* (Chlorophyceae): morphogenesis and evidence for the presence of sporopollenin. *J Phycol* 2008;33:655–65.
- Vogt C. Neige rouge. In: Desor E (ed.) *Excursions et séjours dans les glaciers et les hautes régions des Alpes, de M Agassiz et de ses compagnons de voyage*. Neuchatel and Paris, 1844, 215–24(16; pl. 1: fig. 1-5 (as 'Discerea nivalis').
- Vukić J, Ulqini D, Šanda R. Occurrence of *Knipowitschia goerneri* Ahnelt, 1991 (Gobiidae) in southern Albania confirmed with molecular tools. *J Appl Ichthyol* 2017;33:284–90.
- Wayama M, Ota S, Matsuura H et al. Three-dimensional ultrastructural study of oil and astaxanthin accumulation during encystment in the green alga *Haematococcus pluvialis*. *PLoS One* 2013;8:e53618.
- Wilkinson DM, Koumoutsaris S, Mitchell EAD et al. Modelling the effect of size on the aerial dispersal of microorganism. *J Biogeogr* 2012;39:89–97.
- Wille N. Algologische Notizen IX-XIV. *Nyt Magazin for Naturvidenskaberne* 1903;41:89–185.
- Wrangel FA. Microscopiska och Physiologiska Undersökningar rörande utvecklingen af *Lepraria Kermesina* och dess likhet med den sa kallade röda Snön. Tilläg till Anmärkningarne rörande *Byssus Jolithus* Linn. *Kongl Vetenskaps-Akademiens Handlingar för år 1823, Stockholm 1823*;1:71–95.
- Žárský V, Kalina T, Sulek J. Notes on the sexual reproduction of *Chlamydomonas geitleri* Ettl. *Arch Protistenkd* 1985;130:343–53.
- Zuker M. Mfold web server for nucleic acid folding and hybridization prediction. *Nucleic Acids Res* 2003;31:3406–15.

Sanguina nivaloides and *Sanguina aurantia* gen. et spp. nov. (Chlorophyta):

the taxonomy, phylogeny, biogeography and ecology of two newly recognized algae causing red and orange snow

Supplementary Data

Supplementary Table 1. Samples of *Sanguina nivaloides* from continental Europe, the Svalbard archipelago, North and South America with sample codes, collection date, conductivity (EC; $\mu\text{S cm}^{-1}$), pH, altitude (m a.s.l.), geographic position (GPS), habitat description and location of sampling site. The numbering in the first column corresponds to the data given in Fig. 1.

No.	sample code	Date	EC	pH	altitude	GPS	habitat description	Location	country
1	NK01	18 June 2009	n.a.	n.a.	2300	47°18'N 11°23'E	snow field on limestone	Haferlekarspitze, Nordkette Mountains, Tyrol	Austria
2	4HT	7 July 2014	n.a.	n.a.	2270	47°06'55.0"N 12°17'39.4"E	glacier based snow field, slight slope	Obersulzbachkees, High Tauern	Austria
3	DL07	28 May 2016	8.4	6.2	2380	47°13'42.5"N 11°00'56.9"E	snow on slope	Kühtai, near Lake Gossenkölle, Tyrol	Austria
4	WP122	29 May 2017	n.a.	n.a.	1969	47°13'12.6"N 11°02'25.7"E	snow close to the mountain road	Kühtai, Stockach, Tyrol	Austria
5	WP123	29 May 2017	14	5.81	2352	47°13'35.0"N 11°01'03.1"E	snow close to the road to Schwarzmoos	Kühtai, Stockach, Tyrol	Austria
6	2OT	1 August 2014	n.a.	n.a.	3223	46°46'16.9"N 10°52'23.9"E	glacier based snow field, slight slope	Similaun, Tyrol	Austria
7	CCCryo RS_0022-2003	12 July 2003	n.a.	n.a.	2900	46°58'31.235"N 11°6'29.343"E	dry to slightly wet snow surrounded by glacier	Rotadlkopf, Stubai Glacier, Sölden, Tyrol	Austria

8	P3	29 August 2001	n.a.	n.a.	2800	46°56'N 10°55'E	glacier based snow field next to a road	Sölden, near Rettenbach Glacier, Tyrol	Austria
9	Retten	18 July 2015	n.a.	n.a.	2790	46°56'34.5"N 10°55'29.1"E	snow field with slight slope	Rettenbach Glacier, Tyrol	Austria
10	Tiefen	18 July 2015	n.a.	n.a.	2786	46°55'19.66"N 10°56'53.699"E	snow field with slight slope	Tiefenbach Glacier, Tyrol	Austria
11	1D	11 July 2013	n.a.	n.a.	2298	46°25'23.9"N 11°47'48.5"E	snow field at the end of valley	Pas de San Nicolo, Dolomites	Italy
12	4D	12 July 2013	n.a.	n.a.	2063	46°24'43.4"N 11°45'58.3"E	meadow based snowfield close to a pasture	Forcella dal Pief, Dolomites	Italy
13	9D	12 July 2013	n.a.	n.a.	2668	46°24'11.2"N 11°47'09.0"E	snow field at mountain ridge	Cima de Costabela, Dolomites	Italy
14	5SAR	17 July 2013	n.a.	n.a.	2353	46°48'21.7"N 11°24'09.5"E	rock based snow field close to a lake	Steinwandseen, Sarntal Alps	Italy
15	2RON	17 August 2013	n.a.	n.a.	1939	61°54'25.3"N 09°50'58.9"E	debries based snow field in a saddle	Rondslotett, Rondane	Norway
16	N2	27 June 2015	n.a.	n.a.	1138	61°43'45.7"N 10°12'06.8"E	meadow based snow field close to a lake	NP Rondane, Rondane	Norway
17	N4	9 July 2015	n.a.	n.a.	784	62°03'29.3"N 7°15'47.6"E	meadow based snowfield next to a brook	Geirangen fjord	Norway

18	N5	9 July 2015	n.a.	n.a.	1077	61°36'04.6"N 8°02'27.6"E	meadow based snow field on a slight slope	NP Jotunheimen	Norway
19	NOR4-1	8 September 2015	11	7.1	1145	61°00'42.9"N 7°19'48.8"E	snow field close to the Bjørgavegen road	northeast of Flåm	Norway
20	Zamrznute	4 July 2002	n.a.	n.a.	2013	49°10'32.06"N 20°8'16.79"E	snow field close to lake shore	High Tatra Mountains	Slovakia
21	2SLOV	13 June 2013	n.a.	n.a.	2536	46°26'23.2"N 13°49'49.5"E	steep slope	Veliki Oltar, Julian Alps	Slovenia
22	Furka	26 June 2003	n.a.	n.a.	2431	46°34'22"N 8°25'00"E	snow field in a flat saddle	Furka Pass, Urner Alps	Switzerland
23	CCCRyo RS_0011	8 September 1999	n.a.	n.a.	25	79°44'33"N 10°49'59.998"E	snow fields on rocky south coast	Amsterdamøya, Danskegattet	Svalbard, Norway
26	Sva4	2 July 2016	6.14	6.0	224	78°11'30.4"N 15°32'50.8"E	snow field close to the melting glacier	southwest from Longyearbyen	Svalbard, Norway
27	Sva 10-7	18 July 2010	3.6	5.5	310	78°11.757"N 15°31.319"E	flat snowfield	Tverdalen, south of Longyearbyen	Svalbard, Norway
29	Foxfona	5 August 2017	5.2	6.3	585	78°08.462"N 16°08.992"E	glacier based snow field on a slight slope	Foxfona, southeast from Longyearbyen	Svalbard, Norway
31	CCCRyo RS_0015-2010	4 August 2010	84.0	4.7	15	77°39'44.298"N 14°48'58.903"E	steep snow field stretching down to sea, surrounded by moss vegetation on rock	Midterhuken, southwest of Mariasundet between Bellsund and Van Mijenfjorden, Nathorst Land	Svalbard, Norway

32	CCCRyo RS_0003-2004	6 August 2004	n.a.	n.a.	430	77°34'0.001"N 16°53'59.999"E	almost levelled persistent snow field	northeastern (upper) part of Doktorbreen, Nathorst Land	Svalbard, Norway
33	CCCRyo RS_0014-2013	16 August 2013	25.6	6.1	13	77°1'54.516"N 15°52'20.279"E	icy snow field on shale and carbonate rocks	Gnålodden, Vestre Burgerbukta, Hornsund, Wedel, Jarlsberg Land	Svalbard, Norway
37	redCol	15 July 2017	10	5.5	3731	40°03'26.2"N 105°38'39.6"W	snow field at a bottom of the kettle below Apache peak	Niwot Ridge, Front Range Rocky Mountains	Colorado, USA
38	Saddle	8 July 2017	3	5.44	3540	40°03'21.2"N 105°35'28.9"W	snow field exposed north east to south east	Niwot Ridge, Front Range Rocky Mountains	Colorado, USA
39	Subalpine	8 July 2017	9	5.54	3414	40°02'56.9"N 105°34'57.8"W	south faced snowfield	Niwot Ridge, Front Range Rocky Mts.	Colorado, USA
40	La Hoya	8 December 2016	n.a.	n.a.	1914	42°48'45.7"S 71°15'24.3"W	south-oriented rocky slopes	ski resort La Hoya, close to city Esquel, Patagonia	Argentina
41	Esperanza 3	23 January 2018	n.a.	n.a.	27	63°24'03.5"S 56°59'30.7"W	snow field with slight slope	Hope Bay, Antarctic Peninsula	Antarctica
42	Esperanza 8	10 January 2018	n.a.	n.a.	13	63°23'56.7"S 56°58'48.1"W	flat snow patch above a stream	Hope Bay, Antarctic Peninsula	Antarctica

Supplementary Table 2. Samples of *Sanguina aurantia* from the Svalbard archipelago with sample codes, collection date, conductivity (EC; $\mu\text{S cm}^{-1}$), pH, altitude (m a.s.l.), geographic position (GPS), habitat description and location of sampling site. The numbering in the first column corresponds to the data given in Fig. 1.

No.	sample code	Date	EC	pH	altitude	GPS	habitat description	Location	country
24	RS Camp	20 July 2004	n.a.	5.0	10	78°55.1'N 11°57'E	snow in small creek valley	Ny Alesund, Smithelva, close to camping site	Svalbard, Norway
25	CCCryo RS_0005-2004	30 July 2004	n.a.	n.a.	500	78°10'51.42"N 15°28'44.878"E	snow fields just above side moraine	western side of Longyearbyen	Svalbard, Norway
28	Sva 10-8	18 July 2010	4.7	6.1	319	78°11.780'N 15°31.344'E	flat snowfield	Tverdalen, south of Longyearbyen	Svalbard, Norway
30	CCCryo RS_0006-2004	1 August 2004	1.27	5.0	500	78°9'41.4"N 17°53'31.199"E	almost levelled persistent snow field	Raggfjellet, east of Hellefonna, Sabine Land	Svalbard, Norway
34	CCCryo RS_0017-2010	6 August 2010	n.a.	n.a.	55	77°0'42.156"N 15°32'13.2"E	snow field below bird colony on Fugleberget	Isbjørnhamna, Hornsund, Wedel Jarlsberg Land	Svalbard, Norway
35	CCCryo RS_0018-2010	7 August 2010	6.4	5.3	60	77°0'23.904"N 16°13'17.508"E	top of steep snow field	western side of Treskelen, Wedel Jarlsberg Land	Svalbard, Norway
36	CCCryo RS_0020-2010	9 August 2010	n.a.	4.8	75	76°58'27.48"N 16°22'29.387"E	on rocky gravel, bird colonies above	Chomjakobreen bay, north of Bautaen, Hornsund, Sørkapp Land	Svalbard, Norway

Supplementary Table 3. List of primers used for amplification and Sanger sequencing reactions of 18S rRNA gene, ITS2 rDNA and rbcL markers; (F) forward; (R) reverse.

Primer	Marker	Direction	Sequence	Reference
P2	18S	F	CTGGTTGATTCTGCCAGT	(De Wever <i>et al.</i> 2009)
P4	18S	R	TGATCCTTCYGCAGGTTAC	(De Wever <i>et al.</i> 2009)
18F	18S	F	AACCTGGTTGATCCTGCCAGT	(Katana <i>et al.</i> 2001)
18R	18S	R	TGATCCTTCTGCAGGTTACCTACG	(Katana <i>et al.</i> 2001)
FC	18S	F	GGGAGGTAGTGACAATAAATA	(Matsuzaki <i>et al.</i> 2015)
RF	18S	R	CCCGTGTTGAGTCAAATTAAG	(Matsuzaki <i>et al.</i> 2015)
FA	18S	F	AACCTGGTTGATCCTGCCAGT	(Matsuzaki <i>et al.</i> 2015)
RD	18S	R	GCTGGCAACCAGACTTGCCCTC	(Matsuzaki <i>et al.</i> 2015)
ITS1	ITS2	F	TCCGTAGGTGAACCTGCGG	(White <i>et al.</i> 1990)
ITS5	ITS2	F	GGAAGTAAAAGTCGTAACAAGG	(White <i>et al.</i> 1990)
ITS4	ITS2	R	TCCTCCGCTTATTGATATGC	(White <i>et al.</i> 1990)
SSU	ITS2	F	CTGCGGAAGGATCATTGATTC	(Piercey-Normore and Depriest 2001)
LSU	ITS2	R	AGTTCAGCGGGTGGTCTTG	(Piercey-Normore and Depriest 2001)
AL1500af	ITS1, 5.8S, ITS2	F	GCGCGCTACACTGATGC	(Helms <i>et al.</i> 2001)
LR3	ITS1, 5.8S, ITS2	R	GGTCCGTGTTTCAAGACGG	(Vilgalys and Hester 1990)
TW81	ITS2	F	GGGATCCGTTTCCGTAGGTGAACCTGC	(Goff, Moon and Coleman 1994)
AB28	ITS2	R	GGGATCCATATGCTTAAGTTCAGCGGGT	(Goff, Moon and Coleman 1994)
rbcL1F	rbcL	F	GCTGGTGTTAAAGATTATCG	(Hoham <i>et al.</i> 2002)
rbcL7R	rbcL	R	AAATAAATACCACGGCTACG	(Hoham <i>et al.</i> 2002)
rbcL4R	rbcL	R	GAAAATGAAACGGTCTCTCC	(Hoham <i>et al.</i> 2002)
rbcL10F	rbcL	F	GGTAA CGTWT TTGGT TTCAA AGC	(Hoham <i>et al.</i> 2002)
rbcL8F	rbcL	F	GGTCT TTCAG CTA AA AACTA CGG	(Hoham <i>et al.</i> 2002)
Snow-F3	rbcL	F	CAAGTWGAACGTGACAAATTAAC	(Matsuzaki <i>et al.</i> 2015)
Snow-R12	rbcL	R	CTAAAGTAACTTCACGTTCTCCTTC	(Matsuzaki <i>et al.</i> 2015)
Snow-F0	rbcL	F	TTAAAGCTGGTGTWAAAGAYTAYCGTTT	(Matsuzaki <i>et al.</i> 2015)

Supplementary Table 4. List of *Sanguina nivaloides* samples showing the haplotype codes for ITS2 sequences, sample code, cyst surface morphology, Genbank accession numbers of ITS2/18S/rbcL sequences (¹sequenced in this study), cysts diameters based on scanning electron microscope measurements. Cyst diameters in $\mu\text{m} \pm \text{SD}$ (standard deviation) with n = number of observations. The numbering in the last column corresponds to the data given in Fig. 1. An asterisk (*) indicates a sample, in which ruby cysts were also observed, but rarely. The individual alleles of five specimens with 1-2 heterozygotic positions (redCol, 4HT, 2SLOV, 4D, 9D) were resolved using the PHASE algorithm implemented in DnaSP v.6.0. (Librado and Rozas 2009) and each of these sequences were assigned to two different haplotypes (e.g. redCol_01 is H2, whereas redCol_02 is H8). Note: five field samples (redCol, 4HT, 2SLOV, 4D, 9D) contained two haplotypes per sample which were usually not possible to distinguish in LM. Unless single cell PCR was done, some uncertainty remains, which cell morphotype (and its cell size) is linked to each of these additionally resolved haplotypes (marked with question mark '?'; e.g. 4D_01 as H1 is believed to have smooth cell wall, typical for specimens of haplotype H1, whereas 4D_02 as H14 is supposed to have pronounced papillae). In a few cases cell surface morphology was not recognizable since all cells in that samples were covered by debris).

haplotype code	sample code	Cyst surface morphology	NCBI accession numbers			cysts size (n)	No. according to Fig. 1
			ITS2 rDNA	18S rRNA gene	rbcL		
H1	NK01	Smooth	MK728589 ¹			15.7 ± 3.3 (42)	1
	4HT_01	Covered by debris	MK728590 ¹			28.6 ± 4.5 (40)	2
	DL07	Smooth	MF803749	MF803748	MK733625 ¹	16.6 ± 4.3 (71)	3
	WP122	Smooth	MK728591 ¹			22.5 ± 4.5 (30)	4
	CCCryo RS_0022-2003	Smooth	MK728592 ¹			17.2 ± 2.6 (32)	7
	P3	Smooth	MK728593 ¹			19.4 ± 4.1 (33)	8
	Tiefen	Smooth	MK728594 ¹	MK728635 ¹	MK733623 ¹	15.7 ± 2.2 (58)	10
	1D	Smooth, a few cells with small papillae	MK728595 ¹			17.0 ± 2.2 (40)	11
	5SAR	Smooth	MK728596 ¹			16.7 ± 2.1 (40)	14
	Zamrznute	Smooth, a few cells with small papillae	MK728597 ¹	MK728636 ¹	MK733627 ¹	14.1 ± 3.1 (30)	20
	Furka	Smooth, a few cells with small papillae	MK728598 ¹	MK728646 ¹	MK733626 ¹	14.5 ± 4.0 (65)	22
	CCCryo RS_0015-2010	Smooth	MK728599 ¹	JQ790560	MK733624 ¹	19.7 ± 3.7 (38)	31
	Saddle	Smooth	MK728600 ¹		MK733628 ¹	22.3 ± 3.8 (30)	38
H2	N2	Smooth	MK728601 ¹			24.3 ± 3.5 (53)	16
	N4	Smooth	MK728602 ¹			22.8 ± 3.2 (34)	17
	N5	Smooth	MK728603 ¹	MK728637 ¹	MK733629 ¹	22.4 ± 5.8 (33)	18

	Sva4	Smooth	MK728604 ¹			15.8 ± 2.7 (44)	26
	Sva 10-7	Smooth	MK728605 ¹			18.9 ± 4.1 (47)	27
	Foxfona	Smooth	MK728606 ¹			31.9 ± 2.8 (30)	29
	redCol_01	Smooth	MK728607 ¹			22.0 ± 3.9 (30)	37
	Subalpine	Smooth	MK728608 ¹	MK728638 ¹	MK733630 ¹	25.8 ± 3.2 (47)	39
H3	2RON	Nipples	MK728609 ¹			26.2 ± 6.1 (40)	15
	CCCryo RS_0003-2004	Nipples	MK728610 ¹	MK728639 ¹		14.6 ± 2.6 (39)	32
H4	Retten	Smooth	MK728611 ¹	MK728647 ¹	MK733631 ¹	21.5 ± 4.6 (44)	9
H5	NOR4-1	Smooth (*)	MK728612 ¹	MK728640 ¹		27.0 ± 4.3 (56)	19
H6	CCCryo RS_0014-2013	Smooth	MK728613 ¹	MK728641 ¹	MK733632 ¹	18.9 ± 3.4 (33)	33
H7	CCCryo RS_0011	Smooth, a few cells with short blunt nibs (*)	MK728614 ¹	MK728642 ¹	MK733633 ¹	18.3 ± 3.0 (32)	23
H8	redCol_02	? rarely cells with small papillae	MK728615 ¹				37
	La Hoya	Covered by debris	MK728616 ¹	MK728643 ¹	MK733634 ¹	17.0 ± 4.6 (43)	40
H9	WP123	Smooth	MK728617 ¹		MK733635 ¹	11.9 ± 2.3 (69)	5
H10	2OT	Smooth	MK728618 ¹			14.4 ± 3.2 (40)	6
H11	4D_01	Smooth	MK728619 ¹			17.0 ± 2.3 (40)	12
	2SLOV_01	Smooth	MK728620 ¹			16.9 ± 2.6 (40)	21
H12	2SLOV_02	Smooth	MK728621 ¹				21
H13	4HT_02	Covered by debris	MK728622 ¹				2
H14	4D_02	? cells with pronounced papillae	MK728623 ¹				12
H15	9D_01	Smooth	MK728624 ¹			17.0 ± 2.5 (40)	13
H16	9D_02	Smooth	MK728625 ¹				13
H17	Esperanza_3	Smooth	MK728626 ¹			19.4 ± 3.0 (30)	41
H18	Esperanza_8	Smooth	MK728627 ¹			9.9 ± 1.6 (44)	42

Supplementary Table 5. List of *Sanguina aurantia* samples showing the haplotype codes for ITS2 sequences, sample code, cyst surface morphology, Genbank accession numbers of ITS2/18S/rbcL sequences (¹sequenced in this study), cysts diameters based on scanning electron microscope measurements. Cyst diameters in $\mu\text{m} \pm \text{SD}$ (standard deviation) with n = number of observations. The numbering in the last column corresponds to the data given in Fig. 1.

haplotype code	sample code	Cyst surface morphology	NCBI accession numbers			cysts size (n)	No. according to Fig. 1
			ITS2 rDNA	18S rRNA gene	rbcL		
HA1	RS Camp	The outermost cell wall layer wrinkled, the lower layer smooth	MK728628 ¹		MK733637 ¹	12.6 \pm 1.6 (32)	24
	CCCrysto RS_0005-2004	The outermost cell wall layer wrinkled, the lower layer smooth	MK728629 ¹			10.8 \pm 1.5 (114)	25
	Sva 10-8	The outermost cell wall layer wrinkled, the lower layer smooth	MK728630 ¹			9.3 \pm 1.9 (43)	28
	CCCrysto RS_0006-2004	The outermost cell wall layer wrinkled, the lower layer smooth	MK728631 ¹			10.2 \pm 1.7 (34)	30
	CCCrysto RS_0018-2010	The outermost cell wall layer wrinkled, the lower layer smooth	MK728632 ¹	MK728644 ¹		11.2 \pm 1.7 (46)	35
	CCCrysto RS_0020-2010	The outermost cell wall layer wrinkled, the lower layer smooth	MK728633 ¹		MK733636 ¹	10.4 \pm 1.5 (45)	36
HA2	CCCrysto RS_0017-2010	The outermost cell wall layer wrinkled, the lower layer smooth	MK728634 ¹	MK728645 ¹	MK733638 ¹	11.0 \pm 1.3 (40)	34

Supplementary Table 6. List of the closest known culturable relatives to *Sanguina nivaloides* showing their Genbank accession numbers of 18S rRNA gene and rbcL sequences (¹sequenced in this study).

Taxon	strain designation	Accession number	
		18S rRNA gene	rbcL
cf. <i>Coenochloris</i> sp.	CCCryo 147-01	GU117588	MK728651 ¹
cf. <i>Ploetila</i> sp.	CCCryo 086-99	GU117586	MK728652 ¹
cf. <i>Sphaerocystis</i> sp.	CCCryo 101-99	AF514407	MK728649 ¹
cf. <i>Sphaerocystis</i> sp.	CCCryo 133-01	MK728648 ¹	MK728650 ¹

Supplementary Table 7. Uncorrected (p-distance; %) and corrected pairwise genetic distance (Kimura-2-parameter K2P; %) between analyzed haplotypes of *Sanguina nivaloides* (H1-H18) and *Sanguina aurantia* (HA1 and HA2) field samples based on ITS2 rDNA nucleotide sequence.

	H1	H2	H3	H4	H5	H6	H7	H8	H9	H10	H11	H12	H13	H14	H15	H16	H17	H18	HA1	HA2
H1		0.5	1	0.5	2.5	2	1	1	1.5	0.5	1	1.5	1	1.5	1.5	2	1.5	1.5	3.3	3.8
H2	0.5		0.5	1	2	2.5	1.5	0.5	1	1	0.5	1	1.5	1	1	1.5	1	1	2.8	3.3
H3	1	0.5		1.5	2.5	3	2	1	1.5	1.5	1	1.5	2	1.5	1.5	2	1.5	1.5	3.3	3.8
H4	0.5	1	1.5		3	2.5	1.5	1.5	2	1	1.5	2	1.5	2	1.5	2	2	2	3.8	4.4
H5	2.4	2	2.4	2.9		3.5	2.5	1.5	3	3	2.5	3	3.5	3	3	3.5	3	1.5	3.8	4.4
H6	2	2.4	2.9	2.4	3.4		1	2	2.5	2.5	2.5	3	3	3	3	3.5	3	2.5	4.9	4.4
H7	1	1.5	2	1.5	2.4	1		1	2.5	1.5	1.5	2	2	2	2	2.5	2	1.5	4.4	4.9
H8	1	0.5	1	1.5	1.5	2	1		1.5	1.5	1	1.5	2	1.5	1.5	2	1.5	0.5	3.3	3.8
H9	1.5	1	1.5	2	2.9	2.4	2.4	1.5		2	1.5	2	2.5	2	2	2.5	2	2	3.8	3.3
H10	0.5	1	1.5	1	2.9	2.4	1.5	1.5	2		1.5	2	1.5	2	2	2.5	2	2	3.8	4.4
H11	1	0.5	1	1.5	2.4	2.4	1.5	1	1.5	1.5		0.5	2	0.5	0.5	1	0.5	1.5	3.3	3.8
H12	1.5	1	1.5	2	2.9	2.9	2	1.5	2	2	0.5		2.5	1	1	1.5	1	2	3.8	4.4
H13	1	1.5	2	1.5	3.4	2.9	2	2	2.4	1.5	2	2.4		2.5	2.5	3	2.5	2.5	4.4	4.9
H14	1.5	1	1.5	2	2.9	2.9	2	1.5	2	2	0.5	1	2.4		1	1.5	0.5	2	3.8	4.4
H15	1.5	1	1.5	1.5	2.9	2.9	2	1.5	2	2	0.5	1	2.4	1		0.5	1	2	3.8	4.4
H16	2	1.5	2	2	3.4	3.4	2.4	2	2.4	2.4	1	1.5	2.9	1.5	0.5		1.5	2.5	4.4	4.9
H17	1.5	1	1.5	2	2.9	2.9	2	1.5	2	2	0.5	1	2.4	0.5	1	1.5		2	3.8	4.4
H18	1.5	1	1.5	2	1.5	2.4	1.5	0.5	2	2	1.5	2	2.4	2	2	2.4	2		3.8	4.4
HA1	3.3	2.8	3.3	3.8	3.8	4.7	4.2	3.3	3.8	3.8	3.3	3.8	4.2	3.8	3.8	4.2	3.8	3.8		0.5
HA2	3.8	3.3	3.8	4.2	4.2	4.2	4.7	3.8	3.3	4.2	3.8	4.2	4.7	4.2	4.2	4.7	4.2	4.2	0.5	

Supplementary Table 8. Uncorrected (p-distance; %) and corrected pairwise genetic distance (Kimura-2-parameter K2P; %) between analyzed haplotypes of *Sanguina nivaloides* (H1-H18) and *Sanguina aurantia* (HA1 and HA2) field samples based on 18S rRNA gene nucleotide sequence.

	H1	H2	H3	H4	H5	H6	H7	H8	HA1	HA2
H1		0	0	0	0	0.1	0.2	0.2	0	0
H2	0		0	0	0	0.1	0.1	0.1	0	0
H3	0	0		0	0	0.1	0.1	0.2	0	0
H4	0	0	0		0	0.1	0.1	0.1	0	0
H5	0	0	0	0		0.1	0.1	0.2	0	0
H6	0.1	0.1	0.1	0.1	0.1		0.1	0.2	0.1	0.1
H7	0.2	0.1	0.1	0.1	0.1	0.1		0.2	0.1	0.1
H8	0.2	0.1	0.1	0.1	0.2	0.2	0.2		0.1	0.1
HA1	0	0	0	0	0	0.1	0.1	0.1		0
HA2	0	0	0	0	0	0.1	0.1	0.1	0	

Supplementary Table 9. Uncorrected (p-distance; %) and corrected pairwise genetic distance (Kimura-2-parameter K2P; %) between analyzed haplotypes of *Sanguina nivaloides* (H1-H18) and *Sanguina aurantia* (HA1 and HA2) field samples based on rbcL nucleotide sequence.

	H1	H2	H4	H6	H7	H8	H9	HA1	HA2
H1		0.1	0	2.2	2.2	3.4	0	2.6	3.3
H2	0.1		0.1	2.2	2.2	3.4	0.1	2.6	3.3
H4	0	0.1		2.2	2.2	3.4	0	2.7	3.3
H6	2.1	2.1	2.1		0	3.7	2.2	1.9	2.5
H7	2.1	2.1	2.1	0		3.7	2.2	1.9	2.5
H8	3.2	3.2	3.2	3.5	3.5		3.4	3.6	4.4
H9	0	0.1	0	2.1	2.1	3.2		2.7	3.3
HA1	2.5	2.5	2.6	1.8	1.8	3.4	2.6		0.5
HA2	3.2	3.1	3.2	2.4	2.4	4.1	3.2	0.5	

Supplementary Table 10. Spatial principal component analyses (sPCA) with significance values of the correlation (based on 999 permutation using the Monte Carlo test) for two types of *Sanguina nivaloides* datasets.

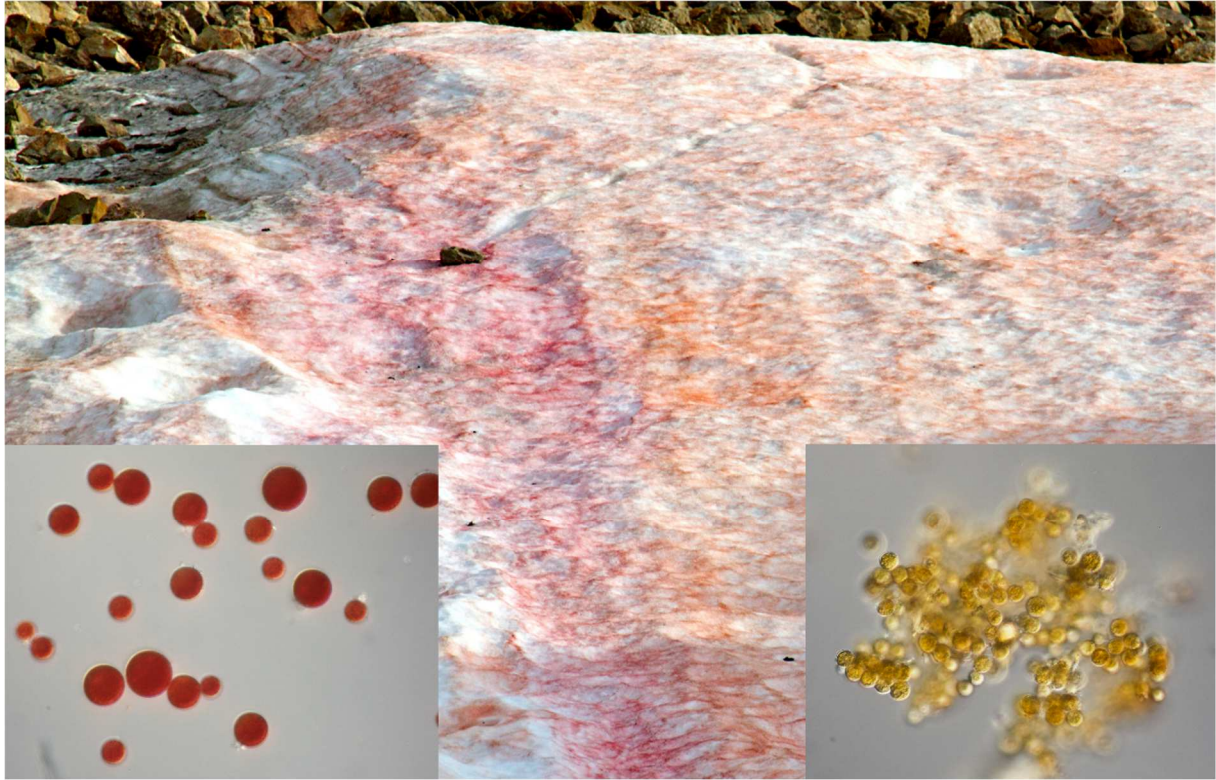
Spatial principal component analyses	p-value	
	global structure	local structure
(a) Europe, America, Antarctica, Svalbard	0.39	0.31
(b) Europe	0.17	0.8

Supplementary Table 11. Mantel test of the genetic similarity and spatial distance of *Sanguina nivaloides* cysts with significance test of distant class in correlogram (based on 1000 repetitions and 1000 permutations, respectively) for two types of datasets.

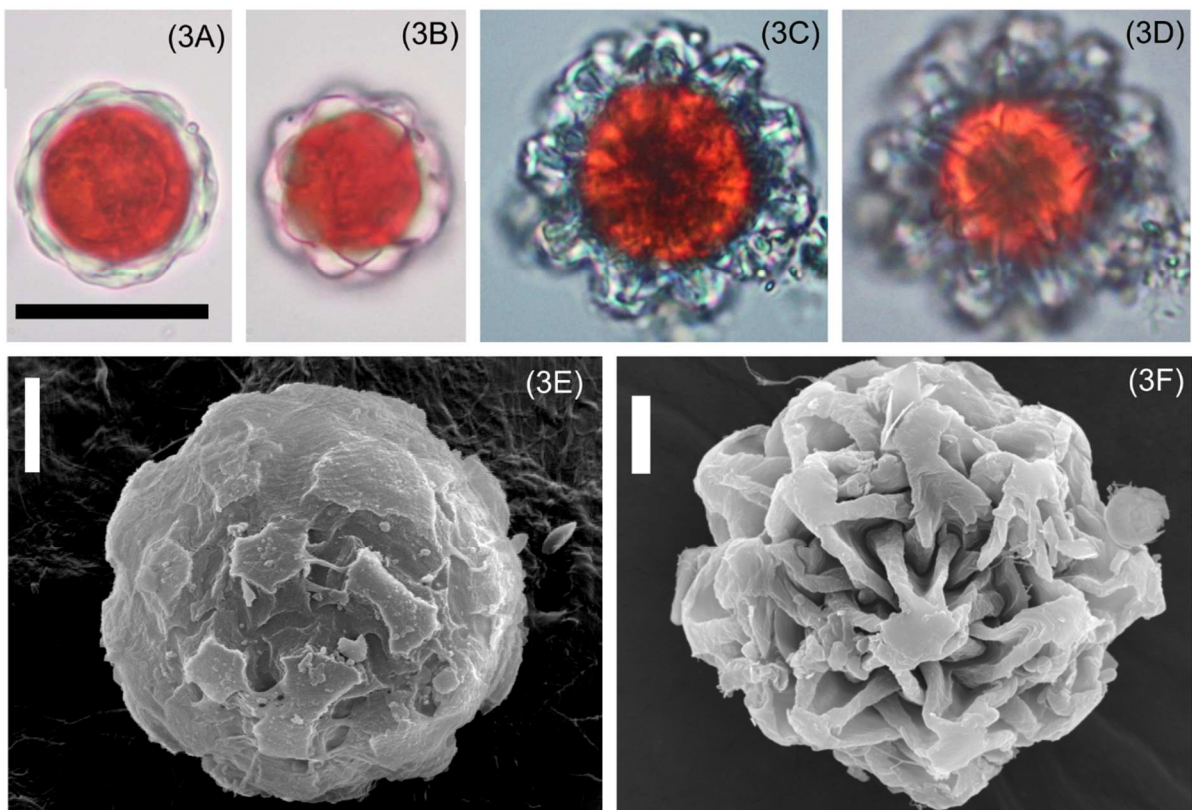
	p-value
(a) Europe, America, Antarctica, Svalbard	0.27
(b) Europe	0.58



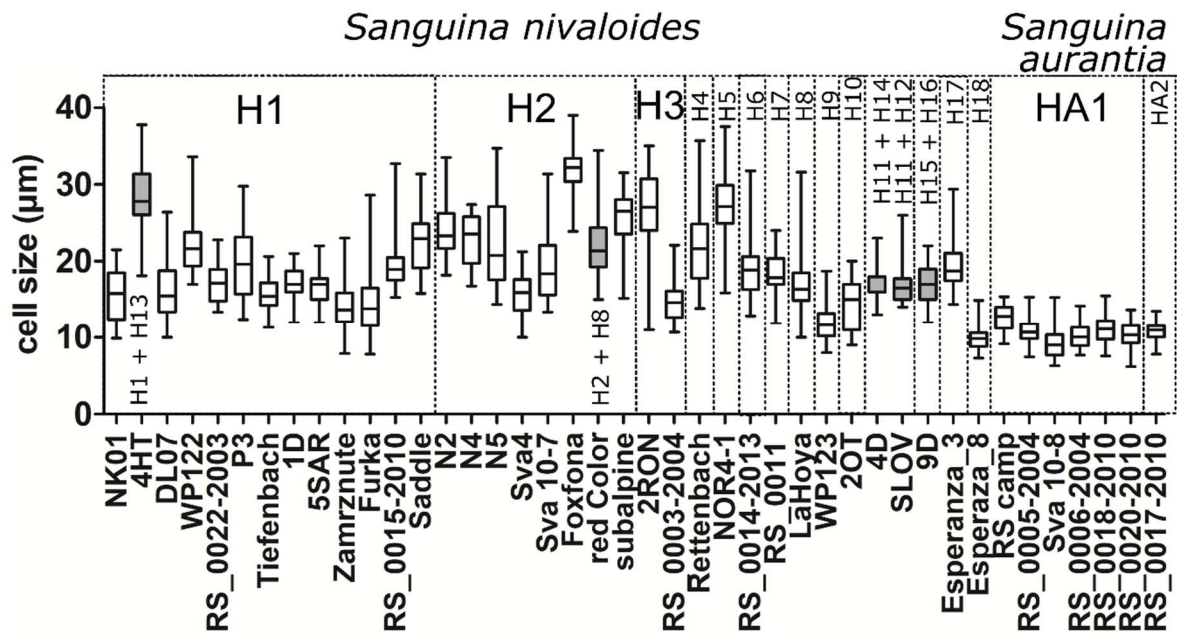
Supplementary Figure 1. Overview of the type locality of *Sanguina nivaloides*, sp. et gen. nov. (Midterhuken, Nathorst Land, Svalbard): (upper) sampling location (red arrowhead) and (lower) a detailed view of the red snowfield during harvest (lower photo with with kind permission of Stephan Hering-Hagenbeck).



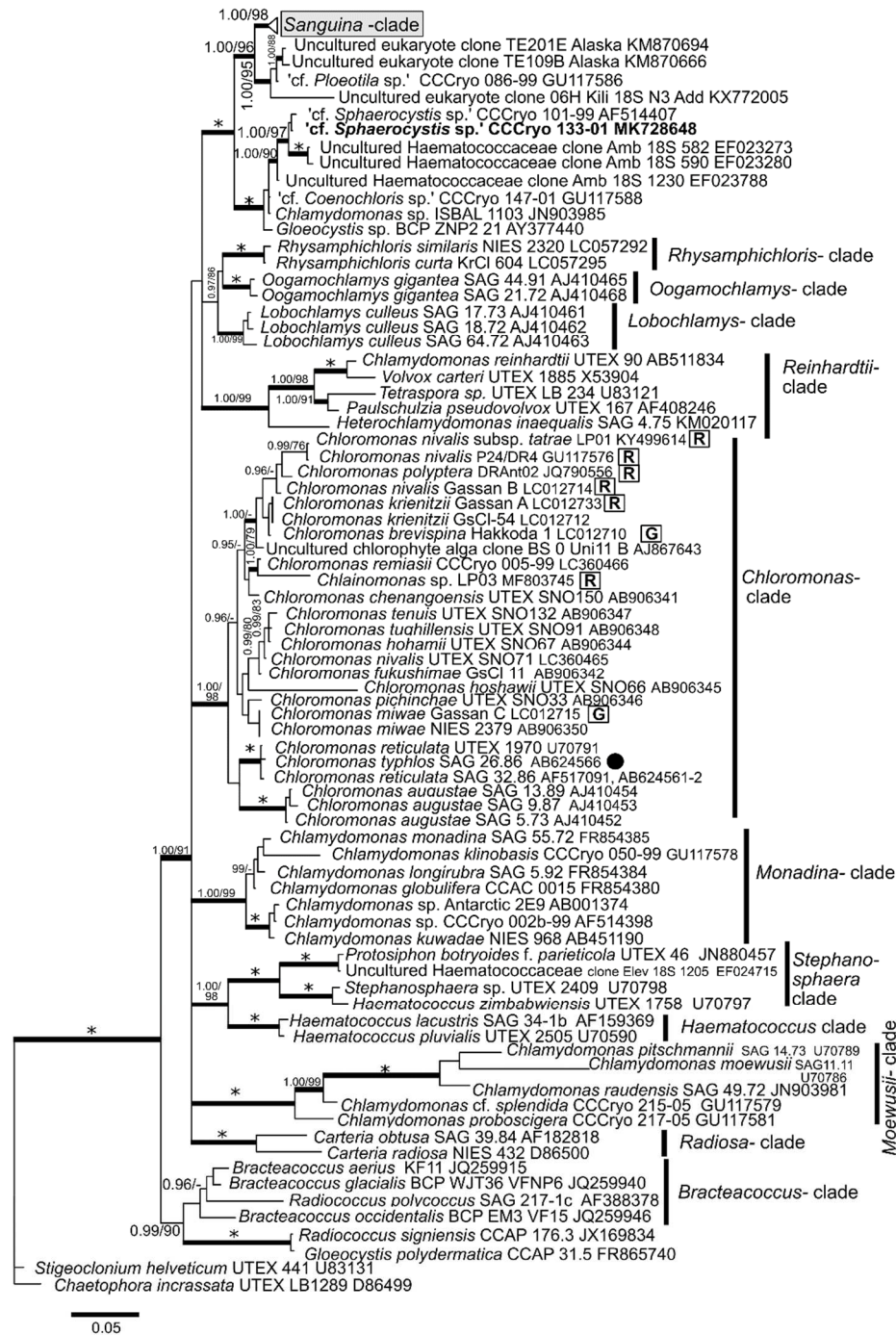
Supplementary Figure 2. Snowfield in a polar habitat on Svalbard (Bautauen Mountain, Hornsund) showing distinct colored patches caused by the co-occurrence of *Sanguina nivaloides* (on the left) and *Sanguina aurantia* (on the right) (sampling location no. 36 in Fig. 1, Supplementary Table 2).



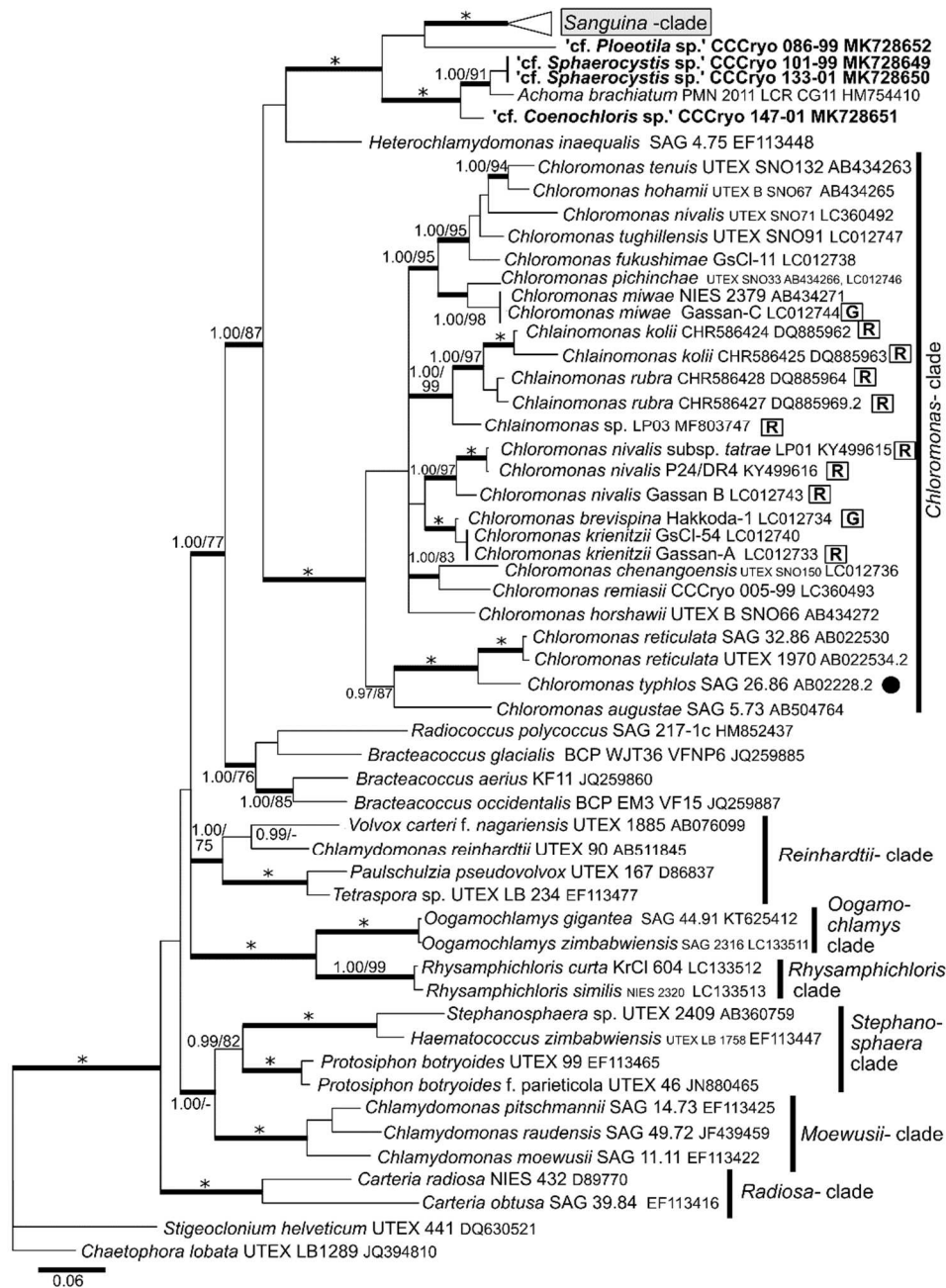
Supplementary Figure 3. Light and scanning electron micrographs of 'ruby' cysts with rosette-like secondary cell wall appearing like mother-of-pearl in the light microscope (scattered in samples RS_0011 and NOR4-1), (A, C) with focus at median cross section, (B, D) with focus on cell surface, note: the mother-of-pearl appearance is not apparent in SEM picture, but show the physical reason behind. Scale bars 20 μm (A-D) and 5 μm (E-F).



Supplementary Figure 4. Cell size ranges of of *Sanguina nivaloides* haplotypes (H1-H18) and *Sanguinea aurantia* haplotypes (HA1 and HA2) in the dataset studied. Boxplots filled in grey indicate five field samples (redCol, 4HT, 2SLOV, 4D, 9D) containing two haplotypes. Boxplots filled in grey indicate five field samples (redCol, 4HT, 2SLOV, 4D, 9D) containing two haplotypes. which were usually indistinguishable in light microscope. Unless single cell PCR was done, some uncertainty remains in this case, which cell size is linked to each of these haplotypes additionally resolved by programme DnaSP v. 6.0. (Librado and Rozas 2009).

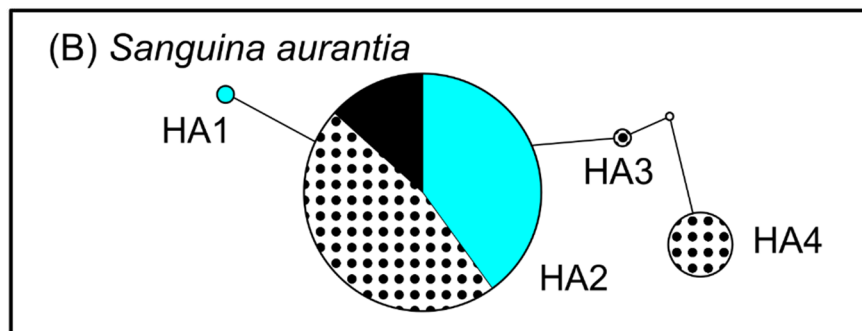
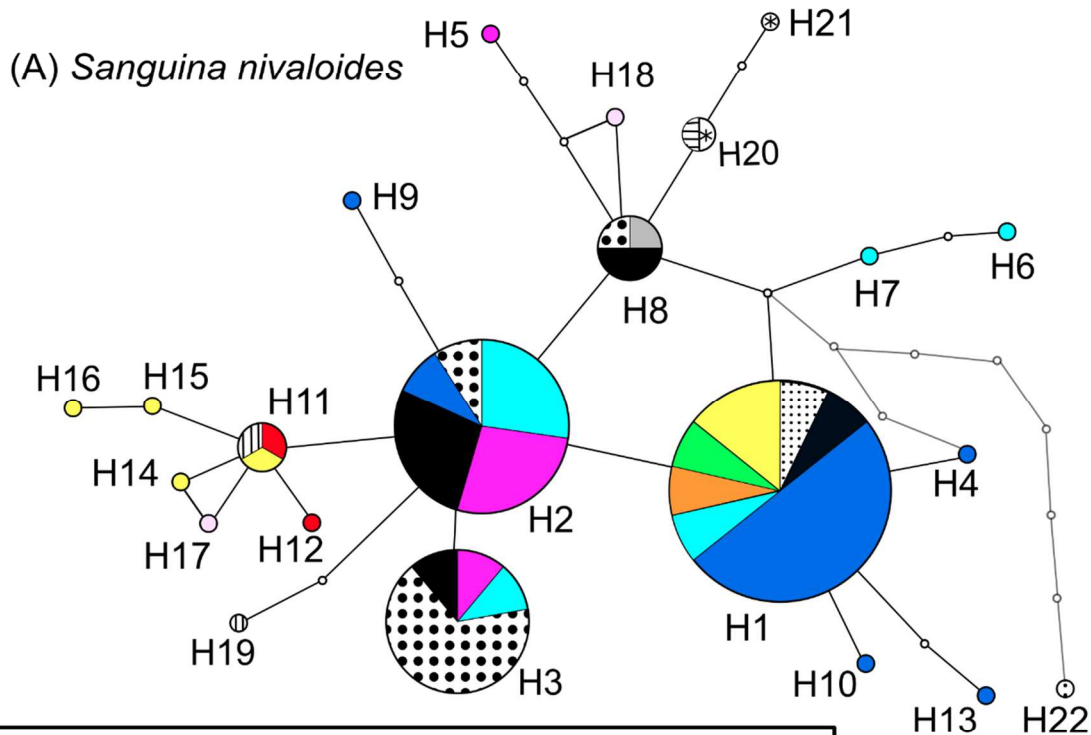
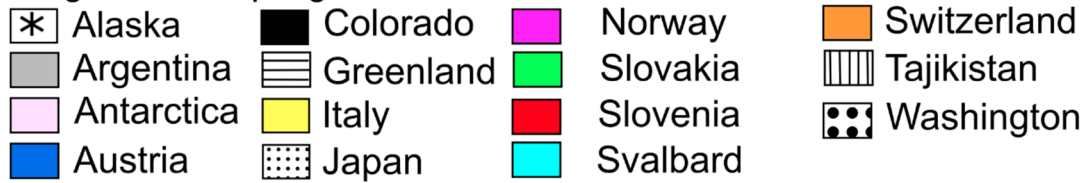


Supplementary Figure 5. 18S rRNA gene based Bayesian phylogenetic tree – full display of the clades except for the *Sanguina* -clade, which is boxed in grey (top). Posterior probabilities (0.95 or more) and bootstrap values from maximum likelihood analyses (75% or more) are shown. Full statistical support (1.00/100) is marked with an asterisk. Thick branches represent nodes receiving the highest posterior probability support (1.00). One newly obtained sequence outside the *Sanguina* -clade is in bold. Accession numbers, strain or field sample codes are indicated after each species name. Sanger sequencing of the field material as a successful strategy if strains are missing (or a complementary approach to link genetical information between field cysts and laboratory flagellate strains) is demonstrated at specimens highlighted in boxes ('R' - red bloom, 'G' - green snow). Position of the strain SAG 26.86 [=IU 1969 original deposition] is marked by full circle, this strain was isolated from snow and formerly believed to cause red snow and thus, labelled as *Chlamydomonas nivalis*.

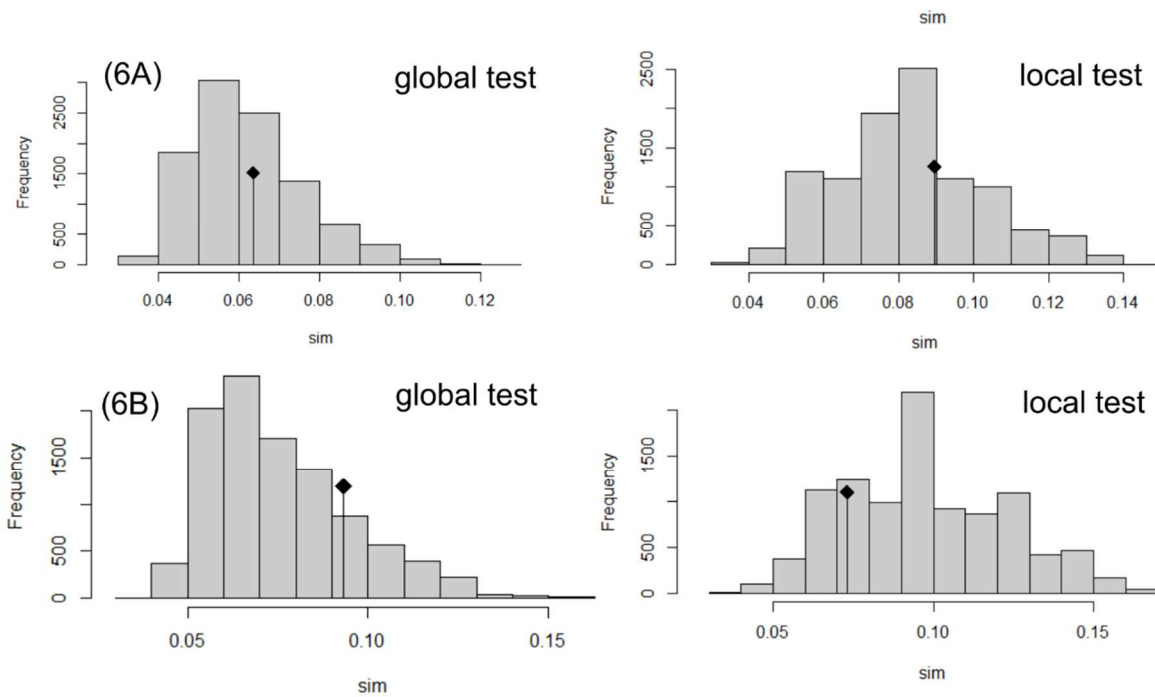


Supplementary Figure 6. rbcL gene based Bayesian phylogenetic tree – full display of the clades except for the *Sanguina*-clade, which is boxed in grey (top). Posterior probabilities (0.95 or more) and bootstrap values from maximum likelihood analyses (75% or more) are shown. Full statistical support (1.00/100) is marked with an asterisk. Thick branches represent nodes receiving the highest posterior probability support (1.00). Four newly obtained sequences outside the *Sanguina*-clade are in bold. Accession numbers, strain or field sample codes are indicated after each species name. Sanger sequencing of the field material as a successful strategy if strains are missing (or a complementary approach to link genetic information between field cysts and lab flagellate strains) is demonstrated at specimens highlighted in boxes (full line - red bloom, dotted line - green snow). Position of the strain SAG 26.86 [=IU 1969 original deposition] is marked by full circle, this strain was isolated from snow and formerly believed to cause red snow and thus, was labelled as *Chlamydomonas nivalis* for a long time.

Region of sampling



Supplementary Figure 7. Geographic distribution of ITS2 haplotypes of *Sanguina nivaloides* and *Sanguina aurantia* based on sequences gained in this study and selected published sequences from Colorado and Washington States, U.S.A. (Brown, Ungerer and Jumpponen 2016), Alaska (AB902998.1), Greenland (AB902971.1), Austrian Alps (GU117577.1, Remias *et al.* 2010), Japan (AB903028.1) and Pamir, Tajikistan (AB902973.1, AB903025.1). Each haplotype network was constructed using a statistical parsimony method under a 95% connection limit. The grey line shows the connections when reducing the TCS connection limit to 90%. Each ball represents a haplotype. The size of the ball is proportional to the number of specimens sampled belonging to that haplotype. The colour represents a country of sampling. Lines connect each haplotype to its most similar relative. Open dots represent mutational steps between haplotypes, one dot indicates a change of 1 base pair.



Supplementary Figure 8. Spatial principal component analyses (sPCA) with histograms of permuted test statistics for *Sanguina nivaloides* field samples, the statistics observed are indicated by a black dot and a segment. Diagram rows: (a) Europe, America, Antarctica, Svalbard (b) Europe only. The output for the global test and local tests are shown in each row on the right and left side respectively. In all cases, plots show that the observed test statistics (black points) are in the range of the most simulated values (histograms), leading to no rejection of the null hypothesis of the absence of a spatial structure, i.e. no spatial structure was detected for *Sanguina nivaloides* indicating that field samples of this species are genetically similar over space.

REFERENCES

- De Wever A, Leliaert F, Verleyen E *et al.* Hidden levels of phylodiversity in Antarctic green algae: further evidence for the existence of glacial refugia. *Proc R Soc Lond, Ser B: Biol Sci* 2009;**276**: 3591-99.
- Goff LJ, Moon D, A., Coleman AW. Molecular delineation of species and species relationships in the red algal agarophytes *Gracilariopsis* and *Gracilaria*. *J Phycol* 1994;**30**: 521-37.
- Helms G, Friedl T, Rambold G *et al.* Identification of photobionts from the lichen family Physciaceae using algal-specific ITS rDNA sequencing. *The Lichenologist* 2001;**33**: 73-86.
- Hoham RW, Bonome TA, Martin CW *et al.* A combined 18S rDNA and *rbcL* phylogenetic analysis of *Chloromonas* and *Chlamydomonas* (Chlorophyceae, Volvocales) emphasizing snow and other cold-temperate habitats. *J Phycol* 2002;**38**: 1051-64.
- Katana A, Kwiatowski J, Spalik K *et al.* Phylogenetic position of *Koliella* (Chlorophyta) as inferred from nuclear and chloroplast small subunit rDNA. *J Phycol* 2001;**37**: 443-51.
- Matsuzaki R, Kawai-Toyooka H, Hara Y *et al.* Revisiting the taxonomic significance of aplanozygote morphologies of two cosmopolitan snow species of the genus *Chloromonas* (Volvocales, Chlorophyceae). *Phycologia* 2015;**54**: 491-502.
- Piercey-Normore MD, Depriest PT. Algal switching among lichen symbioses. *Am J Bot* 2001;**88**: 1490-98.
- Vilgalys R, Hester M. Rapid genetic identification and mapping of enzymatically amplified ribosomal DNA from several *Cryptococcus* species. *J Bacteriol* 1990;**172**: 4238-46.
- White TJ, Bruns T, Lee S *et al.* Amplification and direct sequencing of fungal ribosomal RNA genes for phylogenetics. In: Innis MA, Gelfand DH, Sninsky JJ, White TJ (eds.) *PCR Protocols: A Guide to Methods and Applications*. New York, USA: Academic Press, Inc., 1990, 315-22.

Paper II

**Ecophysiological and morphological comparison of two
populations of *Chlainomonas* sp. (Chlorophyta) causing red snow
on ice-covered lakes in the High Tatras and Austrian Alps**

Procházková L¹, Remias D², Holzinger A³, Řezanka T⁴ & Nedbalová L¹

European Journal of Phycology 53(2): 230–243, 2018

¹ Charles University, Faculty of Science, Department of Ecology, Viničná 7, 128 44 Prague 2,
Czech Republic

² Applied Sciences Upper Austria, Stelzhamerstr. 23, A-4600 Wels, Austria

³ Department of Botany, University of Innsbruck, Austria

⁴ Institute of Microbiology of the Czech Academy of Sciences, Czech Republic

Ecophysiological and morphological comparison of two populations of *Chlainomonas* sp. (Chlorophyta) causing red snow on ice-covered lakes in the High Tatras and Austrian Alps

Lenka Procházková ^a, Daniel Remias^b, Andreas Holzinger ^c, Tomáš Řezanka ^d and Linda Nedbalová^a

^aCharles University, Faculty of Science, Department of Ecology, Viničná 7, CZ-128 44 Prague, Czech Republic; ^bUniversity of Applied Sciences Upper Austria, Stelzhamerstr. 23, A-4600 Wels, Austria; ^cDepartment of Botany, University of Innsbruck, Austria; ^dInstitute of Microbiology of the Czech Academy of Sciences, Czech Republic

ABSTRACT

Based on analyses of multiple molecular markers (18S rDNA, ITS1, ITS2 rDNA, *rbcL*), an alga that causes red snow on the melting ice cover of a high-alpine lake in the High Tatras (Slovakia) was shown to be identical with *Chlainomonas* sp. growing in a similar habitat in the Tyrolean Alps (Austria). Both populations consisted mostly of smooth-walled quadriflagellates. They occurred in slush, and shared similar photosynthetic performances (photoinhibition above 1300 $\mu\text{mol photons m}^{-2} \text{s}^{-1}$), very high levels of polyunsaturated fatty acids (PUFA, 64% and 74% respectively) and abundant astaxanthin accumulation, comparable to the red spores of *Chlamydomonas nivalis* (Bauer) Wille. Physiological differences between the Slovak and Austrian populations included higher levels of α -tocopherol and a 13Z-isomer of astaxanthin in the former. High accumulation of secondary pigments in the Slovak population probably reflected harsher environmental conditions, since the collection was made later in the growing season when cells were exposed to higher irradiance at the surface. Using a polyphasic approach, we compared *Chlainomonas* sp. with *Chlamydomonas nivalis*. The latter causes ‘conventional’ red snow, and shows high photo-physiological plasticity, with high efficiency under low irradiance and no photoinhibition up to 2000 $\mu\text{mol photons m}^{-2} \text{s}^{-1}$. Its PUFA content was significantly lower (50%). An annual cycle of lake-to-snow colonization by *Chlainomonas* sp. from slush layers deeper in the ice cover is proposed. Our results point to an ecologically highly specialized cryoflora species, whose global distribution is likely to be more widespread than previously assumed.

ARTICLE HISTORY Received 30 June 2017; Revised 13 November 2017; Accepted 16 November 2017


KEYWORDS Astaxanthin; *Chlainomonas*; fatty acids; field sample; High Tatras; morphology; photosynthesis; snow algae; ultrastructure; alpine lake

Introduction

Red snow discolouration in alpine and polar regions is caused by many algal species (Kol, 1968; Lutz *et al.*, 2015; Matsuzaki *et al.*, 2015), which in most cases belong to the genera *Chlamydomonas*, *Chloromonas* and *Chlainomonas* (Chlorophyta) (Novis *et al.*, 2008; Brown *et al.*, 2016; Procházková *et al.*, 2018). The genus *Chlainomonas* was established by Christen (1959), with the freshwater species *Chlainomonas ovalis* as the type. Two other species of this genus were described from snow, *C. kolii* (Hardy & Curl) Hoham and *C. rubra* (Stein & Brook) Hoham (Hoham, 1974a,b). Recently, populations of *Chlainomonas* sp. thriving periodically in slush at a high-alpine lake and at a glacier in the Austrian Alps were described (Remias *et al.*, 2016). Despite morphological similarities to spherical immotile red cells of the common snow alga *Chlamydomonas nivalis*, these two *Chlamydo-monadacean* genera are not closely phylogenetically related. Blooms of *Chlainomonas* sp. were restricted to summer snow banks with higher water content, whereas *Chlamydomonas nivalis* was not found in these specific habitats (Remias *et al.*, 2016). However, several questions

concerning the ecology and physiology of *Chlainomonas* sp. remain unanswered. For example, the photosynthetic activity in a broad range of light conditions has not yet been elucidated. Furthermore, change in fatty acid composition is one of the crucial adaptations to cold habitats (De Maayer *et al.*, 2014). The fatty acid profile has not been investigated for this genus so far.

The aim of this study was to compare the ecophysiology and morphology of two populations of *Chlainomonas* sp. causing red snow on melting ice sheets in two high-alpine lakes in different European mountain ranges. We hypothesized that the population in the High Tatras (Slovakia) is the same species as the one in the Tyrolean Alps (Austria). Our intention was (1) to confirm their close phylogenetic relationship; (2) to reveal details of their cytological adaptations to the snow habitat; (3) to evaluate if the spatial distribution of the population in the ice-cover correlates with the availability of liquid water in the snow; (4) to compare the rates of photosynthesis; (5) to analyse the composition of secondary pigments; and (6) to test whether there are any differences

CONTACT Lenka Procházková  lenkacerven@gmail.com

© 2018 The Author(s). Published by Informa UK Limited, trading as Taylor & Francis Group.

This is an Open Access article distributed under the terms of the Creative Commons Attribution License (<http://creativecommons.org/licenses/by/4.0/>), which permits unrestricted use, distribution, and reproduction in any medium, provided the original work is properly cited.

in adaptation strategies between the populations, in terms of fatty acids. Finally, in order to evaluate differences from the snow alga *C. nivalis*, we investigated the same parameters and metabolites of field samples of *C. nivalis* from the Tyrolean Alps. These analyses allowed a comprehensive description of this red-snow species of the genus *Chlainomonas*, which seems to be restricted to extremophilic habitats, including slush layers in lake-ice and glacier surfaces.

Materials and methods

Sampling and snow characterization

The cryoflora causing red snow on the ice cover on Ladové Lake (the High Tatras, Slovakia, LP03) and Gossenkölle Lake (Tyrolean Alps, Austria, DL06) and near Gossenkölle Lake (DL07) was investigated in May and June 2016 (Table 1, Fig. 1). Surface snow was harvested with a sterile shovel, placed in 10 l buckets, and transported the same day to the labora-

Table 1. Samples of *Chlainomonas* sp. from the High Tatras (Slovakia, LP03), Tyrolean Alps (Austria, DL06), and *Chlamydomonas nivalis* from the latter region (DL07) with sample codes, collection date, sampling site, altitude (m) and geographic position (GPS).

Sample	Date	Location	Altitude	GPS
LP03	19 June 2016	snow on ice cover of Ladové Lake	2058	N49° 11.018 E20° 09.649
DL06	27 May 2016	snow on ice cover of Gossenkölle Lake	2411	N47° 13.762 E11° 00.885
DL07	28 May 2016	snow on slope close to Gossenkölle Lake	2380	N47° 13.709 E11° 00.949

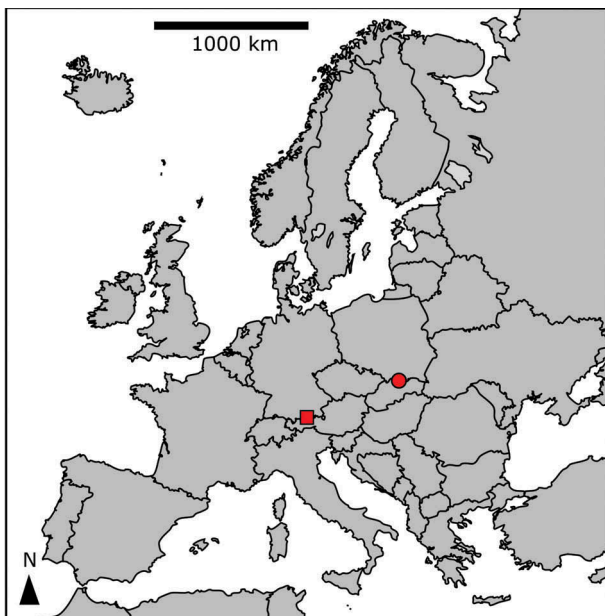


Fig. 1. Sample locations at the High Tatras, Slovakia (circle), and the Tyrolean Alps, Austria (square).

tory. Prior to photosynthesis measurements, samples were slowly melted overnight and kept in the dark at 4–5°C. Electrical conductivity (EC) and pH of the meltwater were obtained with WTW Instruments (Cond 340i and Inolab, Germany) or with HANNA (Combo EC, Romania). Snow water content (SWC) was measured by coring snow with a cylindrical polyvinylchloride corer, according to Procházková *et al.* (2018). The spatial distribution of SWC and cell densities in snow on the ice cover at Lake Gossenkölle were evaluated on 27 May 2016 along a transect from the southern to northern shores (Supplementary fig. S3), at the following distances from the southern shore: 1, 2, 17, 32, 47, 62, 77, 92, 107 and 108 m.

Light and electron microscopy

Light microscopy (LM, magnification 1000×) was performed and preparation of samples for scanning and transmission electron microscopy (SEM and TEM) were carried out in the same manner as described by Procházková *et al.* (2018), with the exception that from the moment of harvest, cells of the thermosensitive *Chlainomonas* sp. were immediately placed in thermos bottles to keep them cool.

Cell counting

In order to quantify the red-snow colouration in the field, we counted the highest cell concentration. An estimation of the mean cell concentration was not intended since there were enormous differences in cell densities at the spatial scale of a dozen cm along the transect in snow at ice cover of Gossenkölle Lake. We took a 10 ml snow subsample from each sampling site (DL06, DL07, LP03) and from these, a further subsample of 0.5 ml snow meltwater was taken and placed in a Kolkwitz plankton-counting chamber (Hydro-Bios, Germany) and processed according to Remias *et al.* (2016).

Isolation of DNA and sequencing

DNA was isolated as described by Procházková *et al.* (2018). The 18S small subunit ribosomal RNA gene (18S rDNA), internal transcribed spacer regions 1 and 2 (ITS1, ITS2 rDNA), and ribulose-1,5-bisphosphate carboxylase/oxygenase large subunit (*rbcL*) gene regions were amplified from DNA isolates by polymerase chain reaction (PCR), using existing primers (Supplementary table S1). Amplification and sequencing reactions for these markers were described by Procházková *et al.* (2018). New sequences were submitted to the NCBI nucleotide sequence database (accession numbers in Supplementary table S2).

Photosynthesis

The light-dependent photosynthesis rates were obtained as the relative electron-transport rate of photosystem II with a fluorometer (PAM 2500, Heinz Walz GmbH, Germany). Cells were exposed to photon flux densities (PFDs) of 5, 34, 67, 104, 201, 366, 622, 984, 1389, 1666 and 2018 $\mu\text{mol photons m}^{-2} \text{s}^{-1}$ for 30 s each at 2°C in a pre-cooled sample chamber (volume of 1 ml). Five independent biological replicates were measured for LP03, DL06 and DL07. After each light exposure, a saturating pulse was applied to detect the effective photochemical quantum yield of photosystem II. A curve of the relative electron-transport rate (rETR) upon PFD was calculated and fitted by the model according to Walsby (1997), assuming photoinhibition. Relative and maximum electro-transport rate (ETR_{max}), initial slope (α) and light saturation point (I_k) were determined (Procházková *et al.*, 2018).

Pigment analysis

Chlorophylls, carotenoids and tocopherols were extracted and quantified according to Remias & Lütz (2007). Briefly, cells were freeze-dried on glass-fibre filters, disrupted with a grinding mill and extracted with dimethylformamide. The analysis was performed with an Agilent 1100 HPLC system with a LiChroSpher C18 column and diode array and fluorescence detectors. Carotenoid standards were obtained from CarotNature (Switzerland).

Lipid extraction and analysis of fatty acid methyl esters (FAMES)

The extraction procedure was based on the method of Bligh & Dyer (1959), and elution was done from a Sep-Pak Vac Silica cartridge 35cc (Waters; 10 g normal-phase silica) by chloroform (neutral lipids), acetone (glycolipids) and methanol (phospholipids) (Saunders & Horrocks, 1984). All classes of lipids were saponified overnight in 10% KOH in methanol at room temperature. The structures of FAMES were confirmed by comparison with GC/MS retention times, and fragmentation patterns with those of standard FAMES (Supelco, Prague) (Řezanka, 1990; Dembitsky *et al.*, 1991). Procedures were described in detail by Procházková *et al.* (2018).

Climatic conditions

For a comparison of the prevailing climate above the snow surface at the sampling localities in the two mountain ranges in the course of a year, radiation, monthly and daily mean air temperature (°C), and monthly cumulative precipitation (mm) were used. For complete description see the Supplementary text.

Results

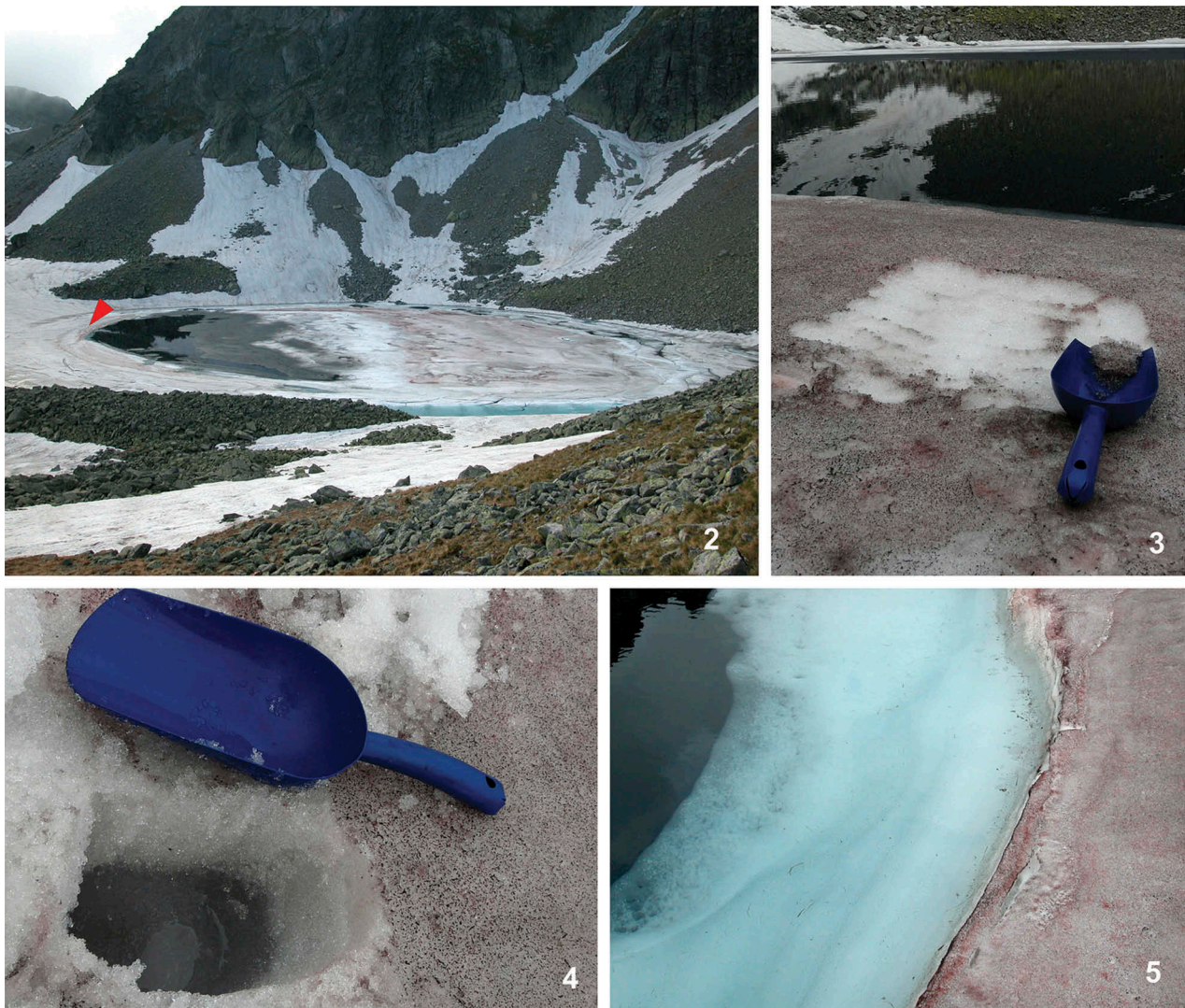
Collection sites and habitat conditions

Red snow caused by *Chlainomonas* sp. was found in late spring 2016 on two still partly ice-covered high-alpine lakes, Ladové Lake in the High Tatras and Gossenkölle Lake in the Tyrolean Alps (Table 1). In the High Tatras, the lake was partly ice-free and red snow was visible on all remaining ice-covered parts (Figs 2–5). The texture of this snow was partly slushy and partly frozen (sample LP03). A prominent soft slush layer, which was apparently soaked by lake water, began approximately 10 cm below the surface. At the Tyrolean location, the snow colouration was visible only close to the lake shore, where melting of the underlying ice was advanced (sample DL06; Supplementary figs S1–S4). The majority of the lake surface was still covered with white snow, and red horizontal patches of snow populated by *Chlainomonas* sp. were hidden several centimetres below the snow surface, close to the interface with the ice cover. One week later, red spots appeared across the entire lake on the surface of the snow. For a comparison ‘terrestrial’ red snow caused by *C. nivalis* was collected near Gossenkölle Lake (sample DL07). This sample was dominated by blood-red mature spores, with a smaller contribution (15%) of young cells in an early stage of development, with green parts of the chloroplasts visible. The habitat conditions of all localities are summarized in Table 2.

Morphology and ultrastructure

The morphology of *Chlainomonas* sp. was characterized by LM (Figs 6–14 for the High Tatras and Supplementary figs S5–S12 for the Tyrolean Alps). The populations at the two locations had very similar morphology. Swimmers of *Chlainomonas* sp. had four flagella. Each flagellum was about as long as the cell (Table 2). The ellipsoidal to nearly spherical flagellates were morphologically variable: many of them possessed a papilla (thickened cell walls with flagellar openings at the anterior pole) and a pseudo-papilla (thickened posterior cell wall) (Fig. 6, Supplementary fig. S5); rarely, the cell wall was entirely detached from the protoplast (Fig. 7). Additionally, swimmers with an equally thin cell wall and papilla (Figs 8, 9, Supplementary figs S6, S7) and swimmers with a collar-like papilla (Fig. 10, Supplementary figs S8–S11) occurred. The protoplast was almost entirely occupied with red pigment. In a few cases, greenish spots of a parietal chloroplast were visible (Fig. 9).

The mean cell sizes of the most common, non-collared flagellates of *Chlainomonas* sp. from both locations are summarized in Table 2. Other life-cycle stages occurred rarely (<5%), and their cell sizes are shown in Supplementary table S3. Flagellates with collared papillae were smaller than



Figs 2–5. Overview of the sampling site of *Chlainomonas* sp. at Ladové Lake (the High Tatras, Slovakia). **Fig. 2.** Red colouration was visible at nearly all ice-covered parts of the lake (mid-June 2016). The harvest spot was close to the southern shore (sample LP03, red arrowhead). **Fig. 3.** Detailed view of red snow after harvest, *Chlainomonas* sp. was present at the surface and down to a depth of 2 cm. **Fig. 4.** Approximately 10 cm below the surface a prominent soft slush layer was noticed, which was apparently soaked by lake water. **Fig. 5.** Detail view of the interface between the lake margin with red snow close to the shore and lake water with edges of a slush layer.

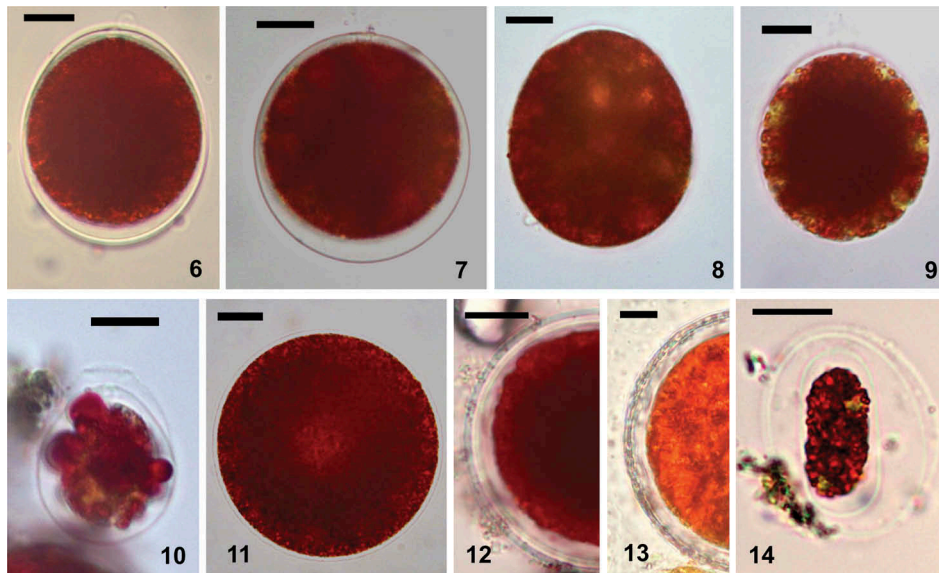
Table 2. Abiotic habitat parameters and cell sizes of snow algae in field samples from the High Tatras (LP03) and Tyrolean Alps (DL06, DL07).

Species (sample)	EC	pH	SWC	Population density ml ⁻¹	Cell length	Cell width
<i>Chlainomonas</i> sp. (LP03)	n.a.	5.8	56.4±3.8	44150±3091	37.7±7.5	35.9±7.3
<i>Chlainomonas</i> sp. (DL06)	2.5	5.8	57.9±1.6	6728±619	30.7±6.2	29±5.9
<i>Chlamydomonas nivalis</i> (DL07)	8.4	6.2	53.9±2.4	56036±3867	16.3±4.2	15.7±4.3

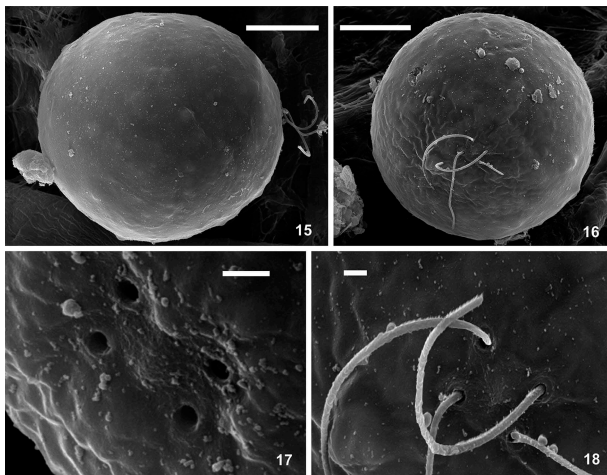
Electrical conductivity (EC; $\mu\text{S cm}^{-1}$), pH of meltwater and snow water content (SWC; %), population density (cells ml⁻¹ meltwater) \pm SD (standard deviation), mean sizes of cells in $\mu\text{m} \pm$ SD, n.a. – not available.

the dominant non-collared flagellates. Immotile stages were ovoid to spherical (Fig. 11). Maintaining field-collected material in melt-water at 4°C in the laboratory for several months helped to reveal other life-cycle stages, which were rarely found in the field. First, mature spores developed from quadriflagellate swimmers, their primary cell wall became hyaline, and a new secondary cell wall was formed below. Sometimes, a third cell wall or multiple layers were also present (Figs 12, 13, Supplementary fig. S12).

Second, smaller oblong red biflagellates enclosed by two layers of a mother cell wall (likely derived from mature spores) appeared in a subsample kept in the same conditions but in the dark (Fig. 14). Further cellular details such as the stigma, cell-wall surface structures such as spines, cell divisions, or other putative stages in the life cycle were not observed. The cell-wall surface of *Chlainomonas* sp. was depicted by SEM (Figs 15–18). A smooth surface was characteristic for swimmers (Figs 15, 16). Four



Figs 6–14. LM micrographs of *Chlainomonas* sp. showing cells from snow at the ice cover of the Ladové Lake directly after harvest (Figs 6–11) and after several months at lab conditions (Figs 12–14). **Figs 6–10.** Morphological variability of swimmers. **Fig. 6.** Typical swimmer possessed papilla and pseudo-papilla (suggested zygote). **Fig. 7.** Rarely, the cell wall was more distant from the protoplast all around. **Figs 8, 9.** Motile cells with a single thin cell wall and a papilla. Note greenish spots of the parietal chloroplasts. **Fig. 10.** A flagellate with a collared papilla. **Fig. 11.** Non-motile stage without partially thickened cell wall, note central brighter region most likely representing the position of the nucleus. **Figs 12, 13.** Mature spores. **Fig. 12.** Smaller spore with hyaline primary cell wall and multiple layers of secondary cell walls. **Fig. 13.** During ageing of spores, the secondary cell wall becomes thicker. **Fig. 14.** Oblong flagellate containing red pigments and a few greenish spots of parietal chloroplasts. It is probably a daughter cell still remaining in the spore. Scale = 10 μm .



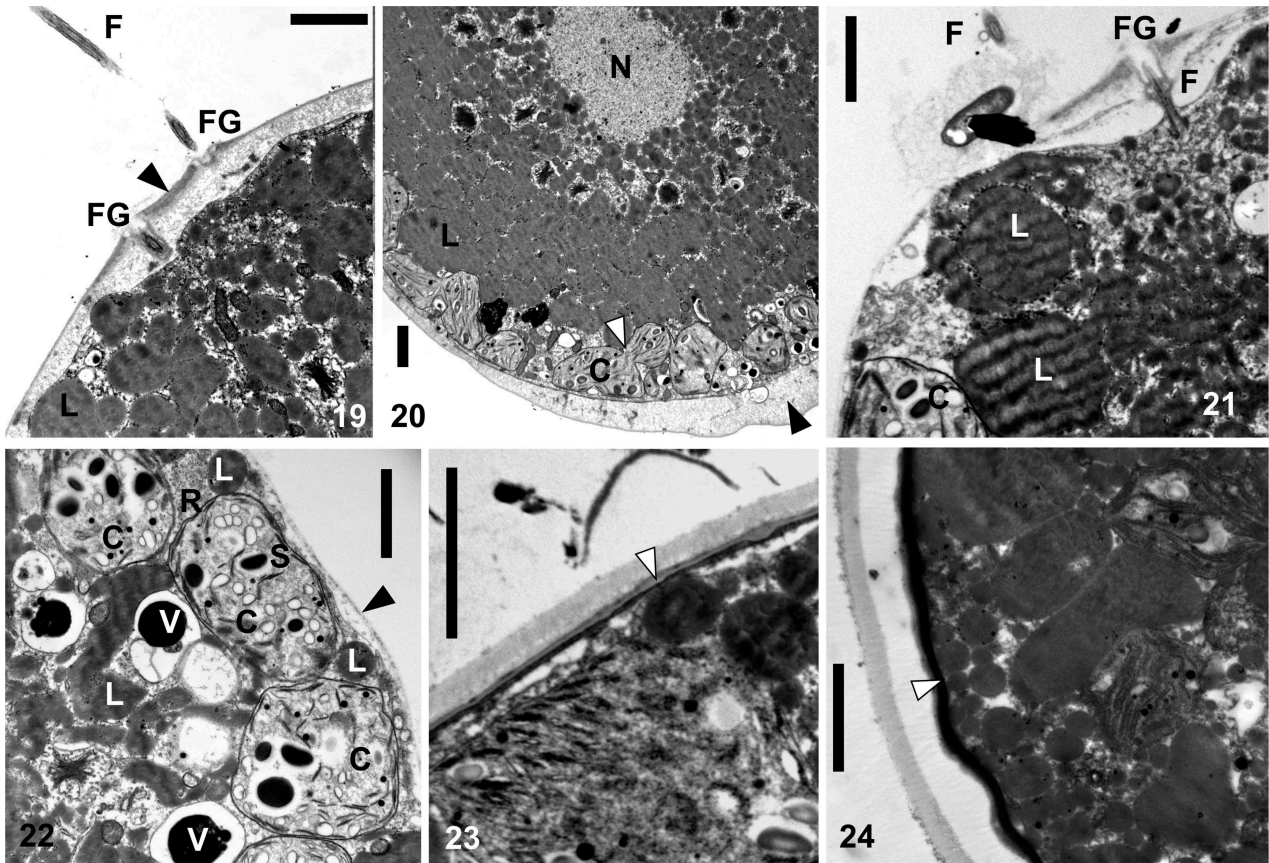
Figs 15–18. SEM micrographs of *Chlainomonas* sp. swimmers from the snow of the Ladové Lake. **Figs 15, 16.** Side and apical view showing the smooth surface of quadriflagellate cells. **Fig. 17.** Detail view of four spherical flagellar grooves in slightly rectangular position. **Fig. 18.** Detail view of two pairs of flagella. Scale = 10 μm (Figs 15, 16) and 1 μm (Figs 17, 18).

spherical flagellar grooves in a subrectangular arrangement were found (Figs 17, 18). Mature spores of *Chlainomonas* sp. possessed fine structures arranged in such a way as to lend an undulating appearance (Supplementary fig. S15, corresponding to Supplementary fig. S12).

The ultrastructure of *Chlainomonas* sp. was analysed by TEM (Figs 19–24 for LP03; Supplementary figs S14, S16, S17 for DL06). The cell walls of most swimmers were thickened at the anterior and posterior ends (Figs 19, 20). A section showing two flagella is depicted in Fig. 19. Small plastids containing starch grains were located parietally (Figs 20, 22). No pyrenoid was observed. The nucleus was positioned centrally and surrounded by many lipid bodies (Fig. 20). Swimmers with a single, uniformly thin cell wall were also found (Figs 8, 9, 21, 22; Supplementary figs S6, S7, S14). Mature spores possessed a trilaminar sheath (secondary wall) surrounded by outer layer(s) of extracellular matrix (Figs 23, 24, Supplementary figs S16, S17). All observed cell stages contained cytoplasmic electron-dense vacuoles, commonly filled with crystalline structures (Fig. 22).

Population density

The population densities of *Chlainomonas* sp. were 6728 ± 619 and 44150 ± 3091 cells ml^{-1} melt-water in the samples from the Tyrolean Alps and the High Tatras, respectively (Table 2). Population densities and SWC were investigated in a 109 m-long south-north transect on the ice cover of Lake Gossenkölle (Supplementary figs S18, S19). The highest values of SWC were reached at sampling points closest to both



Figs 19–24. TEM micrographs of *Chlainomonas* sp. swarmer cells (Figs 19–22) and spores (Figs 23, 24) from the snow of the Ladové Lake. **Figs 19, 20.** A section showing flagellate (F) and two flagella grooves (FG) of a swarmer. Cell wall thickened at the anterior and the posterior of the cell (black arrows). Note small chloroplasts (C) located parietally and a putative process of plastid division (white arrow). Centrally located nucleus (N), likely surrounded by many lipid bodies (L). **Figs 21, 22.** A swarmer with a single, equally thin cell wall (black arrow) with papilla. Section showing one flagella (F) and the flagella groove (FG). Note lipid bodies (L), starch grains (S) in chloroplasts (C), electron dense vacuoles (V) containing a crystalline content and a ribosome rich region (R) close to the cell wall. **Figs 23, 24.** Spherical spore with the trilaminar sheath (secondary cell wall, white arrow). Later outer layers of extracellular matrix are developed. Scale = 2 μm .

lake shores ($89.3 \pm 1.5\%$ and $80.8 \pm 2.9\%$). At points more distant from the lake shores, SWC was significantly lower and ranged from 50.5 ± 2.6 to $57.9 \pm 1.6\%$ (Supplementary fig. S19). The cells were least abundant in the central part of the transect (<400 cells ml^{-1} meltwater), and most abundant in the slushy part, in close proximity to the northern lake shore ($>10\,000$ cells ml^{-1} meltwater) (Supplementary fig. S18). In contrast, the slushy area next to the southern lake shore harboured only one-third as many cells per volume. The spatial variation at the other sampling points of the transect was considerable, ranging from >1500 to <7500 cells ml^{-1} meltwater.

Snow-algal identity inferred from molecular markers

Analyses of the molecular markers 18S rDNA, ITS1 rDNA, ITS2 rDNA and *rbcL* showed that the red snow of the ice covers of both lakes (samples LP03 and DL06) was caused by the same species (100% identity between markers of the two populations).

Furthermore, 18S rDNA and *rbcL* sequences were identical to those of *Chlainomonas* sp. in previous reports (GU117574.1, LN897303; Remias *et al.*, 2010, 2016). The 18S rDNA and ITS2 rDNA for *C. nivalis* (DL07) causing red snow on slopes neighbouring Lake Gossenkölle was, with the exception of one nucleotide change at ITS2 rDNA, identical to a field sample found at a location 40 km south-west (GU117577.1, Remias *et al.*, 2010).

Photosynthesis

Chlainomonas sp. from the High Tatras showed an α value of 0.19 ± 0.02 , a relative ETR_{max} of 25.8 ± 2.3 and an I_k value of 144 ± 26 $\mu\text{mol photons m}^{-2} \text{s}^{-1}$ (Fig. 25). *Chlainomonas* sp. from the Tyrolean Alps showed a similar photosynthetic performance (Fig. 25). In both locations, photoinhibition occurred above 1300 $\mu\text{mol photons m}^{-2} \text{s}^{-1}$. The only significant differences were a one-third lower α value (0.12 ± 0.01), a slightly higher ETR_{max} (29.2 ± 0.9), and a two-fold higher I_k value

($291 \pm 65 \mu\text{mol photons m}^{-2} \text{ s}^{-1}$) for the latter population. In contrast, *C. nivalis* showed signs of photoinhibition beginning only at much higher irradiances ($2000 \mu\text{mol photons m}^{-2} \text{ s}^{-1}$); it also showed a lower ETR_{max} (18.6 ± 1.8) and I_k (76.2 ± 6), but a higher α (0.24).

Pigment composition

The reddish colouration of *Chlainomonas* sp. in the High Tatras and the Austrian Alps was caused by secondary (non-plastidal) carotenoids, which comprised 93% and 88.5% of all pigments, respectively. These pigments were identified as derivatives (likely esters) of the keto-carotenoid astaxanthin (Supplementary figs S20, S21). Chlorophyll-*a* and -*b* comprised 5% and 8% of all pigments, primary (plastidal) carotenoids represented 2% and 3.5% in the pigment pool. For astaxanthin, 44.5% (High Tatras) and 31.9% (Alps) occurred as the native 13Z isomer. The overall ratio of astaxanthin to chl-*a* was 26 and 17 to one, respectively. Other pigment contents are given in Supplementary table S4.

Fatty acid composition

The relative contents of FAs (as % of total lipids and as % of the three major lipid groups) in three snow-algal field samples are shown in Table 3. The Slovak and Austrian populations of *Chlainomonas* sp. had very high levels of polyunsaturated fatty acids (PUFAs; 64.4% and 74.2% of total lipids), whereas the content of saturated acids (SAFAs) did not exceed 27% or 21% (mainly palmitic acid, 16:0 and stearic acid, 18:0), respectively. The contribution of mono-unsaturated fatty acids (MUFAs) was low (<10% of total lipids), with oleic acid (18:1 (9Z)) the most abundant. The major PUFAs were α -linolenic acid (18:3 (9Z,12Z,15Z)), followed by stearidonic acid (18:4 (6Z, 9Z,12Z,15Z)) and linoleic acid (18:2 (9Z,12Z)). For comparison, *C. nivalis* had significantly lower levels of PUFAs (50% of total lipids) (Table 3). The content of SAFAs did not exceed 30%, resulting in a two-fold higher contribution of MUFAs (20% of total lipids) in comparison with *Chlainomonas* sp. Apart from oleic acid, vaccenic acid (18:1 (11Z)) was the second most abundant MUFA. The major PUFAs for *C. nivalis* were the same as for *Chlainomonas* sp. Composition of three major lipid groups differed in saturation of their fatty acids: neutral lipids were composed predominantly of saturated lipids, whereas phospholipids and glycolipids were composed predominantly of PUFAs (Table 3). The total lipid contents of the dry biomass were about 10% for both *Chlainomonas* sp. populations and for *C. nivalis* (Table 3). *Chlamydomonas nivalis* differed in the PUFA profile of its

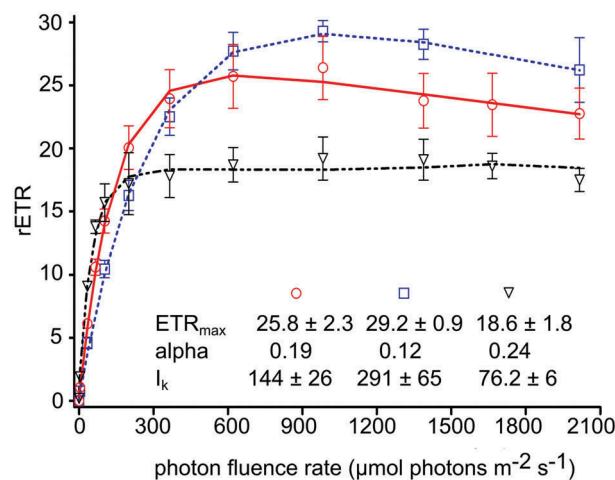


Fig. 25. Comparison of the light-dependent relative electron transport rate (rETR) between two genera causing red snow: *Chlainomonas* sp. swarmers inhabiting ice-covered high alpine lakes (two samples: LP03 (High Tatras) – circles, DL06 (Tyrol Alps) – squares) and *Chlamydomonas nivalis* spores thriving in terrestrial snow habitats (DL07 – triangles). Values of maximum relative electron transfer rate (rETR_{max}), initial slope (α) and saturation irradiance (I_k) for both genera are shown. The data points were fitted with the model of photoinhibition according to Walsby model (1997) assuming photoinhibition. Each symbol represents the mean value of five replicate measurements (\pm SD).

biomembranes (phospholipids and glycolipids) from those of *Chlainomonas* sp. in the nearly 10-fold higher and 3-fold lower contents of vaccenic acid and linoleic acid in *Chlamydomonas nivalis*.

Climatic conditions

The air temperature in close proximity to Ladové Lake and Gossenkölle Lake followed the same pattern over the course of a year (Supplementary fig. S23). The precipitation regime in late spring and early summer differed (Supplementary fig. S24).

Discussion

Taxonomy and related species

Melting ice layers of both high-alpine lakes were populated by the same species. *Chlainomonas* sp. groups among the two other cryoflora species of this genus (see the phylogenetic tree by Remias *et al.*, 2016 in fig. 3). According to their *rbcL* phylogeny, the populations in this study belong to a lineage independent from any other known *Chlainomonas* species (Remias *et al.*, 2016), although their cell size ranges overlap (Supplementary table S3). In order to determine their affiliation, a multigene analysis will be necessary, which is not yet possible because no molecular markers (except *rbcL*) are available for other *Chlainomonas* species. In addition, the sole

Table 3. Snow algal fatty acid composition in % of total lipids (TL) and in % of the three major lipid groups: neutral lipids (NL), phospholipids (PL) and glycolipids (GL).

	<i>Chlainomonas</i> sp. LP03				<i>Chlainomonas</i> sp. DL06				<i>Chlamydomonas nivalis</i> DL07			
	TL	NL	PL	GL	TL	NL	PL	GL	TL	NL	PL	GL
14:0	3.0	5.0	0.9	3.0	1.5	3.9	0.8	0.8	0.7	0.9	0.6	0.5
16:0	19.1	37.8	13.2	7.9	13.3	37.4	4.7	3.5	19.6	53.0	7.8	6.3
16:1 (9Z)	0.7	0.4	0.9	0.9	0.9	0.8	0.9	0.9	1.2	1.5	1.0	0.9
16:1 (11Z)	0.1	0.0	0.4	0.2	0.2	0.2	0.3	0.3	1.3	1.6	1.1	1.0
16:2 (7Z,10Z)	2.0	1.0	2.3	2.3	1.8	0.9	2.1	1.7	1.6	2.0	1.4	1.3
16:3 (4Z, 7Z,10Z)	3.0	2.0	3.4	3.7	3.4	2.0	3.8	4.0	2.1	2.7	1.8	1.6
16:3 (7Z, 10Z, 13Z)	1.4	1.0	2.5	2.2	1.8	1.0	2.7	2.0	0.9	0.4	0.9	1.1
16:4 (4Z, 7Z, 11Z, 13Z)	3.5	2.0	4.2	5.4	4.2	3.0	4.7	4.1	5.6	3.8	6.0	4.7
18:0	4.2	1.0	5.5	6.6	5.7	2.0	10.4	8.5	9.7	2.5	12.1	7.9
18:1 (9Z)	8.1	13.9	3.8	4.9	3.4	6.9	3.8	4.2	9.1	10.1	9.5	9.4
18:1 (11Z)	0.4	1.0	0.7	0.7	0.8	0.6	1.4	1.2	8.3	7.6	11.2	11.8
18:2 (9Z, 12Z)	14.1	12.0	15.1	14.8	11.6	8.9	12.3	14.4	4.3	2.5	4.8	4.7
18:3 (9Z, 12Z, 15Z)	22.2	14.9	26.4	26.7	32.9	18.7	32.2	35.6	26.4	10.1	27.6	32.2
18:4 (6Z, 9Z, 12Z 15Z)	18.2	8.0	20.7	20.7	18.5	13.7	19.9	18.8	9.2	1.3	14.2	16.6
SUFA	26.3	43.8	19.6	17.5	20.5	43.3	15.9	12.8	30.0	56.4	20.5	14.7
MUFA	9.3	15.3	5.8	6.7	5.3	8.5	6.4	6.6	19.9	20.8	22.8	23.1
PUFA	64.4	40.9	74.6	75.8	74.2	48.2	77.7	80.6	50.1	22.8	56.7	62.2

The table shows only fatty acids that have abundances greater than 0.1%. The relative proportion of saturated (SAFA), monounsaturated (MUFA) and polyunsaturated (PUFA) fatty acids is also given.

use of the *rbcL* gene in the phylogeny of *Chloromonadinia* is problematic because unusual gene substitutions, which occur frequently in this group, may result in misleading taxonomic artefacts (Nozaki *et al.*, 2002, 2010). *Chlainomonas* sp. seems to be in close affinity (99% identity at 18S rDNA) to two algae tentatively assigned as ‘*Chloromonas* sp. TA1’ (AB903004.1) and ‘*Chloromonas* sp. TA3’ (AB902981.1), which were isolated from red snow at alpine sites in Japan, at an elevation of 2270 m. However, *Chlainomonas* sp. from Slovakia and Austria represents an independent species from these Japanese snow-algal samples (only 69% similarity at ITS2 rDNA, AB903004.1 and AB902981.1). We refrain from generating a new phylogenetic tree, because for all molecular markers investigated, no new molecular information has become available since the study by Remias *et al.* (2016).

Cytological adaptations to the snow habitat

At both locations, the dominant stages were non-collared ovoid swimmers with four flagella and abundant red pigmentation. Occurrence of swimmers with collar-like papillae (corresponding to the life-cycle stage shown by Novis, 2001, 2002b) would morphologically point to a traditional designation as *Chlainomonas kolii*. However, the proportion of collar-like flagellates in populations is probably a dynamic process (Novis, 2002a). Thus, the taxonomic value of this feature is subject to discussion. Additionally, cell sizes of dark-red oblong biflagellate swimmers corresponded to the morphotype found in populations of both *C. kolii* in New Zealand (Novis, 2002b) and *C. rubra* in North America (Hoham, 1974a). Very probably,

these small oblong biflagellates are daughter cells released from spores after germination, as shown by Hoham (1974a) for *C. kolii*. We hypothesize that the smaller elongate biflagellates represent the vegetative stage, whereas the quadriflagellate swimmers are prolonged planozygotes (as considered by Stein & Brooke, 1964; Hoham, 1974a), which later become spherical and immotile zygotes. The quadriflagellate swimmers of *Chlainomonas* sp. observed here share the arrangement of unequal flagella insertion as described for *C. kolii* (Novis *et al.*, 2008), where the flagellar basal apparatus was organized as two distinct pairs of basal bodies that lack any significant connections. This observation supports the speculation that these stages represent planozygotes originated from a fusion of two biflagellate swimmers. Consequently, the genus *Chlainomonas* might be invalid, in view of the finding that molecular markers place it within the genus *Chloromonas* (Novis *et al.*, 2008), where vegetative swimmers are generally biflagellate. These presumed planozygotes described in this study probably do not have well-developed mechanisms of mechanical resistance or thermostability similar to the mature immotile stages. Thus, their protoplast is quickly damaged after being frozen below 0°C (Hoham, 1975; this study) or when suffering heat stress (Remias *et al.*, 2016; this study). The process of plastid reorganization of *Chloromonas* spp. in the course of their life cycle (Remias *et al.*, 2010; Procházková *et al.*, 2018) seems to be valid also for *Chlainomonas*, as occasionally we found thin-walled swimmers with one or a few larger plastids close to the central part of a cell. The ‘final seasonal stage’ morphotype for *Chlainomonas* sp. had a reticulate surface, which is common for some other members of

Chlamydomonadaceae (VanWinkle-Swift & Rickoll, 1997; Malmberg & VanWinkle-Swift, 2001). The thick-walled mature spores of *Chlainomonas* sp. seem to be adapted to survive harsh conditions, including starvation, mechanical abrasion, freezing and desiccation (Holzinger *et al.*, 2016). Cytokinesis, as reported by Hoham (1974b) and Novis *et al.* (2008), was not noted in this study. As sexual reproduction was not directly observed and attempts to generate a strain were unsuccessful, further details of the life cycle of *Chlainomonas* sp. remain unknown.

Spatial distribution and habitat conditions

The blooms of *Chlainomonas* sp. seem to be an annual phenomenon at Ladové Lake (tentatively identified as '*Chlamydomonas* cf. *nivalis*' by Nedbalová *et al.*, 2006) and at Gossenkölle Lake (Remias *et al.*, 2016) – lakes which share several characteristics of morphometry and limnochemistry (Kamenik *et al.*, 2000; Kopáček *et al.*, 2006). Moreover, both lakes are covered with ice and snow for more than seven months per year (Felip *et al.*, 2002; Šporka *et al.*, 2006), and the ice cover reaches a maximum thickness of 2.5 m (former) or up to one-third of the lake volume (latter). Red snow has never been reported from neighbouring lakes in the same valleys, probably as a result of their geomorphological settings: shallow lakes with rather flat beds usually have less-developed ice cover and associated snow-packs (Šporka *et al.*, 2006). In the two lakes inhabited by *Chlainomonas*, high snow accumulations turn ice covers into complex structures consisting of several ice layers (Sattler *et al.*, 2012). Highly active microbial communities in slush layers of the winter cover (Felip *et al.*, 1999) can be colonizers of the lake water column (Alfreider *et al.*, 1996) and vice versa (Felip *et al.*, 1995). Thus, one may suggest that the *Chlainomonas* population causing red snow on melting lake ice covers is derived from lake slush layers – the algae are released into the water column after complete snowmelt and enter the phytoplankton (Nedbalová *et al.*, 2006). In fact, several large-sized red-pigmented volvocalean cells (tentatively identified as '*Chlamydomonas* sp.', '*Pteromonas*' and '*Chlamydomonas nivalis*') have been found in the slush layers and small pools on the top of the ice cover of Gossenkölle Lake (Felip *et al.*, 2002). In this lake, some of these cell morphotypes most likely represent stages in the life cycle of *Chlainomonas*, as proposed by Novis (2001). Comparison of mean population abundances in lake snow and at the lake shore, the latter being significantly lower (>1000 cells ml^{-1} vs. <50 cells ml^{-1} , Novis, 2002a), support a concept of annual colonization of the lake ice-cover by *Chlainomonas* sp. mainly from the water column

rather than from contributing surface streams. A patchy distribution of *Chlainomonas* sp. along the south-north transect observed in this study (Supplementary fig. S18) corresponds to a considerable spatial variation in population densities within the algal bloom, as also shown for *C. kolii* in New Zealand (Novis, 2002a). A population from the Austrian Alps reached, in the course of our study, comparable densities to previous years (Remias *et al.*, 2016). However, this population was sparse in comparison with the four-fold higher abundances at Ladové Lake, which can be attributed partly to the collection later in the season. Generally *Chlainomonas* sp. was found in slush or nearly completely melted snow on the lake ice cover, but it has also been reported from a glacier in Austria (Remias *et al.*, 2016). In a similar way, *C. kolii* caused snow discolouration in a slush layer (SWC 69%) over snow with a lower density (SWC 46%) (Hardy & Curl, 1968). In our field samples, no cells in the process of division were found. Despite very rare observations of sporangia reported for *C. kolii* (Novis, 2002a), population densities can show significant passive increases, associated partly or even solely with ablation of snow (Novis, 2002a), which can explain the absence of any correlation between the SWC and population densities in this study. Taking these possibilities into account, we assume that cell division and gamete mating are most likely already taking place in the slush layers prior to their exposure to the surface. This generally corresponds to the finding that sexual stages of *Chloromonas* snow algae occur if the SWC is lower (39–50%, L Procházková, unpublished observation; 47–54% observed by Hoham & Duval, 2001).

Morphologically similar algae and their habitat preferences

Three species or subspecies of red snow-causing algae are known from the High Tatras, namely *Chlamydomonas nivalis* (Kol, 1975a, 1975b), *Chloromonas nivalis* subsp. *tatrae* (Kol) Procházková, Remias, Nedbalová & Řezanka (Procházková *et al.*, 2018), and *Chlamydomonas sanguinea* Lagerheim (Kol, 1969). According to Remias *et al.* (2016) this last, poorly morphologically described, species looks very similar to *Chlainomonas* sp. *Chlamydomonas sanguinea* occurred on the Slovak side (Kol, 1975a, 1975b) and probably also on the Polish side of the High Tatras (misidentified as *Chlamydomonas nivalis*; Kawecka, 1981). In the Tyrolean Alps, the first report of *Chlainomonas* was from the small glacier Gamezkogelferner, not far from Gossenkölle Lake (Ettl, 1968), and corresponded to scattered cells found in the course of this study in snow (Supplementary fig. S13). The original description of

Chlainomonas rubra included cells with striking spikes on the wall surface (Stein & Brooke, 1964). The second *Chlainomonas* species living in snow, *C. kolii*, differs from *C. rubra* in the presence of swarmers with a collar-like papilla with an outer, ephemeral cell wall consisting of mosaic plates. Similar to our observation of the habitat preference for *Chlainomonas* sp. in Europe, remarkable blooms of the related *C. kolii* were recorded in the snow of the ice covers of an alpine lake on Mt Philistine and on Canyon Lake, New Zealand (Novis, 2002a, 2002b; Novis *et al.*, 2008), and *C. rubra* in the similar habitats of Squaw Lake and Upper Lena Lake, United States of America (Novis *et al.*, 2008). Therefore, a worldwide distribution of the genus *Chlainomonas* in snowpacks associated with high-alpine lacustrine ecosystems seems to be more common than previously thought. In addition, *C. rubra* is known from snowpacks above the timberline on the volcanic Mt Ruapehu in New Zealand (Hardy, 1966), and from the Vitosha Mountains in Bulgaria (fig. 39 in Lukavský *et al.*, 2009). According to other North American reports, *C. rubra* and *C. kolii* were found beneath or adjacent to coniferous canopies (Stein & Brooke, 1964; Hardy & Curl, 1968; Hoham, 1974a, 1974b).

Photosynthesis

The photosynthetic rates of *Chlainomonas* sp. from both sites were consistent in their relationship to irradiance and in suffering photoinhibition at very high light intensities, from 1300 $\mu\text{mol photons m}^{-2} \text{s}^{-1}$ upwards, which are common at open, high-alpine sites. *Chlainomonas* sp. (DL06) appears to tolerate higher light intensities, where it shows very high photosynthetic performance. Under low light, photosynthesis is less efficient; however, both show similar kinetics. In contrast, the ‘terrestrial’ snow alga *C. nivalis* behaves differently, showing high photophysiological plasticity: high photosynthetic efficiency under low light, but less photoinhibition under high light. As indicated by the I_k , *Chlainomonas* sp. from the High Tatras needs only half the level of irradiance compared with the Tyrolean population to become saturated. This can be explained by the pronounced temperature stress and associated irradiance stress experienced later in the season for the population sampled at Ladové Lake (Supplementary figs S25, S26), in comparison to the population sampled earlier at Gossenkölle Lake. An increased accumulation of *Chlainomonas* sp. at the snow surface is expected as a consequence of rain events (Novis, 2002a), which are more frequent in the High Tatras (Niedzwiedz, 1992). The pronounced topographic shading of Ladové Lake may also contribute to the observed photophysiological differences (Supplementary figs S27, S28; Novikmec *et al.*, 2013), although maximum irradiance

levels during the day can reach comparable levels of 2500 $\mu\text{mol photons m}^{-2} \text{s}^{-1}$ (Sommaruga & Psenner, 1997; Procházková *et al.*, 2018).

Pigments

The high levels of astaxanthin causing the red colouration of *Chlainomonas* sp. are comparable to mature *C. nivalis* obtained from alpine (Bidigare *et al.*, 1993; Remias *et al.*, 2005) and polar regions (Müller *et al.*, 1998). The higher astaxanthin: chlorophyll ratios for the High Tatras population than for the earlier-sampled Austrian Alps population may be a result of the ongoing season, presuming that astaxanthin accumulation is continuous until complete snowmelt due to an active metabolism; alternatively, the amount of chlorophyll could have decreased. This corresponds to a three-fold increase in α -tocopherol (this study), a major antioxidant of the chloroplasts. Similar α -tocopherol to chl-*a* ratios were observed in the ‘red phase’ of two algal strains isolated from Arctic snow and kept in conditions of low nitrogen and high irradiation (CCCY006-99 and 101-99/R2; Leya *et al.*, 2009). Increased accumulation of α -tocopherol during spore maturation was reported for field samples of *C. nivalis* from the Alps (Remias *et al.*, 2010) and in the stationary-growth phase of strains in a screening study by Mudimu *et al.* (2017). The harsher environmental conditions later in the season are in good agreement with the doubled amount of 13Z astaxanthin, which provides advanced protection from UV in relation to all-*trans*-astaxanthin (Supplementary fig. S22). Notably, astaxanthin as a bio-indicator was found in the entire profile of a sediment core (32 cm) taken from the deepest point of Gossenkölle Lake, representing the last 800 years (Kamenik *et al.*, 2000). This may be associated not only with zooplankton grazing on algae containing astaxanthin (Tartarotti *et al.*, 2017), but also with the presence of *Chlainomonas* sp. over time in the lake.

Fatty acid composition

Snow-algal strains are reported as suitable candidates for biotechnological applications (Hulatt *et al.*, 2017). In this study, *Chlainomonas* sp. had a high proportion of PUFAs in the total FA pool. High levels of PUFAs is quite common for aplanozygotes of snow-inhabiting members of the *Chloromonas* clade (Řezanka *et al.*, 2008, 2014). α -Linolenic acid has been found as the dominant unsaturated FA of *Chlainomonas* sp. in other snow algae in this clade (Procházková *et al.*, 2018). On the other hand, stearidonic and linoleic acids were twice as abundant as is typical for all 22 *Chloromonas* species (mean 7.6%

and 6.4%, respectively) screened by Lang *et al.* (2011). Surprisingly, the FA profile of *Chlamydomonas nivalis* from the Austrian Alps was more similar to *Chlainomonas* sp. (e.g. in the dominance of α -linolenic acid) than to arctic field samples associated with the *Chlamydomonas nivalis* clade (oleic acid dominated >45% in sample 9/10 1b of Spijkerman *et al.*, 2012). This suggests that the stage of spore maturation and differences in abiotic habitat parameters connected with latitude (e.g. irradiance, nutrients, water availability) may play a role in FA profiles in species belonging to the same phylogenetic clade (see fig. 4 in Leya *et al.*, 2004). The culture maturation stage was also critical for the FA composition in Zygnematophycean green algae, where upon pre-akinetete formation two unsaturated FAs in particular (oleic acid and linoleic acid) increased drastically (Pichrtová *et al.*, 2016).

In summary, *Chlainomonas* sp. regularly causes red snow on lake-ice cover in the High Tatras and the Austrian Alps, as reported earlier by Remias *et al.* (2016). The differences in ecophysiology and morphology between these two populations illustrate well the influence of harsher conditions, prolonged time for spore maturation and population development during the later part of the growing season. The environmental conditions of the two high-alpine habitats seem to be similar. Several cell morphotypes corresponding to life-cycle stages (biflagellates, flagellates with collar-like papillae, quadriflagellates, mature spores) were found and quadriflagellate swarms were suggested to be prolonged planozygotes. We hypothesize a route of lake-surface colonization by an inoculum originating from sediments, which first incubates in several slush layers prior to the appearance of the visible red colouration at the lake surface. Population patchiness along the spatial transect on the lake-ice cover was shown, no cell division was found, and the SWC varied from slush to nearly completely melted snow. Mating and cell divisions are thus presumed to take place in deeper slush layers and earlier in the season, where the SWC is most likely lower. Both *Chlainomonas* sp. and *C. nivalis* exhibited similar photosynthetic rates during high irradiance, suggesting that these snow algae are well adapted to live in open sites, although they have shown differences in their sensitivity to temperature and in the ultrastructural organization of plastids in mature spores (Remias *et al.*, 2016). Both genera share low levels of primary pigments and a high contribution of non-polar astaxanthin esters. *Chlamydomonas nivalis* had a much lower PUFA content, partly due to the younger spore stages found during the sampling.

Remaining uncertainties about the life cycle of *Chlainomonas* sp. could be resolved by establishing a strain, which likely requires culturable, vegetative states occurring in deep slush layers early in the season. Polyphasic research at other, similar localities (alpine lakes, flat glaciers) with red-snow blooms is needed to assess the cosmopolitan distribution of this species, the morphology of dispersal cells, and the route(s) of colonization of distant locations. Analysis of multiple molecular markers of the other *Chlainomonas* cryoflora taxa would help to determine the exact taxonomic position of each species within the clade.

Acknowledgements

We are grateful to Juliet Brodie and two anonymous reviewers for their critical comments which helped us to improve the manuscript. We thank Janet Reid for the language correction of the paper. We are grateful to Klaus Herburger for his advice on ETR measurements and evaluating the results, and to Siegfried Aigner for assistance with HPLC analysis (both at the University of Innsbruck, Institute of Botany, Austria; K. H. present address: Institute of Molecular Plant Sciences, The University of Edinburgh, UK). We express our sincere thanks to Birgit Sattler (University of Innsbruck, Institute of Ecology, Austria) for providing access to the limnological field station at Kühtai, and to the Stredisko lavínovej prevencie Horskej záchranej služby (Liptovský Hrádok, Slovakia) for providing meteorological data from Ladové Lake. We wish to thank Tomáš Hájek and David Kaftan for their technical support (University of South Bohemia in České Budějovice, Czech Republic) and to Miroslav Hyliš for his logistical assistance (Charles University in Prague, Czech Republic).

Disclosure statement

No potential conflict of interest was reported by the authors.

Funding

This study was supported by the Austrian Science Fund (FWF) grant P 29959-B29 to D. R. and the Czech Science Foundation (GACR) project 17-00027S to T. Ř. The study was further supported by the Austrian Science Fund (FWF) grants P 24242-B16 and I 1951-B16 to A. H.

Supplemental information

The following supplementary material is accessible via the Supplementary Content tab on the article's online page at <https://doi.org/10.1080/09670262.2018.1426789>

Supplementary text. Climatic conditions

Supplementary table S1. List of primers used for amplification of 18S rDNA, ITS1 rDNA, ITS2 rDNA (ITS) and *rbcL* markers.

Supplementary table S2. List of taxa and GenBank accession numbers of nuclear-encoded 18S ribosomal DNA

(rDNA) genes, nuclear rDNA internal transcribed spacer 1 (ITS1) and spacer 2 (ITS2) regions, and the large subunit of RuBisCO (*rbcl*) genes.

Supplementary table S3. List of *Chlainomonas* species causing red snow.

Supplementary table S4. Relative content of pigments and α -tocopherol in ratios to chlorophyll-*a* (=1) in field samples of *Chlainomonas* sp. from the High Tatras (sample LP03) and the Austrian Alps (sample DL06), determined by HPLC.

Supplementary figs S1–S4. Overview of the sampling site of the snow alga *Chlainomonas* sp. at Gossenkölle Lake (Tyrolean Alps, Austria).

Supplementary figs S5–S12. LM micrographs of *Chlainomonas* sp. showing cells from the snow on the ice cover of Gossenkölle Lake after harvest and after several months in lab conditions.

Supplementary fig. S13. A swarmer related to *Chlainomonas rubra* found in red snowfields nearby to Gossenkölle lake.

Supplementary figs S14–S17. TEM and SEM micrographs of *Chlainomonas* sp. from the snow on the ice cover of Gossenkölle Lake.

Supplementary figs S18, S19. Spatial distribution of *Chlainomonas* sp. population and snow water content on the southern-northern transect on the ice cover of Gossenkölle Lake.

Supplementary figs S20, S21. HPL-chromatogram of *Chlainomonas* sp. at 480 nm.

Supplementary fig. S22. Spectral absorbance of all-*trans*-astaxanthin and of the isomer 13Z astaxanthin.

Supplementary figs S23, S24. Prevailing climatic conditions close to habitats of *Chlainomonas* sp.

Supplementary figs S25, S26. Daily mean air temperature in period when the bloom of *Chlainomonas* sp. is expected (May and June 2016) at ice covers of Ladové Lake and Gossenkölle Lake.

Supplementary figs S27, S28. Daily course of photosynthetically active radiation (PAR) in a few contrasting days during May–June.

Supplementary fig. S29. Daily course of PAR (photosynthetic active radiation; $\mu\text{mol photons m}^{-2} \text{s}^{-1}$) during May–June 2016 in the proximity of Gossenkölle Lake.

Author contributions

L. Procházková: original concept, field sampling, molecular laboratory work, PAM measurements, LM, SEM and TEM microscopy, drafting and writing the manuscript; D. Remias: original concept, field sampling, LM microscopy, pigment analysis, drafting, editing the manuscript and financial support; A. Holzinger: editing the manuscript and financial support; T. Řezanka: fatty acid analysis, editing the manuscript and financial support; L. Nedbalová: original concept, editing the manuscript and financial support.

ORCID

Lenka Procházková  <http://orcid.org/0000-0003-3995-6483>

Andreas Holzinger  <http://orcid.org/0000-0002-7745-3978>

Tomáš Řezanka  <http://orcid.org/0000-0002-8704-9645>

References

- Alfreider, A., Pernthaler, J., Amann, R., Sattler, B., Wille, A. & Psenner, R. (1996). Community analysis of the bacterial assemblages in the winter cover and pelagic layers of a high mountain lake by *in situ* hybridization. *Applied and Environmental Microbiology*, **62**: 2138–2144.
- Bigdare, R.R., Ondrusek, M.E., Kennicutt II, M.C., Iturriaga, R., Harvey, H.R., Hoham, R.W. & Macko, S. A. (1993). Evidence for a photoprotective function for secondary carotenoids of snow algae. *Journal of Phycology*, **29**: 427–434.
- Bligh, E.G. & Dyer, W.J. (1959). A rapid method of total lipid extraction and purification. *Canadian Journal of Biochemistry and Physiology*, **37**: 911–917.
- Brown, S.P., Ungerer, M.C. & Jumpponen, A. (2016). A community of clones: snow algae are diverse communities of spatially structured clones. *International Journal of Plant Sciences*, **177**: 432–439.
- Christen, H.R. (1959). Flagellaten aus dem Schützenweiher bei Veltheim. *Mitteilungen der Naturwissenschaftlichen Gesellschaft Winterthur*, **29**: 167–189.
- De Maayer, P., Anderson, D., Cary, C. & Cowan, D.A. (2014). Some like it cold: understanding the survival strategies of psychrophiles. *EMBO Reports*, **15**: 508–517.
- Dembitsky, V.M., Řezanka, T., Bychek, I.A. & Shustov, M. V. (1991). Identification of fatty acids from *Cladonia* lichens. *Phytochemistry*, **30**: 4015–4018.
- Ettl, H. (1968). Ein Beitrag zur Kenntnis der Algenflora Tirols. *Berichte des Naturwissenschaftlich-Medizinischen Vereins in Innsbruck*, **56**: 177–354.
- Felip, M., Camarero, L. & Catalan, J. (1999). Temporal changes of microbial assemblages in the ice and snow cover of a high mountain lake. *Limnology and Oceanography*, **44**: 973–987.
- Felip, M., Sattler, B., Psenner, R., & Catalan, J. (1995). Highly active microbial communities in the ice and snow cover of high mountain lakes. *Applied and Environmental Microbiology*, **61**: 2394–2401
- Felip, M., Wille, A., Sattler, B. & Psenner, R. (2002). Microbial communities in the winter cover and the water column of an alpine lake: system connectivity and uncoupling. *Aquatic Microbial Ecology*, **29**: 123–134.
- Hardy, J.T. (1966). Identification, culture, and physiological ecology of cryophilic algae. Oregon State University, Corvallis. M.S. thesis.
- Hardy, J.T. & Curl, H.J. (1968). Red snow caused by a new species of *Trachelomonas*. *Journal of Phycology*, **4**: 9–12.
- Hoham, R.W. (1974a). *Chlainomonas kolii* (Hardy et Curl) comb. nov. (Chlorophyta, Volvocales), a revision of the snow alga, *Trachelomonas kolii* Hardy et Curl (Euglenophyta, Euglenales). *Journal of Phycology*, **10**: 392–396.
- Hoham, R.W. (1974b). New findings in the life history of the snow alga, *Chlainomonas rubra* (Stein et Brooke) comb. nov. (Chlorophyta, Volvocales). *Syesis*, **7**: 239–247.
- Hoham, R.W. (1975). Optimum temperatures and temperatures ranges for growth of snow algae. *Arctic and Alpine Research*, **7**: 13–24.
- Hoham, R.W. & Duval, B. (2001). Microbial ecology of snow and freshwater ice with emphasis on snow algae. In *Snow Ecology: An Interdisciplinary Examination of Snow-Covered Ecosystems* (Jones, H.G., Pomeroy, J.W., Walker, D.A. & Hoham, R.W., editors), 168–228. Cambridge University Press.

- Holzinger, A., Allen, M.C. & Deheyn, D.D. (2016). Hyperspectral imaging of snow algae and green algae from aeroterrestrial habitats. *Journal of Photochemistry and Photobiology B: Biology*, **162**: 412–420.
- Hulatt, C.J., Berecz, O., Egeland, E.S., Wijffels, R.H. & Kiron, V. (2017). Polar snow algae as a valuable source of lipids? *Bioresource Technology*, **235**: 338–347.
- Kamenik, C., Koinig, K.A., Schmidt, R., Appleby, P.G., Dearing, J.A., & Psenner, R. (2000). Eight hundred years of environmental changes in a high alpine lake (gossenköllesee, tyrol) inferred from sediment records. *Journal of Limnology*, **59** (Suppl. 1): 43–52.
- Kawecka, B. (1981). *Biology and ecology of snow algae*. 2. Formation of aplanospores in *Chlamydomonas nivalis* (Bauer) Wille (Chlorophyta, Volvocales). *Acta Hydrobiologica*, **23**: 211–215.
- Kol, E. (1969). *Chlamydomonas sanguinea* Lagerh. in the High Tatra. *Annales Historico-Naturales Musei Nationalis Hungarici*, **61**: 111–115.
- Kol, E. (1975a). Cryobiological researches in the High Tatra I. *Acta Botanica Academiae Scientiarum Hungaricae*, **21**: 61–75.
- Kol, E. (1975b). Cryobiological researches in the High Tatra II. *Acta Botanica Academiae Scientiarum Hungaricae*, **21**: 279–287.
- Kol, E. (1968). *Kryobiologie. Biologie und Limnologie des Schnees und Eises*. I. *Kryovegetation* (Elster, P. & Ohle, W., editors). *Die Binnengewässer, Band XXIV*. Schweizerbart'sche Verlagsbuchhandlung, Stuttgart.
- Kopáček, J., Stuchlík, E. & Hardekopf, D. (2006). Chemical composition of the Tatra Mountain lakes: recovery from acidification. *Biologia*, **61**: S21–S33.
- Lang, I., Hodac, L., Friedl, T. & Feussner, I. (2011). Fatty acid profiles and their distribution patterns in microalgae: a comprehensive analysis of more than 2000 strains from the SAG culture collection. *BMC Plant Biology*, **11**: 124.
- Leya, T., Müller, T., Ling, H.U. & Fuhr, G.R. (2004). Snow algae from North-Western Spitsbergen (Svalbard). In *The coastal ecosystem of Kongsfjorden, Svalbard: Synopsis of biological research performed at the Koldewey Station in the years 1991–2003 (Berichte zur Polar- und Meeresforschung 492)* (Wiencke, C., editor), 46–54. Bremerhaven.
- Leya, T., Rahn, A., Lütz, C. & Remias, D. (2009). Response of arctic snow and permafrost algae to high light and nitrogen stress by changes in pigment composition and applied aspects for biotechnology. *FEMS Microbiology Ecology*, **67**: 432–443.
- Lukavský, J., Furnadzhieva, S. & Nedbalová, L. (2009). First record of cryoseston in the Vitosha Mountains, Bulgaria. *Nova Hedwigia*, **88**: 97–110.
- Lutz, S., Anesio, A.M., Field, K. & Benning, L.G. (2015). Integrated “Omics”, targeted metabolite and single-cell analyses of arctic snow algae functionality and adaptability. *Frontiers in Microbiology*, **6**: 1–17.
- Malmberg, A.E. & VanWinkle-Swift, K.P. (2001). Zygospore germination in *Chlamydomonas monoica* (Chlorophyta): timing and pattern of secondary zygospore wall degradation in relation to cytoplasmic events. *Journal of Phycology*, **37**: 86–94.
- Matsuzaki, R., Kawai-Toyooka, H., Hara, Y. & Nozaki, H. (2015). Revisiting the taxonomic significance of aplanozygote morphologies of two cosmopolitan snow species of the genus *Chloromonas* (Volvocales, Chlorophyceae). *Phycologia*, **54**: 491–502.
- Mudimu, P., Koopmann, I. K., Rybalka, N., Friedl, T., Schulz, R. & Bilger, W. (2017). Screening of microalgae and cyanobacteria strains for α -tocopherol content at different growth phases and the influence of nitrate reduction on α -tocopherol production. *Journal of Applied Phycology*, **29**: 2867–2875.
- Müller, T., Bleiß, W., Rogaschewski, C.-D.M.S. & Fuhr, G. (1998). Snow algae from northwest Svalbard: their identification, distribution, pigment and nutrient content. *Polar Biology*, **20**: 14–32.
- Nedbalová, L., Stuchlík, E. & Strunecký, O. (2006). Phytoplankton of a mountain lake (Ladové pleso, the Tatra Mountains, Slovakia): seasonal development and first indications of a response to decreased acid deposition. *Biologia*, **61**: S91–S100.
- Niedzwiedz, T. (1992). Climate of the Tatra Mountains. *Mountain Research and Development*, **12**: 131–146.
- Novikmec, M., Svitok, M., Kočický, D., Šporka, F. & Bitušík, P. (2013). Surface water temperature and ice cover of Tatra Mountains lakes depend on altitude, topographic shading, and bathymetry. *Arctic, Antarctic, and Alpine Research*, **45**: 77–87.
- Novis, P.M. (2001). Ecology and taxonomy of alpine algae, Mt Philistine, Arthur's Pass National Park, New Zealand. University of Canterbury, Christchurch, New Zealand. PhD thesis.
- Novis, P.M. (2002a). Ecology of the snow alga *Chlamydomonas kolii* (Chlamydomonadales, Chlorophyta) in New Zealand. *Phycologia*, **41**: 280–292.
- Novis, P.M. (2002b). New records of snow algae for New Zealand, from Mt Philistine, Arthur's Pass National Park. *New Zealand Journal of Botany*, **40**: 297–312.
- Novis, P.M., Hoham, R.W., Beer, T. & Dawson, M. (2008). Two snow species of the quadriflagellate green alga *Chlamydomonas* (Chlorophyta, Volvocales): ultrastructure and phylogenetic position within the *Chloromonas* clade. *Journal of Phycology*, **44**: 1001–1012.
- Nozaki, H., Nakada, T. & Watanabe, S. (2010). Evolutionary origin of *Gloeomonas* (Volvocales, Chlorophyceae), based on ultrastructure of chloroplasts and molecular phylogeny. *Journal of Phycology*, **46**: 195–201.
- Nozaki, H., Onishi, K. & Morita, E. (2002). Differences in pyrenoid morphology are correlated with differences in the *rbcl* genes of members of the *Chloromonas* lineage (Volvocales, Chlorophyceae). *Journal of Molecular Evolution*, **55**: 414–430.
- Pichrtová, M., Arc, E., Stöggel, W., Kranner, I., Hájek, T., Hackl, H. & Holzinger, A. (2016). Formation of lipid bodies and changes in fatty acid composition upon pre-akinete formation in Arctic and Antarctic *Zygnema* (Zygnematophyceae, Streptophyta) strains. *FEMS Microbiology Ecology*, **92**: fiw096.
- Procházková, L., Remias, D., Řezanka, T. & Nedbalová, L. (2018). *Chloromonas nivalis* subsp. *tatrae*, subsp. nov. (Chlamydomonadales, Chlorophyta): re-examination of a snow alga from the High Tatra Mountains (Slovakia). *Fottea*, **18**: 1–18.
- Remias, D., Karsten, U., Lütz, C. & Leya, T. (2010). Physiological and morphological processes in the alpine snow alga *Chloromonas nivalis* (Chlorophyceae) during cyst formation. *Protoplasma*, **243**: 73–86.
- Remias, D. & Lütz, C. (2007). Characterisation of esterified secondary carotenoids and of their isomers in green algae: a HPLC approach. *Algological Studies*, **124**: 85–94.
- Remias, D., Lütz-Meindl, U. & Lütz, C. (2005). Photosynthesis, pigments and ultrastructure of the

- alpine snow alga *Chlamydomonas nivalis*. *European Journal of Phycology*, **40**: 259–268.
- Remias, D., Pichrtová, M., Pangratz, M., Lütz, C. & Holzinger, A. (2016). Ecophysiology, secondary pigments and ultrastructure of *Chlamydomonas* sp. (Chlorophyta) from the European Alps compared with *Chlamydomonas nivalis* forming red snow. *FEMS Microbiology Ecology*, **92**: fiw030.
- Řezanka, T. (1990). Identification of very long polyenoic acids as picolinyl esters by Ag^+ ion-exchange high-performance liquid chromatography, reversed-phase high-performance liquid chromatography and gas chromatography—mass spectrometry. *Journal of Chromatography A*, **513**: 344–348.
- Řezanka, T., Nedbalová, L., Procházková, L. & Sigler, K. (2014). Lipidomic profiling of snow algae by ESI-MS and silver-LC/APCI-MS. *Phytochemistry*, **100**: 34–42.
- Řezanka, T., Nedbalová, L. & Sigler, K. (2008). Unusual medium-chain polyunsaturated fatty acids from the snow alga *Chloromonas brevispina*. *Microbiological Research*, **163**: 373–379.
- Sattler, B., Post, B., Remias, D., Lutz, C., Lettner, H. & Psenner, R. (2012). Cold Alpine regions. In *Life at Extremes. Environments, Organisms, and Strategies for Survival* (Bell, E. editor), 138–154. CABI, Wallingford.
- Saunders, R. D. & Horrocks, L. A. (1984). Simultaneous extraction and preparation for high-performance liquid chromatography of prostaglandins and phospholipids. *Analytical Biochemistry*, **143**: 71–75.
- Sommaruga, R. & Psenner, R. (1997). Ultraviolet radiation in a high mountain lake of the Austrian Alps: air and underwater measurements. *Photochemistry and Photobiology*, **65**: 957–963.
- Spijkerman, E., Wacker, A., Weithoff, G. & Leya, T. (2012). Elemental and fatty acid composition of snow algae in Arctic habitats. *Frontiers in Microbiology*, **3**: 1–15.
- Šporka, F., Livingstone, D.M., Stuchlík, E., Turek, J. & Galas, J. (2006). Water temperatures and ice cover in lakes of the Tatra Mountains. *Biologia*, **61**: S77–S90.
- Stein, J.R. & Brooke, R.C. (1964). Red snow from Mt. Seymour, British Columbia. *Canadian Journal of Botany*, **42**: 1183–1188.
- Tartarotti, B., Trattner, F., Remias, D., Saul, N., Steinberg, C.E.W. & Sommaruga, R. (2017). Distribution and UV protection strategies of zooplankton in clear and glacier-fed alpine lakes. *Scientific Reports*, **7**: 4487. doi: [10.1038/s41598-017-04836-w](https://doi.org/10.1038/s41598-017-04836-w).
- VanWinkle-Swift, K.P. & Rickoll, W.L. (1997). The zygospore wall of *Chlamydomonas monoica* (Chlorophyceae): morphogenesis and evidence for the presence of sporopollenin. *Journal of Phycology*, **33**: 655–665.
- Walsby, A.E. (1997). Modelling the daily integral of photosynthesis by phytoplankton: its dependence on the mean depth of the population. *Hydrobiologia*, **349**: 65–74.

Supplemental information

Climatic conditions

The values for the High Tatras originated from an automatic weather station located on the shore of the Ladové Lake: global radiation (GR, in 2001, unpublished data), precipitation (in 2001, Křeček *et al.*, 2006), air temperature data (in 2016, provided by Stredisko lavínovej prevencie Horskej záchranej služby, Slovakia). Air temperature, irradiance, and precipitation data for the Tyrolean Alps during 2016 were kindly provided by the company Tiwag, Innsbruck (weather station close to Längentaler Stausee, N 47.207149 E 11.005895, 1914 m above sea level). Since this station is located in the same valley as Gossenkölle Lake but at an altitude 500 m lower, monthly mean air temperatures measured at the meteorological station were extrapolated taking the dry adiabatic vertical temperature gradient into account (-0.65°C per increase of 100 m) to estimate air temperature at the elevation of the lake.

Photosynthetically active radiation (PAR, in units of $\mu\text{mol photons m}^{-2} \text{ s}^{-1}$) was calculated from GR (in units of W m^{-2}): multiplied by 50% for the fraction of light in global radiation (output in $\text{J m}^{-2} \text{ s}^{-1}$) and then multiplied by 4.6 (conversion factor for joule to micromole). *In situ* PAR for Gossenkölle Lake (May 28–30, 2017) was monitored using a data logger with built-in sensors and equipped with radiation shields (Minikin QT, EMS Brno, Czech Republic), which was installed on the rock surface close to the lake ice cover.

Supplemental tables

Supplementary Table S1. List of primers used for amplification of 18S rDNA, ITS1 rDNA, ITS2 rDNA (ITS) and *rbcL* markers; F – forward; R – reverse.

Primer	Marker	Direction	Sequence	Reference
P2	18S	F	CTGGTTGATTCTGCCAGT	Gargas & DePriest (1996)
P4	18S	R	TGATCCTTCYGCAGGTTAC	Moon-van der Staay <i>et al.</i> (2000)
TW81	ITS	F	GGGATCCGTTTCCGTAGGTGAACCTGC	Goff <i>et al.</i> (1994)
AB28	ITS	R	GGGATCCATATGCTTAAGTTCAGCGGGT	Goff <i>et al.</i> (1994)
AL1500af	ITS	F	GCGCGCTACACTGATGC	Helms <i>et al.</i> (2001)
LR3	ITS	R	GGTCCGTGTTTCAAGACGG	Vilgalys & Hester (1990)
ITS5	ITS	F	GGAAGTAAAAGTCGTAACAAGG	White <i>et al.</i> (1990)
ITS4	ITS	R	TCCTCCGCTTATTGATATGC	White <i>et al.</i> (1990)
<i>rbcL</i> 1F	<i>rbcL</i>	F	GCTGGTGTTAAAGATTATCG	Hoham <i>et al.</i> (2002)
<i>rbcL</i> 7R	<i>rbcL</i>	R	AAATAAATACCACGGCTACG	Hoham <i>et al.</i> (2002)

Supplementary Table S2. List of taxa and GenBank accession numbers of nuclear-encoded 18S ribosomal DNA (rDNA) genes, nuclear rDNA internal transcribed spacer 1 (ITS1) and spacer 2 (ITS2) regions, and the large subunit of RuBisCO (*rbcL*) genes.

Taxon	Specimen	Accession number			
		18S rDNA	ITS1 rDNA	ITS2 rDNA	<i>rbcL</i>
<i>Chlainomonas</i> sp.	LP03	MF803745	MF803746	MF803746	MF803747
<i>Chlainomonas</i> sp.	DL06	MF803743	MF803743	MF803743	MF803744
<i>Chlamydomonas nivalis</i>	DL07	MF803748		MF803749	

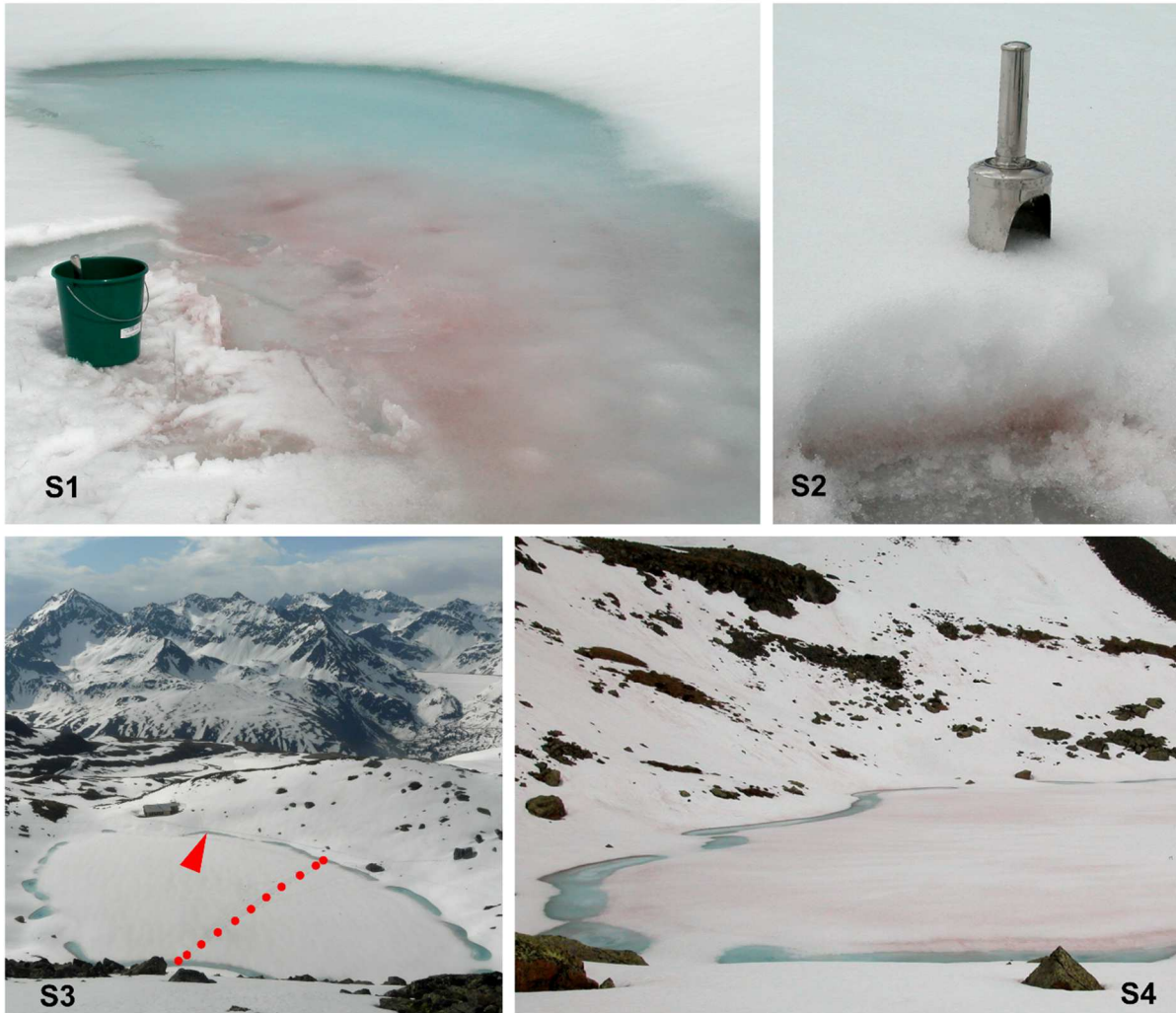
Supplementary Table S3. List of *Chlainomonas* species causing red snow: cell sizes of different life cycle stages in μm ; flagel. = flagellates.

Taxon	Location	life cycle stages					Reference
		uncollar quadriflagel.	collar quadriflagel.	biflagel.	immotile stages	mature spores	
<i>Chlainomonas</i> sp.	Eadové Lake	24–65 \times 24–59	19.1 \times 19	19.4 \times 8.8	65 (85) \times 59 (83)		this study
<i>Chlainomonas</i> sp.	Gossenkölle Lake	20.4–46 \times 19–45.7	23–28 \times 19.5–25.4		46 \times 45.7	20–40	this study
<i>Chlainomonas rubra</i>	Austria	42–55 \times 34–50(70)					Ettl (1968)
<i>Chlainomonas rubra</i>	North America	23–42(60) \times 30–55(90)		17–25 \times 6–10		30–63 \times 25–48	Hoham (1974a, 1974b)
<i>Chlainomonas kolii</i>	New Zealand		(15)20–30 \times (10)15–22	18 \times 10			Novis (2002a)
<i>Chlainomonas kolii</i>	North America		28–38 \times 14–22			13–16 \times 14–19	Hardy & Curl (1968), Hoham (1974a)

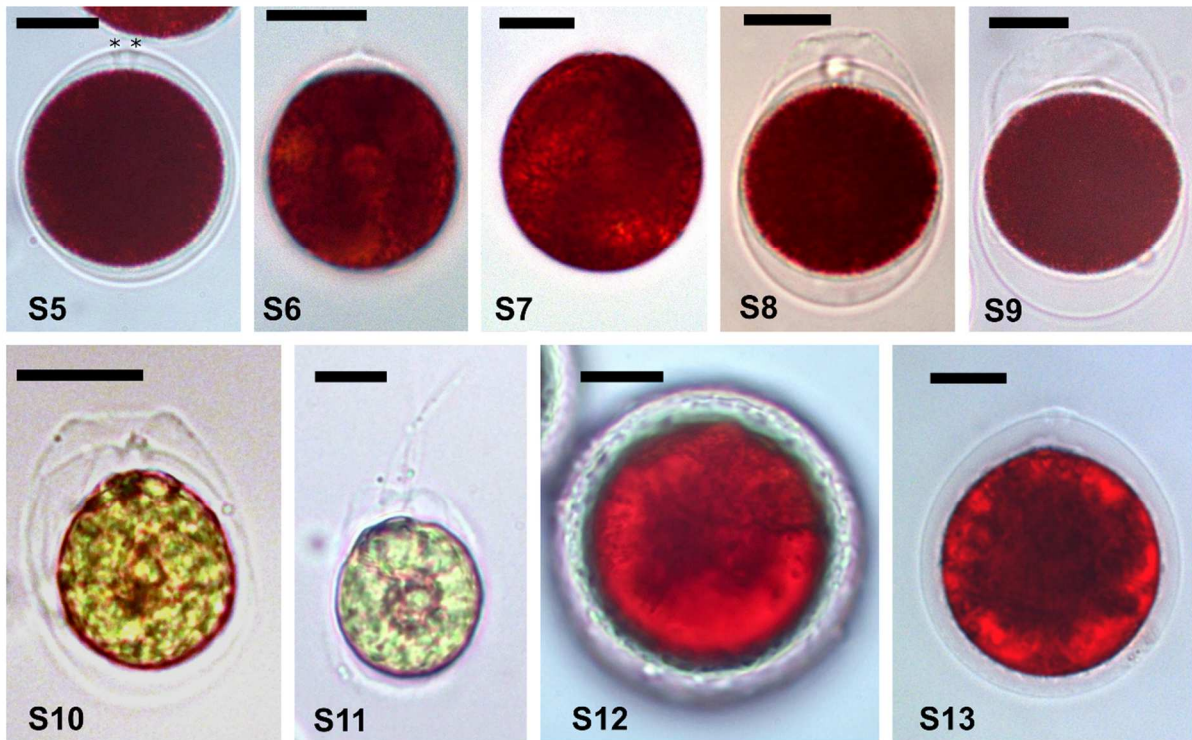
Supplementary Table S4. Relative content of pigments and α -tocopherol in ratios to chlorophyll a (=1) in field samples of *Chlainomonas* sp. from the High Tatras (sample LP03) and the Austrian Alps (sample DL06), determined by HPLC. Note that in LP03 the de-epoxydised xanthophyll-cycle pigment *zea* is present, and it has also a higher content of α -tocopherol. The total amount of astaxanthin (*ast-tot* and *asI-tot* thereof) is 26.178 to 17.594 in favour to LP03. Abbreviations: *neo*, neoxanthin; *vio*, violaxanthin; *ant*, antheraxanthin; *lut*, lutein; *zea*, zeaxanthin; *ech*, echinenone; *chl b*, chlorophyll b; *ast-tot* = astaxanthin all-*trans* plus astaxanthin esters; *asi-tot*, total amount of astaxanthin *cis*-isomers (mainly 13Z); α -toc, α -tocopherol; n.d., not detected.

	Neo	Vio	Ant	Lut	Zea	Ech	Chl <i>b</i>	Ast-tot	AsI-tot	α -toc
LP03	0.05	0.177	0.00	0.252	0.026	0.00	0.444	14.531	11.648	0.397
DL06	0.053	0.018	0.00	0.359	n. d.	0.00	0.583	11.981	5.613	0.122

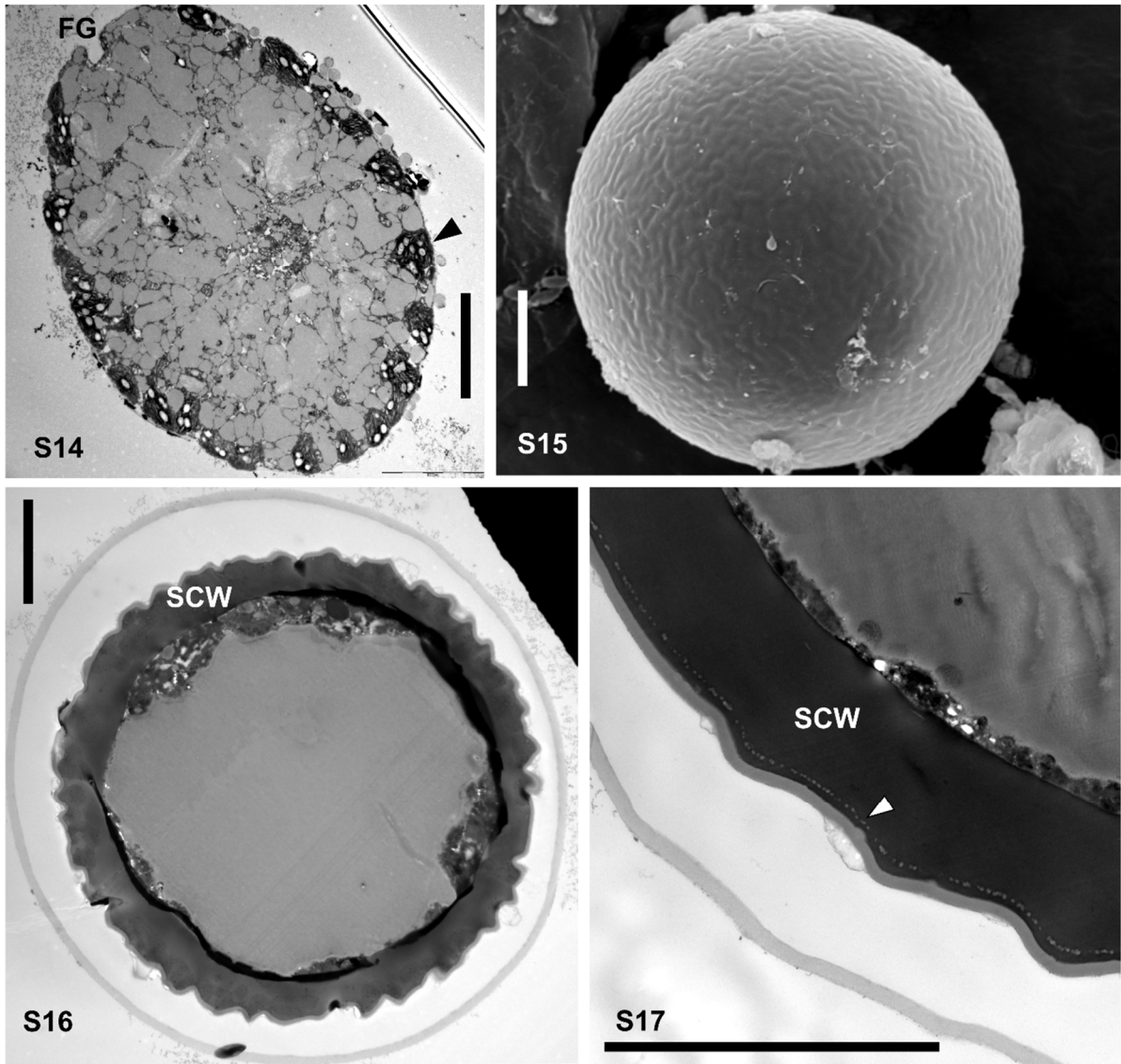
Supplemental figures



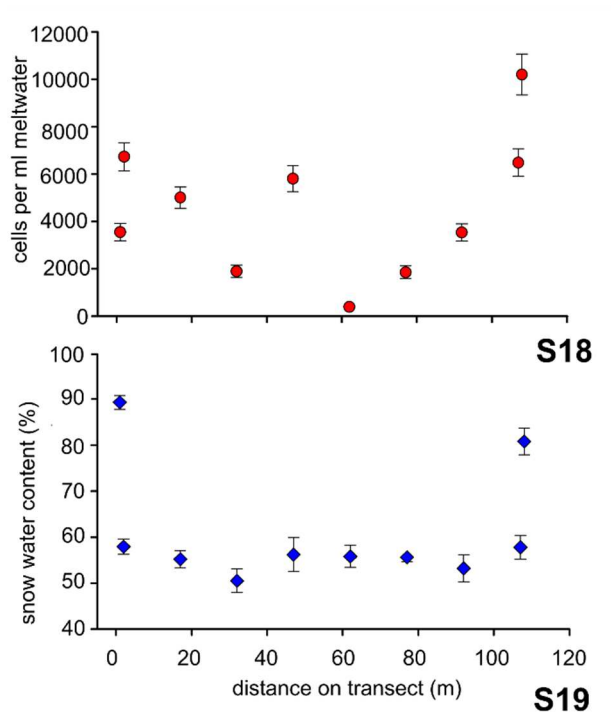
Supplementary Figs S1–S4. Overview of the sampling site of the snow alga *Chlainomonas* sp. at Gossenkölle Lake (Tyrolean Alps, Austria). **Fig. S1.** During harvest, the snow colouration was visible only close to the lake margin, where melting of the underlying ice was advanced (late May 2016), detail view of red snow after harvest (sample DL06). **Fig. S2.** The majority of the lake surface was still covered by white snow and red horizontal patches of snow were hidden several cm below the snow surface, close to the interface with the ice cover. **Fig. S3.** Population densities and snow water contents were investigated in a 109 m long southern-northern transect on the ice cover of the lake. The main sampling location (DL06) was close to the southern shore (red arrowhead). **Fig. S4.** Red spots appeared one week later across the entire lake snow surface, most likely due to ongoing melting processes (early June 2016).



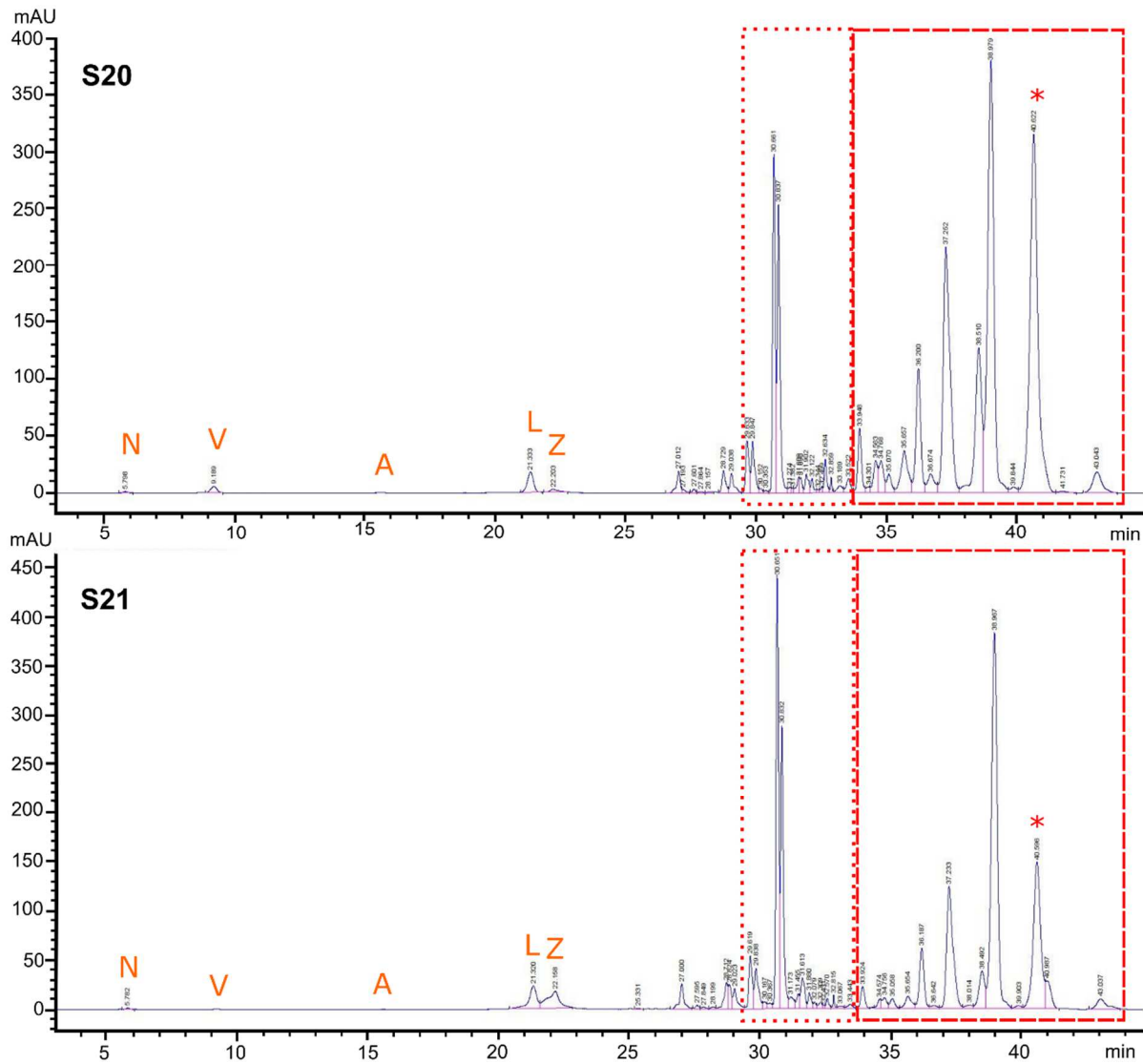
Supplementary Figs S5–S12. LM micrographs of *Chlainomonas* sp. showing cells from the snow on the ice cover of Gossenkölle Lake after harvest (Figs S5–S9, living cells; Figs S10–S11, fixed material with acid Lugol’s solution) and after several months at lab conditions (Fig. S12). **Figs S5–S11.** Morphological variability of swarmers. **Fig. S5.** Most abundant swarmers possessed papilla and pseudo-papilla (presumably a zygote), two pairs of flagella grooves of a swarmer marked with asterisk. **Figs S6, S7.** Swarmers with equally thin cell wall and more or less apparent papilla. **Figs S8–S11.** Flagellates with collar papilla. **Fig. S9.** A cell in a process of losing the collar. **Fig. S12.** Mature spores with thick secondary cell wall. **Fig. S13.** A swarmer related to *Chlainomonas rubra* found in red snowfields nearby to Gossenkölle Lake. Note the secondary cell wall equally distant from protoplast and small projections of the inner cell wall. Scale bar = 10 μ m.



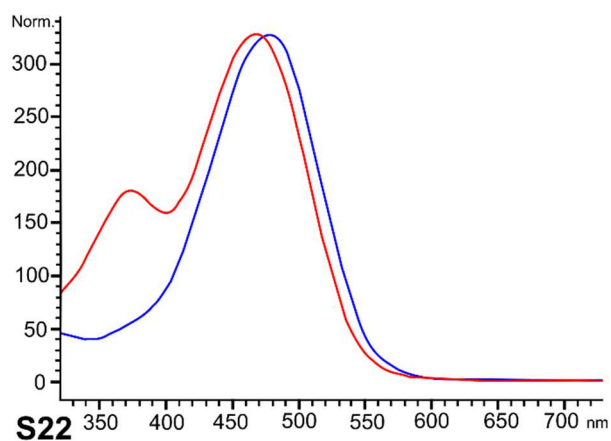
Supplementary Figs S14–S17. TEM and SEM micrographs of *Chlainomonas* sp. from the snow on the ice cover of Gossenkölle Lake. **Fig. S14.** Swarmer with equally thin cell wall, parietal plastids (black arrow) and flagellar groove (FG). **Figs S15–S17.** Mature spore after several months at lab conditions, note undulating fine surface structures (corresponding to Fig. S12). Section of a trilaminar sheath (white arrow) and fully developed secondary cell wall (SCW), surrounded by extracellular matrix. Scale bar = 5 μm .



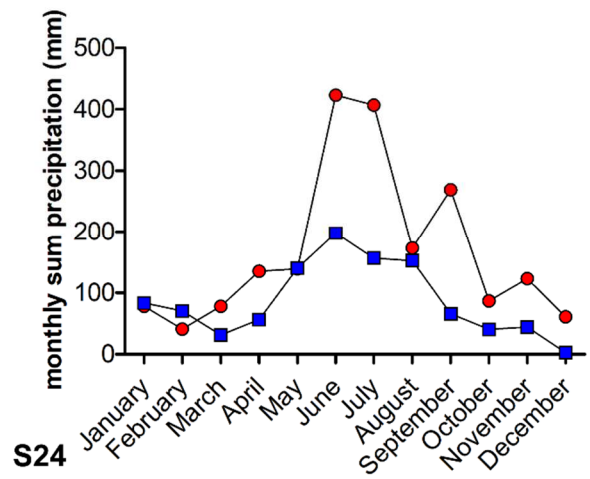
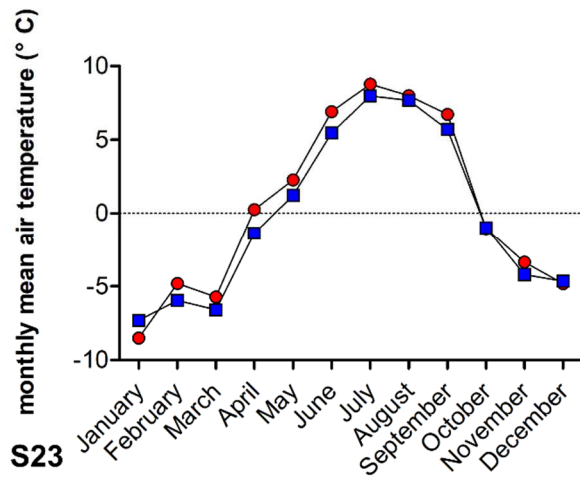
Supplementary Figs S18, S19. Spatial distribution of *Chlainomonas* sp. population (red circles) and snow water content (SWC, blue boxes) on the southern-northern transect on the ice cover of Gossenkölle Lake. Each point of population density and SWC represents the mean of two and three measurements, respectively. Standard deviation is indicated.



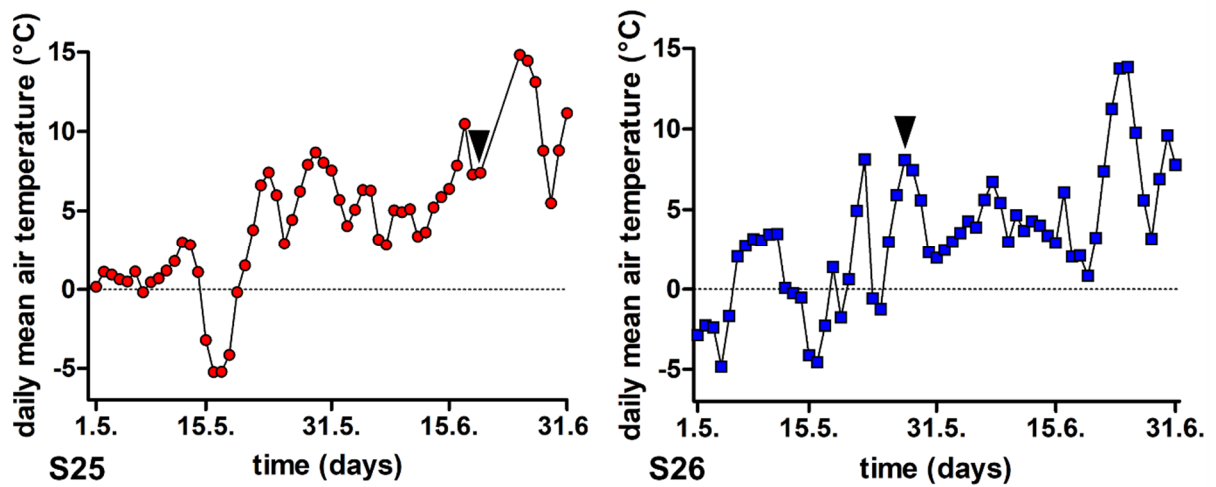
Supplementary Figs S20, S21. HPL-chromatogram of *Chlainomonas* sp. at 480 nm. **Fig. S20.** Sample harvested in the High Tatras. **Fig. S21.** Sample harvested in the Tyrol Alps. Two groups of peaks are indicated: Astaxanthin-monoesters (red dotted line), astaxanthin-diester (red dashed line). Abbreviations: N, neoxanthin; V, violaxanthin; A, antheraxanthin; L, lutein; Z, zeaxanthin; 13Z isomers astaxanthin indicated by asterisk.



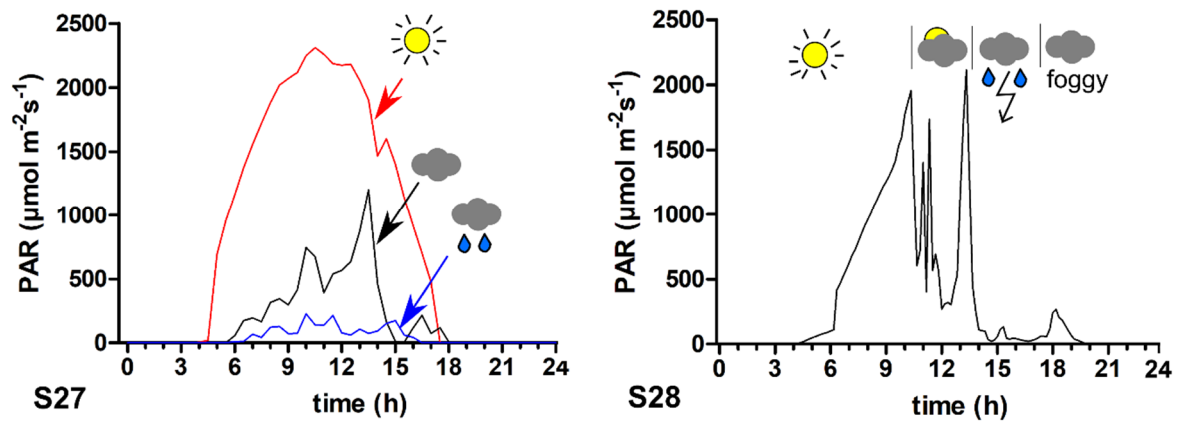
Supplementary Fig. S22. Spectral absorbance of all-*trans*-astaxanthin (blue line, maximum around 478 nm) and of the isomer 13Z astaxanthin with a similar maximum absorbance but providing additional UV protection (red line, shoulder at 371 nm). Peaks with these spectra were found in both *Chlainomonas* sp. samples.



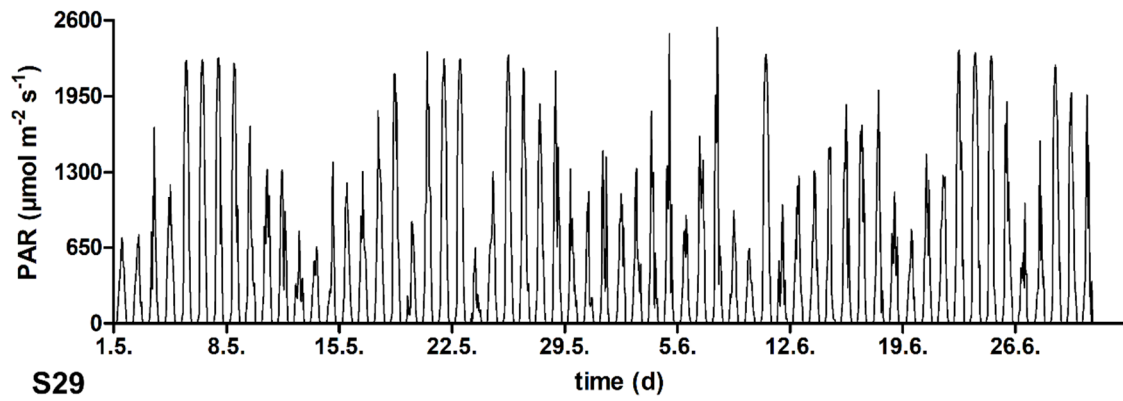
Supplementary Figs S23, S24. Prevailing climatic conditions close to habitats of *Chlainomonas* sp. (L'adové Lake – circles, Gossenkölle Lake – boxes). **Fig. S23.** Monthly sum of precipitation (mm). **Fig. S24.** Monthly mean air temperature (°C).



Supplementary Figs S25, S26. Daily mean air temperature in period when the bloom of *Chlainomonas* sp. is expected (May and June 2016) at ice covers of Ladové Lake (red circles) and Gossenkölle Lake (blue squares). Black arrows indicate the date of red snow harvest in course of this study. Despite comparable prevailing air temperatures at both dates of sampling, there was a much longer period of time since the last freezing events at Ladové Lake (one month) in comparison to Gossenkölle Lake (two days), thus indicating an advanced snowmelt and associated higher exposure of cells to the irradiance on the snow surface in the former.



Supplementary Figs S27, S28. Daily course of photosynthetically active radiation (PAR) in a few contrasting days during May-June. **Fig. S27.** At Ladové Lake: sunny (red line, 23. 5. 2001), cloudy (black line, 1. 6. 2001) and rainy day (blue line, 19. 6. 2001). **Fig. S28.** Changeable weather conditions during one day *in situ* at Gossenkölle Lake (30. 5. 2017) from sunny to cloudy, rainy and then foggy. Note the difference in timing of sunset at both lakes in studied period caused partly by actual weather conditions and partly by different topographic shading: Ladové Lake is surrounded by mountain peaks except on the south and south-southwest and thus it receives less direct solar input. In contrast, Gossenkölle Lake is surrounded by mountain peaks only to the north, and is less affected by more-distant peaks to the northwest, which means that sunshine at this location continues until the late evening.



Supplementary Fig. S29. Daily course of PAR (photosynthetic active radiation; $\mu\text{mol photons m}^{-2} \text{s}^{-1}$) during May-June 2016 in the proximity to Gossenkölle Lake.

ADDITIONAL REFERENCES

- Gargas, A. & DePriest, P. T. (1996). A nomenclature for fungal PCR primers with examples from intron-containing SSU rDNA. *Mycologia*, **88**(5): 745–748.
- Goff, L.J., Moon, D.A. & Coleman, A.W. (1994). Molecular delineation of species and species relationships in the red algal agarophytes *Gracillariopsis* and *Gracilaria* (Gracilariales). *Journal of Phycology*, **30**: 521–537.
- Helms, G., Friedl, T., Rambold, G. & Mayerhofer, H. (2001). Identification of photobionts from the lichen family Physciaceae using algal-specific ITS rDNA sequences. *Lichenologist*, **33**: 73–86.
- Hoham, R.W., Bonome, T.A., Martin, C.W. & Leebens-Mach, J.H. (2002). A combined 18S rDNA and *rbcL* phylogenetic analysis of *Chloromonas* and *Chlamydomonas* (Chlorophyceae, Volvocales) emphasizing snow and other cold-temperature habitats. *Journal of Phycology*, **38**: 1051–1064.
- Křeček, J., Turek, J., Ljungren, E., Stuchlík, E. & Šporka, F. (2006). Hydrological processes in small catchments of mountain headwater lakes: The Tatra Mountains. *Biologia*, **61**: S1–S10. <https://doi.org/10.2478/s11756-006-0115-8>
- Moon-van der Staay, S.Y., van der Staay, G.W.M., Guillou, L. & Vaultot, D. (2000). Abundance and diversity of prymnesiophytes in the picoplankton community from the equatorial Pacific Ocean inferred from 18 rDNA sequences. *Limnology and Oceanography*, **45**(1): 98–109.
- Vilgalys, R. & Hester, M. (1990). Rapid genetic identification and mapping of enzymatically amplified ribosomal DANN from several *Cryptococcus* species. *Journal of Bacteriology*, **175**: 4238–4246.
- White, T.J., Bruns, T., Lee, S.J.W.T. & Taylor, J.W. (1990). Amplification and direct sequencing of fungal ribosomal RNA genes for phylogenetics. *PCR protocols: a guide*

to methods and applications, **18(1)**: 315–322.

Paper III

**Ecophysiology of *Chloromonas hindakii*, sp. nov. (Chlorophyceae),
causing orange snow blooms at different light conditions**

Procházková L¹, Remias D², Řezanka T³ & Nedbalová L¹

Microorganisms 7(10): 434, 2019

¹ *Department of Ecology, Faculty of Science, Charles University, Viničná 7, 12844 Prague,
Czech Republic*

² *School of Engineering, University of Applied Sciences Upper Austria, Stelzhamerstr. 23, 4600
Wels, Austria*

³ *The Czech Academy of Sciences, Institute of Microbiology, Vídeňská 1083, 142 20 Prague,
Czech Republic*



Article

Ecophysiology of *Chloromonas hindakii* sp. nov. (Chlorophyceae), Causing Orange Snow Blooms at Different Light Conditions

Lenka Procházková ^{1,*} , Daniel Remias ² , Tomáš Řezanka ³ and Linda Nedbalová ¹ ¹ Department of Ecology, Faculty of Science, Charles University, Viničná 7, 12844 Prague, Czech Republic² School of Engineering, University of Applied Sciences Upper Austria, Stelzhamerstr. 23, 4600 Wels, Austria³ The Czech Academy of Sciences, Institute of Microbiology, Vídeňská 1083, 142 20 Prague, Czech Republic

* Correspondence: lenkacerven@gmail.com; Tel.: +420-221-95-1809

Received: 20 August 2019; Accepted: 2 October 2019; Published: 10 October 2019



Abstract: Slowly melting snowfields in mountain and polar regions are habitats of snow algae. Orange blooms were sampled in three European mountain ranges. The cysts within the blooms morphologically resembled those of *Chloromonas nivalis* (Chlorophyceae). Molecular and morphological traits of field and cultured material showed that they represent a new species, *Chloromonas hindakii* sp. nov. The performance of photosystem II was evaluated by fluorometry. For the first time for a snow alga, cyst stages collected in a wide altitudinal gradient and the laboratory strain were compared. The results showed that cysts were well adapted to medium and high irradiance. Cysts from high light conditions became photoinhibited at three times higher irradiances ($600 \mu\text{mol photons m}^{-2} \text{s}^{-1}$) than those from low light conditions, or likewise compared to cultured flagellates. Therefore, the physiologic light preferences reflected the conditions in the original habitat. A high content of polyunsaturated fatty acids (about 60% of total lipids) and the accumulation of the carotenoid astaxanthin was observed. They are regarded as adaptations to cope with extreme environmental conditions of snow that include low temperatures, freeze-thaw cycles, and variable light intensity. The intraspecific ability of adaptation of the photosynthetic apparatus to different irradiance regimes seems to be advantageous for thriving in different snow habitats.

Keywords: cryoflora; photosynthesis; cysts; environmental sample; astaxanthin; fatty acids

1. Introduction

For microalgae, snow and ice surfaces are habitats characterized by a multitude of abiotic stresses, including low nutrients, diurnal freeze-thaw cycles, high UV and photosynthetically active radiation (PAR) at the surface, and an overall short growing season. In these ecosystems, diverse algal communities develop distinct snow discolorations and exhibit individual cellular metabolic profiles [1]. The organisms responsible for such a phenomenon mainly belong to green algae [2,3]. Prominent genera thriving in snow are *Chloromonas* [4] and *Sanguina* (formerly assigned to *Chlamydomonas*) [5].

These microalgae are essential primary producers in such an extreme ecosystem (e.g., [6]), where phototrophic life is restricted to a few specialized organisms. For instance, they provide a basic ecosystem, e.g., for snow bacteria [7], fungi [8], and ciliated protozoa [9]. Snow algae microbial communities play an important role in snow food webs and supply nutrients that are delivered throughout the ecosystem (e.g., supraglacial and periglacial environments) [10].

Insight in complex feedbacks between snow and climate were recently done by [11]. Snow in the mid-latitudes appears to be most sensitive to climate change [12], and mid-latitude areas below 1200 m a.s.l. are assumed to suffer complete snow loss by the end of 21st century [13]. Therefore,

snow microbial communities of mid-latitude mountains urgently deserve focused research before their habitats are gone forever.

Organisms living in melting snow have to be well adapted. A key factor for photoautotrophic life is the plasticity of the photosynthetic apparatus, necessary for balancing energy consumption and conversion [14], because light conditions in snow are very variable from surface to deeper layers [15]. At the beginning of the season, cells are deep in the snowpack, thus subject to absence of light. Due to the combination of ongoing melting and upwards migration of flagellates, they become exposed in surface layers to higher light conditions [16]. Thus, constant adjustment of the photosynthetic apparatus is required spatially and temporally in the course of a few weeks. Additionally, snowfields can be quite different in regard of light conditions depending on being shaded, partly shaded under canopy, or permanently exposed at sites without trees. This led to the earlier conclusion that red snow, which is usually fully exposed, comprises species with high light tolerance, whereas green snow, which is usually found at shaded places, is taxonomically different and does not tolerate excessive irradiation [17].

Rapid light curves, acquired either via oxygen turnover or by fluorometry of the plastidal electron transport rates, demonstrate the adaptation of snow algal photosystems (i.e., to low temperatures). This was performed with monospecific blooms like *Chloromonas* (*C.*) *nivalis* [18], *C. polyptera* [19], *C. nivalis* subsp. *tatrae* [20], *Chloromonas brevispina* [21], *Scotiella cryophila* [22], and *Sanguina nivaloides* (formerly classified as “*Chlamydomonas nivalis*”) [23]. However, these studies used only field samples collected at a certain locality, and to our knowledge, there were no efforts yet to compare either the autecological photophysiology of a single species collected from different mountain ranges, or differently exposed sites in terms of PAR. The first ecophysiological comparison of cryoflora populations from two mountain ranges was done in the case of *Chlamydomonas* sp. [16]. However, data on flagellated stages based on laboratory strains or field samples were not available. Thus, the range of light adaptation remained unknown; also the differences between two life cycle stages of typical snow algae in the order Chlamydomonadales (flagellates vs. immotile cysts) were never determined before.

C. nivalis (Chodat) Hoham et Mullet was regarded as a cosmopolitan species living in polar and mid-latitude mountainous regions. The taxon was usually identified solely based on the morphology of fusiform cysts bearing elongated cell wall flanges, which usually dominate field blooms. However, molecular studies showed that it comprises multiple taxa, which were recently independently described, e.g., *C. muramotoi* [4].

The cysts used in this study that cause orange snow in mid-latitude mountains in central Europe resembled those of *C. nivalis* as well, but were revealed to be a new taxon of its own by analyses of multiple DNA marker regions. It is described here as *C. hindakii* Procházková & Remias sp. nov., based on molecular and morphologic characteristics of vegetative flagellates and immotile cysts. The aim was not only to describe morphology and ecology, but also to compare the two main life cycle stages in terms of photobiology and fatty acids profiles. Since we were able to find blooms of this species at habitats with quite different conditions of irradiance, we were able to test the hypothesis that populations from high light conditions get photoinhibited at higher irradiances than those from low light conditions. Finally, the carotenoid composition of the reddish cysts was investigated. To sum up, the results of this study are a showcase, helping to understand the geographical distribution, taxonomy, habitat preferences, and intraspecific physiological variability of a new species of snow alga in the snow melting period.

2. Materials and Methods

2.1. Sampling and Snow Characteristics

Orange colored spots of snow were investigated in May and June in the years 2017–2019 in the High Tatra (Slovakia, Poland), Krkonoše, and Jeseníky Mountains (the Czech Republic) (Figure 1, Table 1, Figure S1).

For sampling, the selection of virtually monospecific spots was done with a field microscope according to [5]. Orange snow was harvested with a sterile shovel, placed in 5 l buckets, 1 l thermos bottles, or 50 mL centrifugation tubes, and transported the same day to the laboratory. Prior to photosynthesis measurements, samples were melted gently at darkness overnight at 4–5 °C. Electrical conductivity (EC) and pH of the meltwater were obtained with WTW Instruments (Cond 340i and Inolab, Germany) or with HANNA (Combo EC, ftb Romania). Snow water equivalent (SWE; referred to as ‘snow water content’ in the following reference) was carried out as described previously [20].

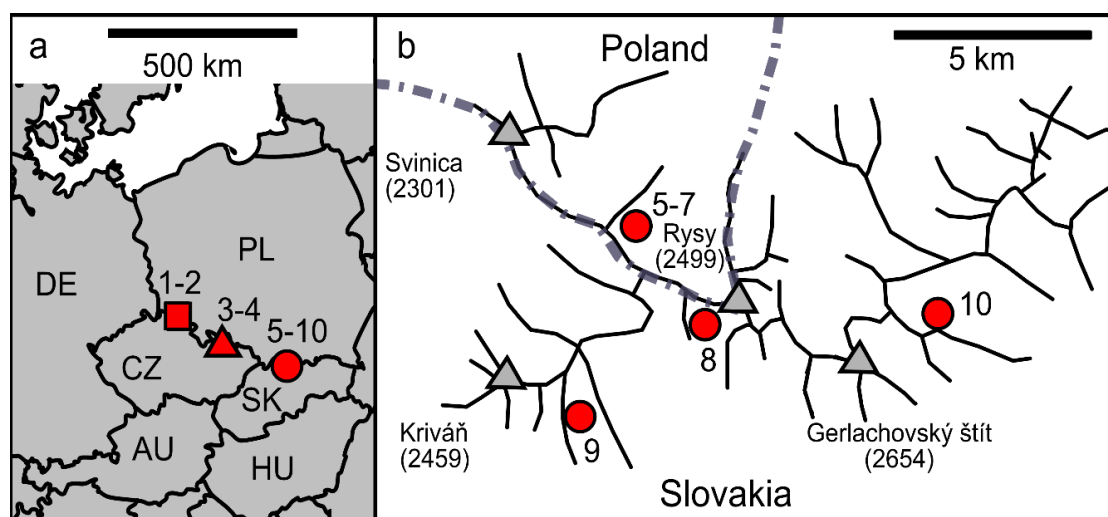


Figure 1. Sampling locations of *Chloromonas hindakii* sp. nov. in (a) Krkonoše, Czech Republic (square), Jeseníky, Czech Republic (triangle), and at the High Tatras, Slovakia and Poland (circle), with codes of the European countries (AU, Austria; CZ, Czech Republic; DE, Germany; HU, Hungary; PL, Poland; SK, Slovakia); (b) Detailed map of the High Tatras, showing principal peaks with their elevation in meters (triangles).

Table 1. Sampling locations of *Chloromonas hindakii* sp. nov. from Krkonoše, Jeseníky, and High (H.) Tatra Mountains with sample codes, collection date, sampling site, altitude (m a.s.l.) and geographic position (GPS) (CZ, Czech Republic; PL, Poland; SK, Slovakia). The numbers in parentheses indicate position in the map of Figure 1 (L., Lake).

Sample	Date	Location	Altitude	GPS
DD2	11.5.2017	CZ (1), Krkonoše, Dlouhý důl	984	N50°43.231 E15°39.433
Rozcestí	12.5.2017	CZ (2), Krkonoše, close to Na Rozcestí	1349	N50°42.327 E15°40.368
Jes19-1	8.5.2019	CZ (3), Jeseníky, close to U Výrovky	1137	N50°06.673 E17°10.967
Jes19-6	9.5.2019	CZ (4), Jeseníky, next to Sněžná kotlina	1157	N50°08.121 E17°08.817
LP06	14.6.2017	PL (5), H. Tatras, Dolina za Mnichem	1858	N49°11.656 E20°03.146
WP129	15.6.2017	PL (6), H. Tatras, Dolina za Mnichem	2082	N49°11.424 E20°03.153
WP130	15.6.2017	PL (7), H. Tatras, ice-covered Zadni Mnichow L.	2038	N49°11.403 E20°03.101
WP136	15.6.2017	SK (8), H. Tatras, Mengusovská dolina	1976	N49°10.475 E20°04.910
NW	18.6.2017	SK (9), H. Tatras, shore of Nižné Wahlenberg.L.	2061	N49°9.543 E20°1.612
WP194	17.6.2018	SK (10), H. Tatras, Velká Studená dolina	2022	N49°10.540 E20°09.414

2.2. Strain Isolation

For obtaining a unialgal strain of *C. hindakii* sp. nov., a subsample of WP129 (containing only sedimented cysts, no flagellates observed) with visible orange coloration was put into sterile 2 mL cryotubes and the meltwater replaced with deionized water. For induction of germination of the cysts, the cells were kept at 1 °C during the day (14 h) resp. −1 °C during the night (10 h) in a Percival LT-36VL (CLF Plant Climatics, Wertingen, Germany). The light intensity generated by fluorescent tubes was approximately 40–70 $\mu\text{mol PAR m}^{-2} \text{s}^{-1}$. After several weeks, many cysts developed daughter

cells (Figure S2), and subsequently, green flagellates were present in the supernatant; 10 µL aliquots of the latter were transferred into liquid 0.6 N Bold's Basal Medium (BBM) [24] and irradiation was dimmed to 20–30 µmol PAR m⁻² s⁻¹. In the next step, the culture was used for genetics, microscopy, fluorometry, and lipid analysis. This strain was deposited as CCCryo 531-19 at the Culture Collection of Cryophilic Algae in Germany.

2.3. Light and Electron Microscopy

Light microscopy (LM) was performed with an Olympus BX43 at 1000× magnification using oil immersion, equipped with Nomarski Contrast and an Olympus DP27 camera or digital camera DXM 1200F (Nikon, Melville, NY, USA), using cellSens Entry Imaging Software. Scanning and transmission electron microscopy (SEM and TEM) were carried out as described previously [20].

2.4. Isolation of DNA, PCR, Sequencing

DNA isolation was carried out with a DNeasy Plant Mini Kit (Qiagen, Germany), as in [20]. If less than 20 mg wet biomass was available, DNA was extracted using the Instagene Matrix Kit (Bio-Rad Laboratories, Hercules, CA, USA) according to [25]. The 18S small subunit ribosomal RNA gene (18S rDNA), internal transcribed spacer region 2 (ITS2 rDNA), and ribulose-1,5-bisphosphate carboxylase/oxygenase large subunit (*rbcL*) marker regions were amplified from DNA isolates by polymerase chain reaction (PCR) using existing primers (Table 2). Amplification reactions were described in [20]. PCR products were purified and sequenced using an Applied Biosystems automated sequencer (ABI 3730xl) at Macrogen Europe (Amsterdam, Netherlands). The obtained sequences of *C. hindakii* sp. nov. were submitted to NCBI Nucleotide sequence database (accession numbers at Table 3).

Table 2. List of primers used for amplification of 18S rDNA, ITS1 rDNA, ITS2 rDNA (ITS), and *rbcL* markers (F, forward; R, reverse).

Primer	Marker	Direction	Sequence	Reference
SSU	ITS2	F	CTGCGGAAGGATCATTGATTC	[26]
LSU	ITS2	R	AGTTCAGCGGGTGGTCTTG	[26]
ITS5	ITS2	F	GGAAGTAAAAGTCGTAACAAGG	[27]
ITS1	ITS2	F	TCCGTAGGTGAACCTGCCG	[27]
ITS4	ITS2	R	TCCTCCGCTTATTGATATGC	[27]
Al1500af	ITS2	F	GCGCGCTACACTGATGC	[28]
LR3	ITS2	R	GGTCCGTGTTTCAAGACGG	[29]
18F2	18S	F	AACCTGGTTGATCCTGCCAGT	[30]
18R2	18S	R	TGATCCTTCTGCAGGTTACCTACG	[30]
<i>rbcL</i> 1F	<i>rbcL</i>	F	CTGCTTTATACTGCGAAACTGC	[31]
<i>rbcL</i> 7R	<i>rbcL</i>	R	AAATAAATACCACGGCTACG	[31]

Table 3. List of marker sequences for the authentic strain of *Chloromonas hindakii* and field samples, indicating the Genbank accession numbers for ITS2 rDNA/18S rDNA/*rbcL* sequences.

Sample/Strain Code	NCBI Accession Numbers		
	ITS2 rDNA	18S rDNA	<i>rbcL</i>
WP129 (= CCCryo 531-19)	MN251865	MN251865	MN251877
DD2	MN251866	MN251874	MN251878
Rozcestí	MN251867	MN251875	MN251879
Jes19-1	MN251868		
Jes19-6	MN251869	MN251876	
LP06	MN251870		
WP136	MN251871		
NW	MN251872		MN251880
WP194	MN251873		MN251881

2.5. ITS2 rRNA Secondary Structure Prediction and Phylogenetic Analysis

The methods of annotation and prediction of the secondary structure of the nuclear rDNA ITS2 region were the same as in [20]. The secondary structure of nuclear rDNA ITS2 of *C. hindakii* sp. nov. was drawn using VARNA version 3.9 [32]. The 18S rDNA alignment contained 40 sequences (1567 bp) examined in previous studies [4,22], as well as three specimens of field-collected cysts and *C. hindakii* strain WP129 (= CCCryo 531-19); the *rbcL* matrix consisted of 37 sequences (924 bp), as well as four specimens of field-collected cysts and *C. hindakii* strain WP129 (= CCCryo 531-19); the mesophilic species of the genus *Chloromonas sensu* [33] or the *Chloromonadinia* clade [34] were selected as the outgroup. The best-fit nucleotide substitution model was estimated by jModeltest 2.0.1 [35]. Based on the Akaike Information Criterion, the GTR+I+G model was selected for 18rDNA. Three partitions were set for *rbcL* gene sequences and the following substitution models were applied: TIM1+I+G (first codon position), K80+I (second codon position), and GTR+I+G (third codon position). The 18S rDNA and *rbcL* phylogenetic trees were inferred by Bayesian inference (BI) and maximum likelihood (ML) according to [36], with the minor modification that Markov Chain Monte Carlo runs were carried out for three million generations in BI. Convergence of the two cold chains was checked by the average standard deviation of split frequencies (0.000533 and 0.00105 for 18S rDNA and *rbcL* dataset, respectively). Bootstrap analyses and Bayesian posterior probabilities were performed as described by [36].

2.6. Photosynthesis

In vivo chlorophyll fluorescence parameters were obtained with a pulse–amplitude modulated fluorometer (PAM 2000, Heinz Walz GmbH, Germany) in a 0.6 mL chamber and cooled with an ice bath to approximately 2 °C. To obtain the relative electron transport rates (rETR) and the light saturation point I_k , cells were exposed to photon flux densities (PFD) of 5, 9, 34, 67, 104, 201, 366, 622, 984, 1389, 1666, and 2018 $\mu\text{mol photons m}^{-2} \text{s}^{-1}$ for 30 s each. Four independent replicates were measured. For further details, see [20].

2.7. Pigment Analysis

Carotenoids and chlorophylls were analyzed by HPLC (Agilent 1200 ChemStation) equipped with a quaternary pump and a diode array detector at 450 nm, using a reversed phase YMC C30 Carotenoids column (YMC Europe, Dinslaken, Germany), ID 300 mm \times 4.6 mm at 25 °C. α -tocopherol was simultaneously measured with a fluorescence detector (Em/Ex = 295/325 nm). The flow rate was 1 mL min^{-1} , analysis time was 20 min following an 8 min post-run prior next injection. The mobile phases were (A) methanol (gradient grade), (B) methyl *tert*-butyl ether (MTBE; HPLC grade) with 1.3% deionized water (*w/w*), and (C) MTBE (HPLC grade). The linear solvent gradient was: From 0 to 4 min at 82% A, 18% B, from 4 to 12 min to 50% A, 0% B, 50% C, from 12 to 20 min to 20% A, 80% C. Post-run was 20% A, 0% B, 80% C from 20 to 23 min, from 23 to 24 min to 82% A, 18% B, and then kept for 4 min. Cells were lyophilized for 48 h and frozen at -25 °C prior use. Extraction was performed with a porcelain mortar and pestle (Z247464 and Z247502, Sigma-Aldrich), using liquid nitrogen for 2 min of precooling and during grinding of cells for 1 min. The cell powder (approximately 10–50 mg) was suspended in approximately 5 mL of chloroform/dichloromethane (2/1) with 1 mM BHT (butylated hydroxytoluene) as antioxidants, the suspension grinded for another minute, and then transferred with a glass pipette into 50 mL plastic tubes for a subsequent post-extraction for at least 12 h at -25 °C. Afterwards, the supernatant was gently evaporated at 30 °C and resuspended in a defined volume of organic solvents (usually 5 mL) composed of 82% mobile phase A and 18% mobile phase B. Prior to injection, the extracts were centrifuged for 10 min at 10,000 $\times g$ and 1 °C. Peak identification was done by peak retention time and peak spectrum in relation to calibration standards (Sigma-Aldrich, Darmstadt, Germany).

2.8. Lipid Extraction and Fatty Acid Methyl Esters Analysis (FAMES)

The extraction procedure was based on the method of [37], and elution was done from a Sep-Pak Vac Silica cartridge 35cc (Waters; 10 g normal-phase silica) by chloroform (neutral lipids), acetone (glycolipids), and methanol (phospholipids) [38]. All classes of lipids were saponified overnight in 10% KOH in methanol at room temperature. The structures of FAMES were confirmed by comparison with Gas Chromatography/Mass Spectrometry retention times and fragmentation patterns with those of standard FAMES (Supelco, Prague) method of [39,40]. Procedures were described in detail by [20].

3. Results

3.1. Habitat Conditions

In the High Tatra (Slovakia, Poland), and Krkonoše and Jeseníky Mountains (Czech Republic), orange snow fields were found in May and June 2017 and 2019 at altitudes from 984 to 2082 m a.s.l. (Figure 2, Table 1). The habitat conditions of these localities are shown in Table 4. The orange blooms occurred at open sites above timberline (snow surface: Samples “WP194”, “WP129”, “WP130”, “WP136”; for “LP06”, spots were visible at the surface but the main bloom was harvested at 3–5 cm depth), a semi-shaded site above timberline (close to a boulder, sample “NW”), below dwarf pines (“Rozcestí”). Below timberline, the species was found at open sites (at avalanche slopes, data not shown), semi-shaded (samples “DD2”, “Jes19-1”), and full-shaded sites (“Jes19-6”). For the purpose of rapid light curves measurements, a sample from high light conditions (WP194) and samples from low light conditions (LP06 and DD2) were investigated.

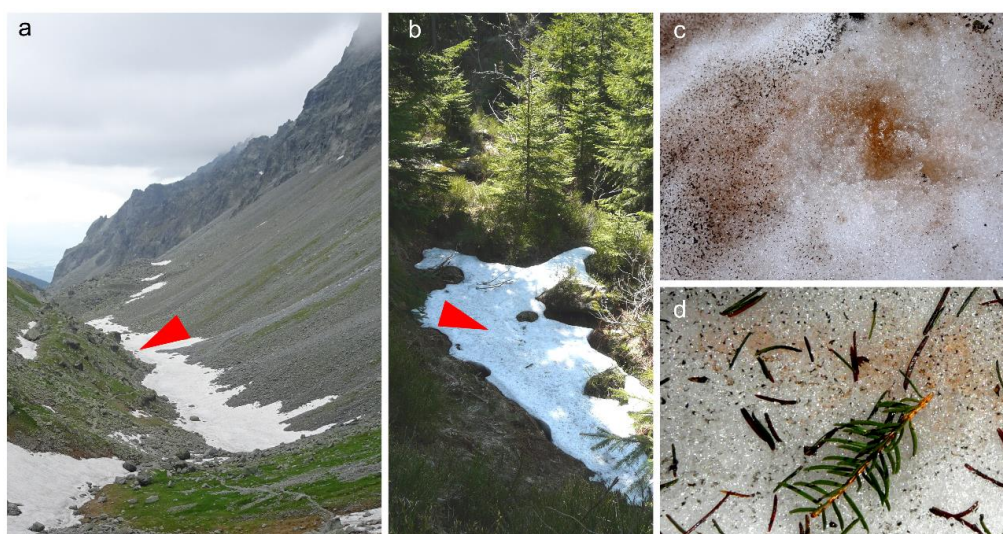


Figure 2. Two representative sampling sites of *Chloromonas hindakii* indicated by red arrowheads and detailed views of the orange snow blooms. (a,c) Open site above timberline (i.e., high light conditions) in the High Tatra Mountains (sample WP194) and (b,d) semi-shaded site close to spruce trees (i.e., low light conditions) in the Krkonoše Mountains (sample DD2).

3.2. Maximal Population Density and Morphology of Field-Collected Cysts

The population densities reached from 19,950 to 79,100 orange cysts mL⁻¹ meltwater (Table 4). Neither green nor orange flagellates were observed in the field material. Cell wall surfaces and intracellular organization were observed by light and electron microscopy (Figure 3). The fusiform cysts with wall surface structures corresponded to those of the aplanozygote of *C. nivalis*, as proposed by [41]. Cells were 18.5–34.3 µm long and 11.9–23.1 µm wide, with a length to width ratio of 1.2:1.9 (Figure S3). Typically, there were 7–10 flanges at the equatorial plane. Wall flanges were either straight or slightly undulating. SEM showed that four prominent flanges always joined at the apex and antapex

of the cell, and these flanges ran from one pole to the other. Other wall flanges were shorter and terminated either isolated in the subapex zone, or less often, fused with another flanges. The cytoplasm was dominated by orange–reddish pigmented compartments. Mature cysts had small chloroplast discs (data not shown). The daughter cells within the cysts were smooth-walled (Figure 3e).

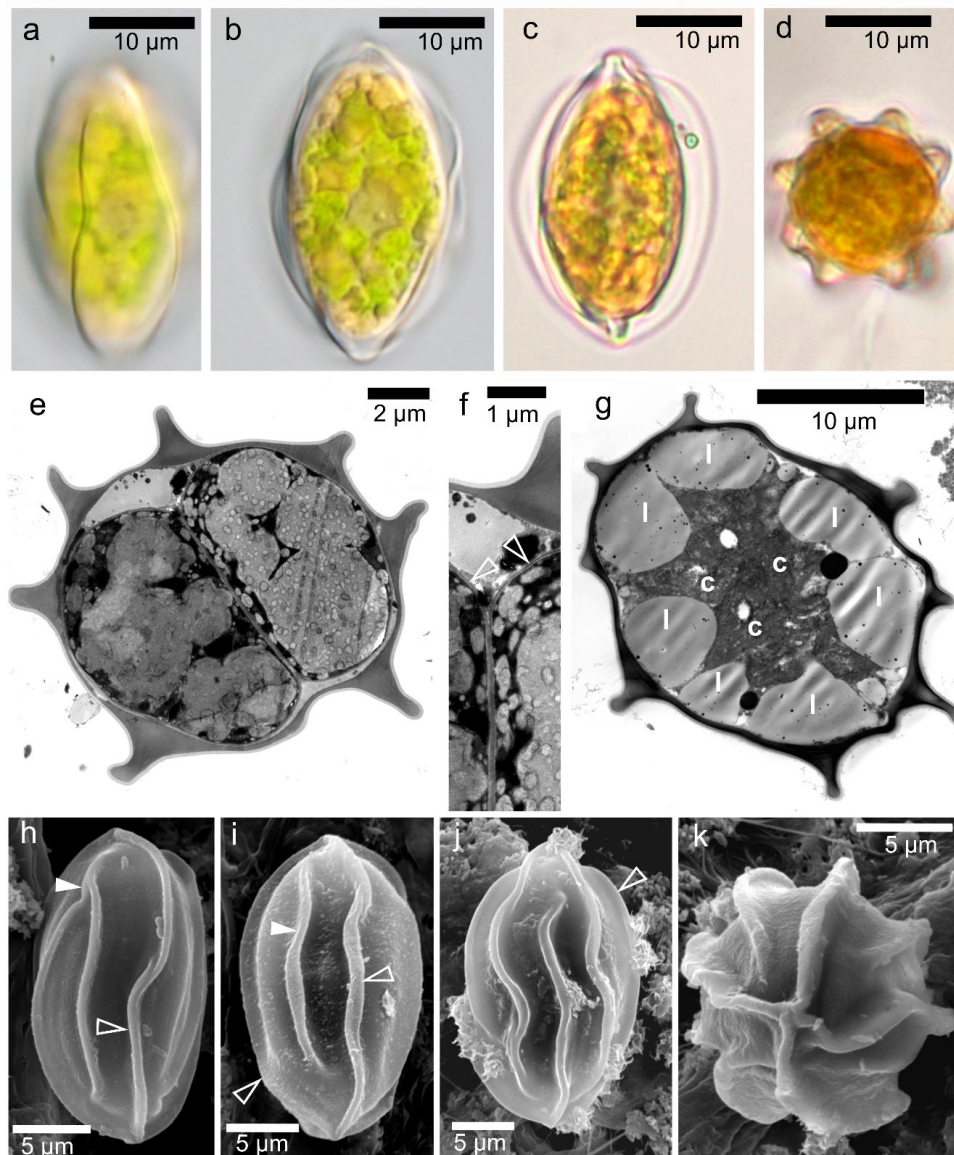


Figure 3. Light and electron microscopy of field-collected cysts of *Chloromonas hindakii* sp. nov.—samples Jes 19-1 (a,b), WP129 (c,d), WP194 (e,f,h–k), and DD2 (g). (a–d) Light micrographs. (a) Surface view showing cell wall flanges. (b,c) Optical sections, showing cytoplasm containing reddish astaxanthin depots and greenish chloroplast (b) and prominent wall flanges reaching the cell apices (c). (d) A cell in upright position, showing eight cell wall flanges. (e–g) Transmission electron micrographs. (e) Cell cross-section showing cleavages within the mother cell wall. (f) A detailed view of the newly formed cell wall of two daughter cells (empty arrowheads). (g) The cytoplasm of mature cysts occupied by large peripheral lipid bodies (l) with centrally located chloroplasts (c). (h–k) Scanning electron micrographs, showing characteristic organization of the cell ornamentation. An empty arrowhead indicates a flange reaching from pole to antapex. (h) Two flanges joining or a bifurcation of one flange into two independents (white arrowheads). (i) An isolated furcated flange (white arrowhead), (j) Slightly undulating flanges. (k) Apical view of a cell presenting eight flanges in total. Four of them are usually running from apex to antapex.

Table 4. Abiotic habitat parameters and cell sizes of *Chloromonas hindakii* field samples from the Krkonoše, Jeseníky, and High Tatra Mountains. Electrical conductivity (EC; $\mu\text{S}\cdot\text{cm}^{-1}$), pH of meltwater and snow water content (SWE; %), maximal population density \pm standard deviation (SD), average sizes of cells in $\mu\text{m} \pm$ SD, length to width ratio (L:W ratio) \pm SD are shown.

Sample	EC	pH	SWE	Cells Per mL Meltwater	Cell Length	Cell Width	L:W Ratio
DD2	14	5.7	48.7 \pm 0.3	19,950 \pm 2000	25.5 \pm 2	16.3 \pm 1.4	1.57 \pm 0.1
Rozcestí	9	5.9	-	-	25.0 \pm 2.1	16.6 \pm 1.5	1.51 \pm 0.1
Jes19-1	28	7.0	-	60,800 \pm 6080	27.3 \pm 2.1	17.9 \pm 2.2	1.53 \pm 0.1
Jes19-6	33	6.9	-	43,050 \pm 4300	30.3 \pm 2.1	19.7 \pm 1.7	1.54 \pm 0.1
LP06	5.2	5.5	55.9 \pm 2.1	54,150 \pm 5400	25.2 \pm 2	16.4 \pm 1.5	1.54 \pm 0.1
WP129	-	-	-	-	23.7 \pm 1.2	15.0 \pm 0.8	1.52 \pm 0.1
WP130	-	-	-	47,100 \pm 4700	-	-	-
WP136	-	-	-	79,100 \pm 7900	23.5 \pm 2.3	15.6 \pm 2.1	1.52 \pm 0.1
NW	-	-	-	-	23.0 \pm 2.1	15.0 \pm 1.4	1.54 \pm 0.1
WP194	5.1	6.8	60.8 \pm 5.97	21,900 \pm 2100	26.8 \pm 1.4	17.6 \pm 1.4	1.53 \pm 0.1

3.3. Phylogeny and Comparative Analysis of Internal Transcribed Spacer 2

The sequences of 18S rDNA and *rbcL* among the strain WP129 (= CCCryo 531-19) and field-collected cysts were identical. According to phylogenies of 18S rDNA (Figure 4) and *rbcL* (Figure 5), this species is a member of “*Chloromonas* clade B” *sensu* [4]. *Chloromonas hindakii* is related to *Chloromonas nivalis* Gassan-B (11 bp different out of 1650 bp in 18S rDNA), *Chloromonas polyptera* DRAnt023 (15 bp different out of 1653 bp in 18S rDNA), *Scotiella cryophila* K-1 (21 bp out of 1680 bp in 18S rDNA), and *Chloromonas nivalis* subsp. *tatrae* LP01 (34 bp out of 1683 bp in 18S rDNA). The new species formed a well supported subclade with other specimens of field cysts identified as *Chloromonas nivalis* P24/DR4 from the Austrian Alps and *Chloromonas nivalis* subsp. *tatrae* from the High Tatra Mountains (Slovakia) in 18S rDNA phylogeny. In contrast, the new species formed a well supported subclade together with *Scotiella cryophila* K-1 from the Austrian Alps in the *rbcL* phylogeny. Within all investigated samples (Table 3), the number of nucleotide differences in the entire ITS2 region ranged from 0 to 4 bp, and no compensatory base changes (CBCs) were detected (Figure 6). Conversely, one CBC was found between strain WP129 (= CCCryo 531-19) and an uncultured environmental clone ALBC6 from Switzerland (Figure S4), and between strain WP129 (= CCCryo 531-19) and *Chloromonas nivalis* Gassan-B from Japan (Figure S5), even near to the 5' apex of III helix, the most conserved part of ITS2 [42].

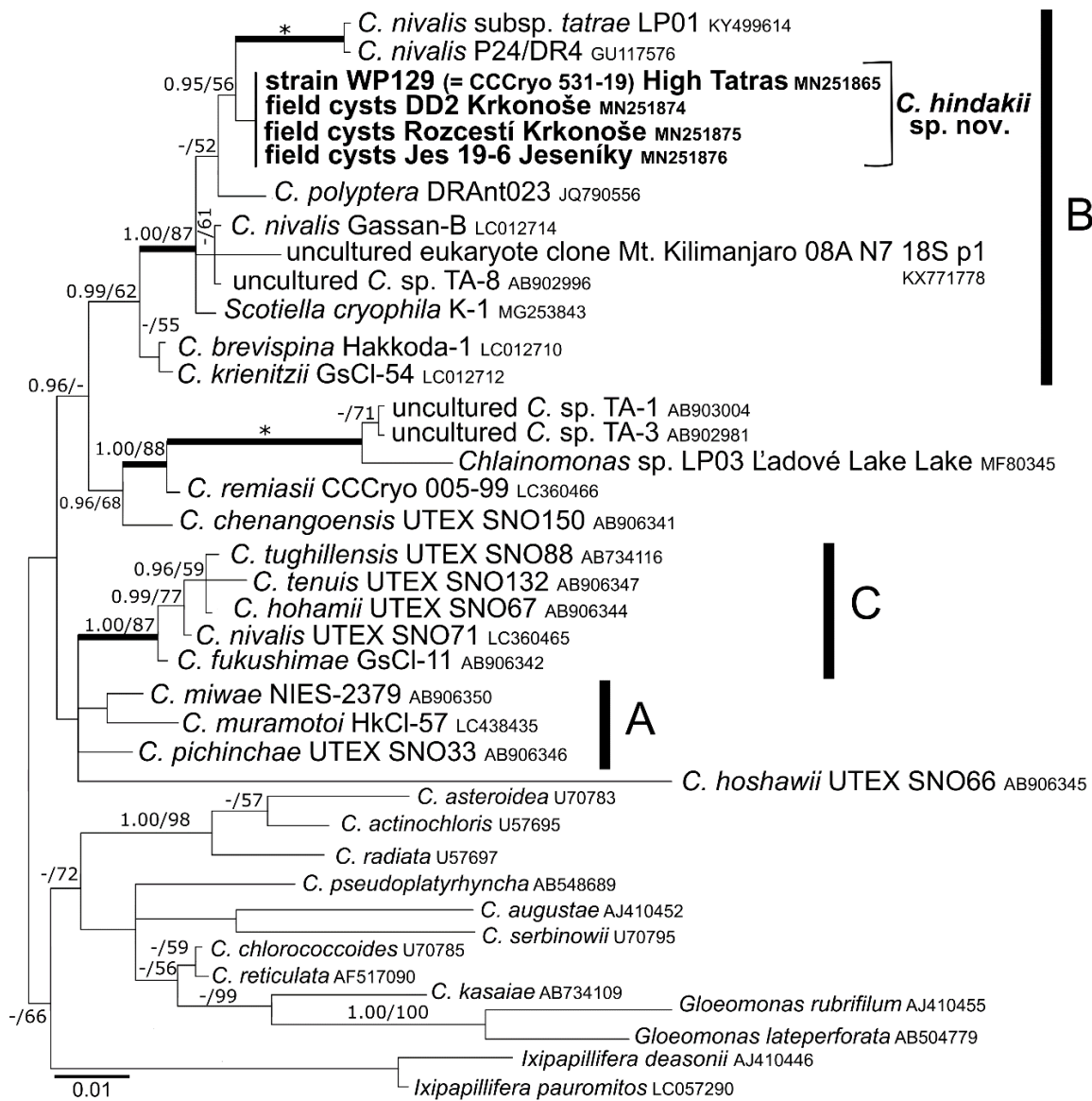


Figure 4. 18S ribosomal RNA gene-based Bayesian phylogenetic tree of *Chloromonas* focusing on snow-inhabiting species. *C.* = *Chloromonas*. The labeled clades ‘A’, ‘B’, and ‘C’ correspond to [4]. Posterior probabilities (0.95 or more) and bootstrap values from maximum likelihood analyses (50% or more) are shown. Full statistical support (1.00/100) is marked with an asterisk. Thick branches represent nodes receiving the highest posterior probability support (1.00). Newly obtained sequences are in bold. Accession numbers, strain, or field sample codes are indicated after each species name.

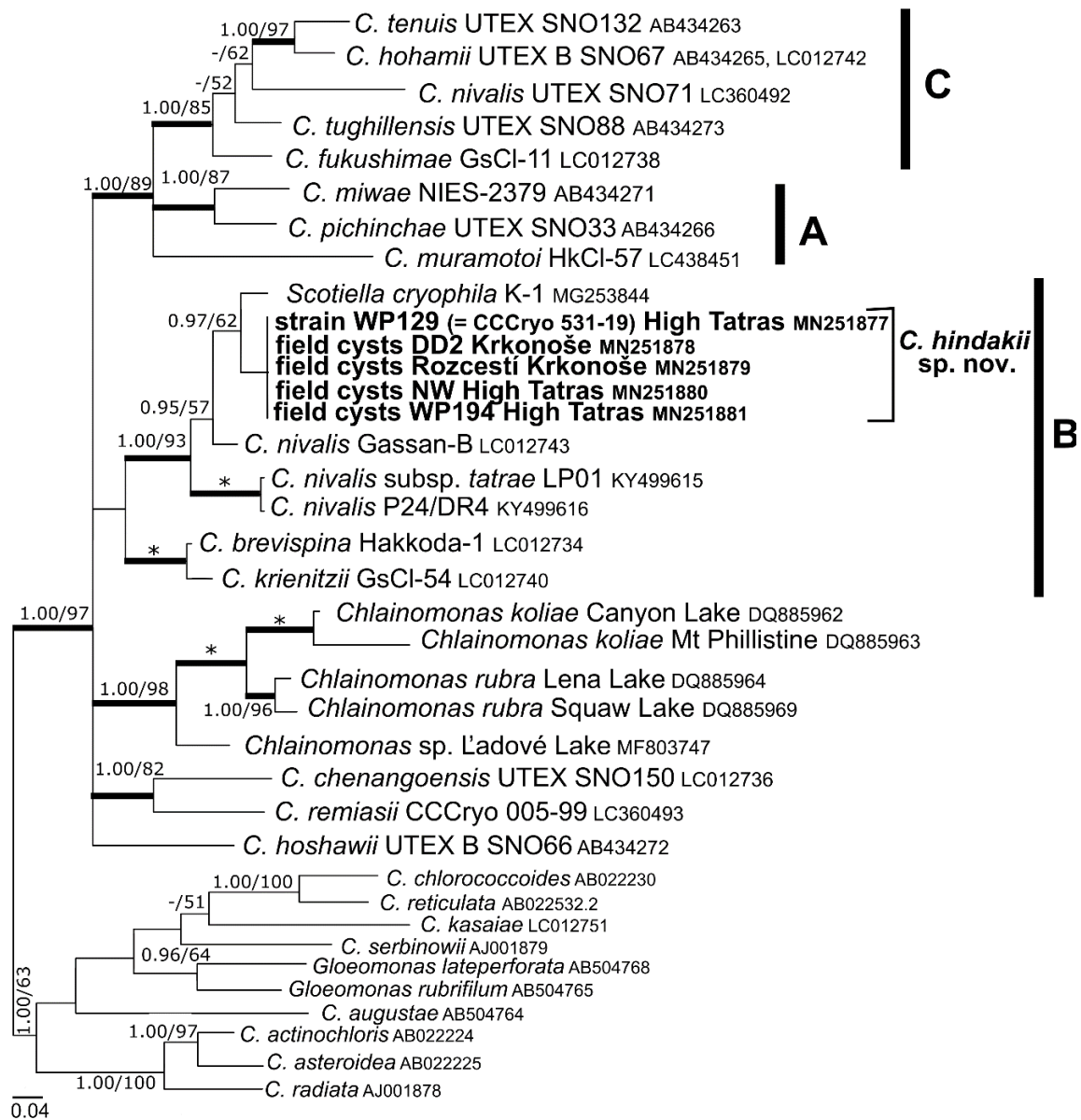


Figure 5. *rbcL* gene-based Bayesian phylogenetic tree of *Chloromonas* focusing on snow-inhabiting species. *C.* = *Chloromonas*. The labeled clades 'A', 'B', and 'C' correspond to [4]. Posterior probabilities (0.95 or more) and bootstrap values from maximum likelihood analyses (50% or more) are shown. Full statistical support (1.00/100) is marked with an asterisk. Thick branches represent nodes receiving the highest posterior probability support (1.00). Newly obtained sequences are in bold. Accession numbers, strain, or field sample codes are indicated after each species name.

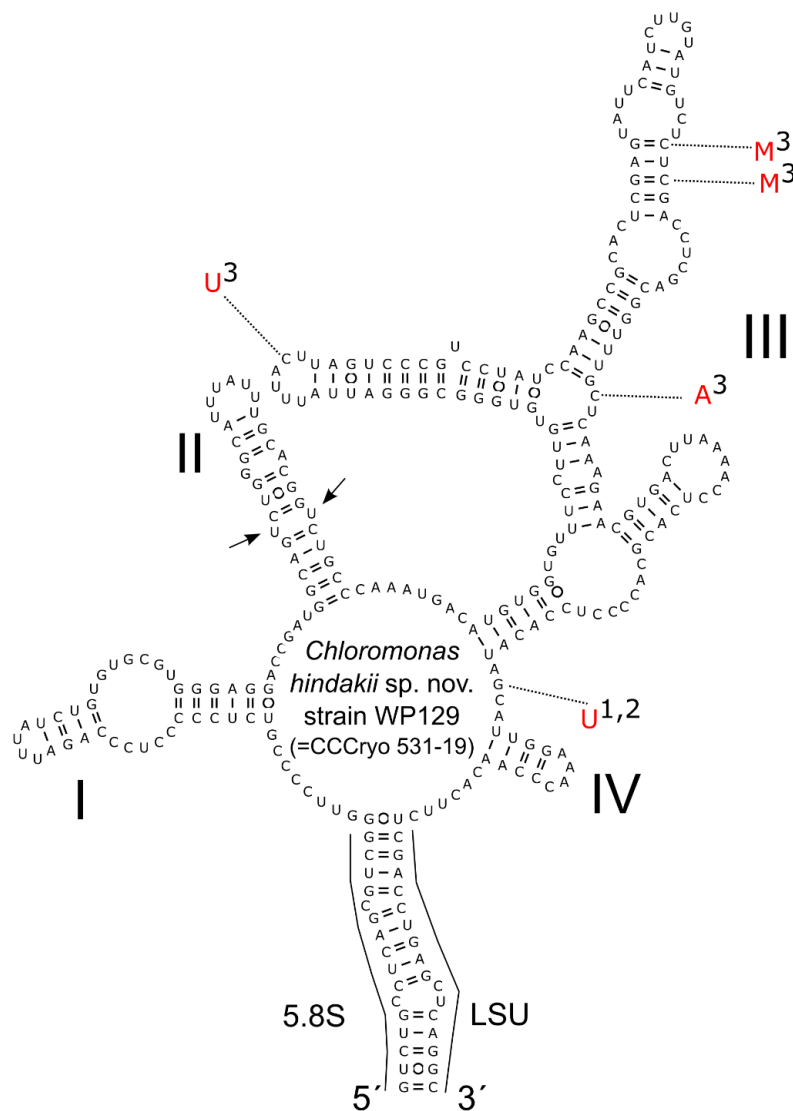


Figure 6. Intraspecific variability in the secondary structure of ITS2 rDNA transcripts of *Chloromonas hindakii* sp. nov.—comparison between the type strain WP129 (= CCCr1o 531-19) (accession number MN251865) and field-collected cysts from different localities. The marker was identical for the strain and the following field samples: Rozcestí (MN251867), Jes19-6 (MN251869), LP06 (MN251870), NW (MN251872), WP194 (MN251873). It differed by 1–4 bp in comparison with the field samples (1-DD2, MN251866; 2-Jes19-1, MN251868; 3-WP136, MN251871). Helices are labeled with Latin numbers: I–IV. Nucleotide differences of the field samples are described in red outside the structure and linked by dotted lines. Note the U–U mismatch in helix II (arrows).

3.4. Morphology of Vegetative Cells of *Chloromonas hindakii* sp. nov.

The strain consisted of green and solitary cells, bean-shaped with a rounded posterior end, 7–12.5 µm wide and 17–24.5 µm long (Figure 7). Cells had two equal flagella (if present) at the anterior end, a single chloroplast not fully occupying the posterior end of the protoplast (Figure 7a), two contractile vacuoles near the base of the flagella (Figure 7a), and the wall had no prominent anterior papilla (Figure 7b). The compact, elongated to slightly bean-shaped chloroplast had an emargination in the median region where the nucleus is usually located. The plastid was further lacking an eyespot and pyrenoids. The nucleus was almost spherical, located in the ventral half in the middle of the protoplast (Figure 7b). Asexual reproduction occurred via zoospore (autospore) formation. Generally, two, four, or rarely, eight daughter cells were produced within the parental wall (Figure 7c–e). Sexual reproduction

was not observed in the culture, even under nitrogen starvation; nor was the formation of cysts or accumulation of secondary reddish pigments. For testing temperature preferences, cells of *C. hindakii* were exposed to 15 °C but started to decay after 2 weeks, whereas at 5 °C they grew well long-term, and likewise at 1 °C (data not shown).

Figure 7f shows an overview of a flagellate by TEM. The papilla was small and flattened (Figure 7g). Cytokinesis took place in equatorial position of the cell (Figure 7h), resulting either in two spherical cells surrounded by undulating cytoplasmic membrane only (Figure 7i), or resulting in two elongated cells per sporangium with a prominent rough endoplasmic reticulum (indicating active metabolism). The daughter cells already possessed flagella (see an ultrastructure trait marked with “f”) (Transversal section, Figure 7j). Prior the release from the mother cell, the flagellates developed their own cell wall. The majority released flagellates were bean-shaped, but unusual spherical cells were also observed. Older, mature flagellates contained numerous small discoid chloroplasts with starch grains (Figure 7k).

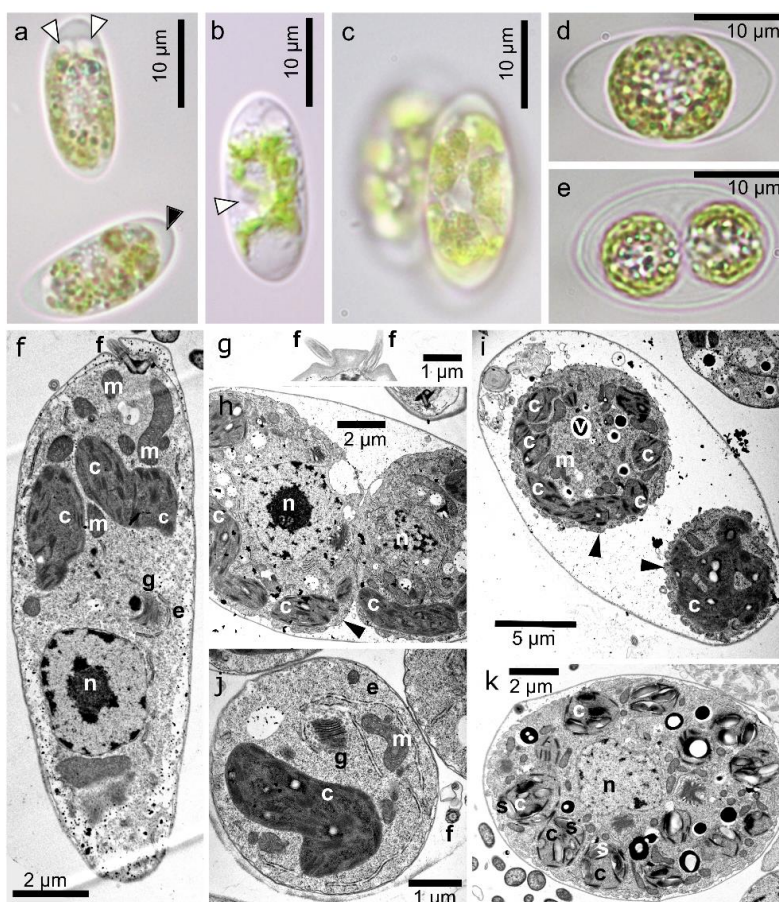


Figure 7. LM and TEM of vegetative cells of *Chloromonas hindakii* sp. nov. strain WP129 (= CCCryo 531-19): (a–e) LM. (a) Optical section of the cell, showing two contractile vacuoles (white arrowheads) and a chloroplast not totally occupying the posterior end of the protoplast (black arrowhead) within the cell. (b) Position of the nucleus (white arrowhead) within the cell. (c) Sporangium and plate-like sections of the plastid. (d,e) Development of two spherical daughter cells. (f–k) TEM. The following structures are labeled: Undulating plasmatic membrane (arrowhead), chloroplast (c), endoplasmic reticulum (e), flagellum (f), Golgi body (g), mitochondrion (m), nucleus (n), starch (s), vacuole with crystalline content (v). (f) Longitudinal cell section, showing position of nucleus. (g) Papilla shape. (h) Cell cleavage. (i) Two spherical daughter cells in mother cell wall, still lacking own cell wall. (j) Detail of one out of four spherical daughter cells with newly developed cell wall, still inside the sporangium wall. Note prominent rough endoplasmic reticulum. (k) Transversal cell section of an older cell with many discoid chloroplasts including starch grains.

3.5. Taxonomic Treatment

***Chloromonas hindakii* Procházková & Remias sp. nov. (Figures 3 and 7)**

DESCRIPTION: Vegetative cells solitary, having two equal flagella, two contractile vacuoles near the base of the flagella, a single chloroplast, single spherical nucleus positioned in the ventral half at the middle of the cell, without prominent anterior papilla. Cells elongate, kidney-shaped or bean-shaped with rounded posterior end; 7–11.5 μm wide and 17–24.5 μm long. A single chloroplast not occupying the posterior end of the protoplast and lacking eyespot and pyrenoid. Asexual reproduction by formation of two, four, or eight zoospores within the parental cell. Cell aggregates not observed in old cultures. Sexual reproduction unknown. Zygotes or cysts elongate to fusiform, 18.5–34.3 μm long and 11.9–23.1 μm wide, with length to width ratio within a range of 1.2–1.9. Cell walls with rib-like surface structures, such flanges are either straight or slightly undulating. Four prominent flanges always join at the apex and antapex of the cell, and they run entirely from one pole to the other. Further wall flanges are shorter, i.e., terminating either isolated at the subapical zone or less often fusing with another flange, or representing solitary flanges. The cytoplasm of cysts or zygotes usually contains reddish carotenoid droplets. The species differs from any other described representatives of the genus *Chloromonas* in the nuclear 18S rDNA, ITS rDNA, and plastid *rbcL* gene sequences (accession numbers: MN251865, MN251865, and MN251877, respectively).

HOLOTYPE: Specimen WP129 deposited at the Culture Collection of Algae of Charles University in Prague (CAUP), Czech Republic; material consists of resin-embedded vegetative cells from culture strain WP129.

AUTHENTIC STRAIN: WP129. The strain was deposited at the Culture Collection of Cryophilic Algae (CCryo, Available online: <http://cccryo.fraunhofer.de/web/strains>) in Potsdam, Germany, as a living culture, strain number CCryo 531-19.

TYPE LOCALITY: N49°11.424 E20°03.153, snowfield at Dolina za Mnichem, High Tatra Mountains, Powiat tatrzański, Bukowina Tatrzańska, Lesser Poland, Poland.

OTHER DISTRIBUTIONS: High Tatra Mountains (Slovakia), and Krkonoše and Jeseníky Mountains (Czech Republic).

ETYMOLOGY: The species epithet '*hindakii*' is *in memoriam* to Prof. František Hindák (1937–2019), a Slovak phycologist with influential contributions on microscopic algae. He described many new genera and species, including snow algae (e.g., [43,44]), and was one of the pioneers in successfully cultivating snow algae at laboratory conditions [45].

3.6. Photosynthesis

The photosynthetic activity of *C. hindakii* sampled at locations with different light conditions was tested and rapid light curves generated (Figure 8). Additionally, the performance of field cysts was compared with the laboratorial strain. Generally, the cysts were not dormant in terms of photosynthesis, as indicated by rETR. For the strain, and field cysts from low light conditions (below dwarf pine or 5 cm below the snow surface at a site above timberline), photoinhibition occurred above 200 $\mu\text{mol PAR m}^{-2} \text{ s}^{-1}$. The strain showed an α value of 0.23, a relative ETRmax of 6.6 ± 2.3 , and an I_k value of $33 \pm 8 \mu\text{mol PAR m}^{-2} \text{ s}^{-1}$. Field cysts from low light conditions had one-quarter lower alpha values (0.17 and 0.16) and two-fold higher I_k (73 and 78). In contrast, cysts from the snow surface above timberline (i.e., high light conditions) showed later signs of photoinhibition, starting from three times higher irradiances (600 $\mu\text{mol photons m}^{-2} \text{ s}^{-1}$); they also showed a two-fold higher ETRmax (14.5 ± 1) and four times higher I_k (129 ± 27), but a nearly twice lower α (0.13), when compared to the strain.

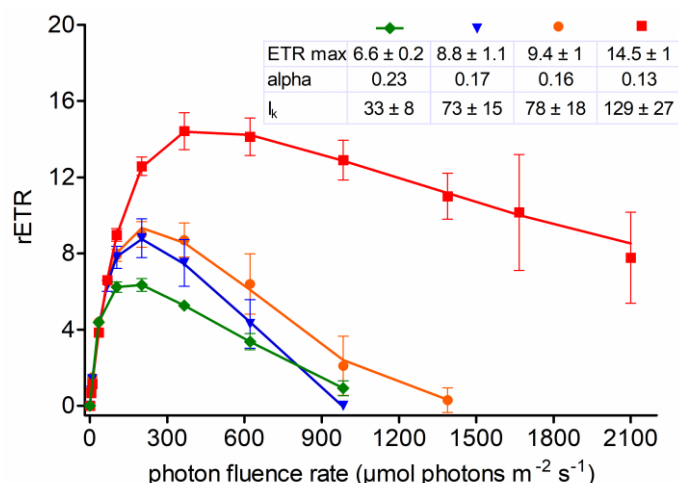


Figure 8. Rapid light curves showing the intraspecific photosynthetic flexibility of *Chloromonas hindakii* sp. nov. The effect of increasing photon fluence rates (x-axis) on the relative electron transport rate (rETR; y-axis) of chloroplasts was measured for vegetative flagellates (green diamonds, strain WP129 (= CCCryo 531-19) grown in the lab) and non-motile field-collected cysts (blue triangles—semi-shaded site close to a spruce canopy, sample DD2; orange circles—site above timberline, population located mainly 3–5 cm below snow surface, sample LP06; red boxes—site above timberline, population at snow surface, sample WP194). Values are means of four replicate measurements ($n = 4$, \pm SD). The data points were fitted to the photoinhibition model of [46].

3.7. Pigment Composition

The orange pigmentation of cysts of *C. hindakii* was caused by the secondary (non-plastid) carotenoid astaxanthin. Its abundance and those of other pigments and α -tocopherol was calculated in reference to chlorophyll-*a* (Table 5). Astaxanthin comprised 19.8% and 22.1% of all pigments, respectively (WP194, LP06). At HPLC, it occurred in a range of several peaks with identical absorption spectra, all of them likely esters with different fatty acids (Figure S6). Chlorophylls (*a* and *b*) comprised 57.7% and 57.6% of all pigments, primary (plastid) carotenoids represented 22.5% and 20.3% of the pigment pool. The overall ratio of cysts for astaxanthin to chl-*a* was 0.4 and 0.5, respectively. Further details are given in Table 5. In contrast, the laboratorial strain always stayed green (data not shown).

Table 5. Relative cellular content of carotenoids, chlorophyll *b*, and α -tocopherol in relation to chlorophyll *a* (= 1) in field samples of *Chloromonas hindakii* sp. nov. from the High Tatras at the Slovak side (sample WP194; high light conditions) and at the Polish side (LP06; low light conditions), determined by HPLC. Abbreviations: n & v, neoxanthin and violaxanthin; lut, lutein; zea, zeaxanthin; chl *b*, chlorophyll *b*; β -car, β -carotene; ast, astaxanthin (free/unesterified); ast-E, astaxanthin derivatives (esters); ast-tot, astaxanthin in total (free and derivatives); α -toc; α -tocopherol; n.d., not detected.

Sample	N&V	Lut	Zea	Chl <i>b</i>	β -car	Ast	Ast-E	Ast-tot	α -toc
WP194	0.120	0.315	n.d.	0.227	0.014	0.037	0.385	0.422	0.085
LP06	0.135	0.277	n.d.	0.273	0.020	0.012	0.476	0.488	0.080

3.8. Fatty Acid (FA) Composition

The relative content of FAs (percentage of total lipids and percentage of the three major lipid groups) in *C. hindakii* is given in Table 6. FAs with 14 to 18 C prevailed in field cysts and the strain (WP129). Cells showed high levels of PUFAs (65.8% and 58.1%, respectively, of total lipids), whereas the content of saturated acids (SAFA) did not exceed 23% (mainly palmitic acid, 16:0). The main monounsaturated fatty acid (MUFA) was oleic acid (18:1 (9Z), $9.8 \pm 3.6\%$ and 9.4%). The major PUFAs

were identical for field cysts and the strain flagellates but differed in relative proportions. The dominant PUFA was α -linolenic acid (18:3 (9Z,12Z,15Z), 25.9 \pm 3.7% and 31.6%, respectively). Flagellates had three times higher content of hexadecatetraenoic acid (16:4 (4Z,7Z,11Z,13Z), 28.5 \pm 4.6%) than cysts (10.3%) and similar levels of stearidonic acid (18:4 (6Z,9Z,12Z,15Z), 5.9 \pm 0.2 and 4.7%). Only minor differences in the FA composition between the three lipid classes of vegetative flagellates were observed (Table 6). PUFAs dominated the neutral lipids, phospholipids, and glycolipids (63.8%, 65.1%, and 75%, respectively). α -linolenic acid was up to twice higher in phospholipids than in neutral and glycolipids.

Table 6. Cellular fatty acid composition of *Chloromonas hindakii* sp. nov. vegetative strain WP129 (= CCCryo 531-19) cultivated at 1 °C ($n = 3$) compared to field-collected cysts (from sample Rozcestí) in % of total lipids (TL) and in % of the three major lipid groups: Neutral lipids (NL), phospholipids (PL), and glycolipids (GL). The table shows only fatty acids that have abundances greater than 0.1%. The relative proportion of saturated (SAFA), monounsaturated (MUFA), and polyunsaturated (PUFA) fatty acids is also given.

Fatty Acid	WP129 (= CCCryo 531-19)				Rozcestí
	TL	NL	PL	GL	TL
14:0	0.7 \pm 0.5	0.8 \pm 0.6	1.1 \pm 0.3	0	0.5
16:0	14.7 \pm 6.1	15.6 \pm 8.3	15.7 \pm 1.4	10.4 \pm 0.9	19.2
16:1 (9Z)	0.3 \pm 0.1	0	2.5 \pm 1.3	0	1.9
16:1 (7Z)	0.4 \pm 0.3	0.5 \pm 0.5	0	0	2.1
3t-16:1	0	0	4.6 \pm 0.1	0	0
16:2 (7Z,10Z)	0	0	0	0	3.2
16:3 (4Z,7Z,10Z)	0	0	0	0	0.3
16:3 (7Z,10Z,13Z)	2.1 \pm 1.1	1.9 \pm 1.4	1.5 \pm 0.2	3.6 \pm 0.3	2.7
16:4 (4Z,7Z,11Z,13Z)	28.5 \pm 4.6	30.6 \pm 6.1	12.1 \pm 0.6	29.5 \pm 1.6	10.3
18:0	7.3 \pm 6.8	6.7 \pm 8.9	1.5 \pm 0.6	14.5 \pm 3.6	1.3
18:1 (11Z)	0.5 \pm 0.3	0.5 \pm 0.4	1.1 \pm 0.3	0	7.5
18:1 (9Z)	9.8 \pm 3.6	12.1 \pm 5.2	8.4 \pm 1.1	0	9.4
18:2 (9Z,12Z)	3.4 \pm 0.8	3.9 \pm 1.0	3.4 \pm 0.1	1.2 \pm 0.7	4.8
18:3 (9Z,12Z,15Z)	25.9 \pm 3.7	21.4 \pm 3.7	44.7 \pm 1.7	33.2 \pm 8.4	31.6
18:3 (6Z,9Z,12Z)	0	0	0	0	0.5
18:4 (6Z,9Z,12Z,15Z)	5.9 \pm 0.2	6.0 \pm 1.6	3.3 \pm 1.1	7.4 \pm 4.7	4.7
SAFA	22.7 \pm 10.9	23.1 \pm 13.5	18.4 \pm 1.0	25.0 \pm 3.6	21
MUFA	11.5 \pm 3.6	13.1 \pm 5.0	16.6 \pm 0.8	0	20.9
PUFA	65.8 \pm 9.9	63.8 \pm 8.5	65.1 \pm 1.5	75.0 \pm 3.6	58.1

4. Discussion

4.1. Geographic Distribution and Ecology

Based on the discoveries in several mountain ranges of Poland, Slovakia, and the Czech Republic, *C. hindakii* sp. nov. seems to be a common member of the local cryoflora. Remarkably, it causes orange blooms both below and above timberline, contrary to many other snow algae, which usually thrive either in exposed or shaded habitats. The distribution of the species, at altitudinal gradient, ranged from montane to subalpine and alpine vegetation belt; e.g., for Krkonoše Mountains, see [47] (p. 271). The discoloration may vary; along with lower population densities, the snow was once reported to be pinkish [48]. A further, hitherto unidentified snow alga with eyespot and prominent cellular tail from the same sampling region reported as '*C. nivalis*' [48] is not in accordance to the morphology of *C. hindakii* (compare Figure 2b,c in [48] to Figure 7a,b in this study). However, in the study of [48], cysts morphologically identical to *C. hindakii* were found in Krkonoše at a wide altitudinal gradient from 740 to 1545 m a.s.l., at shaded (broad leaf and spruce trees) as well as at open sites (assigned to *C. nivalis*, see Figure 2e–g in [48]). Moreover, *C. hindakii* may occur also in other mountains in Slovakia [49]. Moreover, it may be found in the Bulgarian Vitosha Mountains, since [50] reported morphologically corresponding cysts in term of cell size, prominent cell apices, and number and organization of longitudinal cell wall flanges. The overall geographic distribution of *C. hindakii*, including further

regions like the European Alps, is not known yet, but distinct morphologic traits reported in this study and deposited molecular marker sequences should help for a future correct recognition.

4.2. Taxonomy and Related Species

To our knowledge, the vegetative strain of *C. hindakii* is the first available with a “*C. nivalis*-like” morphology of cysts (fusiform cells with prominent cell wall flanges) within the *Chloromonas* ‘snow clade B’ (*sensu* [4]). In many cases for snow algae, cysts were not made to germinate for generating a flagellate culture. Comparative analysis of the ITS2 rRNA secondary structure showed that *C. hindakii* is closely genetically related to an uncultured environmental clone, ALBC6, from a glacier forefield in Switzerland (accession number JX435348, [51]) and to *C. nivalis* Gassan-B from snow in Japan (accession number LC012758, [52]), indicating that the closest relatives also thrive in cold habitats. However, by using solely light microscopy, the cysts of *C. hindakii* have probably been reported several times as those of *C. nivalis* (as “*Scotiella nivalis*”) in the Krkonoše [48,53–56] and High Tatra Mountains [49,57–60]. On the other hand, this is the first report about cryoflora from the Jeseníky Mountains. By the help of electron microscopy and molecular methods, it was possible to describe this new species out of the “collective” taxon *C. nivalis*. This goes along with the description of further new snow algae like *C. hoshawii* or *C. remiasii*, which were formerly assigned to *C. nivalis* as well [61].

4.3. Morphology of the Field Cysts

Field-collected cysts in snow identifiable by LM as the cosmopolitan taxon *C. nivalis* were recently shown to represent multiple species [61]. Detailed morphological comparisons of the cyst (i.e., cell wall flanges distribution and characterization [20]) and flagellates [61] is crucial for classical species determination. Morphologically, cysts of *C. hindakii* differ from its close molecular relative *Scotiella cryophila* K-1 in having significantly less elongated cysts (the latter has length to width ratios from 2.1 to 4.7 [22]). Moreover, *C. hindakii* cysts differ from genetically distinct *C. nivalis* in the Austrian Alps [18], and *C. nivalis* subsp. *tatrae* [20] in the High Tatras in their cell size (larger cysts) and more prominent cell wall flanges. The number of cell wall flanges when observed at equatorial position is lower for the new species compared to *C. nivalis* subsp. *tatrae* (the latter has (9)10 to 12(14) flanges). These two species co-occurred occasionally in the High Tatra Mountains (own observations). Aplanozygotes of *C. nivalis* from North America [41] possess a lower number of flanges at cross-section (six to eight), are similarly large (16–37 $\mu\text{m} \times 10\text{--}27 \mu\text{m}$), but lack fusing/diverting flanges apart from the apex; however, here are no sequences available for these cysts yet. In addition, the identity of several vegetative *Chloromonas* strains isolated from the collection sites of *C. nivalis* in North America [41] is still unknown, and morphological details of their source material are missing (i.e., UTEX SNO16, UTEX SNO17, UTEX SNO18, UTEX SNO19, and UTEX SNO21). Matsuzaki et al. [4] reported for *C. muramotoi* a regular cell wall flange organization (i.e., four long flanges reached to both poles of the cell) similar to *C. hindakii*; however, *C. muramotoi* can be discriminated by its markedly smaller cell sizes (9.1–13.4 μm wide and 15.6–22.4 μm long). Moreover, a bifurcation of wall flanges was not observed for *C. muramotoi* and shorter flanges were only medially located (i.e., not reaching subapical cell regions). In this aspect, the new species is somehow similar to another snow alga, *C. miwae*, which, however, is smaller (10–16 μm wide and 20–26 μm long) and lacks visible accumulation of secondary carotenoids [52]. Mature cysts of *C. hindakii* have small chloroplast discs like all other cysts of *Chloromonas* species dwelling in snow (e.g., see chloroplast shape in Figure 22 in [20]). To conclude, it is generally possible to distinguish the cysts of *C. hindakii* morphologically from cysts of other snow algae.

4.4. Morphology of the Strain and Context to *C. nivalis*

The vegetative flagellates of *C. hindakii* differ from the five other most similar looking elongate to bean-shaped *Chloromonas* species isolated from snow as follows: The chloroplast of *C. hindakii* does not occupy the posterior ending of the protoplast, in contrast to *C. krienitzii* [52]. *C. hindakii* is larger in size than *C. fukushimae* when kept at the same cultivation conditions (4–9 $\mu\text{m} \times 15\text{--}23 \mu\text{m}$; [62]) and

develops only rarely eight zoospores in zoosporangia. Large cell aggregates were not observed in old cultures of *Chloromonas hindakii* in opposition to *Chloromonas polyptera*, where aggregates are made up of more than 16 cells [63]. *Chloromonas hindakii* differs in chloroplast morphology from *C. rostafinskii*—the latter has a cup-shaped chloroplast [64]. *Chloromonas hindakii* differs from *Chloromonas rubroleosa* in papilla shape and number of contractile vacuoles near the base of flagella—the latter has prominent bimamillate papilla and four contractile vacuoles [65]. Additionally, the vegetative morphology of *C. hindakii* is different from species not possessing bean-shaped flagellates, such as the North American strain UTEX SNO71 [4], which was recently proposed to represent the ‘true’ *C. nivalis* [4,41]. The latter has tear drop-shaped flagellates with a prominent posterior end. However, Robert Chodat’s type locality of *C. nivalis* in France close to Mont Blanc has not yet been resurveyed for revealing the molecular identity of its population. Moreover, in the original description the flagellate morphology is missing [66]. Recent molecular data suggest that species with a *C. nivalis*-like morphology of cysts evolved several times in the history of snow-thriving *Chloromonas* species [4,52,61].

4.5. Photobiology of Field Cysts vs. Laboratorial Strain

The rapid light curves from different habitats showed a high intraspecific flexibility of *C. hindakii* in terms of light acclimation, reflecting the occurrence in semi-shaded locations close to spruce canopy, below dwarf pine vegetation, as well as in exposed sites above timberline. This likely indicates the capabilities of the photosynthetic apparatus in regard to changeable short- and long-term incident irradiations, such as (a) diurnal changes due to topographic or/and vegetation shadings [48], (b) the distance of the cells from the snow surface during melting season [16], and (c) actual weather situation (e.g., sunny vs. cloudy day; [67]).

The fluorometric measurements of cysts showed that the photosystem II was well adapted to medium-to-high levels of irradiation. The cysts from the high light conditions (red graph in Figure 8) became photoinhibited at much higher irradiances than cysts from low light conditions (blue and orange graphs in Figure 8) or the laboratory strain, which was grown at low-light conditions (green graph in Figure 8). At open sites, at a snow depth of 20 cm, usually less than 5% of incident irradiation may be available [15]. Thus, in case of this study, the cysts found at an alpine location 5 cm below snow surface (sample LP06) perceived similarly low PAR like the cells at snow surface below spruce canopy (sample DD2). As a consequence, the characteristics of the rapid light curves (i.e., α , I_k and ETR values) of cells from these two different shaded sites are similar, which indicates that acclimation of the photosynthesis to certain snow depths is similar for *C. hindakii* with acclimation to a snow surface at semi-shaded site. Semi-shaded sites below timberline differ from open sites above timberline in the amplitude of PAR; for the former in the Krkonoše Mountains it reaches up to $\sim 1300 \mu\text{mol photons m}^{-2} \text{ s}^{-1}$ [48]. In contrast, the cysts from open alpine sites (sample WP194) in the High Tatra Mountains were exposed to PAR exceeding $2000 \mu\text{mol photon m}^{-2} \text{ s}^{-1}$ (see Supplementary Figure S27 in [16]). Likewise, other species were still able to perform positively at such high irradiances, and the light saturation (optimal) irradiance (i.e., I_k) of *C. hindakii* was nearly as high as those for cysts of *C. nivalis* and *C. nivalis* subsp. *tatrae*, causing reddish/brownish snow [18,20]. In contrast, the strain of *C. hindakii* exhibited a similarly low I_k and high light utilization efficiency (α value) to those recorded for cysts of the snow alga *Scotiella cryophila* caused green subsurface stripes at a depth of 20 cm below the snow surface [22]. In other words, photosynthesis was adapted to low light conditions. The high intraspecific flexibility of *C. hindakii*’s response to different light conditions allows this species to colonize, respectively survive at changeable conditions in snow.

4.6. Pigments and Fatty Acid Composition

The average levels of astaxanthin that cause the reddish coloration of *C. hindakii* are comparable to mature cysts of *C. nivalis* from the Austrian Alps [18]. Still, the astaxanthin to chlorophyll *a* ratio is three times lower than for *C. nivalis* subsp. *tatrae* from exposed sites at the High Tatras [20]. The main role of astaxanthin is likely to act as sunscreen against excessive visible and harmful UV irradiation.

On the other hand, too much astaxanthin would shade the plastids too much, thus decreasing the photosynthetic performance at sites with lower irradiation levels. Apparently, this species has developed a compromise. Probably, the accumulation of astaxanthin reflects the extent of endogenous cyst maturation, regardless of whether the cells are found at high light or at low light conditions (i.e., WP194 had similar astaxanthin to chl-*a* ratio like LP06). The laboratorial strain of *C. hindakii* produces no astaxanthin (data not shown), different to other microalgae feasible for biotechnology [68].

With the same protocol as for pigments, the plastid antioxidant α -tocopherol was quantified. The cysts of *C. hindakii* showed one magnitude higher concentrations than *C. nivalis* from the Austrian Alps [18], but the quantities were similarly low to cells that cause red snow (*Sanguina nivaloides*, referred as *Chlamydomonas nivalis* in [23]). The accumulation of vitamin E was reported to increase during the maturation process of *Chlamydomonas* sp. cysts under harsh environmental conditions in the late melting season [16].

In both stages, the strain and the field cysts of *C. hindakii* had a high level of PUFAs, which is regarded as an adaptation to cold conditions [69]. High levels of PUFAs are common also for other snow-dwelling *Chloromonas* species (e.g., see FAs composition in Table 5 in [20]) and algae living in other cold habitats such as lake ice [70]. Hexadecatetraenoic acid was present in flagellates of *C. hindakii* at relatively high levels of total FAs (~30%); its production in *C. hindakii* was the same as in a strain of *C. remiasii* CCCryo 005-99 isolated from snow in the Arctic and kept under nitrogen deficient conditions [71]. A likewise high accumulation of hexadecatetraenoic acid was found in edible marine macroalgae *Undularia pinnatifida* and *Ulva pertusa* [72]. This fatty acid extracted from algae was shown to have physiological effects on the human health [73]; it inhibited production of leukotrienes involved in several inflammatory and allergic reactions (e.g., [74]). What is more, alpine and polar microalgal strains are promising candidates for biotechnology [75], also in outdoor bioreactors at low temperature conditions [76]. Higher levels of saturated palmitic acid and monounsaturated oleic acid in *C. hindakii* correspond to similar amounts found in other strains of genus *Chloromonas* [77].

5. Conclusions

Molecular phylogenetic assays, in combination with morphological observation of cysts (likely zygotes) and vegetative flagellates, demonstrated that *C. hindakii* is a new species within a group of morphologically and taxonomically closely related cryoflora phytoflagellates, and most of them were formerly associated with the collective taxon *C. nivalis*. An unialgal vegetative strain with motile flagellates was established from field-collected cysts under suitable laboratorial conditions simulating the temperature of melting snow. For further detail in physiological, cytological, or closer molecular investigations, a clonal strain should be derived from a single cell. *C. hindakii* occurred at very different altitudes from the montane belt to subalpine and alpine locations of mid-latitude mountains, and it exhibited an infraspecific photosynthetic flexibility accordingly. This study shows for the first time for a snow alga that populations from high light conditions get photoinhibited at higher irradiances than those harvested from low light conditions. The physiologic light preferences reflected the light conditions in the original habitat. PUFAs prevailed in the lipids of *C. hindakii*, and astaxanthin was the pigment responsible for the orange coloration of the snow bloom. Generally, the response of a cold-adapted alga exposed to different light conditions can be investigated, along with screening which responses are activated (e.g., effect on pigments, proteins), as done for *Koliella antarctica* [78]. In future, the intraspecific variability among populations of other snow algae and its relation to the incident irradiation may be tested.

Supplementary Materials: The following are available online at <http://www.mdpi.com/2076-2607/7/10/434/s1>

Author Contributions: Conceptualization, L.P., D.R., and L.N.; data curation, L.P.; formal analysis, L.P.; funding acquisition, D.R. and L.N.; investigation, L.P., D.R., and T.Ř.; methodology, L.P. and D.R.; project administration, D.R. and L.N.; resources, L.P., D.R., and L.N.; supervision, L.N.; visualization, L.P.; writing—original draft, L.P.; writing—review and editing, L.P. and D.R.

Funding: This research was funded by the Czech Science Foundation (GACR) projects 18-02634S granted to L.N. and L.P., 17-00027S granted to T.Ř., and by the Austrian Science Fund (FWF) project P29959 granted to D.R.

Acknowledgments: We are grateful to David Kaftan for assistance in the field, and to Tomáš Hájek for technician support (both: University of South Bohemia in České Budějovice, Czech Republic). Open Access Funding by the Austrian Science Fund (FWF).

Conflicts of Interest: The authors declare no conflicts of interest.

References

1. Davey, M.P.; Norman, L.; Sterk, P.; Huete-Ortega, M.; Bunbury, F.; Loh, B.K.W.; Stockton, S.; Peck, L.S.; Convey, P.; Newsham, K.K.; et al. Snow algae communities in Antarctica—Metabolic and taxonomic composition. *New Phytol.* **2019**, *222*, 1242–1255. [[CrossRef](#)]
2. Anesio, A.M.; Lutz, S.; Christmas, N.A.M.; Benning, L.G. The microbiome of glaciers and ice sheets. *NPJ Biofilms Microbiomes* **2017**, *3*, 10. [[CrossRef](#)] [[PubMed](#)]
3. Cvetkovska, M.; Hüner, N.P.A.; Smith, D.R. Chilling out: The evolution and diversification of psychrophilic algae with a focus on Chlamydomonadales. *Polar Biol.* **2017**, *40*, 1169–1184. [[CrossRef](#)]
4. Matsuzaki, R.; Nozaki, H.; Takeuchi, N.; Hara, Y.; Kawachi, M. Taxonomic re-examination of “*Chloromonas nivalis* (Volvocales, Chlorophyceae) zygotes” from Japan and description of *C. muramotoi* sp. nov. *PLoS ONE* **2019**, *14*, e0210986. [[CrossRef](#)] [[PubMed](#)]
5. Procházková, L.; Leya, T.; Křížková, H.; Nedbalová, L. *Sanguina nivaloides* and *Sanguina aurantia* gen. et spp. nov. (Chlorophyta): The taxonomy, phylogeny, biogeography and ecology of two newly recognised algae causing red and orange snow. *FEMS Microbiol. Ecol.* **2019**, *95*, fiz064. [[CrossRef](#)] [[PubMed](#)]
6. Vimercati, L.; Solon, A.J.; Krinsky, A.; Arán, P.; Porazinska, D.L.; Darcy, J.L.; Dorador, C.; Schmidt, S.K. Nieves penitentes are a new habitat for snow algae in one of the most extreme high-elevation environments on Earth. *Arct. Antarct. Alp. Res.* **2019**, *51*, 190–200. [[CrossRef](#)]
7. Terashima, M.; Umezawa, K.; Mori, S.; Kojima, H.; Fukui, M. Microbial community analysis of colored snow from an alpine snowfield in Northern Japan reveals the prevalence of Betaproteobacteria with snow algae. *Front. Microbiol.* **2017**, *8*, 1481. [[CrossRef](#)] [[PubMed](#)]
8. Brown, S.P.; Olson, B.J.S.C.; Jumpponen, A. Fungi and algae co-occur in snow: An issue of shared habitat or algal facilitation of heterotrophs? *Arct. Antarct. Alp. Res.* **2015**, *47*, 729–749. [[CrossRef](#)]
9. Bidigare, R.R.; Ondrusek, M.E.; Kennicutt II, M.C.; Iturriaga, R.; Harvey, H.R.; Hoham, R.W.; Macko, S.A. Evidence for a photoprotective function for secondary carotenoids of snow algae. *J. Phycol.* **1993**, *29*, 427–434. [[CrossRef](#)]
10. Hamilton, T.L.; Havig, J. Primary productivity of snow algae communities on stratovolcanoes of the Pacific Northwest. *Geobiology* **2017**, *15*, 280–295. [[CrossRef](#)]
11. Thackeray, C.W.; Derksen, C.; Fletcher, C.G.; Hall, A. Snow and climate: Feedbacks, drivers, and indices of change. *Curr. Clim. Chang. Rep.* **2019**, 1–12. [[CrossRef](#)]
12. Mudryk, L.R.; Kushner, P.J.; Derksen, C.; Thackeray, C. Snow cover response to temperature in observational and climate model ensembles. *Geophys. Res. Lett.* **2017**, *44*, 919–926. [[CrossRef](#)]
13. Marty, C.; Schlögl, S.; Bavay, M.; Lehning, M. How much can we save? Impact of different emission scenarios on future snow cover in the Alps. *Cryosphere* **2017**, *11*, 517–529. [[CrossRef](#)]
14. Morgan-Kiss, R.M.; Priscu, J.C.; Pockock, T.; Gudynaite-Savitch, L.; Huner, N.P.A. Adaptation and acclimation of photosynthetic microorganisms to permanently cold environments. *Microbiol. Mol. Biol. R.* **2006**, *70*, 222–252. [[CrossRef](#)] [[PubMed](#)]
15. Gorton, H.L.; Vogelmann, T.C. Ultraviolet radiation and the snow alga *Chlamydomonas nivalis* (Bauer) Wille. *Photochem. Photobiol.* **2003**, *77*, 608–615. [[CrossRef](#)]
16. Procházková, L.; Remias, D.; Holzinger, A.; Řezanka, T.; Nedbalová, L. Ecophysiological and morphological comparison of two populations of *Chlainomonas* sp. (Chlorophyta) causing red snow on ice-covered lakes in the High Tatras and Austrian Alps. *Eur. J. Phycol.* **2018**, *53*, 230–243. [[CrossRef](#)] [[PubMed](#)]
17. Remias, D. Cell structure and physiology of alpine snow and ice algae. In *Plants in Alpine Regions. Cell physiology of Adaption and Survival Strategies*; Lütz, C., Ed.; Springer: Berlin/Heidelberg, Germany, 2012; pp. 175–186.

18. Remias, D.; Karsten, U.; Lütz, C.; Leya, T. Physiological and morphological processes in the Alpine snow alga *Chloromonas nivalis* (Chlorophyceae) during cyst formation. *Protoplasma* **2010**, *243*, 73–86. [[CrossRef](#)] [[PubMed](#)]
19. Remias, D.; Wastian, H.; Lütz, C.; Leya, T. Insights into the biology and phylogeny of *Chloromonas polyptera* (Chlorophyta), an alga causing orange snow in Maritime Antarctica. *Antarct. Sci.* **2013**, *25*, 648–656. [[CrossRef](#)]
20. Procházková, L.; Remias, D.; Řezanka, T.; Nedbalová, L. *Chloromonas nivalis* subsp. *tatrae*, subsp. nov. (Chlamydomonadales, Chlorophyta): Re-examination of a snow alga from the High Tatra Mountains (Slovakia). *Fottea* **2018**, *18*, 1–18.
21. Kvíderová, J.; Stibal, M.; Nedbalová, L.; Kaštovská, K. The first record of snow algae vitality in situ by variable fluorescence of chlorophyll. *Czech Phycol.* **2005**, *5*, 69–77.
22. Remias, D.; Procházková, L.; Holzinger, A.; Nedbalová, L. Ecology, cytology and phylogeny of the snow alga *Scotiella cryophila* K-1 (Chlamydomonadales, Chlorophyta) from the Austrian Alps. *Phycologia* **2018**, *57*, 581–592. [[CrossRef](#)] [[PubMed](#)]
23. Remias, D.; Lütz-Meindl, U.; Lütz, C. Photosynthesis, pigments and ultrastructure of the alpine snow alga *Chlamydomonas nivalis*. *Eur. J. Phycol.* **2005**, *40*, 259–268. [[CrossRef](#)]
24. Bischoff, H.W.; Bold, H.C. Phycological studies. IV. Some soil algae from Enchanted Rock and related algal species. *Univ. Texas Publ.* **1963**, 6318, 95.
25. Remias, D.; Pichtrová, M.; Pangratz, M.; Lütz, C.; Holzinger, A. Ecophysiology, secondary pigments and ultrastructure of *Chlainomonas* sp. (Chlorophyta) from the European Alps compared with *Chlamydomonas nivalis* forming red snow. *FEMS Microbiol. Ecol.* **2016**, *92*, fiw030. [[CrossRef](#)] [[PubMed](#)]
26. Piercey-Normore, M.D.; DePriest, P.T. Algal switching among lichen symbioses. *Am. J. Bot.* **2001**, *88*, 1490–1498. [[CrossRef](#)] [[PubMed](#)]
27. White, T.J.; Bruns, T.; Lee, S.; Taylor, J. Amplification and direct sequencing of fungal ribosomal RNA Genes for phylogenetics. In *PCR Protocols—A Guide to Methods and Applications*; Innis, M.A., Gelfand, D.H., Sninsky, J.J., White, T.J., Eds.; Academic Press: Cambridge, MA, USA, 1990; Volume 18, pp. 315–322.
28. Helms, G.; Friedl, T.; Rambold, G.; Mayrhofer, H. Identification of photobionts from the lichen family Physciaceae using algal-specific ITS rDNA sequencing. *Lichenologist* **2001**, *33*, 73–86. [[CrossRef](#)]
29. Vilgalys, R.; Hester, M. Rapid genetic identification and mapping of enzymatically amplified ribosomal DNA from several *Cryptococcus* species. *J. Bacteriol.* **1990**, *172*, 4238–4246. [[CrossRef](#)]
30. Katana, A.; Kwiatowski, J.; Spalik, K.; Zakryś, B.; Szalacha, E.; Szymańska, H. Phylogenetic position of *Koliella* (Chlorophyta) as inferred from nuclear and chloroplast small subunit rDNA. *J. Phycol.* **2001**, *37*, 443–451. [[CrossRef](#)]
31. Hoham, R.W.; Bonome, T.A.; Martin, C.W.; Leebens-Mack, J.H. A combined 18S rDNA and *rbcL* phylogenetic analysis of *Chloromonas* and *Chlamydomonas* (Chlorophyceae, Volvocales) emphasizing snow and other cold-temperature habitats. *J. Phycol.* **2002**, *38*, 1051–1064. [[CrossRef](#)]
32. Darty, K.; Denise, A.; Ponty, Y. VARNA: Interactive drawing and editing of the RNA secondary structure. *Bioinformatics* **2009**, *25*, 1974–1975. [[CrossRef](#)]
33. Pröschold, T.; Marin, B.; Schlösser, U.G.; Melkonian, M. Molecular phylogeny and taxonomic revision of *Chlamydomonas* (Chlorophyta). I. Emendation of *Chlamydomonas* Ehrenberg and *Chloromonas* Gobi, and description of *Oogamochlamys* gen. nov. and gen. nov. and *Lobochlamys* gen. nov. *Protist* **2001**, *152*, 265–300. [[CrossRef](#)]
34. Nakada, T.; Misawa, K.; Nozaki, H. Molecular systematics of Volvocales (Chlorophyceae, Chlorophyta) based on exhaustive 18S rRNA phylogenetic analyses. *Mol. Phylogenet. Evol.* **2008**, *48*, 281–291. [[CrossRef](#)] [[PubMed](#)]
35. Posada, D. jModelTest: Phylogenetic model averaging. *Mol. Biol. Evol.* **2008**, *25*, 1253–1256. [[CrossRef](#)] [[PubMed](#)]
36. Nedbalová, L.; Mihál, M.; Kvíderová, J.; Procházková, L.; Řezanka, T.; Elster, J. Identity, ecology and ecophysiology of planktic green algae dominating in ice-covered lakes on James Ross Island (northeastern Antarctic Peninsula). *Extremophiles* **2017**, *21*, 187–200. [[CrossRef](#)] [[PubMed](#)]
37. Bligh, E.G.; Dyer, W.J. A rapid method of total lipid extraction and purification. *Can. J. Biochem. Phys.* **1959**, *37*, 911–917. [[CrossRef](#)]

38. Saunders, R.D.; Horrocks, L.A. Simultaneous extraction and preparation for high-performance liquid chromatography of prostaglandins and phospholipids. *Anal. Biochem.* **1984**, *143*, 71–75. [[CrossRef](#)]
39. Řezanka, T. Identification of very long polyenoic acids as picolinyl esters by Ag⁺ ion-exchange high-performance liquid chromatography, reversed-phase high-performance liquid chromatography and gas chromatography—mass spectrometry. *J. Chromatogr. A* **1990**, *513*, 344–348. [[CrossRef](#)]
40. Dembitsky, V.M.; Řezanka, T.; Bychek, I.A.; Shustov, M.V. Identification of fatty acids from *Cladonia* lichens. *Phytochemistry* **1991**, *30*, 4015–4018. [[CrossRef](#)]
41. Hoham, R.W.; Mullet, J.E. The life history and ecology of the snow alga *Chloromonas cryophila* sp. nov. (Chlorophyta, Volvocales). *Phycologia* **1977**, *16*, 53–68. [[CrossRef](#)]
42. Coleman, A.W. Pan-eukaryote ITS2 homologies revealed by RNA secondary structure. *Nucleic Acids Res.* **2007**, *35*, 3322–3329. [[CrossRef](#)]
43. Hindák, F. Brownish snow in the High Tatras. *Biologia* **1969**, 80–85.
44. Javornický, P.; Hindák, F. *Cryptomonas frigoris* spec. nova (Cryptophyceae), the new cyst-forming flagellate from the snow of the High Tatras. *Biologia* **1970**, *25*, 241–250. [[PubMed](#)]
45. Hindák, F.; Komárek, J. Cultivation of cryosestonic alga *Koliella* (Kol) Hind. *Biol. Plant.* **1968**, *10*, 95–97. [[CrossRef](#)]
46. Walsby, A.E. Modelling the daily integral of photosynthesis by phytoplankton: Its dependence on the mean depth of the population. *Hydrobiologia* **1997**, *349*, 65–74. [[CrossRef](#)]
47. Chytrý, M. Current Vegetation of the Czech Republic. In *Flora and Vegetation of the Czech Republic*; Chytrý, M., Danihelka, J., Kaplan, Z., Pyšek, P., Eds.; Springer: Cham, Switzerland, 2017; pp. 229–337.
48. Nedbalová, L.; Kociánová, M.; Lukavský, J. Ecology of snow algae in the Giant Mts. *Opera Corcon.* **2008**, *45*, 59–68.
49. Hanzelová, M.; Vido, J.; Škvarenina, J.; Nalevanková, P.; Perháčová, Z. Microorganisms in summer snow patches in selected high mountain ranges of Slovakia. *Biologia* **2018**, *73*, 1177–1186. [[CrossRef](#)]
50. Lukavský, J.; Furnadzhieva, S.; Nedbalová, L. First record of cryoseston in the Vitosha Mountains (Bulgaria). *Nova Hedwig.* **2009**, *88*, 97–110. [[CrossRef](#)]
51. Frey, B.; Bühler, L.; Schmutz, S.; Zumsteg, A.; Furrer, G. Molecular characterization of phototrophic microorganisms in the forefield of a receding glacier in the Swiss Alps. *Environ. Res. Lett.* **2013**, *8*, 15033. [[CrossRef](#)]
52. Matsuzaki, R.; Kawai-Toyooka, H.; Hara, Y.; Nozaki, H. Revisiting the taxonomic significance of aplanozygote morphologies of two cosmopolitan snow species of the genus *Chloromonas* (Volvocales, Chlorophyceae). *Phycologia* **2015**, *54*, 491–502. [[CrossRef](#)]
53. Kociánová, M.; Štursová, H.; Štursa, J.; Vaněk, J.; Vávra, V. Nové nálezy červeného sněhu v Krkonoších. [New records of red snow in the Krkonoše Mountains]. *Opera Corcon.* **1989**, *26*, 151–158.
54. Stibal, M. Ecological and physiological characteristics of snow algae from Czech and Slovak mountains. *Czech Phycol.* **2003**, *3*, 141–152.
55. Komárek, J.; Nedbalová, L. Green cryosestic algae. In *Algae and Cyanobacteria in Extreme Environments*; Seckbach, J., Ed.; Springer: Berlin/Heidelberg, Germany, 2007; pp. 321–342.
56. Jehlička, J.; Culka, A.; Nedbalová, L. Colonization of snow by microorganisms as revealed using miniature Raman spectrometers—Possibilities for detecting carotenoids of psychrophiles on Mars? *Astrobiology.* **2016**, *16*, 1–12. [[CrossRef](#)] [[PubMed](#)]
57. Lukavský, J. Algal flora of lakes in the High Tatra Mountains (Slovakia). *Hydrobiologia* **1994**, *274*, 65–74. [[CrossRef](#)]
58. Kol, E. Cryobiological researches in the High Tatra I. *Acta Bot. Hung.* **1975**, *21*, 61–75.
59. Kol, E. Cryobiological researches in the High Tatra II. *Acta Bot. Hung.* **1975**, *21*, 279–287.
60. Osterrothová, K.; Culka, A.; Němečková, K.; Nedbalová, L.; Procházková, L.; Jehlička, J. Analyzing carotenoids of snow algae by Raman microspectroscopy and high-performance liquid chromatography. *Spectrochim. Acta Part A* **2019**, *212*, 262–271. [[CrossRef](#)] [[PubMed](#)]
61. Matsuzaki, R.; Nozaki, H.; Kawachi, M. Taxonomic revision of *Chloromonas nivalis* (Volvocales, Chlorophyceae) strains, with the new description of two snow-inhabiting *Chloromonas* species. *PLoS ONE* **2018**, *13*, e0193603. [[CrossRef](#)]

62. Matsuzaki, R.; Hara, Y.; Nozaki, H. A taxonomic study of snow *Chloromonas* species (Volvocales, Chlorophyceae) based on light and electron microscopy and molecular analysis of cultured material. *Phycologia* **2014**, *53*, 293–304. [[CrossRef](#)]
63. Ling, H.U.; Seppelt, R.D. Snow algae of the Windmill Islands, continental Antarctica. 3. *Chloromonas* polyptera (Volvocales, Chlorophyta). *Polar Biol.* **1998**, *20*, 320–324. [[CrossRef](#)]
64. Starmach, K.; Kawecka, B. The yellowish-green snow in the valley Za Mnichem in the Tatra Mountains. *Limnol. Investig. Tatra Mt. Dunajec River Basin* **1965**, *11*, 75–80.
65. Ling, H.U.; Seppelt, R.D. Snow algae of the Windmill Islands, continental Antarctica. 2. *Chloromonas* rubroleosa sp. nov. (Volvocales, Chlorophyta), an alga of red snow. *Eur. J. Phycol.* **1993**, *28*, 77–84. [[CrossRef](#)]
66. Chodat, R. *Algues vertes de la Suisse, A. Pleurococcoïdes–Chroolépoides*; K.J. Wyss: Berne, Switzerland, 1902; pp. 145–146.
67. Stibal, M.; Elster, J. Seasonal and diel changes in photosynthetic activity of the snow alga *Chlamydomonas nivalis* (Chlorophyceae) from Svalbard determined by pulse amplitude modulation fluorometry. *FEMS Microbiol. Ecol.* **2007**, *59*, 265–273. [[CrossRef](#)] [[PubMed](#)]
68. Molino, A.; Iovine, A.; Casella, P.; Mehariya, S.; Chianese, S.; Cerbone, A.; Rimauro, J.; Musmarra, D. Microalgae characterization for consolidated and new application in human food, animal feed and nutraceuticals. *Int. J. Environ. Res. Pu.* **2018**, *15*, 2436. [[CrossRef](#)] [[PubMed](#)]
69. Leya, T. Snow algae: Adaptation strategies to survive on snow and ice. In *Polyextremophiles. Life Under Multiple Forms of Stress*; Seckbach, J., Oren, A., Stan-Lotter, H., Eds.; Springer: Berlin/Heidelberg, Germany, 2013; Volume 27, pp. 401–423.
70. Osipova, S.; Dudareva, L.; Bondarenko, N.; Nasarova, A.; Sokolova, N.; Obolkina, L.; Glyzina, O.; Timoshkin, O. Temporal variation in fatty acid composition of *Ulothrix zonata* (Chlorophyta) from ice and benthic communities of Lake Baikal. *Phycologia* **2009**, *48*, 130–135. [[CrossRef](#)]
71. Spijkerman, E.; Wacker, A.; Weithoff, G.; Leya, T. Elemental and fatty acid composition of snow algae in Arctic habitats. *Front. Microbiol.* **2012**, *3*, 1–15. [[CrossRef](#)] [[PubMed](#)]
72. Ishihara, K.; Murata, M.; Kaneniwa, M.; Saito, H.; Komatsu, W.; Shinohara, K. Purification of stearidonic acid (18:4(n-3)) and hexadecatetraenoic acid (16:4(n-3)) from algal fatty acid with lipase and medium pressure liquid chromatography. *Biosci. Biotech. Bioch.* **2000**, *64*, 2454–2457. [[CrossRef](#)]
73. Ishihara, K.; Murata, M.; Kaneniwa, M.; Saito, H.; Shinohara, K.; Maeda-Yamamoto, M. Inhibition of icosanoid production in MC/9 mouse mast cells by n-3 polyunsaturated fatty acids isolated from edible marine algae. *Biosci. Biotech. Bioch.* **1998**, *62*, 1412–1415. [[CrossRef](#)]
74. Calder, P.C. Polyunsaturated fatty acids and inflammatory processes: New twists in an old tale. *Biochimie* **2009**, *91*, 791–795. [[CrossRef](#)]
75. Suzuki, H.; Hulatt, C.J.; Wijffels, R.H.; Kiron, V. Growth and LC-PUFA production of the cold-adapted microalga *Koliella antarctica* in photobioreactors. *J. Appl. Phycol.* **2019**, *31*, 981–997. [[CrossRef](#)]
76. Řezanka, T.; Nedbalová, L.; Lukavský, J.; Strížek, A.; Sigler, K. Pilot cultivation of the green alga *Monoraphidium* sp. producing a high content of polyunsaturated fatty acids in a low-temperature environment. *Algal Res.* **2017**, *22*, 160–165. [[CrossRef](#)]
77. Lang, I.; Hodač, L.; Friedl, T.; Feussner, I. Fatty acid profiles and their distribution patterns in microalgae: A comprehensive analysis of more than 2000 strains from the SAG culture collection. *BMC Plant Biol.* **2011**, *11*, 124. [[CrossRef](#)] [[PubMed](#)]
78. La Rocca, N.; Sciuto, K.; Meneghesso, A.; Moro, I.; Rascio, N.; Morosinotto, T. Photosynthesis in extreme environments: Responses to different light regimes in the Antarctic alga *Koliella antarctica*. *Physiol. Plantarum.* **2015**, *153*, 654–667. [[CrossRef](#)] [[PubMed](#)]



Supplementary Information

Ecophysiology of *Chloromonas hindakii* sp. nov. (Chlorophyceae), Causing Orange Snow Blooms at Different Light Conditions

Lenka Procházková, Daniel Remias, Tomáš Řezanka and Linda Nedbalová



Figure S1. Type locality of *Chloromonas hindakii* sp. nov. at Dolina za Mnicem, Powiat tatrzański, Bukowina Tatrzańska, High Tatra Mountains, Poland: (a) overview of the sampling location, (b) detail view of the orange snow spot during harvest (sample WP129, June 2017).

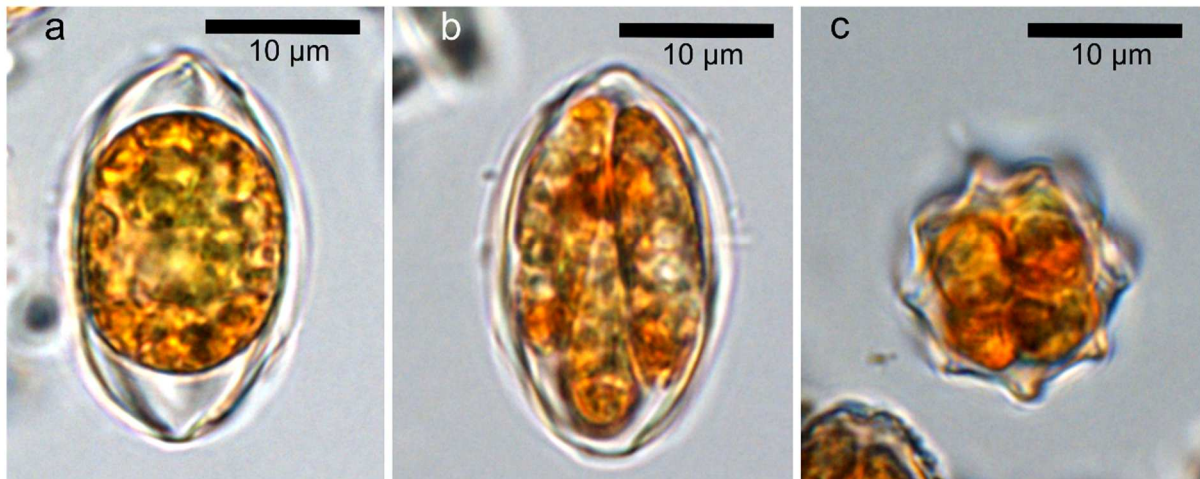


Figure S2. Light microscopy of field-collected material of *Chloromonas hindakii* sp. nov. (sample WP129). The cysts were kept in deionized water for several weeks at temperatures around the freezing point to provoke cell division (putative meiosis). (a) Old cyst, preparing for meiosis (or mitosis) by contracting the protoplast. In a consecutive step, (b) four elongated cells developed, still surrounded by the mother cell wall, lateral view, (c) apical view of the smooth walled daughter cells.

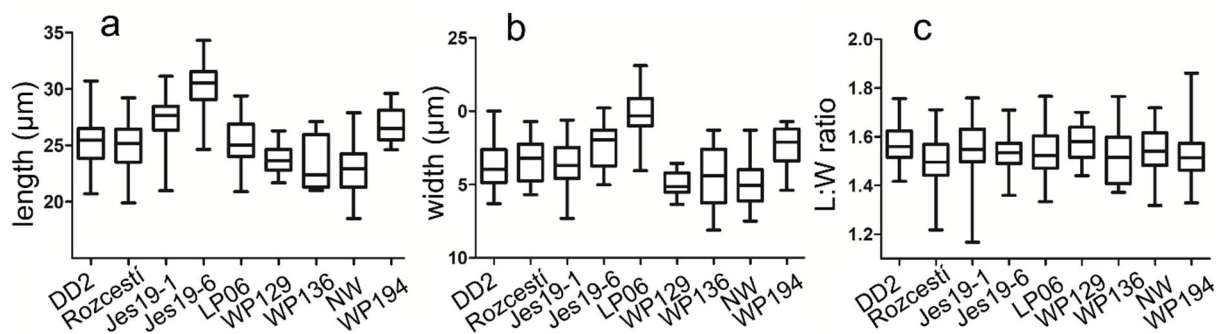


Figure S3. Cell size ranges of field-collected cysts of *Chloromonas hindakii* sp. nov. from the Krkonoše Mountains, the High Tatras and the Jeseníky Mountains after harvest (DD2, n = 40; Rozcestí, n = 32; LP06, n = 44; WP129, n = 21; WP136, n = 9; NW = 38; WP194, n = 31; Jes19-1, n = 33; Jes19-6, n = 36): (a) length, (b) width, (c) length to width ratio.

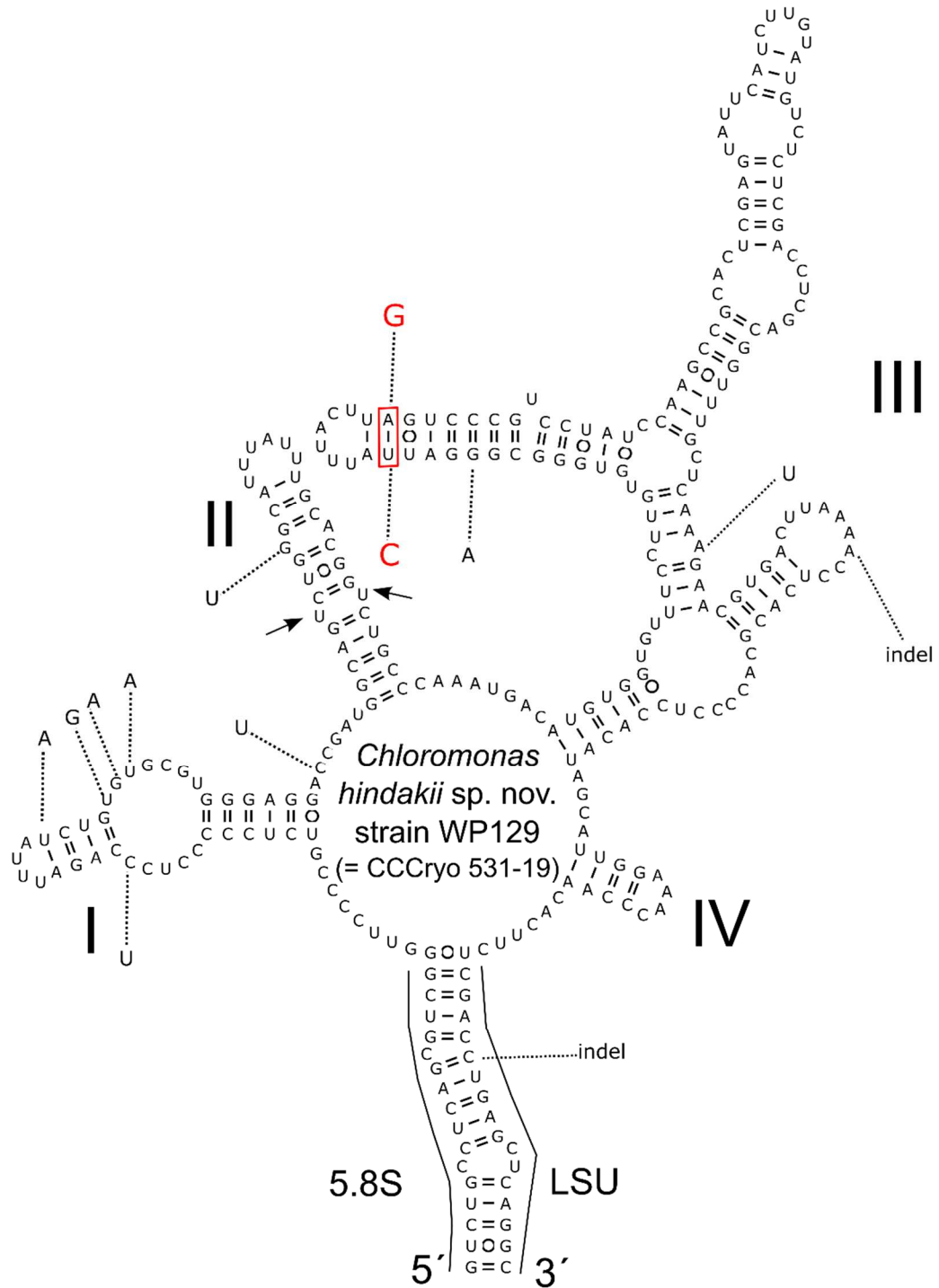


Figure S4. Comparison of the secondary structure of ITS2 rDNA transcripts between *Chloromonas hindakii* sp. nov. strain WP129 (= CCCryo 531-19, accession number MN251865) and the Uncultured Chlorophyte clone ALBC6 from Swiss Alps (accession number JX435348; [51]). Helices are labelled with Latin numbers: I-IV. Nucleotide differences of the second species are described in red outside the structure and linked by dotted lines. Compensatory base change in the 5' end of helix III between both algae is indicated by a rectangle. Note the U-U mismatch in helix II (arrows).

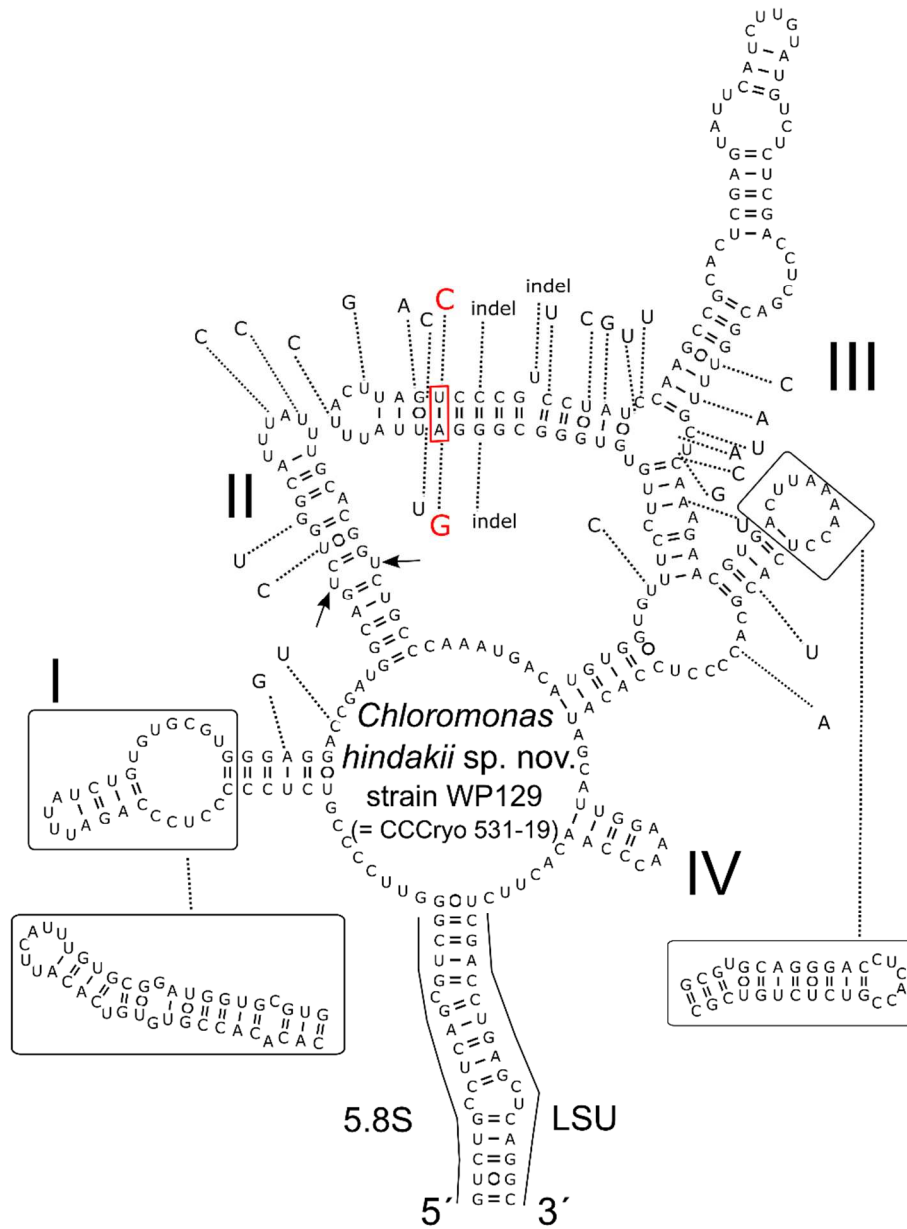


Figure S5. Comparison of the secondary structure of ITS2 rDNA transcripts between *Chloromonas hindakii* sp. nov. strain WP129 (= CCCryo 531-19, accession number MN251865) and *Chloromonas nivalis* Gassan-B from Japan (accession number LC012758, [52]). Helices are labelled with Latin numbers: I–IV. Nucleotide differences of the second species are described in red outside the structure and linked by dotted lines. Compensatory base change in the 5′-end of helix III between both algae is indicated by a rectangle. Note the U–U mismatch in helix II (arrows).

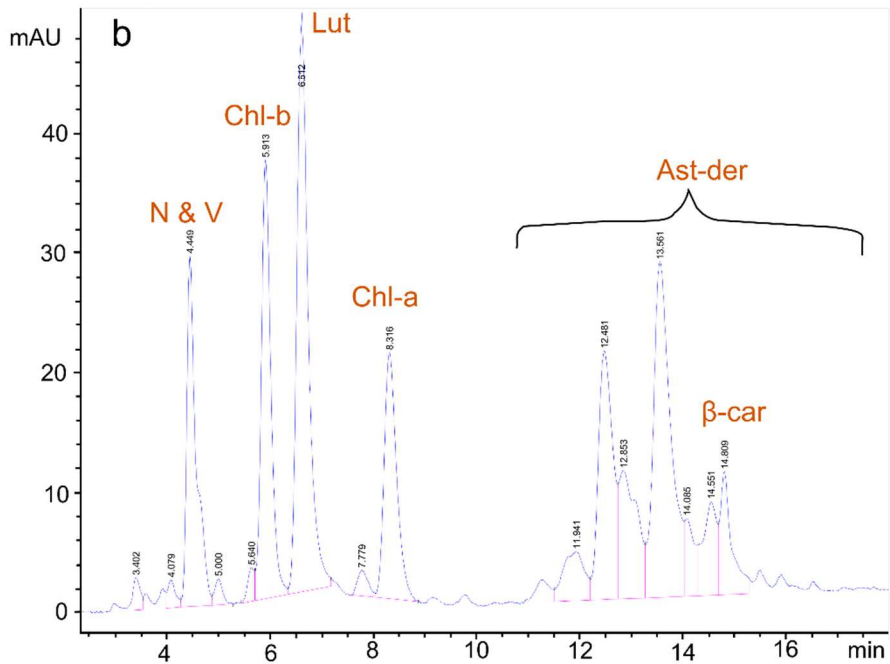
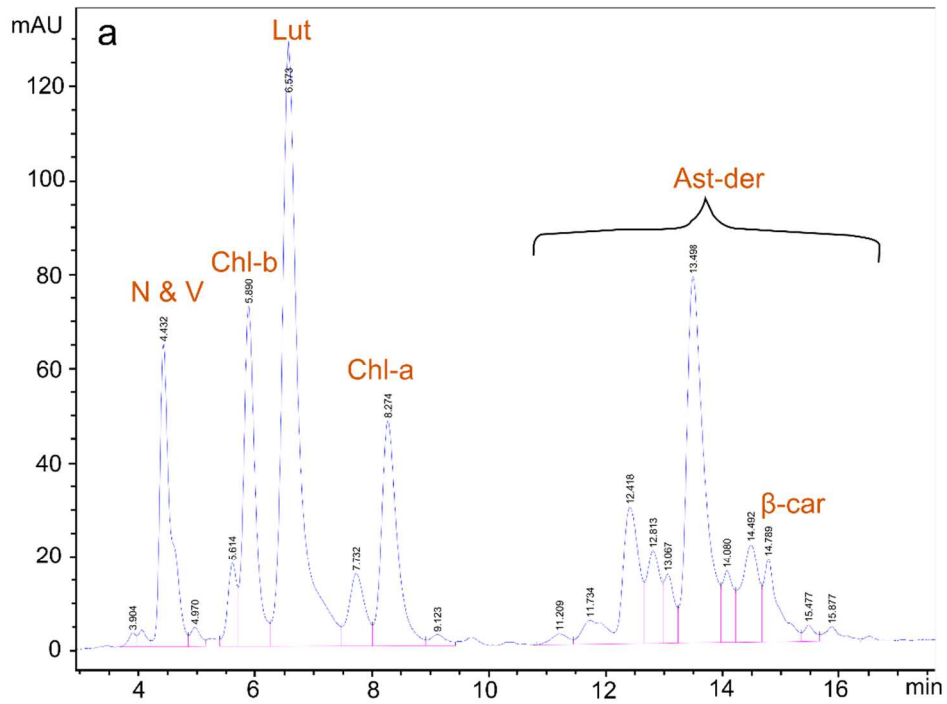


Figure S6. HPL-chromatogram of field-collected cysts of *Chloromonas hindakii* sp. nov. at 450 nm showing the main pigments. (a) Sample WP194 (high light conditions) from the Slovak side of the High Tatras. (b) Sample LP06 (low light conditions) from the Polish side of the High Tatras. Abbreviations: N, neoxanthin; V, violaxanthin; Lut, lutein; Chl-b, chlorophyll b; Chl-a, chlorophyll a; β -car, β -carotene; Ast-der, Astaxanthin derivatives (pooled).

Paper IV

Chloromonas nivalis subsp. *tatrae*, subsp. nov.

(Chlamydomonadales, Chlorophyta): re-examination of a snow alga
from the High Tatra Mountains (Slovakia)

Procházková L¹, Remias D², Řezanka T³ & Nedbalová L¹

Fottea 18(1): 1–18, 2018

¹ Charles University, Faculty of Science, Department of Ecology, Viničná 7, CZ–128 44 Prague,
Czech Republic

² University of Applied Sciences Upper Austria, Stelzhamerstraße 23, A–4600 Wels, Austria

³ Institute of Microbiology CAS, Vídeňská 1083, CZ–142 20 Prague, Czech Republic

***Chloromonas nivalis* subsp. *tatrae*, subsp. nov. (Chlamydomonadales, Chlorophyta): re-examination of a snow alga from the High Tatra Mountains (Slovakia)**

Lenka PROCHÁZKOVÁ^{1*}, Daniel REMIAS², Tomáš ŘEZANKA³ & Linda NEDBALOVÁ¹

¹ Charles University, Faculty of Science, Department of Ecology, Viničná 7, CZ-128 44 Prague, Czech Republic; Corresponding author e-mail: lenkacerven@gmail.com

² University of Applied Sciences Upper Austria, Stelzhamerstraße 23, A-4600 Wels, Austria

³ Institute of Microbiology CAS, Videňská 1083, CZ-142 20 Prague, Czech Republic

Abstract: Melting snow fields populated by aplanozygotes of the genus *Chloromonas* (Chlamydomonadales, Chlorophyta) are found in polar and alpine habitats. In the High Tatra Mountains (Slovakia), cells causing blooms of brownish-red snow designated as *Scotiella tatrae* KOL turned out to be genetically (18S, ITS1 and ITS2 rDNA, *rbcL*) very closely related to *Chloromonas nivalis* (CHODAT) HOHAM et MULLET from the Austrian Alps. Therefore, *Sc. tatrae* is transferred into the latter taxon and reduced to a subspecies as *Cr. nivalis* subsp. *tatrae*. Both exhibit a similar photosynthetic performance, thrive in similar habitats at open sites above timberline, but differ in astaxanthin accumulation and number of aplanozygote cell wall flanges. In a field sample of *Cr. nivalis* subsp. *tatrae*, polyunsaturated fatty acids formed nearly 50 % of total lipids, dominating in phospholipids and glycolipids. *Cr. nivalis* subsp. *tatrae* represents likely a variation of a common cryoflora species with distinct morphology.

Key words: aplanozygote, astaxanthin, *Chloromonas nivalis*, fatty acids, field sample, High Tatra Mountains, photosynthesis, snow algae, *Scotiella*, ultrastructure

INTRODUCTION

Snow inhabiting algae are polyextremophiles in terms like habitat temperature, incident irradiation or availability of liquid water and nutrients. They have been reported from many mountainous and polar regions, where melting snow packs persist until summer (HOHAM & DUVAL 2001). Cryoflora draws attention not only because of greenish to reddish snow discolorations, but also due to striking morphologic and physiologic strategies in course of its adaptation (KOMÁREK & NEDBALOVÁ 2007), especially in comparison with their ‘conventional’ mesophilic relatives. CVETKOVSKA et al. (2016) summarized the evolutionary origin and diversity of psychrophilic algae, showing that Chlorophyta harbour more than a third of all known photo-psychrophiles (plastid-bearing protists metabolically active and able to reproduce at temperatures permanently close to the freezing point of water, which do not tolerate temperatures > 20 °C). Generally, psychrophiles occur in a great variety of habitats and exhibit strategies like anti-freeze proteins or accumulation of compatible solutes like glycine (DE MAAYER et al. 2014).

The Tatra Mountains, which are located mainly in northern Slovakia and to a smaller part in southern Poland, are the topmost part of the Carpathian Arc. The relief of this mountain range is very complex due to glacial events (ZASADNI & KLAPYTA 2014). The presence of red snow in the Tatra Mountains was already reported several centuries ago (BUCHHOLZ 1783). The high cryoflora biodiversity of this massif was summarized by KOL (1975a, b).

The genus *Scotiella* (*Sc.*) was established by FRITSCH (1912) with the snow alga *Sc. antarctica* FRITSCH as the type. It is characterized by striking cell wall surface structures like flanges, and daughter cells were said to possess the same ribbed morphology already before being released from the mother cell. Many fusiform snow algae inhabiting polar areas and high alpine zones were initially believed to be a member of this genus (KOL 1968). However, the true nature of *Scotiella*-stages as aplanozygotes (‘aplano-’= immotile according to Ettl & GARTNER 2014) in the life cycle of a *Chloromonas* (*Cr.*)-like flagellate was revealed decades after the initial description by HOHAM & MULLET (1977), who showed that vegetative daughter

cells lack any cell wall ornamentation. Thus, several *Scotiella* like species inhabiting snow were transferred to the genus *Chloromonas* (HOHAM & MULLET 1978), e.g. *Sc. antarctica* was considered to be a zygotic stage of *Cr. nivalis* (CHODAT) HOHAM & MULLET, however the synonymy has been later questioned due to different cell flange morphology between these two species (NOVIS 2002). The genus *Scotiella* is now regarded as an artificial group of species retained for those taxons which's reproduction is unknown (HANAGATA 1998).

In this work, we studied populations collected close to the type locality of *Sc. tatrae* in the High Tatras, more than 50 years after the initial description by KOL (1965). All investigations were undertaken with field material, since cultures are not available yet, most likely because continuous growth under laboratory conditions was, to our knowledge, so far unsuccessful. The overall aim of this study was to evaluate abiotic habitat parameters, to check the phylogenetic position of *Sc. tatrae* using molecular and morphological traits, to measure the photosynthetic activity under varying light conditions, to describe the pigments which cause the secondary reddish colouration and finally, taking a putative adaptation to low temperatures into account, analysing the repertoire of fatty acids (FAs) occurring in membranes and cellular lipid depots.

The results were compared with the closest relatives, which is especially *Cr. nivalis*, from snow fields in the Austrian Alps.

MATERIAL AND METHODS

Sampling and snow characteristics. The cryoflora of brownish–red snow fields in the High Tatra Mts. (Slovakia) was investigated in June 2016 (Fig. 1). Exact geographic position, sampling date, elevation and corresponding sample code are summarized in Table 1. Surface snow samples were harvested either with a sterile plastic shovel and a 10 l bucket (sample ‘LP01’) or directly transferred into 50 ml sterile plastic tubes (other two samples). Samples were transported the same day to a field laboratory in close proximity. Prior to physiological measurements, the snow was gently melted over night at 4 °C to 5 °C and kept in its own melt water in the dark.

Electrical conductivity (EC) and pH of melt water samples were obtained with HANNA (Combo EC, Romania) and WTW Instruments (Inolab pH, Germany), respectively. Snow density was measured by coring snow with a cylindrical polyvinylchloride corer (length 72 cm, diameter 3.7 cm, volume 0.774 l). All cores were taken in the layer visually containing a bloom of snow algae and were orientated parallel to the surface of the snowbank according to HOHAM (1975). Cores were then transferred into plastic bags and the weight of each core was immediately measured by a spring balance Medio Line (precision 2 g, Pesola, Switzerland; similarly to KRÍSTEK et al. 2011). Three independent random cores were averaged. The snow water content (SWC) was expressed in percent and calculated as (weight of a snow core divided by the weight of water of the same volume as the core) × 100.

Light and electron microscopy. Light microscopy (LM) was conducted using an Olympus BX43 (Olympus corporation, Japan) equipped with a digital camera DXM 1200F (Nikon, USA). Microphotographs were processed using the QuickPHOTO Camera 3.0 software (Promicra, Czech Republic). The same software was used to measure cell sizes. Preparation of samples for scanning and transmission electron microscopy (SEM and TEM, respectively) included joint steps: samples were fixed in 1.25% glutaraldehyde in 50 mM cacodylate buffer (pH 7.0) for 2 hours at 4 °C, two times washed in cacodylate buffer at 4 °C for 15 minutes, postfixed in 1% OsO₄ overnight at 4 °C, three times washed in distilled water, gradually dehydrated through an ascending ethanol series (until 70% ethanol in 4 °C, then switched to room temperature). For SEM, fixed cells were transferred into a critical point drying chamber (Bal–Tec CPD 030). After gold–coating, specimens were examined with a JEOL 6380 LV SEM at 25 kV. For TEM, cells were embedded in Araldine and Poly/Bed® 812 mixture (SPI–CHEM, USA). Ultrathin sections were cut with a diamond knife, stained using uranyl acetate and lead citrate. TEM grids were examined with a JEOL 1011 TEM (JEOL Ltd., Japan) at 80 kV. Microphotographs were taken with a Veleta CCD camera equipped with Olympus image analysis software (Olympus Soft Imaging Solution, Germany) and later modified by iTEM 5.1 (Germany Soft Imaging Solution, Germany).

Cell counting and cultivation. A 10 ml subsample was taken at Capie Lake shore snow field (location LP01) in order to determine the cell concentration. After snow melt and homogenisation by shaking, a subsample of 0.01 ml was put into a Cyrus I chamber (Meopta, Czech Republic) for counting under a light microscope. Two replicates were analysed, each with a grid area of 1 cm². More than 200 cells were counted for one run. Attempts were made to culture the dominating snow algal species. For this, cells were placed a day after sampling on petri dishes containing BBM medium 1.5% agar (BISCHOFF & BOLD 1963) and kept at 3 °C under continuous illumination of 20 μmol.photons.m⁻².s⁻¹. Light

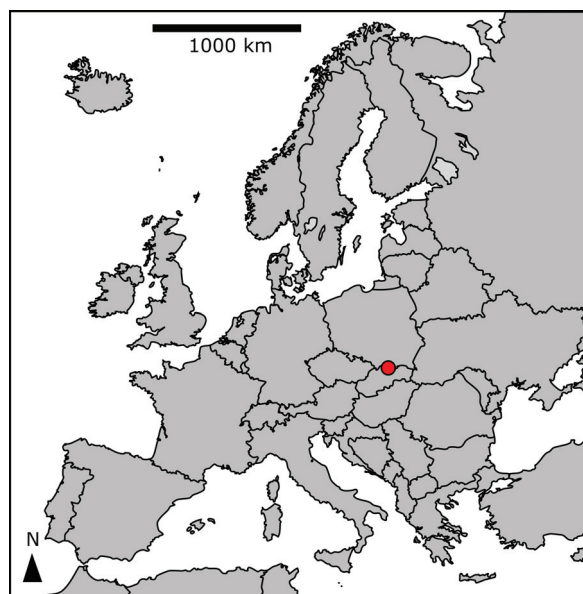


Fig. 1. Location of the High Tatra Mountains, Slovakia (marked with a red circle).

Table 1. Samples of *Chloromonas nivalis* subsp. *tatrae* from the High Tatra Mountains with sample codes, collection date, sampling site, altitude (m a.s.l.) and geographic position (GPS).

Sample/reference	Date	Location	Altitude	GPS
LP01 (this study)	18 June 2016	shore of Capie Lake	2073	N49°10.081 E20°02.279
KOL (1965)	22 June 1932	shore and ice cover of Okružle Lake	2000	N49°10.242 E20°02.178

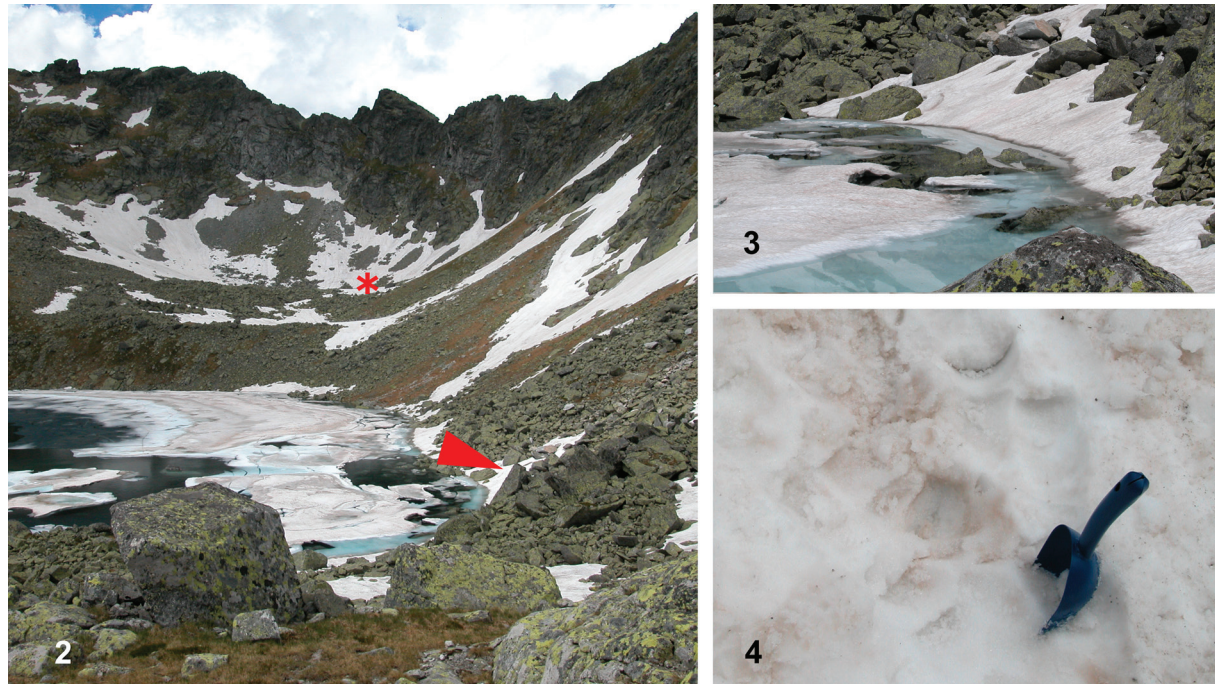


Fig. 2–4. Overview of sampling sites of *Chloromonas nivalis* subsp. *tatrae*: (2) sampling location of this study next to Capie Lake (code LP01, red arrowhead) and the first observation in 1932 in Okružle Lake (asterisk); (3) coloured snowfields at LP01 (4) detail view of brownish–red snow after harvest.

microscopy of field samples kept in their original meltwater was performed ~100 days after sampling to verify the development of daughter cells.

Isolation of DNA, sequencing, ITS2 rRNA secondary structure prediction and phylogenetic analysis. DNA was isolated from the sample LP01 with a DNeasy Plant Mini Kit (Qiagen). Cells were mechanically disrupted by shaking for 15 min (30 Hz) in the presence of glass beads (3 mm diameter, Sigma–Aldrich) in a Mixer Mill MM 400 (Retsch, Germany). Then, samples were put in freezer at -20°C for half an hour. Subsequently, DNA was isolated in accordance with the manufacturer’s procedure. Quality and concentration of DNA was measured on the NanoDrop® ND–1000 Spectrophotometer (NanoDrop Technologies, Inc.).

The 18S small subunit ribosomal RNA gene (18S rDNA), internal transcribed spacer regions 1 and 2 (ITS1, ITS2 rDNA) and ribulose–1,5–bisphosphate carboxylase/oxygenase large subunit (*rbcL*) gene regions were amplified from DNA isolates by PCR using existing primers (Table 2). Amplification reactions for 18S rDNA was performed using cycle parameters according to KATANA et al. (2001) with minor modification that duration of initial denaturation was prolonged for 10 min and annealing temperatures were

50°C , 58°C and 61°C . Amplification reactions for *rbcL* gene were performed using cycle parameters according to HOHAM et al. (2002) with minor change that three different annealing temperatures were applied (53°C , 55°C , 59°C). Each 20 μl of PCR reaction for 18S and *rbcL* amplification contained 5 μl of DNA isolates (diluted to concentration of 5 $\text{ng}\ \mu\text{l}^{-1}$), 0.8 μl of each 10 μM primer, 1.6 μl of 25 mM MgCl_2 , 1.5 μl of 2 mM dNTPs, 2 μl of 10 \times Taq buffer + KCl-MgCl_2 , 7.8 μl sterile Milli–Q water, and 0.5 μl of 1 $\text{U}\cdot\mu\text{l}^{-1}$ Taq DNA polymerase (Fermentas, USA). Amplification reactions for ITS2 rDNA region were performed using cycle parameters according to GOFF & MOON (1993) with minor modification that the gradient of annealing temperature was included (56°C , 58°C , 61°C , 64°C). Each 35 μl PCR reaction contained 1 μl of DNA isolates (diluted to concentration of 5 $\text{ng}\ \mu\text{l}^{-1}$), 1.4 μl of each 10 μM primer, 2.8 μl of 25 mM MgCl_2 , 2.6 μl of 2 mM dNTPs, 3.5 μl of 10 \times buffer Taq buffer + KCl-MgCl_2 , 21.8 μl sterile Milli–Q water, and 0.5 μl of 1 $\text{U}\cdot\mu\text{l}^{-1}$ Taq DNA polymerase (Fermentas). The PCR products were stained with bromophenol loading dye, quantified on 1.5% agarose gel, stained with GelRed. The amplification products were purified and sequenced using an Applied Biosystems automated sequencer (ABI 3730 \times 1) at Macrogen (Korea). The newly obtained sequences were

Table 2. List of primers used for amplification of 18S rDNA, ITS1 rDNA, ITS2 rDNA (ITS) and *rbcL* markers; (F) forward; (R) reverse.

Primer	Marker	Direction	Sequence	Reference
SSU	ITS	F	CTGCGGAAGGATCATTGATTC	PIERCEY–NORMORE & DEPRIEST (2001)
LSU	ITS	R	AGTTCAGCGGGTGGTCTTG	PIERCEY–NORMORE & DEPRIEST (2001)
Al1500af	ITS	F	GCGCGCTACACTGATGC	HELMS et al. (2001)
LR3	ITS	R	GGTCCGTGTTTCAAGACGG	VILGALYS & HESTER (1990)
<i>rbcL</i> 1F	<i>rbcL</i>	F	CTGCTTTTACTGCGAAACTGC	HOHAM et al. (2002)
<i>rbcL</i> 7R	<i>rbcL</i>	R	AAATAAATACCACGGCTACG	HOHAM et al. (2002)
<i>rbcL</i> 10F	<i>rbcL</i>	F	GGTAACGTWTTTGTTCAAAGC	HOHAM et al. (2002)
<i>rbcL</i> 14R	<i>rbcL</i>	R	CGTTCWCCTTCAAGTTTACC	HOHAM et al. (2002)
<i>rbcL</i> 19F	<i>rbcL</i>	F	CTCAATCGTTCATGCGTTGG	HOHAM et al. (2002)
<i>rbcL</i> 4R	<i>rbcL</i>	R	GAAAATGAAACGGTCTCTCC	HOHAM et al. (2002)
18S1F	18S	F	CTGCTTTTACTGCGAAACTGC	HOHAM et al. (2002)
34F	18S	F	GTCTCAAAGATTAAGCCATGC	MIKHAILYUK et al. (2008)
895R	18S	R	AAATCCAAGAATTTACCTC	MIKHAILYUK et al. (2008)
18F	18S	F	AACCTGGTTGATCCTGCCAGT	KATANA et al. (2001)
18R	18S	R	TGATCCTTCTGCAGGTTACCTACG	KATANA et al. (2001)
1122R	18S	R	CAATTCCTTTAAGTTTCAGCC	MIKHAILYUK et al. (2008)

submitted to NCBI Nucleotide sequence database (accession numbers for *Cr. nivalis* subsp. *tatrae* LP01: 18S, ITS1, ITS2 – KY499614, *rbcL* – KY499615; *Cr. nivalis* P24/DR4: *rbcL* – KY499616).

The nuclear rDNA ITS2 region was identified using a web interface at the ITS2 database showing position of 5.8S and 26S motives (<http://its2.bioapps.biozentrum.uni-wuerzburg.de/cgi-bin/index.pl?annotator>; KOETSCHAN et al. 2010). The sequence was then folded with 5.8S–LSU stem regions using the Mfold server accessible at <http://mfold.rna.albany.edu/?q5mfold> (ZUKER 2003). A model of the secondary structure consistent with the specific features of nuclear rDNA ITS2 was selected: four helixes, U–U mismatch in helix II, and the UGGU motif near the 5′-end site apex of helix III (COLEMAN 2007).

Photosynthesis. *In vivo* chlorophyll fluorescence parameters were obtained in a chamber for liquid samples at approximately 0 °C with a pulse–amplitude modulated fluorometer (PAM 2000, Heinz Walz GmbH, Germany). To gain sufficient biomass, cells were concentrated by passive sedimentation of melt water in a 1 l plastic cylinder overnight and the pellet was then used for measurements. Prior measurement, algae were kept in the snow meltwater in the dark for 30 minutes. Then, cells were exposed to photon flux densities (PFDs) of 5, 34, 66, 104, 201, 366, 622, 984, 1389, 1666 and 2018 $\mu\text{mol} \cdot \text{photons} \cdot \text{m}^{-2} \cdot \text{s}^{-1}$ for 30 seconds each. Four replicate measurements were carried out. After each light exposure, a saturating pulse was given to detect effective photochemical quantum yield of photosystem II (PS II):

$$Y(\text{II}) = (F_m' - F) / F_m' \quad (\text{GENTY et al., 1989})$$

where F_m' = maximal fluorescence yield emitted by

chlorophyll–a in PS II when PSII reaction centres are closed by a saturation pulse and F = minimum fluorescence yield at steady state.

Afterwards, the relative electron transport rate of PSII (rETR) was calculated as follows:

$$\text{rETR} = Y(\text{II}) \times \text{PFD} \times P_{\text{PSII}} / P_{\text{PPS}} \times \text{ETR-Factor}$$

where $Y(\text{II})$ = the effective PSII quantum efficiency, PFD = photon flux density, $P_{\text{PSII}} / P_{\text{PPS}}$ = photons absorbed by PS II relative to photons absorbed by all photosynthetic pigments (default value 0.5), ETR-Factor = an empirical corrective factor (default value 0.84), which considers fraction of incident photons absorbed by the chlorophyll *a* molecules in PSII.

A curve of rETR upon PFD was calculated and fitted by the mathematical model according to WALSBY (1997) where photoinhibition is assumed. Presence of photoinhibition was indicated by $\beta < 0$:

$$\text{rETR} = \text{ETR}_{\text{max}} (1 - \exp(-\alpha \times \text{PFD} / \text{ETR}_{\text{max}})) + \beta \times \text{PFD}$$

where rETR = relative electron transport rate of PSII, rETR_{max} = maximum relative electron transport rate of PSII, α = initial slope alpha and β = slope of the curve at high irradiances. PFD = photon flux density. The parameters ETR_{max} , α and β were found using the Solver software in Microsoft Excel.

If $\beta > 0$ (no photoinhibition), curve of rETR upon PFD was calculated and fitted according to model WEBB et al. (1974) where photoinhibition is not assumed:

$$rETR = ETR_{\max} (1 - \exp(-\alpha \times PFD/ETR_{\max}))$$

The fitting model with a lower sum of squared deviations was chosen.

Pigment analysis. Chlorophylls and carotenoids were isolated and determined by a protocol optimized for snow algae described by REMIAS & LÜTZ (2007) and REMIAS et al. (2013). Briefly, cells were lyophilized on glass fibre filters and broken in a shaking mill and using quartz balls and mill jars pre-cooled with liquid nitrogen. Extraction was performed with dimethylformamide (Sigma–Aldrich) and compounds were identified and quantified by high performance liquid chromatography with diode array detector (Agilent ChemStation 1100).

Lipid extraction. The extraction procedure was based on the method of BLIGH & DYER (1959), except that 2–propanol was substituted for methanol, since 2–propanol does not serve as a substrate for phospholipases (KATES & VOLCANI 1996). The alcohol–water mixture was cooled, one part chloroform was added and the lipids from the lyophilized cells were extracted for 30 min. Insoluble material was sedimented by centrifugation and the supernatant was separated into two phases. The aqueous phase was aspirated off and the chloroform phase was washed three times with two parts 1 M KCl each. The resulting chloroform phase was evaporated to dryness under reduced pressure. 10 mg of total lipid extract in 1 ml of chloroform was applied to Sep–Pak Vac Silica cartridge 35cc (Waters; 10 g normal–phase silica), and then eluted with 30 ml each of the following solvents: chloroform (neutral lipids), acetone (glycolipids), and methanol (phospholipids) at 4 ml min^{−1} (SAUNDERS & HORROCKS 1984). The eluates of each lipid class were then evaporated prior further analysis.

Fatty acid methyl esters analysis (FAMES). The lipids (neutral lipids, glycolipids and phospholipids) (~5 mg of total dry weight) were saponified overnight in 10% KOH–MeOH at room temperature. A FA fraction obtained from saponification was partitioned between alkali solution (pH 9) and diethylether to remove basic and neutral components. The aqueous phase, containing FAs, was acidified to pH 2 and extracted with hexane. The FA fraction was methylated using CH₂N₂. Gas chromatography coupled with mass spectrometry (GC–MS) of FAMES mixture was done on a Finnigan 1020 B with electron ionization (EI) mode. Splitless injection was at 100 °C, and a fused silica capillary column (Supelcowax 10; 60 m × 0.25 mm i.d., 0.25 mm film thickness; Supelco, Prague) was used. The temperature program was as follows: 100 °C for 1 min, subsequently increasing at 20 °C min^{−1} to 180 °C and at 2 °C min^{−1} to 250 °C, which was maintained for 1 min.

The carrier gas was helium at a linear velocity of 60 cm.s^{−1}. All spectra were scanned within the range of m/z 50–500. The structures of FAMES were confirmed by comparison of retention times and fragmentation patterns with those of standard FAMES (Supelco, Prague) (REZANKA 1990; DEMBITSKY et al. 1991).

Statistical analysis. Cell sizes (length, width, length to width ratio) of *Sc. tatrae* (LP01) were compared with those from *Cr. nivalis* at the Austrian Alps, (P12, P24/DR4, DR43, GK05, GK09; collection data of these field samples in Table S1 and in REMIAS et al. 2010). Kruskal–Wallis test was used for testing the hypothesis that cell size median of all *Cr. nivalis* samples from the Austrian Alps is not different. Moreover, Mann–Whitney test was used for testing the hypothesis that the median of two groups is identical (*Sc. tatrae* vs. *Cr. nivalis*).

RESULTS

Collection sites and habitat conditions

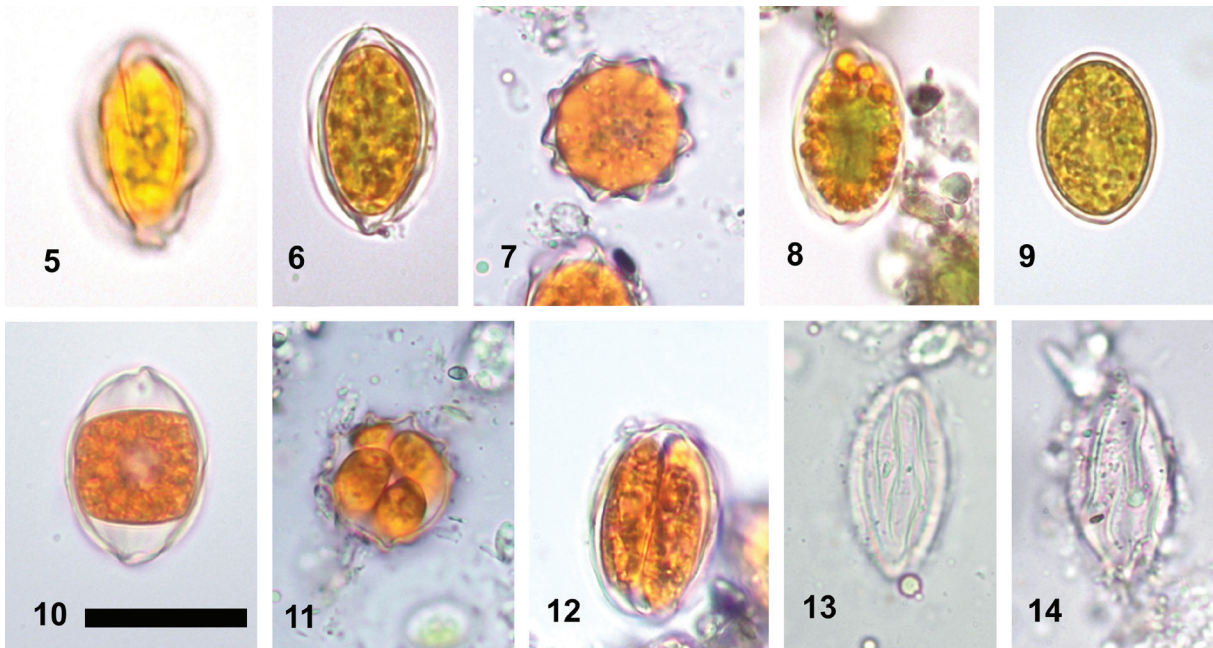
In the High Tatra Mountains (Slovakia), brownish–red snow fields were found during June 2016 at elevations of approximately 2000 m a. s. l. (Figs 2–4). A site in the vicinity to the locality of the first observation of the snow alga *Sc. tatrae* was sampled: the coloured snow was harvested at the shore of Capie Lake in Mlynická Valley (sample LP01) (Table 1). The population contained virtually only cells with a morphology according to *Sc. tatrae*. Scattered cells of the fungi *Chionaster nivalis* BOHLIN (WILLE) occurred. The habitat conditions of this locality are shown in Table 3. Moreover, snowfields dominated mainly by morphotype *Cr. nivalis* and rarely of *Sc. tatrae* were found in other sampling spots slightly distant from the Okružle Lake (at the shore of Vyšné Kozie Lake in Mlynická Valley – 0.5 km far away; at the shore of Upper Sesterske Lake in Velká Studená Valley – about 10 km far away).

Morphology and ultrastructure

Cell wall surface and intercellular organisation of field samples was described by light and electron microscopy (Figs 5–27). The fusiform cells of *Sc. tatrae* were taxonomically determined by their characteristic surface structures, and the harvested cell stage was tentatively designated as an aplanozygote on the basis of the life cycle proposed by HOHAM & MULLET (1977). The

Table 3. Abiotic habitat parameters and cell sizes of *Chloromonas nivalis* subsp. *tatrae* field samples from the High Tatra Mountains. Electrical conductivity (EC; µS.cm^{−1}), pH of meltwater and snow water content (SWC; %), population density ± SD (standard deviation), average sizes of cells in µm ± SD, length to width ratio (L:W ratio) ± SD and number of cell wall flanges counted at equatorial region of cell in cross–section view are shown.

Sample/reference	EC	pH	SWC	cells per ml meltwater	cell length	cell width	L:W ratio	flanges
LP01 (this study)	15	5.7	52.6±3.8	19950±1995	19.8±1.3	12.8±0.9	1.55 ± 0.12	(9)10–12(14)
KOL (1965)	–	5.2	–	–	18–24	12–15	–	10–12



Figs 5–14. LM micrographs of *Chloromonas nivalis* subsp. *tatrae* subsp. nov.: (5–9) mature aplanozygotes which dominated the field sample, (5–6) cell wall flanges, (7) focus at cross section view of cells in upright position, showing 10 cell wall flanges, (8) cytoplasm containing peripheral reddish astaxanthin depots and central greenish spots of the chloroplast, (9) young aplanozygotes with smooth cell walls were rarely present; (10) ‘old’ cells, preparing for division (most likely meiotic) by contracting the protoplast after being kept in original meltwater for ~100 days; (11–12) in a subsequent step, four elongate daughter cells were developed, still surrounded by the mother cell wall, (11) apical and (12) lateral view of the smooth walled daughter cells; (13–14) empty secondary cell walls showing (13) straight and (14) slightly undulating cell flanges. Scale bar 20 μm .

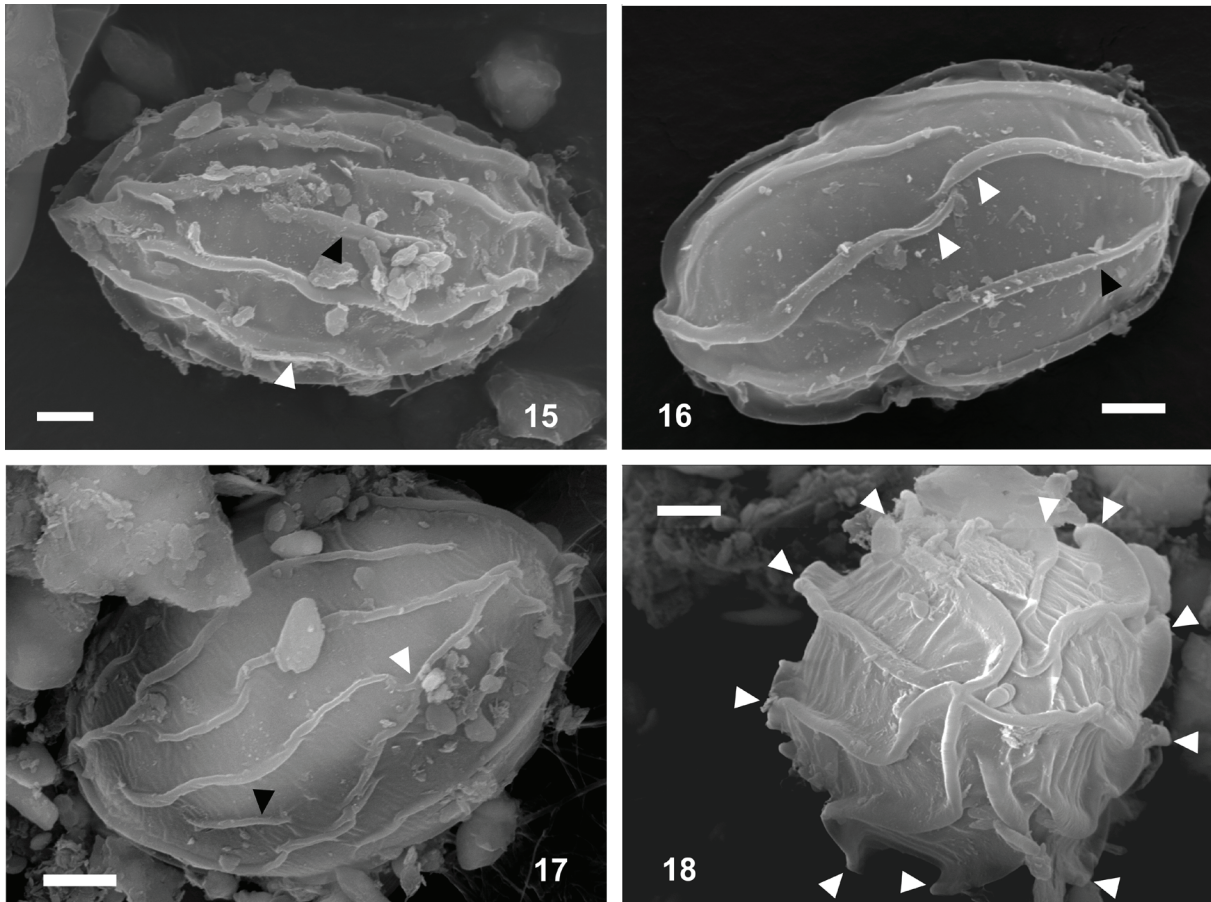
ornamented cell wall structures were made of straight to sometimes slightly undulated flanges (Figs 5–6, 13–14), and LM showed that (9)10–12(14) flanges per cell were present in equatorial region, which became evident at cross-section view (Fig. 7). The average cell sizes are summarised in Table 3. The cytoplasm was almost entirely occupied by lipid bodies containing a secondary pigmentation, thus causing an overall orange impression of the cells (Fig. 8). Rarely, young aplanozygotes surrounded by a smooth (primary) cell wall were observed (Fig. 9). SEM confirmed the presence of 10 to 14 flanges (Fig. 18), and further details of their arrangement could be observed: most common were flanges reaching from pole to pole (Fig. 15) and from one pole nearly to the antapex (Fig. 16). Rarely, flanges reached from one pole only to the equatorial position of the cell (Fig. 16), bifurcations (Fig. 17) or isolated shorter flanges (Fig. 15) also occurred. In a few cases all these secondary surface structures were found on a single aplanozygote. The ultrastructure observed by TEM is presented in Figs 19–27. Three different life cycle stages were recognized. Firstly, ovoid young aplanozygotes still without cell wall flanges, usually with one compact chloroplast containing starch grains (Fig. 19). In a few cases, an undulated cell membrane was found (Fig. 19). Moreover, mitochondria were observed (Fig. 20). Well-developed Golgi bodies and a cytoplasm rich in vesicles and ribosomes indicated an active metabolism (Fig. 21). Vacuoles full of electron dense, sometimes crystalline content were also present

(Fig. 21). Secondly, intermediate aplanozygotes with flanges at the secondary cell wall surface, but still surrounded by a primary cell wall were observed (Figs 22–25). Thirdly, and prevailing in the sample, ‘mature’ aplanozygotes with fully developed flanges. The majority of the cytoplasmatic volume was occupied by large lipid bodies (containing secondary pigments) (Figs. 26–27). Instead of a compact chloroplast, several smaller spherical plastids located around the nucleus were present. Starch grains were very small or absent. Other life cycle stages like vegetative flagellates or any cleaving activities (formation of daughter cells) were not observed directly after sampling.

In order to discriminate *Sc. tatrae* from its’ closest relative, *Cr. nivalis* from the Austrian Alps, cell sizes of aplanozygotes of both snow algae were compared. *Sc. tatrae* aplanozygotes were significantly smaller in term of cell length (17.6–23.1, median 19.5 vs. 18.35–27 μm , median 22.4), width (10.9–16.2, median 12.9 vs. 10.6–16 μm , median 13.2) and length to width ratio (1.33–1.8, median 1.55 vs. 1.38–2.04, median 1.7) (Figs S1–S4). However, significant differences in cell sizes were found also among samples of *Cr. nivalis* (Table. 4).

Population density and cultivation assay

The population density of *Sc. tatrae* (LP01) was $19\,950 \pm 1995$ cells. ml^{-1} meltwater (Table 3). Cultivation assays were unsuccessful, and no cell cleavages have been observed up to three months after inoculation on



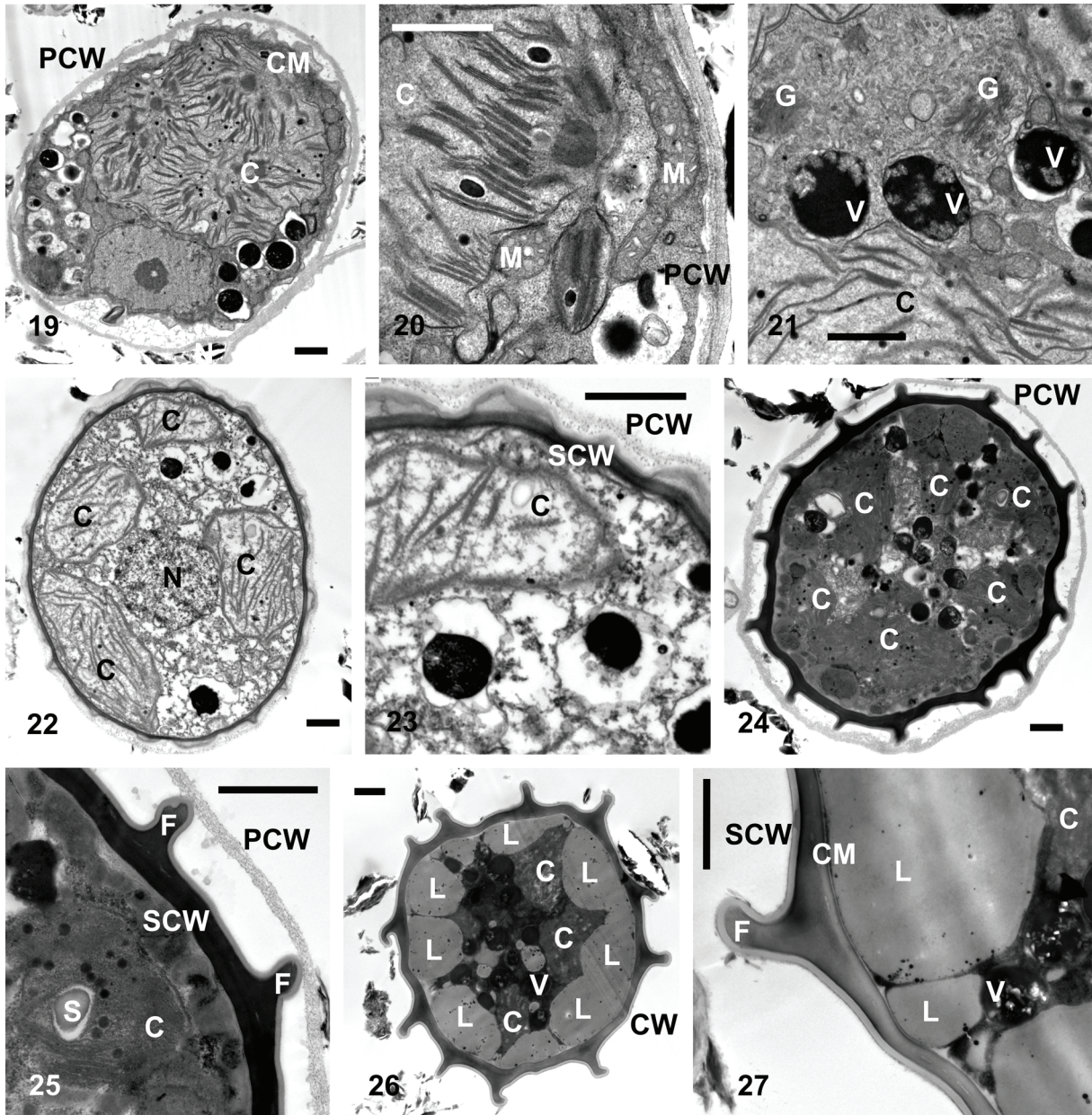
Figs 15–18. SEM micrographs of mature aplanozygotes of *Chloromonas nivalis* subsp. *tatrae* subsp. nov.: (15) cell wall flange reaching from pole to pole (white arrow) and an isolated short flange (black arrow); (16) the flange reaches from pole nearly to antapex (black arrow) and two flanges are reaching from opposite cell poles and finally touching at the equatorial region of the cell (white arrows); (17) two flanges join together, respectively a bifurcation of one flange into two independent is shown (white arrow), moreover, an isolated short flange is present (black arrow); (18) apical view of a cell presenting 10 flanges in total (white arrows). Scale bars 2 μ m.

solid medium. However, in a field sample kept in its original meltwater for approximately 100 days, many cells started to contract the protoplast (Fig. 10) and to generate four elongate daughter cells (4.5–6.7 μ m wide \times 15.4–20.4 μ m long), still surrounded by the mother cell wall (Figs 11–12). The constant number of four daughter cells points to foregoing meiotic divisions. The daughter cell pigmentation was similarly orange–greenish like that of the mother cell before cleavage.

Phylogenetic analysis

The phylogenetic affiliation of *Sc. tatrae* was elucidated based on molecular analysis of three nuclear (18S rDNA, ITS1 rDNA, ITS2 rDNA) and one plastid marker (*rbcL*). The 18S rDNA gene sequence of *Sc. tatrae* was identical with *Cr. nivalis* from the Austrian Alps (sample P24/DR4, accession number GU117576.1, REMIAS et al. 2010) except for two ambiguous bases at the end of the P24/DR4 sequence resulting in identity 99.9% (identical 1697 from 1699 bases). This affiliation was supported by comparing the secondary structures of the ITS2 region between the Slovak and the Austrian populations (letters outside the structure

indicate differences; Fig. 28): Twenty nucleotide differences were found, one in the helices I and II, both of them were located in single stranded regions, ten differences in the most conserved helix III and eight changes in expansion segments between the III. helix and LSU stem. There was no compensatory base change (CBC; changes on both sides of structures which maintain the pairing between nucleotides). One hemi–CBC (hCBC; change only on one side maintaining the pairing) was found in helix III (A–U in *Cr. nivalis* vs. A–G in *Sc. tatrae*, marked by asterisk in Fig. 28). ITS2 rDNA identity was 94.5% (identical 342 out of 362 bp). A close affiliation between both taxa was deduced also from a pairwise comparison of the variable nuclear marker ITS1 rDNA, revealing 98.4% identity (identical 308 of 313 bp; three substitution detected and two ambiguous bases in the P24/DR4 sequence). There was no other more similar ITS2 sequence in public databases which can be used for secondary structure comparison with *Sc. tatrae* since other hits in BLAST search showed identity less than 76% and query cover less than 57%. The plastid marker (*rbcL*) of *Sc. tatrae* was 99.6% identical with the corresponding of *Cr. nivalis* P24/



Figs 19–27. TEM micrographs of *Chloromonas nivalis* subsp. *tatrae* subsp. nov.: (19–21) young ovoid aplanozygotes, (19) young cyst with nucleus (N) smooth primary cell wall (PCW) one compact chloroplast (C) and an undulated cell membrane (CM), (20) detail of a young cyst, additionally showing mitochondria (M), (21) detail of the cytoplasm showing numerous ribosomes and Golgi stacks (G), indicating high metabolic activity, and vacuoles (V) occupied by electron dense, partly crystalline material; (22–25) intermediate aplanozygotes, (22) several smaller peripheral chloroplasts (C) and the nucleus (N), (23) a detail showing a chloroplast (C), the primary (PCW) and the secondary cell wall (SCW), (24) flanges at the secondary cell wall surface surrounded by the primary cell wall (PCW), (25) detail of the primary cell wall (PCW) and the bi-layered secondary cell wall (SCW) with surface flanges (F), peripheral chloroplasts (C) including starch grain (S); (26–27) mature aplanozygotes, (26) fully developed flanges, cytoplasm occupied by large peripheral lipid bodies (L), whereas electron dense vacuoles (V) and chloroplasts (C) are centrally located, (27) detail of the bilayered secondary cell wall (SCW), cell membrane (CM), fully developed flange (F), chloroplast (C) and crystalline content of electron dense vacuoles (V). Scale bars 1 μ m.

DR4 (560 out of 562 bp, two ambiguous bases in P24/DR4 sequence were present in one codon, thus one amino acid in the product of translation was labelled as 'X', sequenced in this study) and showed a sister relationship to *Cr.* sp. 'Gassan B' from Japan (identity 96.5 %, identical 1004 out of 1039 bp, sequence LC012743.1, see the phylogenetic tree – Fig. S14 in MATSUZAKI et al. 2015).

Photosynthesis

In order to test the photosynthetic activity of this snow alga, the performance of field samples was measured under different light levels at the temperature of the melting snow habitat (photosynthesis/irradiance-curves). In general, aplanozygotes of *Sc. tatrae* were physiologically active and exhibited an α value of 0.19 ± 0.01 , a relative ETR_{max} of 21.8 ± 1.0 and an

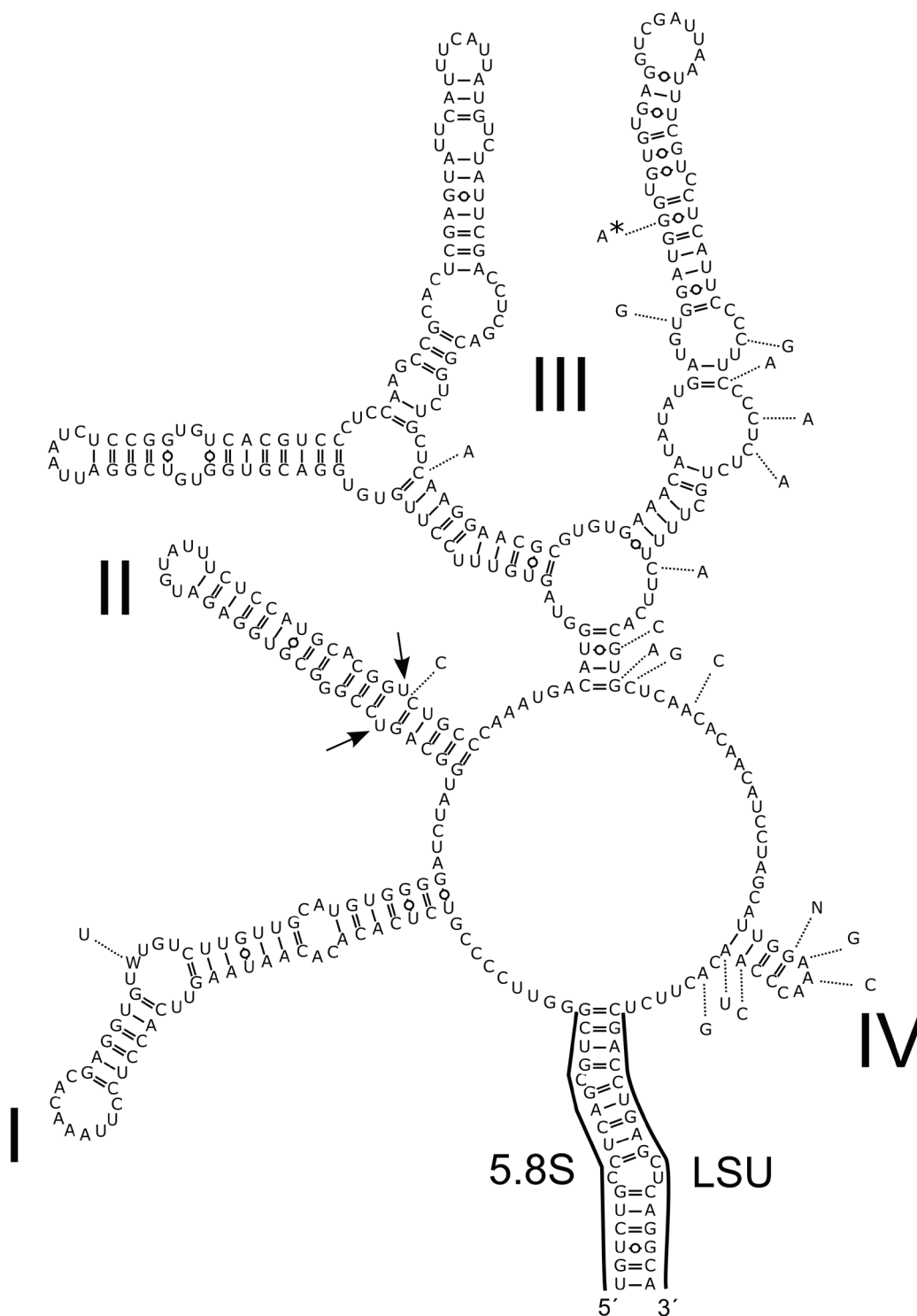


Fig. 28. Comparison of secondary structure of ITS2 rDNA transcripts between *Chloromonas nivalis* subsp. *tatrae* (accession number: KY499614, this study) and *Chloromonas nivalis* from the Austrian Alps (accession number GU117576.1, REMIAS et al. 2010). Note the U–U mismatch in the helix II (arrowheads). Differences characteristic for the latter are shown by nucleotides outside of the structure. The asterisk indicates hemi-compensatory base change.

I_k value of $149 \pm 18 \mu\text{mol} \cdot \text{photons} \cdot \text{m}^{-2} \cdot \text{s}^{-1}$ (Fig. 29). Photoinhibition was noticed from $600 \mu\text{mol} \cdot \text{m}^{-2} \cdot \text{s}^{-1}$ on. For comparison, values of *Cr. nivalis* from the Austrian Alps (from REMIAS et al. 2010) were integrated in Fig. 29 and showed a likewise photosynthetic performance. The only difference was a lower parameter I_k about one

third for *Cr. nivalis* ($I_k = 106 \mu\text{mol} \cdot \text{photons} \cdot \text{m}^{-2} \cdot \text{s}^{-1}$). The irradiance level from which on *Cr. nivalis* was subject to photoinhibition is not known, because application of higher irradiance levels in REMIAS et al. (2010) were not possible due to technical reasons.

Table 4. Statistical significance in differences of aplanozygotes length, width and length to width ratio (L:W) between *Cr. nivalis* subsp. *tatrae* from the High Tatra Mts. and *Cr. nivalis* from the Austrian Alps, and among latter group; ns – not significant.

	<i>Cr. nivalis</i> subsp. <i>tatrae</i> vs. <i>Cr. nivalis</i>	among <i>Cr. nivalis</i>
Length	<0.0001	<0.005
Width	<0.05	<0.05
L:W ratio	<0.0001	n.s.

Pigments

In mature aplanozygotes, chlorophyll-*a* and -*b* accounted for 46.6%, primary (plastidal) carotenoids 12.0% and secondary (non-plastidal) carotenoids 41.4%. The latter were identified as derivatives of the keto-carotenoid astaxanthin by their spectral absorbance and occurred as 3 peaks. Their late retention times the non-polar region (compared to non-derivative astaxanthin standard) of the chromatogram point to the presence of astaxanthin esterified with a variety of different FAs. The ratio astaxanthin to chlorophyll-*a* was 1.465. Other secondary carotenoids were not detected.

Fatty acid composition

The relative content of FAs (as % of total lipids and as % in the three major lipid groups) in *Sc. tatrae* is given in Table 5. FAs with 14 to 18 carbon atoms were detected. The cells had a high level of PUFAs (49 % in total lipids), whereas the content of saturated acids did not exceed 34 % (formed mainly by palmitic acid, 16:0). The main monounsaturated fatty acid (MUFA) was oleic acid (18:1n9, 14 %). The major PUFA were α -linolenic acid (18:3n3, 19%), followed by linoleic acid (18:2n6, 10 %), hexadecatetraenoic acid (16:4n3, 7 %) and steariadic acid (18:4n3, 6 %). There were significant differences in FA composition among the three major lipid classes. The level of saturated lipids was the highest in neutral lipids (48 %), whereas PUFAs were dominant in phospholipids (67.1 %) and glycolipids (69 %) (Table 5). The total lipid content in the biomass was 17.6 % (of dry weight).

Taxonomic treatment

***Chloromonas nivalis* subsp. *tatrae* (KOL) PROCHÁZKOVÁ, REMIAS, ŘEZANKA et NEDBALOVÁ subsp. nov.**

Synonym: *Scotiella tatrae* KOL 1965: 147, figs 1–5, 8–11.

Basionym: *Pteromonas nivalis* CHODAT 1902: 145, fig. 70.

Description: mature zygote (causing the coloured snow phenomenon) elongate to somewhat fusiform, 16.4–24.0 μm long, 10.0–16.2 μm wide, length to width ratio 1.55–1.64, one nucleus, single axial chloroplast or several smaller spherical ones, abundant peripheral lipid globules containing orange carotenoids

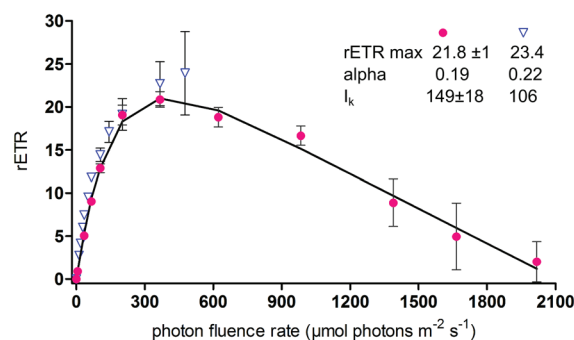


Fig. 29. Comparison of the light-dependent relative electron transfer rate (rETR) between the aplanozygotes of *Chloromonas nivalis* subsp. *tatrae* (full circles, this study) and *Chloromonas nivalis* from the Austrian Alps (open triangles, REMIAS et al. 2010). Values of maximum relative electron transfer rate ($rETR_{max}$), initial slope (α) and saturation irradiance (I_k) for both species are shown. The data points were fitted with the model of photoinhibition according to WALSBY (1997). Each symbol represents the mean value of four and three replicate measurements (\pm SD) for the former and latter species, respectively.

(astaxanthin to chlorophyll ratio \sim 1.5), two layered cell wall, most frequently 10–12 flanges, rarely less (9) or more (up to 14) in the equatorial region of the cell surface; aplanozygote division into four daughter cells, which are smooth-walled elongate 15.4–20.4 μm long, 4.5–6.7 μm wide; occurring in open sites above timberline; flagellates unknown; no pyrenoid or stigma visible; young zygote smooth-walled still without flanges, one compact chloroplast.

Holotype: specimen LP01 deposited at Herbarium of CAUP (Charles University in Prague), material consists of gold coated aplanozygotes.

Iconotype: Figs 5–27.

Etymology: The species epithet *tatrae* is based on the name of the geographic region, the Tatra Mountains, where it was found. It is genitive of the substantive 'Tatra' and this form corresponds with former description of '*Sc. tatrae*' done by Kol.

Type locality: Snow fields close to the rocky shore of Capie Lake (Mlynická Valley), High Tatra Mountains, Poprad District, Slovakia.

Distribution: so far known from snowfields on shores of four alpine lakes: Okružle Lake, Capie Lake, Vyšné Kozie Lake (Mlynická Valley) and Upper Sesterske Lake (Velká Studená Valley) in the High Tatra Mountains, Slovakia.

Remarks: Any deposited material from the first observation of '*Sc. tatrae*' is unknown. KOL (1965) reported 10–12 cell wall flanges on basis of LM. *Cr. nivalis* subsp. *tatrae* differs from *Cr. nivalis* sensu CHODAT (1902) in having mostly 10 or more flanges on cross-section instead of 8–9. Besides, *Cr. nivalis* in the Austrian Alps (REMIAS et al. 2010) differs from subsp. *tatrae* physiologically in the accumulation of

Table 5. Fatty acid composition (as % of total lipids and three major lipid groups) of *Chloromonas nivalis* subsp. *tatrae* field sample (LP01). The table gives only those fatty acids that have abundances greater than 0.1%. The relative proportion of saturated (SAFA), monounsaturated (MUFA) and polyunsaturated (PUFA) fatty acids is also given.

Fatty acid	% total lipids	% neutral lipids	% phospholipids	% glycolipids
14:0	0.1	0.1	0.1	0.1
16:0	23.2	37.3	15.2	13.8
16:1n9	0.9	0.8	1.0	0.9
16:1n7	1.2	1.5	1.3	1.1
16:2n6	1.4	1.5	1.8	1.7
16:3n4	1.7	1.8	2.3	2.1
16:3n3	1.4	1.1	1.5	1.7
16:4n3	6.7	3.2	7.6	8.5
17:1n8	0.4	0.2	0.3	0.5
18:0	10.1	10.8	4.3	5.3
18:1n9	14.1	18.1	9.8	8.5
18:1n7	1.1	1.2	0.9	0.8
18:2n6	10.3	6.4	15.2	12.5
18:3n6	2.0	1.1	2.2	2.1
18:3n3	19.3	12.8	26.7	28.7
18:4n3	6.1	2.1	9.8	11.7
SAFA	33.4	48.2	19.6	19.2
MUFA	17.7	21.8	13.3	11.8
PUFA	48.9	30.0	67.1	69.0

secondary carotenoids (about three times lower astaxanthin to chl-a ratio in mature cells for the former) and slightly larger cell sizes of aplanozygotes: (18.4–27 × 10.6–16 μm). Aplanozygotes of *Cr. nivalis* from North America (HOHAM et MULLET 1977) possess a lower number of flanges at cross-section (six to eight), are larger (16–37 × 10–27 μm) and lack fusing/diverting flanges apart from the apex (the latter are typical for *Cr. nivalis* from the Austrian Alps and for *Cr. nivalis* subsp. *tatrae*).

DISCUSSION

Scotiella tatrae was initially described from red and pink snow in the High Tatra Mountains at Okružle Lake, 2000 m a.s.l. (formerly Döller Lake) where it developed an almost monospecific bloom (KOL 1965). In a much lower extend, *Cr. nivalis* was also present, but no exact proportion to the former was given ('in einer kleineren Menge' according to KOL 1965). In that report, scattered cells of *Chlamydomonas* (*Cd.*)

nivalis (BAUER) WILLE, fungi *Chionaster nivalis* and *Chionaster bicornis* KOL were found as well. We collected our sample from a snow field close to the shore of Capie Lake, which is situated about 150 m south from the place of the initial observation (Fig. 2). Generally, the subspecies *tatrae* seems to be restricted to the High Tatra Mountains and can thus be likely regarded as endemic. A single report of scattered cells from elsewhere (Kühtai region, 2500 m a. s. l., Tyrolean Alps, Austria) by KOL (1970) should be questioned, because such observation of *Sc. tatrae* in Austrian Alps has never been repeated in spite of intensive cryobiological research of this region (REMIAS et al. 2010).

For the population harvested in course of this study, the new name combination *Cr. nivalis* subsp. *tatrae* is proposed, since it shows a very close molecular affiliation to *Cr. nivalis* from the Austrian Alps based on the investigated molecular markers (18S rDNA, ITS1 rDNA, ITS2 rDNA, *rbcL*). CBCs in ITS2 secondary structures correlate with Ernst Mayr's biological species concept (COLEMAN 2009). This hypothesis is also referred to as the CBC species concept. In our study, no CBCs in conserved parts (helices II and III) were detected, however, nucleotide difference in this

variable marker between *Cr. nivalis* subsp. *tatrae* and *Cr. nivalis* of about 5.5 % suggests that a molecular divergence between them is ongoing. In comparison, it was nearly two fold higher than in two strains of *Cd. reinhardtii* P. A. DANGEARD, NIES-2463 and SAG 11-32a, which can cross and produce zygotes (3.3 %, NAKADA et al. 2010). On the other hand, it was slightly less than that between *Microglena basinuclata* DEMCHENKO, MIKHAILYUK & PRÖSCHOLD and *M. monadina* (EHRENBERG) STEIN (5.9 %), recently separated taxa based on polyphasic approach including several CBCs in helix III (DEMACHENKO et al. 2012). On the other hand, even in absence of any CBC, algae may belong to the different species with a probability of 0.24 (WOLF et al. 2013) because total loss of gamete compatibility may be observed sooner than any CBC appear in the most conserved region of helix III (COLEMAN 2009). Between *Cr. nivalis* and subsp. *tatrae*, there were found similarities in the intracellular organization of aplanozygotes, cell sizes, photosynthetic performance and type of preferred habitat (see REMIAS et al. 2010). However, the significant differences in cell wall surface organization, a feature of taxonomic relevance, that seems to be stable considering no detectable changes since first descriptions of this snow alga several decades ago, justified the setup of a new subspecies. It remains open, if hybrids between subsp. *tatrae* and the main form of *Cr. nivalis* occur.

Ecology

Low electrical conductivities and slightly acidic pH were characteristic for the habitat of *Cr. nivalis* subsp. *tatrae* (Table 3). These findings are in good agreement with environmental conditions recorded for *Cr. nivalis* in the Austrian Alps (pH = 4–6.2, EC = 2.8–7.2 $\mu\text{S}\cdot\text{m}^{-2}\cdot\text{s}^{-1}$; REMIAS et al. 2010). pH values of snow meltwater with algae present were summarised in HOHAM et al. (2007). They ranged from 3.8 to 8.1, with *Cr. pichincha* WILLE in the most acidic environment close to coniferous trees (HOHAM 1975) and *Cr. polyptera* (FRITSCH) HOHAM, MULLET & ROEMER in the most alkaline meltwater influenced by a guano input from close penguin colonies (LING & SEPPELT 1998). Similarly high pH of meltwater (7.7–7.9) was caused by input of volcanic ash (LUTZ et al. 2015). Meltwater conductivities with snow algae present varied from <1 to 950 $\mu\text{S}\cdot\text{m}^{-2}\cdot\text{s}^{-1}$. For instance, the very low values were found in arctic habitats of red orange cells affiliated to clade of *Cd. nivalis* (EC= 0.83) and *Cr. nivalis* (EC= 7.4) in Svalbard (MÜLLER et al. 1998). High EC was reported from the environment of *Cr. polyptera* in Antarctica in close proximity to bird colonies (LING & SEPPELT 1998). The snow water contents in snow surface samples containing *Cr. nivalis* subsp. *tatrae* are in good agreement with *Cr. nivalis* (45–52 %; HOHAM & MULLET 1977). This parameter is influenced by air temperatures during day and depends also to the depth of sampling (HOHAM & MULLET 1977). Generally, the

availability of liquid water in the snow influences the life cycle development of *Chloromonas* snow algae: sexual stages occur if SWC is lower (47–54 %), whereas the asexual phase dominate during a higher SWC values (57–63 %, HOHAM & DUVAL 2001). The population density of *Cr. nivalis* subsp. *tatrae* was twice times higher than the detection limit from which on snow discolouration can be recognized by bare eyes ($>10^4$ cells per ml^{-1} of meltwater; HOHAM & DUVAL 2001). Generally, the intensity of colouration may change in dependence on the cellular pigment composition, prevailing life cycle stage and the seasonality. Due to melt water flush out processes, cryoflora can have an important impact on biota feeding on algae in adjacent lakes. The period of serious acidification of the High Tatra lakes in the 20th century was accompanied with a decrease of phytoplankton biomass to nearly zero values. The inflow of cryoflora (probably mainly *Cr. nivalis* subsp. *tatrae*) into Ochrúhle Lake was thus believed to be the key food supply for planktonic calanoid copepod *Arctodiapomus alpinus* IMHOF that enabled its survival despite of the acidification-induced processes of oligotrofication (HOŘICKÁ et al. 2006).

Morphology and ultrastructure

The aplanozygote sizes of ‘rediscovered’ populations of *Sc. tatrae* ($16.4\text{--}24 \times 10\text{--}16.2 \mu\text{m}$) fit to the original description ($18\text{--}24 \times 12\text{--}15 \mu\text{m}$; KOL 1965). The morphological similarity of ‘*Sc. tatrae*’ and *Cr. nivalis* (formerly *Sc. nivalis*) was confirmed earlier by a cluster analysis where all species with *Scotiella*-like morphology were included (KOMÁROMY 1982). The striking difference is a morphologic variation: most commonly 10 to 12 flanges per cell in cross-section typical are a constant feature for *Cr. nivalis* subsp. *tatrae*. On the contrary, *Cr. nivalis* aplanozygotes from the Austrian Alps have usually 8 to 9 flanges only (REMIAS et al. 2010). In both taxa, the organization of flanges is consistent, except for the rare case of two flanges reaching from opposite cell poles and finally touching at the equatorial region of the cell (Fig. 16), which has not been observed in *Cr. nivalis* from Alps. The aplanozygote sizes of the new subspecies were slightly smaller than those of the relative from the Alps. However, a large variability of aplanozygote lengths among samples of *Cr. nivalis* (Fig. S1, Table 4) is probably reflecting individual growth conditions depending on the date of sampling in course of the season, and furthermore the abiotic microhabitat and weather conditions before sampling. The known life cycle of *Cr. nivalis* comprises vegetative flagellates which cleave into two, four, eight or sixteen daughter cells. Daughter cells behave as zoospores or gametes. Generative fusion of two gametes leads to development of a quadriflagellate motile zygote. After a while, loss of flagella takes place (transformation to an aplanozygote), the primary cell wall is shed and exposing the developing secondary wall structures of the zygote (HOHAM & MULLET

1977). For *Cr. nivalis* for the Alps, swarmers with four flagella were many times found in the field, another indication of sexual reproduction is the empty shed cell wall directly after the putative fusion (REMIAS et al. 2010). As subsp. *tatrae* is closely related to the main form, assumption was made that observed cells were aplanozygotes indeed. This concept is supported by the observation of a fading primary cell wall in this study, surrounding young aplanozygotes ('PCW' in Figs 19–20). The secondary aplanozygote cell wall is formed below ('SCW' in Figs 22–25) and later made of two distinguishable layers, whereat the inner layer is more electron-dense (Figs 26–27). Differently to our own field observations, LING & SEPPELT (1998) and HOHAM et al. (2002) reported that two snow algal species from the genus *Chloromonas* can form cysts directly from vegetative flagellates without sexual fusion (vegetative hypnoblasts). *Cr. nivalis* subsp. *tatrae* zygotes started to cleave in original meltwater approximately 100 days after sampling and developed four elongate daughter cells. Timing of cleavage and daughter cell shapes were consistent with observation for *Cr. nivalis* from the North America. Cell sizes were about one third larger for the latter one (6–10 µm × 19–28 µm in HOHAM & MULLETT (1977).

Cytosolic, electron dense vacuoles, commonly filled with striking crystalline structures at the TEM level (Fig. 21), play a role in intracellular polyphosphate and polyamine storage (OTA et al. 2016). Despite their abundant presence, they have been frequently neglected for microalgae. *Cr. nivalis* subsp. *tatrae* possesses these membrane-bound depots, like many other snow algae (REMIAS 2012). Accordingly, ubiquitous lipid bodies play a significant role to overcome demanding situations in the beginning of the seasonal life cycle (e. g. as storage of energy for flagellate migration towards snow surface in spring). Their localization at the cell periphery, together with the accompanying accumulation of astaxanthin, provides a protection of centrally located organelles like chloroplast and nucleus against harmful UV or excessive visible irradiation. The reorganization of a single chloroplast of vegetative cells (Fig. 19 – note thylakoids arranged in distinct clusters, a putative preparation for plastid rearrangement) into several smaller sections during aplanozygote maturation (Figs 22, 26) has been observed at all known species of *Chloromonas* from snow (REMIAS et al. 2010). Several plastids types may be present in a single species during its life cycle, such as occur in *Cr. chenangoensis* HOHAM, BERMAN, ROGERS, FELIO, RYBA et MILLER and *Cr. tughillensis* HOHAM, BERMAN, ROGERS, FELIO, RYBA et MILLER from snow (HOHAM et al. 2006). Thus, paying attention only to vegetative stages of chlamydomonads kept in laboratory cultures can lead to partly misleading conclusions in case much emphasis is placed on chloroplast morphology (MATSUZAKI et al. 2014, 2015), but the change of plastid shapes during life cycle is not considered. Physiological adaptation of observed

intracellular reorganisation may be following: this raise in plastid membrane surface to volume ratio provides probably advantages due to better metabolite exchange for survival in drastically changing cold habitats at the end of growing season. Also the development secondary cell wall flanges during aplanozygote maturation can be generally regarded as a mechanism of mechanical protection, which becomes effective after complete snowmelt and cells are subject to draught when exposed at bare rock surfaces (REMIAS 2012).

Other genetically and morphologically related snow algal species

Zygotes of *Cr. cf. nivalis* have been recorded from all continents except Australia (KOL 1968; DUVAL et al. 1999). However, according to 18S rDNA and *rbcl* phylogeny, *Cr. nivalis*-like aplanozygotes were found in at least four independent lineages, and each lineage is located in a different geographic region (Japan, Svalbard, North America and Europe; see the phylogenetic tree in Fig. S13 in MATSUZAKI et al. 2015), suggesting a geographical barrier of dispersion or isolation. Another explanation could be an independent snow colonization several times in the evolution history of '*Cr. cf. nivalis*'.

Zygotes of the snow alga *Cr. pichincha* from the North America were reported to resemble '*Sc. tatrae*' in number of flanges per cell [(6)9–11(15)] and cell size (17–20 × 11–14 µm) (HOHAM 1975). Accordingly, HOHAM & MULLETT (1978) suggested in their taxonomic notice that '*Sc. tatrae*' is a zygotic stage of *Cr. pichincha*. However, strain *Cr. pichincha* UTEX SNO 33 is well separated from the *Cr. nivalis* from the Austrian Alps according to 18S phylogeny (see Fig. S13 in MATSUZAKI et al. 2015). Independent evolution can be inferred also from ecology, because *Cr. pichincha* prefers shaded habitat under heavy forest canopy (HOHAM 1975) whereas *Cr. nivalis* subsp. *tatrae* causes blooms at exposed sites above timberline. *Cr. hohamii* LING & SEPPELT is another morphologically related snow algae, however with a higher numbers of usually undulating flanges per cell [12–16(20)] (HOHAM et al. 1983; LING & SEPPELT 1998). Additionally, it has, like in the case of *Cr. pichincha*, a different molecular affiliation than *Cr. nivalis* subsp. *tatrae*. The 18S rDNA sequence of *Cr. hohamii* UTEX SNO 67 represents an independent lineage (see Fig. S13 in MATSUZAKI et al. 2015) which is also supported by a different geographical distribution (HOHAM et al. 1983, LING & SEPPELT 1998). The sister lineage to *Cr. nivalis* from the Austrian Alps (and thus to *Cr. nivalis* subsp. *tatrae*) is represented by *Cr. polyptera* (based on 18S phylogeny in MATSUZAKI et al. 2015), a snow algae described from Maritime Antarctica (FRITSCH 1912). The putative vegetative hypnoblasts of this species occur in coastal, penguin-influenced places and differ morphologically in possessing a very high number of flanges (18–23 per cell; AKIYAMA 1979), in preference of neutral to alkaline pH

(6.7–8.1; LING & SEPPELT 1998) and in elevated supply of nutrients from bird colonies (electrical conductivity 56–950 $\mu\text{S}\cdot\text{cm}^{-1}$ in LING & SEPPELT 1998; 42–95 $\mu\text{S}\cdot\text{cm}^{-1}$ in REMIAS et al. 2013). Contrary, habitat conditions *Cr. nivalis* subsp. *tatrae* are characterised by low conductivities and slightly acidic pH (Table 3).

Recent approaches use effective high-throughput sequencing protocols to elucidate OTUs (operational taxonomic units) and their abundances in whole cryoflora communities, thus describing the biodiversity of snow microbiomes (LUTZ et al. 2016). Apparently, the use of a single gene for eukaryotes, especially when only sections of the conservative 18S rDNA are available by this method in the context of Chlorophyta, does not provide sufficient resolution to reflect the actual taxonomic richness. *Cr. nivalis* subsp. *tatrae* is an example that a ‘rare’ or regionally distributed taxon could be overseen depending on the used gene, because clear morphologic differences to the standard form of *Cr. nivalis* cannot be evaluated by using 18S rDNA.

Pigment composition

The survival of microalgae at exposed, nutrient-poor snow surfaces frequently goes along with the accumulation of secondary carotenoids (REMIAS 2012). On the one hand, these pigments effectively absorb excessive visible and near ultraviolet irradiation, thus protecting the photosystems against photoinhibition (BIDIGARE et al. 1993). On the other hand, carotenoids are nitrogen-free compounds which can be abundantly synthesized also in nitrogen-poor habitats. So far, Chlorophycean snow algae have been reported to accumulate exclusively astaxanthin and derivatives, which are stored in cytoplasmic lipid globules (REMIAS et al. 2016). It is the same with *Cr. nivalis* subsp. *tatrae*, which’s pigments have, to our knowledge, been analysed for the first time. Generally, the cellular amount of astaxanthin in microalgae is illustrated as a relative ratio to chlorophyll (BIDIGARE et al. 1993; REMIAS & LÜTZ 2007). This ratio reflects either the level of aplanozygotes maturity during life cycle (the higher ratio, the older the cells; REMIAS et al. 2010), or in a tentative chemotaxonomical approach, it shows a distinct range of ratios found for certain clades or taxa. For example, the astaxanthin to chlorophyll ratio was three times higher for mature aplanozygotes of *Cr. nivalis* subsp. *tatrae* than that of comparable cells of *Cr. nivalis* from the Austrian Alps (REMIAS et al. 2010). This suggests a higher tolerance to excessive irradiation for the former population, but still five times lower values in comparison with dark red cells of the common snow alga *Cd. nivalis*, which is usually found at the most exposed high alpine and polar sites (REMIAS et al. 2005). The relative proportions of pigment classes in aplanozygotes of *Cr. nivalis* subsp. *tatrae* and *Cr. nivalis* (REMIAS et al. 2013) slightly differ, containing twice as many secondary carotenoids, but one third less primary carotenoids and one quarter less chlorophylls for the former alga. In both

cases, astaxanthin was the only secondary carotenoid. Accordingly, the cellular astaxanthin content reflects the specific snow coloration such as brownish–red for subsp. *tatrae* or blood– to crimson red snow for *Cd. nivalis* (REMIAS et al. 2005).

Photosynthesis

The adaptation of *Cr. nivalis* subsp. *tatrae* to rather high irradiation conditions can be deduced not only from abundant levels of astaxanthin, but also from its photosynthetic performance, such as high light saturation point ($I_k = 149$), light saturation rate ($\text{ETR}_{\text{max}} = 21.8$) and the irradiance level from which on, photoinhibition takes place ($600 \mu\text{mol photons m}^{-2}\cdot\text{s}^{-1}$). Moreover, photosynthesis showed positive rETR values even at irradiance levels ($< 2100 \mu\text{mol photons m}^{-2}\cdot\text{s}^{-1}$) close to full sunlight (up to $2500 \mu\text{mol photons m}^{-2}\cdot\text{s}^{-1}$ at Ľadové Lake with an elevation of 2057 m, the High Tatra Mountains; unpublished results from the automatic meteorological station). Cells may be subject to such irradiances and have to cope with photoinhibition when they are accumulated on snow surface due to proceeding snow melt. Additionally, this species is also able to perform well under low light conditions: Since penetration of irradiation decreases logarithmically with depth of snow column (GORTON & VOGELMAN 2003), a high alpha value of 0.19 supports cells located a few centimetres below the snow surface to perform positively. In comparison, mature aplanozygotes of *Cr. nivalis* from the Austrian Alps seems to be saturated by light at slightly lower irradiance levels ($I_k = 106$) what is probably related to their lower astaxanthin content. Flagellate stages of *Cr. nivalis* are lacking secondary pigments (HOHAM & MULLET 1977). One of their protective mechanisms against high irradiance is believed to be the active migration to deeper parts of the snow pack (KVÍDEROVÁ 2010). Diurnal decrease of rETR and alpha value during noon and successful recovery a few hours later in response to irradiance at open sites was documented for vegetative flagellates tentatively designed as *Cr. cf. nivalis* (KVÍDEROVÁ 2010). The preference of low irradiances (about $100 \mu\text{mol photons m}^{-2}\cdot\text{s}^{-1}$) for flagellate stages of *Cr. nivalis* originating from shady sites was demonstrated (STIBAL 2003). Similar irradiance levels below tree canopy were found in the upper 5 cm of snowpacks containing populations of *Cr. hohamii* and *Cr. nivalis* in the North America (HOHAM et al. 1998) and were proven to be optimal for mating of *Cr. tughillensis* and *Cr. chenangoensis* at lab conditions (HOHAM et al. 2006). In our study, we have shown physiological borders for photosynthesis of aplanozygotes of *Cr. nivalis* subsp. *tatrae*, whereas growing optima of vegetative stages remain unknown due to a lack of cultures.

Fatty acid composition

The desaturation of FAs in biomembranes is considered as one of the main mechanisms of adaptation and acclimation of photosynthetic microorganism to cold

environments (MORGAN–KISS et al. 2006). The number and position of double bonds together with FA chain length markedly influence melting point (MP) of FA and thus fluidity, permeability and stability of biological membranes (e.g. MP = –11.58 °C for α -linolenic acid; MP = 65.45 °C for palmitic acid, 16:0; KNOTHE & DUNN 2009). For example, the levels of oleic acid (18:1n9) and α -linolenic acid (18:3n3) decreased in thylakoid membranes upon increase of exposure temperatures from low to mesophilic (LUKEŠ et al. 2014). The α -linolenic acid as the dominant unsaturated FA in cells of *Cr. nivalis* subsp. *tatrae* (19.3 % in total lipids) is consistent with profiles of other *Chloromonas* species harvested from snow (*Cr. pichincha*, 22.9–25.7%; ŘEZANKA et al. 2014) or of a strain kept in nitrogen deficient medium (*Cr. nivalis* CCCryo 005–99, ~35%; SPIJKERMAN et al. 2012). A high contribution of this FA seems to be typical for all 22 *Chloromonas* species screened in the study of LANG et al. (2011) (average 27 %). On the contrary, snow algae from a different clade related to *Cd. nivalis*, show a dominance of oleic acid (~59 %; BIDIGARE 1993; ~45 %; SPIJKERMAN et al. 2012), suggesting that phylogenetic aspects can play a role in native FA patterns within the Chlamydomonadales. This study showed that FAs containing C16 and C18 chains with 0 to 4 double bonds were dominating in aplanozygotes of *Cr. nivalis* subsp. *tatrae*. A different profile with dominating medium to long chain FAs of C11 to C18 chains with 0 to 5 double bonds were found in snow dwelling flagellates of *Cr. brevispina* (FRITSCH) HOHAM, ROEMER & MULLETT (ŘEZANKA et al. 2008). The high level of PUFAs of *Cr. nivalis* subsp. *tatrae* (48%) is comparable with field samples of other *Chloromonas* species from snow (*Cr. brevispina*, 74%, ŘEZANKA et al. 2008; *Cr. pichincha*, 59–70%, ŘEZANKA et al. 2014) and reflects a suitable strategy for life at temperatures close freezing point (KVIDEROVÁ 2010). The proportion of PUFAs in *Cr. nivalis* subsp. *tatrae* was nearly 70% in lipid groups associated with membranes, and it was twice lower in neutral lipids which are likely deposited in cytosolic lipid bodies as storage products (THOMPSON 1996). Generally, this is in agreement with data published on other microalgae, where PUFA content of the glycolipid and phospholipid fractions was higher than that of the neutral lipid fraction (e.g. HENDERSON et al. 1998). However, this pattern is extremely pronounced in *Cr. nivalis* subsp. *tatrae* suggesting that the high accumulation of PUFAs in membranes is important for its survival in the harsh snow environment.

CONCLUSION

In summary, *Cr. nivalis* subsp. *tatrae* can be presumably regarded as an endemic variation of a common cryoflora species. It has been found so far only in the High Tatra Mountains (Slovakia). According to the analysis of several molecular markers, it is closely

related to *Cr. nivalis* from the Austrian Alps. Despite having similar physiological performance and ecological requirements, they differ in the abundance of secondary carotenoids and certain morphological traits. Aplanozygotes (*Cr. hohamii* and *Cr. pichincha*) and putative vegetative hypnoblasts (*Cr. polyptera*) of further morphologically similar species living in snow can be distinguished by different habitat ecology, molecular traits and morphological details like number of flanges. High levels of polyunsaturated fatty acids were detected especially in membrane lipids. The taxonomic affiliation of *Cr. cf. nivalis*-like species inhabiting further localities in the High Tatra Mountains listed in (KOL 1975a, b) and LUKAVSKÝ (1994) is still unclear. A phylogenetic position of other *Scotiella* species associated with snow (e.g. *Sc. norvegica* KOL) is lacking. To our experience, establishing cultures from aplanozygotes remains difficult. A polyphasic approach including molecular analysis of multiple DNA regions, description of ecology, cytology and physiology might help to reveal species identity of snow algae and evaluate biodiversity of polar and alpine regions.

ACKNOWLEDGEMENTS

This work was supported by Czech Science Foundation (GACR) project 17–00027S. We are grateful to Tomáš Hájek (University of South Bohemia in České Budějovice, Czech Republic) for technical assistance and Siegfried Aigner (University of Innsbruck, Institute of Botany, Austria) for assistance with HPLC analysis. We thank an anonymous reviewer for constructive comments.

REFERENCES

- AKIYAMA, M. (1979): Some ecological and taxonomic observations on the colored snow algae found in Rumpa and Skarvsnes, Antarctica. – Mem. Natl. Inst. Polar Res. Spec. Issue 11: 27–34.
- BIDIGARE, R.R.; ONDRUSEK, M.E.; ITURRIAGA, R.; HARVEY, H.R.; HOHAM, R.W. & MACKO, S.A. (1993): Evidence for a photoprotective function for secondary carotenoids of snow algae. – J. Phycol. 29: 427–434.
- BISCHOFF, H.W. & BOLD, H.C. (1963): Phycological studies. IV. Some soil algae from Enchanted Rock and related algal species. – University of Texas, Publications 6318: 1–95.
- BLIGH, E.G. & DYER, W.J. (1959): A rapid method of total lipid extraction and purification. – Can. J. Biochem. Physiol. 37: 911–917.
- BUCHHOLZ, J. (1793): Beschreibung des wundervollen Karpatischen Schnee–Gebirges. – Ung. Mag. Pressburg, 3–47.
- CHODAT, R. (1902): Algues vertes de la Suisse. Pleurococcoïdes – Chrooléoïdes. Beiträge Kryptogamenflora der Schweiz. Band I, Heft 3. – pp. 1–373. Berne: Druck und Verlag von K.–J. Wyss, Libraire–Éditeur.
- COLEMAN, A.W. (2007): Pan–eukaryote ITS2 homologies revealed by RNA secondary structure. – Nucleic Acids Res. 35: 3322–3329.
- COLEMAN, A. (2009): Is there a molecular key to the level of ‘biological species’ in eukaryotes? A DNA guide.

- Mol. Phylogenet. Evol. 50: 197–203.
- CVETKOVSKA, M.; HÜNER, N.P.M. & SMITH, D.R. (2016): Chilling out: the evolution and diversification of psychrophilic algae with a focus on Chlamydomonadales. – Polar Biol., doi:10.1007/s00300-016-2045-4.
- DEMACHENKO, E.; MIKHAILYUK, T.; COLEMAN, A. & PRÖSCHOLD, T. (2012): Generic and species concepts in *Microglena* (previously the *Chlamydomonas monadina* group) revised using an integrate approach. – Eur. J. Phycol., 47: 264–290.
- DEMBITSKY, V.M.; ŘEZANKA, T.; BYCHEK, I.A. & SHUSTOV, M.V. (1991): Identification of fatty-acids from *Cladonia* lichens. – Phytochemistry 30: 4015–4018.
- DE MAAYER, P.; ANDERSON, D.; CARY, C. & COWAN, D.A. (2014): Some like it cold: understanding the survival strategies of psychrophiles. – EMBO Rep. 15: 508–517.
- DUVAL, B.; DUVAL, E. & HOHAM, R.W. (1999): Snow algae of the Sierra Nevada, Spain, and High Atlas mountains of Morocco. – Internat. Microbiol. 2: 39–42.
- ETTL, H. & GÄRTNER, G. (2014): Syllabus der Boden-, Luft- und Flechtenalgen. – 773 pp., Springer, Berlin, Heidelberg.
- FRICTSCH, F.E. (1912): Freshwater algae collected in the South Orkneys by Mr. R. N. Rudmose Brown, B.Sc. of the Scottish National Antarctic Expedition, 1902–04. – J. Linn. Soc. London Botany 40: 293–338.
- GENTY, B.; BRIANTAIS, J.-M. & BAKER, N.R. (1989): The relationship between the quantum yield of photosynthetic electron transport and quenching of chlorophyll fluorescence. – Biochim. Biophys. Acta (BBA) – General Subjects 990: 87–92.
- GOFF, L.J. & MOON, D.A. (1993): PCR amplification of nuclear and plastid genes from algal herbarium specimens and algal spores. – J. Phycol. 29: 381–384.
- GORTON, H.L. & VOGELMAN, T.C. (2003): Ultraviolet Radiation and the Snow Alga *Chlamydomonas nivalis* (Bauer) Wille. – Photochem. Photobiol. 77: 608–615.
- HANAGATA, N. (1998): Phylogeny of the subfamily Scotiellocoystoideae (Chlorophyceae, Chlorophyta) and related taxa inferred from 18S ribosomal RNA gene. – J. Phycol. 24: 1049–1054.
- HELMS, G.; FRIEDL, T.; RAMBOLD, G. & MAYRHOFER, H. (2001): Identification of photobionts from the lichen family Physciaceae using algal-specific ITS rDNA sequences. – Lichenologist 33: 73–86.
- HENDERSON, R.J.; HEGSETH, E.N. & PARK, M.T. (1998): Seasonal variation in lipid and fatty acid composition of ice algae from the Barents Sea. – Polar Biol. 20: 48–55.
- HOHAM, R.W. (1975): The life history and ecology of the snow alga *Chloromonas pichincha* (Chlorophyta, Volvocales). – Phycologia 14: 213–226.
- HOHAM, R.W. & MULLET, J.E. (1977): The life history and ecology of the snow alga *Chloromonas cryophila* sp. nov. (Chlorophyta, Volvocales). – Phycologia 16: 53–68.
- HOHAM, R.W. & MULLET, J.E. (1978): *Chloromonas nivalis* (Chod.) Hoh. & Mull. comb. nov., and additional comments on the snow alga, *Scotiella*. – Phycologia 17: 106.
- HOHAM, R.W. & DUVAL, B. (2001): Microbial ecology of snow and freshwater ice. – In: JONES, H.G.; POMEROY, J.W.; WALKER, D.A. & HOHAM, R.W. (eds): Snow Ecology: An Interdisciplinary Examination of Snow-Covered Ecosystems. – pp. 168–228, Cambridge University Press, Cambridge.
- HOHAM, R.W.; MULLET, J.E. & ROEMER, S.C. (1983): The life history and ecology of the snow alga *Chloromonas polyptera* comb. nov. (Chloropyta, Volvocales). – Can. J. Bot. 61: 2416–2429.
- HOHAM, R.W.; SCHLAG, E.M.; KANG, J.Y.; HASSELWANDER, A.J.; BEHRSTOCK, A.F.; BLACKBURN, I.R.; JOHNSON, R.C. & ROEMER, S.C. (1998): The effects of irradiance levels and spectral composition on mating strategies in the snow alga, *Chloromonas* sp.-D, from the Tughill Plateau, New York State. – Hydrol. Process. 12: 1627–1639.
- HOHAM, R.W.; BONOME, T.A.; MARTIN, C.W. & LEEBENS-MACK, J.H. (2002): A combined 18S rDNA and *rbcL* phylogenetic analyses of *Chloromonas* and *Chlamydomonas* (Chlorophyceae, Volvocales) emphasizing snow and other cold-temperature habitats. – J. Phycol. 38: 1051–1064.
- HOHAM, R.W.; BERMAN, J.D.; ROGERS, H.S.; FELIO, J.H.; RYBA, J.B. & MILLER, P.R. (2006): Two new species of green snow algae from Upstate New York, *Chloromonas chenangoensis* sp. nov. and *Chloromonas tughillensis* sp. nov. (Volvocales, Chlorophyceae) and the effects of light on their life cycle development. – Phycologia 45: 319–330.
- HOHAM, R.W.; FILBIN, R.W.; FREY, F.M.; PUSACK, T.J.; RYBA, J.B.; McDERMOTT, P.D. & FIELDS, R.A. (2007): The Optimum pH of the green snow algae, *Chloromonas tughillensis* and *Chloromonas chenangoensis*, from Upstate New York. – Arct. Antarct. Alp. Res. 39: 65–73.
- HOŘICKÁ, Z.; STUHLÍK, E.; HUDEC, I.; ČERNÝ, M. & FOTT, J. (2006): Acidification and the structure of crustacean zooplankton in mountain lakes: The Tatra Mountains (Slovakia, Poland). – Biologia, 61/Suppl. 18: S121–S134.
- KATANA, A.; KWIATOWSKI, J.; SPALIK, K.; ZAKRYŚ, B.; SZALACHA, E. & SZYMAŃSKA, H. (2001): Phylogenetic position of *Koliella* (Chlorophyta) as inferred from nuclear and chloroplast small subunit rDNA. – J. Phycol. 37: 443–451.
- KATES, M. & VOLCANI, B.E. (1996): Biosynthetic pathways for phosphatidylsulfocholine, the sulfonium analogue of phosphatidylcholine, in diatoms. – In: KIENE, R.P.; VISSCHER, P.T.; KELLER, M.D. & KIRST, G.O. (eds): Biological and Environmental Chemistry of DMSP and Related Sulfonium Compounds. – pp. 109–119, Springer, New York.
- KNOTHE, G. & DUNN, R.O. (2009): A comprehensive evaluation of the melting points of fatty acids and esters determined by differential scanning calorimetry. – J. Am. Oil Chem. Soc. 86: 843–856.
- KOL, E. (1965): Roter Schnee von *Scotiella* in der Hohen Tatra. – Ann. Hist.-Nat. Mus. Natl. Hung. 57: 146–148.
- KOL, E. (1968): Kryobiologie I. Kryovegetation. – In: ELSTER, J. & OHLE, W. (eds): Die Binnengewässer 24. – 216 pp., Schweizerbart, Stuttgart.
- KOL, E. (1970): Vom roten Schnee der Tiroler Alpen. – Ann. Hist.-Nat. Mus. Natl. Hung. 62: 129–136.
- KOL, E. (1975a): Cryobiological researches in the High Tatra I. – Acta Bot. Hung. 21: 61–75.
- KOL, E. (1975b): Cryobiological researches in the High Tatra

- II. – Acta Bot. Hung. 21: 279–287.
- KOETSCHAN, C.; FÖRSTER, F.; KELLER, A.; SCHLEICHER, T.; RUDERISCH, B.; SCHWARZ, R.; MÜLLER, T.; WOLF, M. & SCHULTZ, J. (2010): The ITS2 Database III – sequences and structures for phylogeny. – Nucleic Acids Res. 38: D275–279.
- KOMÁREK, J. & NEDBALOVÁ, L. (2007): Green cryosestic algae. – In: SECKBACH, J. (ed.): Algae and Cyanobacteria in Extreme Environments. – pp. 321–342, Springer, Dordrecht.
- KOMÁROMY, Z.P. (1982): Application of cluster analysis in the taxonomy of *Scotiella* species (Chlorophyceae). – Arch. Hydrobiol. Suppl. 60: 432–438.
- KŘÍSTEK, Š.; HOLUŠA, J.; URBAŇCOVÁ, N.; TROMBIK, J. & DRÁPELA, K. (2011): Expeditionary measurements of snow in extensively forested Carpathian Mountains: evaluating parameters variability. – Carpath. J. Earth Environ. Sci. 6: 45–58.
- KVÍDEROVÁ, J. (2010): Characterization of the community of snow algae and their photochemical performance *in situ* in the Giant Mountains, Czech Republic. – Arct. Antarct. Alp. Res., 42: 210–218.
- LANG, I.; HODAČ, L.; FRIEDL, T. & FEUSSNER, I. (2011): Fatty acid profiles and their distribution patterns in microalgae: a comprehensive analysis of more than 2000 strains from the SAG culture collection. – BMC Plant Biol. 11: 124.
- LING, H.U. & SEPPELT, R.D. (1998): Snow algae of the Windmill Islands, continental Antarctica. 3. *Chloromonas polyptera* (Volvocales, Chlorophyta). – Polar Biol. 20: 320–324.
- LUKAVSKÝ, J. (1994): Algal flora of lakes in the High Tatra Mts. (Slovakia). – Hydrobiologia: 274: 65–74.
- LUKEŠ, M.; PROCHÁZKOVÁ, L.; SHMIDT, V.; NEDBALOVÁ, L. & KAFTAN, D. (2014): Temperature dependence of photosynthesis and thylakoid lipid composition in the red snow alga *Chlamydomonas* cf. *nivalis* (Chlorophyceae). – FEMS Microbiol. Ecol. 89: 303–315.
- LUTZ, S.; ANESIO, A.M.; EDWARDS, A. & BENNING, L.G. (2015): Microbial diversity on Icelandic glaciers and ice caps. – Front Microbiol 6: 307.
- LUTZ, S.; ANESIO, A.M.; RAISWELL, R.; EDWARDS, A.; NEWTON, R.J.; GILL, F. & BENNING, L. – G. (2016): The biogeography of red snow microbiomes and their role in melting arctic glaciers. – Nat. Commun. 7: 11968, doi:10.1038/ncomms11968.
- MATSUZAKI, R.; HARA, Y. & NOZAKI, H. (2014): A taxonomic study of snow *Chloromonas* species (Volvocales, Chlorophyceae) based on light and electron microscopy and molecular analysis of cultured material. – Phycologia 53: 293–304.
- MATSUZAKI, R.; KAWAI-TOYOOKA, H.; HARA, Y. & NOZAKI, H. (2015): Revisiting the taxonomic significance of aplanozygote morphologies of two cosmopolitan snow species of the genus *Chloromonas* (Volvocales, Chlorophyceae). – Phycologia 54: 491–502.
- MIKHAILYUK, T.I.; SLUIMAN, H.J.; MASSALSKI, A.; MUDIMU, O.; DEMCHENKO, E.M.; KONDRATYUK, S.Y. & FRIEDL, T. 2008. New streptophyte green algae from terrestrial habitats and an assessment of the genus *Interfilum* (Klebsormidiophyceae, Streptophyta). – J. Phycol. 44: 1586–1603.
- MORGAN-KISS, R.; IVANOV, A.G.; WILLIAMS, J.; KHAN, M. & HUNER, N.P.A. (2006): Differential thermal effects on the energy distribution between photosystem II and photosystem I in thylakoid membranes of a psychrophilic and mesophilic alga. – Biochim. Biophys. Acta 1561: 251–265.
- MÜLLER, T.; BLEIß, W.; MARTIN, C.–D.; ROGASCHESKI, S. & FUHR, G. (1998): Snow algae from northwest Svalbard: their identification, distribution, pigment and nutrient content. – Polar Biol. 20: 14–32.
- NAKADA, T.; SHINKAWA, H.; ITO, T. & TOMITA, M. (2010): Recharacterization of *Chlamydomonas reinhardtii* and its relatives with new isolates from Japan. – J. Plant Res. 123: 67–78.
- NOVIS, P. (2002): New records of snow algae for New Zealand, from the Mt Philistine, Arthur's Pass National Park. – New J. Zeal. Bot., 40: 297–312.
- OTA, S.; YOSHIHARA, M.; YAMAZAKI, T.; TAKESHITA, T.; HIRATA, A.; KONOMI, M.; OSHIMA, K., HATTORIM, M.; BIŠOVÁ, K.; ZACHLEDER, V. & KAWANO, S. (2016): Deciphering the relationship among phosphate dynamics, electron–dense body and lipid accumulation in the green alga *Parachlorella kessleri*. – Sci. Rep. 6: 25731, doi: 10.1038/srep25731.
- PIERCEY–NORMORE, M. D. & DEPRIEST, P.T. (2001): Algal–switching among lichen symbioses. – Am. J. Bot. 88: 1490–1498.
- REMIAS, D. (2012): Cell structure and physiology of alpine snow and ice algae. – In: LÜTZ, C. (ed.): Plants in Alpine Regions. Cell Physiology of Adaption and Survival Strategies. – pp. 175–186, Springer, Wien.
- REMIAS, D. & LÜTZ, C. (2007): Characterisation of esterified secondary carotenoids and of their isomers in green algae: a HPLC approach. – Algological Studies 124: 85–94.
- REMIAS, D.; LÜTZ–MEINDL, U. & LÜTZ, C. (2005): Photosynthesis, pigments and ultrastructure of the alpine snow alga *Chlamydomonas nivalis*. – Eur. J. Phycol. 40: 259–268.
- REMIAS, D.; KARSTEN, U.; LÜTZ, C. & LEYA, T. (2010): Physiological and morphological processes in the Alpine snow alga *Chloromonas nivalis* (Chlorophyceae) during cyst formation. – Protoplasma 243: 73–86.
- REMIAS, D.; WASTIAN, H.; LÜTZ, C. & LEYA, T. (2013): Insights into the biology and phylogeny of *Chloromonas polyptera* (Chlorophyta), an alga causing orange snow in Maritime Antarctica. – Antarct. Sci. 25: 648–656.
- REMIAS, D.; PICHRTOVÁ, M.; PANGRATZ, M.; LÜTZ, C. & HOLZINGER, A. (2016): Ecophysiology, secondary pigments and ultrastructure of *Chlainomonas* sp. (Chlorophyta) from the European Alps compared with *Chlamydomonas nivalis* forming red snow. – FEMS Microbiol. Ecol. 92: fiw030.
- ŘEZANKA, T. (1990): Identification of very long polyenoic acids as picolinyl esters by Ag⁺ ion–exchange high–performance liquid–chromatography, reversed–phase high–performance liquid–chromatography and gas–chromatography mass–spectrometry. – J. Chromatogr. 513: 344–348.
- ŘEZANKA, T.; NEDBALOVÁ, L. & SIGLER, K. (2008): Unusual medium–chain polyunsaturated fatty acids from the snow alga *Chloromonas brevispina*. – Microbiol. Res. 163: 373–379.
- ŘEZANKA, T.; NEDBALOVÁ, L.; PROCHÁZKOVÁ, L. & SIGLER, K. (2014): Lipidomic profiling of snow algae by ESI–MS

- and silver –LC/APCI–MS. – *Phytochemistry* 100: 34–42.
- SAUNDERS, R.D. & HORROCKS, L.A. (1984): Simultaneous extraction and preparation for high–performance liquid chromatography of prostaglandins and phospholipids. – *Anal. Biochem.* 143: 71–75.
- SPIJKERMAN, E.; WACKER, A.; WEITHOFF, G. & LEYA, T. (2012): Elemental and fatty acid composition of snow algae in Arctic habitats. – *Front. Microbiol.* 3: 380.
- STIBAL, M. (2003): Ecological and physiological characteristics of snow algae from Czech and Slovak mountains. – *Czech Phycology* 3: 141–152.
- THOMPSON, G.A. (1996): Lipids and membrane function in green algae. – *Biochim. Biophys. Acta* 1302: 17–45.
- VILGALYS, R. & HESTER, M. (1990): Rapid genetic identification and mapping of enzymatically amplified ribosomal DNA from several *Cryptococcus* species. – *J. Bacteriol.* 172: 4238–4246.
- WALSBY, A.E. (1997): Modelling the daily integral of photosynthesis by phytoplankton: its dependence on the mean depth of the population. – *Hydrobiologia* 349: 65–74.
- WEBB, W.L.; NEWTON, M. & STARR, D. (1974): Carbon dioxide exchange of *Alnus rubra*. A mathematical model. – *Oecologia* 17: 281–291.
- WOLF, M.; CHEN, S.; SONG, J.; ANKENBRAND, M. & MÜLLER, T. (2013): Compensatory base changes in ITS2 secondary structures correlated with the biologic species concept despite intragenomic variability in ITS2 sequences – a proof of concept. – *PLOS ONE* 8: e66726.
- ZASADNI, J. & KLAPYTA, P. (2014): The Tatra Mountains during the Last Glacial Maximum. – *J. Maps* 10: 440–456.
- ZUKER, D.J. (2003): Mfold web server for nucleic acid folding and hybridization prediction. – *Nucleic Acids Res.* 31: 3406–3415.

Supplementary material

the following supplementary material is available for this article:

Table S1. Collection data and sample codes of mature aplanozygotes of *Chloromonas nivalis* from exposed snow fields in the Austrian Alps.

Fig S1. Comparison of lengths of mature aplanozygotes between *Chloromonas nivalis* subsp. *tatrae* (LP01) and *Chloromonas nivalis* from the Austrian Alps (P12, P24/DR4, DR43, GK05, GK09).

Fig S2–S4. Comparison of lengths, widths and length to width ratio (L:W) of mature aplanozygotes between *Chloromonas nivalis* subsp. *tatrae* (one sample) and *Chloromonas nivalis* from the Austrian Alps (five samples).

This material is available as part of the online article (<http://fottea.czechphycology.cz/contents>)

© Czech Phycological Society (2018)

Received January 26, 2017

Accepted March 15, 2017

Table S1. Collection data and sample codes of mature aplanozygotes of *Chloromonas nivalis* from exposed snow fields in the Austrian Alps. Electrical conductivity (EC; $\mu\text{S}\cdot\text{cm}^{-1}$) and pH of meltwater are given. Furthermore, sizes of cells in $\mu\text{m} \pm \text{SD}$ (standard deviation), length to width ratio (L:W ratio) $\pm \text{SD}$ and snow colour are shown; n/a– not available.

Code	Date	Location, Altitude (m)	EC	pH	cell length	cell width	L:W ratio	snow colour
P12	16 June 2002	Kalkkögel, 1950	n/a	n/a	22.8 ± 1.5	13.19 ± 0.9	1.73 ± 0.1	orange
P24/DR4	19 August 2004	Kühtai, 2478	3.6	6.0	21.5 ± 1.6	12.95 ± 1.3	1.67 ± 0.11	orange/brown
DR43	24 July 2008	Kühtai, 2503	4.9	4.6	21.8 ± 1.8	12.6 ± 1.0	1.73 ± 0.11	yellow/brown
GK05	3 June 2009	Kühtai, 2419	5.4	6.2	22.0 ± 1.6	13.4 ± 1.1	1.65 ± 0.15	orange/brown
GK09	1 July 2009	Kühtai, 2463	7.2	5.4	23.5 ± 1.8	14.0 ± 1.0	1.69 ± 0.13	pink

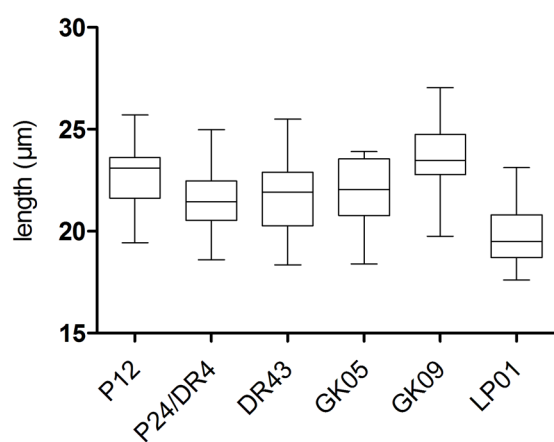


Fig S1. Comparison of lengths of mature aplanozygotes between *Chloromonas nivalis* subsp. *tatrae* (LP01) and *Chloromonas nivalis* from the Austrian Alps (P12, P24/DR4, DR43, GK05, GK09). Details of sample locations are listed in Table 1 and Table S1. Note that the reported size of *Scotiella tatrae* was 18–24 μm (KOL 1965).

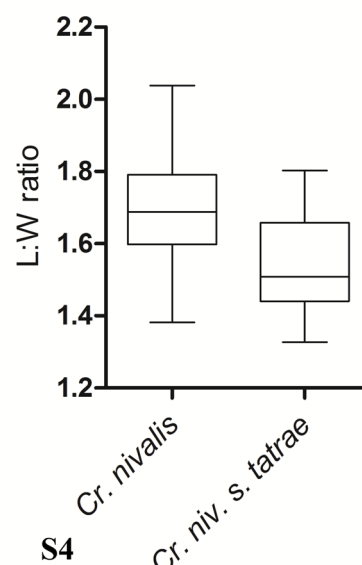
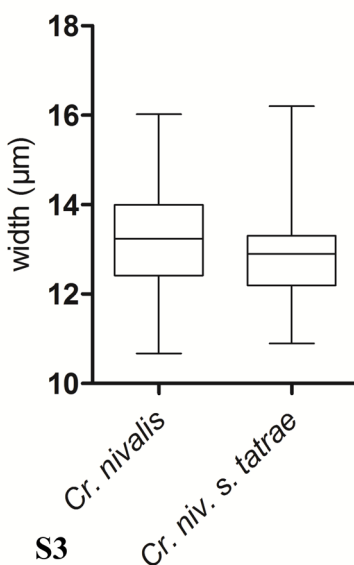
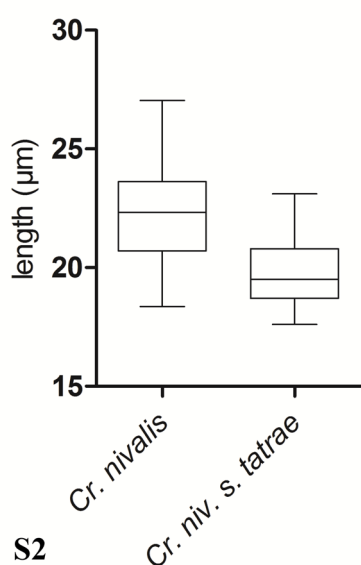


Fig S2–S4. Comparison of lengths, widths and length to width ratio (L:W) of mature aplanozygotes between *Chloromonas nivalis* subsp. *tatrae* (one sample) and *Chloromonas nivalis* from the Austrian Alps (five samples). Note that the reported cell lengths and widths of *Scotiella tatrae* were 18–24 μm and 12–15 μm , respectively (KOL 1965). Statistical significance of differences is shown in Table 4.

Paper V

Ecology, cytology and phylogeny of the snow alga *Scotiella cryophila* K-1 (Chlamydomonadales, Chlorophyta) from the Austrian Alps

Remias D^{1*}, Procházková L^{2*}, Holzinger A³ & Nedbalová L²

Phycologia 57(5): 581–592, 2018

¹ *University of Applied Sciences, Campus Wels, Stelzhamerstr. 23, A-4600 Wels, Austria*

² *Charles University, Faculty of Science, Department of Ecology, Viničná 7, CZ-128 44 Prague,
Czech Republic*

³ *University of Innsbruck, Department of Botany, Sternwartestr. 15, A-6020 Innsbruck, Austria*

*DR and LP contributed equally to this work

Ecology, cytology and phylogeny of the snow alga *Scotiella cryophila* K-1 (Chlamydomonadales, Chlorophyta) from the Austrian Alps

DANIEL REMIAS^{1*}†, LENKA PROCHÁZKOVÁ²†, ANDREAS HOLZINGER³ AND LINDA NEDBALOVÁ²

¹University of Applied Sciences, Campus Wels, Stelzhamerstr. 23, A-4600 Wels, Austria

²Charles University, Faculty of Science, Department of Ecology, Viničná 7, CZ-128 44 Prague, Czech Republic

³University of Innsbruck, Department of Botany, Sternwartestr. 15, A-6020 Innsbruck, Austria

ABSTRACT: Long-lasting, slowly melting snowfields in mountainous regions are frequently populated by specialised microalgae whose diversity is still vastly underestimated. Cysts causing sub-surficial green snow were collected in the Austrian Alps, Tyrol, and morphologically accorded to the snow alga *Scotiella cryophila sensu* Chodat, initially described from Switzerland. The cytology and photobiology of this population were investigated to understand mechanisms of adaptation to the harsh habitat. Cysts of *S. cryophila* K-1 had secondary cell walls with pronounced rib-like surface structures and contained several small spherical plastids. The cytoplasm was dominated by lipid bodies, which developed reddish secondary pigmentation. Partial life cycle observations showed that daughter cells lacked structured cell walls. Cysts performed active photosynthesis at temperature conditions close to the freezing point and were photoinhibited at irradiances greater than 70 $\mu\text{mol m}^{-2} \text{s}^{-1}$. This corresponded exactly to habitat conditions 20 to 40 cm below the snow surface. Phylogenetic analyses using 18S rDNA, *rbcL* and ITS2 rDNA sequences indicated that *S. cryophila* K-1 is related to *Chloromonas*, known to contain several snow algae. The taxon forms an independent lineage and is clearly genetically distinct from the type strain of *Chloromonas rosae* var. *psychrophila* from North America that is supposed to have morphologically identical cysts. For a taxonomic treatment including a species assignment of *S. cryophila* K-1 from Europe within *Chloromonas*, flagellates will have to be cultivated from cysts or from acquired field material for a detailed morphological description. Acquisition and genetic analysis of cysts that resemble *S. cryophila* from America could elucidate their relationship to European samples.

KEY WORDS: Cryoflora, Cryospheric algae, Cysts, Extremophiles, Fluorometry, Ultrastructure

INTRODUCTION

Blooms of snow algae can cause green, orange, yellow or red snow discolourations, depending on prevailing cell pigmentation (Hoham & Duval 2001; Anesio *et al.* 2017). In a global context, snow and glacial algae are considered to play a role in accelerating Arctic snow melt due to albedo reduction driven by their abundant secondary pigments. Thus, they should be incorporated into climate models (Lutz *et al.* 2016; Ganey *et al.* 2017). Members of Chlamydomonadaceae (Chlorophyceae) dominate these extreme habitats, most likely because of (1) morphological and physiological adaptations of their life cycles to low or comparable high temperatures before and after snowmelt, (2) temporary or restricted availability of liquid water, or (3) extreme ultraviolet and visible irradiation at the snow surface (Komárek & Nedbalová 2007; Lukeš *et al.* 2014; Cvetkovska *et al.* 2017).

We investigated a snow alga that morphologically matches the previously described *Scotiella cryophila* Chodat (Chloro-

ophyceae, Chodat 1922). This species is not known to cause striking monospecific blooms at the snow surface, unlike many other snow algae. The alga investigated here was collected in the Kühtai region (K-1) of the Austrian Alps and characterised by its cytology, photobiology and phylogeny. It was initially described from Switzerland (Chodat 1922), and scattered cells were further reported from the Giant Mountains in the Czech Republic (Nedbalová *et al.* 2008), the High Tatra Mountains in Slovakia (Kol 1968), Scotland (Light & Belcher 1968), Greenland (Kol 1968) and North America (Arizona, New York and Vermont; Hoham *et al.* 2002). This taxon is recognized by having oblong, immotile, fusiform cells with undulating or alternating surface ribs, several disc-like plastids and occasional reddish pigmented ‘droplets’ close to the cell poles. Species of *Scotiella* were initially considered to develop daughter cells with the same ribbed wall morphology as the mother cells. Later, it was shown that daughter cells of several species of ‘*Scotiella*’ inhabiting snow lack any cell wall ornamentation, and the stage of *Scotiella* was recognized either as a vegetative cyst or a generative zygote (Hoham & Mullet 1977). Thus, these taxa were transferred to the genus *Chloromonas* (e.g. Hoham & Mullet 1978). Using a strain isolated from snow in the White Mountains, Arizona, *Chloromonas rosae* var. *psychrophila* Hoham, Bonome, Martin, & Leebens-Mack was proposed as a synonym of *S. cryophila* (Hoham *et al.* 2002). However, it is unknown if the type strain of *C. rosae* var. *psychrophila* (consisting of flagellates) is genetically identical to the cysts that caused the field bloom. Furthermore, it is not clear if snow algae with identical cyst

* Corresponding author (daniel.remias@fh-wels.at).

† DR and LP contributed equally to this work.

DOI: 10.2216/18-45.1

© 2018 International Phycological Society. This is an open access article distributed under the terms of the Creative Commons Attribution Non-commercial License (CC-BY-NC). This license permits copying and redistribution in any medium or format as long as proper attribution is given and the use is non-commercial in nature. For more information, see: <http://creativecommons.org/licenses/by-nc/4.0/>.

morphology from elsewhere belong to the same species or not.

The major aim of this study was to determine if the cyst population of the Kühtai region 1 (K-1) of *Scotiella cryophila* from the European Alps was morphologically and phylogenetically related to other similar extremophilic algae living in snow. Because harvested cells dominated sub-surficial layers, covered by a white snow pack, we wanted to determine whether the photobiology was adapted to low irradiances. This is ecologically significant, since light penetration through snow decreases logarithmically with depth (Gorton *et al.* 2001). Finally, in order to find the correct phylogenetic position, a combination of the three molecular markers (18S rDNA, *rbcL* and ITS2) was applied. This revealed that the type strain of *Chloromonas rosae* var. *psychrophila* (UTEX SNO47) from North America is not related to the blooms of *S. cryophila* K-1 in alpine snow in Europe. Since *Scotiella* is invalid for species where daughter cells have smooth walls instead of ribbed ones, and the epithet *cryophila* already exists in *Chloromonas* (Hoham & Mullet 1977), a *nomen novum* for this taxon will be necessary once flagellates can be described.

MATERIAL AND METHODS

The green cryoflora was collected 5 June 2009 (sample GK02) and 30 May 2017 (sample WP125) in Austria (Tyrol, district Imst at Kühtai Valley, between Schwarzmooos and Gossenkölle Lake). Global positioning system locations and altitude were 47°13.748'N, 11°00.704'E, 2432 m (GK02) and 47°13.754'N, 11°00.718'E, 2435 m (WP125), respectively. First, surface snow was removed, and then cells at depths of about 20–30 cm were harvested into buckets with a stainless steel shovel. Snow was gently melted at 4°C in the dark. Some of the cells were intentionally kept at these conditions in the meltwater and additionally illuminated with approximately 40 $\mu\text{mol photons m}^{-2} \text{ s}^{-1}$ for several weeks to follow the further development of the cysts. Electrical conductivity and pH of the meltwater were measured immediately after melting with a conductometer from WTW Instruments (Weilheim, Germany). Light conditions in the snow were acquired with a PMA2100 logger equipped with a photosynthetic active radiation (PAR) sensor PMA2131 (Solar Light, Glenside, Pennsylvania USA). Light microscopy (LM) and cell size measurements were performed with a Zeiss Axiovert 200M, photomicrographs taken with an AxioCam MRc5 (Zeiss, Oberkochen, Germany). The protocols described in Procházková *et al.* (2018a) were used to determine cell concentration per meltwater volume and to study cell wall structure by scanning electron microscopy (SEM). The ultrastructure of the cells was investigated by transmission electron microscopy (TEM) according to Remias *et al.* (2010). Permanently cryopreserved cysts of *Scotiella cryophila* K-1 collected 5 June 2009 (field sample GK02) were deposited at the Culture Collection of Algae of Charles University in Prague (CAUP), Czech Republic.

For evaluation of the light-dependent plastid photon flux rates, *in vivo* chlorophyll fluorescence measurements were

performed with a PAM 2500 in a 0.6 ml suspension cuvette KS-2500 (Walz GmbH, Effeltrich, Germany) at 1°C. To measure the relative electron transport rate (rETR) and the light saturation point I_k , cells from sample WP125 were exposed to photon flux densities (PFD) of 5, 9, 34, 67, 104, 201 $\mu\text{mol photons m}^{-2} \text{ s}^{-1}$ for 30 seconds each. Four independent replicates were measured. For further details see Procházková *et al.* (2018a).

For genetic analyses, the type strain of *Chloromonas rosae* var. *psychrophila* SNO47 was acquired from UTEX (Houston, Texas USA).

Total genomic DNA was extracted according to Procházková *et al.* (2018a). The 18S small subunit ribosomal RNA gene (18S rDNA), internal transcribed spacer regions 1 and 2 (ITS1, ITS2 rDNA) and ribulose-1,5-bisphosphate carboxylase/oxygenase large subunit (*rbcL*) gene regions were amplified from DNA isolates by polymerase chain reaction using existing primers (Table S1). Amplification and sequencing reactions for these markers were identical to those described by Procházková *et al.* (2018a). The obtained sequences were submitted to the National Center for Biotechnology Information (NCBI) Nucleotide sequence database (accession numbers Table S2). The methods of annotation and prediction of the secondary structure of the nuclear rDNA ITS2 region were the same as those described by Procházková *et al.* (2018a). The ITS2 sequences of *Scotiella cryophila* K-1 (this study) and *Chloromonas nivalis* Gassan-B (Matsuzaki *et al.* 2015) were aligned using the sequence-structure analysis in 4SALE (Seibel *et al.* 2006, 2008) in order to find compensatory base changes (CBCs). Manual validation and correction of alignment were included. The secondary structure of nuclear rDNA ITS2 was drawn using VARNA version 3.9 (Darty *et al.* 2009). 18S rDNA alignment contained 41 sequences (1668 bp); *rbcL* matrix consisted of 38 sequences (1128 bp); members of the clade of *Reinhardtii*, the clade of *Oogamochlamys* and the clade of *Carteria sensu* Pröschold *et al.* (2001) were selected as the outgroup. The best-fit nucleotide substitution model was estimated by jModeltest 2.0.1 (Posada 2008). Based on the Akaike Information Criterion, the 'TIM1 + I + G' model was selected for 18rDNA. Three partitions were set for *rbcL* gene sequences and the following substitution models were applied: 'TIM1 + I + G' (first codon position), 'GTR + I + G' (second codon position) and 'TIM3 + I + G' (third codon position). The 18S rDNA and *rbcL* phylogenetic trees were inferred by Bayesian inference (BI) and maximum likelihood (ML) according to Nedbalová *et al.* (2017), with the minor modification that Markov Chain Monte Carlo runs were carried out for three million generations in BI. Convergence of the two cold chains was checked by the average standard deviation of split frequencies (0.000738 and 0.000943 for 18S rDNA and *rbcL* dataset, respectively). Bootstrap analyses and Bayesian posterior probabilities were performed as described by Nedbalová *et al.* (2017).

For evaluating the additional growth of *Scotiella cryophila* K-1 during cyst maturation, length, width and the length to width ratio determined directly after the harvest (GK02, WP125) were compared with those kept for 3 months in laboratory conditions (GK02 old, WP125 old). Statistical

analyses followed Procházková *et al.* (2018a), and the Mann–Whitney test was used for testing the hypothesis that the median of two groups was identical.

RESULTS

Habitat description

The sampling location in the Austrian Alps (47°13.748'N, 11°00.704'E) was flat and slightly southwest orientated. The snowfield was exposed above timberline, the underground was scree, and some larger granite rocks were not snow covered (Fig. S1). In June 2009, the snow surface was red and dominated by spherical cysts of *Chlamydomonas nivalis* (Bauer) Wille to approximately 10 cm depth. After removing about 20 cm of snow, a band of green snow dominated by oblong fusiform cysts was found and harvested (GK02). Eight years later, in late May 2017, the surface at practically the same location appeared uncoloured; however, a green band at 20 to 30 cm depth with the same species (WP125) was found and harvested (Fig. S2). Further algae that co-occurred in 2017 were scattered cells of *C. nivalis*, *Chloromonas brevispina* (Fritsch) Hoham, Roemer & Mullet and an undetermined unicellular biflagellate chrysophyte. The water content of this snow layer was $49.2 \pm 3.2\%$. The meltwater had an electrical conductivity of $7.0 \mu\text{S cm}^{-1}$ and a pH of 5.5 in 2009, and $9.0 \mu\text{S cm}^{-1}$ and pH of 5.1 in 2017. At noon, PAR 20 cm below the snow surface accounted for 2% of surface amounts during sunny weather (40 vs $2062 \mu\text{mol m}^{-2} \text{s}^{-1}$) and 1.4% in cloudy conditions (12 vs $836 \mu\text{mol m}^{-2} \text{s}^{-1}$). In 2017, the concentration at the margin of the bloom was $1325 \text{ cells ml}^{-1}$ snow meltwater.

Morphological description

The elongate cysts had a fusiform shape (Fig. 1), were $33.3 \pm 3.0 \mu\text{m}$ long (mean \pm s; $n=92$) and $10.5 \pm 2.0 \mu\text{m}$ wide, with a length to width ratio from 2.1 to 4.7 (3.3 ± 0.5 ; WP125 and GK02 averaged together; sizes of each sample shown separately in Figs S3–S5). Many cells were in the process of shedding a smooth outer cell wall (Fig. 2), leaving a secondary wall with straight to undulate ribs (Figs 3, 4), which sometimes alternated toward the cell poles. The cytoplasm of young cysts was dominated by a parietal chloroplast, which was obviously rearranged during maturation to irregular band-like sections, and finally into small spherical plastids (Fig. 5). During sampling, only a few cells contained reddish lipid globules; however, after aging for 3 months at low irradiance in laboratory conditions, virtually all cells developed peripheral secondary pigmentation (Fig. S6). Under the same conditions, many cells underwent two cell divisions. First, the protoplast contracted by becoming rounder (Fig. 6), then it cleaved into four, smooth-walled, oblong daughter cells (Fig. 7). Concurrently, the cysts grew slightly (to $36.1 \pm 2.6 \mu\text{m}$ long, $12.5 \pm 1.4 \mu\text{m}$ wide; sample WP125). Mature cysts (3 months after harvest) were significantly wider and had a lower length to width ratio than cysts when harvested (both $P < 0.01$); whereas, the influence of ageing on cyst lengths was not significant (Figs S3–S5). Motile flagellates were never observed.

The arrangement of the characteristic cell wall surface ribs, which were sometimes difficult to observe by LM, was depicted by SEM (Figs 8–11): some ribs reached from one pole nearly to the antapex (Fig. 8), sometimes fusing or diverging (Fig. 9); moreover, an isolated short rib could be present (Fig. 10). The most prominent rib could have two lateral secondary ribs (Fig. 11). In median cross section, usually six to ten ribs were present. TEM revealed that cyst cell walls had up to three layers (Fig. 12) and some prominent wall ribs were secondarily ribbed (Fig. 13). Mature cysts were covered by an electron-dense innermost cell wall, peripheral lipid bodies surrounding the nucleus and several roundish plastids (Figs 14–16).

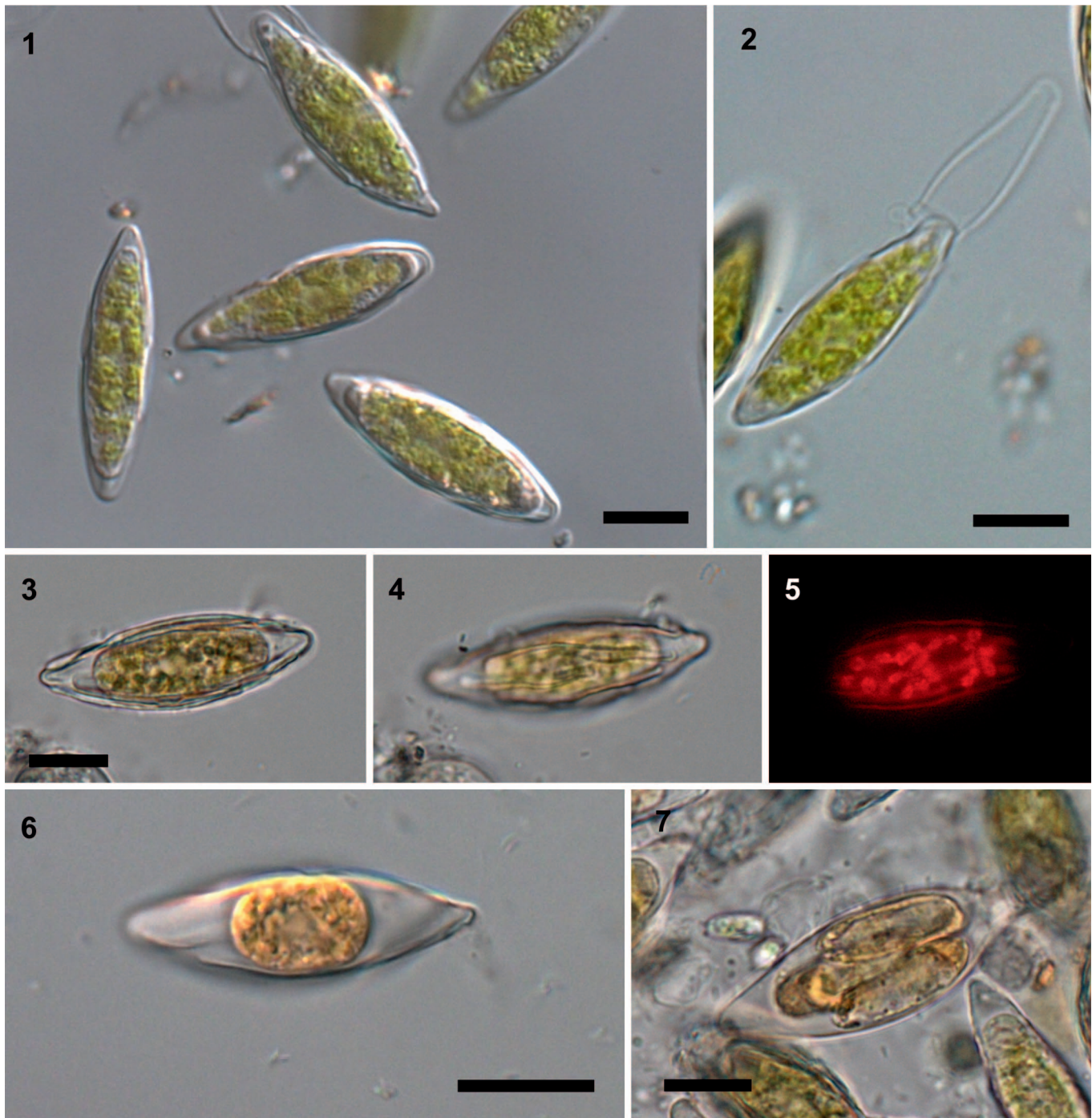
Photosynthesis

The light-dependent relative electron transport rates revealed the extent of adaptation of photosystem II to the low-light habitat conditions. *Scotiella cryophila* K-1 (sample WP125) exhibited an alpha (slope of the light-limited region of the photosynthesis-irradiance curve) of 0.24 ± 0.01 , a relative ETR_{max} of 3.9 ± 0.2 and an I_k value of $27 \pm 2 \mu\text{mol photons m}^{-2} \text{s}^{-1}$ (Fig. 17). Photoinhibition occurred above approximately $70 \mu\text{mol photons m}^{-2} \text{s}^{-1}$.

Molecular phylogeny

With the NCBI basic local alignment search tool server, the closest hit for the ITS2 variable marker of *Scotiella cryophila* K-1 was *Chloromonas nivalis* Gassan-B (LC012714, Matsuzaki *et al.* 2015), a snow alga sampled from Japanese mountains. Still, these two field samples were independent taxa because several CBCs in helices II–III of the ITS2 rDNA secondary structure were present (Fig. 18). For ITS1 of *S. cryophila* K-1 (MG253843), no hits with more than 90% identity were found. In contrast, UTEX SNO47, the type strain of *Chloromonas rosae* var. *psychrophila*, turned out to be genetically identical (ITS1) and nearly identical (ITS2), except for one nucleotide change in the middle part of helix I, to *Chloromonas reticulata* CCCryo 213-05 (= UTEX 1970 = SAG 29.83) (MG253846 vs HQ404885).

In 18S and *rbcL* phylogenies, *Scotiella cryophila* K-1 was placed in a well-supported clade ‘B’ consisting of several species of *Chloromonas* causing snow discoloration (Figs 19, 20). Its closest relatives were *Chloromonas polyptera* (Fritsch) Hoham, Mullet & Roemer from Antarctica, *Chloromonas nivalis* (Chodat) Hoham & Mullet from the Austrian Alps, *Chloromonas nivalis* subsp. *tatrae* (Kol) Procházková, Remias, Řezanka & Nedbalová from the High Tatras in Slovakia, *Chloromonas nivalis* Gassan-B, uncultured *Chloromonas* sp. TA8 (both from Japan) and an uncultured eukaryote from a periglacial environment at Mount Kilimanjaro in Tanzania. Strain UTEX SNO47 was in the clade ‘A1’ *sensu* Hoham *et al.* (2002; corresponding to the clade of ‘*Chloromonas reticulata*’ *sensu* Pröschold *et al.* 2001), which was confirmed by 18S rDNA and *rbcL* phylogenetic trees (Figs 19, 20). For *rbcL*, the sequence of strain UTEX SNO47 was identical to Hoham *et al.* (2002 comparison of MG253847 and AF517073). For 18S rDNA, the new sequence of this strain (MG253845) was identical to Hoham *et al.* (2002) except for a single nucleotide gap in the initial sequencing (AF517093), which was not shared in the whole 18S rDNA alignment.



Figs 1–7. Light micrographs of cysts of *Scotiella cryophila* K-1 (sample GK02, if not stated). Scale bars = 10 μ m.

Figs 1–2. Young cysts.

Fig. 1. Overview with a group of typical immotile cells with inconspicuous secondary structured cell walls.

Fig. 2. Primary cell wall is shed.

Figs 3–5. A mature cell (WP125) at bright field and fluorescence mode.

Fig. 3. Cell focused at median plane.

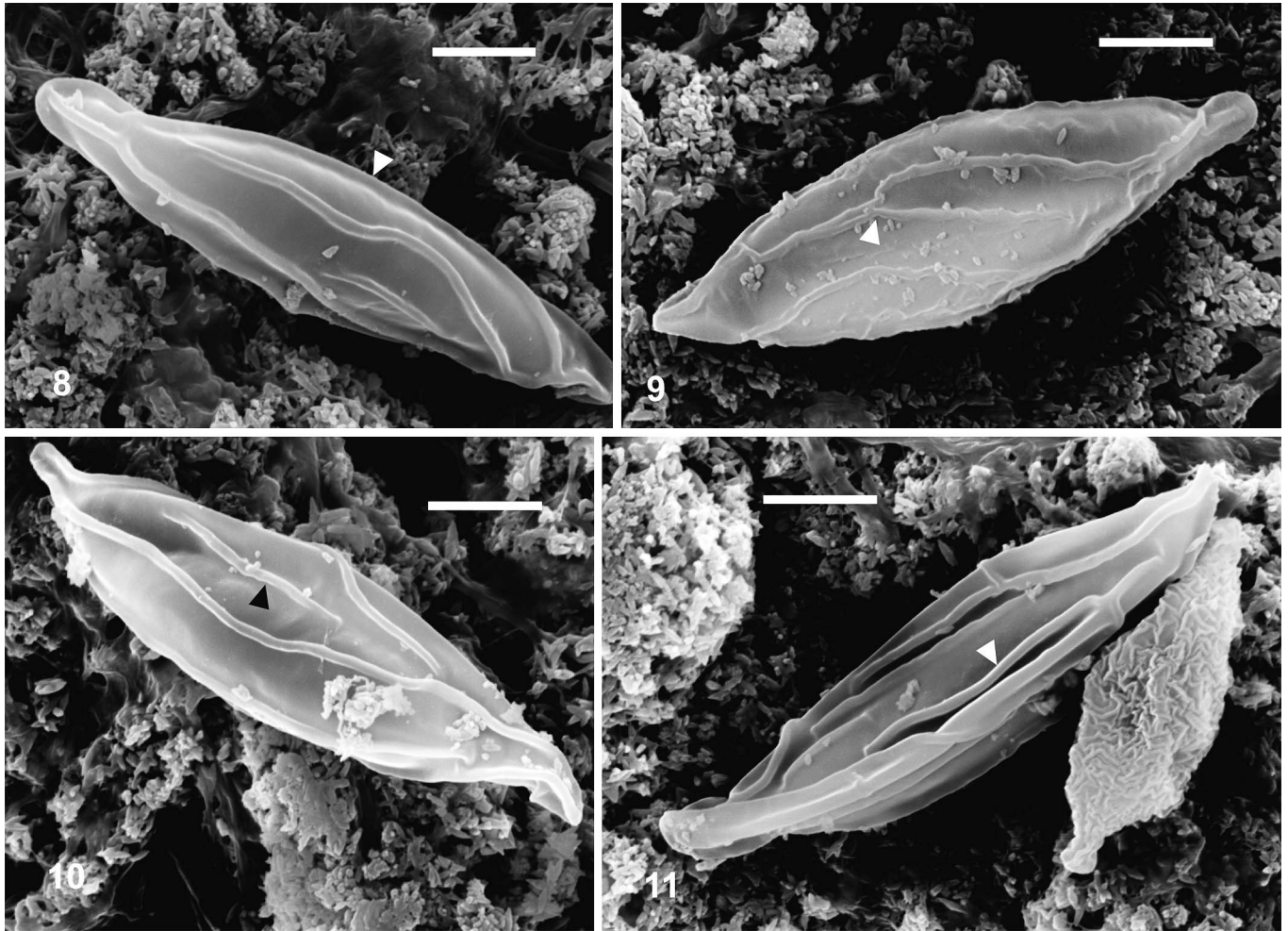
Fig. 4. Cell focused on top revealing characteristic longitudinal cell wall ribs.

Fig. 5. Chlorophyll-autofluorescence showing spherical plastids.

Figs 6–7. Old cysts 3 months after sampling.

Fig. 6. Contracted protoplast likely prior to cell division. Note the orange colour caused by secondary carotenoids (WP125).

Fig. 7. Four smooth-walled, oblong daughter cells inside mother cell, three of them visible.



Figs 8–11. Scanning electron micrographs of mature cysts of *Scotiella cryophila* K-1 (WP125). Scale bar = 5 μ m.

Fig. 8. A cell wall rib reaching from pole nearly to antapex (arrowhead).

Fig. 9. A bifurcation of one flange into two independent ones is shown (arrowhead).

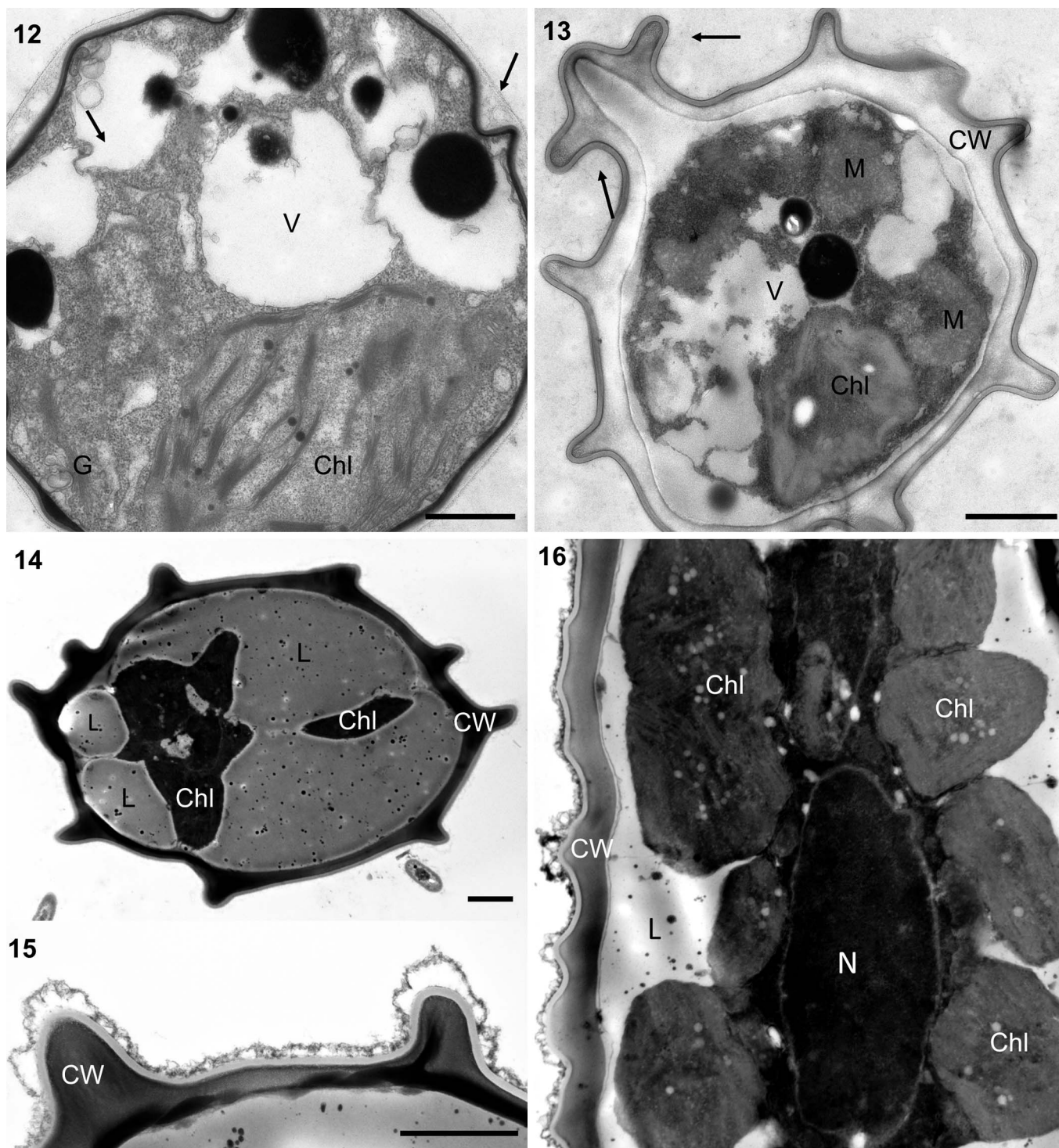
Fig. 10. An isolated short rib (arrowhead).

Fig. 11. Note the main rib on top, which is composed of at least two twisted ribs (arrowhead); the most prominent rib can have two lateral secondary ribs.

DISCUSSION

Scotiella cryophila sensu Chodat is a rather neglected snow alga, probably because it has been reported less frequently than other cryoflora such as *Chlamydomonas nivalis* (Remias *et al.* 2005) or *Chloromonas brevispina* (Hoham *et al.* 1979). In this study, the sampled snow field consisted of a virtually pure population of cysts. Scattered cysts of *S. cryophila* were found in many snow fields from other regions (Stein & Brooke 1964; Kol 1970; Whitford & Kim 1971). *Scotiella cryophila* cysts associated with *Chloromonas rosae* var. *psychrophila* dominate the green snow packs at Whiteface Mountain, Adirondacks, New York (Hoham *et al.* 2008). The fact that after 8 years the population was found again at more or less the same spot in the Tyrol Alps indicates a local occurrence (site fidelity) and implies that the mature cysts rest directly on the dry rock ground after snow melt, where they may accumulate over years and develop a kind of ‘seed bank’ for germination during suitable spring conditions. The cell stages present during harvest exhibited the typical morphology of immotile

stages of *Chloromonas*, which dominate snow pack for most of the season. Different from many snow algae of the genus *Chloromonas*, *S. cryophila* K-1 likely produces asexual cysts directly out of biflagellate swimmers. This was reported for field material of *C. rosae* var. *psychrophila* by Hoham *et al.* (2002). *Scotiella cryophila* K-1 is distinguished from its close relative *Chloromonas nivalis* in having significantly elongated cysts with length to width ratios from 2.1 to 4.7 (this study) vs 1.4 to 2.1 for more ellipsoidal to ovoid cysts of the latter species (Procházková *et al.* 2018a). Consequently, *S. cryophila* K-1 should not be confused with *C. nivalis*. Also, the other species of cryoflora of this genus have shorter cysts of broad-ellipsoidal shape (e.g. length to width ratios of 1.1–1.8 for *Chloromonas polyptera*; unpublished data, D.R.), or 1.3–1.8 for *Chloromonas nivalis* subsp. *tatrae*, Procházková *et al.* 2018a). Furthermore, the cell wall ribs of other species are more pronounced and clearly visible with LM. The cysts of *S. cryophila* K-1 and associated cryoflora species of *Chloromonas* share morphological and cytological traits: flagellar loss, contractive vacuoles and possibly an eyespot, shedding a non-



Figs 12–16. TEM micrographs of *Scotiella cryophila* K-1. Abbreviations: Chl, chloroplast; CW, cell wall; G, Golgi stacks; M, mitochondrion; N, nucleus; L, lipid; V, vacuole. Scale bar: 1 μ m.

Figs 12–13. Transverse section of young cysts (GK02).

Fig. 12. Single compact chloroplast and large vacuoles, primary wall still present (arrows).

Fig. 13. Young electron translucent cell wall ribs and one rib secondary ribbed (arrows).

Figs 14–16. Cross sections of mature cysts with fully developed cell wall ribs (WP125).

Fig. 14. Cytoplasm occupied by several large peripheral lipid bodies.

Fig. 15. Detail of the bi-layered secondary cell wall, the inner layer is electron dense.

Fig. 16. Longitudinal section of a cyst showing a detailed view of the cytoplasm containing several roundish plastids close to the nucleus.

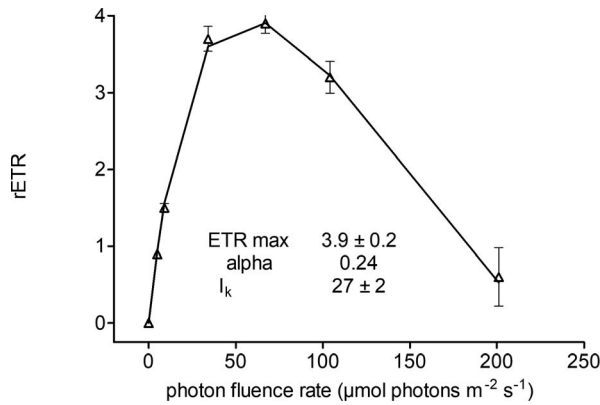


Fig. 17. Effect of increasing photon fluence rates (x-axis) on the relative electron transport rate (rETR; y-axis) of chloroplasts in non-motile stages of *Scotiella cryophila* K-1 (sample WP125). Values are means of four replicate measurements ($\pm s$). The data points were fitted to the photoinhibition model of Walsby (1997).

ribbed primary cell wall during maturation, releasing a structured secondary cell wall, having small spherical or discoid plastids instead of a compact chloroplast and accumulation of secondary reddish pigments.

Fluorometric measurement demonstrated that the photosystem II of green cysts of *Scotiella cryophila* K-1 is adapted to low light conditions. The light compensation point could not be acquired by pulse amplitude modulation but since I_k had occurred at a PFD of $27 \mu\text{mol m}^{-2} \text{s}^{-1}$ and photoinhibition started from about $70 \mu\text{mol photons m}^{-2} \text{s}^{-1}$, it is obvious that these stages must have a positive photosynthetic balance at PFDs between 12 and $40 \mu\text{mol m}^{-2} \text{s}^{-1}$ PAR, which occurred 20 cm below the surface. Hoham *et al.* (2006) reported that slightly higher irradiation of 95 and 115 $\mu\text{mol m}^{-2} \text{s}^{-1}$ were optimal for sexual reproduction of the snow algae *Chloromonas tughillensis* and *Chloromonas chenangoensis*, respectively. Furthermore, *Chloromonas rosae* var. *psychrophila* from North America grew at low irradiances (Hoham *et al.* 1998), thus with the same light conditions as the cysts studied here. However, once the cysts reach the snow surface due to ongoing melting, they would be subject to severe light stress if they did not rearrange their photosynthetic apparatus to high irradiance. Alternatively, cells should produce protective carotenoids like astaxanthin. Light adaptations must have taken place in the course of cyst maturation, as indicated by observation of surficial populations of *S. cryophila* from snow fields partly shaded by a

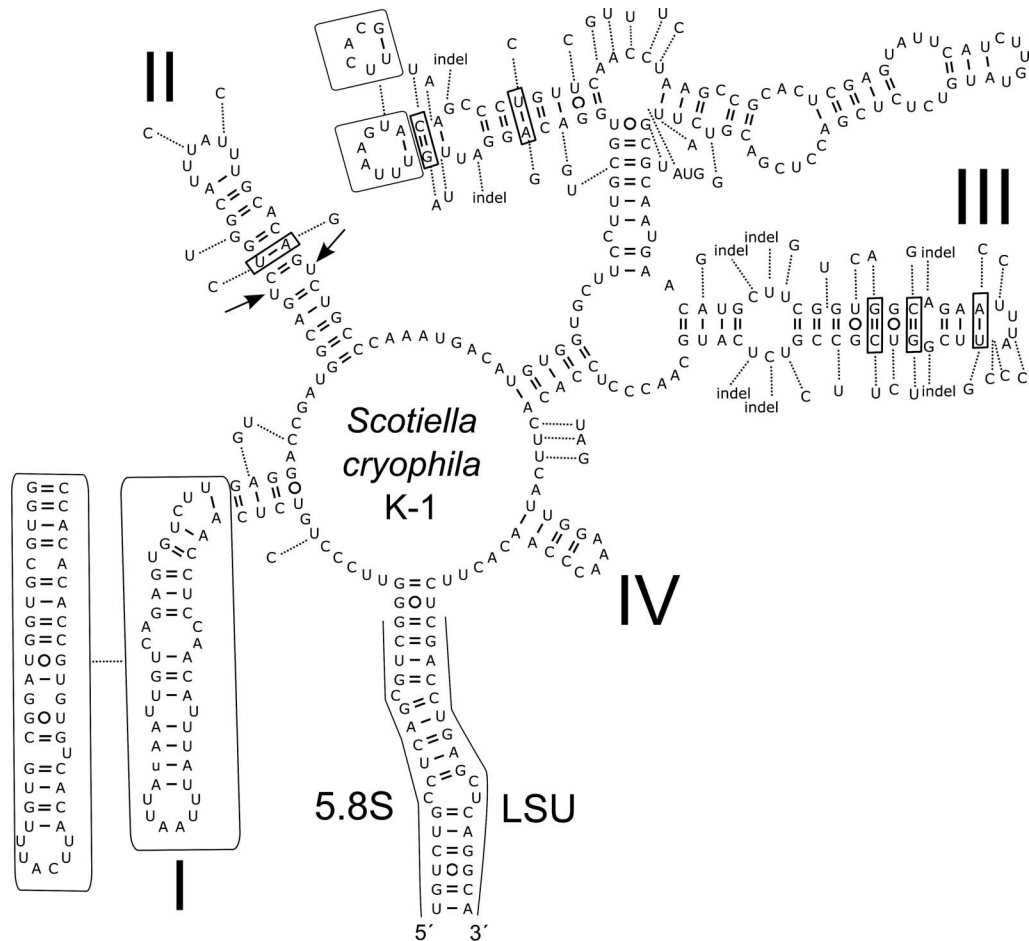


Fig. 18. Comparison of the secondary structure of ITS2 rDNA transcripts between *Scotiella cryophila* K-1 from the Austrian Alps (accession number MG253843, this study) and *Chloromonas nivalis* Gassan-B from Japan (accession number LC012758, Matsuzaki *et al.* 2015). Helices are labelled with Latin numbers. Nucleotide differences of the second species are outside the structure and linked by dotted lines. Compensatory base changes between both algae are indicated by rectangles. Note the U-U mismatch in helix II (arrows).

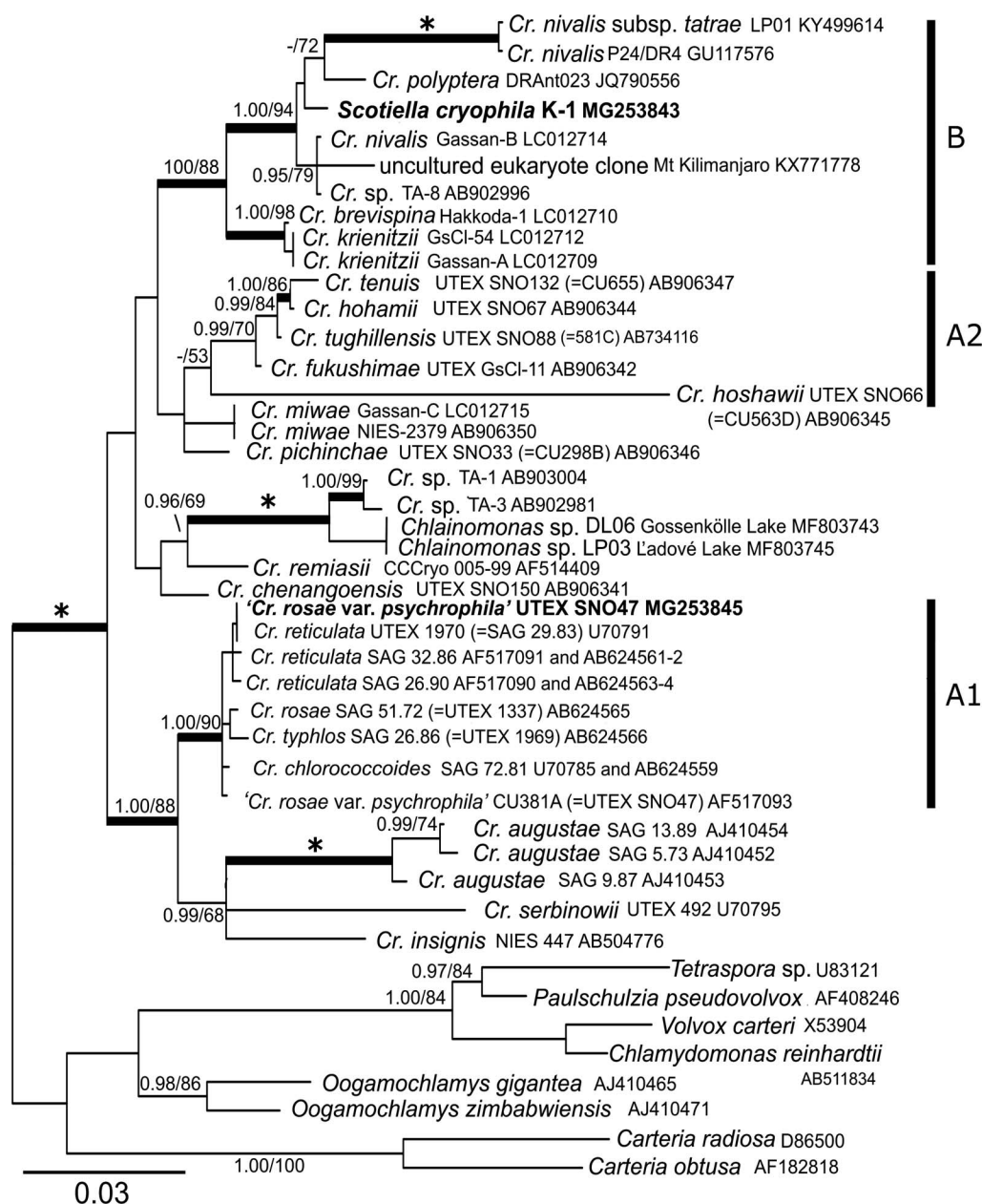


Fig. 19. 18S ribosomal DNA gene-based Bayesian phylogenetic tree of *Chloromonas* focusing on snow-inhabiting species and selected mesophilic relatives. *Cr.* = *Chloromonas*. The labelled clades 'A1' and 'A2' correspond to Hoham *et al.* (2002), clade 'B' is according to Matsuzaki *et al.* (2015). Posterior probabilities (0.95 or more) and bootstrap values from maximum likelihood analyses (50% or more) are shown. Full statistical support (1.00/100) is marked with an asterisk. Thick branches represent nodes receiving the highest posterior probability support (1.00). Newly obtained sequences are in bold. Accession numbers, strain or field sample codes are indicated after each species name.

sparse canopy (Nedbalová *et al.* 2008). The light regime (open exposures) of the Austrian site of cysts that resemble *S. cryophila* is very different from locations of *C. rosae* var. *psychrophila* in North America, which were usually associated with coniferous trees that shade the snow banks (Hoham *et al.* 2008). Nonetheless, microhabitat light conditions seem to be similar, since *S. cryophila* K-1 caused green snow at least 20 cm below the snow surface.

Phylogenetically, all species of *Chloromonas* investigated to date that thrive exclusively in snow are members of the closely related clades 'A2' (Hoham *et al.* 2002) and 'B'

(Matsuzaki *et al.* 2015). The type strain of *Chloromonas rosae* var. *psychrophila* (UTEX SNO47) was closely related to *C. rosae* SAG 26.90 (Hoham *et al.* 2002). Additionally, Matsuzaki *et al.* (2012) assigned the latter strain to *Chloromonas reticulata* based on multigene analysis and observations with light and electron microscopy. The absence of any CBCs in the ITS2 secondary structure between UTEX SNO47 and SAG 26.90 indicates that UTEX SNO47 belongs to *C. reticulata*. Generally, a phylogeny based solely on the conservative 18S rDNA marker does not provide sufficient resolution to discriminate between inde-

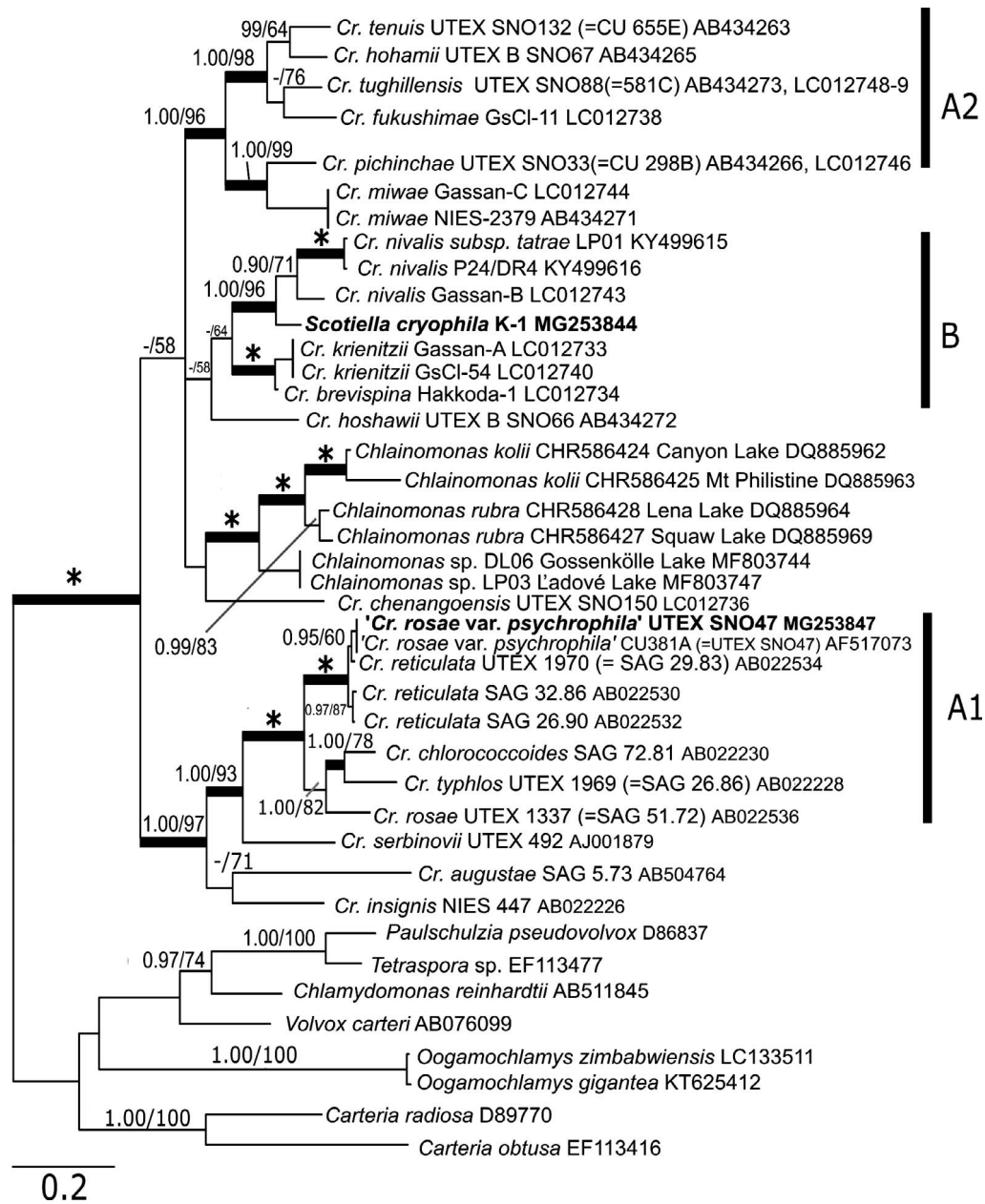


Fig. 20. *rbcL* gene-based Bayesian phylogenetic tree of the genus *Chloromonas* including snow-inhabiting species and mesophilic relatives. *Cr.* = *Chloromonas*. The labelled clades 'A1' and 'A2' correspond to Hoham *et al.* (2002), clade 'B' is according to Matsuzaki *et al.* (2015). Posterior probabilities (0.95 or more) and bootstrap values from maximum likelihood analyses (50% or more) are shown. Full statistical support (1.00/100) is marked with an asterisk. Thick branches represent nodes receiving the highest posterior probability support (1.00). Newly obtained sequences are in bold. Accession numbers, strain or field sample codes are indicated after each species name.

pendent species, as indicated by low bootstrap values of some branches (only posterior probabilities > 95% shown in our phylogenetic trees). For example, *C. polyptera*, *C. nivalis* and *S. cryophila* K-1 seemingly form a monophyletic clade where any subclades are less supported. Nevertheless, an 18S rDNA based phylogeny of snow algae may at least reveal the taxonomic context between related species. The *rbcL* marker verified the topology of the clades. Finally, with the help of the variable ITS2 rDNA marker, lineages of closely related species (e.g. *S. cryophila* K-1 and *C. nivalis* Gassan-B) were successfully resolved.

At the sampling site of *Scotiella cryophila* K-1 in the Tyrolean Alps, the slightly acidic pH and very low electrical conductivity values of meltwater were similar to rainwater and typical of other snow fields in the same region (Remias *et al.* 2010). North American populations of *Chloromonas rosae* var. *psychrophila* occurred in habitats with pH and conductivity values in the same range (Hoham *et al.* 1989, 2007, 2008). The snow water content was, however, lower than in slush on an almost frozen, high alpine lake about 50 m away from the sampling site, where a different cryoflora of *Chlainomonas*

sp. persisted (Procházková *et al.* 2018b). *Scotiella cryophila* K-1 was found in comparably low concentrations, thus causing no striking snow discolourations, or it was reported as an additional component in blooms dominated by other species above the treeline (Remias *et al.* 2005) or at both forested and non-forested slopes (Nedbalová *et al.* 2008). So far, it has not been reported from polar habitats like the well investigated Arctic Archipelago of Svalbard (Kvídárová 2012). Kol (1959) found *S. cryophila* at Cape York in Greenland and described a new and larger variety, *S. cryophila* var. *groenlandica* Kol, with well-developed, straight ribs from pole to pole and cell sizes of $33\text{--}42 \times 15\text{--}18 \mu\text{m}$. However, this latter taxon has neither been observed again, nor is a strain available, thus a molecular proof is not possible. Moreover, the drawings of these cells do not closely resemble *S. cryophila* K-1.

Generally, the average cell sizes of mature cysts may reflect how suitable the habitat conditions were in the course of a season (e.g. nutrient and water availability, freeze–thaw events, light regime). As a consequence, we think that the samples of this study are identical to *Scotiella cryophila* initially described by Chodat (1922), though he gave lower dimensions of size ranges from a comparable habitat in the Swiss Alps ($12\text{--}30 \mu\text{m} \times 6\text{--}10 \mu\text{m}$). Since we found larger than average sizes for old cysts producing daughter cells, further growth during maturation seems to be possible (observed also for North American samples; R. Hoham, pers. comm.), and maybe the smaller sizes reported by Chodat included flagellate-like younger stages, which we did not find. Such stages likely occur very early in the melting season, when the alpine snow becomes waterlogged at the end of March (results found by DR, data not shown). While the putatively sensitive flagellates enable a migration within a waterlogged snow pack to a certain extent, the immotile stages can be regarded as robust. This reflects their thick walled structures, and the carotenoids accumulated in cytoplasmic lipid bodies are powerful antioxidants and absorbers of excessive ultraviolet (UV) and PAR (Remias 2012). Moreover, incorporated secondary metabolites, which were probably reflected by the electron-dense innermost wall layer (Figs 14–15), could also protect against harmful UV irradiation. *S. cryophila* K-1 shares these strategies with other snow algae, e.g. *Chloromonas brevispina* (Hoham *et al.* 1979), *C. nivalis* (Remias *et al.* 2010) and *C. polyptera* (Remias *et al.* 2013).

The morphology of swimmers and the complete life cycle of *Scotiella cryophila* K-1 from Europe remain unknown. Interestingly, morphologically identical cysts in field material from North America (Hoham *et al.* 2002), addressed as *Chloromonas rosae* var. *psychrophila*, had multiple plastids and sizes comparable with those of this study ($28\text{--}31 \mu\text{m} \times 10\text{--}18 \mu\text{m}$). Conductivity, pH values and light regime of the North American and the Austrian microhabitats of cysts of *S. cryophila* were similar but it remains unresolved if these field cysts from America were genetically identical to *S. cryophila* K-1 from Europe. Accordingly, we found scattered cells of *S. cryophila* recently in Iceland (Snæfjellsjökul, July 2017, DR, pers. obs.), the cell sizes were again in the range of the Austrian and North American samples.

A question that remains is why vegetative cells of '*Chloromonas rosae* var. *psychrophila*' and cysts of *Scotiella cryophila* K-1 are placed in different parts of the phylogenetic tree. An explanation could be that cysts similar to *S. cryophila* K-1 are produced by different species worldwide. This phenomenon was reported by Matsuzaki *et al.* (2015) for *C. nivalis*. Also, for *C. reticulata* (e.g. SAG 29.83, SAG 32.86, SAG 26.90) the morphology of stages of '*Scotiella*' is still unknown. Moreover, no molecular proof was given that the type strain UTEX SNO47 of '*C. rosae* var. *psychrophila*' (or any other strains in the UTEX collection deposited under this taxon) and cysts resembling *S. cryophila* from the Americas are genetically identical, which should be revealed by molecular protocols.

In summary, we characterised the morphology, physiology and phylogenetic position of a snow algae causing monospecific green blooms in the Austrian Alps that most likely represent the previously described *Scotiella cryophila* (Chodat 1922). Other physiological aspects, such as the occurrence of antifreeze agents, accumulation of soluble carbohydrates (osmolytes), presence of ice binding proteins (Raymond 2014) or the fatty acid composition (e.g. Procházková *et al.* 2018a), have not yet been studied.

The biodiversity of cryoflora is still not thoroughly explored. Molecular and life cycle studies including both field blooms and strains isolated from snow are needed to answer general ecological questions. Do a few globally distributed species of Chlamydomonadaceae dominate melting snow fields, or are local taxa with distinct distribution but similar morphology of immotile stages more common? Long distance dispersal strategies of snow algae have hardly been investigated. New techniques like high-throughput-sequencing of several molecular markers (e.g. 18S, ITS2) will be a support in establishing biogeography of snow algae (Lutz *et al.* 2016). In addition, molecular re-investigations of strains from North American sites, which were designated as *Chloromonas rosae* var. *psychrophila*, and field cysts, which are morphologically identical to *Scotiella cryophila* Chodat, are needed. Resampling of the type locality of this latter taxon in western Switzerland could be useful. Similarly, a phylogenetic position of *S. cryophila* var. *groenlandica* is lacking. Mechanisms of physiologic adaptation remain unexplained, such as drastic cellular changes like photo acclimation to low light below the snow surface and high-light exposure at the surface in the course of a few weeks. Finally, what are the mechanisms that cause cyst germination?

ACKNOWLEDGEMENTS

The authors acknowledge grants from the Austrian Science Fund (FWF): P 29959 to DR, I 1951-B16 to AH, Czech Science Foundation (GACR) project 18-02634S to LP and LN. We would like to thank Sabrina Obwegeser (University of Innsbruck) for help in TEM sectioning and image generation (sample GK02). We express sincere thanks to Birgit Sattler (University of Innsbruck, Institute of Ecology, Austria) for providing access to the limnologic field station at Kühtai.

SUPPLEMENTARY DATA

Supplementary data associated with this article can be found online at <http://dx.doi.org/10.2216/18-45.1.s1>.

REFERENCES

- ANESIO A.M., LUTZ S., CHRISTMAS N.A.M. & BENNING L.G. 2017. The microbiome of glaciers and ice sheets. *NPJ Biofilms and Microbiomes* 3: 1–11.
- CHODAT R. 1922. Matériaux pour l'histoire des algues de la Suisse. *Bulletin de la Société Botanique de Genève* 13: 66–114.
- CVETKOVSKA M., HÜNER N.P.A. & SMITH D.R. 2017. Chilling out: the evolution and diversification of psychrophilic algae with a focus on Chlamydomonadales. *Polar Biology* 40: 1169–1184.
- DARTY K., DENISE A. & PONTY Y. 2009. VARNA: Interactive drawing and editing of the RNA secondary structure. *Bioinformatics* 25: 1974–1975.
- GANEY G.Q., LOSO M.G., BURGESS A.B. & DIAL R.J. 2017. The role of microbes in snowmelt and radiative forcing on an Alaskan icefield. *Nature Geoscience* 10: 754–759.
- GORTON H.L., WILLIAMS W.E. & VOGELMANN T.C. 2001. The light environment and cellular optics of the snow alga *Chlamydomonas nivalis* (Bauer) Wille. *Photochemistry and Photobiology* 73: 611–620.
- HOHAM R.W. & DUVAL B. 2001. Microbial ecology of snow and freshwater ice with emphasis on snow algae. In: *Snow Ecology: an interdisciplinary examination of snow-covered ecosystems* (Ed. by H.G. Jones, J.W. Pomeroy, D.A. Walker & R.W. Hoham), pp. 168–228. Cambridge University Press, Cambridge, UK.
- HOHAM R.W. & MULLET J.E. 1977. The life history and ecology of the snow alga *Chloromonas cryophila* sp. nov. (Chlorophyta, Volvocales). *Phycologia* 16: 53–68.
- HOHAM R.W. & MULLET J.E. 1978. *Chloromonas nivalis* (Chod.) Hoh. & Mull. Comb. Nov., and additional comments on the snow alga, *Scotiella*. *Phycologia* 17: 106–107.
- HOHAM R.W., ROEMER S.C. & MULLET J.E. 1979. The life history and ecology of the snow alga *Chloromonas brevispina* comb. nov. (Chlorophyta, Volvocales). *Phycologia* 18: 55–70.
- HOHAM R.W., YATSKO C.P., GERMAIN L. & JONES H.G. 1989. Recent discoveries of snow algae in Upstate New York and Quebec Province and preliminary reports on related snow chemistry. In: *Proceedings of the 46th annual eastern snow conference*; 1989 June 8–9; Quebec City (Ed. by J.E. Lewis), pp. 196–200.
- HOHAM R.W., SCHLAG E.M., KANG J.Y., HASSELWANDER A.J., BEHRSTOCK A.F., BLACKBURN I.R., JOHNSON R.C. & ROEMER S.C. 1998. The effects of irradiance levels and spectral composition on mating strategies in the snow alga, *Chloromonas* sp. -D, from the Tughill Plateau, New York State. *Hydrological Processes* 12: 1627–1639.
- HOHAM R.W., BONOME T.A., MARTIN C.W. & LEEBENS-MACK J.H. 2002. A combined 18S rDNA and rbcL phylogenetic analysis of *Chloromonas* and *Chlamydomonas* (Chlorophyceae, Volvocales) emphasizing snow and other cold-temperature habitats. *Journal of Phycology* 38: 1051–1064.
- HOHAM R.W., BERMAN J.D., ROGERS H.S., FELIO J.H., RYBA J.B. & MILLER P.R. 2006. Two new species of green snow algae from Upstate New York, *Chloromonas chenangoensis* sp. nov. and *Chloromonas tughillensis* sp. nov. (Volvocales, Chlorophyceae) and the effects of light on their life cycle development. *Phycologia* 45: 319–330.
- HOHAM R.W., FILBIN R.W., FREY F.M., PUSACK T.J., RYBA J.B., McDERMOTT P.D. & FIELDS R.A. 2007. The optimum pH of the green snow alga, *Chloromonas tughillensis* and *Chloromonas chenangoensis*, from Upstate New York. *Arctic, Antarctic, and Alpine Research* 39: 65–73.
- HOHAM R.W., McCAY T.S., POIRIER M.B. & BELL T. 2008. Balsam fir leaf litter extract stimulates growth of the green snow alga *Chloromonas rosae* var. *psychrophila* (Chlorophyta, Volvocales) from Whiteface Mountain, New York. *Nova Hedwigia* 86: 133–140.
- KOL E. 1959. The red snow of Greenland I. West Greenland. *Acta Botanica Academiae Scientiarum Hungaricae* 5: 57–70.
- KOL E. 1968. Kryobiologie. Biologie und Limnologie des Schnees und Eises. I. Kryovegetation. In: *Die Binnengewässer* (Ed. by H.J. Elster & W. Ohle), Band XXIV. Schweizerbart'sche Verlagsbuchhandlung, Stuttgart, Germany. 216 pp.
- KOL E. 1970. Vom roten Schnee der Tiroler Alpen. *Annales Historico-Naturales Musei Nationalis Hungarici* 62: 129–136.
- KOMÁREK J. & NEDBALOVÁ L. 2007. Green cryosestic algae. In: *Algae and cyanobacteria in extreme environments* (Ed. by J. Seckbach), pp. 321–342. Springer, Dordrecht, Netherlands.
- KVĚDEROVÁ J. 2012. Research on cryosestic communities in Svalbard: the snow algae of temporary snowfields in Petunia-bukta, Central Svalbard. *Czech Polar Reports* 2: 8–19.
- LIGHT J.J. & BELCHER J.H. 1968. A snow microflora in the Cairngorm Mountains, Scotland. *British Phycological Bulletin* 3: 471–473.
- LUKEŠ M., PROCHÁZKOVÁ L., SHMIDT V., NEDBALOVÁ L. & KAFTAN D. 2014. Temperature dependence of photosynthesis and thylakoid lipid composition in the red snow alga *Chlamydomonas* cf. *nivalis* (Chlorophyceae). *FEMS Microbiology Ecology* 89: 303–315.
- LUTZ S., ANESIO A.M., RAISWELL R., EDWARDS A., NEWTON R.J., GILL F. & BENNING L.G. 2016. The biogeography of red snow microbiomes and their role in melting arctic glaciers. *Nature Communications* 7: 11968.
- MATSUZAKI R., HARA Y. & NOZAKI H. 2012. A taxonomic revision of *Chloromonas reticulata* (Volvocales, Chlorophyceae), the type species of the genus *Chloromonas*, based on multigene phylogeny and comparative light and electron microscopy. *Phycologia* 51: 74–85.
- MATSUZAKI R., KAWAI-TOYOOKA H., HARA Y. & NOZAKI H. 2015. Revisiting the taxonomic significance of aplanozygote morphologies of two cosmopolitan snow species of the genus *Chloromonas* (Volvocales, Chlorophyceae). *Phycologia* 54: 491–502.
- NEDBALOVÁ L., KOCIÁNOVÁ M. & LUKAVSKÝ J. 2008. Ecology of snow algae in the Giant Mts. *Opera Corcontica* 45: 59–68.
- NEDBALOVÁ L., MIHÁL M., KVĚDEROVÁ J., PROCHÁZKOVÁ L., ŘEZANKA T. & ELSTER J. 2017. Identity, ecology and ecophysiology of planktic green algae dominating in ice-covered lakes on James Ross Island (northeastern Antarctic Peninsula). *Extremophiles* 21: 187–200.
- POSADA D. 2008. jModelTest: Phylogenetic model averaging. *Molecular Biology and Evolution* 25: 1253–1256.
- PROCHÁZKOVÁ L., REMIAS D., ŘEZANKA T. & NEDBALOVÁ L. 2018a. *Chloromonas nivalis* subsp. *tatrae*, subsp. nov. (Chlamydomonadales, Chlorophyta): re-examination of a snow alga from the High Tatras Mountains (Slovakia). *Fottea* 18: 1–18.
- PROCHÁZKOVÁ L., REMIAS D., HOLZINGER A., ŘEZANKA T. & NEDBALOVÁ L. 2018b. Ecophysiological and morphological comparison of two populations of *Chlamydomonas* sp. (Chlorophyta) causing red snow on ice-covered lakes in the High Tatras and Austrian Alps. *European Journal of Phycology* 53: 230–243.
- PRÖSCHOLD T., MARIN B., SCHLÖSSER U.G. & MELKONIAN M. 2001. Molecular phylogeny and taxonomic revision of (Chlorophyta). I. Emendation of *Chlamydomonas* Ehrenberg and *Chloromonas* Gobi, and description of *Oogamochlamys* gen. nov. and *Lobochlamys* gen. nov. *Protist* 152: 265–300.
- RAYMOND J.A. 2014. The ice-binding proteins of a snow alga, *Chloromonas brevispina*: probable acquisition by horizontal gene transfer. *Extremophiles* 18: 987–994.
- REMIAS D. 2012. Cell structure and physiology of alpine snow and ice algae. In: *Plants in alpine regions. Cell physiology of adaptation and survival strategies* (Ed. by C. Lütz), pp. 175–186. Springer, Vienna.
- REMIAS D., LÜTZ-MEINDL U. & LÜTZ C. 2005. Photosynthesis, pigments and ultrastructure of the alpine snow alga *Chlamydomonas nivalis*. *European Journal of Phycology* 40: 259–268.
- REMIAS D., KARSTEN U., LÜTZ C. & LEYA T. 2010. Physiological and morphological processes in the Alpine snow alga *Chloromonas nivalis* (Chlorophyceae) during cyst formation. *Protoplasma* 243: 73–86.
- REMIAS D., WASTIAN H., LÜTZ C. & LEYA T. 2013. Insights into the biology and phylogeny of *Chloromonas polyptera* (Chlorophyta), an alga causing orange snow in Maritime Antarctica. *Antarctic Science* 25: 648–656.
- SEIBEL P.N., MÜLLER T., DANDEKAR T., SCHULTZ J. & WOLF M. 2006. 4SALE – a tool for synchronous RNA sequence and

- secondary structure alignment and editing. *BMC Bioinformatics* 7: 498.
- SEIBEL P.N., MÜLLER T., DANDEKAR T. & WOLF M. 2008. Synchronous visual analysis and editing of RNA sequence and secondary structure alignments using 4SALE. *BMC Research Notes* 1: 91.
- STEIN J.R. & BROOKE R.C. 1964. Red snow from Mt. Seymour, British Columbia. *Canadian Journal of Botany* 42: 1183–1188.
- WALSBY A.E. 1997. Modelling the daily integral of photosynthesis by phytoplankton: its dependence on the mean depth of the population. *Hydrobiologia* 349: 65–74.
- WHITFORD L.A. & KIM Y.C. 1971. Algae from alpine areas in Rocky Mountain National Park, Colorado. *The American Midland Naturalist* 85: 425–430.

Received 26 April 2018; accepted 27 April 2018

Supplemental Material

Ecology, cytology and phylogeny of the snow alga *Scotiella cryophila* K-1 (Chlamydomonadales, Chlorophyta) from the Austrian Alps

DANIEL REMIAS¹, LENKA PROCHÁZKOVÁ², ANDREAS HOLZINGER³ AND LINDA NEDBALOVÁ²

¹University of Applied Sciences, Campus Wels, Stelzhamerstr. 23, A-4600 Wels, Austria

²Charles University, Faculty of Science, Department of Ecology, Viničná 7, CZ-128 44

Prague, Czech Republic

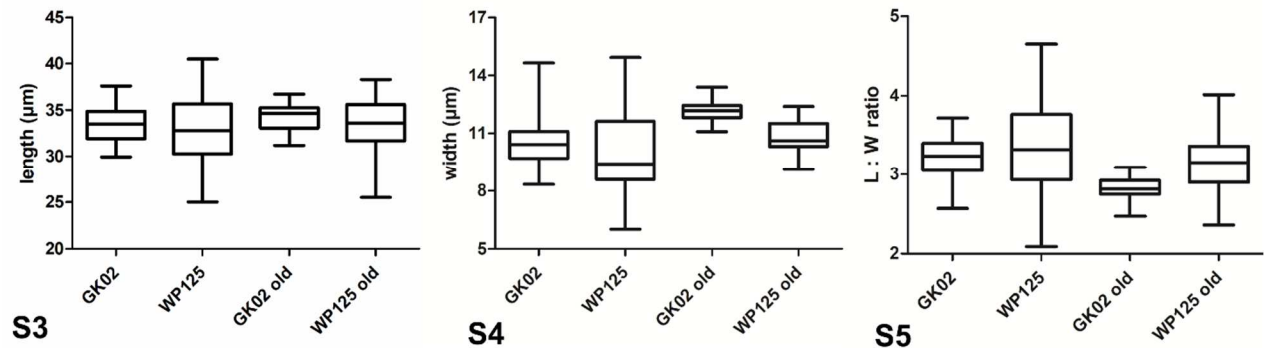
³University of Innsbruck, Department of Botany, Sternwartestr. 15, A-6020 Innsbruck, Austria



Figs S1-S2. Overview of sampling sites of *Scotiella cryophila* K-1 from Kühtai, Tyrol, Alps, Austria. Photos taken at 30 May 2017.

Fig. S1. A flat, open site above timberline close to Gossenkölle Lake.

Fig. S2. Detail view of the green snow after digging to a depth of approximately 20 to 40 cm.



Figs S3-S5. Cell size ranges of cysts of *Scotiella cryophila* K-1 from the Austrian Alps in the moment of harvest (GK02, n = 28; WP125, n = 51) and three months later (GK02 old, n = 14; WP125 old, n = 31). L:W ratio = length to width ratio.



Fig. S6: Mature cysts of *Scotiella cryophila* K-1. Left cell with reddish lipids at each cell pole. Scale bar = 10 µm.

Table S1. List of primers used for amplification of 18S rDNA, ITS1 rDNA, ITS2 rDNA (ITS) and *rbcL* markers; (F) forward; (R) reverse.

Primer	Marker	Direction	Sequence	Reference
18F	18S	F	AACCTGGTTGATCCTGCCAGT	(Katana <i>et al.</i> 2001)
18R	18S	R	TGATCCTTCTGCAGGTTACCTACG	(Katana <i>et al.</i> 2001)
FC	18S	F	GGGAGGTAGTGACAATAAATA	(Matsuzaki <i>et al.</i> 2015)
RF	18S	R	CCCGTGTTGAGTCAAATTAAG	(Matsuzaki <i>et al.</i> 2015)
AL1500af	ITS	F	GCGCGCTACACTGATGC	(Helms <i>et al.</i> 2001)
LR3	ITS	R	GGTCCGTGTTTCAAGACGG	(Vilgalys & Hester 1990)
ITS5	ITS	F	GGAAGTAAAAGTCGTAACAAGG	(White <i>et al.</i> 1990)
ITS4	ITS	R	TCCTCCGCTTATTGATATGC	(White <i>et al.</i> 1990)
Snow-F0	<i>rbcL</i>	F	TTAAAGCTGGTGTWAAAGAYTAYCGTTT	Matsuzaki <i>et al.</i> 2015
Snow-R2	<i>rbcL</i>	R	AARTCTAAWCCACCACGTAAACA	(Matsuzaki <i>et al.</i> 2015)
Snow-F3	<i>rbcL</i>	F	CAAGTWGAACGTGACAAATTAAC	(Matsuzaki <i>et al.</i> 2015)
<i>rbcL</i> 14R	<i>rbcL</i>	R	CGTTCWCCTTCAAGTTTACC	(Hoham <i>et al.</i> 2002)
Snow-F4	<i>rbcL</i>	F	GAACGTGACAAATTAACAAATA	(Matsuzaki <i>et al.</i> 2015)
Snow-R12	<i>rbcL</i>	R	CTAAAGTAACTTCACGTTCTCCTTC	(Matsuzaki <i>et al.</i> 2015)
<i>rbcL</i> 1F	<i>rbcL</i>	F	GCTGGTGTTAAAGATTATCG	(Hoham <i>et al.</i> 2002)
<i>rbcL</i> 7R	<i>rbcL</i>	R	AAATAAATACCACGGCTACG	(Hoham <i>et al.</i> 2002)

Table S2. List of taxa and GenBank accession numbers of newly obtained sequences of nuclear-encoded 18S ribosomal DNA (rDNA) genes, nuclear rDNA internal transcribed spacer 1 (ITS1) and spacer 2 (ITS2) regions, and the large subunit of RuBisCO (*rbcL*) genes.

Taxon	Specimen/strain	Accession number			
		18S rDNA	ITS1 rDNA	ITS2 rDNA	<i>rbcL</i>
<i>Scotiella cryophila</i> K-1	GK02,WP125	MG253843	MG253843	MG253843	MG253844
<i>Chloromonas rosae</i> var. <i>psychrophila</i>	UTEX SNO47	MG253845	MG253846	MG253846	MG253847

ADDITIONAL REFERENCES:

- HELMS G., FRIEDL T., RAMBOLD G. & MAYRHOFER H. 2001. Identification of photobionts from the lichen family Physciaceae using algal-specific ITS rDNA sequencing. *The Lichenologist* 33: 73–86.
- KATANA A., KWIATOWSKI J., SPALIK K., ZAKRYŚ B., SZALACHA E. & SZYMAŃSKA H. 2001. Phylogenetic position of *Koliella* (Chlorophyta) as inferred from nuclear and chloroplast small subunit rDNA. *Journal of Phycology* 37: 443–451.
- VILGALYS R. & HESTER M. 1990. Rapid genetic identification and mapping of enzymatically amplified ribosomal DNA from several *Cryptococcus* species. *Journal of Bacteriology* 172: 4238–4246.
- WHITE T.J., BRUNS T., LEE S. & TAYLOR J. 1990. Amplification and direct sequencing of fungal ribosomal RNA Genes for phylogenetics. *PCR Protocols: A Guide to Methods and Applications* 18: 315–322.

Paper VI

Two new *Kremastochryopsis* species,

***K. austriaca* sp. nov. and *K. americana* sp. nov. (Chrysophyceae)**

Remias D¹, Procházková L², Nedbalová L² & Andersen R³ (in press):

Journal of Phycology, doi: 10.1111/jpy.12937

¹ School of Engineering, University of Applied Sciences Upper Austria, 4600 Wels, Austria

² Department of Ecology, Faculty of Science, Charles University, 12844 Prague, Czech Republic

³ Friday Harbor Laboratories, University of Washington, Friday Harbor, Washington DC

98250, USA

TWO NEW *KREMASTOCHRYSOPSIS* SPECIES, *K. AUSTRIACA* SP. NOV. AND *K. AMERICANA* SP. NOV. (CHRYSTOPHYCEAE)¹

Daniel Remias² 

School of Engineering, University of Applied Sciences Upper Austria, 4600 Wels, Austria

Lenka Procházková, Linda Nedbalová 

Department of Ecology, Faculty of Science, Charles University, 12844 Prague, Czech Republic

and Robert A. Andersen

Friday Harbor Laboratories, University of Washington, Friday Harbor, Washington DC 98250, USA

Melting summer snow in the Austrian Alps exhibited a yellowish bloom that was mainly comprised of an unidentified unicellular chrysophyte. Molecular data (18S rRNA and *rbcL* genes) showed a close relationship to published sequences from an American pond alga formerly identified as *Kremastochrysis* sp. The genera *Kremastochrysis* and *Kremastochryopsis* are morphologically distinguished by the number of flagella observed with the light microscope, and therefore we assigned the Austrian snow alga and an American pond alga to the genus *Kremastochryopsis*. Transmission and scanning electron microscopy revealed that swimming cells had two flagella oriented in opposite directions, typical for the Hibberdiales. Molecular phylogenetic analyses showed that both new species were closely related to *Hibberdia*. *Kremastochryopsis ocellata*, the type species and only known species, has two chloroplasts per cell and the zoospores have red eyespots. Our two organisms had only a single chloroplast and no zoospore eyespot, but their gene sequences differed substantially. Therefore, we described two new species, *Kremastochryopsis austriaca* sp. nov. and *Kremastochryopsis americana* sp. nov. When grown in culture, both taxa showed a characteristic hyponeustonic growth (hanging below the water surface), whereas older immotile cells grew at the bottom of the culture vessel. Ecologically, *Kremastochryopsis austriaca* sp. nov., which caused snow discolorations, had no close phylogenetic relationships to other psychrophilic chrysophytes, for example, *Chromulina chionophila*, *Hydrurus* sp., and *Ochromonas*-like flagellates.

Key index words: *Chromophyton*; *Kremastochrysis*; psychrophilic; snow algae; substitutional saturation

The Chrysophyceae is a diverse class of heterokont (stramenopile) microorganisms that occur in a variety of freshwater and marine habitats (Pascher 1912, 1913, Bourrelly 1957, Starmach 1985, Nicholls and Wujek 2015). Several chrysophytes (e.g., *Chromophyton*, *Chrysotilos*, *Kremastochrysis*, and *Kremastochryopsis*) are associated with the air–water interface, or neuston. Of these, *Kremastochrysis* and *Kremastochryopsis* hang down from the air–water interface and are hyponeustonic organisms (Pascher 1942). Conversely, the more commonly occurring *Chromophyton* grows up from the air–water interface and is an epineustonic organism (Woronin 1880, Lund 1942, Vischer 1943, Petersen and Hansen 1958). *Kremastochrysis* has been rarely reported since its description by Pascher (1942). The type species, *Kremastochrysis pendens*, has a single chloroplast, and its zoospores have two flagella but no eyespot was reported. Pascher (1942) described a second species, *Kremastochrysis ocellata*, that has two chloroplasts, and its zoospores are uniflagellate and possess an eyespot on one of the plastids. Bourrelly (1957) proposed the genus *Kremastochryopsis* (*Kremastochryopsis ocellata*) because of its single visible flagellum when viewed with a light microscope. Thus, *Kremastochrysis* and *Kremastochryopsis* differ by number of flagella visible by light microscopy. Finally, a third species, *Kremastochrysis minor* Catalan has been described (Catalan 1987).

The occurrence of one or two flagella (and their relative lengths) has long been an important character for classifying taxa in the Chrysophyceae (e.g., Pascher 1913; Chromulinales, Isochrysidales, and Ochromonadales). This character reached a pinnacle when Bourrelly (1965) established subclasses within the Chrysophyceae based on flagellar patterns (see also Bourrelly 1981, Starmach 1985, Andersen 2007). Electron microscopy showed that a second, very short flagellum was present on organisms previously believed to be uniflagellates (e.g., Rouiller and Fauré-Fremiet 1958, Belcher and Swale

¹Received 21 March 2019. Accepted 10 September 2019.

²Author for correspondence: email daniel.remias@fh-wels.at.

1 1967, 1971, Hibberd 1976, Andersen 1986, 1989).
 2 However, despite the discovery of a second flagel-
 3 lum for “uniflagellate” organisms, classification
 4 based upon flagellar number has persisted and is
 5 supported by molecular evidence. One early molec-
 6 ular phylogenetic study suggested that uniflagellate
 7 and biflagellate lineages may be monophyletic, sup-
 8 porting the Pascher/Bourrelly classifications (Anders-
 9 sen et al. 1999). However, more recent molecular
 10 phylogenetic studies recovered only smaller clades
 11 that were strictly uniflagellate or biflagellate, while a
 12 few clades were recovered with both flagellar types
 13 (e.g., Andersen 2007, Grossmann et al. 2016, Ander-
 14 sen et al. 2017, Pusztai and Škaloud 2019). Today,
 15 flagellar number (as viewed in the light microscope)
 16 carries phylogenetic signal for smaller clades, but
 17 these clades characterize orders, families or genera,
 18 not subclasses.

19 This paper addresses the molecular phylogenetic
 20 relationships for two new species of *Kremastochryso-*
 21 *psis*. One strain was previously identified as *Kremas-*
 22 *tochrysis* sp. (Andersen 2007) and the other strain
 23 was recently isolated from melting alpine snow, that
 24 is, a non-hyponeustonic habitat. We discuss the rela-
 25 tionships of *Kremastochrysis*, *Kremastochryso-*
 26 *psis* and related chrysophytes, including comments about
 27 snow habitats.

MATERIALS AND METHODS

32 *Collection, culturing, and microscopy.* Strain DR75b was col-
 33 lected from melting snow at an alpine meadow May 5,
 34 2017 in Austria, province Tyrol, district Imst, east of
 35 Kühtai village. The GPS was 47°13.223 N, 11°02.431 E, at
 36 an elevation of 1998 m. A unialgal strain was isolated from
 37 petri dishes with solidified DY-Vm medium (Na₂HPO₄·H₂O
 38 substituted for Na₂ β-glycerophosphate; [https://ncma.bigelow.org/media/wysiwyg/Algal_recipes/NCMA_algal_med-
 39 ium_DY-V.pdf](https://ncma.bigelow.org/media/wysiwyg/Algal_recipes/NCMA_algal_medium_DY-V.pdf)) and 1.6% agar, kept at 5°C. Strain CCMP
 40 260 was collected from a pond in Massachusetts, USA, by
 41 Ralph Lewin, but other information is missing (e.g., date,
 42 precise location). For morphological studies, both strains
 43 were grown at room temperature (varying between 10°C
 44 and 25°C) in DY-V medium (with Na₂ β-glycerophosphate)
 45 or in a biphasic soil-water medium. Cells were observed
 46 with a Leica DM RB light microscope (Leica Microsystems
 47 Inc., Buffalo Grove, IL, USA) equipped with differential
 48 interference contrast, phase contrast, brightfield, and dark-
 49 field optics; cells were photographed using a Canon T6i
 DSLR camera (Canon USA Inc., Melville, NY, USA).

50 For transmission electron microscopy, strain DR75b was
 51 grown at 1°C and fixed as described previously
 52 (Procházková et al. 2018). TEM grids were examined with a
 53 JEOL 1011 TEM (JEOL Ltd., Tokyo, Japan) at 80 kV. Pho-
 54 tomicrographs were taken with a Veleta CCD camera
 55 equipped with Olympus image analysis software (Olympus
 56 Soft Imaging Solution, Germany) and modified using iTEM
 57 5.1 (Germany Soft Imaging Solution, Germany). For scan-
 58 ning electron microscopy, strain DR75b was grown at 5°C
 59 and strain CCMP260 was grown at 18°C; both strains were
 60 fixed as described in Hanousková et al. (2019). SEM gold-
 coated coverslips were observed at 80V with a JEOL 6380
 LV (JEOL Ltd.).

Molecular phylogeny. Total genomic DNA was extracted
 from strain DR75b as described in Procházková et al. (2018).
 The 18S rRNA and *rbcL* gene regions were amplified from
 DNA isolates by PCR using existing primers. For the 18S
 rRNA gene sequence, there were two PCR reactions: the for-
 ward primer SSUIF (CCT GGT TGA TCC TGC CAG T;
 Medlin et al. 1988) with the reverse primer SSU1295R (TCA
 GCC TTG CGA CCA TAC) and the forward primer SSU1065F
 (TCA GAG GTG AAA TTC TTG GAT T) with the reverse pri-
 mer SSU1954R (CCT TGT TAC GAC TTC TCC TTC C; Yang
 et al. 2012). For the *rbcL* sequence, there was one reaction
 using the forward primer *rbcL*46F (CGT TAY GAA TCT GGT
 GTA ATH CC) and the reverse primer *rbcL*1425R (GTA TCT
 GTT GAW GWA TAG TCR AA; Andersen et al. 2017). Ampli-
 fication and sequencing reactions for these markers were
 identical to those described by Procházková et al. (2018).
 The newly generated sequences of the strain DR75b are avail-
 able under GenBank accession numbers: MK614366 – 18S
 rRNA gene; MK614367 – *rbcL*. The sequences of the second
 investigated strain CCMP260 were published in previous stud-
 ies (Andersen et al. 1999, Andersen 2007).

Two different alignments were constructed for the phylo-
 genetic analyses, based on the 18S rRNA and *rbcL* gene
 sequences. The sequences were selected according to the
 publications of Kristiansen and Škaloud (2017) and Andersen
 (2007) to encompass all chrysophycean lineages. The 18S
 rRNA gene alignment contained 88 sequences (1581 bp); the
 initial *rbcL* matrix consisted of 49 sequences (921 bp). Sec-
 ond, to remove saturated nucleotide sites of the third *rbcL*
 codon partition, a modified site-stripping approach was
 applied (Waddell et al. 1999, Škaloud et al. 2013). Site-
 specific rates were calculated with the “Substitution Rates”
 standard analysis implemented in HyPhy (Pond et al. 2005),
 under a global GTR+G+I model using the inferred Maximum
 Likelihood phylogeny as a guide tree. 66% of fast-evolving
 sites in the third codon position of *rbcL* were removed using
 SiteStripper (Verbruggen 2012), according to the rates file
 generated in HyPhy. The stripped *rbcL* alignment was 816 bp
 long. Third, an *rbcL* matrix consisting of first and second *rbcL*
 codon positions only was prepared (alignment was 614 bp
 long). The outgroup taxa (*Synchroma* and *Nannochloropsis*)
 were selected according to the results of the recent multigene
 phylogenetic analysis of stramenopiles by Yang et al. (2012).
 The best-fit nucleotide substitution model was estimated by
 jModeltest 2.0.1 (Posada 2008). Based on the Akaike Informa-
 tion Criterion, the ‘GTR+I+G’ model was selected for 18S
 rRNA gene. Three partitions were set for *rbcL* gene sequences
 and GTR+I+G substitution model was applied for each of
 three codon positions. The 18S rRNA gene and *rbcL* phyloge-
 netic trees were inferred by Bayesian Inference and Maxi-
 mum Likelihood according to Nedbalová et al. (2017), with
 the minor modification that Markov Chain Monte Carlo runs
 were carried out for three million generations in Bayesian
 Interference. Convergence of the two cold chains was
 checked by the average standard deviation of split frequen-
 cies (0.001228 and 0.001004 for 18S rRNA gene and *rbcL* data
 set, respectively). Bootstrap analyses and Bayesian posterior
 probabilities were performed as described by Nedbalová et al.
 (2017).

RESULTS

Description. *Kremastochryopsis austriaca* Remias,
 Procházková & R. A. Andersen sp. nov. (Figs. 1–3)

Diagnosis: Non-motile vegetative cells without cell
 walls, ~(4)5–8(10) μm diameter; cells with one
 chloroplast, up to three contractile vacuoles, lipid

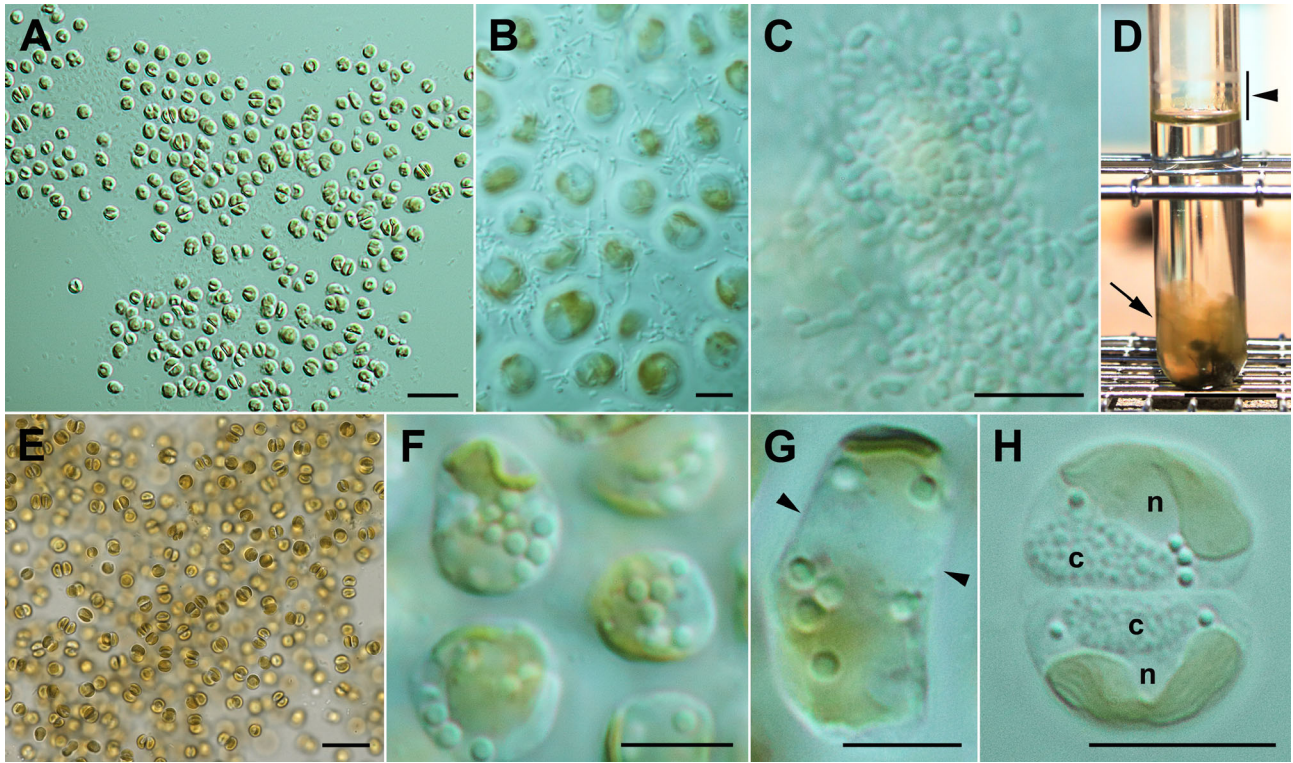


FIG. 1. *Kremastochryopsis austriaca* sp. nov. (A) Monolayer of cells below the air–water interface. Scale bar = 20 μ m. (B) Cells just below the air–water interface surrounded by bacteria. Scale bar = 5 μ m. (C) Bacterial plaques above the cells exactly at the air–water interface. Scale bar = 5 μ m. (D) Test tube (20 mm diameter) showing dried cells above the air–water interface (bar, arrowhead) caused by evaporation from the test tube and a cloud of palmelloid cells near the bottom of the tube (arrow). Biphasic soil–water medium. Scale bar = 20 mm. (E) Palmelloid cell mass from near the bottom of a test tube, likely rich in carotenoids. DY-V medium. Scale bar = 20 μ m. (F) Non-motile cells showing the parietal chloroplast and lipid droplets. Scale bar = 5 μ m. (G) A rectangular dividing cell showing the future division plane (arrowheads). Scale bar = 5 μ m. (H) Two daughter cells showing typical hemispherical shapes. Note the granular chrysolaminarin vacuoles (c) and the nuclei (n). Scale bar = 5 μ m.

droplets, and chrysolaminarin vacuole; both non-motile and motile cells capable of cell division; zoospores formed directly from vegetative cells; zoospores generally oval in shape, 4–6 \times 6–8 μ m; zoospores uniflagellate, with one plastid and no eyespot; cysts not observed; 18S rRNA and *rbcL* gene sequences distinctive.

Holotype here designated: NY 02666691; a permanent microscope slide prepared from culture strain DR75b and deposited in the New York Botanical Garden herbarium, New York City, NY USA.

Isotype here designated: NY 02666692; a permanent microscope slide prepared from culture strain DR75b and deposited in the New York Botanical Garden herbarium, New York City, NY USA.

Isotype here designated: WU 0106471; cells embedded in a resin block from strain DR75b and deposited in the herbarium of the University of Vienna, Austria.

Type locality: Kühltai, district Imst, Tyrol, Austria, Europe; melting winter snow above an alpine meadow (47°13.223'N, 11°02.431'E).

Etymology: the specific epithet “austriaca” refers to Austria, the country where the alga was collected.

***Kremastochryopsis americana* R. A. Andersen, Procházková & Remias sp. nov.** (Figs. 3, 4)

Diagnosis: Non-motile vegetative cells without cell walls, ~(4)5–10(12) μ m in diameter; cells with one chloroplast, 1–2 contractile vacuoles; lipid droplets, and chrysolaminarin vacuole; both non-motile and motile cells capable of cell division; zoospores were oval in shape, 5–6 \times 6–10 μ m, uniflagellate when viewed in the light microscope, with one plastid and no eyespot, 1–2 contractile vacuoles, chrysolaminarin vacuole and fat droplets; cysts not observed; 18S rRNA and *rbcL* gene sequences distinctive.

Holotype here designated: NY 02666693; a permanent microscope slide prepared from culture strain CCMP260 and deposited in the New York Botanical Garden herbarium, New York City, NY USA.

Isotype here designated: NY 02666694; a permanent microscope slide prepared from culture strain CCMP260 and deposited in the New York Botanical Garden herbarium, New York City, NY USA.

Type locality: unknown pond, Massachusetts (presumably near Woods Hole), USA.

Etymology: the epithet “Americana” refers to the continent where the alga was collected.

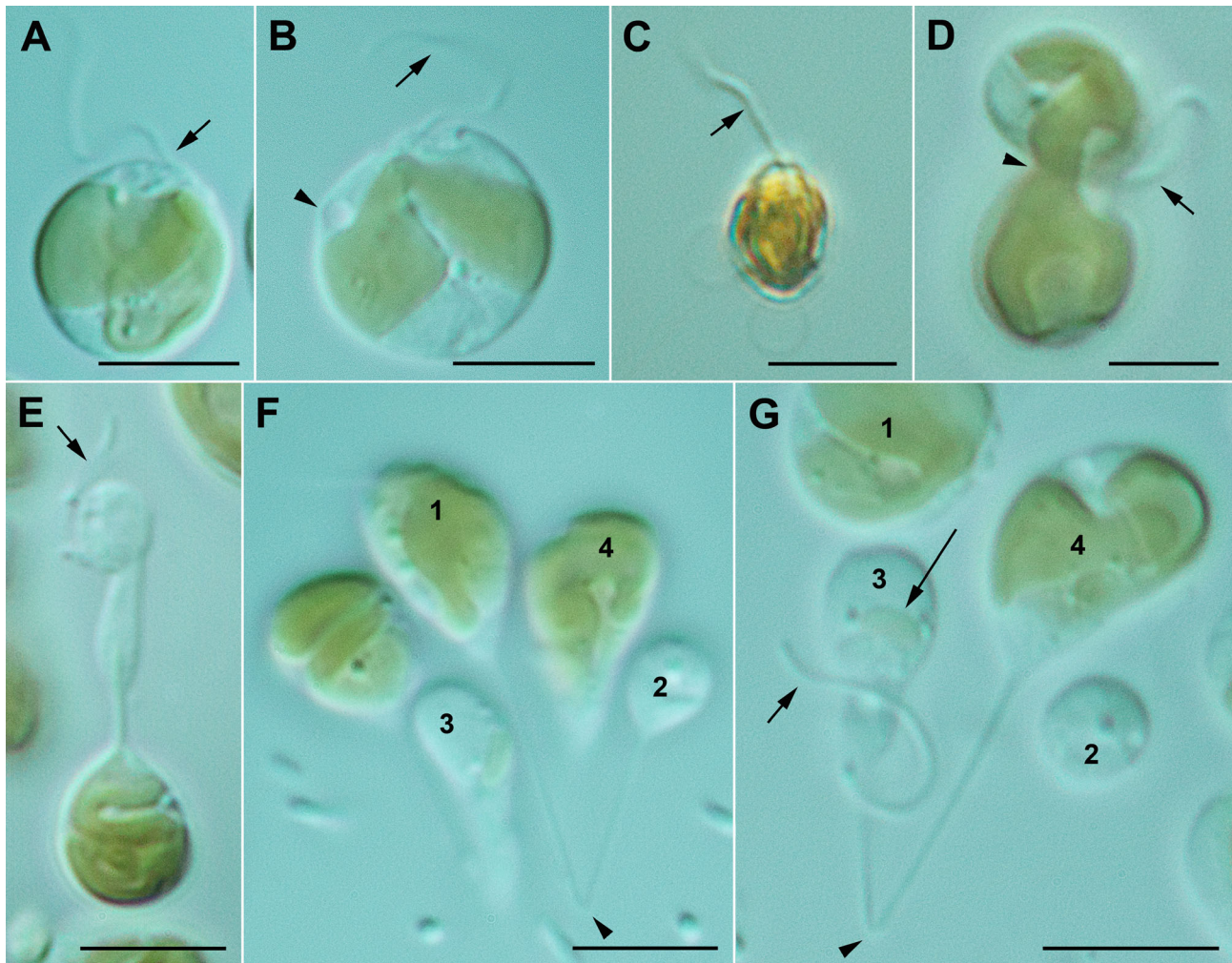


FIG. 2. *Kremastochryopsis austriaca* sp. nov. Scale bars = 5 μ m. (A) Flagellate cell showing the flagellum (arrow) and contractile vacuole (arrowhead). (B) Flagellate cell showing the flagellum (arrow) and contractile vacuole (arrowhead). Note the narrow bridge connecting the two chloroplast lobes. (C) Flagellate cell stained with Lugol's solution showing a single flagellum (arrow). Note that there is no evidence of a second flagellum. (D) A dividing flagellate cell. Note that one future daughter cell has a flagellum but the other does not. Note the chloroplast lobe pinching at the plane where the daughter cells are pinching apart. (E) An odd dividing flagellate cell where one future daughter cell has a flagellum (arrow) but lacks a chloroplast. (F) Image showing a long thin cytoplasmic strand (arrowhead) that connects cells 1 and 2. Note that cell 2 is smaller and lacks a chloroplast. Cell 1 had a flagellum but it is out of the plane of view. (G) Image similar to F but focused slightly different to show the cytoplasmic strain connecting cells 3 and 4. Note the flagellum on the smaller cell (short arrow) and the very small chloroplast in cell 3 (long arrow).

***Kremastochryopsis pendens* Pascher lectotype specimen designated here: figure 9** in Pascher, A. 1942. *Beiheft zum Botanischen Centralblatt. Abteilung A. Morphologie und Physiologie der Pflanzen* 61:467.

***Kremastochryopsis ocellata* (Pascher) Bourrelly lectotype specimen designated here: figure 12c** in Pascher, A. 1942. *Beiheft zum Botanischen Centralblatt. Abteilung A. Morphologie und Physiologie der Pflanzen* 61:470.

Kremastochryopsis austriaca sp. nov. strain DR75b grew just below the air–water interface (hyponeustonically) when grown in DY-V or soil–water medium. These cells formed a monolayer that was composed of immobile and swimming cells (Fig. 1A). Bacteria formed a covering around and over the cells (Fig. 1, B and C). In older cultures,

cells grew at the air–water interface and at the bottom of the culture tube (Fig. 1D). Cells at the bottom of test tubes formed palmelloid “clouds” of cells held together by a colonial gel (Fig. 1E). The gel margin stained with brilliant cresyl blue (not shown). Immobile cells were (4)5–8(10) μ m in size, lacked a cell wall, had a single parietal chloroplast, 1–2 contractile vacuoles, a chrysolaminarin vacuole, and several lipid droplets (Fig. 1, F–H). The chloroplast was sometimes deeply lobed, but always connected by a bridge between the two lobes. Immobile cells divided by first elongating and dividing the chloroplast into two plastids (Fig. 1G) and then by forming hemispherical daughter cells after cytokinesis was completed (Fig. 1H).

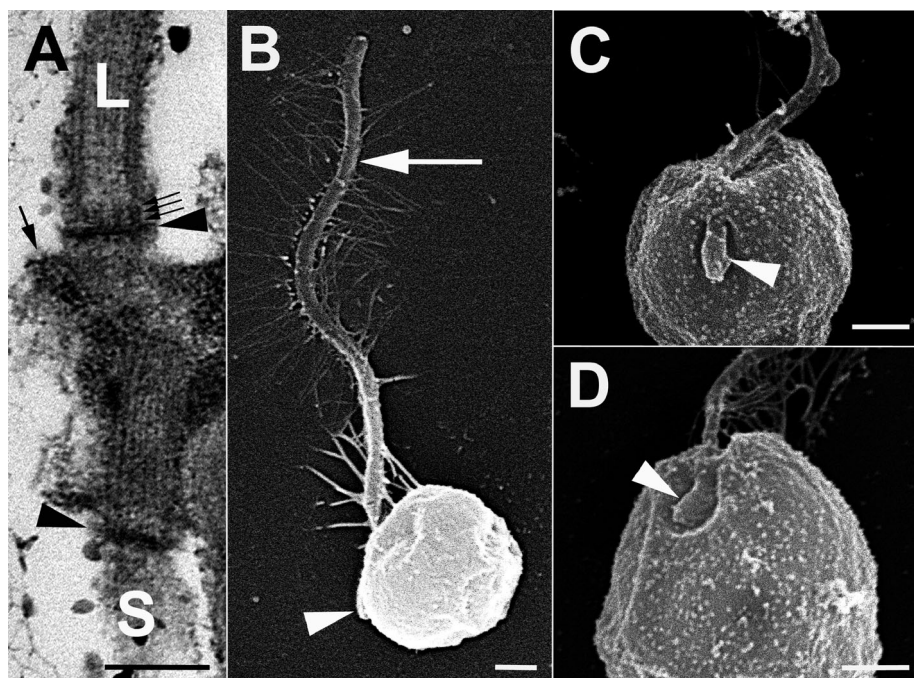


FIG. 3. *Kremastochryopsis austriaca* sp. nov. and *K. americana* sp. nov. (A) *K. austriaca*. TEM image of the long flagellum (L), short flagellum (S), and their basal bodies. Note the dense transitional plates (arrowheads), the three-gyre transitional helix (small arrows), and the microtubules of root R₁ (large arrow). Scale bar = 200 nm. (B) *K. austriaca*. SEM image showing the long flagellum (arrow) and hidden short flagellum (arrowhead). Note that the cell shrank during dehydration. Scale bar = 400 nm. (C) *K. austriaca*. SEM image showing the short flagellum (arrowhead) lying in a shallow depression. Scale bar = 500 nm. (D) *K. americana*. SEM image showing the short flagellum (arrowhead) lying in a shallow depression. Scale bar = 500 nm.

Motile cells were typically 5–8 μm with a single visible flagellum; no eyespot was observed. Swimming cells were spherical to pyriform to oval in shape and had a single parietal chloroplast, 1–3 contractile vacuoles, a chrysolaminarin vacuole but rarely had lipid droplets (Fig. 2, A and B). When stained with Lugol's solution, a second flagellum was not visible (Fig. 2C). Motile cells divided by forming dumbbell shapes and the two daughter cells were separated by a pinching or centripetal constriction type of cytokinesis (Fig. 2D). The plastid typically divided during cytokinesis (Fig. 2D). In some cases, the chloroplast failed to divide, or if divided then failed to segregate, into the two daughter cells, and consequently one of the daughter cells was formed without a chloroplast (Fig. 2, E and F). In some cases, a tiny plastid was observed in one daughter cell but the other daughter cell had a very large plastid (Fig. 2G). For hyponeustonic cells, the two swimming cells separated and rapidly transformed into the typical flagellate cell morphology. Stalked cells occurred when cells attached to around the test tube margin at the air–water interface, and often these cells remained connected by a cytoplasmic strain (Fig. 2, F and G).

Observations using transmission electron microscopy were limited because of the poor fixation quality. Cells had two flagella when viewed with TEM (Fig. 3A). The two flagella were arranged

nearly opposite of each other ($\sim 180^\circ$ orientation of the two basal bodies), and the basal bodies overlapped at their proximal ends. The transitional plates of both flagella were dense, and a transitional helix with three gyres was observed (Fig. 3A). The proximal end of the R₁ root (R₃ root with Moestrup's [2000] system) was present but the fixation quality did not allow for reconstruction of the flagellar apparatus. Observations using scanning electron microscopy showed one long flagellum bearing mastigonemes (Fig. 3B) and one very short second flagellum (Fig. 3, B and C). Both flagella laid in a shallow depression (Fig. 3C).

Kremastochryopsis americana sp. nov. strain CCMP260 grew hyponeustonically just below the air–water meniscus in recently transferred cultures; bacteria grew at or above the air–water interface (Fig. 4A). In older cultures, many cells sank to the bottom of the test tube, and cells formed cloud-like masses with cells held together by a thin colonial gel (not shown). The gel margin stained with brilliant cresyl blue but the watery gel matrix did not stain (not shown). Non-motile vegetative cells were naked (without a cell wall), typically 5–10 μm in diameter, and they contained a single chloroplast, chrysolaminarin vacuole, lipid droplets, and one or two contractile vacuoles (Fig. 4B). When cells were severely flattened by the microscope slide/coverslip, then the chrysolaminarin vacuole became granular,

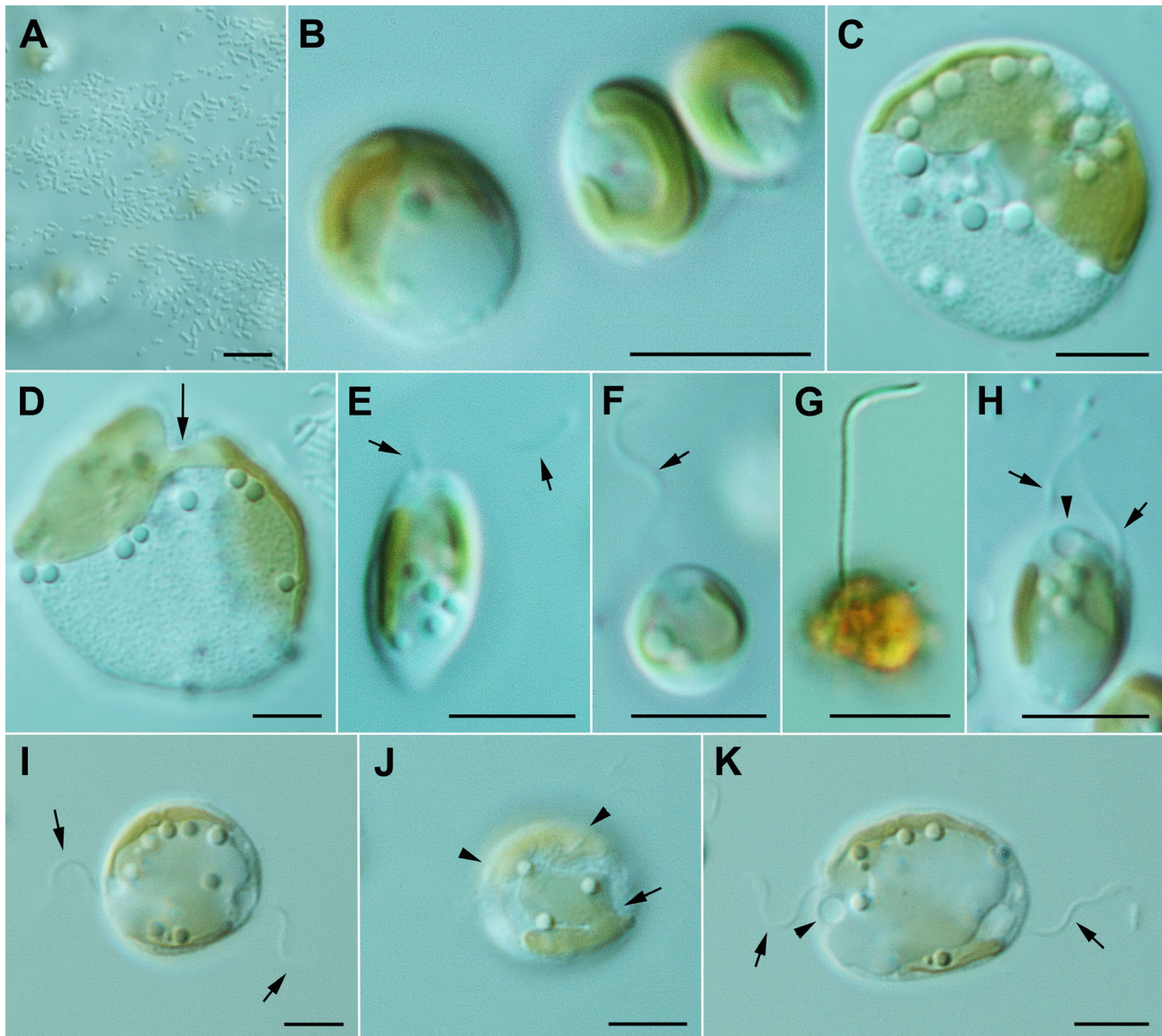


FIG. 4. *Kremastochryopsis americana* sp. nov. Scale bars = 5 μ m. (A) Image of the air–water interface showing the bacterial plaques and algal cells out of focus below the interface. (B) Three vegetative cells showing the parietal chloroplast. (C) A large and very flattened cell showing the bilobed chloroplast, numerous lipid droplets and a granular chrysolaminarin vacuole. (D) A large, flattened cell showing the bridge (arrow) between the two chloroplast lobes. (E) An elongate swimming cell with a single flagellum (arrows). (F) A spherical swimming cell with a single flagellum (arrow). (G) A swimming cell stained with Lugol's solution showing the single flagellum but no evidence of a second flagellum. (H) A dividing swimming cell showing the two visible flagella (arrows) and a contractile vacuole (arrowhead). (I–K) Three images of the same dividing flagellate cell: (I) The cell has flagella at the opposite poles of the cell (arrows). (J) A different focal plane showing that the chloroplast had already divided. Note the upper plastid (arrowheads) and the lower plastid with a deep division between the chloroplast lobes (arrow). (K) The same cell several minutes later that was more elongated. Note the two flagella (arrows) and the contractile vacuole (arrowhead).

showing a papillose consistency (Fig. 4, C and D); such flattened cells reached diameters of nearly 20 μ m before bursting. The chloroplast in smaller cells was parietal and rarely lobed (Fig. 4 B); however, in larger cells, the plastids were bilobed (Fig. 4, C and D). When plastids were deeply lobed, a small bridge between the lobes was visible (Fig. 4D). Cell division of immobile cells was like that described for strain DR75b.

Motile cells were typically 5–6 μ m wide and 6–10 μ m long. They contained a single visible flagellum that was inserted at the anterior end of the cell (Fig. 4, E–G). The chloroplast was parietal and usually trough-shaped, and it lacked a red eyespot (Fig. 4, E and F). The flagellum was 1–1.5 times as long as the cell and beat with a sinusoidal wave motion. The flagellum appeared longer on cells stained with Lugol's solution, but this was due to

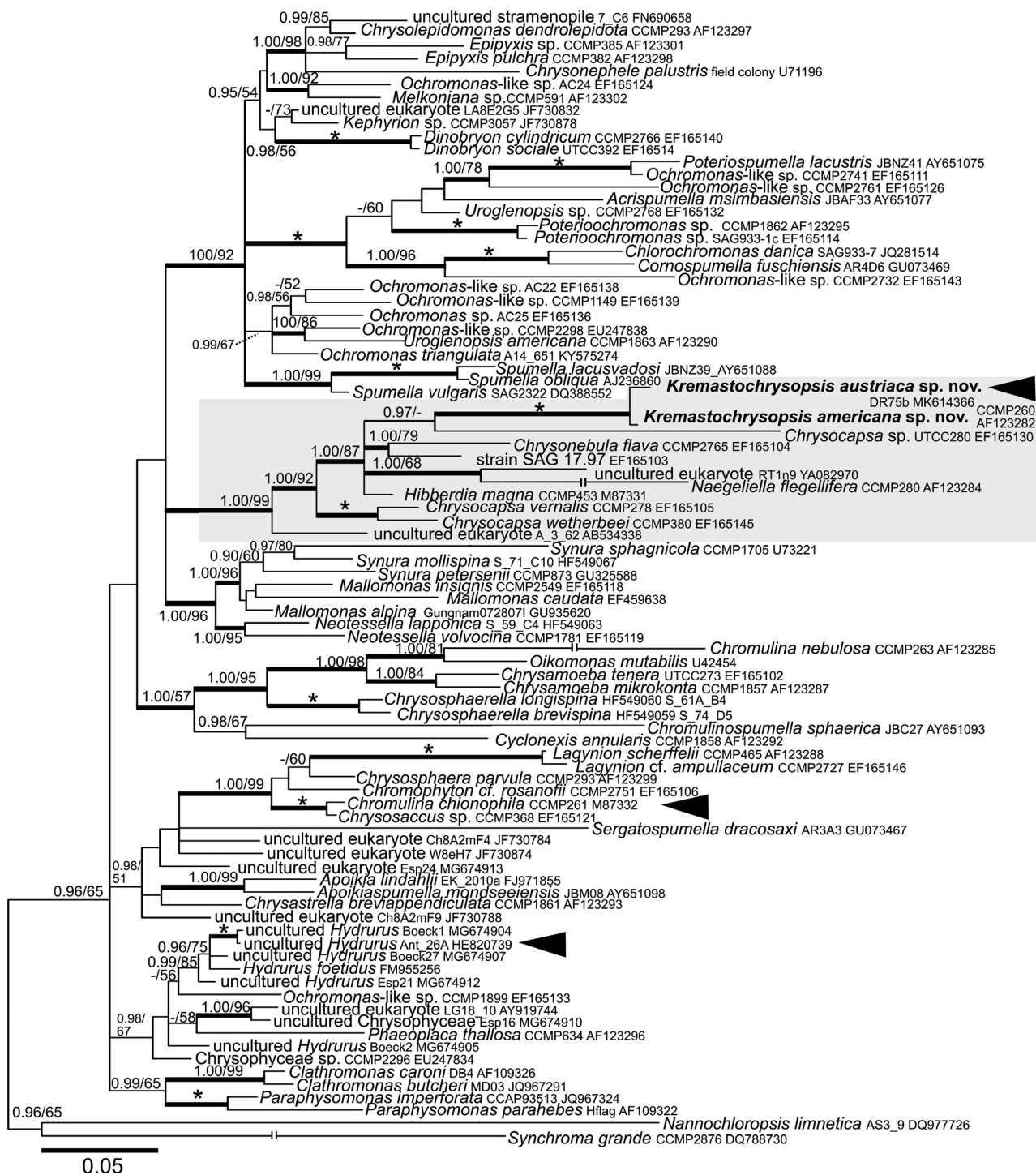


FIG. 5. Bayesian phylogenetic tree based on the 18S rRNA gene. The newly described species are in bold. Accession numbers, strain and field sample codes are indicated after each species name. The scale bar shows the estimated number of substitutions per site. Origin in snow is indicated by black arrowheads for relevant species. The Hibberdiales clade is highlighted in a grey box. Posterior probabilities (0.95 or more) and bootstrap values from maximum likelihood analyses (50% or more) are shown. Full statistical support (1.00/100) is marked with an asterisk. Thick branches represent nodes receiving the highest posterior probability support (1.00). For *Naegeliella flagellifera*, *Chromulina nebulosa*, and *Synchronoma grande* branch lengths were shortened by 50% for graphic reasons.

shrinkage of the cytoplasm (Fig. 4G). Flagellate cells underwent cell division by producing a second immature flagellum via flagellar transformation

(Fig. 4H). The two flagella moved to opposite sides of the mother cell, but the cell remained spheroid in shape (Fig. 4I). The chloroplast divided before

1 there was evidence of cytokinesis (Fig. 4J). Gradu-
 2 ally, the mother cell elongated (Fig. 4K), and then
 3 cytokinesis occurred quickly to produce two daugh-
 4 ter cells. Unlike strain DR75b, CCMP260 rarely pro-
 5 duced colorless daughter cells or stalked cells.

6 No TEM was attempted for *Kremastochrysoptis amer-*
 7 *icana*. SEM observations showed a very short second
 8 flagellum that laid in a shallow depression
 9 (Fig. 3D).

10 Molecular phylogenetic analyses**. The 18S
 11 rRNA gene for the two species differed by 11
 12 nucleotides (out of 1554 bp), and the *rbcL* differed
 13 by 14 nucleotides (out of 1035 bp). Based on 18S
 14 rRNA gene and *rbcL* phylogenies (Figs. 5, 6), *Kre-*
 15 *mastochrysoptis austriaca* sp. nov. and *K. americana* sp.
 16 nov. represented an independent, well-supported
 17 lineage within the well-supported order Hibber-
 18 diales. These two new species were closely related
 19 sister taxa in the 18S rRNA gene tree, and they were
 20 in turn sister to strain UTCC280, tentatively identi-
 21 fied as *Chrysocapsa* sp. In the *rbcL* tree, *Kre-*
 22 *mastochrysoptis* occupied a clade with *Hibberdia magna*,
 23 *Chrysonobula flava*, and strain SAG 17.97. The phylo-
 24 genies inferred from the two markers that they were
 25 partly incongruent: the *rbcL* phylogenetic tree gen-
 26 erally had lower support values for internal
 27 branches, resulting in less resolution of taxonomic
 28 relationships (Fig. 6). A possible saturation of the
 29 *rbcL* data set was checked, the strength of the phylo-
 30 genetic signal versus noise was assessed for the 18S
 31 rRNA gene and different *rbcL* codon partitions
 32 (Fig. S1 in the Supporting Information). The signifi-
 33 cant saturation was revealed for the third *rbcL*
 34 codon partition (Fig. S1C). Neither removal of the
 35 saturated nucleotide sites by the site-stripping
 36 method nor total deletion of the third *rbcL* codon
 37 from alignment improved the reconstructed phy-
 38 logeny (Figs. S2 and S3 in the Supporting Informa-
 39 tion). Still, the *rbcL* phylogeny based on the initial
 40 *rbcL* alignment was more congruent with the 18S
 41 rRNA gene phylogeny than were the two other *rbcL*
 42 trees where nucleotide positions were removed.

DISCUSSION

46 *Morphology and classification.* *Kremastochrysoptis* is a
 47 poorly known genus that was first described from
 48 bog waters near Františkovy Lázně, Czech Republic
 49 (Pascher 1942). The primary defining character of
 50 the genus is its hyponeustonic habit, that is, cells
 51 hanging below the water surface. *Kremastochrysoptis pen-*
 52 *dens*, the type species, has a single chloroplast. Its
 53 vegetative cells are 8–11 μm in diameter, and its
 54 zoospores have two flagella visible with a light
 55 microscope but no eyespot. *Kremastochrysoptis minor* was
 56 described from a small pond in Castellví de Rosanes
 57 in northeastern Spain (Catalan 1987); vegetative
 58 cells of *Kremastochrysoptis minor* are 6–7 μm , with a sin-
 59 gle parietal chloroplast that occupies the surface far-
 60 thest from the water surface. Its zoospores are

biflagellate, 5 μm in diameter (or elliptical,
 5 \times 9 μm in size), and each zoospore has a single
 chloroplast. Both vegetative and zoospore chloro-
 plasts have an eyespot.

Prior to our paper, there was only a single species
 of *Kremastochrysoptis*, *Kremastochrysoptis ocellata*, which
 has two chloroplasts per cell; the vegetative cells are
 up to 25 μm and the zoospores have one LM visible
 flagellum and a red eyespot on one plastid.

Unfortunately, these *Kremastochrysoptis* and *Kre-*
mastochrysoptis species have not been reported again.
 Catalan (1987) designated an ink drawing as the
 holotype (iconotype) for *Kremastochrysoptis minor*, but
 Pascher (1942) did not designate a holotype for
 either of his two taxa. Therefore, no biological
 material was used for the nomenclatural type speci-
 mens and no DNA can be obtained from the icono-
 type. Ideally, recollection of Pascher's two taxa from
 the type locality and gene sequencing would be the
 best approach because one could establish DNA
 sequences for the type species (e.g., see Andersen
 et al. 2017). Such a search for the type species from
 the type locality is beyond the scope of this study,
 and therefore we identified our strains as *Kre-*
mastochrysoptis based upon their light microscopic mor-
 phology. For nomenclatural purposes, we
 designated an ink drawing as the lectotype speci-
 men for each of Pascher's taxa.

The cells of *Chrysotilos ferrea* resemble those of
Kremastochrysoptis. *Chrysotilos ferrea* is also a neu-
 stonic organism and it was found in very shallow
 pools formed by melted snow at mountain mead-
 ows near Lunz, Austria (Pascher 1931). Cells are 7–
 9 μm in size with a single parietal chloroplast; it
 produces dorsoventrally flattened uniflagellate zoos-
 pores (as viewed by light microscopy) with an eye-
 spot. The cells form yellow-brown to black-brown
 flakes (up to 1 mm) on the water surface, but it is
 unclear if these are epineustonic or hyponeustonic
 layers. A thin gelatinous envelope surrounds the
 cells of a flake. A second species, *Chrysotilos tatra-*
ica, was described from the epineuston of a small pools
 near the cable car station Gubałówka, Zakopane
 (Krakow region), Poland (Czosnowski 1948). The
 vegetative cells are spherical, 7–9 μm in diameter,
 with a single golden chloroplast with a small eye-
 spot. Uniflagellate zoospores are 7–10 μm by 5.5–
 7 μm . Thus, *Chrysotilos* vegetative and swimming
 cells are similar to *Kremastochrysoptis*, but there are
 two important differences that separate the genera.
 First, *Chrysotilos* produces pseudocysts-shell-like
 structures that become heavily impregnated with
 iron (Pascher 1931, Czosnowski 1948). The pseudo-
 cysts typically have two parts, upper and lower
 “halves.” Furthermore, *Chrysotilos* produces sporang-
 ia-like structures that contain 2–32 or more cells.
 While *Kremastochrysoptis* may produce palmelloid
 colonies in old cultures, the cells are evenly dis-
 persed and they are never enclosed to produce a
 sporangium-like structure.

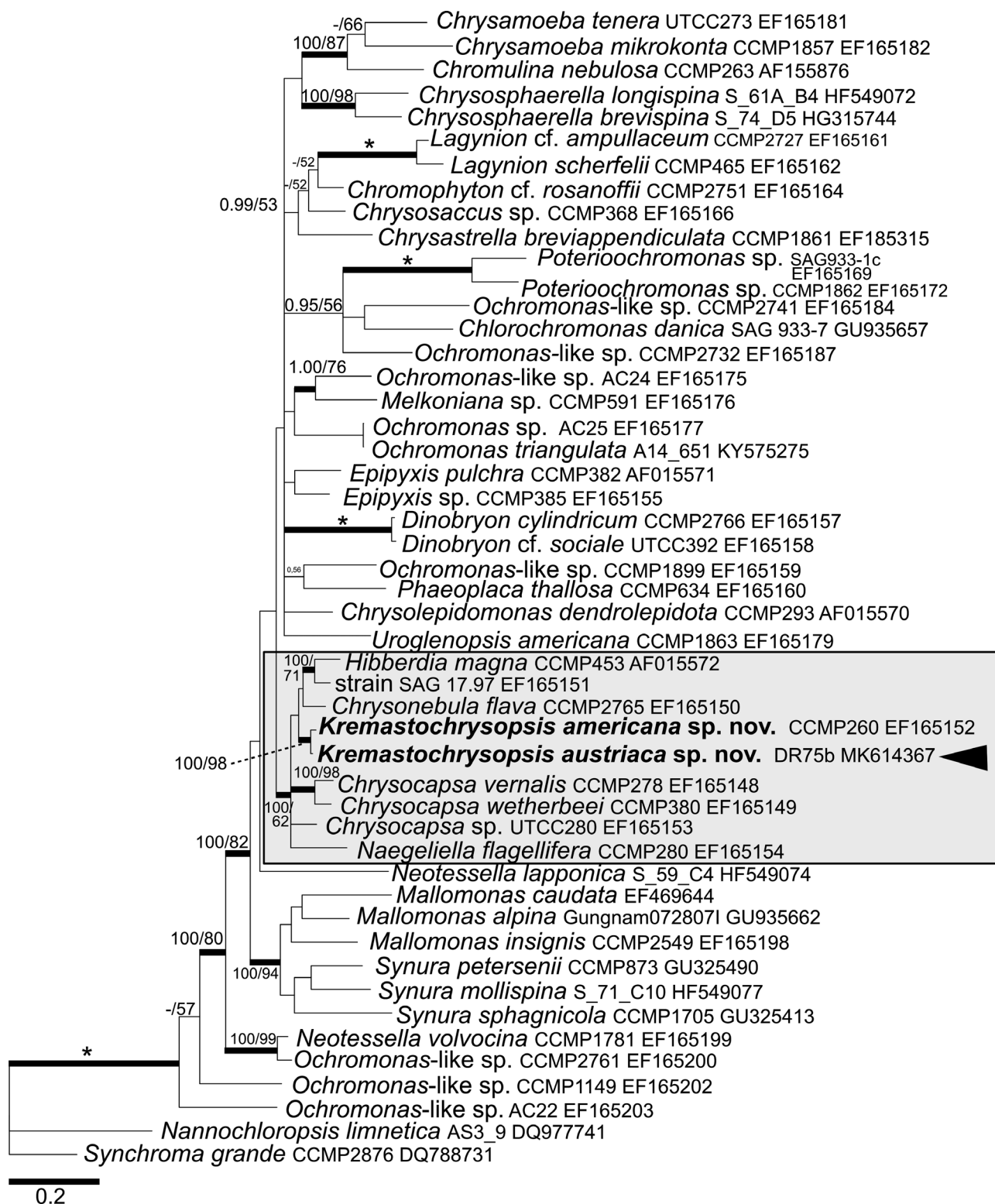


FIG. 6. Bayesian phylogenetic tree based on the *rbcL* gene. The newly described species are in bold. Accession numbers, strain, or field sample codes are indicated after each species name. The scale bar shows the estimated number of substitutions per site. Origin in snow is indicated by black arrowhead for relevant species. The Hibberdiales clade is highlighted in a grey box. Posterior probabilities (0.95 or more) and bootstrap values from maximum likelihood analyses (50% or more) are shown. Full statistical support (1.00/100) is marked with an asterisk. Thick branches represent nodes receiving the highest posterior probability support (1.00).

1 Finally, because *Kremastochryopsis austriaca* was col-
 2 lected in melting snow rather than the neuston, we
 3 compare our strains to the uniflagellate snow alga,
 4 *Chromulina chionophila*. *Chromulina chionophila* has
 5 flattened cells, one flagellum (as viewed in the light
 6 microscope), and an eyespot in the chloroplast
 7 (Stein 1963). *Chromulina chionophila* differs from our
 8 new species because of the flattened cells and the
 9 eyespot. There is some resemblance between the
 10 swimming cells of *Chrysotilos* and *Chromulina chiono-*
 11 *phila*, but the latter does not form pseudocysts or
 12 sporangia.

13 *Molecular phylogeny.* Our phylogenies (18S rRNA
 14 and *rbcL* genes) show that both of our new *Kremas-*
 15 *tochryopsis* species are members of monophyletic
 16 Hibberdiales clade. *Kremastochryopsis austriaca*
 17 showed no close phylogenetic relation to other
 18 chrysophytes causing blooms in melting snow
 19 (Figs. 5, 6), for example, *Chromulina chionophila*
 20 (Hoham 1975), *Hydrurus* sp. (Remias et al. 2013),
 21 or *Ochromonas*-like flagellates (Tanabe et al. 2011).

22 *Ecology.* The occurrence of *Kremastochryopsis aus-*
 23 *triaca* in melting mountain snow causing a yellowish
 24 bloom was surprising because other members of the
 25 Hibberdiales are known from standing or flowing
 26 waters. Previous studies found that *Kremastochryopsis*
 27 *austriaca* occurred together with other “snow algae
 28 genera,” for example, *Chloromonas* and *Sanguina*
 29 (Remias et al. 2018, Procházková et al. 2019). While
 30 additional studies must be made, it seems probable
 31 that *K. austriaca* is distributed in other areas of the
 32 Austrian Alps.

33 DR acknowledges funding from the Austrian Science Fund
 34 (FWF): P29959. LP and LN acknowledge funding from the
 35 Czech Science Foundation (GACR): 18-02634. We are grate-
 36 ful to Pavel Škaloud (Charles University, Prague, Czech
 37 Republic) for consultations about applying the modified site-
 38 stripping approach. We express our thanks to Ivan Čepička
 39 and Miroslav Hylíš (both: Charles University, Prague, Czech
 40 Republic) for their recommendations concerning chemical
 41 fixation for scanning electron microscopy and the flagellar
 42 apparatus observation.

43 Andersen, R. A. 1986. Some new observations on *Saccochrysis*
 44 *piriformis* Korsh. emend. Andersen (Chrysophyceae). In
 45 Kristiansen, J. & Andersen, R. A. [Eds.] *Chrysophytes: Aspects*
 46 *and Problems*. Cambridge University Press, NewYork, pp.
 47 107–17.

48 Andersen, R. A. 1989. Absolute orientation of the flagellar appa-
 49 ratus of *Hibberdia magna* comb. nov. (Chrysophyceae). *Nord.*
 50 *J. Bot.* 8:653–69.

51 Andersen, R. A. 2007. Molecular systematics of the Chrysophyceae
 52 and Synurophyceae. In Lewis, J. & Brodie, J. [Eds.] *Unravel-*
 53 *ing the Algae: The Past, Present and Future of Algal Systematics*.
 54 Taylor and Francis, Boca Raton, Florida, USA, pp. 283–311.

55 Andersen, R. A., Graf, L., Malakhov, Y. & Yoon, H. S. 2017. Redis-
 56 covery of the *Ochromonas* type species *Ochromonas triangulata*
 57 (Chrysophyceae) from its type locality (Lake Veysove,
 58 Donetsk region, Ukraine). *Phycologia* 56:591–604.

59 Andersen, R. A., Van de Peer, Y., Potter, D., Sexton, J. P., Kawa-
 60 chi, M. & Lajeunesse, T. 1999. Phylogenetic analysis of the
 SSU rRNA from members of the Chrysophyceae. *Protist*
 150:71–84.

Belcher, J. H. & Swale, E. M. F. 1967. *Chromulina placentula* sp.
 nov. (Chrysophyceae), a freshwater nanoplankton flagellate.
Br. Phycol. Bull. 3:257–67.

Belcher, J. H. & Swale, E. M. F. 1971. The microanatomy of
Phaeaster pascheri Scherffel (Chrysophyceae). *Br. Phycol. J.*
 6:157–69.

Bourrelly, P. 1957. Recherches sur les Chrysophycées. Morphologie,
 Phylogénie, Systématique. *Revue Algologique Mémoire Hors-*
 4 *Série* 1:1–412.

Bourrelly, P. 1965. La classification des Chrysophycées: ses
 problèmes. *Rev. Algol.* 9:56–60.

Bourrelly, P. 1981. *Les Algues d'eau douce, algues jaunes et brunes*, vol.
 2. Boubée, Paris, 517 pp.

Catalan, J. 1987. *Kremastochrysis minor* sp. nov.: a neustonic mem-
 ber of the Chrysophyceae. *Br. Phycol. J.* 22:257–60.

Czosnowski, J. 1948. O zakwicie neustonowym *Chrysotilos tatraica* n.
 sp. na Gebalówce pod Zakopanem. *Poznanski Tow. Przyj. Nauk*
 11. *Prace Kom. Biol.* 47:47–52.

Doflein, F. 1923. Untersuchungen über Chrysomonaden III.
 Arten von *Chromulina* und *Ochromonas* aus dem badischen
 Schwarzwald und ihre Cystenbildung. IV. Über einige aus
 dem Schwarzwald stammende, dort noch nicht bekannte
 oder neue Chrysomonaden. *Arch. Protistenkunde* 46:267–
 327.

Grossmann, L., Bock, C., Schwiert, M. & Boenigk, J. 2016. Small
 but manifold – hidden diversity in “*Spumella*-like flagellates”.
J. Eukaryot. Microbiol. 63:419–39.

Hanousková, P., Táborský, P. & Čepička, I. 2019. *Dactylomonas*
 gen. nov., a novel lineage of heterolobosean flagellates with
 unique ultrastructure, closely related to the amoeba *Sele-*
 5 *naion koniopes* Park, De Jonckheere & Simpson, 2012.
J. Eukaryot. Microbiol. 66:120–39.

Hibberd, D. J. 1976. The ultrastructure and taxonomy of the
 Chrysophyceae and Prymnesiophyceae (Haptophyceae): a
 survey with some new observations on the ultrastructure of
 the Chrysophyceae. *Bot. J. Linn. Soc.* 72:55–80.

Hoham, R. W. 1975. Optimum temperatures and temperature
 ranges for growth of snow algae. *Arct. Alp. Res.* 7:13–24.

Kristiansen, J. & Škaloud, P. 2017. Chrysophyta. In Archibald, J.
 M., Simpson, A. G. B. & Slamovits, C. H. [Eds.] *Handbook of*
 6 *the Protists*. Springer International Publishing AG, ????, pp.
 331–66.

Lund, J. W. G. 1942. Contributions to our knowledge of British
 Chrysophyceae. *New Phytol.* 41:274–92.

Lund, J. W. G. 1953. New or rare British Chrysophyceae. II.
Hyalobryon polymorphum n. sp. and *Chrysonobula holmesii*
 n. gen., n. sp.. *New Phytol.* 52:114–23.

Medlin, L., Elwood, H. J., Stickel, S. & Sogin, M. L. 1988. The
 characterization of enzymatically amplified eukaryotic 16S-
 like rRNA-coding regions. *Gene* 71:491–9.

Moestrup, Ø. 2000. The flagellate cytoskeleton. In Leadbeater, B.
 S. C. & Green, J. C. [Ed.] *The Flagellates: Unity, Diversity and*
 8 *Evolution*. Taylor & Francis, London, pp. 69–94.

Nedbalová, L., Mihál, L., Kvíderová, J., Procházková, L., Řezanka,
 T. & Elster, J. 2017. Identity, ecology and ecophysiology of
 planktic green algae dominating in ice-covered lakes on
 James Ross Island (northeastern Antarctic Peninsula). *Extre-*
 9 *mophiles* 21:187–200.

Nicholls, K. H. & Wujek, D. E. 2015. Chrysophyceae and
 Phaeothamniophyceae. In Wehr, J. D., Sheath, R. G. & Koci-
 10 olek, J. P. [Eds.] *Aquatic Ecology, Freshwater Algae of North Amer-*
ica, 2nd ed. Academic Press, Cambridge, Massachusetts, USA,
 pp. 537–86.

Pascher, A. 1912. Über Rhizopoden- und Palmellastadien bei
 Flagellaten (Chrysomonaden), nebst einer Übersicht über
 die braunen Flagellaten. *Arch. Protistenkd.* 25:153–200.

Pascher, A. 1913. Chrysomonadinae. In Pascher, A. [Ed.] *Die Süs-*
 11 *swasser-Flora Deutschlands, Österreichs und der Schweiz*. G Fischer,
 Jena, Heft 2, ?????, pp. 7–95.

Pascher, A. 1931. Über eigenartige zweischalige Dauerstadien bei
 zwei tetrasporalen Chrysophyceen (Chrysocapsalen). *Arch.*
 12 *Protistenkunde* 73:73–103.

- Pascher, A. 1942. Über einige mit Schwimmschirmchen versehen Organismen der Wasseroberfläche. *Beiheft zum Botanischen Centralblatt. Abteilung A. Morphologie und Physiologie der Pflanzen* 61:462–87.
- Petersen, J. B. & Hansen, J. B. 1958. On some neuston organisms I. *Saertryk af Bot. Tidsskr.* 54:93–110.
- Pond, S. L. K., Frost, S. D. W. & Muse, S. V. 2005. HyPhy: hypothesis testing using phylogenies. *Bioinformatics* 21:676–9.
- Posada, D. 2008. jModelTest: phylogenetic model averaging. *Mol. Biol. Evol.* 25:1253–6.
- Procházková, L., Leya, T., Krížková, H. & Nedbalová, L. 2019. *Sanguina nivaloides* and *Sanguina aurantia* gen. et spp. nov. (Chlorophyta): the taxonomy, phylogeny, biogeography and ecology of two newly recognised algae causing red and orange snow. *FEMS Microbiol. Ecol.* 95:fiz064.
- Procházková, L., Remias, D., Rezsanka, T. & Nedbalová, L. 2018. *Chloromonas nivalis* subsp. *tatrae*, subsp. nov. (Chlamydomonadales, Chlorophyta): re-examination of a snow alga from the High Tatra Mountains (Slovakia). *Fottea* 18:1–18.
- Pusztai, M. & Škaloud, P. 2019. Elucidating the evolution and diversity of *Uroglena*-like colonial flagellates (Chrysophyceae), polyphyletic origin of the morphotype. *Eur. J. Phycol.* 54:404–16.
- Remias, D., Jost, S., Boenigk, J., Wastian, J. & Lütz, C. 2013. *Hydrurus*-related golden algae (Chrysophyceae) cause yellow snow in polar summer snowfields. *Phycol. Res.* 61:277–85.
- Remias, D., Procházková, L., Holzinger, A. & Nedbalová, L. 2018. Ecology, cytology and phylogeny of the snow alga *Scotiella cryophila* K-1 (Chlamydomonadales, Chlorophyta) from the Austrian Alps. *Phycologia* 57:581–92.
- Rouiller, C. & Fauré-Fremiet, E. 1958. Structure fine d'un flagellé chrysomonadien: *Chromulina psammobia*. *Exp. Cell Res.* 14:47–67.
- Škaloud, P., Kristiansen, J. & Škaloudová, M. 2013. Developments in the taxonomy of silica-scaled chrysophytes – from morphological and ultrastructural to molecular approaches. *Nordic J. Bot.* 31:385–402.
- Starmach, K. 1966. Über neue und seltene Chrysophyceae in der Algenflora Polens. *Acta Hydrobiol.* 8:5–14.
- Starmach, K. 1972. *Chrysocapsa vernalis* n. sp. and *Chrysocapsella mucoophila* n. sp. (Chrysophyceae) grown in frog spawn. *Bull. Acad. Polon. Sci. Ser. Sci. Biol. Cl. II.* 20:671–5.
- Starmach, K. 1985. Chrysophyceae und Haptophyceae. In Ettl, H., Gerloff, J., Heynig, H. & Mollenhauer, D. [Eds.] *Süßwasserflora von Mitteleuropa, Band 1*. Gustav Fischer Verlag, Stuttgart, 515 pp.
- Stein, J. R. 1963. A *Chromulina* (Chrysophyceae) from snow. *Can. J. Bot.* 41:1367–70.
- Tanabe, Y., Shitara, T., Kashino, Y., Hara, Y. & Kudoh, S. 2011. Utilizing the effective xanthophyll cycle for blooming of *Ochromonas smithii* and *O. itoi* (Chrysophyceae) on the snow surface. *PLoS ONE* 6:e14690.
- Verbruggen, H. 2012. SiteStripper v.1.01. GNU General Public License. <http://www.phycoweb.net/software/SiteStripper/index.html>
- Vischer, W. 1943. Über die Goldalge *Chromophyton rosanoffii* Woronin. *Berichte der Schweizer Botanische Gesellschaft* 53:91–101.
- Waddell, P. J., Cao, Y., Hauf, J. & Hasegawa, M. 1999. Using novel phylogenetic methods to evaluate mammalian mtDNA, including amino acid-invariant sites-LogDet plus site stripping, to detect internal conflicts in the data, with special reference to the positions of hedgehog, armadillo and elephant. *Syst. Biol.* 48:31–53.
- Woronin, A. 1880. *Chromophyton rosanoffii*. *Botanische Zeitung* 38:625–31 & 641–48.
- Yang, E. C., Boo, G. H., Kim, H. J., Cho, S. M., Boo, S. M., Andersen, R. A. & Yoon, H. S. 2012. Supermatrix data highlight

the phylogenetic relationships of photosynthetic Stramenopiles. *Protist* 163:217–31.

Supporting Information

Additional Supporting Information may be found in the online version of this article at the publisher's web site:

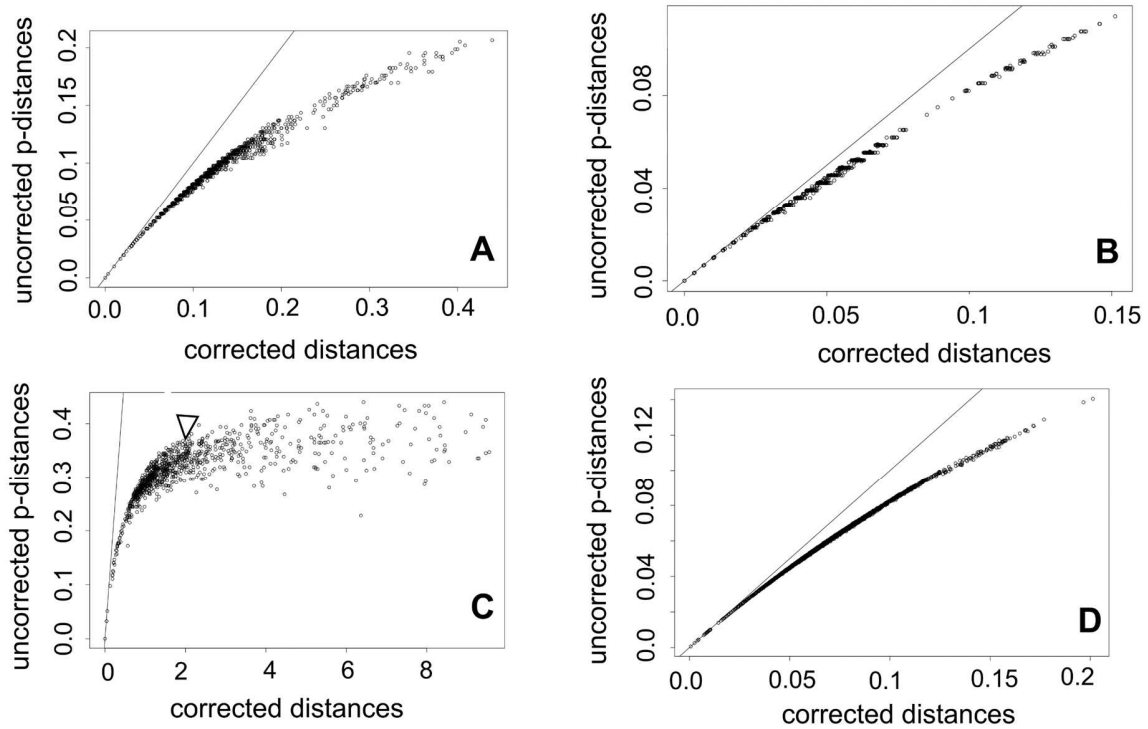
Figure S1. Plots of DNA codon substitutional saturation. Maximum likelihood-corrected distances are plotted against uncorrected p-distances for the first (A), second (B) and third (C) codon position of the *rbcl* gene, and (D) the 18S rRNA gene dataset. Strong curving of saturation plots indicates the significant saturation of molecular datasets. The lowest corrected distance used for removal of fast-evolving sites is indicated by an arrow.

Figure S2. Bayesian phylogenetic tree of Chrysophyta based on the partitioned *rbcl* dataset after removal of saturated sites by the site-stripping method. The newly described species are in bold. Origin in snow is indicated for relevant species. The Hibberdiales clade is highlighted in a grey box. Posterior probabilities (0.95 or more) and bootstrap values from maximum likelihood analyses (50% or more) are shown. Full statistical support (1.00/100) is marked with an asterisk. Thick branches represent nodes receiving the highest posterior probability support (1.00). Accession numbers, strain or field sample codes are indicated after each species name. The scale bar shows the estimated number of substitutions per site.

Figure S3. Bayesian phylogenetic tree of Chrysophyta based on the partitioned *rbcl* dataset after removal of the third codon positions. The newly described species are in bold. Origin in snow is indicated for relevant species. The Hibberdiales clade is highlighted in a grey box. Posterior probabilities (0.95 or more) and bootstrap values from maximum likelihood analyses (50% or more) are shown. Full statistical support (1.00/100) is marked with an asterisk. Thick branches represent nodes receiving the highest posterior probability support (1.00). Accession numbers, strain or field sample codes are indicated after each species name. The scale bar shows the estimated number of substitutions per site.

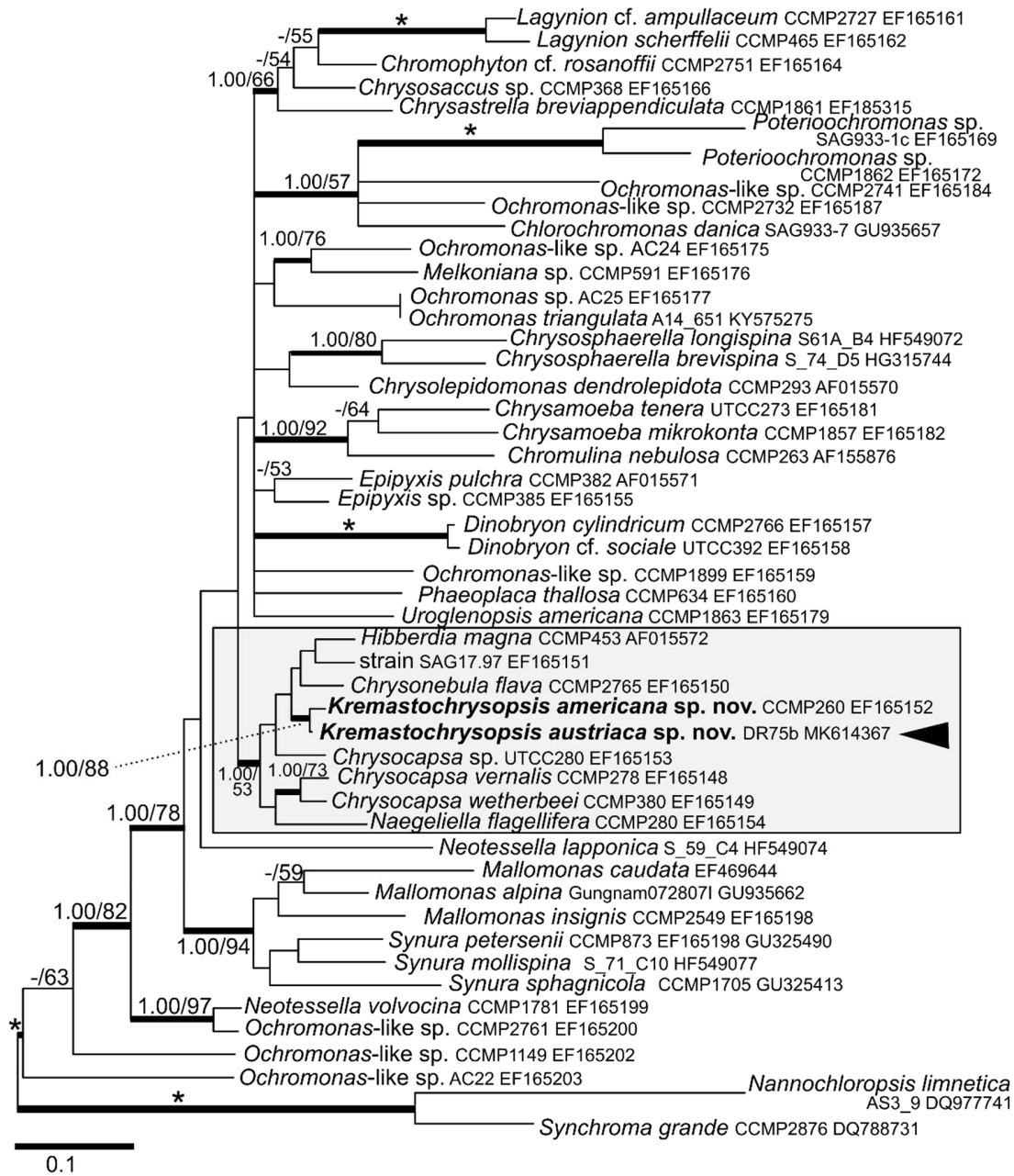
1

Supporting Information



2

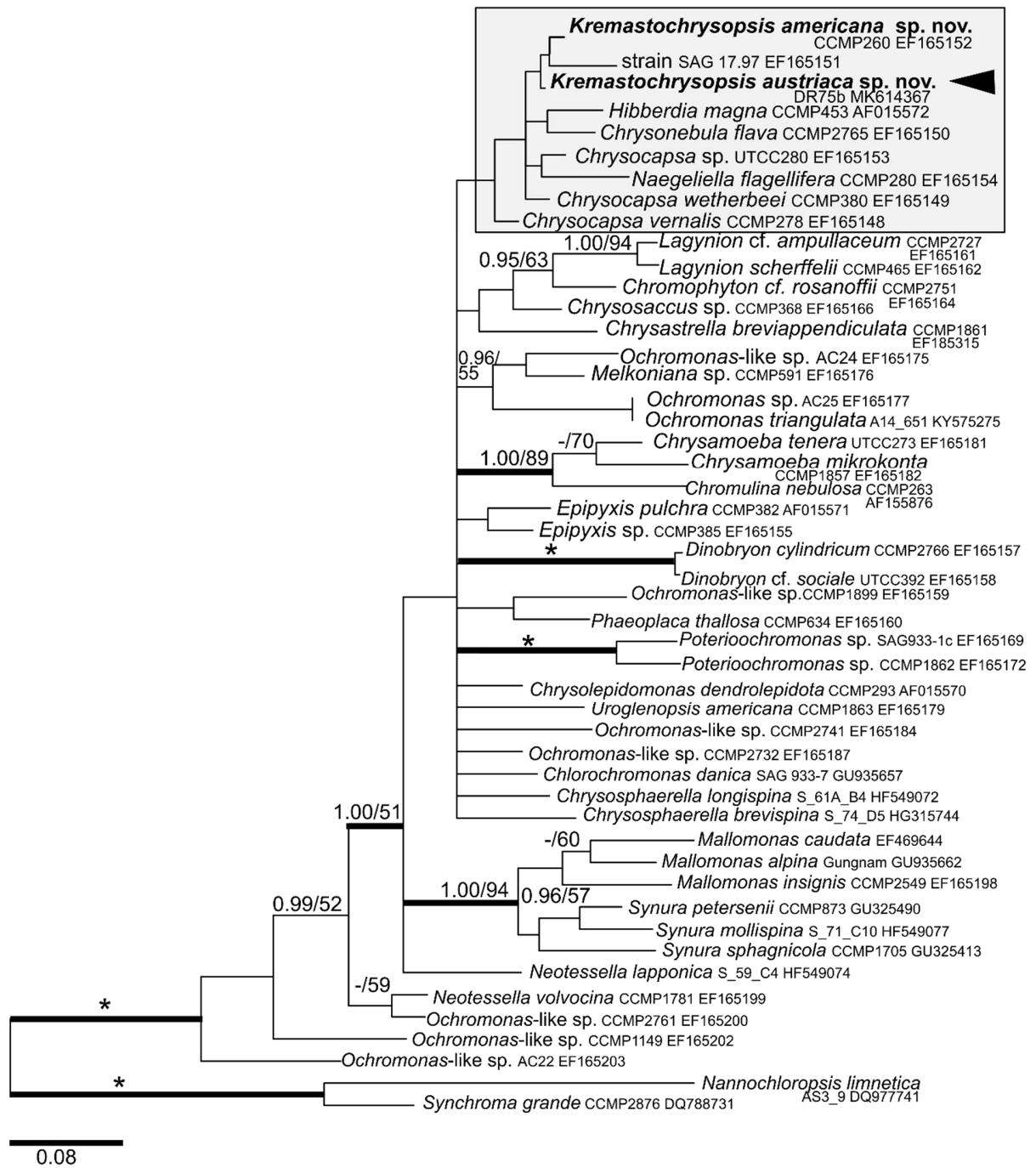
3 **Figure S1.** Plots of DNA codon substitutional saturation. Maximum likelihood-corrected
4 distances are plotted against uncorrected p-distances for the first (A), second (B) and third (C)
5 codon position of the *rbcL* gene, and (D) the 18S rRNA gene dataset. Strong curving of
6 saturation plots indicates the significant saturation of molecular datasets. The lowest corrected
7 distance used for removal of fast-evolving sites is indicated by an arrow.



9

10 **Figure S2.** Bayesian phylogenetic tree of Chrysophyta based on the partitioned *rbcL* dataset after
 11 removal of saturated sites by the site-stripping method. The newly described species are in bold.
 12 Origin in snow is indicated for relevant species. The Hibberdiales-clade is highlighted in a grey
 13 box. Posterior probabilities (0.95 or more) and bootstrap values from maximum likelihood

- 14 analyses (50% or more) are shown. Full statistical support (1.00/100) is marked with an asterisk.
- 15 Thick branches represent nodes receiving the highest posterior probability support (1.00).
- 16 Accession numbers, strain or field sample codes are indicated after each species name. The scale
- 17 bar shows the estimated number of substitutions per site.
- 18



19

20 **Figure S3.** Bayesian phylogenetic tree of Chrysophyta based on the partitioned *rbcL* dataset after
 21 removal of the third codon positions. The newly described species are in bold. Origin in snow is
 22 indicated for relevant species. The Hibberdiales-clade is highlighted in a grey box. Posterior
 23 probabilities (0.95 or more) and bootstrap values from maximum likelihood analyses (50% or

24 more) are shown. Full statistical support (1.00/100) is marked with an asterisk. Thick branches
25 represent nodes receiving the highest posterior probability support (1.00). Accession numbers,
26 strain or field sample codes are indicated after each species name. The scale bar shows the
27 estimated number of substitutions per site.

Paper VII

Evaluating amplicon high-throughput sequencing data of microalgae living in melting snow: improvements and limitations

Lutz S^{1*}, Procházková L^{2*}, Benning LG^{1,3,4}, Nedbalová L^{2,5} & Remias D⁶

Fottea 19(2): 115–131, 2019

¹ *GFZ German Research Centre for Geosciences, Telegrafenberg, 14473 Potsdam, Germany;
current address: Agroscope, Müller-Thurgau-Strasse 29, 8820 Wädenswil, Switzerland*

² *Department of Ecology, Faculty of Science, Charles University, Viničná 7, 128 44 Prague 2,
Czech Republic*

³ *School of Earth & Environment, University of Leeds, Woodhouse Lane, Leeds LS2 9JT, UK*

⁴ *Department of Earth Sciences, Free University of Berlin, 12249 Berlin, Germany*

⁵ *The Czech Academy of Sciences, Institute of Botany, Dukelská 135, 379 82 Třeboň, Czech
Republic*

⁶ *University of Applied Sciences Upper Austria, Stelzhamerstr. 23, 4600 Wels, Austria*

***SL and LP contributed equally to this work**

Evaluating amplicon high-throughput sequencing data of microalgae living in melting snow: improvements and limitations

Stefanie LUTZ^{1*}, Lenka PROCHÁZKOVÁ^{2*}, Liane G. BENNING^{1,3,4}, Linda NEDBALOVÁ^{2,5}
& Daniel REMIAS⁶

¹GFZ German Research Centre for Geosciences, Telegrafenberg, 14473 Potsdam, Germany; *Corresponding author e-mail: stefanie.lutz@agroscope.admin.ch; current address: Agroscope, Müller-Thurgau-Strasse 29, 8820 Wädenswil, Switzerland

²Department of Ecology, Faculty of Science, Charles University, Viničná 7, 128 44 Prague 2, Czech Republic; *Corresponding author e-mail: lenkacerven@gmail.com

³School of Earth & Environment, University of Leeds, Woodhouse Lane, Leeds LS2 9JT, UK

⁴Department of Earth Sciences, Free University of Berlin, 12249 Berlin, Germany

⁵The Czech Academy of Sciences, Institute of Botany, Dukelská 135, 379 82 Třeboň, Czech Republic

⁶University of Applied Sciences Upper Austria, Stelzhamerstr. 23, 4600 Wels, Austria

Abstract: Melting snowfields are dominated by closely related green algae. Although microscopy-based classification are evaluable distinction tools, they can be challenging and may not reveal the diversity. High-throughput sequencing (HTS) allows for a comprehensive community evaluation but has been rarely used in such ecosystems. We found that assigning taxonomy to DNA sequences strongly depends on the quality of the reference databases. Furthermore, for an accurate identification, a combination of manual inspection of automated assignments, and oligotyping of the abundant 18S OTUs and ITS2 secondary structure analyses were needed. The use of one marker can be misleading because of low variability (18S) or the scarcity of references (ITS2). Our evaluation reveals that HTS outputs need to be thoroughly checked when the organisms are poorly represented in databases. We recommend an optimized workflow including consistent sampling, a two-molecular marker approach, light microscopy-based guidance, generation of appropriate reference sequences and a final manual verification of taxonomic assignments as a best approach for accurate diversity analyses.

Key words: 18S rDNA, ITS2 rDNA, high-throughput sequencing, Illumina, oligotyping, OTU clustering, red snow, Sanger, secondary structure, snow algae

INTRODUCTION

In alpine and polar regions, psychrophilic microalgae can cause a distinct colouration of melting snow from green to different shades of yellow, orange and red (ANESIO et al. 2017; HOHAM & DUVAL 2001; KOL 1968; KOMÁREK & NEDBALOVÁ 2007; LEYA 2013; LUTZ et al. 2016). Snow algae have evolved a range of adaptive strategies to overcome a multitude of environmental stresses including low temperatures, freezing, desiccation, nutrient scarcity and extreme irradiation. Thus, they are of general interest to study a wide range of fundamental cellular processes. These eukaryotic photoautotrophs mostly belong to the Chlamydomonadaceae (Chlorophyceae) and their carotenoid-rich immotile stages (cysts), which are adapted to harsh conditions, are predominately found throughout the melt season (REMIAS et al. 2010).

Traditionally, the red snow phenomenon has been

associated with *Chlamydomonas nivalis* (F.A. Bauer) Wille (KOL 1968). Yet, a plethora of further species can be found in melting snow including *Chlainomonas* sp. Christen (REMIAS et al. 2016), *Chloromonas nivalis* (Chodat) Hoham et Mullet (PROCHÁZKOVÁ et al. 2018a; REMIAS et al. 2010) or *Chloromonas brevispina* (F.E. Fritsch) Hoham, Roemer et Mullet (MATSUZAKI et al. 2015). Nonetheless, we are only scratching the surface of snow algal diversity characterization and the above-mentioned species likely constitute a small proportion of the true diversity. For many taxa, no strains are available because the germination of cysts collected in the field was not successful (PROCHÁZKOVÁ et al. 2018a; own observations). Moreover, cells of one species transgress through a variety of morphological and physiologic changes during their life cycle. This poses another challenge for the microscopy-based identification and classification.

In contrast, high-throughput sequencing (HTS) allows for a comprehensive assessment of the microbial

community composition of a natural ecosystem. With its broad application in many other environments (GROSSMANN et al. 2016), it is striking how rarely such approaches have been used for psychrophilic algae. So far a few studies have targeted snow algal communities in the Arctic (LUTZ et al. 2015a; LUTZ et al. 2015b; LUTZ et al. 2016, 2017; SEGAWA et al. 2018), in the US (BROWN et al. 2016), in Japan (TERASHIMA et al. 2017) and in Antarctica (SEGAWA et al. 2018). However, HTS data on European Alpine communities is completely absent in the literature.

The nature of HTS to produce large datasets in a mostly automated way comes at a cost; i.e., some of the data processing steps are to a certain degree a ‘black box’. In addition, several technical biases must be taken in account. These may include effects due to extreme GC/AT ratios (OYOLA et al. 2012), the choice of primers and library preparation methods (SCHIRMER et al. 2015), annealing temperature (SCHMIDT et al. 2013), DNA polymerase (BRANDARIZ-FONTES et al. 2015), amplicon size variability (SCHIRMER et al. 2015) or from the sequencing technology itself (SCHLOSS et al. 2011).

Several DNA markers, which are being employed for algal species delimitation, have been summarized in LELIAERT et al. (2014). Comprehensive 18S rDNA marker reference databases such as Silva (QUAST et al. 2012), PR2 (GUILLOU et al. 2013) or EukRef (CAMPO et al. 2018) exist. However, the 18S rDNA marker is not sufficiently variable to distinguish among closely related taxa (HALL et al. 2010). In contrast, the internal nuclear rDNA transcribed spacer 2 (ITS2 rDNA) inherits high taxonomic resolution, but also in some cases high intragenomic variation (THORNHILL et al. 2007; SIMON & WEISS 2008; ALANAGREH et al. 2017), which may affect OTU (Operational Taxonomic Unit) clustering and taxonomic identification. Since the rRNA cassette can vary in copy numbers per organism and the ITS regions are free to independently drift within the same organism, a potential overestimation of OTUs may occur, especially in some fungal species (i.e., one species can split into several OTUs (LINDNER & BANIK 2011; LINDNER et al. 2013)). Nevertheless, intergenic variation of ITS2 in algae is generally considered low compared to fungi. Moreover, there is a dearth of appropriate ITS2 rDNA reference sequences (YAO et al. 2010; BUCHHEIM et al. 2011) that can be used for algae. Hence, for any accurate diversity evaluation of cryophilic algae diversity in environmental samples at least a two-marker approach is advisable (CHASE & FAY 2009).

In a methodologically motivated approach, we evaluated the application of HTS for the characterization of snow algal communities in the extreme habitat of melting European Alpine snowfields. We present a case study that aims to improve the application of HTS techniques for accurate diversity assessments in such ‘less common’ and ‘less well-studied’ ecosystems. To do this we (1) investigated the suitability of the two markers 18S and ITS2 rDNA for amplicon high-throughput

sequencing; (2) evaluated the importance of completion and curation of reference databases for correct taxonomic assignments of environmental sequences; (3) complemented our HTS data with traditional Sanger sequencing data to gain more and longer reference sequences; (4) cross-correlated the sequencing data with traditional microscopic observations; (5) tested different strategies for taxonomic assignments (QIIME, Blast and a final manual refinement) in order to reveal potential differences; and (6) to delineate cryptic diversity of dominant species, we performed oligotyping of the most abundant 18S rDNA OTUs and assessed species boundaries by ITS2 rDNA transcript secondary structures comparison.

MATERIAL AND METHODS

The overall workflow we followed in this study is shown in Fig. 1.

Field work and sample preparation. The samples were collected from a non-permanent, flat snow field in the Kühtai region of the Tyrolean Alps in Austria (Table 1). The site was dominated by an alpine meadow covered by a melting snow pack with characteristic reddish surface coloration. For HTS, two field samples (sample 1, sample 2) containing mixed communities of several snow algae were harvested in the summers of 2015 and 2016 (Table 1). For Sanger sequencing cells from virtually monospecific patches were collected and identified by light microscopy. The Sanger samples were each dominated by one of the locally abundant taxa: *Chlamydomonas nivalis* (sample 3 collected in 2016 and described in PROCHÁZKOVÁ et al. 2018b), *Scotiella cryophila* (sample 4 collected in 2009 and described in REMIAS et al. 2018) and *Chloromonas brevispina* (sample 5; collected in 2016 and described here). The 2016 Sanger and HTS samples (samples 1, 2 and 5; Table 1) were collected about two to three weeks earlier in the melting season than sample 1 collected in 2015 or sample 4 collected in 2009. Cell harvest was performed as previously described by PROCHÁZKOVÁ et al. (2018a) using a sterilized stainless steel shovel, putting the snow into sterile sampling bags and keeping it cold/frozen until returning to the laboratories for microscopic analyses and DNA extractions. The presence of algae and the species composition were evaluated using an Evolution field microscope (Pyser SGI, USA). For HTS, we intentionally used two different sampling approaches: In 2015 (sample 1) sampling included the complete snow column from the snow surface to the soil layer (approximately 30 cm; Fig. S1), whereas in 2016 (sample 2) surface and ground snow were not harvested (Fig. S2) to avoid allochthonous organisms (airborne and soil algae can occur in snow, STIBAL & ELSTER 2005).

Light Microscopy. Cells were analyzed in the laboratory with a Nikon Eclipse 80i light microscope equipped with a Plan Fluor 1.3 100× objective and a Nikon DS-5M digital camera.

Sanger sequencing of locally abundant taxa. 18S rDNA and ITS2 rDNA sequences of *Chloromonas brevispina* K-2 (sample 5) were gained in course of this study, whereas Sanger sequences from two other species were recently published – *Chlamydomonas nivalis* DL07 (sample 3; PROCHÁZKOVÁ et al. 2018b) and *Scotiella cryophila* K-1 (sample 4; REMIAS et al. 2018). These three sequences were used for the generation of a custom reference sequence database and are available at

Table 1. Overview of snow algae samples from Kühtai in the Austrian Alps with three locally abundant taxa (causing virtually monospecies bloom) harvested for Sanger sequencing and two samples of mixed cryoflora communities collected for HTS. Sample number (code), collection date, sampling altitude (m a.s.l.) and geographic position (GPS) are shown.

Sample (code)	Date	Altitude (m)	GPS	Sequencing	Reference
Sample 1 (WP79)	11.06.2015	2300	N47°13.422 E11°01.310	HTS	this study
Sample 2 (WP99)	31.05.2016	2299	N47°13.416 E11°01.260	HTS	this study
Sample 3 (DL07)	28.05.2016	2380	N47°13.709 E11°00.949	Sanger	PROCHÁZKOVÁ et al. 2018b
Sample 4 (K-1)	05.06.2009	2432	N47°13.748 E11°00.704	Sanger	REMIAS et al. 2018
Sample 5 (K-2)	28.05.2016	2430	N47°13.753 E11°00.737	Sanger	this study

Table 2. Overview of HTS data. Number of 18S rDNA and ITS2 sequences before and after quality filtering, as well as the number and percentage of sequences assigned to green algal taxa (the remaining sequences were mostly assigned to Fungi, Alveolata and Rhizaria; data not shown).

Marker	Samples	No. of sequences before quality filtering	No. of sequences after quality filtering	No. and percentage of sequences assigned to green algae
18S	Sample 1	221837	184921	88795 (48.0%)
	Sample 2	294484	248269	119722 (48.2%)
ITS2	Sample 1	187543	116446	81022 (69.6%)
	Sample 2	204224	156958	108889 (69.4%)

NCBI under the accession numbers listed in Table S3. Total genomic DNA was isolated from the *Chlamydomonas nivalis* dominated sample 3 with the DNeasy Plant Mini kit (Qiagen) as previously described (PROCHÁZKOVÁ et al. 2018a). Sample 55, containing *Chloromonas brevispina* was lower in biomass (<20 mg wet weight), and thus, DNA was extracted using the Instagene Matrix (Bio-Rad Laboratories, USA) following the protocols described in Remias et al. (2016). Isolated DNA was diluted to a concentration of 5 ng.µl⁻¹ and the 18S and ITS2 rDNA regions were amplified using existing primers (Table S1). Polymerase chain reactions (PCR) were performed according to Procházková et al. (2018a). The PCR products were stained with bromophenol loading dye, quantified on a 1.5% agarose gel and stained with GelRed (Biotium). The amplification products were purified and sequenced on the Applied Biosystems automated sequencer (ABI 3730×1) at Macrogen (Netherlands). Chromatogram data of forward and reverse sequences of both markers were visually inspected and edited in the program FinchTV 1.4.0 (Geospiza, USA). The contig of each marker was assembled in SeqMan 5.06 (DNASTAR Inc., USA).

High-throughput sequencing. DNA was extracted from both field samples (sample 1 and 2) using the PowerSoil® DNA Isolation kit (MoBio Laboratories). The 18S and ITS2 rDNA amplicons were prepared according to the Illumina “16S Metagenomic Sequencing Library Preparation” guide

(ILLUMINA). In brief, 18S rDNA genes were amplified using the eukaryotic primers 528F (5' GCGGTAATTCCAGCTCCAA) and 706R (5' AATCCRAGAATTTACCTCT; CHEUNG et al. 2010) spanning the V4–V5 hypervariable regions. ITS2 rDNA genes were amplified using the primers 5.8SbF (5' GATGAAGAACGCAGCG; MIKHAILYUK et al. 2008) and ITS4R (5' TCCTCCGCTTATTGATATGC; WHITE et al. 1990). All primers were tagged with the Illumina adapter sequences. PCR was performed using KAPA HiFi HotStart ReadyMix. Initial denaturation at 95 °C for 3 min was followed by 25 cycles of denaturation at 95 °C for 30 s, annealing at 55 °C for 30 s and elongation at 72 °C for 30 s. Final elongation was at 72 °C for 5 min. All PCRs were carried out in reaction volumes of 25 µl containing 12.5 µl of ReadyMix, each 5 µl of the forward and reverse primer and 12.5 ng of DNA template in 2.5 µl. All pre-amplification steps were done in a laminar flow hood with DNA-free certified plastic ware and filter tips. Amplicons were barcoded using the Nextera XT Index kit. The pooled library was sequenced on the Illumina MiSeq using paired 300 bp (base pairs) reads at the University of Bristol Genomics Facility. 18S and ITS2 rDNA raw sequences have been deposited to the European Nucleotide Archive (ENA) under accession number PRJEB24479.

Quality filtering of HTS sequences and ITS2 extraction. The sequencing quality of each de-multiplexed fastq file was analyzed using the FastQC software (<http://www.bioinformatics>).

babraham.ac.uk/projects/fastqc/). The low quality 3' ends of all reads were trimmed. All forward reads were trimmed by 20 bp and all reverse reads by 100 bp. All other processing steps were performed in Qiime (CAPORASO et al. 2010). The trimmed paired end reads were joined before further processing and additionally filtered only allowing a minimum Phred quality score of Q20. Reads that could not be joined or were below the quality cut-off were excluded from the analysis. Chimeric sequences were removed using USEARCH 6.1.

The software ITSx (BENGTSSON-PALME et al. 2013) was used to extract the ITS2 rDNA regions from all sequences to avoid the inclusion of the highly conserved neighbouring genes (i.e., 5.8S and 28S). Inclusion of these regions in the identification process would otherwise lead to misleading results. HMMER (EDDY 1996) was used to predict the origin of the sequences (e.g., Chlorophyta, Fungi) based on Hidden Markov Models.

Clustering sequences into OTUs and creation of OTU table.

In general, fragments of 18S rDNA sequences of phytoplankton assemblages and prokaryotic and eukaryotic alpine permafrost communities are clustered into OTUs at 97% similarity in HTS studies (FREY et al. 2016; TRAGIN et al. 2017). A far stricter threshold for clustering and species assignment is required for this marker when snow algal communities dominated by Chlamydomonadales are investigated. Several species in this group are very closely related and they differ in some cases by only one bp over the length of the amplicon (e.g. *Chloromonas fukushimae* GsCl-11 (AB906342) and *Chloromonas tughillensis* UTEX SNO91 (AB906348)). Therefore, OTUs were picked *de novo* and clustered at 99.5% similarity for the conserved 18S rDNA marker.

In contrast, ITS2 is more variable and was thus clustered at 94.0% similarity. The chosen threshold is in par with several findings on the level of identity of algal ITS2 rDNA.

In *Gonium pectorale* less than 5% of the nucleotide positions differ in pairwise comparisons and less than 7% vary between all clones (COLEMAN et al. 1993). Similarly, only few nucleotide differences have been reported among strains of *Chloromonas reticulata* (3.4–4.1%), and of *Chlamydomonas reinhardtii* NIES-2463 and SAG 11-32a (3.3%), with the latter one being able to cross and produce zygotes (MATSUZAKI et al. 2015). A similar low identity threshold for OTU picking (95%) as in our case was also successfully applied during Illumina barcoding of soil fungal communities (SCHMIDT et al. 2013).

Singletons (OTUs containing only 1 sequence, likely derived from sequencing errors) were removed from both the 18S and ITS2 rDNA data sets prior to further analysis. The OTU tables were created by counting the number of times an OTU appeared in each sample and adding the taxonomic predictions to each OTU.

Identification of OTUs. The objective of this final process was to define species boundaries. In order to do so, the representative sequences (i.e., the cluster seeds in the OTU picking process) of the 50 most abundant 18S and ITS2 rDNA OTUs (comprising >85% and >98% of the total community, respectively) were used.

Three different strategies for taxonomic assignments of each OTU from environmental samples were tested:

Strategy A (basic version): The BLAST (KENT 2002) assignment method implemented in Qiime was used with the default minimum percent similarity of 90% to consider a database match a hit (unless a customized script is being used to overwrite the default setting and to increase the similarity threshold). The publicly available and Qiime-compatible Silva database (release 128) (QUAST et al. 2012) was used for the assignment of the 18S rDNA data set and extended, with 223 additional sequences of psychrophilic algae kindly provided by Dr. Thomas Leya from the CCCryo – Culture Collection of

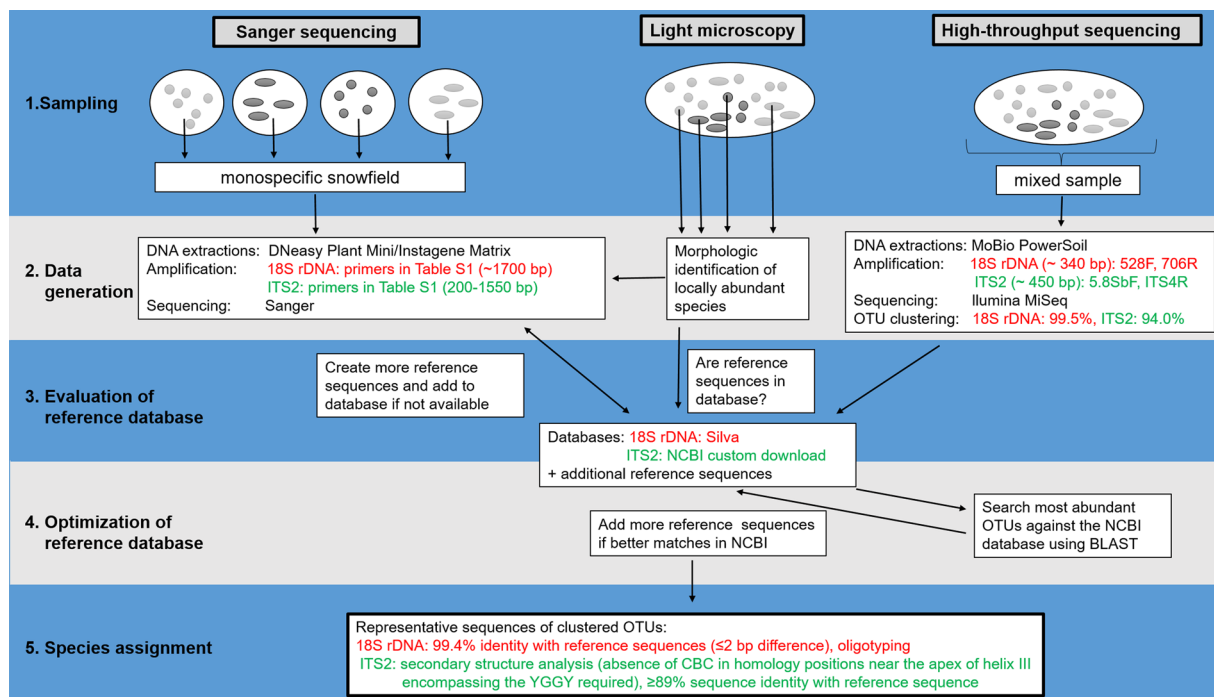


Fig. 1. Schematic workflow for the optimised molecular evaluation of snow algal community structures and diversity, which heavily relies on the combined power of light microscopy, Sanger sequencing and amplicon high-throughput sequencing. All details on the markers 18S rDNA and ITS2 are highlighted in red and green, respectively.

Cryophilic Algae (Fraunhofer IZI–BB). Sequences assigned to Opisthokonta, Amoebozoa, Alveolata and Rhizaria were removed from the OTU table. For the taxonomic assignment of the ITS2 rDNA sequences, a custom database with the limited number of available reference sequences for (psychrophilic) green algae was downloaded from NCBI (Table S2).

Strategy B (extended version): The basic version was improved by adding reference sequences of the locally abundant taxa derived from Sanger sequencing (see above) to the custom reference database.

Strategy C (further extended version): All the steps were done as in the extended version. Additionally, manual comparisons were carried out for the representative sequences of the OTUs with their respective reference sequences (pairwise blast). A manual search of each OTU representative sequence against NCBI was performed (megablast). Additional reference sequences were added to the custom based database, if the search resulted in a better sequence identity match than the one with its respective reference sequence. A verification of sequence identities for 18S (including oligotyping) and ITS2 (including secondary structures comparisons) was performed. Hereafter, we define these unique ITS2 sequences among one species as “haplotypes”.

Manual identification of OTUs (Strategy C [further extended version] in detail). Representative sequences of the most abundant 18S and ITS2 OTUs were manually submitted to the

BLAST (KENT 2002) web server to search NCBI for close hits to algal taxa. The used BLAST nucleotides parameters were the following: megablast (highly similar sequences), ‘others’ as database search set, uncultured/environmental sequences were included, other algorithm parameters were kept with default values.

In case of 18S rDNA, an identity threshold of ~99.4% (i.e., 2 bp nucleotide difference in a 342 bp sequence) had to be passed in order to be considered as a database match. Sequences below this threshold were recorded as “no blast hit”. A stricter identity threshold could inflate the diversity due to potential sequencing errors (BRADLEY et al. 2016).

To discover cryptic diversity in the 18S rDNA data, the three most abundant OTUs of this marker were further subjected to oligotyping, a high-resolution method that uses Shannon entropy to evaluate the most information-rich nucleotide position in an amplicon data set (EREN et al. 2013; LUTZ et al. 2018). All sequences contained in one OTU were extracted individually and trimmed to the same length of 340 bp using Fastx Trimmer (http://hannonlab.cshl.edu/fastx_toolkit/). The number of components (i.e., nucleotide position with the highest entropy) to be used was chosen based on the entropy analysis of the sequence alignment. Noise filtering was carried out using a minimum substantive abundance of 50.

In order to assess species boundaries using ITS2 rDNA, three steps were carried out: (1) A minimum similarity

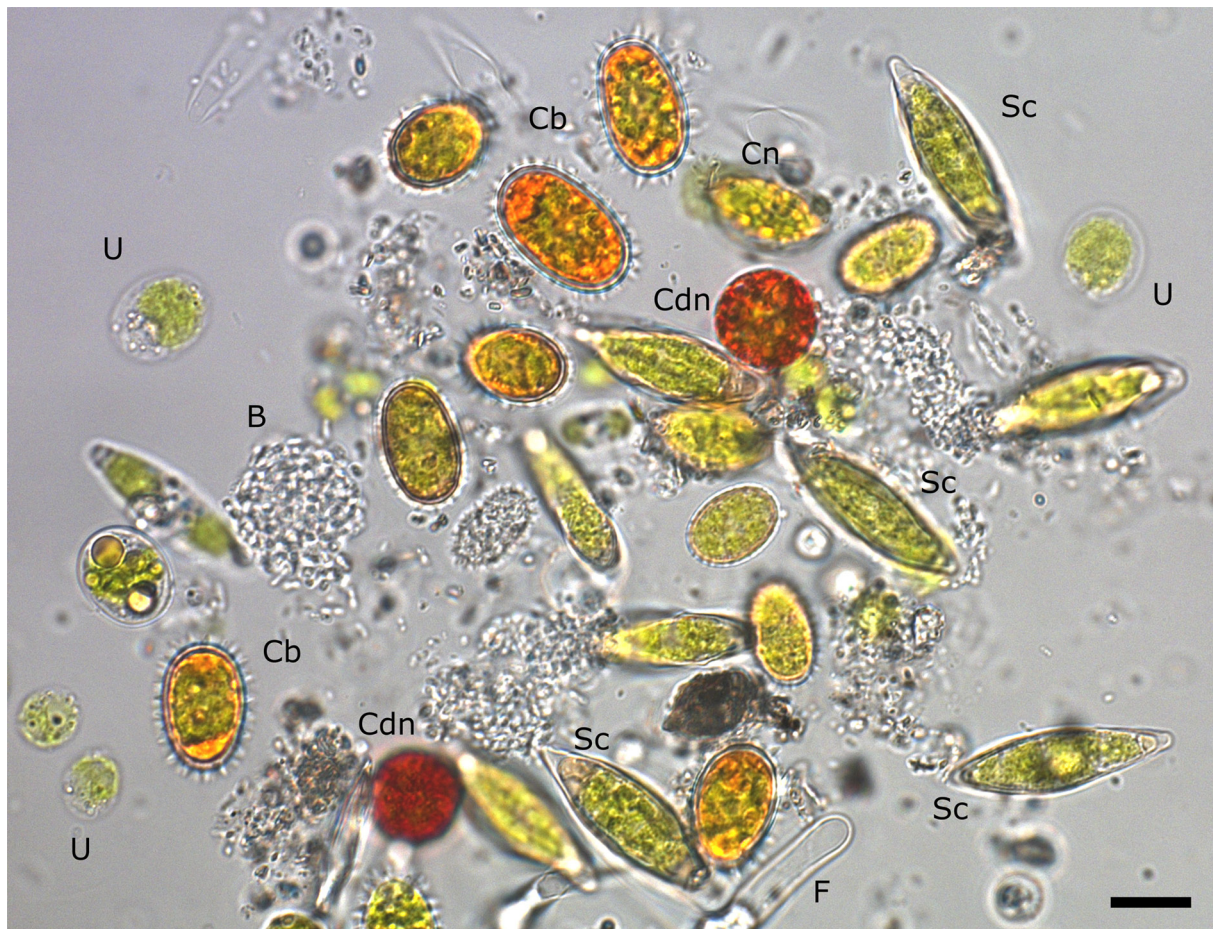


Fig. 2. Light micrograph of cells in field sample 1. The three locally abundant snow algae identified using morphological features were *Cr. brevispina* (Cb), *Scotiella cryophila* (Sc) and *Cd. nivalis* (Cdn). Other cells observed in this sample were *Cr. nivalis* (Cn), unknown unicellular green alga (U), fungus (F) or bacteria (B). Scale bar 10 μ m.

Table 3. Algal community structure based on the 18S rDNA data set. The ten most abundant OTUs were selected (>78% of the community). The table shows the discrepancies between OTU assignments using three strategies: (A) basic version using Qiime and the Silva database, (B) extended version using Qiime and additional reference sequences of the locally abundant taxa (underlined) and (C) further extended version using final manual verification of taxa assignments at NCBI, only allowing up to 2 bp nucleotide difference to the respective reference sequence (sequences below this threshold were recorded as “no blast hit”). A comprehensive list of the 50 most abundant OTUs with corresponding OTU identification numbers can be found in Table S4.

OTU ID	Sample 1 (%)	Sample 2 (%)	(A) Qiime + Silva	(B) Qiime + Silva + local references	(C) Qiime + Silva + local references + manual verification
denovo14334	33.0	66.8	<i>Chloromonas</i> sp. Gassan–A LC012753.1	<i>Chloromonas brevispina</i> K–2	Ambiguous hits: <i>Chloromonas brevispina</i> K–2, <i>Scotiella cryophila</i> K–1, <i>Chloromonas</i> sp. TA AB902996, <i>Chloromonas</i> sp. Gassan–B LC012714.1
denovo45654	18.7	0.1	<i>Mesotaenium</i> sp. AG–2009–1 FM992335.1	<i>Ancylonema nordenskiöldii</i> AF514397.2	<i>Ancylonema nordenskiöldii</i> AF514397.2
denovo36485	0.9	13.6	Uncultured <i>Chlamydomonadaceae</i> AB902971.1	<i>Chlamydomonas nivalis</i> DL07	<i>Chlamydomonas nivalis</i> DL07
denovo40226	8.2	0	<i>Botrydiopsis constricta</i> AJ579339.1	<i>Botrydiopsis constricta</i> AJ579339.1	<i>Botrydiopsis constricta</i> AJ579339.1
denovo15070	4.6	1.0	Uncultured <i>Chloromonas</i> AB903008.1	<i>Chloromonas</i> cf. <i>alpina</i> CCCryo 033–99 HQ404865.1	<i>Chloromonas platystigma</i> strain CCCryo 020–99
denovo20542	4.6	0	Uncultured <i>Dunaliellaceae</i> EF023287.1	Uncultured <i>Dunaliellaceae</i> EF023287.1	<i>Chloroidium saccharophilum</i> isolate HST10K KX024691.1
denovo101	3.2	1.1	<i>Chloromonas</i> sp. D–CU581C AF517086.1	<i>Chloromonas</i> cf. <i>rostafinskii</i> CCCryo 025–99 AF514402.1	Ambiguous hits: <i>Chloromonas</i> sp. NIES–2379 AB906350.1, <i>Chloromonas rostafinskii</i> strain CCCryo 025–99 AF514402.1
denovo23251	3.0	<0.1	<i>Chloromonas</i> sp. Gassan–A LC012753.1	<i>Chloromonas brevispina</i> K–2	Ambiguous hits: <i>Chloromonas brevispina</i> K–2, <i>Chloromonas</i> sp. Hakkoda–1 LC012710.1, <i>Chloromonas</i> sp. Gassan–A LC012709.1
denovo30051	0.4	1.9	Uncultured <i>Chloromonas</i> AB902984.1	Uncultured <i>Chloromonas</i> AB902984.1	No blast hit
denovo36086	2.1	0	<i>Prasiola furfuracea</i> AF189073.1	<i>Prasiola furfuracea</i> AF189073.1	No blast hit
	21.3	15.5	Other	Other	Other

Table 4. Oligotyping of the three most abundant 18S rDNA OTUs (sequences shown in Table S5). The table shows individual oligotypes that were conflated in the three most abundant 18S rDNA OTUs (Table 3), but were not detected by conventional OTU clustering. The refined taxonomic assignments and their respective relative abundances were then used for the final description of the snow algal community composition in Figure 5. For instance, OTU ‘denovo14334’ was assigned to *Chloromonas brevispina* K–2 (Sample 1: 33%). However, oligotyping revealed that only one oligotype within this OTU corresponded to this species, which decreased its relative abundance from 33.0% to 23.4%.

OTU Oligotype	Taxa assignment	Similarity (%)	Sample 1 (%)	Sample 2 (%)
denovo14334	Ambiguous hits: <i>Chloromonas brevispina</i> K–2, <i>Scotiella cryophila</i> K–1, <i>Chloromonas</i> sp. TA AB902996, <i>Chloromonas</i> sp. Gassan–B LC012714.1	99.4	33.0	66.8
TTT	Uncultured snow algae LC371427.1, LC371425.1, LC371423.1, LC371419.1, LC371414.1	100	1.0	60.7
TCT	<i>Chloromonas brevispina</i> K–2, <i>Chloromonas</i> sp. Gassan–A LC012753.1, <i>Chloromonas</i> sp. Hakkoda–1 LC012710.1	100	23.4	<0.1
CTT	<i>Chloromonas</i> sp. Gassan–B LC012714, uncultured <i>Chloromonas</i> sp. ANT1 AB903007.1 and <i>Chloromonas</i> sp. TA8 AB902996.1, <i>Chloromonas polyptera</i> JQ790556.1, uncultured Viridiplantae HQ188979.1	100	8.5	0.2
TTC	28 hits	>99	0.1	5.9
denovo45654	<i>Ancylonema nordenskiöldii</i> AF514397.2	100	18.7	0.1
A	<i>Ancylonema nordenskiöldii</i> AF514397.2	100	17.2	0.1
C	<i>Mesotaenium berggrenii</i> var. <i>alaskana</i> JF430424.1, <i>Mesotaenium</i> sp. AG–2009–1 FM992335.1	99.4	1.5	<0.1
denovo36485	<i>Chlamydomonas nivalis</i> DL07	100	0.9	13.6
T	<i>Chlamydomonas nivalis</i> DL07, 14 hits including several <i>Chlamydomonas nivalis</i> and uncultured snow algae strains	100	0.8	12.3
C	14 hits including several <i>Chlamydomonas nivalis</i> and uncultured snow algae strains	100	0.1	1.3

of $\geq 89.0\%$ between an OTU and the reference sequence had to be passed to be considered as a database match. (2) If an OTU passed this identity threshold, it was retained for the creation of ITS2 rDNA transcript secondary structures. (3) The absence of a CBC in the homology positions of the ITS2 in comparison to an OTU with the reference sequence near the 5′-apex of helix III in the ITS2 secondary structure was required in order to be assigned to this reference taxon. A suggested schematic overview of taxonomic assignment of environmental ITS2 rDNA sequences from environmental samples is shown in Fig. S3. In detail, the ITS2 sequences were folded using the Mfold server (<http://mfold.rna.albany.edu/?q=5mfold>; ZUKER 2003; note: HTS delivers DNA based data, but during RNA folding, thymine [‘T’] is converted to uracil [‘U’]). The model of the secondary structure with the minimum free energy that was consistent with the specific features of nuclear rDNA ITS2 and that contained four helices and U–U mismatch in helix II (COLEMAN 2007) was selected. The ITS2 sequences and secondary structures were automatically and synchronously aligned (SCHULTZ & WOLF 2009) using 4SALE (SEIBEL et al. 2006, 2008), and subsequently manually validated and corrected. First, structure based information (i.e., consensus of all secondary structures and all secondary structures displayed separately) was visually inspected to detect misaligned sequences. This was followed by the manual

editing of the secondary structure in order to provide accurate sequence–structure alignments in the context sensitive editing mode (i.e., sequences and secondary structure information are used to validate whether a binding in the context is possible or not). The alignment consisted of the reference species and all OTUs assigned to this species based on preliminary pairwise comparisons in BLAST. Species delimitation was performed in 4SALE and was based on the detection of CBCs (Compensatory Base Changes), both nucleotides of a paired site mutate while the pairing itself stays stable (e.g., paired sites A–U mutated into G–C). A search for CBCs can only be performed in homologous positions of the ITS2 molecule, which can be unambiguously aligned. For Chlorophyceae, the consensus secondary structure model of ITS2 was identified and the conservation level of individual ITS2 sequence positions (i.e., a position is conserved above 70%) in the alignment was specified (CAISOVÁ et al. 2013). Comparisons of the ITS2 secondary structure prediction of the reference sequences gained from Sanger sequencing and those from the HTS data set that were preliminarily assigned to those reference sequences were performed. Based on these comparisons, species boundaries between OTUs and the number of haplotypes for each reference species was assessed. Even a single CBC in helices II and III of the ITS2 secondary structure may indicate sexual incompatibility as has been shown in crossing experiments

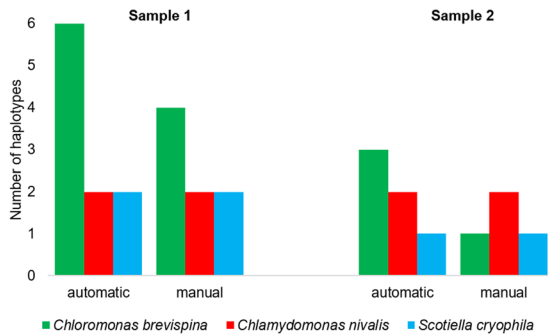


Fig. 3. Analysis of the 38 most abundant OTUs of both samples: Comparison of haplotype diversity of the three locally abundant species (*Chloromonas brevispina* K-2, *Chlamydomonas nivalis* DL07, *Scotiella cryophila* K-1; identified by light microscopy) between an evaluation based on automatic species assignment via Qiime and a manual assignment according to the CBC species concept (comparison of the ITS2 rDNA transcript secondary structures). A sequence identity of $\geq 89.0\%$ and an absence of CBCs in homologous positions near the 5' apex of helix III were required in comparison to a reference species for an assignment to each taxon.

(COLEMAN 2000, 2009). One CBC in the most conserved part of helix III region of the ITS2 encompassing the YGGY motif (the most conserved region of the ITS2 secondary structures of eukaryotes; COLEMAN 2007) suggested the separation of two sister species which differ in their cell morphology, i.e., *Chloromonas reticulata* and *Chloromonas chlorococcoides* (MATSUZAKI et al. 2012). It has been shown that the probability of a CBC representing two distinct species is 93% (WOLF et al. 2013). The secondary structure of nuclear rDNA ITS2 was drawn using VARNA version 3.9 (DARTY et al. 2009).

Evaluation of the different strategies for taxonomic assignments. Nonmetric multidimensional scaling (NMDS) based on Bray–Curtis distances was performed using the program CANOCO 5 (TER BRAAK & ŠMILAUER 2012) to visualize the differences in taxonomic assignments based on 18S and ITS2 rDNA and among the three strategies used (A, B, C, see above).

RESULTS

Community composition based on light microscopy

The most abundant algal taxa identified in both samples 1 and 2 were *Chloromonas brevispina*, *Chlamydomonas nivalis* and *Scotiella cryophila*. All cells of these species were immotile cysts containing a secondary red carotenoid pigmentation, more or less masking the chlorophylls (Fig. 2, Fig. S4). The macroscopic appearance of the snow was red at the surface, turning greenish deeper in the snow at the spot where sample 1 was collected (Fig. S1) and yellowish where sample 2 was collected. Sample 1 additionally contained several other, unidentified unicellular green algae. The microscopic identification of the sample 5 revealed solely *Chloromonas brevispina*. The microscopic identifications of the dominant algae in samples 3 and 4 have been described previously (PROCHÁZKOVÁ et al. 2018b; REMIAS et al. 2018).

Output of the Sanger sequencing of the locally abundant taxa

Long sequences of multiple DNA regions containing 18S (about 1700 bp) and ITS2 rDNA (~200–1550 bp, Fig. 1) were obtained from the samples with virtually monospecific blooms of the three locally abundant taxa. The primers used (Table S1) amplified a larger fragment than ITS2. The actual length of the ITS2 rDNA for Chlorophyta (most common photosynthetic members of snow communities) varies between taxa in a range between 180 and 480 bp (BUCHHEIM et al. 2011). For instance, the AL1500af and LR3 primers (Table S1) are complementary to the end of 18S rDNA and 26S rDNA, and therefore resulting in the amplification of an approximately 1550 bp region.

Output of the 18S rDNA HTS data

A total of 433,190 18S rDNA sequences passed the quality control and 208,517 sequences could be assigned to green algal taxa (Table 2). The remainder of the sequences was assigned mostly to fungi, as well as Alveolata and Rhizaria (data not shown). 50 OTUs made up $>87\%$ of the total community composition (Table S4) and they were selected for the data evaluation and workflow optimization (Fig. 1). An overview of the ten most abundant OTUs ($>78\%$ of the total community) can be found in Table 3. The largest proportion of the sequences (sample 1: 33.0%, sample 2: 66.8%) was clustered in one OTU ‘denovo14334’ (99.4% similarity).

Evaluation of the different strategies for taxonomic assignments in 18S rDNA

Strategy A (basic version): The initial species assignment solely using the Qiime-compatible Silva database resulted in *Chloromonas* sp. Gassan–A LC012753.1 (Table 3 – column (1)). Other abundant OTUs were assigned to *Mesotaenium* sp. and several “uncultured *Chloromonas* and *Chlamydomonadaceae*” without a species affiliation (Table 3). **Strategy B (extended version):** The inclusion of the reference sequences of the locally abundant taxa into custom reference sequence database resulted in new assignments (26 out of the 50 most abundant OTUs) and in some cases in the clarification of the species assignment (Table S4 – column (2)). For instance, the “uncultured *Chlamydomonadaceae*” was identified as *Chlamydomonas nivalis* (sample 1: 0.9%, sample 2: 13.6%). **Strategy C (further extended version):** The representative sequences of the 50 most abundant OTUs in 18S rDNA were subjected to a manual BLAST search against NCBI GenBank (since the taxa assignments in Qiime (CAPORASO et al. 2010) uses a low default value of 90% minimum percent similarity to assign taxonomies to OTUs). The aim was to verify the actual percentage of identity, and whether closer hits not present in the Silva database occurred. Indeed, the manual verification step improved the taxonomic assignment of another eight taxa. However, it also revealed that 15 OTUs shared the same identity with several species. For

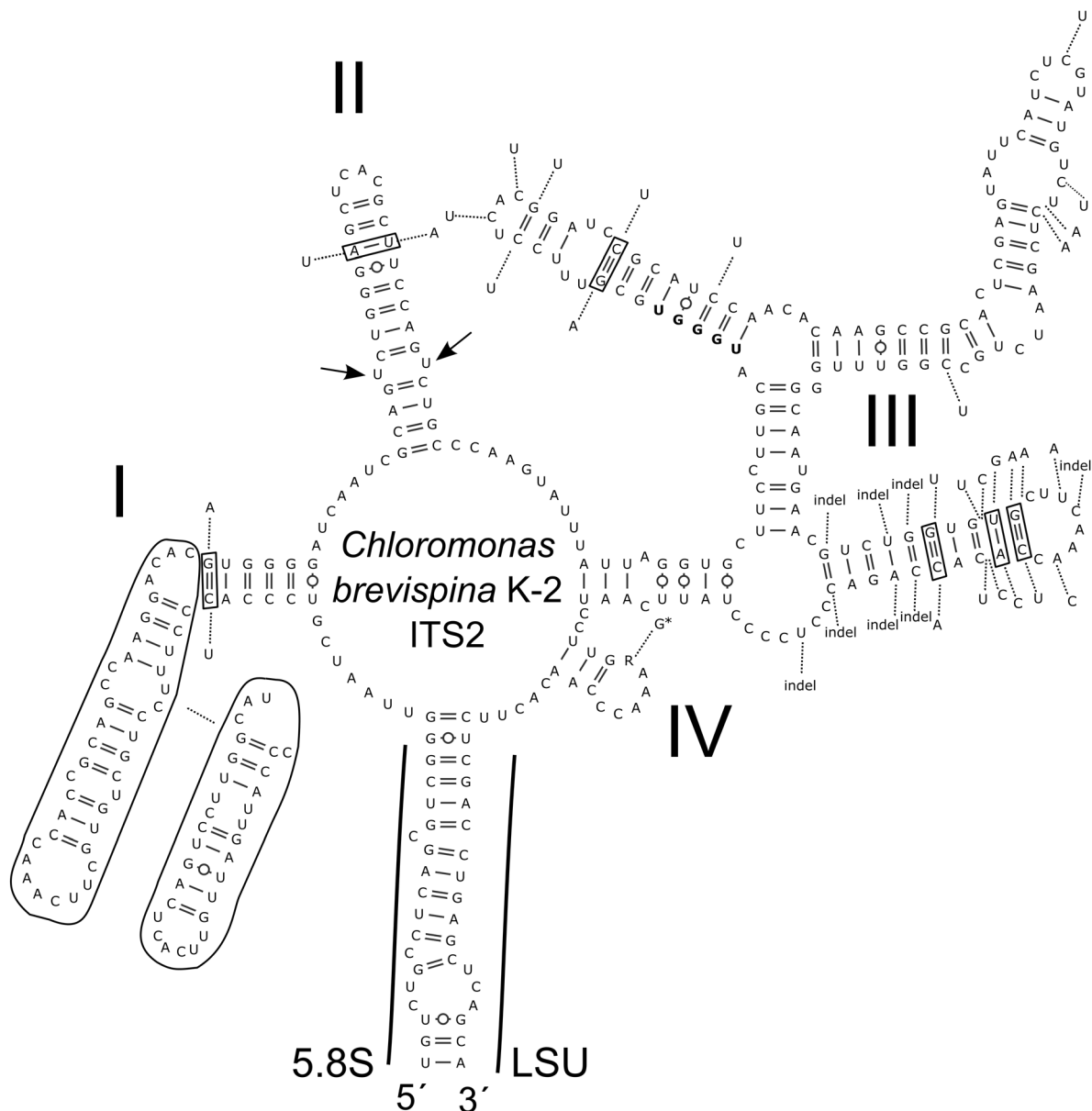


Fig. 4. Secondary structure of the ITS2 rDNA transcript *Chloromonas brevispina* K-2 (accession number MG791868). Differences between this species and the closely related OTU 'denovo99' are shown by nucleotides outside the structure linked by dotted lines. The U-U mismatch in helix II is indicated by arrows and the YGGY motif on the 5' side near the apex of helix III is in bold. CBCs in conserved parts of the structure are indicated by rectangles. The most significant CBC is located near the 5' apex of III helix. In addition, *Chloromonas brevispina* K-2 was identical with OTU 'denovo107' except for one ambiguous base (marked by an asterisk in helix IV).

instance, a vast number of *Chloromonas* species shared more than 99% identity in the hypervariable V3–V4 region of the 18S rDNA sequences (Table 3 and Table S4). This was the case for *Chloromonas brevispina* K-2, *Chloromonas* sp. TA 8 (AB902996.1), *Chloromonas* sp. Gassan-A (LC012714.1), *Chloromonas* sp. Gassan-B (LC012714.1), *Chloromonas polyptera* (JQ790556) and *Chloromonas* sp. Hakkoda-1 (LC012710.1), as well as *Scotiella cryophila* K-1 (MG253843; considering two ambiguous positions in the reference which can code for the same nucleotides). The same situation applied to *Raphidonema sempervirens* (AF514410.2), *Raphidonema*

nivale (AB488604.1) and *Stichococcus* sp. (KP081395.1), which also shared more than 99% identity. Thus, those OTUs were not assigned unambiguously at one species level (see ambiguous hits in Tables 3 and Table S4). The most abundant OTU, denovo14334, showed a difference of 1 bp to *Chloromonas brevispina* K-2, *Chloromonas* sp. TA 8 (AB902996.1), *Chloromonas* sp. B (LC012714.1) and *Scotiella cryophila* K-1 (MG253843). Thus, several species are likely conflated in this OTU. In addition, several OTUs showed differences of more than 2 bp to the closest reference and their assignment was therefore discarded in this step and recorded as “no blast hit”

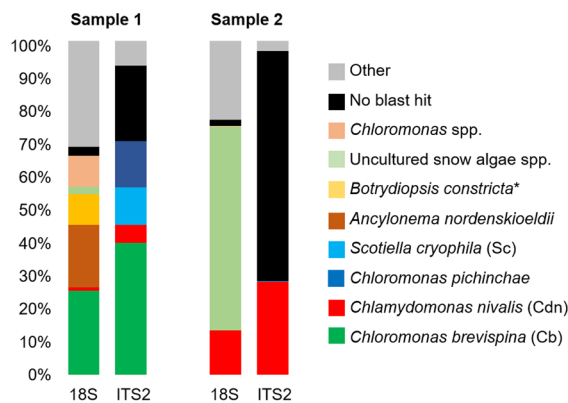


Fig. 5. Snow algal community composition after all optimization steps comprising all taxa with a minimum relative abundance of 5%. Full details can be found in Tables S4 and S6. Some discrepancies still prevailed between the 18S and ITS2 rDNA data sets, in particular in terms of the percentage of sequences with an unambiguous species assignment. Soil algae, which were only present in sample 1, are highlighted with an asterisk. Less abundant taxa are summarised in ‘Other’. Species abbreviations in brackets are referring to cells identified by light microscopy. Sequences below the similarity threshold of 94.5% and of 89.0% for 18S rDNA and ITS2, respectively, were recorded as “no blast hit”.

(2 OTUs in Table 3 – column (3), and 15 OTUs in Table S4 – column (3)). The percentage of sequence cover in the pairwise comparison with the reference sequence was also considered. For example, the OTU denovo30674 was initially assigned to *Prototheca cutis* (AB470468.1; < 2 bp difference). Yet, manual post-processing revealed that the sequence cover was only 18%. Thus, this assignment was discarded.

Furthermore, based on light microscopic observations and known species distribution patterns for this European Alpine region, some taxa assignments had to be scrutinized despite a very high similarity of the amplicon sequences with the suggested affiliations. These included *Ancylonema nordenskiöldii*, which mainly thrives on glacial surfaces of Polar Regions (LUTZ et al. 2018; REMIAS et al. 2012), and *Chloromonas polyptera*, which can be found in Maritime Antarctica near penguin rookeries (REMIAS et al. 2013).

Since several OTUs seemed to contain multiple taxa, oligotyping was carried out for further refinement of the taxonomic assignments. OTU ‘denovo14334’ consisted of four oligotypes, of which the most abundant shared 100% similarity with *Chloromonas brevispina* K–2 in sample 1 and several uncultured snow algae species in sample 2 (Table 4, Table S5). Oligotyping of the sequences grouped in the OTUs ‘denovo45654’ and ‘denovo36485’ also resulted in the resolution of another two oligotypes in each OTU.

Output of the ITS2 rDNA HTS data

A total of 273,404 ITS2 rDNA sequences passed the quality control and 189,922 sequences could be assigned to Chlorophyta (Table 2). The remainder of the sequences was assigned to mostly Fungi and Alveolata

(Table S6). An overview of the 10 most abundant OTUs (>88% of the total community) can be found in Table 5. 38 OTUs made up >98% of the total community composition (Table S7) and were selected for the data evaluation and workflow optimization (Fig. 1, Fig. S3). All sequence–structure alignments of ITS2 transcripts and ITS2 secondary structures of these most abundant OTUs, together with their reference sequences, can be found in the Supplementary Material (Figs S5–S24).

Evaluation of the different strategies for taxonomic assignments in the ITS2

Strategy A (basic version): The initial assignments based on the limited number of sequences available at NCBI resulted in species assignments for 17 out of the 38 OTUs (Table S7 – column (1)). Strategy B (extended version): After including the Sanger derived reference sequences of the three locally abundant taxa into custom reference sequence database, eight assignments for denovo OTUs were improved (Table S7 – column (2)) and one OTU previously without blast hit could be newly assigned (i.e. denovo63 to *Scotiella cryophila* K–1). *Chloromonas brevispina* K–2 and *Scotiella cryophila* K–1 contributed significantly to the pool of detected sequences. Strategy C (further extended version): After conducting ITS2 rDNA transcript secondary structure analyses and CBC detection in the most conserved part close to 5′-apex of III helix, the haplotype diversity of locally abundant *Chloromonas brevispina* revealed to be lower than expected from the HTS output (Fig. 3 – column ‘automatic’), whereas it did not change for *Scotiella cryophila* and *Chlamydomonas nivalis*. In the analysis of the 38 most abundant OTUs, which comprised >98% of the community (Table S7), one dominant and up to three rare haplotypes for each of three locally abundant species was recovered (Fig. 3 – column ‘manual’, Table S7). The dominant one was shown to be 100% identical with the reference sequence of a locally abundant taxon (Fig. 4, Figs S11, S16). For instance, the dominant haplotype of *Scotiella cryophila* K–1 in sample 1 accounted for 8,853 reads, whereas the second haplotype comprised 194 reads. The major haplotype of *Chlamydomonas nivalis* DL07 in sample 2 included 30,734 reads and the second haplotype only 61 reads. The major haplotype of *Chloromonas brevispina* K–2 in sample 1 was represented by 32,258 reads and the second haplotype by 155 reads only. The most abundant OTU ‘denovo99’ (59% of sequences in sample 2), which had previously been assigned to *Chloromonas brevispina* K–2, had six CBCs in the conservative regions (including one CBC in the most conserved apex of helix III close to the 5′ end) of the ITS2 structure in comparison with the reference sequence (Fig. 4). Considering that the presence of at least one CBC between two organisms in the most conserved regions of ITS2 is predicting a failure to cross sexually (COLEMAN 2009), we infer that OTU ‘denovo99’ might represent an independent though undescribed species. Furthermore, several OTU taxonomic assignments were below the chosen similarity threshold

of 89% with respect to the reference sequences. The suitability of the used ITS2 identity threshold was verified by checking the presence of CBCs in all representative OTUs, also those with a lower similarity threshold. These included the three OTUs (denovo142, denovo254 and denovo127) initially assigned to *Chloromonas* cf. *rostafinskii* (HQ404863.1). Indeed, they had several CBCs in the most conserved 5' end of helix III (Figs S12–S14). Consequently, these unknown species contributed to 22.5% of the unidentified ITS2 diversity in sample 1. Another OTU with an identity above the threshold of 89% was 'denovo100', which shared 92% identity with *Chloromonas pichincha* CCryo 261–06. A single CBC outside the most conserved part in helix III was detected in this case when the secondary structures of these sequences were compared (Figs S6, S7). Therefore, OTU 'denovo100' was also assigned to *Chloromonas pichincha*. Similarly, four CBCs were found between OTU 'denovo44' and *Scotiella cryophila*. They were located in helix III but outside its most conserved part (Figs. S15, S16), therefore these CBCs were treated as intraspecific variability (and maybe as an intragenomic variability) and OTU 'denovo44' was assigned to *Scotiella cryophila*. In addition, OTU 'denovo85' was 95% identical with the reference species and no CBC was found. Thus, 'denovo85' was assigned to *Chloromonas pichincha* (Fig. S6, S7).

Comparison of community compositions obtained with HTS using 18S and ITS2

The differences in the algal community structure obtained using the two markers is summarised in the NMDS ordination graphs (Figs. S25–S26). Whereas the 18S rDNA dataset resulted in a very similar taxonomic composition of both samples, ITS2 based analysis clearly separated the samples. The discrepant outcomes of the different assignment strategies are clearly visible for both markers. The presence of *Chloromonas brevispina* K–2 and *Chlamydomonas nivalis* DL07 were confirmed by both the 18S and the ITS2 rDNA data. Whereas *Scotiella cryophila* K–1 was one of the more abundant species in the ITS2 data in sample 1 (11.1%), it could not be unambiguously assigned in the 18S data (Table 3 and Table S4, denovo14334). Several other, less frequent species, (e.g. *Chloromonas* sp. Hakkoda–1 (LC012710.1), *Chloromonas platystigma* (AF514401.1), *Chloroidium saccharophilum* (KX024691.1), *Chloromonas* cf. *rostafinskii* (AF514402.1) could be detected in the 18S rDNA data, yet, were absent in the ITS2 data.

In contrast, the 18S rDNA data of sample 2 was dominated by a taxon sharing 100% similarity with several uncultured snow algal species, and *Chlamydomonas nivalis* (18S: 13.6%, ITS2: 28.3%; Tables 3 and 5, Figure 5). A considerably higher abundance of sequences with no species assignment was present in the ITS2 data sets (sample 1: 22.5%, sample 2: 68.6%) in comparison to the 18S rDNA data sets (sample 1: 3.6%, sample 2: 3.0%; Fig. 5). However, the vast majority of unassigned sequences

in sample 2 was represented by a single dominant OTU (denovo99; 86% of all sequences without species assignment) closely related to *Chloromonas brevispina* K–2 (Fig. 4), and the abundance of *Chloromonas brevispina* K–2 was negligible (<10 reads). In contrast, in sample 1 *Chloromonas brevispina* K–2 represented the dominant abundant OTU and denovo99 was much less abundant. In sample 1, allochthonous soil algae like *Botrydiopsis constricta* (AJ579339.1), *Botrydiopsis callosa* (AJ579340.1), *Heterococcus pleurococcoides/fuornensis/chodatii* (Xanthophyceae; BROADY 1976; NEGRISOLO et al. 2004), *Chloroidium saccharophilum* (KX024691.1; DARIENKO et al. 2010), *Lobosphaera* sp. (KT119889.1), *Lobosphaera incisa* (KM020046.1) and *Lobosphaera tirolensis* (Chlorophyta; AB006051.1; KARSTEN et al. 2005) were present (Tables S4 and A7). In contrast, these species were absent in sample 2 (when surface and soil–near snow were avoided during sample collection). This highlights the importance of a consistent sampling strategy when the aim is to compare species composition and abundances between different sites (Fig. S2).

DISCUSSION

Approaches to create a custom reference database of locally abundant taxa

Here, we show that by generating reference sequences of the locally abundant taxa and including them into the custom reference databases, the number of the identified OTUs increased. The use of monospecific snow algae blooms is advisable for obtaining long reference sequences of multiple DNA regions by Sanger sequencing. However, environmental sequences can be tricky and must be of high quality when used as references for HTS data (RIMET et al. 2018). A polyphasic approach (i.e., collectively using genetic, chemotaxonomic and phenotypic methods) is required to determine accurately the taxonomic identity of species found in field samples (MATSUZAKI et al. 2015). Alternatively, single cells with identifiable morphologies, can be picked out of mixed samples for single–cell sequencing to link morphology to genotype (BOCK et al. 2014). Light microscopy evaluations of cell morphologies should be conducted for each sample (directly after collection) to investigate which species might be present in the sequencing results. Qualitative light microscopic observation and identification may help link a phenotype of the most dominant morphotype with a genotype of the dominant OTU (e.g., OTU 'denovo99' prevailing in sample 2 is closely related to *Chloromonas brevispina* K–2 and they most likely share similar morphologies). The number of haplotypes of dominant species within a bloom might be revealed and compared with reports from elsewhere. For instance, a low haplotype diversity of *Chlamydomonas nivalis* DL07 is in par with previous findings on red snow from North America (BROWN et al. 2016).

Table 5. Algal community structure based on the ITS2 data set, comprising the ten most abundant OTUs that made up >88% of the community. The table shows discrepancies between OTU assignments using three strategies: (A) basic version using Qiime and a custom database downloaded from NCBI, (B) extended version using Qiime and additional reference sequences of the locally abundant taxa (underlined), and (C) further extended version using final manual verification of taxa assignments which required $\geq 89.0\%$ similarity (sequences below this threshold were recorded as “no blast hit”) and the absence of compensatory base changes (CBC) in homology positions near the 5′-apex of helix III. A comprehensive list comprising the 38 most abundant taxa with their corresponding OTU identification numbers can be found in the Table S7. Our results reveal that the manual verification including secondary structure prediction and CBC search is essential, and thus, highly recommended.

OTU ID	Sample 1 (%)	Sample 2 (%)	(A) Qiime + NCBI database	(B) Qiime + NCBI database + local references	(C) Qiime + NCBI database + local references + manual verification (sequence similarity (%), sequence cover (%))
denovo99	1.8	59.1	<i>Chloromonas</i> sp. CCCryo289-06 HQ404893.1	<i>Chloromonas brevispina</i> K-2	No blast hit (88%, 83%, 6 CBC when compared denovo99 and <i>Chloromonas brevispina</i> K-2 – one CBC out of it is located in the most conserved part of structure, i.e. in top close to the 5′ end of III helix, see Fig. 4)
denovo20	5.5	28.2	<i>Chlamydomonas nivalis</i> GU117577.1	<i>Chlamydomonas nivalis</i> DL07	<i>Chlamydomonas nivalis</i> DL07 (100%, 100%)
denovo107	39.8	<0.1	<i>Chloromonas</i> sp. CCCryo289-06 HQ404893.1	<i>Chloromonas brevispina</i> K-2	<i>Chloromonas brevispina</i> K-2 (100% identical except for one nucleotide – instead of ‘R’ in reference sequence, there was ‘G’, 100%)
denovo100	13.7	<0.1	<i>Chloromonas pichincha</i> HQ404889.1	<i>Chloromonas pichincha</i> HQ404889.1	<i>Chloromonas pichincha</i> HQ404889.1 (92%, 100%, 1 CBC in helix III [outside the most conserved part] when compared denovo100 and <i>Chloromonas pichincha</i> , see Figs S6, S7)
denovo63	10.9	0.2	No blast hit	<i>Scotiella cryophila</i> K-1	<i>Scotiella cryophila</i> K-1 (100%, 100%)
denovo142	8.2	1.7	<i>Chloromonas rostaffinskii</i> HQ404863.1	<i>Chloromonas rostaffinskii</i> HQ404863.1	No blast hit (79%, 60% – denovo142 vs. <i>Chloromonas rostaffinskii</i> : 86%, 77% – denovo142 vs. <i>Chloromonas miwae</i> LC012762.1, four CBCs [one CBC out of it is located in the most conserved part of the structure, i.e., in the top close to the 5′ end of III helix] when compared denovo142 and <i>Chloromonas miwae</i> , sequence–structure alignment in Fig. S12)
denovo130	1.4	3.5	No blast hit	No blast hit	No blast hit (no significant similarity found)
denovo181	4.1	0	No blast hit	No blast hit	No blast hit (82%, 87%, <i>Desmococcus endolithicus</i> KX094830.1; five CBCs – one in helix II and four CBCs in helix III, see Figs S19, S20)

Table 5 Cont.

denovo254	3.1	0.1	<i>Chloromonas rostafinskii</i> HQ404863.1	<i>Chloromonas rostafinskii</i> HQ404863.1	No blast hit (82%, 48% – denovo254 vs. <i>Chloromonas rostafinskii</i> : 88%, 84% – denovo254 vs. <i>Chloromonas miwae</i> LC012762.1, three CBCs [one out of in the most conserved part of the structure] when compared denovo254 and <i>Chloromonas miwae</i> , see Figs S12, S14)
denovo23	0.1	2.2	No blast hit	No blast hit	No blast hit (no significant similarity found)
	11.4	5.0	Other	Other	Other

The 18S rDNA marker and its limitations

Currently, a considerably higher number of 18S rDNA reference sequences exists in public databases compared to ITS2 rDNA. Therefore, 18S rDNA seems to be the obvious marker of choice for high-throughput studies of eukaryotic communities. Several other gene loci, e.g. *tufA* (VIEIRA et al. 2016) and *rbcL* (HALL et al. 2010; ZOU et al. 2016), have been recommended as the promising DNA barcode for some green algae (HALL et al. 2010). However, *tufA* records for the genus *Chloromonas*, which is frequently found in snow, are currently scarce in the NCBI database. Currently, the HTS technology limits the chosen marker to only a fraction of its actual length. The chosen V4–V5 region is the most variable region of the 18S rDNA gene for snow algal taxa, yet, the variability was not sufficient and unambiguous species assignments were often not feasible (Table 3). The most abundant 18S rDNA OTU was assigned to *Chloromonas brevispina* K–2. However, there was likely a ‘hidden’ diversity to a certain extent, since many different *Chloromonas* species can share up to 100% identity of this marker. An oligotyping approach (manual taxonomic assignment strategy C, further extended version), could resolve some of the “hidden” diversity for species with a difference of 1 bp in the sequenced amplicon. Therefore, this approach is highly recommended for further refinements of data sets that are characterized by very low variability, which is not detectable by conventional clustering of operational taxonomic units where 97% or 98% clustering levels are applied. Furthermore, due to the possibility of identical reference sequences of species that are not present in the habitat, it is essential to check alignments with the reference sequences manually. For instance, *Chloromonas polyptera* has been reported in HTS studies from several places in the northern hemisphere (LUTZ et al. 2015; TERASHIMA et al. 2017), yet, these results seem to be caused by ambiguous species assignments. For instance, TERASHIMA et al. (2017) reported 100% identity in the 18S rDNA of their OTU44 with *Chloromonas polyptera* (JQ790556). However, the sequenced gene fragment also shares 100% identity with *Chloromonas*

sp. Gassan B (LC012714.1), *Chloromonas* sp. ANT1 (AB903007.1), *Chloromonas* sp. TA8 (AB902996.1) and an uncultured ‘Viridiplantae’ clone (HQ188979.1). In summary, 18S rDNA amplicons do not adequately identify taxa on the species level in several taxonomic groups (XIAO et al. 2014).

Advantages of the ITS2 marker

In contrast to the 18S rDNA marker, Illumina reads can span the entire region of ITS2 rDNA. This hypervariable molecular marker provides a much higher resolution than 18S rDNA. The prediction of the ITS2 rDNA transcript secondary structures allowed a thorough identification of the haplotype diversity (manual taxonomic assignment strategy C, further extended version). It is therefore a powerful tool to delete wrong OTU assignments and represents an appropriate way of describing the true biodiversity (e.g., in sample 2 the most abundant OTU ‘denovo99’ is not *Chloromonas brevispina* K–2). Nevertheless, the methodological approach of ITS2 rRNA secondary structure prediction of each OTU is currently immensely time-consuming. The process is partly automatized (e.g., using Mfold, 4SALE), yet, significant input of manual validation and correction is still required. WOLF et al. (2013) reported a probability of ~0.99 that no intragenomic CBC took place, based on the comparison of ITS2 of 178 species of land plants. However, some *Chloromonas* species in snow possess intragenomic CBCs (MATSUZAKI et al. 2015). As a consequence, evaluation of CBCs detection should be carried out carefully; i.e., not only the pure presence or absence of CBCs, but also the exact position in the ITS2 molecule (i.e., whether it is in or outside the most conserved part) and the overall level of genetic difference of ITS2 between OTUs should be taken into account. For instance, among three OTUs from aplanozygotes and strains of *C. miwae*, one CBC was observed between specimen Gassan–C/strain NIES–2379 and strain NIES–2380 (MATSUZAKI et al. 2015). This CBC was located outside the most conserved branch of helix III and the genetic differences in the nuclear rDNA ITS2 region between

the aplanozygote specimen and the *C. miwae* strain were only 0.0 to 0.4% (see Fig. S15 in MATSUZAKI et al. 2015). Thus, both field specimens and the strain are regarded as one species. As a consequence, species boundaries in our proposed HTS approach rely on CBCs in the most conserved part of helix III only (i.e., close to its 5' apex).

A two-marker approach is mandatory

None of the two markers adequately described the community composition, either due to their low resolution (18S) or due to the lack of reference sequences (ITS2). Moreover, the output can also be partly influenced by library production biases and primer inefficiencies. Combining the strengths of both markers is thus recommended, particular in less-well studied environments. In addition, one marker can guide the data optimization of the other marker. Despite its low resolution, the 18S marker can provide guidance, which ITS2 rDNA reference sequences need to be generated and vice versa. Depending on the used markers, the estimated community composition may differ, mainly as a result of different primer specificity (VĚTROVSKÝ et al. 2016). The use of different markers can also address different aspects of community composition analyses: (a) the comparison of single-copy versus multi-copy markers provides better relative abundance approximations, (b) in contrast to non-coding markers, coding genes can be used to identify pseudogenes and construct phylogenetic (TONK et al. 2013; VĚTROVSKÝ et al. 2016). The potential of multi-marker approaches has been highlighted for species discovery in metabarcoding studies (MARCELINO & VERBRUGGEN 2016), as well as for assessing the effectiveness to distinguish cryptic species in a model morphospecies (EVANS et al. 2007).

Advantages, limitations and perspectives of HTS for community composition analyses

HTS allowed a more comprehensive assessment of the prevailing biodiversity than traditional Sanger sequencing and light microscopic observations. In addition to the detection of low-abundant taxa, a multitude of sequences, which did not match any references in the databases, were generated. Some of these likely represent new species (e.g., OTU 'denovo99'). Strain-based taxonomic studies or accurate species determination of monospecific field blooms by Sanger sequencing (to gain complete reads of the target marker) are required to increase the number of reference sequences. On the other hand, Sanger sequencing can be problematic for unrecognized mixed communities in terms of chromatogram corrections unless cloning is involved. Alternatively, putative monospecies snowfields can be sampled for HTS studies to evaluate the biodiversity and for the detection of any intragenomic variations of ITS2.

The quality of the reference databases is crucial for identification of various microorganisms including dinophytes (SOEHNER et al. 2012), diatoms (VISCO et al. 2015) and cryptophytes (HOEF-EMDEN 2012). New entries must be continuously updated. The Qiime-compatible

Silva database delivers reference sequences in one batch; yet, an updated version is only released about once a year. In contrast, NCBI is under continuous revision and therefore we recommend that new potential reference sequences are added manually to the Qiime-compatible Silva database prior to use. Only such optimized data can then be used for further evaluations including phylogeography and phylogenetic studies based on the generation of multi-locus sequence data in a fast and cost-effective way (McCORMACK et al. 2013). Alternatively, the use of the PR2 database (GUILLOU et al. 2013) may offer a better taxonomic assignment than Silva, especially for green algae.

In this methodological case study, we evaluated the application of high-throughput sequencing on an unconventional ecosystem of melting snowfields. Based on light microscopic observations, the investigated snowfields were dominated by three algal species, which were however not always reflected in the sequencing dataset. Consequently, HTS data need to be handled with care if applied on habitats or groups of organisms that are (highly) underrepresented in molecular databases. Currently, the need to generate appropriate reference sequences for the key taxa in the studied environment is an inevitable task for such studies. Furthermore, the two-marker approach, a consistent sampling strategy, light microscopy-based guidance and a final manual verification of all taxonomic assignments are strongly recommended.

ACKNOWLEDGEMENTS

The authors would like to thank Prof. Andreas Holzinger for providing access to his lab at the Institute of Botany, Dr. Birgit Sattler (Institute of Ecology) for providing access to the Limnological Station in Kühtai, both at the University of Innsbruck, Austria, and Dr. Thomas Leya (Fraunhofer IZI-BB, Potsdam-Golm, Germany) for providing access to his CCCryo 18S rDNA database. DR acknowledges funding from the Austrian Science Fund (FWF): P29959. SL and LGB acknowledge funding from the Helmholtz Recruiting Initiative (award number I-044-16-01). LP and LN acknowledge funding from the Czech Science Foundation (GACR) project 18-02634S and from the Institutional Research Concept RVO67985939 (LN).

REFERENCES

- ALANAGREH, L.; PEGG, C.; HARIKUMAR, A. & BUCHHEIM, M. (2017): Assessing intragenomic variation of the internal transcribed spacer two: Adapting the Illumina metagenomics protocol. – *PLOS one* 12: e0181491.
- ANESIO, A.M.; LUTZ, S.; CHRISMAS, N.A.M. & BENNING, L.G. (2017): The microbiome of glaciers and ice sheets. – *Npj Biofilms and Microbiomes* 3: 10.
- BENGTSSON-PALME, J.; RYBERG, M.; HARTMANN, M.; BRANCO, S.; WANG, Z.; GODHE, A.; DE WIT, P.; GARCÍA-SÁNCHEZ, M.; EBERSBERGER, I.; DE SOUSA, F.; AMEND, A.; JUMPPONEN, A.; UNTERSEHER, M.; KRISTIANSSON, E.; ABARENKOV, K.; BERTRAND, Y.J.K.; SANLI, K.; ERIKSSON, K.M.; VIK, U.; VELDRE, V. & NILSSON, R.H. (2013): Improved software detection and extraction of ITS1 and ITS2 from ribosomal ITS sequences of fungi and other eukaryotes for analysis of environmental sequencing data. – *Methods*

- in Ecology and Evolution 4: 914–919.
- BOCK, C.; MEDINGER, R.; JOST, S.; PSENNER, R. & BOENIGK, J. (2014): Seasonal variation of planktonic chrysophytes with special focus on *Dinobryon*. – Fotia 14: 179–190.
- BRADLEY, I.M.; PINTO, A.J. & GUEST, J.S. (2016): Design and Evaluation of Illumina MiSeq-Compatible, 18S rRNA gene-specific primers for improved characterization of mixed phototrophic communities. – Applied and Environmental Microbiology 82: 5878–5891.
- BRANDARIZ-FONTES, C.; CAMACHO-SANCHEZ, M.; VILÀ, C.; VEGA-PLA, J.L.; RICO, C. & LEONARD, J.A. (2015): Effect of the enzyme and PCR conditions on the quality of high-throughput DNA sequencing results. – Scientific Reports 5: 8056.
- BROADY, P.A. (1976): Six new species of terrestrial algae from Signy Island, South Orkney Islands, Antarctica. – British Phycological Journal 11: 387–405.
- BROWN, S.P.; UNGERER, M.C. & JUMPPONEN, A. (2016): A Community of Clones: Snow Algae Are Diverse Communities of Spatially Structured Clones. – International Journal of Plant Sciences 177: 432–439.
- BUCHHEIM, M.A.; KELLER, A.; KOETSCHAN, C.; FÖRSTER, F.; MERGET, B.; WOLF, M. & M. (2011): Internal Transcribed Spacer 2 (nu ITS2 rRNA) Sequence-Structure Phylogenetics: Towards an Automated Reconstruction of the Green Algal Tree of Life. – PLoS ONE 6: e16931.
- CAISOVÁ, L.; MARIN, B. & MELKONIAN, M. (2013): A Consensus Secondary Structure of ITS2 in the Chlorophyta Identified by Phylogenetic Reconstruction. – Annals of Anatomy 164: 482–496.
- CAMPO, J. DEL; KOLISKO, M.; BOSCARO, V.; SANTOFERRARA, L.F.; NENAROKOV, S.; MASSANA, R.; GUILLOU, L.; SIMPSON, A.; BERNEY, C.; DE VARGAS, C.; BROWN, M.W.; KEELING, P.J. & PARFREY, L.W. (2018): EukRef: Phylogenetic curation of ribosomal RNA to enhance understanding of eukaryotic diversity and distribution. – PLOS Biology 16: e2005849.
- CAPORASO, J.G.; KUCZYNSKI, J.; STOMBAUGH, J.; BITTINGER, K.; BUSHMAN, F.D.; COSTELLO, E.K.; FIERER, N.; PEÑA, A.G.; GOODRICH, J.K.; GORDON, J.I.; HUTTLEY, G.A.; KELLEY, S.T.; KNIGHTS, D.; KOENIG, J.E.; LEY, R.E.; LOZUPONE, C.A.; McDONALD, D.; MUEGGE, B.D.; PIRRUNG, M.; REEDER, J.; SEVINSKY, J.R.; TURNBAUGH, P.J.; WALTERS, W.A.; WIDMANN, J.; YATSUNENKO, T.; ZANEVELD, J. & KNIGHT, R. (2010): QIIME allows analysis of high-throughput community sequencing data. – Nature Methods 7: 335–336.
- CHASE, M.W. & FAY, M.F. (2009): Ecology. Barcoding of plants and fungi. – Science 325: 682–683.
- CHEUNG, M.K.; AU, C.H.; CHU, K.H.; KWAN, H.S. & WONG, C.K. (2010): Composition and genetic diversity of picoeukaryotes in subtropical coastal waters as revealed by 454 pyrosequencing. – The ISME Journal 4: 1053–1059.
- COLEMAN, A. (2007): Pan-eukaryote ITS2 homologies revealed by RNA secondary structure. – Nucleic Acids Research 35: 3322–3329.
- COLEMAN, A.W. (2000): The significance of a coincidence between evolutionary landmarks found in mating affinity and a DNA sequence. – Protist 151: 1–9.
- COLEMAN, A.W. (2009): Is there a molecular key to the level of “biological species” in eukaryotes? A DNA guide. – Molecular Phylogenetics and Evolution 50: 197–203.
- COLEMAN, A.W.; SUAREZ, A. & GOFF, L.J. (1993): Molecular delineation of species and syngens in Volvocacean green algae (Chlorophyta). – Journal of Phycology 30: 80–90.
- DARIENKO, T.; GUSTAVS, L.; MUDIMU, O.; MENENDEZ, C.R.; SCHUMANN, R.; KARSTEN, U.; FRIEDL, T. & PRÖSCHOLD, T. (2010): *Chloroidium*, a common terrestrial coccoid green alga previously assigned to Chlorella (Trebouxiophyceae, Chlorophyta). – European Journal of Phycology 45: 79–95.
- DARTY, K.; DENISE, A. & PONTY, Y. (2009): VARNA: Interactive drawing and editing of the RNA secondary structure. – Bioinformatics 25: 1974–1975.
- EDDY, S.R. (1996): Hidden Markov models. – Current Opinion in Structural Biology 6: 361–365.
- EREN, A.M.; MAIGNIEN, L.; SUL, W.J.; MURPHY, L.G.; GRIM, S.L.; MORRISON, H.G. & SOGIN, M.L. (2013): Oligotyping: differentiating between closely related microbial taxa using 16S rRNA gene data. – Methods in Ecology and Evolution 4: 1111–1119.
- EVANS, K. M.; WORTLEY, A. H. & MANN, D. G. (2007): An assessment of potential diatom “barcode” genes (cox1, rbcL, 18S and ITS rDNA) and their effectiveness in determining relationships in *Sellaphora* (Bacillariophyta). – Protist 158: 349–364.
- FREY, B.; RIME, T.; PHILLIPS, M.; STIERLI, B.; HAJDAS, I.; WIDMER, F. & HARTMANN, M. (2016): Microbial diversity in European alpine permafrost and active layers. – FEMS Microbiology Ecology 92: 1–17.
- GROSSMANN, L.; BEISSER, D.; BOCK, C.; CHATZINOTAS, A.; JENSEN, M.; PREISFELD, A.; PSENNER, R.; RAHMANN, S.; WODNIOK, S. & BOENIGK, J. (2016): Trade-off between taxon diversity and functional diversity in European lake ecosystems. – Molecular Ecology 25: 5876–5888.
- GUILLOU, L.; BACHAR, D.; AUDIC, S.; BASS, D.; BERNEY, C.; BITTNER, L.; BOUTTE, C.; BURGAUD, G.; DE VARGAS, C.; DECELLE, J.; DEL CAMPO, J.; DOLAN, J.R.; DUNTHORN, M.; EDVARDSEN, B.; HOLZMANN, M.; KOOISTRA, W.H.C.F.; LARA, E.; LE BESCOT, N.; LOGARES, R.; MASSANA, F.M.R.; MONTRESOR, M.; MORARD, R.; NOT, F.; PAWLOWSKI, J.; PROBERT, I.; SAUVADET, A.-L.; SIANO, R.; STOECK, T.; VAULOT, D.; ZIMMERMANN, P. & CHRISTEN, R. (2013): The Protist Ribosomal Reference database (PR2): a catalog of unicellular eukaryote Small Sub-Unit rRNA sequences with curated taxonomy. – Nucleic Acids Research 41: D597–D604.
- HALL, J.D.; FUČÍKOVÁ, K.; LO, C.; LEWIS, L.A. & KAROL, K.G. (2010): An assessment of proposed DNA barcodes in freshwater green algae. – Cryptogamie, Algologie 31: 529–555.
- HOHAM, R.W. & DUVAL, B. (2001): Microbial ecology of snow and freshwater ice with emphasis on snow algae. – In: JONES, H.G.; POMEROY, J.W.; WALKER, D.A. & HOHAM, R. (eds.) Snow Ecology. An Interdisciplinary Examination of Snow-covered Ecosystems. – pp. 168–228, Cambridge University Press, Cambridge.
- HOEF-EMDEN, K. (2012): Pitfalls of establishing DNA barcoding systems in protists: the Cryptophyceae as a test case. – PLoS One 7: e43652.
- HOHAM, R.W.; ROEMER, S.C. & MULLET, J.E. (1979): The life history and ecology of the snow alga *Chloromonas brevispina* comb. nov. (Chlorophyta, Volvocales). – Phycologia 18: 55–70.
- ILLUMINA: 16S Metagenomic Sequencing Library Preparation Preparing 16S Ribosomal RNA Gene Amplicons for the Illumina MiSeq System. 1–28. (support.illumina.com/documents/documentation/chemistry_documentation/16s/16s-metagenomic-library-prep-guide-15044223-b.pdf). Accessed 13 August 2014.
- KARSTEN, U.; FRIEDL, T.; SCHUMANN, R.; HOYER, K. & LEMBCKE, S. (2005): Mycosporine-like amino acids and phylogenies in green algae: *Prasiola* and its relatives from the Trebouxiophyceae (Chlorophyta). – Journal of Phycology 41: 557 Stuttgart: 566.

- KENT, W.J. (2002): BLAT—the BLAST-like alignment tool. — *Genome Research* 12: 656–664.
- KOL, E. (1968): Kryobiologie; Biologie und Limnologie des Schnees und Eises. Die Binnengewässer (Vol. 24). — 216 pp., Schweizerbart'sche Verlagsbuchhandlung, Stuttgart.
- KOMÁREK, J. & NEDBALOVÁ, L. (2007): Green Cryosestic Algae. — In: SECKBACH, J. (ed.): *Algae and Cyanobacteria in Extreme Environments*. — pp. 321–342, Springer, Netherlands.
- LELIAERT, F.; VERBRUGGEN, H.; VANORMELINGEN, P.; STEEN, F.; LÓPEZ–BAUTISTA, J.M.; ZUCCARELLO, G.C. & DE CLERCK, O. (2014): DNA-based species delimitation in algae. — *European Journal of Phycology* 49: 179–196.
- LEYA, T. (2013): Snow algae: adaptation strategies to survive on snow and ice. — In: SECKBACH, J.; OREN, A. & STAN–LOTTER, H. (eds.): *Polyextremophiles*. — pp. 401–423, Springer, Cham.
- LINDNER, D.L. & BANIK, M.T. (2011): Intragenomic variation in the ITS rDNA region obscures phylogenetic relationships and inflates estimates of operational taxonomic units in genus *Laetiporus*. — *Mycologia* 103: 731–740.
- LINDNER, D.L.; CARLSEN, T.; HENRIK NILSSON, R.; DAVEY, M.; SCHUMACHER, T. & KAUSERUD, H. (2013): Employing 454 amplicon pyrosequencing to reveal intragenomic divergence in the internal transcribed spacer rDNA region in fungi. — *Ecology and Evolution* 3: 1751–1764.
- LUTZ, S.; ANESIO, A.M.; EDWARDS, A. & BENNING, L.G. (2015): Microbial diversity on icelandic glaciers and ice caps. — *Frontiers in Microbiology* 6: 307.
- LUTZ, S.; ANESIO, A.M.; EDWARDS, A. & BENNING, L.G. (2017): Linking microbial diversity and functionality of arctic glacial surface habitats. — *Environmental Microbiology* 19: 551–565.
- LUTZ, S.; ANESIO, A.M.; FIELD, K. & BENNING, L.G. (2015): Integrated “Omics”, targeted metabolite and single-cell analyses of arctic snow algae functionality and adaptability. — *Frontiers in Microbiology* 6: 1323.
- LUTZ, S.; ANESIO, A.M.; RAISWELL, R.; EDWARDS, A.; NEWTON, R.J.; GILL, F. & BENNING, L.G. (2016): The biogeography of red snow microbiomes and their role in melting arctic glaciers. — *Nature Communications* 7: 11968.
- LUTZ, S.; MCCUTCHEON, J.; MCQUAID, J.B. & BENNING, L.G. (2018): The diversity of ice algal communities on the Greenland Ice Sheet as revealed by oligotyping. — *Microbial Genomics* 4: e000159.
- MARCELINO, V. R. & VERBRUGGEN, H. (2016): Multi-marker metabarcoding of coral skeletons reveals a rich microbiome and diverse evolutionary origins of endolithic algae. — *Scientific Reports* 6: 31508.
- MATSUZAKI, R.; HARA, Y. & NOZAKI, H. (2012): A taxonomic revision of *Chloromonas reticulata* (Volvocales, Chlorophyceae), the type species of the genus *Chloromonas*, based on multigene phylogeny and comparative light and electron microscopy. — *Phycologia* 51: 74–85.
- MATSUZAKI, R.; KAWAI–TOYOOKA, H.; HARA, Y. & NOZAKI, H. (2015): Revisiting the taxonomic significance of aplanozygote morphologies of two cosmopolitan snow species of the genus *Chloromonas* (Volvocales, Chlorophyceae). — *Phycologia* 54: 491–502.
- MCCORMACK, J.E.; HIRD, S.M.; ZELLMER, A.J.; CARSTENS, B.C. & BRUMFIELD, R.T. (2013): Applications of next-generation sequencing to phylogeography and phylogenetics. — *Molecular Phylogenetics and Evolution* 66: 526–538.
- MIKHAILYUK, T.I.; SLUIMAN, H.J.; MASSALSKI, A.; MUDIMU, O.; DEMCHENKO, E.M.; KONDRATYUK, S.Y. & FRIEDL, T. (2008): New streptophyte green algae from terrestrial habitats and an assessment of the genus *Interfilum* (Klebsormidiophyceae, Streptophyta). — *Journal of Phycology* 44: 1586–1603.
- NEGRISOLO, E.; MAISTRO, S.; INCARBONE, M.; MORO, I.; DALLA VALLE, L.; BROADY, P.A. & ANDREOLI, C. (2004): Morphological convergence characterizes the evolution of Xanthophyceae (Heterokontophyta): evidence from nuclear SSU rDNA and plastidial rbcL genes. — *Molecular Phylogenetics and Evolution* 33: 156–170.
- NOVIS, P.M. (2002): Ecology of the snow alga *Chlainomonas kolii* (Chlamydomonadales, Chlorophyta) in New Zealand. — *Phycologia* 41: 280–292.
- OYOLA, S.O.; OTTO, T.D.; GU, Y.; MASLEN, G.; MANSKE, M.; CAMPINO, S.; TURNER, D.; MACINNIS, B.; KWIATOWSKI, D.; SWERDLOW, H. & QUAIL, M.A. (2012): Optimizing illumina next-generation sequencing library preparation for extremely AT-biased genomes. — *BMC Genomics* 13: 1.
- PROCHÁZKOVÁ, L.; REMIAS, D.; HOLZINGER, A.; ŘEZANKA, T. & NEDBALOVÁ, L. (2018b): Ecophysiological and morphological comparison of two populations of *Chlainomonas* sp. (Chlorophyta) causing red snow on ice-covered lakes in the High Tatras and Austrian Alps. — *European Journal of Phycology* 53: 230–243.
- PROCHÁZKOVÁ, L.; REMIAS, D.; ŘEZANKA, T. & NEDBALOVÁ, L. (2018a): *Chloromonas nivalis* subsp. *tatrae*, subsp. nov. (Chlamydomonadales, Chlorophyta): Re-examination of a snow alga from the High Tatra Mountains (Slovakia). — *Fottea* 18: 1–18.
- QUAST, C.; PRUESSE, E.; YILMAZ, P.; GERKEN, J.; SCHWEER, T.; YARZA, P.; PEPLIES, J. & GLÖCKNER, F.O. (2013): The SILVA ribosomal RNA gene database project: Improved data processing and web-based tools. — *Nucleic Acids Research* 41: D590–D596.
- REMIAS, D. (2012): Cell structure and physiology of alpine snow and ice algae. — In: LÜTZ, C. (ed.): *Plants in Alpine Regions*. — pp. 175–185, Springer, Vienna.
- REMIAS, D.; HOLZINGER, A.; AIGNER, S. & LÜTZ, C. (2012): Ecophysiology and ultrastructure of *Ancylonema nordenskiöldii* (Zygnematales, Streptophyta), causing brown ice on glaciers in Svalbard (high arctic). — *Polar Biology* 35: 899–908.
- REMIAS, D.; KARSTEN, U.; LÜTZ, C. & LEYA, T. (2010): Physiological and morphological processes in the alpine snow alga *Chloromonas nivalis* (Chlorophyceae) during cyst formation. — *Protoplasma* 243: 73–86.
- REMIAS, D.; LÜTZ–MEINDL, U. & LÜTZ, C. (2005): Photosynthesis, pigments and ultrastructure of the alpine snow alga *Chlamydomonas nivalis*. — *European Journal of Phycology* 40: 259–268.
- REMIAS, D.; PICHRTOVÁ, M.; PANGRAZ, M.; LÜTZ, C. & HOLZINGER, A. (2016): Ecophysiology, secondary pigments and ultrastructure of *Chlainomonas* sp. (Chlorophyta) from the European Alps compared with *Chlamydomonas nivalis* forming red snow. — *FEMS Microbiology Ecology* 92: fiw030.
- REMIAS, D.; PROCHÁZKOVÁ, L.; HOLZINGER, A. & NEDBALOVÁ, L. (2018): Ecology, cytology and phylogeny of the snow alga *Scotiella cryophila* K-1 (Chlorophyceae) from the Austrian Alps. — *Phycologia* 57: 581–592.
- REMIAS, D.; WASTIAN, H.; LÜTZ, C. & LEYA, T. (2013): Insights into the biology and phylogeny of *Chloromonas polyptera* (Chlorophyta), an alga causing orange snow in Maritime Antarctica. — *Antarctic Science* 25: 648–656.
- RIMET, F.; ABARCA, N.; BOUCHEZ, A.; KUSBER, W.H.; JAHN, R.; KAHLERT, M.; KECK, F.; KELLY, M.G.; MANN, D.G.; PIUZ, A.; TROBAJO, R.; TAPOLCZAI, K.; VASSELON, V. & ZIMMERMANN, J. (2018): The potential of High-Throughput Sequencing (HTS) of natural samples as a source of primary taxonomic information for reference libraries

- of diatom barcodes. – *Fottea* 18: 37–54.
- SCHIRMER, M.; IJAZ, U.Z.; D'AMORE, R.; HALL, N.; SLOAN, W.T. & QUINCE, C. (2015): Insight into biases and sequencing errors for amplicon sequencing with the Illumina MiSeq platform. – *Nucleic Acids Research* 43: e37.
- SCHLOSS, P.D.; GEVERS, D. & WESTCOTT, S.L. (2011): Reducing the effects of PCR amplification and sequencing Artifacts on 16S rRNA-based studies. – *PLoS One* 6: e27310.
- SCHMIDT, P.A.; BÁLINT, M.; GRESHAKE, B.; BANDOW, C.; RÖMBKE, J. & SCHMITT, I. (2013): Illumina metabarcoding of a soil fungal community. – *Soil Biology and Biochemistry* 65: 128–132.
- SCHULTZ, J. & WOLF, M. (2009): ITS2 sequence–structure analysis in phylogenetics: A how–to manual for molecular systematics. – *Molecular Phylogenetics and Evolution* 52: 520–523.
- SEGAWA, T.; MATSUZAKI, R.; TAKEUCHI, N.; AKIYOSHI, A.; NAVARRO, F.; SUGIYAMA, S.; YONEZAWA, T. & MORI, H. (2018): Bipolar dispersal of red–snow algae. – *Nature Communications* 9: 3094.
- SEIBEL, P.N.; MÜLLER, T.; DANDEKAR, T.; SCHULTZ, J. & WOLF, M. (2006): 4SALE – a tool for synchronous RNA sequence and secondary structure alignment and editing. – *BMC Bioinformatics* 7: 498.
- SEIBEL, P.N.; MÜLLER, T.; DANDEKAR, T. & WOLF, M. (2008): Synchronous visual analysis and editing of RNA sequence and secondary structure alignments using 4SALE. – *BMC Research Notes* 1: 91.
- SIMON, U. & WEISS, M. (2008): Intragenomic variation of fungal ribosomal genes is higher than previously thought. – *Molecular Biology and Evolution* 25: 2251–2254.
- SOEHNER, S.; ZINSSMEISTER, C.; KIRSCH, M. & GOTTSCHLING, M. (2012): Who am I—and if so, how many? Species diversity of calcareous dinophytes (Thoracosphaeraceae, Peridinales) in the Mediterranean Sea. – *Organisms Diversity & Evolution* 12: 339–348.
- STIBAL, M. & ELSTER, J. (2005): Growth and morphology variation as a response to changing environmental factors in two Arctic species of *Raphidonema* (Trebouxiophyceae) from snow and soil. – *Polar Biology* 28: 558–567.
- TER BRAAK, C.J.F. & ŠMILAUER, P. (2012): CANOCO reference manual and user's guide: Software for ordination (version 5.0). – 496 pp. Microcomputer Power, Ithaca, NY.
- TERASHIMA, M.; UMEZAWA, K.; MORI, S.; KOJIMA, H. & FUKUI, M. (2017): Microbial community analysis of colored snow from an alpine snowfield in Northern Japan reveals the prevalence of Betaproteobacteria with snow algae. – *Frontiers in Microbiology* 8: 1–13.
- THORNHILL, D.J.; LAJEUNESSE, T.C. & SANTOS, S.R. (2007): Measuring rDNA diversity in eukaryotic microbial systems: how intragenomic variation, pseudogenes, and PCR artifacts confound biodiversity estimates. – *Molecular Ecology* 16: 5326–5340.
- TONK, L.; BONGAERTS, P.; SAMPAYO, E. M. & HOEGH–GULDBERG, O. (2013): SymbioGBR: a web–based database of *Symbiodinium* associated with cnidarian hosts on the Great Barrier Reef. – *BMC Ecology* 13: 7.
- TRAGIN, M.; ZINGONE, A. & VAULOT, D. (2017): Comparison of coastal phytoplankton composition estimated from the V4 and V9 regions of 18S rRNA gene with a focus on photosynthetic groups and especially Chlorophyta. – *Environmental Microbiology* 20: 506–520.
- VĚTROVSKÝ, T.; KOLAŘÍK, M.; ŽIFČÁKOVÁ, L.; ZELENKA, T. & BALDRIAN, P. (2016): The rpb2 gene represents a viable alternative molecular marker for the analysis of environmental fungal communities. – *Molecular Ecology Resources* 16: 388–401.
- VIEIRA, H.H.; BAGATINI, I.L.; GUINART, C.M. & VIEIRA, A.A.H. (2016): tufA gene as molecular marker for freshwater Chlorophyceae. – *Algae* 31: 155–165.
- VISCO, J. A.; APOTHÉLOZ–PERRET–GENTIL, L.; CORDONIER, A.; ESLING, P.; PILLET, L. & PAWLOWSKI, J. (2015): Environmental monitoring: inferring the diatom index from next–generation sequencing data. *Environmental science & technology* 49: 7597–7605.
- WHITE, T.J.; BRUNS, T.; LEE, S. & TAYLOR, J. (1990): Amplification and direct sequencing of fungal ribosomal RNA genes for phylogenetics. – In: INNIS, M.A.; GELFAND, D. H.; SNINSKY, J. J. & WHITE, T. J. (eds.): *PCR Protocols*. – pp. 315–322, Elsevier.
- WOLF, M.; CHEN, S.; SONG, J.; ANKENBRAND, M. & MÜLLER, T. (2013): Compensatory Base Changes in ITS2 Secondary Structures Correlate with the Biological Species Concept Despite Intra-genomic Variability in ITS2 Sequences – A Proof of Concept. – *PLoS One* 8: e66726.
- XIAO, X.; SOGGE, H.; LAGESEN, K.; TOOMING–KLUNDERUD, A.; JAKOBSEN, K.S. & ROHRLACK, T. (2014): Use of High Throughput Sequencing and Light Microscopy Show Contrasting Results in a Study of Phytoplankton Occurrence in a Freshwater Environment. – *PLoS One* 9: e106510.
- YAO, H.; SONG, J.; LIU, C.; LUO, K.; HAN, J.; LI, Y.; PANG, X.; XU, H.; ZHU, Y.; XIAO, P. & CHEN, S. (2010): Use of ITS2 Region as the Universal DNA Barcode for Plants and Animals. – *PLoS One* 5: e13102.
- ZOU, S.; FEI, C.; WANG, C.; GAO, Z.; BAO, Y.; HE, M. & WANG, C. (2016): How DNA barcoding can be more effective in microalgae identification: a case of cryptic diversity revelation in *Scenedesmus* (Chlorophyceae). – *Scientific reports* 6: 36822.
- ZUKER, M. (2003): Mfold web server for nucleic acid folding and hybridization prediction. – *Nucleic Acids Research* 31: 3406–3415.

Supplementary material

the following supplementary material is available for this article:

Supplementary material is available for this article.

This material is available as part of the online article (<http://fottea.czechphycology.cz/contents>)

Data sharing and data accessibility

18S and ITS2 rDNA amplicon sequences have been deposited to the European Nucleotide Archive (ENA) under accession number PRJEB24479 (Please note that data has been deposited but not been released yet, and they will be made public upon manuscript acceptance). Sanger sequences of reference species were deposited in NCBI under accession numbers listed in supplementary Table S5. All other data are presented in this manuscript and in the further supplemental files.



Fig. S1. a) Red snow surface (sample 1) caused by microalgae at Kühtai, Tyrolean Alps, Austria. b) The discoloration reached several centimetres down, changing from red to green.

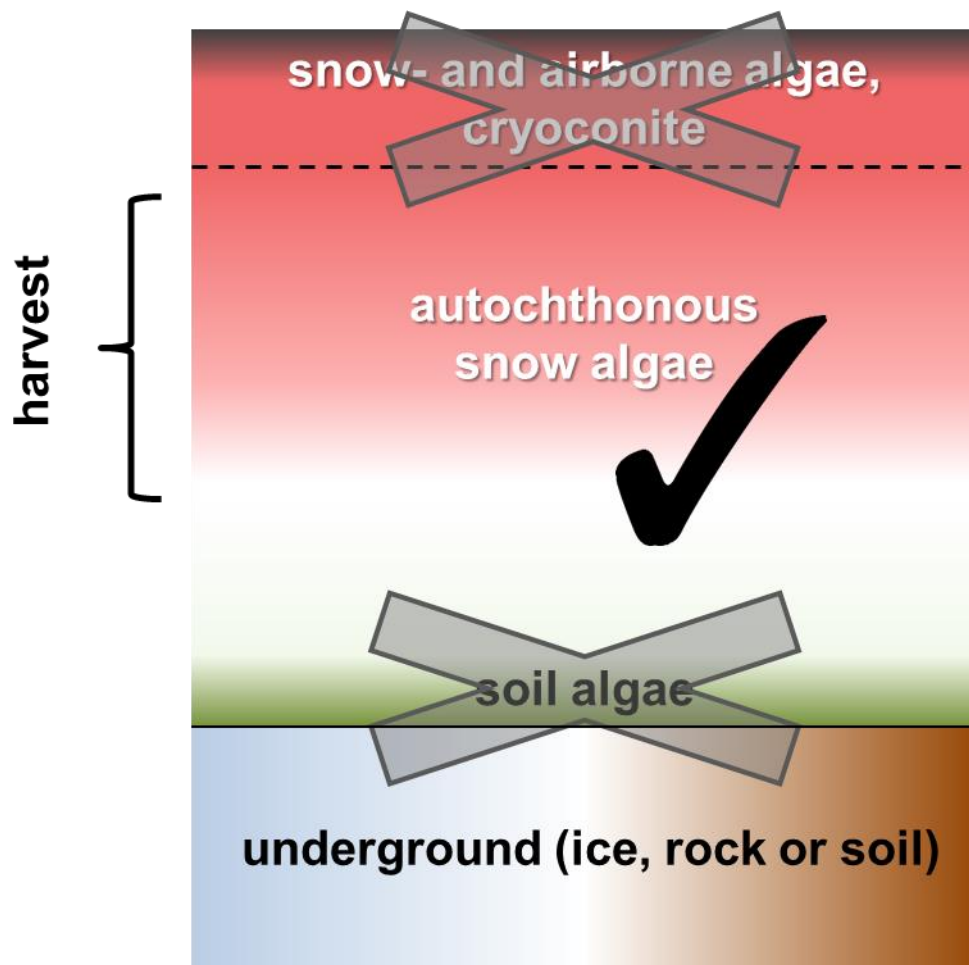


Fig. S2. Vertical scheme of a melting snowfield showing the best practice of 'true' (autochthonous) snow algae sampling. In order to avoid allochthonous organisms (airborne, soil bound), the uppermost surface and lowermost ground centimeters of snow should not be harvested. A consistent sampling strategy is important when the aim is to compare microbial diversity and abundances between different sites. Exceptions may be steep slopes in polar regions, where snow algae populations are surface based, and thus, surface layer cannot be omitted.

ACTIVITY	HOW	AIM
1. selection of sequences	<ul style="list-style-type: none"> pairwise BLAST search: - against NCBI custom download library - against additional reference sequences 	<ul style="list-style-type: none"> - generation of dataset of ITS2 sequences: reference sequence and all OTUs which passed the identity threshold of $\geq 94.0\%$ when compared to this reference sequence
2. individual RNA structure prediction	<ul style="list-style-type: none"> - carry out for each of the sequences in the ITS2 dataset at server MFold: http://unafold.rna.albany.edu/?q=mfold - ITS2 sequences are pasted into window at RNA Folding Form and folded - note: HTS delivers DNA based data, but during RNA folding, thymine ['T'] are converted to uracil ['U'] 	<ul style="list-style-type: none"> - selection of the model of the secondary structure with the minimum free energy having specific features (4 helices, U-U mismatch in helix II, UGGU motif in helix III) - saving Vienna file (XFasta format, i.e. fasta file with line containing structural information in bracket-dot-bracket notation below the sequence)
3. sequence and secondary structure alignment	<ul style="list-style-type: none"> - paste sequences in MEGA - in each row is ITS2 rRNA sequence followed by its structural information - load this *fas file into 4SALE 4SALE available here: http://4sale.bioapps.biozentrum.uni-wuerzburg.de/quickstart.html 	<ul style="list-style-type: none"> - performing sequence and secondary structure alignment in the first step automatically via Clustal - inspection of the secondary structure (structure viewer, detection of misaligned sequences, gap, conservation, alignment column position, helix position), - monitoring structure information and manual editing (in edit mode) - mapping alignment to consensual structure
4. analyzing CBCs	<ul style="list-style-type: none"> - in homologous positions of the ITS2 molecule which are unambiguously aligned 4SALE -> Window -> CBC Table , -> Export CBC matrix - inspection of positions of CBCs in consensual model of ITS2 molecule via structure viewer 	<ul style="list-style-type: none"> - visualisation of structural differences - marked CBCs in the CBC table are highlighted in the alignment and the structure window - presence of at least one CBC near the 5'-apex of helix III of ITS2 may predict a failure to sexually cross
5. secondary structure drawing	<ul style="list-style-type: none"> - VARNA (visualisation Applet for RNA) http://varna.lri.fr/ - edit in graphic programme Inkscape https://inkscape.org/en/ 	<ul style="list-style-type: none"> - graphical output of secondary structure of ITS2 rRNA, and comparison nucleotide differences between OTUs assigned to the same reference sequence and visualisation of CBCs positions (if any)

Fig. S3. Schematic workflow for taxonomic assignments of environmental ITS2 OTUs from environmental samples of snow algal communities where Chlamydomonadaceae prevail. For this taxonomic group the CBC species concept (in frame of a polyphasic approach) was successfully applied (e.g., MATSUZAKI et al.2015). The aim of the process is to get sequence-structure alignments of selected OTUs with their reference sequences and then search for compensatory base changes (CBCs) in homologous positions near the 5'- apex of helix III encompassing the YGGY motif (the most conserved region of the ITS2 secondary structure of eukaryotes).

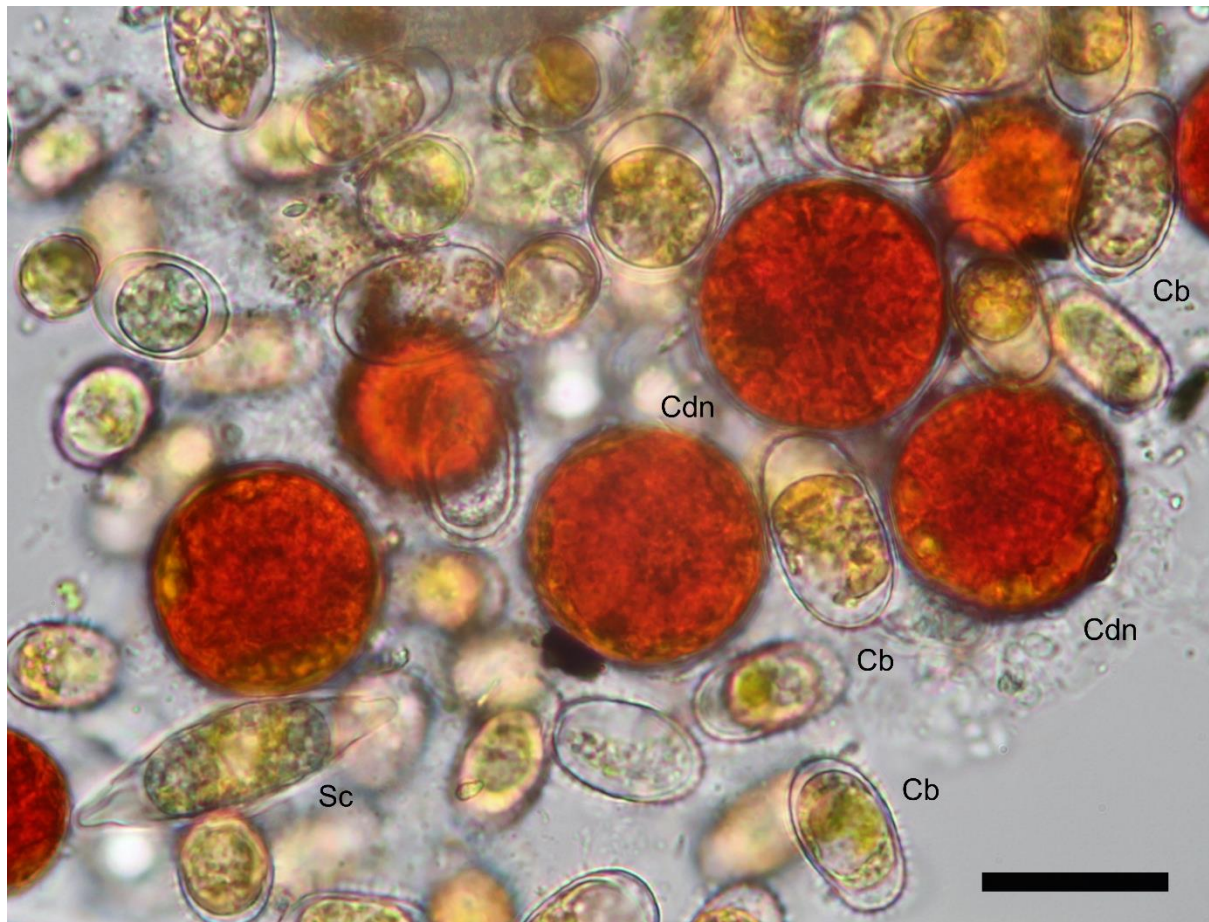


Fig. S4. Light micrograph of cells in field sample 2. The three locally abundant snow algae identified using morphological features were *Cr. brevispina* (Cb; later identified by HTS and secondary structure prediction as an undescribed species - OTU denovo99), *Scotiella cryophila* K-1 (Sc) and *Cd. nivalis* (Cdn). Scale bar: 20 μm .

```

          10      20      30      40      50      60
Cr. brevispina  GGUUAUUGUCCACCCUUUCCUG-C-UGUGCUUCAAAACCACCGCA--G-CCA-AG-GA
((.....(((((((((((((--(-((.....))))))--)-..-)))-)
denovo107      GGUUAUUGUCCACCCUUUCCUG-C-UGUGCUUCAAAACCACCGCA--G-CCA-AG-GA
((.....(((((((((((((--(-((.....))))))--)-..-)))-)
denovo249      GGUUAUUGUCCACCCUUCUCCUG-C-UGUGCUUCAAAACCACCGCA--G-CCG-AG-GA
((.....(((((((((((((--(-((.....))))))--)-..-)))-)
denovo173      GGUUAUUGUCCACCCUUUCCUG-C-UGUGCUUCAAAACCACCGCA--G-CCA-AG-GA
((.....(((((((((((((--(-((.....))))))--)-..-)))-)
denovo99       GGUUAUUGUCCAUCCAUU--G-A-U-UG-UUCA-C--U-CA--GUCCU-UG-G-
((.....(((((((---(-(-((.....-.-.-.-))---))..-)))-)
denovo266      GGUCCUGUCUCAACCUCCA--ACAUU-UAUUUA--U--UAUAAUG-UCAGAGUGU
((.....((((((((((---(((-((.....-.-.-)))))..-)))-)
denovo248      GGUUAUUGUCCAUCCAUU--G-A-U-UG-UUCA-C--U-CA--GUCCU-UG-G-
((.....(((((((---(-(-((.....-.-.-))---))..-)))-)

          70      80      90      100     110     120
Cr. brevispina  CACGUGGGGAUCAUUGCAGUCUGGGAGCUCACGCUUC-CAGUCUGCCCAAGUAUUUAUU
.....))))).(((.((((((((.....))))-)))).).....(((
denovo107      CACGUGGGGAUCAUUGCAGUCUGGGAGCUCACGCUUC-CAGUCUGCCCAAGUAUUUAUU
.....))))).(((.((((((((.....))))-)))).).....(((
denovo249      CACGUGGGGAUCAUUGCAGUCUGGGAGCUCACGCUUC-CAGUCUGCCCAAGUAUUUA-U
.....))))).(((.((((((((.....))))-)))).).....-((
denovo173      CACGUGGGGAUCAUUGCAGUCUGGGAGCUCACGCUUC-CAGUCUGCCCAAGUAUUUA-U
.....))))).(((.((((((((.....))))-)))).).....-((
denovo99       CAUAUGGGGAUCAUUGCAGUCUGGGUGCUCACGCAUC-CAGUCUGCCCAAGUAUUUAUU
.....))))).(((.((((((((.....))))-)))).).....(((
denovo266      C-U-UGAGGACCGAUGGCAGUCUGGGCAUUUAU-UUGCACAGUCUGCCCAAAUGAC-A-U
.-.))))).....(((((((---(-((.....-)))))..-)))-).....-((
denovo248      CAUAUGGGGAUCAUUGCAGUCUGGGUGCUCACGCAUC-CAGUCUGCCCAAGUAUUUAUU
.....))))).(((.((((((((.....))))-)))).).....((
```

	190	200	210	220	230	240
					
<i>Cr. brevispina</i>	UCGAGUAUUC	AUCUCGUAUGUCUC	UCGAA-UCUGCCGGUUUGGGCAAUGAACGU	----	C	
	(((((((((.....(((.....))).....-))))-..))..))))))..))))..))..((----(
denovo107	UCGAGUAUUC	AUCUCGUAUGUCUC	UCGAA-UCUGCCGGUUUGGGCAAUGAACGU	----	C	
	(((((((((.....(((.....))).....-))))-..))..))))))..))))..))..((----(
denovo249	UCGAGUAUUC	AUCUCGUAUGUCUC	UCGACCUC-GACGGUUUGCUCAAUGA	-A----	C	
	(((((((((.....(((.....))).....-)))).....-..))))))..))))..))..--.....(
denovo173	UCGAGUAUUC	AUCUCGUAUGUCUC	UCGAA-UCUGCCGGUUUGGGCAAUGAACAUUCUU			
	(((((((((.....(((.....))).....-))))-..))..))))))..))))..))..((....(
denovo99	UCGAGUAUUC	AUCUUGUAUGUUUAUCGAA-UCUGCUGGUUUUGGGCAAUGAAC	U	----	C	
	(((((((((.....(((.....))).....-))))-..))..))))))..))))..))..((----(
denovo266	UCGAGUAUUC	AUCUCGUAUGUCUC	UCGAA-UCUGCCGGUUUGGGCAAUGAACGU	----	C	
	(((((((((.....(((.....))).....-))))-..))..))))))..))))..))..((----(
denovo248	UCGAGUAUUC	AUCUUGUAUGUUUC	UCGAC-UUCGACAGCUUGCGUCAGAUCCU	----	C	
	(((((((((.....(((.....))).....-))))-..))..))))))..))))..))..((----(
	250	260	270	280	290	300
					
<i>Cr. brevispina</i>	UGGUG----	U-G-CUUCAAAC-C-A--	CACCAG-----	ACCCUCCCC--	UAUUCAA	
	(((((((((----(-.....-)-)---))))))-----)).....-))))..))					
denovo107	UGGUG----	U-G-CUUCAAAC-C-A--	CACCAG-----	ACCCUCCCC--	UAUUCAA	
	(((((((((----(-.....-)-)---))))))-----)).....-))))..))					
denovo249	--GUG----	A-CUU-AAACCU	---CAC-G-----	CA-CC-CCUC-	CACAU	
	--(((-----(-.....-)-)---))--)-----).....-))))..))-					
denovo173	--GGUGGCA-GAA-UUU-A---	UUCGGUCGCC-GUCUCAUGCAAC-	CCUCCACACU-U-			
	-(((((((.....(((.....-))))..))))))-.....))))..))..-))))..))-					
denovo99	--UUG-UCG-AACUA-AAAC-U-CCU-CAA-G-----	A-CC-CCCC-UAUUCAA				
	--(((---(-.....-)-).....))--)-----).....-))))..))					
denovo266	UGGUG----	U-G-CUUCAAAC-C-A--	CACCAG-----	ACCCUCCCC--	UAUUCAA	
	(((((((((----(-.....-)-)---))))))-----)).....-))))..))					
denovo248	--UUG-A-C-A-CUU-G---	U-GC-CAA-G-----	A-CU-UGU-	CACCAU		
	--(((---(-.....-)-).....))--)-----).....-))))..))					



Fig. S5. Sequence-structure alignment of nuclear ribosomal DNA internal transcribed spacer 2 transcripts from *Chloromonas brevispina* K-2 (accession number MG791868) and the most abundant OTUs, which were preliminary assigned to this reference taxon using Qiime. (Note: HTS delivers DNA based data, but during RNA folding, thymine ['T'] is converted to uracil ['U']).

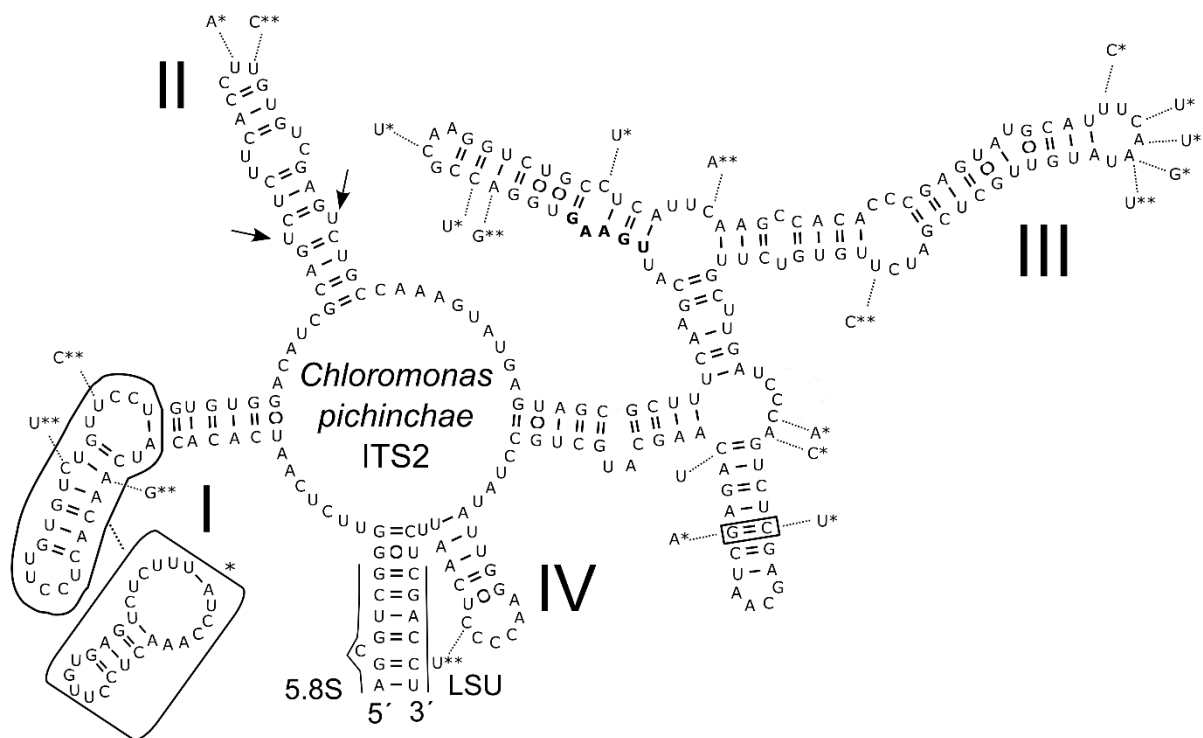


Fig. S7. Comparison of the secondary structure of ITS2 rDNA transcripts between *Chloromonas pichincae* CCCryo 261-06 (accession number HQ404889.1) and the closely related OTU ‘denovo100’ and OTU ‘denovo85’. Differences characteristic for both OTUs are shown by nucleotides outside the structure and are linked by dotted lines. One asterisk means that the difference was detected only in OTU ‘denovo100’, and double asterisks imply that the difference were detected in OTU ‘denovo85’; middle and top part of helix I (encircled) represent an expansion segment, whose length is not conserved and in which positions are <70% conserved according to consensual secondary structure model of Chlorophyceae (CAISOVÁ et al.2013). Therefore, this part of helix I characteristic for OTU ‘denovo100’ is shown outside the structure and is linked by dotted lines. A single compensatory base change (CBC) in comparison with the reference sequence was found in OTU ‘denovo100’ but outside the most conserved part of helix III (the most conserved is close to the 5’ end of III helix) and, therefore, this CBC represents intraspecific variability of *Chloromonas pichincae*. OTU ‘denovo85’ had no CBC when compared to the reference species, and thus, was assigned to *Chloromonas pichincae*. (Note: HTS delivers DNA based data, but during RNA folding, thymine [‘T’] is converted to uracil [‘U’])

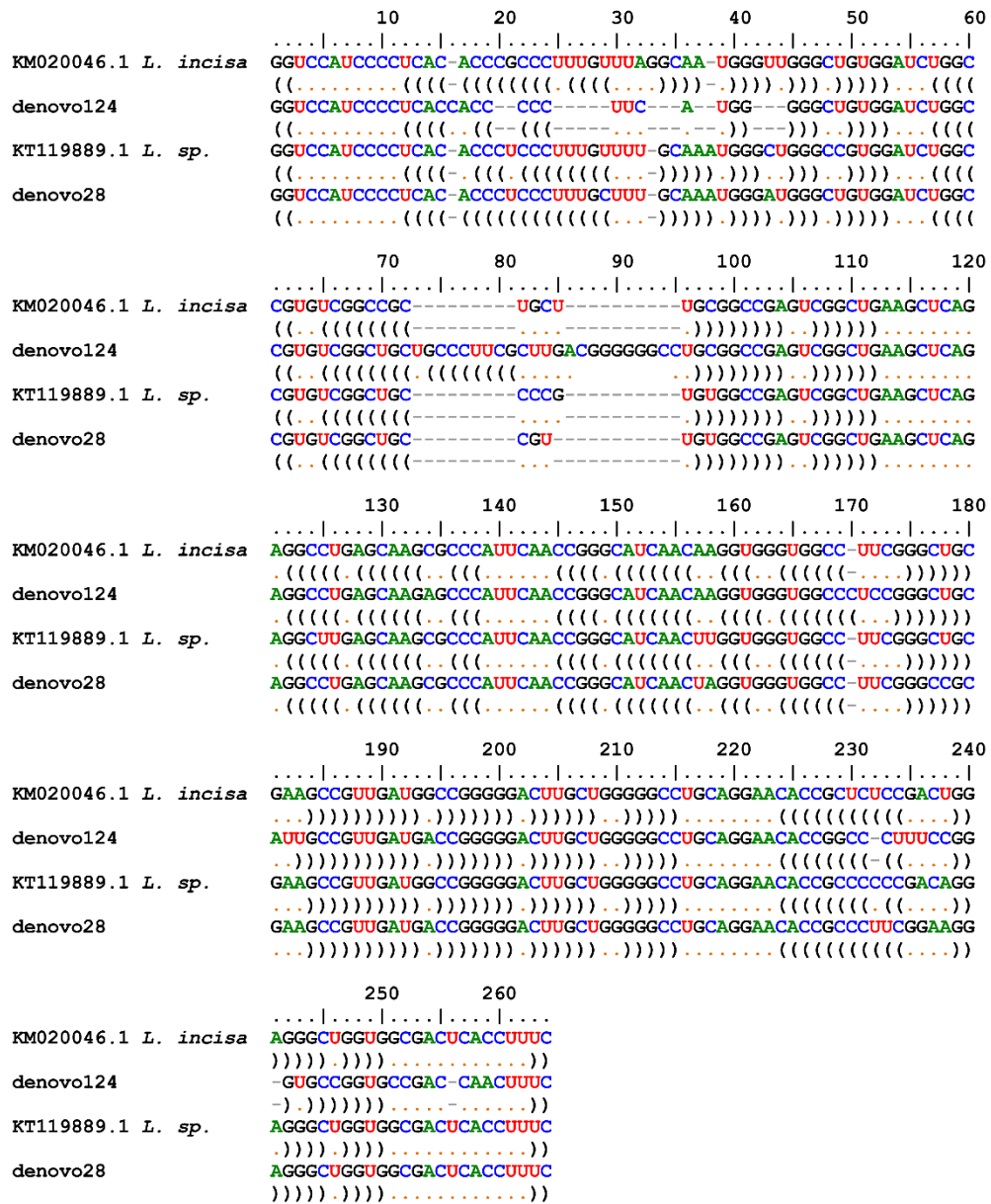


Fig. S8. Sequence-structure alignment of nuclear ribosomal DNA internal transcribed spacer 2 transcripts from *Lobosphaera incisa* SAG 2466 (accession number KM020046.1), OTU ‘denovo124’, *Lobosphaera* sp. K-1 (accession number KT119889.1) and OTU ‘denovo28’. No compensatory base change (CBC) was found in the dataset. Thus, both OTUs were assigned to species *Lobosphaera incisa* (Note: HTS delivers DNA based data, but during RNA folding, thymine [‘T’] is converted to uracil [‘U’])

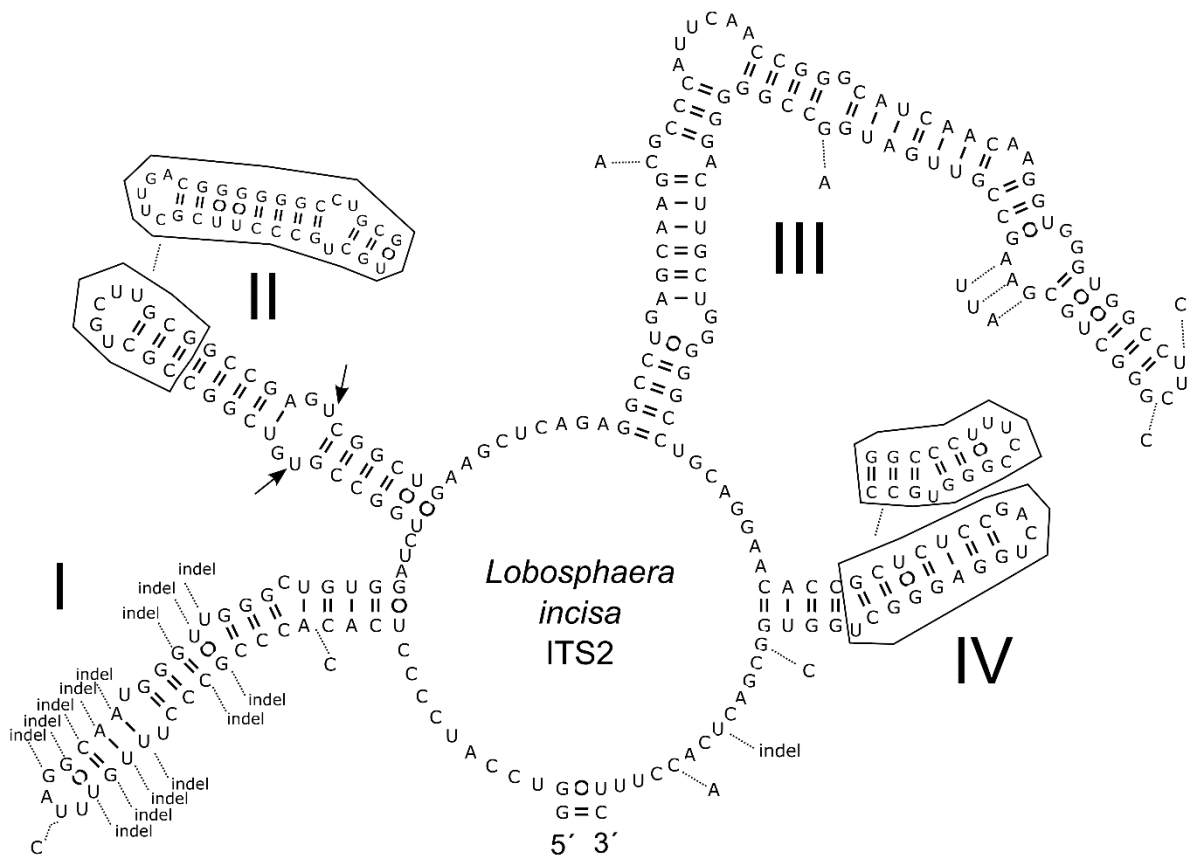


Fig. S9. Comparison of the secondary structure of ITS2 rDNA transcripts between *Lobosphaera incisa* SAG 2466 (accession number KM020046.1) and the closely related OTU ‘denovo124’. Differences characteristic for the latter are shown by nucleotides outside the structure and are linked by dotted lines. Top of helix II and helix IV (encircled) represent one of expansion segments, whose length is not conserved and in which positions are <70% conserved according to consensual secondary structure model of Chlorophyceae (CAISOVÁ et al. 2013). Therefore, this part of helix II and helix IV characteristic for OTU ‘denovo124’ is shown outside the structure and is linked by dotted lines. No CBC was found between *Lobosphaera incisa* SAG 2466 and OTU ‘denovo124’ suggesting that OTU ‘denovo124’ can be assigned to species *Lobosphaera incisa*. (Note: HTS delivers DNA based data, but during RNA folding, thymine [‘T’] is converted to uracil [‘U’])

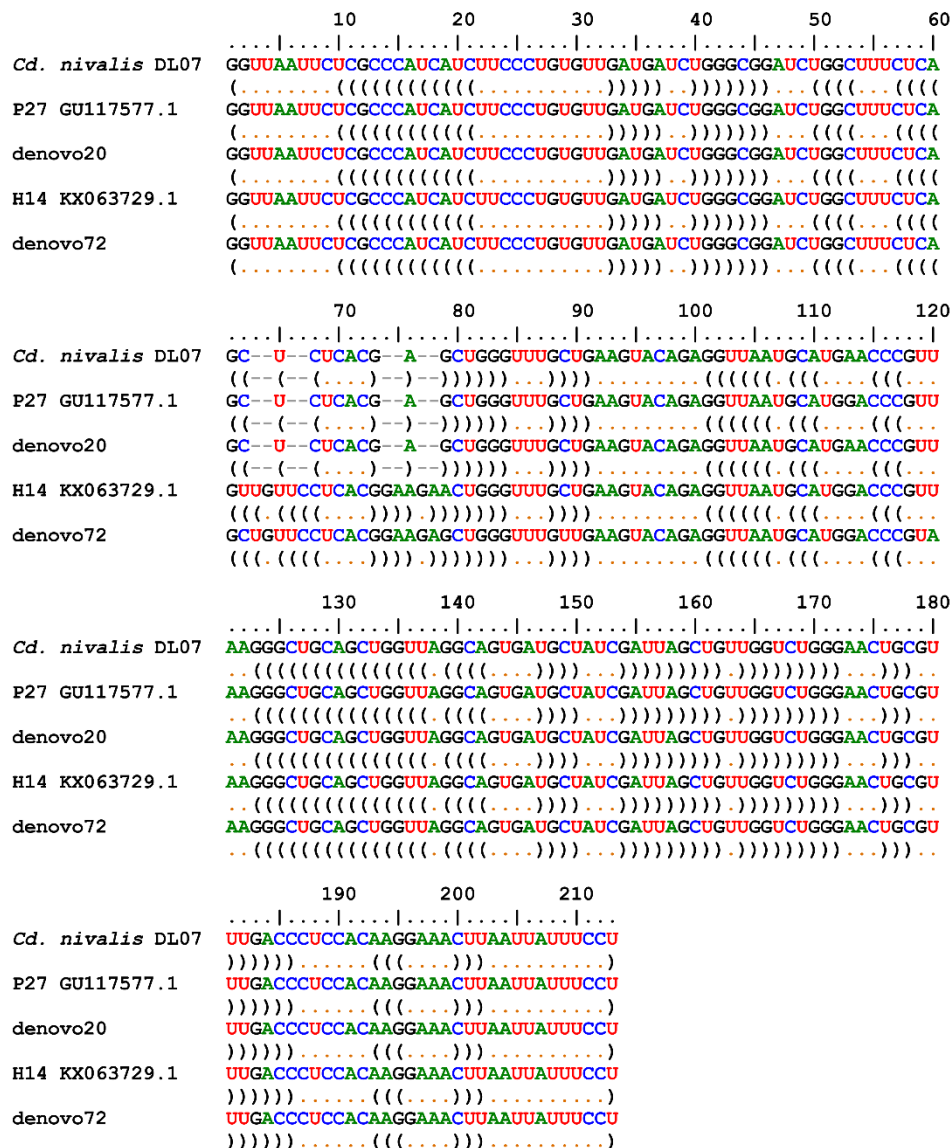


Fig. S10. Sequence-structure alignment of nuclear ribosomal DNA ITS2 transcripts from *Chlamydomonas nivalis* DL07 (accession number MF803749.1) and the most abundant OTUs, which were preliminary assigned to this reference taxon using Qiime. *Chlamydomonas nivalis* P27 (accession number GU117577.1) picked up by Qiime differs from *Chlamydomonas nivalis* DL07 by single nucleotide position in a single strand region in helix III. Note that the sequence of ‘denovo20’ is identical with the reference sequence of DL07. (Note: HTS delivers DNA based data, but during RNA folding, thymine [‘T’] is converted to uracil [‘U’])

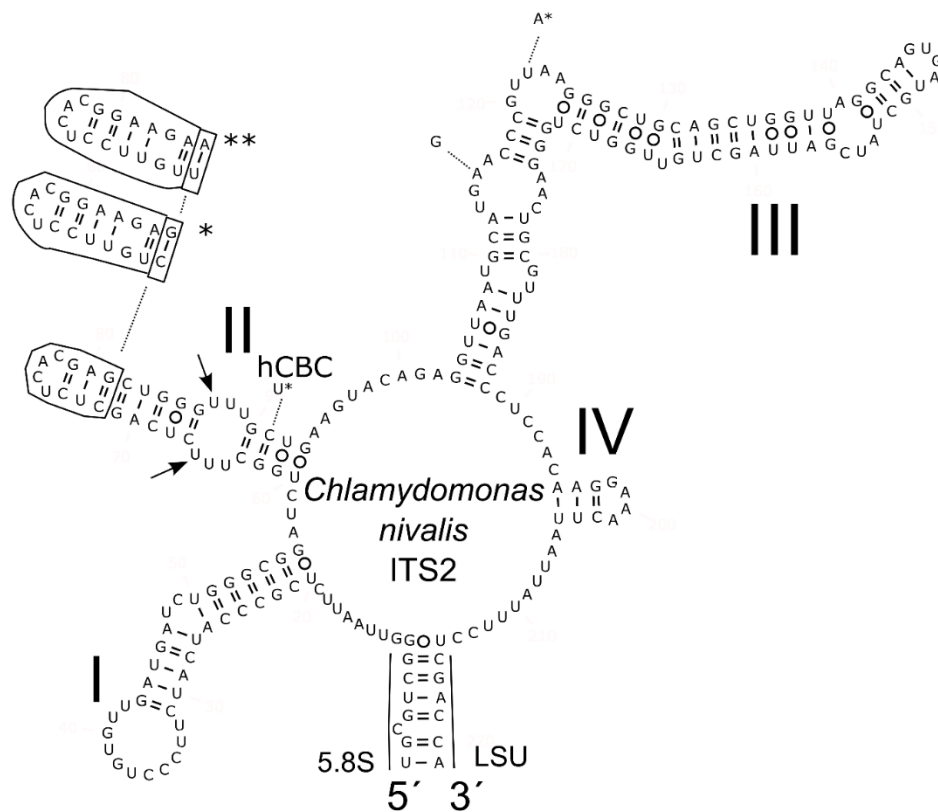


Fig. S11. Comparison of the secondary structure of ITS2 rDNA transcripts between *Chlamydomonas nivalis* DL07 (accession number MF803749.1), *Chlamydomonas nivalis* P27 (accession number GU117577.1), *Chlamydomonas* clone H14 (accession number KX063729.1), and the closely related OTU ‘denovo20’ and OTU ‘denovo72’. OTU ‘denovo20’ was 100% identical with the reference sequence of *Chlamydomonas nivalis* DL07. Differences characteristic for *Chlamydomonas nivalis* P27, OTU denovo72 and clone H14 are shown by nucleotides outside the structure and are linked by dotted lines. Single nucleotide difference in helix III was shared in all three specimens (i.e., ‘G’ instead of ‘A’). One asterisk means that the difference was detected only in OTU ‘denovo72’, and double asterisks imply that the difference was detected in clone H14. Top part of helix I (encircled) represent an expansion segments, whose length are not conserved and in which positions are <70% conserved according to consensual secondary structure model of Chlorophyceae (CAISOVÁ et al. 2013). Therefore, this part of helix I characteristic for OTU ‘denovo72’ and clone H14 are shown outside the structure and are linked by dotted lines. There was no CBC between ‘denovo72’ and reference sequence DL07, the sequence identity was 93%. Interestingly, ITS2 of ‘denovo72’ has higher sequence similarity of 98% with uncultured *Chlamydomonas* clone H14 (accession number KX063729.1) but there is one CBC in helix II between ‘denovo72’ and clone H14 (in the 13th nucleotide in helix II). A CBC at the same position in the structure is present also when reference sequence DL07 and clone H14 are compared. Single hemi-CBC (hCBC) in the basal part of helix I was found when compared *Chlamydomonas nivalis* DL07 and OTU ‘denovo72’. Absence of any CBC in the helix III among all these sequences suggest that all these OTUs can be assigned to the same species. (Note: HTS delivers DNA based data, but during RNA folding, thymine [‘T’] is converted to uracil [‘U’])

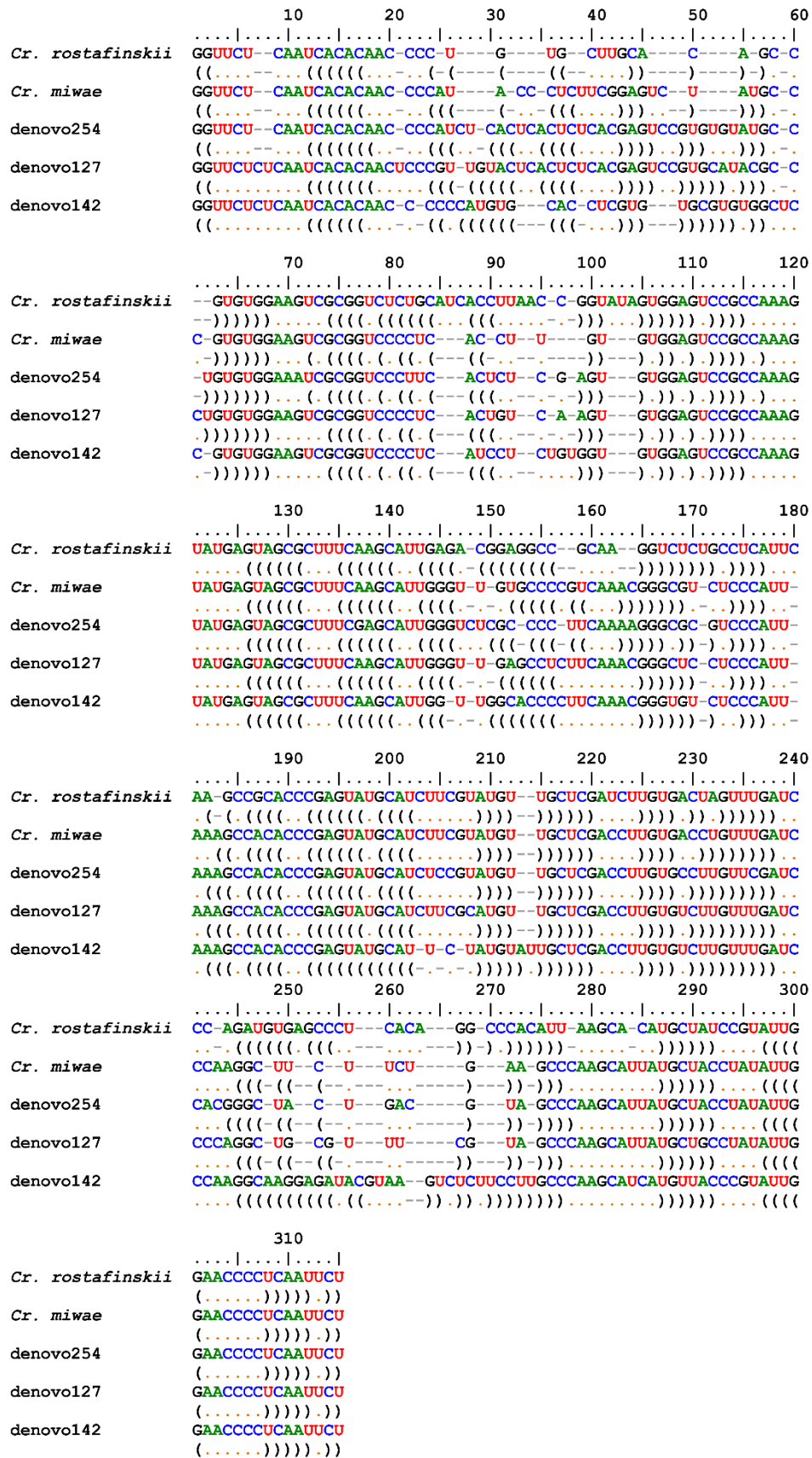


Fig. S12. Sequence-structure alignment of nuclear ribosomal DNA internal transcribed spacer 2 transcripts from *Chloromonas rostafinskii* CCCryo 010-99 (accession number

HQ404863.1) and the most abundant OTUs, which were preliminary assigned to this reference taxon using Qiime. Further search in NCBI revealed that a better hit in term of higher sequence identity of 86-90% for these OTUs was represented by *Chloromonas miwae* NIES-2379 (accession number LC012762.1). As a contrast ITS2 of *Chloromonas rostafinskii* had sequence similarity with these three OTUs between 77-85% only. Compensatory base changes (CBC) in comparison with the reference sequence of *Chloromonas miwae* were found in helix III in OTU 'denovo254' (three CBCs), OTU 'denovo127' (two CBCs) and OTU 'denovo142' (four CBCs). Thus, three OTUs represent probably independent taxa. (Note: HTS delivers DNA based data, but during RNA folding, thymine ['T'] is converted to uracil ['U'])

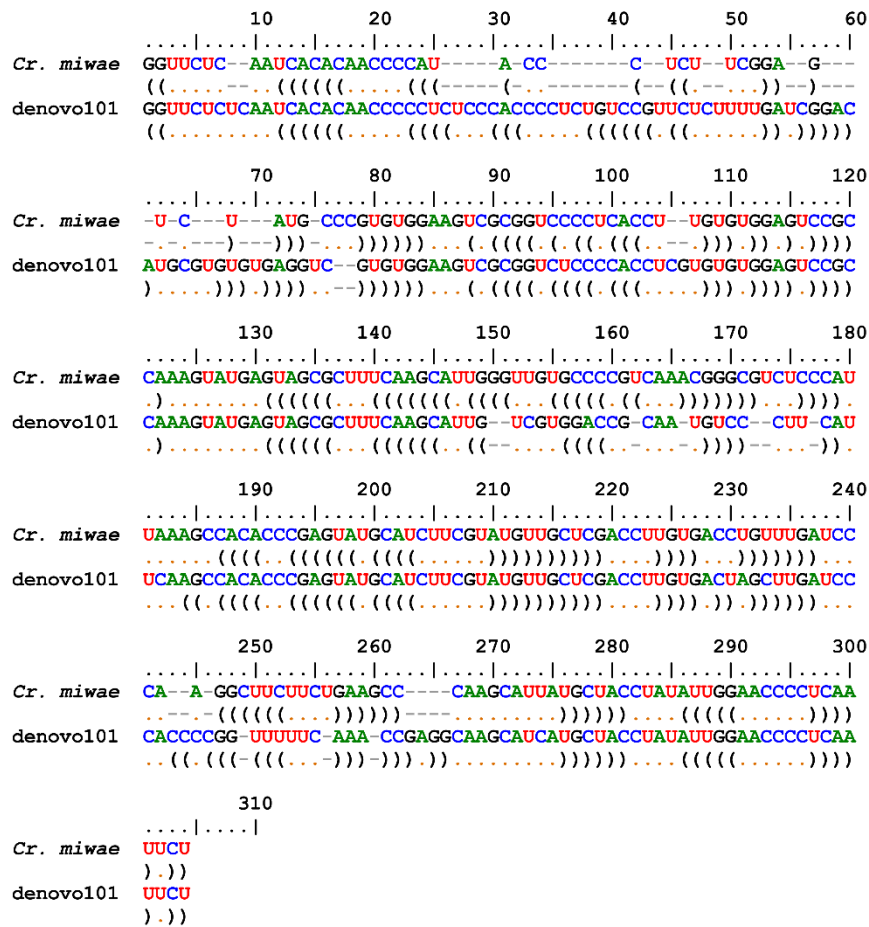


Fig. S13. Sequence-structure alignment of nuclear ribosomal DNA ITS2 transcripts from *Chloromonas miwae* NIES-2379 (accession number LC012762.1) and OTU 'denovo101'. No blast hit was initially found against custom download database using Qiime. Further manual search in NCBI revealed 84% sequence similarity shared with *Chloromonas miwae* NIES-2379. Three compensatory base changes (CBCs) in comparison with the reference sequence of *Chloromonas miwae* were found in helix III, two out of the most conserved part of the structure, i.e., in the top close to the 5' end of III helix. Thus OTU 'denovo101' represents likely an independent taxon. (Note: HTS delivers DNA based data, but during RNA folding, thymine ['T'] is converted to uracil ['U'])

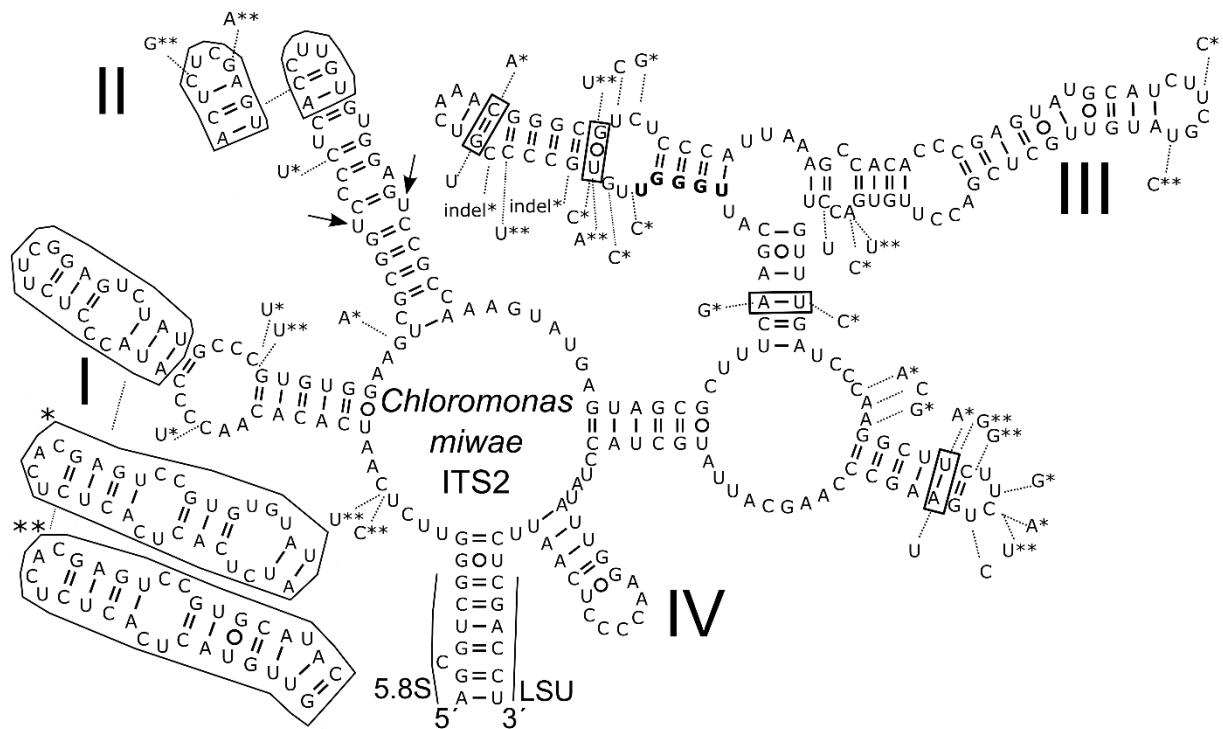


Fig. S14. Comparison of the secondary structure of ITS2 rDNA transcripts between *Chloromonas miwae* NIES-2379 (accession number LC012762) and the closely related OTU ‘denovo254’ and OTU ‘denovo127’. Differences characteristic for both OTUs are shown by nucleotides outside the structure and are linked by dotted lines. One asterisk means that the difference was detected only in OTU ‘denovo254’, and double asterisks imply that the difference were detected in OTU ‘denovo127’. Middle and top part of helix I and top part of helix II (encircled) represent expansion segments, whose length are not conserved and in which positions are <70% conserved according to consensual secondary structure model of Chlorophyceae (CAISOVÁ et al. 2013). Therefore, these parts of helix I and II characteristic for OTU ‘denovo254’ and ‘denovo127’ are shown outside the structure and are linked by dotted lines. CBSs between ITS2 sequences of *Chloromonas miwae* NIES-2379, OTU ‘denovo254’ and OTU ‘denovo127’ are indicated by rectangles in the helix III, one out of these CBS is located in the most conserved part of helix III suggesting that both OTUs represent probably two independent species. (Note: HTS delivers DNA based data, but during RNA folding, thymine [‘T’] is converted to uracil [‘U’])

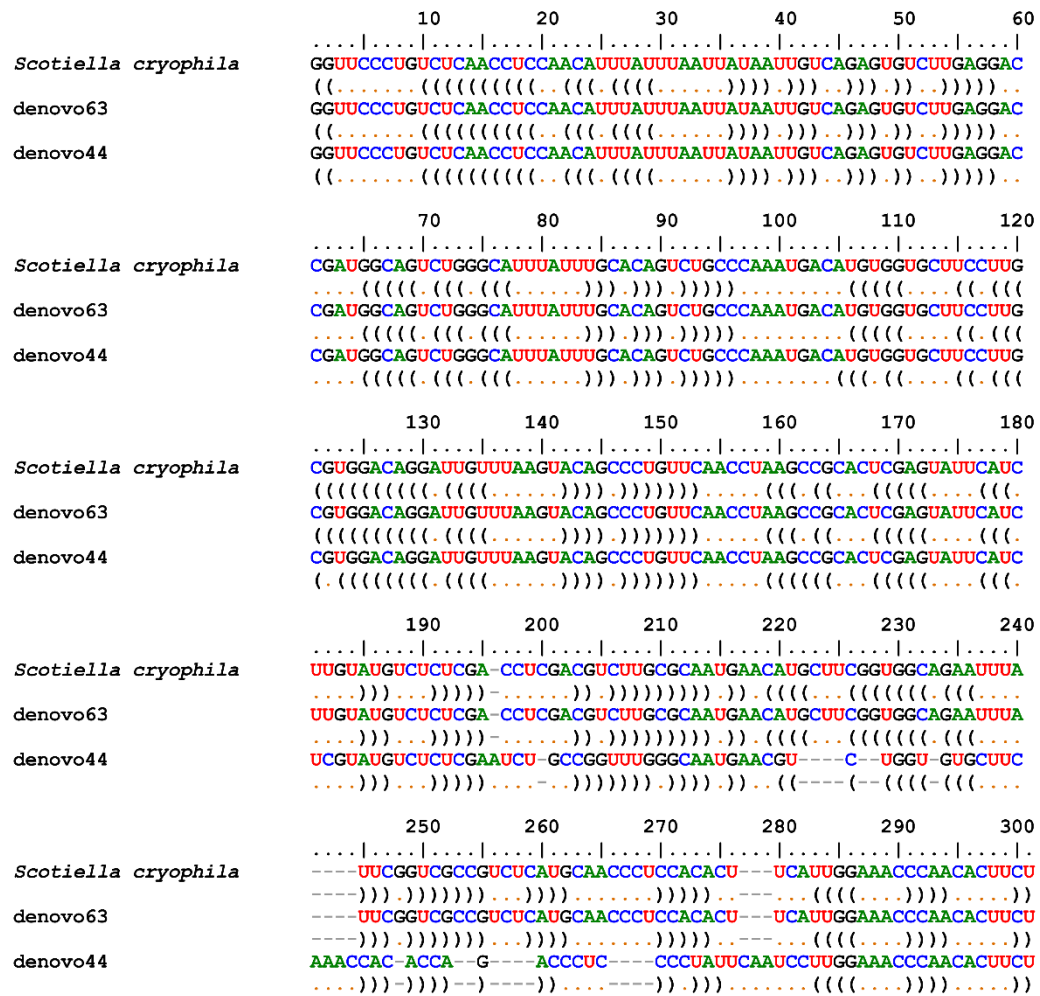


Fig. S15. Sequence-structure alignment of nuclear ribosomal DNA ITS2 transcripts from *Scotiella cryophila* K-1 (accession number MG253843.1) and the most abundant OTUs, which were preliminary assigned to this reference taxon using Qiime. Note that the sequence of 'denovo63' is identical with the reference sequence. (Note: HTS delivers DNA based data, but during RNA folding, thymine ['T'] is converted to uracil ['U'])

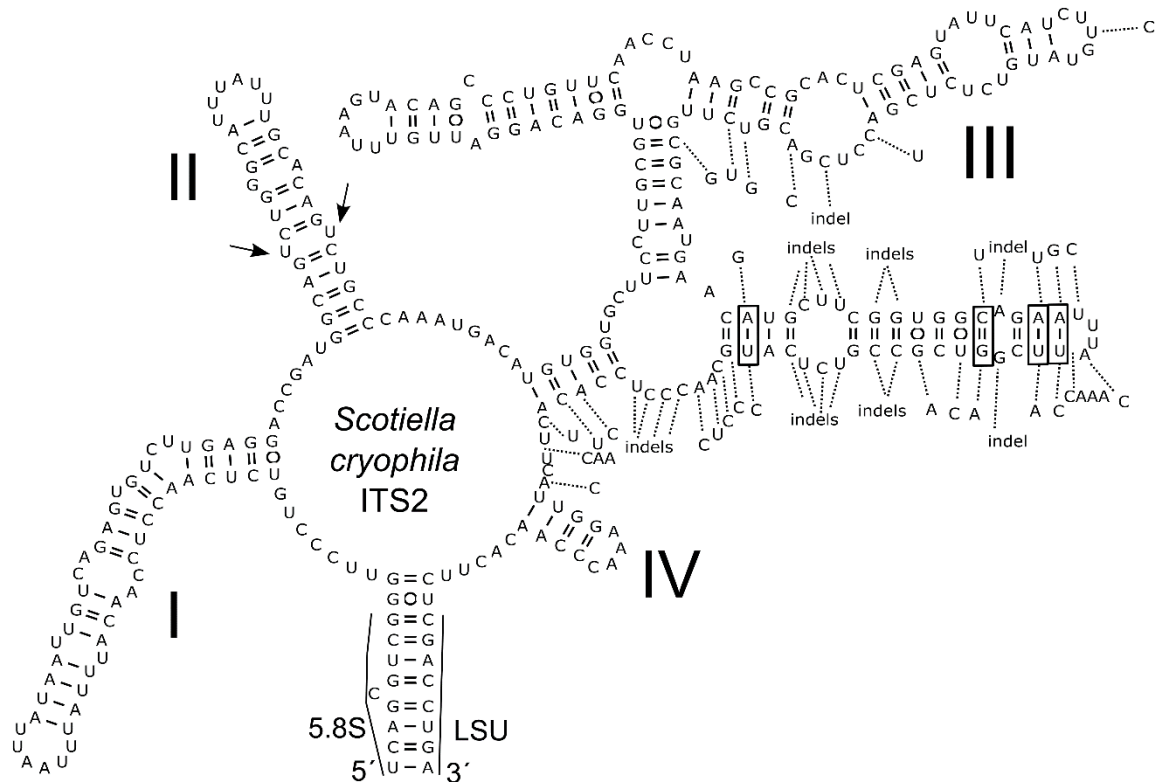


Fig. S16. Comparison of the secondary structure of ITS2 rDNA transcripts between *Scotiella cryophila* K-1 (accession number MG253843.1) and the closely related OTU ‘denovo63’ and OTU ‘denovo44’. OTU ‘denovo63’ was 100% identical with reference sequence. Differences characteristic for the OTU ‘denovo44’ are shown by nucleotides outside the structure and are linked by dotted lines. Each out of four compensatory base changes between ITS2 sequences of *Scotiella cryophila* K-1 and OTU ‘denovo44’ is indicated by a rectangle in the helix III and are found outside the most conserved part of helix III (the most conserved is close to the 5’ end of III helix), therefore, ‘denovo44’ can be assigned to *Scotiella cryophila*. (Note: HTS delivers DNA based data, but during RNA folding, thymine [‘T’] is converted to uracil [‘U’])

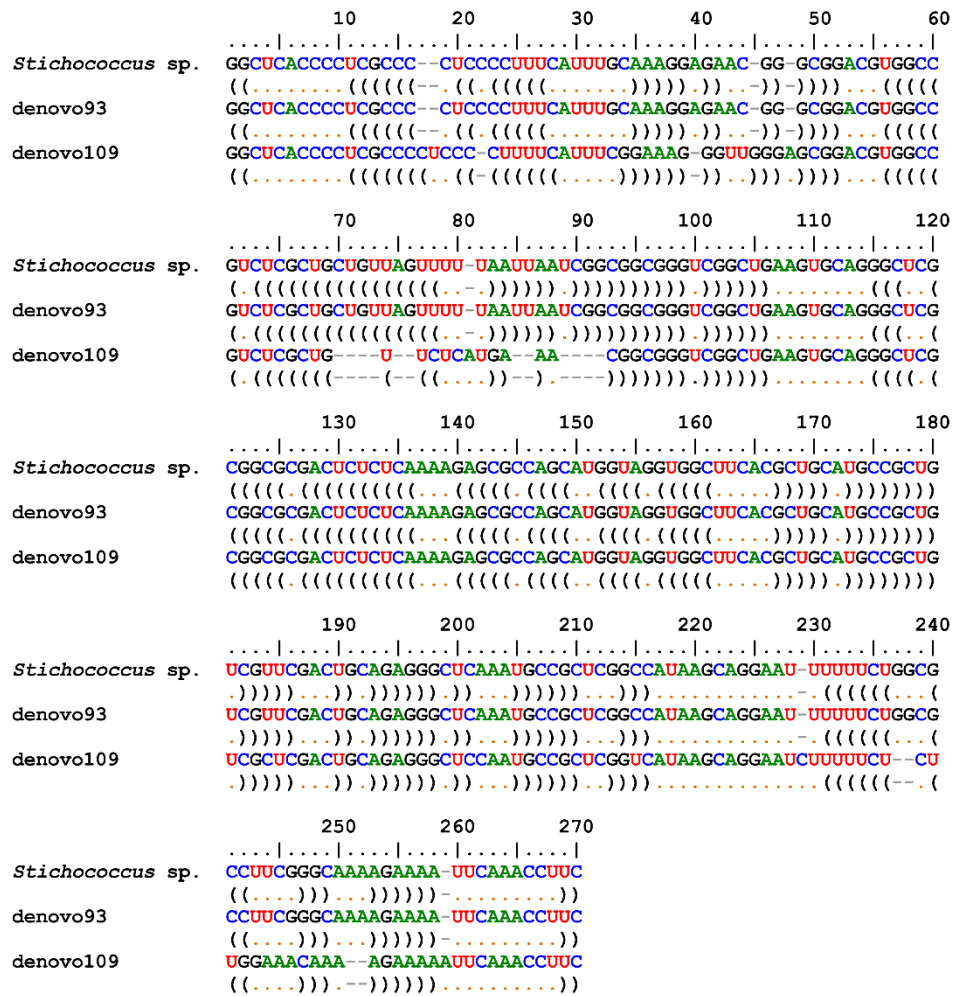


Fig. S17. Sequence-structure alignment of nuclear ribosomal DNA internal transcribed spacer 2 transcripts from *Stichococcus* sp. SAG 2482 (accession number KX094848.1) and the most abundant OTUs, which were preliminary assigned to this reference taxon using Qiime. Note that the sequence of OTU ‘denovo93’ is identical with the reference sequence. (Note: HTS delivers DNA based data, but during RNA folding, thymine [‘T’] is converted to uracil [‘U’])

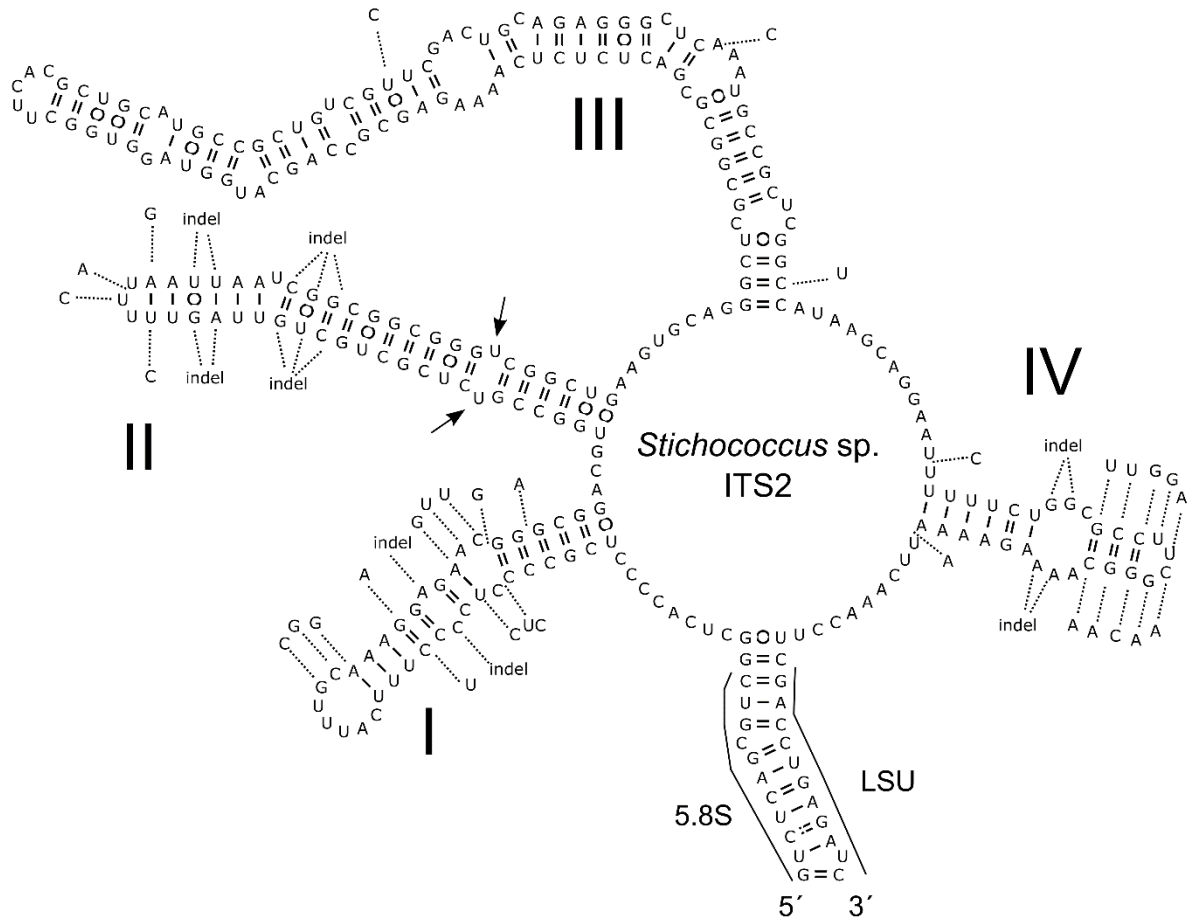


Fig. S18. Comparison of the secondary structure of ITS2 rDNA transcripts between *Stichococcus* sp. (accession number KX094848.1) and the closely related OTU ‘denovo93’ and OTU ‘denovo109’. OTU ‘denovo93’ was 100% identical with reference sequence. Differences characteristic for the OTU ‘denovo109’ are shown by nucleotides outside the structure and are linked by dotted lines. For OTU ‘denovo109’ vs. reference species – six pairs of nucleotide differences at both side of structures keeping pairing were found in variable parts of the structure (the middle part of helix I, the terminal part of helix II, helix IV, i.e. no true CBCs). However, one hemi-CBC (a change at one side of the structure in the conserved part) was found in the conserved bottom part of helix III (this site was reported to be conserved across all 56 ITS2 sequences of *Stichococcus* spp. analyzed in study of (HODAČ et al. 2016). (Note: HTS delivers DNA based data, but during RNA folding, thymine [‘T’] is converted to uracil [‘U’])

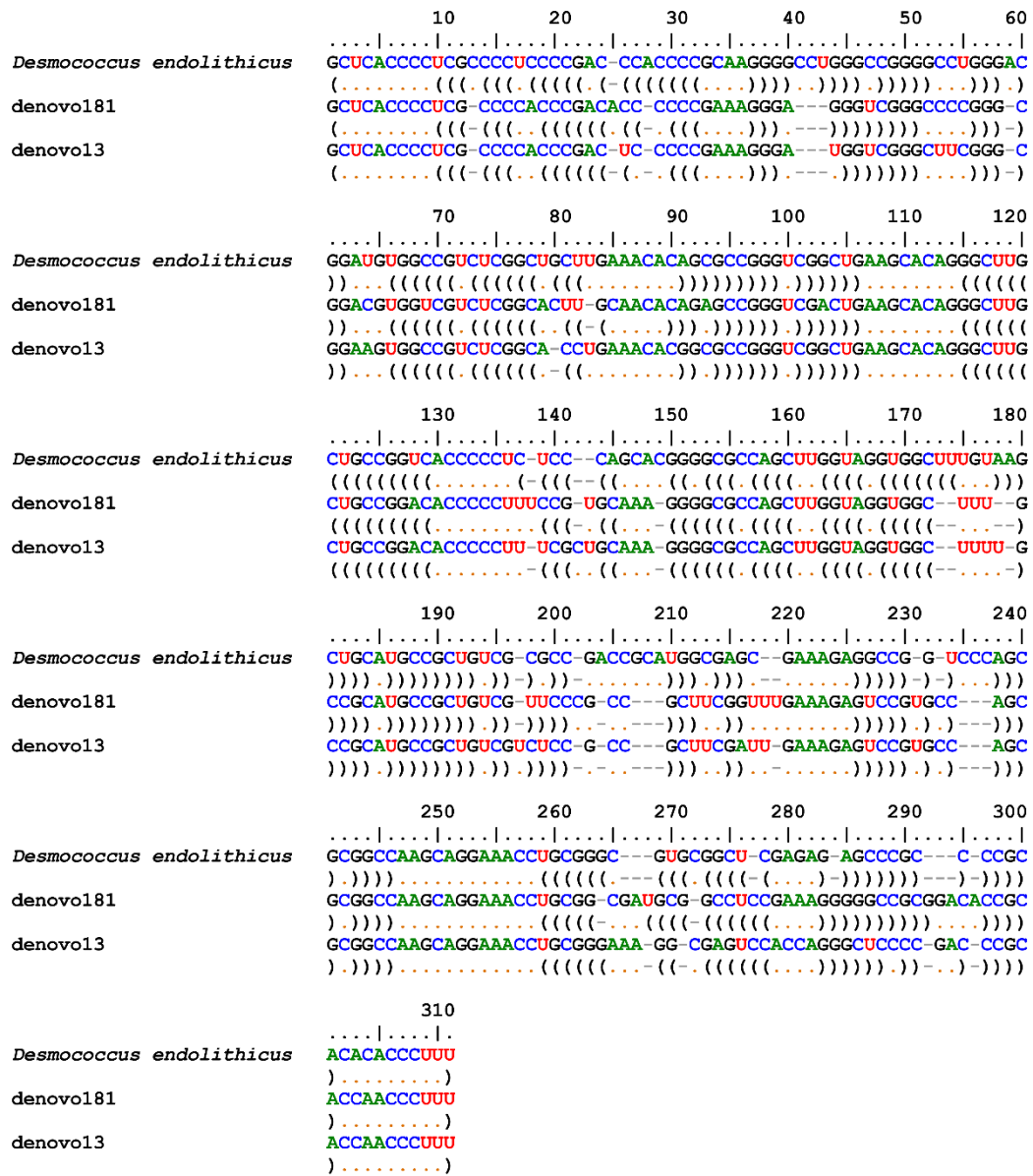


Fig. S19. Sequence-structure alignment of nuclear ribosomal DNA ITS2 transcripts from *Desmococcus endolithicus* SAG 25.92 (accession number KX094830.1) and the most abundant OTUs, which were preliminary assigned to this reference taxon using Qiime. (Note: HTS delivers DNA based data, but during RNA folding, thymine [‘T’] is converted to uracil [‘U’])

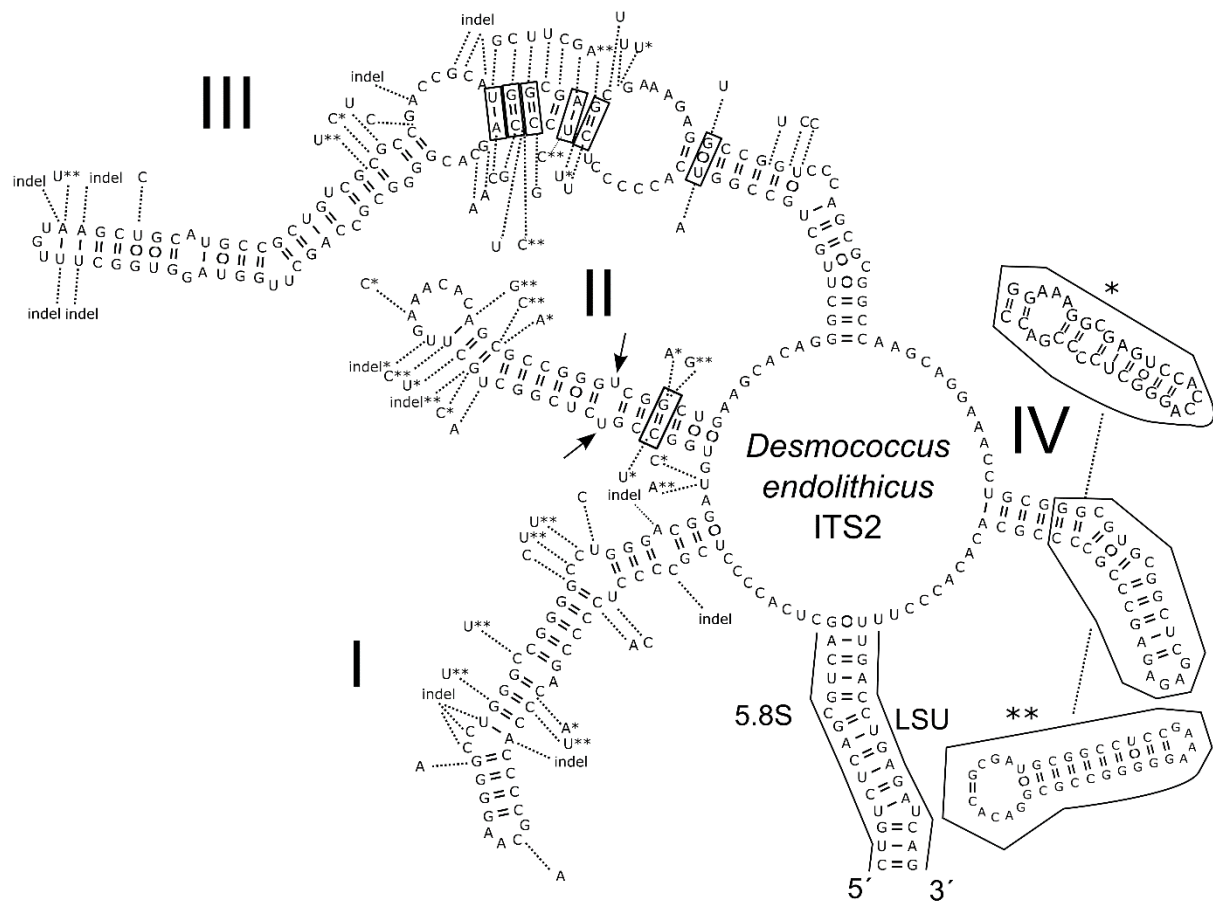


Fig. S20. Comparison of the secondary structure of ITS2 rDNA transcripts between *Desmococcus endolithicus* SAG 25.92 (accession number KX094830.1) and the closely related OTU ‘denovo181’ and OTU ‘denovo13’. Differences characteristic for these OTUs are shown by nucleotides outside the structure and are linked by dotted lines. One asterisk means that the difference was detected only in OTU ‘denovo181’, and double asterisks imply that the difference were detected in OTU ‘denovo13’; middle and top part of helix IV (encircled) represent an expansion segment, whose length is not conserved and in which positions are <70% conserved according to consensual secondary structure model of Chlorophyceae (CAISOVÁ et al. 2013). Therefore, this part of helix IV characteristic for both OTUs is shown outside the structure and is linked by dotted lines. Compensatory base changes between ITS2 sequences of *Desmococcus endolithicus* SAG 25.92 and OTU ‘denovo181’, and between *Desmococcus endolithicus* SAG 25.92 and OTU ‘denovo13’ are indicated by rectangles in the helix II and in the helix III. OTUdenovo181 and OTUdenovo13 had five and four CBCs, respectively, in conserved parts of the ITS2 secondary structure in comparison with the reference sequence. Moreover, ITS2 sequence similarities between *Desmococcus endolithicus* SAG 25.92 vs. OTU ‘denovo181’ and OTU ‘denovo13’ were only 82% and 84%, respectively (e.g. below the suggested identity threshold <89%). (Note: HTS delivers DNA based data, but during RNA folding, thymine [‘T’] is converted to uracil [‘U’])

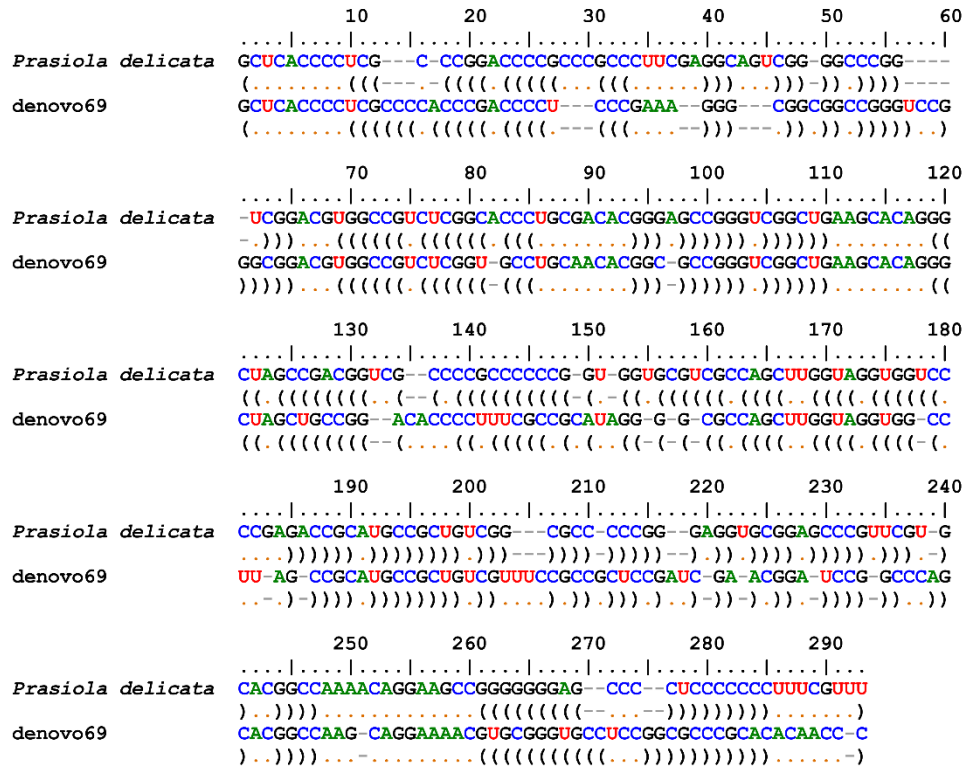


Fig. S21. Sequence-structure alignment of nuclear ribosomal DNA internal transcribed spacer 2 transcripts from *Prasiola delicata* isolate I34S (accession number MF801375.1) and OTU 'denovo69'. No blast hit was initially found against custom download database using Qiime. Further manual search in NCBI revealed 82% sequence similarity shared with *Prasiola delicata* isolate I34S. (Note: HTS delivers DNA based data, but during RNA folding, thymine ['T'] is converted to uracil ['U'])

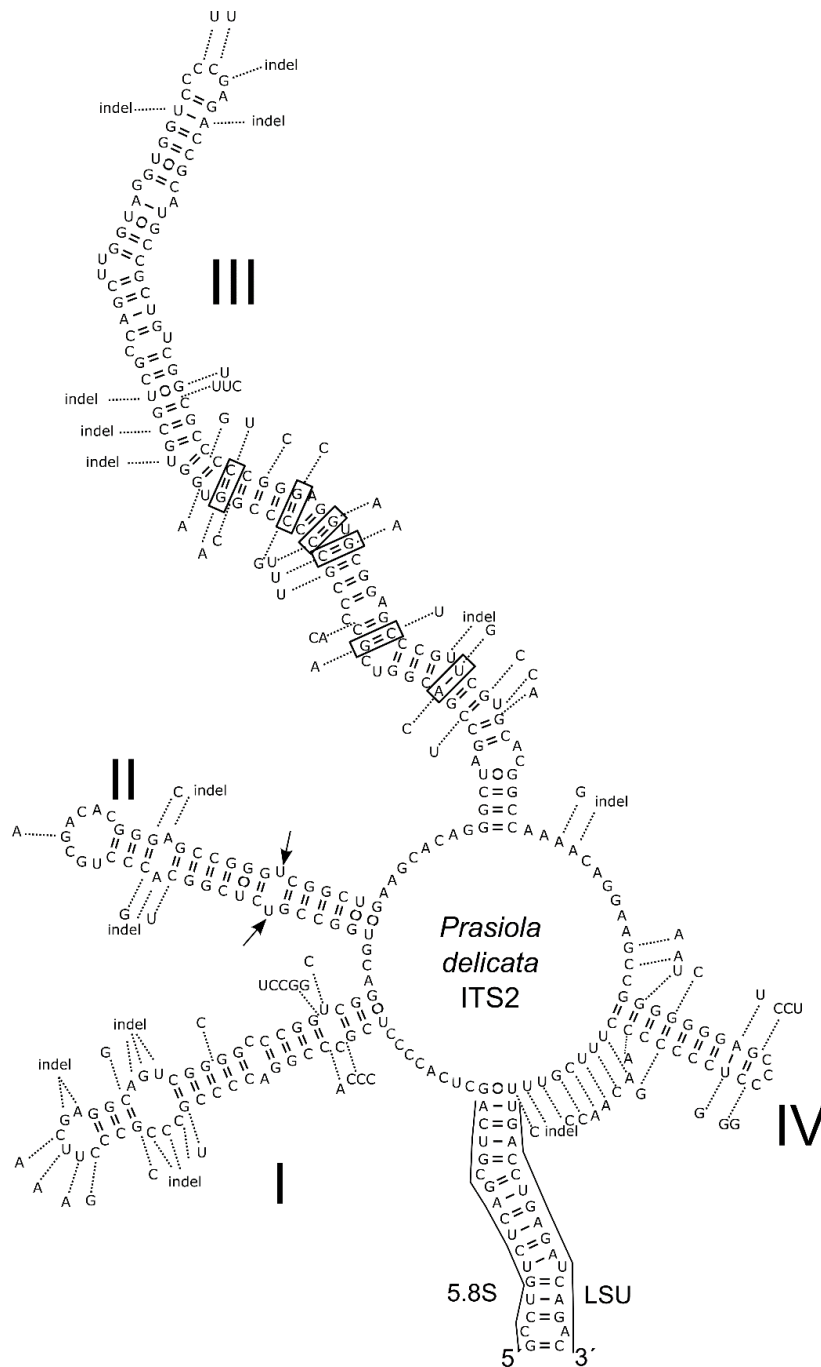


Fig. S22. Comparison of the secondary structure of ITS2 rDNA transcripts between *Prasiola delicata* isolate I34S (accession number MF801375.1) and OTU ‘denovo69’. Differences characteristic for this OTU are shown by nucleotides outside the structure and are linked by dotted lines. Compensatory base changes in conserved parts of the structure are indicated by rectangles. OTU ‘denovo69’ had six CBCs in helix III of the ITS2 secondary structure in comparison with the reference sequence. Moreover, ITS2 sequence similarities between *Prasiola delicata* isolate I34S and OTU ‘denovo69’ were only 82% (i.e. below the suggested identity threshold <89%). (Note: HTS delivers DNA based data, but during RNA folding, thymine [‘T’] is converted to uracil [‘U’])

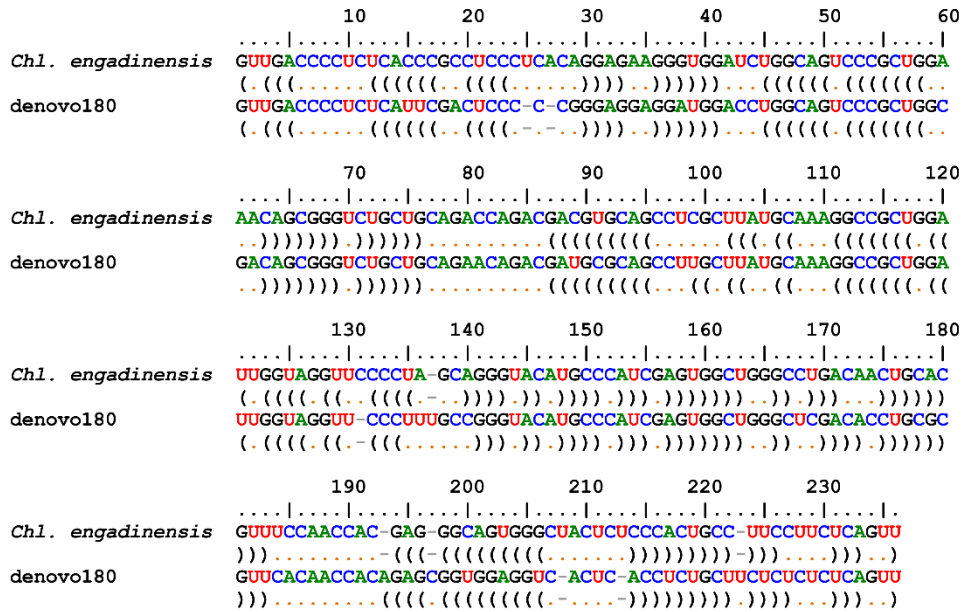


Fig. S23. Sequence-structure alignment of nuclear ribosomal DNA internal transcribed spacer 2 transcripts from *Chlorocloster engadinensis* SAG 812-1 (accession number FM946011.1) and OTU 'denovo180'. No blast hit was initially found against custom download database using Qiime. Further manual search in NCBI revealed 84% sequence similarity shared with *Chlorocloster engadinensis* SAG 812-1. (Note: HTS delivers DNA based data, but during RNA folding, thymine ['T'] is converted to uracil ['U'])

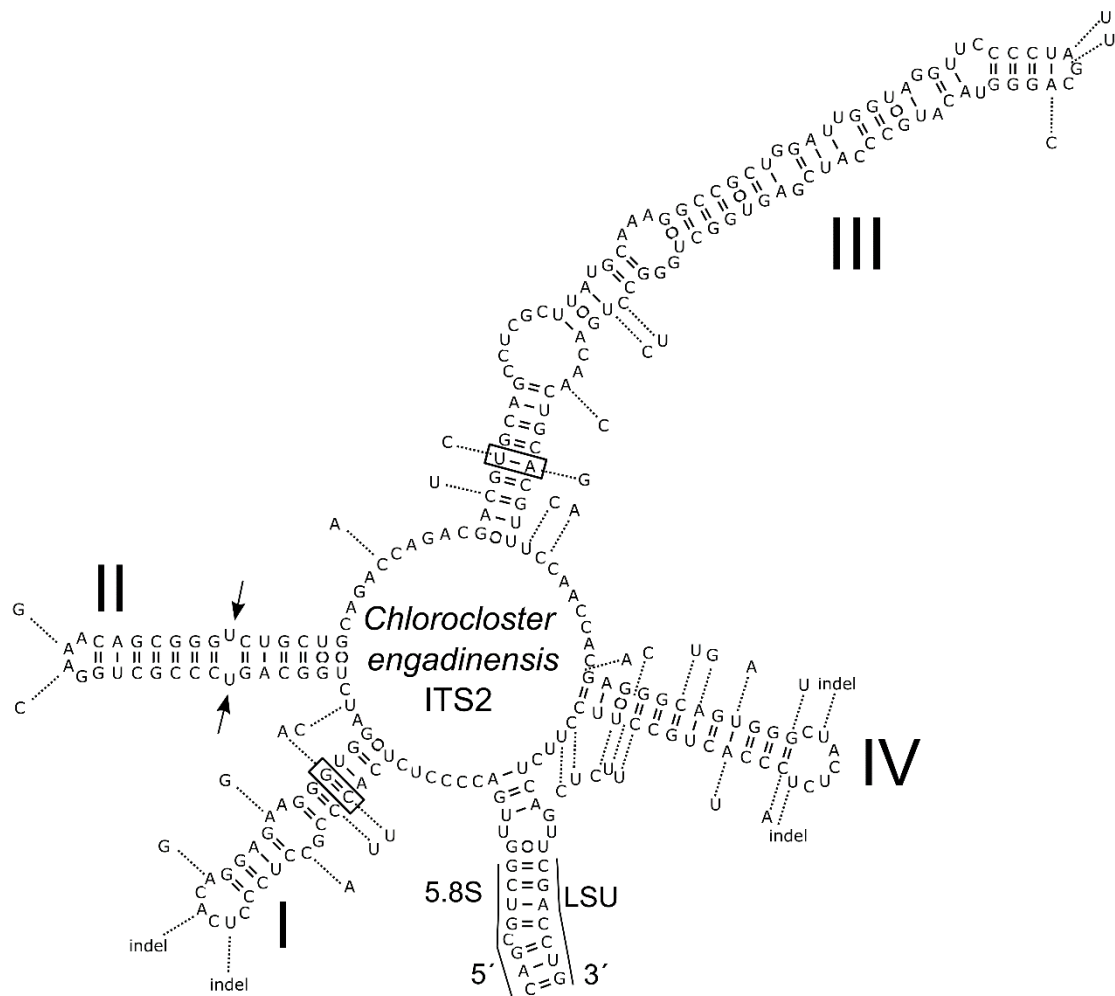


Fig. S24. Comparison of the secondary structure of ITS2 rDNA transcripts between *Chlorocloster engadinensis* SAG 812-1 (accession number FM946011.1) and OTU ‘denovo180’. Differences characteristic for this OTU are shown by nucleotides outside the structure and are linked by dotted lines. Compensatory base changes in conserved parts of the structure are indicated by rectangles. OTU ‘denovo180’ had one CBC in basal part of helix I and one CBC in basal part of helix III in comparison with the reference sequence. Moreover, ITS2 sequence similarities between OTU ‘denovo180’ and its closest hit in NCBI, *Chlorocloster engadinensis* SAG 812-1, were only 84% (i.e. below the suggested identity threshold <89%). (Note: HTS delivers DNA based data, but during RNA folding, thymine [‘T’] is converted to uracil [‘U’])

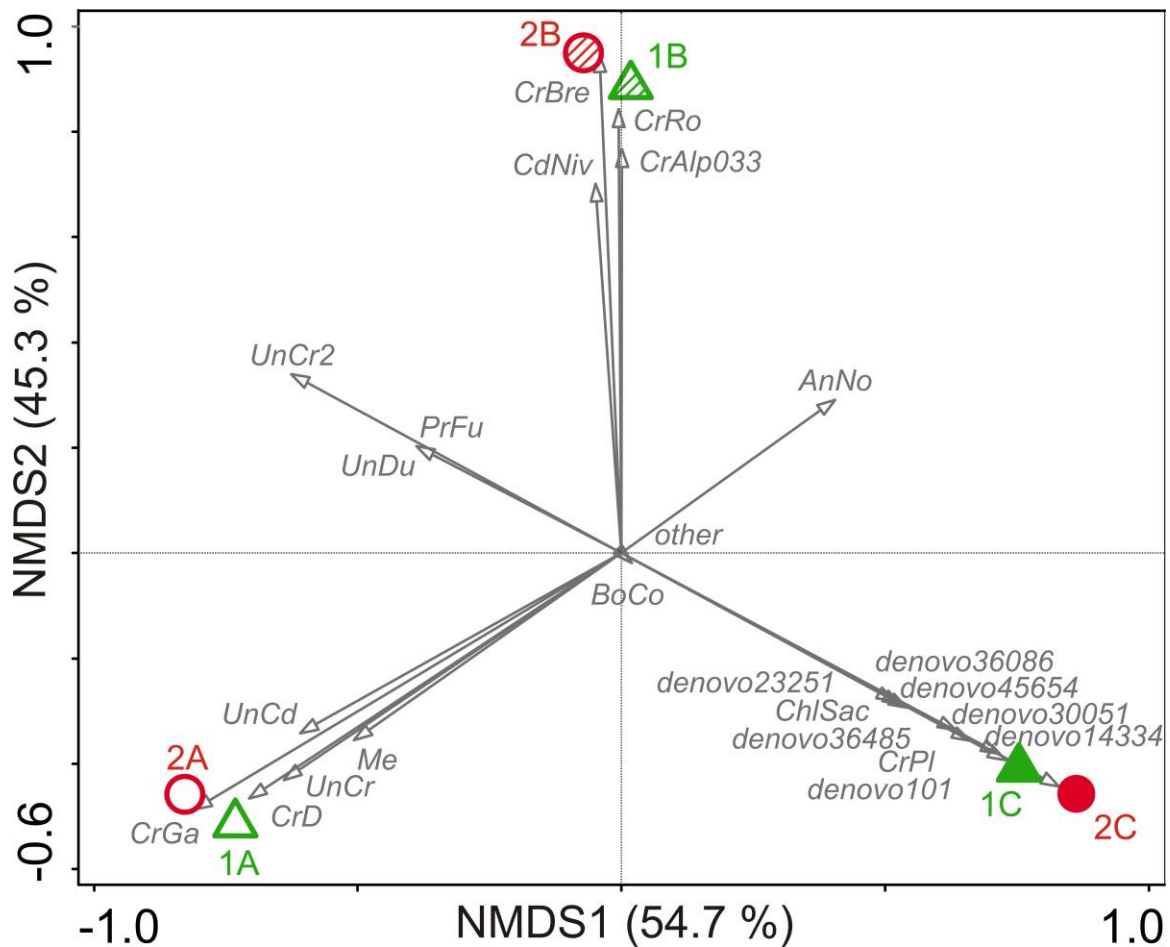


Fig. S25. Nonmetric multidimensional scaling (NMDS) ordination describing the differences in taxonomic composition of the two samples (sample 1 – green, sample 2 – red) based on 18S rDNA data analysed using the three strategies of taxonomic assignment (A, B, C – for details, see the text). Values within parentheses show % of variance explained by each axis.

Source of the data for NMDS ordination: Table 5.

Acronyms:

- AnNo* *Ancydonema nordenskiöldii* AF514397.2
- BoCo* *Botrydiopsis constricta* AJ579339.1
- CdNiv* *Chlamydomonas nivalis* DL07 MF803748
- CrAlp033* *Chloromonas cf. alpina* CCCryo 033-99 HQ404865.1
- CrBre* *Chloromonas brevispina* K-2 MG791867
- CrD* *Chloromonas* sp. D-CU581C AF517086.1
- CrGa* *Chloromonas* sp. Gassan-A LC012753.1
- CrPl* *Chloromonas platystigma* strain CCCryo 020-99 AF514401.1
- CrRo* *Chloromonas cf. rostafinskii* CCCryo 025-99 AF514402.1
- ChlSac* *Chloroidium saccharophilum* isolate HST10K KX024691.1
- Me* *Mesotaenium* sp. AG-2009-1 FM992335.1
- PrFu* *Prasiola furfuracea* AF189073.1
- UnCd* Uncultured Chlamydomonadaceae AB902971.1
- UnCr* Uncultured *Chloromonas* AB903008.1
- UnCr2* Uncultured *Chloromonas* AB902984.1
- UnDu* Uncultured Dunaliellaceae EF023287.1

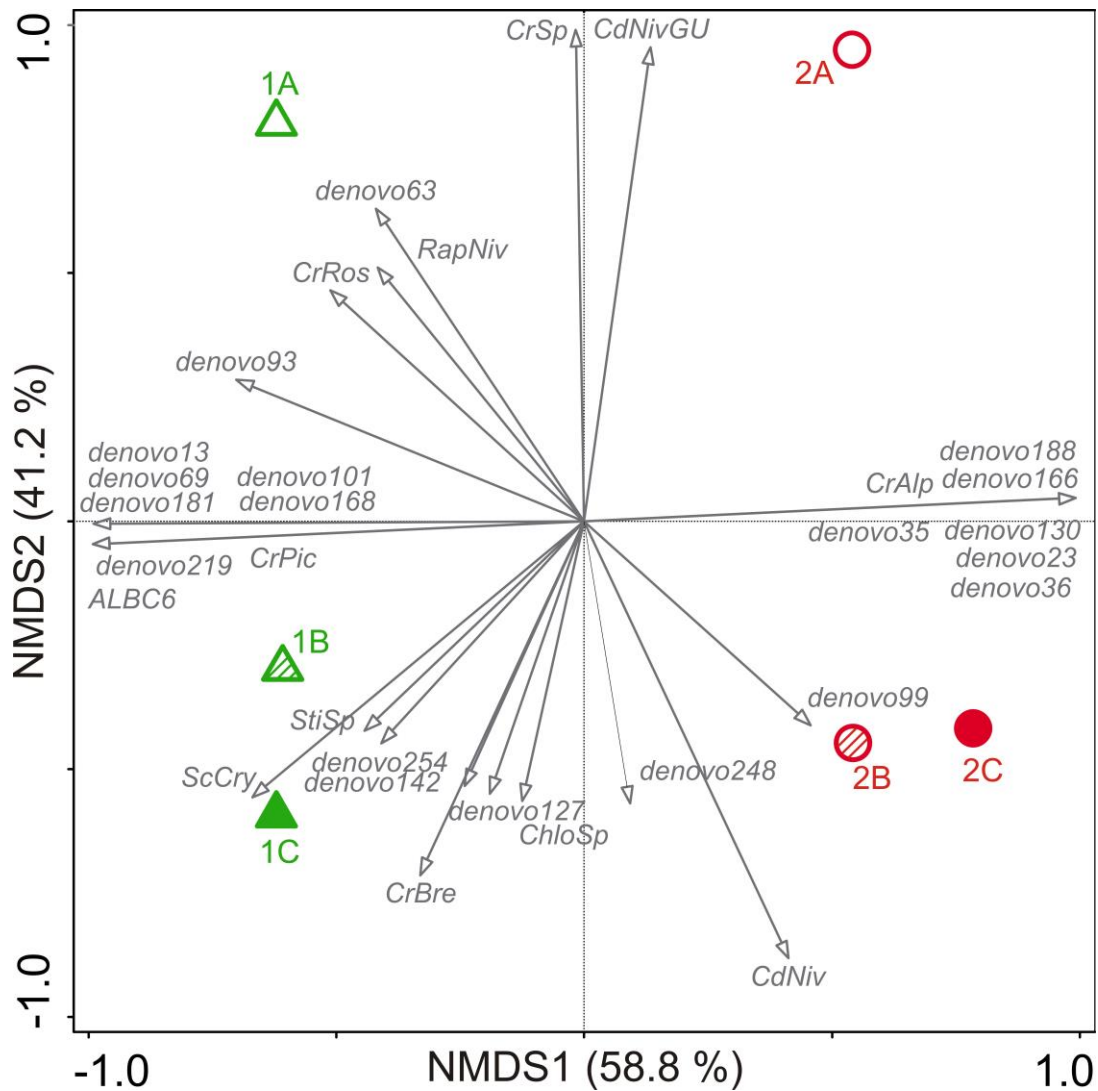


Fig. S26. Nonmetric multidimensional scaling (NMDS) ordination describing the differences in taxonomic composition of the two samples (sample 1 – green, sample 2 – red) based on ITS2 data analysed using the three strategies of taxonomic assignment (A, B, C – for details, see the text). Values within parentheses show % of variance explained by each axis. Source of the data for NMDS ordination: Table S7.

Acronyms:

<i>ALBC6</i>	Uncultured Chlorophyte clone ALBC6 JX435348
<i>CdNiv</i>	<i>Chlamydomonas nivalis</i> DL07 MF803749
<i>CdNivGU</i>	<i>Chlamydomonas nivalis</i> GU117577
<i>CrAlp</i>	<i>Chloromonas alpina</i> CCCryo032-99 HQ404864
<i>CrBre</i>	<i>Chloromonas brevispina</i> K-2 MG791868
<i>CrPic</i>	<i>Chloromonas pichincha</i> CCCryo 2616-06 HQ404889
<i>CrRos</i>	<i>Chloromonas rostafinskii</i> HQ404863
<i>CrSp</i>	<i>Chloromonas</i> sp. CCCryo 289-06 HQ404893
<i>ChloSp</i>	uncultured <i>Chlorella</i> sp.5 AB90311
<i>RapNiv</i>	<i>Raphidonema nivale</i> AJ431676
<i>ScCry</i>	<i>Scotiella cryophila</i> K-1 MG253843
<i>StiSp</i>	<i>Stichococcus</i> sp. SAG 2482 KX094848

Table S1. List of primers used for amplification and Sanger sequencing reactions of 18S rDNA and ITS2 rDNA markers; (F) forward; (R) reverse.

Primer	Marker	Direction	Sequence	Reference
P2	18S	F	CTGGTTGATTCTGCCAGT	(MOON-VAN DER STAAY et al. 2000)
P4	18S	R	TGATCCTTCYGCAGGTTAC	(MOON-VAN DER STAAY et al. 2000)
FA	18S	F	AACCTGGTTGATCCTGCCAGT	(MATSUZAKI et al. 2015)
RD	18S	R	GCTGGCACCAGACTTGCCCTC	(MATSUZAKI et al. 2015)
FC	18S	F	GGGAGGTAGTGACAATAAATA	(MATSUZAKI et al. 2015)
RF	18S	R	CCCGTGTTGAGTCAAATTAAG	(MATSUZAKI et al. 2015)
FE	18S	F	GGGAGTATGGTCGCAAGGCTG	(MATSUZAKI et al. 2015)
RB	18S	R	TGATCCTTCTGCAGGTTACCTAC	(MATSUZAKI et al. 2015)
AL1500af	ITS	F	GCGCGCTACACTGATGC	(HELMS et al. 2001)
LR3	ITS	R	GGTCCGTGTTTCAAGACGG	(VILGALYS & HESTER 1990)
ITS5	ITS	F	GGAAGTAAAAGTCGTAACAAGG	(WHITE et al. 1990)
ITS4	ITS	R	TCCTCCGCTTATTGATATGC	(WHITE et al. 1990)
SSU	ITS	F	CTGCGGAAGGATCATTGATTC	(PIERCEY-NORMORE & DEPRIEST 2001)
LSU	ITS	R	AGTTCAGCGGGTGGTCTTG	(PIERCEY-NORMORE & DEPRIEST 2001)

Supplemental References

- CAISOVÁ, L.; MARIN, B. & MELKONIAN, M. (2013): A Consensus Secondary Structure of ITS2 in the Chlorophyta Identified by Phylogenetic Reconstruction. – *Annals of Anatomy* 164: 482–496.
- HELMS, G.; FRIEDL, T.; RAMBOLD, G. & MAYRHOFER, H. (2001): Identification of photobionts from the lichen family Physciaceae using algal-specific ITS rDNA sequencing. – *The Lichenologist* 33(1): 73–86.
- HODAČ, L.; HALLMANN, C.; SPITZER, K.; ELSTER, J.; FABHAUER, F.; BRINKMANN, N.; ... FRIEDL, T. (2016): Widespread green algae *Chlorella* and *Stichococcus* exhibit polar-temperate and tropical-temperate biogeography. – *FEMS Microbiology Ecology* 92(8): 1–16.
- MATSUZAKI, R.; KAWAI-TOYOOKA, H.; HARA, Y. & NOZAKI, H. (2015): Revisiting the taxonomic significance of aplanozygote morphologies of two cosmopolitan snow species of the genus *Chloromonas* (Volvocales, Chlorophyceae). – *Phycologia* 54(5): 491–502.
- MOON-VAN DER STAAY, S.Y.; VAN DER STAAY, G.W.M.; GUILLOU, L.; VAULOT, D.; CLAUSTRE, H. & MEDLIN, L.K. (2000): Abundance and diversity of prymnesiophytes in the picoplankton community from the equatorial Pacific Ocean inferred from 18S rDNA sequences. – *Limnology and Oceanography* 45(1): 98–109.
- PIERCEY-NORMORE, M.D. & DEPRIEST, P.T. (2001): Algal switching among lichen symbioses. – *American Journal of Botany* 88(8): 1490–1498.
- VILGALYS, R. & HESTER, M. (1990): Rapid genetic identification and mapping of enzymatically amplified ribosomal DNA from several *Cryptococcus* species. – *Journal of Bacteriology* 172(8): 4238–4246.
- WHITE, T.J.; BRUNS, T.; LEE, S. & TAYLOR, J. (1990): Amplification and direct sequencing of fungal ribosomal RNA genes for phylogenetics. In: M. A. INNIS; D. H. GELFAND; J. J. SNINSKY, & T. J. WHITE (eds.): *PCR Protocols*. – pp. 315–322, Elsevier.

Table S2. ITS2 reference sequences downloaded from NCBI for the custom-built database

Taxon	Specimen/strain designation	Accession number ITS2 rDNA
<i>Chlamydomonas reinhardtii</i>	CC620	U66954.2
<i>Chlamydomonas</i> sp.		AF033295.1
<i>Raphidonema nivale</i>	CCAP 470/4	AJ431676.1
<i>Raphidonema sempervirens</i>	CCAP 470/6	AJ431674.1
<i>Spirogyra</i> sp.	GRS2	KM453687.1
<i>Klebsormidium</i> sp.	SAG 2065	EU434032.1
<i>Mesostigma viride</i>		EC732140.1
<i>Chloromonas nivalis</i>	P24/DR4	GU117576.1
<i>Chloromonas nivalis</i>	CCCryo_005-99	HQ404862.1
<i>Chloromonas pichincae</i>	CCCryo_261-06	HQ404889.1
<i>Chloromonas</i> sp.	CCCryo 207-05	HQ404883.1
<i>Chloromonas alpina</i>	CCCryo 033-99	HQ404865.1
<i>Chloromonas alpina</i>	CCCryo 032-99	HQ404864.1
<i>Chloromonas</i> sp.	CCCryo 289-06	HQ404893.1
<i>Chloromonas rostafinskii</i>	CCCryo 010-99	HQ404863.1
<i>Chloromonas pichincae</i>	CCCryo 192-04	HQ404880.1
<i>Chlamydomonas nivalis</i>	P27/DR1	GU117577.1
<i>Chloromonas</i> sp.	JP13	AB902970.1
Uncultured Chlorophyta	clone ALBC6	JX435348.1

Table S3. List of reference species locally abundant in the studied Austrian alpine snowfields and the GenBank accession numbers of encoded 18S rDNA and ITS2 rDNA markers.

Taxon	accession number	
	18S rDNA	ITS2 rDNA
<i>Chlamydomonas nivalis</i> DL07	MF803748	MF803749
<i>Scotiella cryophila</i> K-1	MG253843	MG253843
<i>Chloromonas brevispina</i> K-2	MG791867	MG791868

Table S4. Algal community compositions based on the 18S rDNA data sets comprising the 50 most abundant OTUs that made up >87% of the community. The table shows the discrepancies between OTU assignments using three strategies: (A) basic version using Qiime and the publicly available Silva database, (B) extended version using Qiime and additional reference sequences of the locally abundant taxa (underlined), and (C) further extended version using the final manual verification of taxa assignments in NCBI, only allowing a 2 bp nucleotide difference ($\geq 99.4\%$ identity; sequences below this threshold were recorded as “no blast hit”). With the respective reference sequence in order to be recorded as a match. Ambiguous hits are sequences that share all the same level of similarity with an inspected OTU, and thus they cannot be assigned unambiguously. Our results reveal that the manual verification in NCBI is essential and, thus, highly recommended.

OTU ID	Sample 1 [%]	Sample 2 [%]	(A) Qiime + Silva	(B) Qiime + Silva + local references	(C) Qiime + Silva + local references + manual verification
denovo14334	33.0	66.8	<i>Chloromonas</i> sp. Gassan-A LC012753.1	<u><i>Chloromonas brevispina</i> K-2</u>	Ambiguous hits: <u><i>Chloromonas brevispina</i> K-2</u> <u><i>Scotiella cryophila</i> K-1</u> <i>Chloromonas</i> sp. TA 8 AB902996 <i>Chloromonas</i> sp. Gassan-B LC012714
denovo45654	18.7	0.1	<i>Mesotaenium</i> sp. AG-2009-1 FM992335.1	<i>Ancylonema nordenskioldii</i> AF514397.2	<i>Ancylonema nordenskioldii</i> AF514397.2
denovo36485	0.9	13.6	Uncultured Chlamydomonadaceae AB902971.1	<u><i>Chlamydomonas nivalis</i> DL07</u>	<u><i>Chlamydomonas nivalis</i> DL07</u>
denovo40226	8.2	0	<i>Botrydiopsis constricta</i> AJ579339.1	<i>Botrydiopsis constricta</i> AJ579339.1	<i>Botrydiopsis constricta</i> AJ579339.1
denovo15070	4.6	1.0	Uncultured <i>Chloromonas</i> AB903008.1	<i>Chloromonas</i> cf. <i>alpina</i> CCCryo 033-99 HQ404865.1	<i>Chloromonas platystigma</i> strain CCCryo 020-99 AF514401.1
denovo20542	4.6	0	Uncultured Dunaliellaceae EF023287.1	Uncultured Dunaliellaceae EF023287.1	<i>Chloroidium saccharophilum</i> isolate HST10K KX024691.1
denovo101	3.2	1.1	<i>Chloromonas</i> sp. D-CU581C AF517086.1	<i>Chloromonas</i> cf. <i>rostaftinskii</i> CCCryo 025-99 AF514402.1	Ambiguous hits: <i>Chloromonas</i> sp. NIES-2379 AB906350.1, <i>Chloromonas rostaftinskii</i> strain CCCryo 025-99 AF514402.1
denovo23251	3.0	<0.1	<i>Chloromonas</i> sp. Gassan-A LC012753.1	<u><i>Chloromonas brevispina</i> K-2</u>	Ambiguous hits: <u><i>Chloromonas brevispina</i> K-2</u> <i>Chloromonas</i> sp. Hakkoda-1 LC012710.1, <i>Chloromonas</i> sp. Gassan-A LC012709.1
denovo30051	0.4	1.9	<i>Chloromonas</i> sp. JP15 AB902984.1	<i>Chloromonas</i> sp. JP15 AB902984.1	No blast hits
denovo36086	2.1	0	<i>Prasiola furfuracea</i> AF189073.1	<i>Prasiola furfuracea</i> AF189073.1	No blast hits
denovo2551	1.6	0.1	<i>Chloromonas</i> sp. Gassan-A LC012753.1	<i>Chloromonas</i> sp. TA 8 AB902996.1	Ambiguous hits: <u><i>Scotiella cryophila</i> K-1</u> <i>Chloromonas</i> sp. Gassan-B LC012714
denovo44194	0.9	0.4	<i>Chloromonas</i> sp. D-CU581C AF517086.1	<i>Chloromonas tughillensis</i> UTEX_SNO_88 AB734116.1	No blast hit

denovo30674	0.1	1.0	<i>Prototheca cutis</i> AB470468.1	<i>Prototheca cutis</i> AB470468.1	No blast hit
denovo32383	1.1	0	<i>Chloromonas tughillensis</i> UTEX_SNO_88 AB734116.1	<i>Chloromonas tughillensis</i> UTEX_SNO_88 AB734116.1	<i>Chloromonas fukushima</i> AB906342
denovo12840	0	1.0	<i>Chloromonas</i> sp. JP15 AB902984.1	<i>Chloromonas</i> sp. JP15 AB902984.1	Ambiguous hits: >40 sequences including <i>Chloromonas</i> sp. TA 9 AB903024.1
denovo12413	0	1.0	<i>Chlamydomonas</i> sp. GL1 AB902971.1	<i>Chlamydomonas nivalis</i> DL07	<i>Chlamydomonas nivalis</i> DL07
denovo14574	0	0.9	<i>Chlamydomonas</i> sp. GL1 AB902971.1	<i>Chlamydomonas nivalis</i> DL07	<i>Chlamydomonas nivalis</i> DL07
denovo18060	0	0.8	<i>Chloromonas</i> sp. GL4 AB903027.1	<i>Chloromonas</i> sp. GL4 AB903027.1	Uncultured eukaryote clone ALA5117773
denovo44928	0.1	0.7	Uncultured eukaryote clone TE107A KM870650.1	Uncultured eukaryote clone TE107A KM870650.1	Uncultured eukaryote clone TE107A KM870650.1
denovo25214	0.8	0	<i>Botrydiopsis callosa</i> AJ579340.1	<i>Botrydiopsis callosa</i> AJ579340.1	<i>Botrydiopsis callosa</i> AJ579340.1
denovo18262	0	0.7	<i>Hydrurus</i> sp. Sva 10_3 HE820740.1	Uncultured <i>Hydrurus</i> HE820740.1	<i>Hydrurus foetidus</i> FM955256.1
denovo12567	0.1	0.5	<i>Chloromonas</i> sp. Gassan-A LC012753.1	<i>Chloromonas brevispina</i> K-2	Ambiguous hits 7 sequences including: <i>Chloromonas brevispina</i> K-2 <i>Scotiella cryophila</i> K-1 <i>Chloromonas</i> sp. Gassan-B LC012714.1 <i>Chloromonas polyptera</i> JQ790556.1
denovo40835	0	0.4	<i>Chloromonas</i> sp. Gassan-A LC012753.1	<i>Chloromonas brevispina</i> K-2	No blast hit
denovo40500	0.1	0.2	<i>Chloromonas</i> sp. Gassan-A LC012753.1	<i>Chloromonas brevispina</i> K-2	Ambiguous hits: <i>Chloromonas brevispina</i> K-2 <i>Scotiella cryophila</i> K-1 <i>Chloromonas</i> sp. Gassan-B LC012714.1
denovo46231	0	0.3	<i>Chloromonas</i> sp. AL4 AB903027.1	<i>Chloromonas</i> sp. AL4 AB903027.1	<i>Chloromonas</i> sp. AL4 AB903027.1
denovo48297	0	0.3	<i>Chloromonas</i> sp. Hakkoda-1 LC012710.1	<i>Chloromonas brevispina</i> K-2	No blast hit
denovo45502	0	0.3	<i>Botrydiopsis constricta</i> AJ579339.1	<i>Botrydiopsis constricta</i> AJ579339.1	Botrydiopsidaceae sp. AM695636.1
denovo24516	0.3	0	<i>Raphidonema sempervirens</i> AJ309939.1	<i>Raphidonema sempervirens</i> AF514410.2	Ambiguous hits: >40 sequences including <i>Raphidonema sempervirens</i> AF514410.2 <i>Stichococcus</i> sp. KP08194
denovo21882	0.3	0	<i>Heterococcus fuornensis</i> AM490821.1	<i>Heterococcus fuornensis</i> AM490821.1	Ambiguous hits: 6 sequences including <i>Heterococcus chodatii</i> AM490822.1 <i>Heterococcus fuornensis</i> AM490821.1 <i>Heterococcus pleurococcoides</i> AJ579335.1
denovo29189	0.2	0	<i>Stichococcus bacillaris</i> JQ315605.1	<i>Stichococcus jenerensis</i> DQ275461.1	Ambiguous hits 4 sequences including <i>Stichococcus</i> sp. SAG 2482 KP081395.1 <i>Stichococcus</i> sp. KP081396.1
denovo34115	0.2	0	<i>Chloromonas</i> sp. JP15 AB902984.1	<i>Chloromonas</i> sp. JP15 AB902984.1	Ambiguous hits: >40 sequences including

					<i>Chloromonas</i> sp. TA9 AB903024.1 <i>Chloromonas</i> sp. SV3 AB903022.1 <i>Chloromonas</i> sp. PA2 AB903020.1
denovo16044	0.2	0	<i>Chloromonas</i> sp. Gassan-A LC012753.1	<i>Chloromonas</i> sp. Hakkoda-1 LC012710.1	Ambiguous hits: <i>Chloromonas</i> sp. Hakkoda-1 LC012710.1 <i>Chloromonas</i> sp. Gassan-A LC012709.1
denovo4533	0.1	0.2	<i>Chloromonas</i> sp. Gassan-A LC012753.1	<u><i>Chloromonas brevispina</i> K-2</u>	Ambiguous hits: 8 sequences including <u><i>Chloromonas brevispina</i> WP124</u> <u><i>Scotiella cryophila</i> K-1</u> <i>Chloromonas</i> sp. Gassan B LC012714.1 <i>Chloromonas polyptera</i> JQ790556.1
denovo31489	0.2	0	<i>Prasiola furfuracea</i> AF189073.1	<i>Stichococcus bacillaris</i> SAG 379-1b AJ311637.1	No blast hit
denovo17414	0	0.2	<i>Chloromonas</i> sp. D-CU581C AF517086.1	<i>Chloromonas nivalis</i> CCCryo-005-99	No blast hit
denovo47016	0	0.2	<i>Chloromonas</i> sp. Gassan-A LC012753.1	<u><i>Chloromonas brevispina</i> K-2</u>	Ambiguous hits: 8 sequences including <u><i>Scotiella cryophila</i> K-1</u> <i>Chloromonas</i> sp. Gassan-B LC012714.1 <i>Chloromonas polyptera</i> JQ790556.1
denovo38221	0.2	0	<i>Prototheca cutis</i> AB470468.1	<i>Prototheca cutis</i> AB470468.1	No blast hit
denovo13893	0	0.2	<i>Chlamydomonas</i> sp. GL1 AB902971.1	<u><i>Chlamydomonas nivalis</i> DL07</u>	No blast hit
denovo16269	0	0.2	uncultured Chlamydomonadaceae HW01/1 GU117574.1	<i>Chlainomonas</i> sp. MF803743	<i>Chlainomonas</i> sp. DL06 MF803743
denovo43924	0	0.2	<i>Chloromonas</i> sp. Gassan-A LC012753.1	<u><i>Chloromonas brevispina</i> K-2</u>	No blast hit
denovo34049	0.2	0	<i>Chloromonas</i> sp. Hakkoda-1 LC012710.1	<i>Chloromonas</i> sp. Hakkoda LC012710.1	No blast hit
denovo24547	0.1	0	<i>Mesotaenium</i> sp. AG-2009-1 FM992335.1	<i>Ancylonema nordenskioldii</i> AF514397.2	<i>Ancylonema nordenskioldii</i> AF514397.2
denovo15255	0.1	0	uncultured Dunaliellaceae EF023287.1	uncultured Dunaliellaceae EF023287.1	No blast hit
denovo28329	0.1	0	<i>Heterococcus fuorensis</i> AM490821.1	<i>Heterococcus fuorensis</i> AM490821.1	No blast hit
denovo23345	0.1	0	<i>Mesotaenium</i> sp. AG-2009-1 FM992335.1	<i>Ancylonema nordenskioldii</i> AF514397.2	<i>Ancylonema nordenskioldii</i> AF514397.2
denovo18826	0	0.1	<i>Raphidonema sempervirens</i> AJ309939.1	<i>Raphidonema sempervirens</i> AF514410.2	Ambiguous hits: >20 sequences including <i>Raphidonema sempervirens</i> AF514410.2 <i>Raphidonema nivale</i> AB488604.1 <i>Koliella sempervirens</i> AM412750.1 <u><i>Chlamydomonas nivalis</i> DL07</u>
denovo34529	0	0.1	<i>Chlamydomonadas</i> sp. GL1 AB902971.1	<u><i>Chlamydomonas nivalis</i> DL07</u>	<u><i>Chlamydomonas nivalis</i> DL07</u>
denovo9133	0	0.1	<i>Chloromonas</i> sp. Gassan-A LC012753.1	<u><i>Chloromonas brevispina</i> K-2</u>	No blast hit
denovo44422	0	0.1	<i>Hydrurus foetidus</i> FM955256.1	<i>Hydrurus foetidus</i> FM955256.1	<i>Hydrurus foetidus</i> FM955256.1
denovo8805	0	0.1	<i>Chloromonas</i> sp. Gassan-A LC012753.1	<i>Chloromonas cf. rostafinskii</i> HQ404863	No blast hit
Other	13.7	4.9			

Table S5. Oligotype sequences of the three most abundant 18S rDNA OTUs .

OTU ID	Oligotype ID	Sequence
denovo14434	TTT	GCGGTAATTCCAGCTCCAATAGCGTATATTTAAGTTGTTGCAGTAAAAAGCTCGTAGTTGGATTCGGGTGGGTTGCAATGGTCCGGTTCGCTGTGTACTGTT GCGGCCTTCCTTTCTGCCGGGGACGGGCTCTTGGGCTTCATTGTCTGGGATCCGGAGTCGGCGAGGTTACTTTGAGTAAATTAGAGTGTTCAAAGCAAGCTTA CGCTCTGAATACATTAGCATGGAATAACACGATAGGACTCTGGCCTATCTTGTGGTCTGTAGGACTGGAGTAATGATTAAGAGGGACAGTCGGGGGCATTG TATTTCAATTGTCAGAGGTGAAATCTTGGGA
	TTC	GCGGTAATTCCAGCTCCAATAGCGTATATTTAAGTTGTTGCAGTAAAAAGCTCGTAGTTGGATTCGGGTGGGTTGCAATGGTCCGGTTCGCTGTGTACTGTT GCGGCCTTCCTTTCTGCCGGGGACGGGCTCTTGGGCTTCATTGTCTGGGATCCGGAGTCGGCGAGGTTACTTTGAGTAAATTAGAGTGTTCAAAGCAAGCTTA CGCTCTGAATACATTAGCATGGAATAACACGATAGGACTCTGGCCTATCTTGTGGTCTGTAGGACTGGAGTAATGATTAAGAGGGACAGTCGGGGGCATTG TATTTCAATTGTCAGAGGTGAAATCTCCTCGGA
	TCT	GCGGTAATTCCAGCTCCAATAGCGTATATTTAAGTTGTTGCAGTAAAAAGCTCGTAGTTGGATTCGGGTGGGTTGCAATGGTCCGGTTCGCTGTGTACTGTT GCGGCCTTCCTTTCTGCCGGGGACGGGCTCTTGGGCTTCACTGTCTGGGATCCGGAGTCGGCGAGGTTACTTTGAGTAAATTAGAGTGTTCAAAGCAAGCTTA CGCTCTGAATACATTAGCATGGAATAACACGATAGGACTCTGGCCTATCTTGTGGTCTGTAGGACTGGAGTAATGATTAAGAGGGACAGTCGGGGGCATTG TATTTCAATTGTCAGAGGTGAAATCTTGGGA
	CTT	GCGGTAATTCCAGCTCCAATAGCGTATATTTAAGTTGTTGCAGTAAAAAGCTCGTAGTTGGATTCGGGTGGGTTGCAACGGTCCGGTTCGCTGTGTACTGTT GCGGCCTTCCTTTCTGCCGGGGACGGGCTCTTGGGCTTCATTGTCTGGGATCCGGAGTCGGCGAGGTTACTTTGAGTAAATTAGAGTGTTCAAAGCAAGCTTA CGCTCTGAATACATTAGCATGGAATAACACGATAGGACTCTGGCCTATCTTGTGGTCTGTAGGACTGGAGTAATGATTAAGAGGGACAGTCGGGGGCATTG TATTTCAATTGTCAGAGGTGAAATCTTGGGA
denovo36485	T	GCGGTAATTCCAGCTCCAATAGCGTATATTTAAGTTGTTGCAGTAAAAAGCTCGTAGTTGGATTCGGGTGGGTTGCGTCCGGTTCGCTGTGTACTGTT TTGAGCCTTCCTTTCTGCCGGGGACGGGTTCTGGGCCTACGGTTTGGGACTCGGAGTCGGCGAGGTTACTTTGAGTAAATTAGAGTGTTCAAAGCAAGCCT ACGCTCTGAATACATTAGCATGGAATAACGCGATAGGACTCTGGCCTATCTTGTGGTCTGTAGGACTGGAGTAATGATTAAGAGGGACAGTCGGGGGCATTG GTATTTCAATTGTCAGAGGTGAAATCTTGGG
	C	GCGGTAATTCCAGCTCCAATAGCGTATATTTAAGTTGTTGCAGTAAAAAGCTCGTAGTTGGATTCGGGTGGGTTGCGTCCGGTTCGCTGTGTACTGTT TTGAGCCTTCCTTTCTGCCGGGGACGGGTTCTGGGCCTACGGTTTGGGACTCGGAGTCGGCGAGGTTACTTTGAGTAAATTAGAGTGTTCAAAGCAAGCCT ACGCTCTGAATACATTAGCATGGAATAACGCGATAGGACTCTGGCCTATCTTGTGGTCTGTAGGACTGGAGTAATGATTAAGAGGGACAGTCGGGGGCATTG GTATTTCAATTGTCAGAGGTGAAATCTCCTCGG
denovo45654	C	GCGGTAATTCCAGCTCCAATAGCGTATATTTAAGTTGTTGCAGTAAAAAGCTCGTAGTTGGATTTGGGTTGGTGTGGTTCGGTCTGCTTTCTAGTTGAACTGG CTACTCCATCCTTCTTCCGGGGACGCGTTCTGGCCTTCAATTGGCTGGGACGCGGAGTCGGCGATGTTACTTTGAAAAAATTAGAGTGTTCAAAGCAGGCCTA CGCTCTGAATACATTAGCATGGAATAACGTGATAGGACTCTGGTCTTATTGTGTGGTCTTCCGGACCGGAGTAATGATTAATAGGGACAGTTGGGGGCATTG GTATTTCAATTGTCAGAGGTGAAATCTTGGG
	A	GCGGTAATTCCAGCTCCAATAGCGTATATTTAAGTTGTTGCAGTAAAAAGCTCGTAGTTGGATTTGGGTTGGTGTGGTTCGGTCTGCTTTCTAGTTGAACTGG CTACTCCATCCTTCTTCCGGGGACGCGTTCTGGCCTTAATTGGCTGGGACGCGGAGTCGGCGATGTTACTTTGAAAAAATTAGAGTGTTCAAAGCAGGCCTA CGCTCTGAATACATTAGCATGGAATAACGTGATAGGACTCTGGTCTTATTGTGTGGTCTTCCGGACCGGAGTAATGATTAATAGGGACAGTTGGGGGCATTG GTATTTCAATTGTCAGAGGTGAAATCTTGGG

Table S6. Output of the ITSx software. ITS2 regions were extracted from all sequences to avoid the inclusion of the highly conserved neighbouring genes (i.e., 5.8S and 28S). Inclusion of these regions in the identification process would otherwise lead to misleading results. HMMER was used to predict the origin of the sequences (e.g., Chlorophyta, Fungi) based on Hidden Markov Models.

Number of sequences in input file:	273404
Sequences detected as ITS by ITSx:	273309
On main strand:	273239
On complementary strand:	70
Sequences detected as chimeric by ITSx:	0
ITS sequences by preliminary origin	
Alveolates:	35443
Amoebozoa:	0
Bacillariophyta:	1
Brown algae:	2
Bryophytes:	0
Euglenozoa:	0
Eustigmatophytes:	0
Fungi:	47293
Green algae:	189922
Liverworts:	0
Metazoa:	11
Microsporidia:	0
Oomycetes:	1
Prymnesiophytes:	0
Raphidophytes:	0
Red algae:	0
Rhizaria:	0
Synurophyceae:	0
Tracheophyta:	636

Table S7. Algal community composition based on the ITS2 data set and comprising the 38 most abundant OTUs that made up >98% of the community. Table shows the discrepancies between OTU assignments using three strategies: (A) basic version using Qiime and a custom database downloaded from NCBI, (B) extended version using Qiime and additional reference sequences of the locally abundant taxa (underlined), and (C) further extended version using final manual verification of taxa assignments. The latter one comprised the comparison of the representative sequences of the OTUs with their respective reference sequences in terms of sequence identities ($\geq 89.0\%$ similarity required; sequences below this threshold were recorded as “no blast hit”) and their secondary structures (absence of compensatory base changes (CBC) in homological positions near the 5’- apex of helix III [the most conserved region of the ITS2 secondary structure of eukaryotes] required). Our results reveal that the manual verification including secondary structure prediction and CBC search is essential, and thus, highly recommended.

OTU ID	WP79 [%]	WP99 [%]	(A) Qiime + NCBI database	(B) Qiime + NCBI database + local references	(C) Qiime + NCBI database + local references + manual verification (sequence similarity [%], sequence cover [%])
denovo99	1.8	59.1	<i>Chloromonas</i> sp. CCCryo289-06 HQ404893.1	<u><i>Chloromonas brevispina</i> K-2</u>	No blast hit (88%, 83%, 6 CBC when compared denovo99 and <i>Chloromonas brevispina</i> K-2 – one CBC out of it is located in the most conserved part of the structure, i.e., in the top close to the 5’ end of III helix, see Fig. 4)
denovo20	5.5	28.2	<i>Chlamydomonas nivalis</i> GU117577.1	<u><i>Chlamydomonas nivalis</i> DL07</u>	<u><i>Chlamydomonas nivalis</i> DL07</u> (100%, 100%)
denovo107	39.8	<0.1	<i>Chloromonas</i> sp. CCCryo289-06 HQ404893.1	<u><i>Chloromonas brevispina</i> K-2</u>	<u><i>Chloromonas brevispina</i> K-2</u> (100% identical except for one nucleotide - instead of R in reference sequence, there was G, 100%)
denovo100	13.7	<0.1	<i>Chloromonas pichincae</i> HQ404889.1	<i>Chloromonas pichincae</i> HQ404889.1	<i>Chloromonas pichincae</i> HQ404889.1 (92%, 100%, 1 CBC in helix III [outside the most conserved part] when compared denovo100 and <i>Chloromonas pichincae</i> , see Figs S6, S7)
denovo63	10.9	0.2	No blast hit	<u><i>Scotiella cryophila</i> K-1</u>	<u><i>Scotiella cryophila</i> K-1</u> (100%, 100%)
denovo142	8.2	1.7	<i>Chloromonas rostafinskii</i> HQ404863.1	<i>Chloromonas rostafinskii</i> HQ404863.1	No blast hit (79%, 60% - denovo142 vs. <i>Chloromonas rostafinskii</i> : 86%, 77% - denovo142 vs. <i>Chloromonas miwae</i> LC012762.1, four CBCs [one CBC out of it is located in the most conserved part of the structure, i.e., in the top close to the 5’ end of III helix] when compared denovo142 and <i>Chloromonas miwae</i> , sequence-structure alignment in Fig. S12)
denovo130	1.4	3.5	No blast hit	No blast hit	No blast hit (no significant similarity found)
denovo181	4.1	0	No blast hit	No blast hit	No blast hit (82%, 87%, <i>Desmococcus endolithicus</i> KX094830.1; five CBCs – one in helix II and four CBCs in helix III, see Figs S19, S20)
denovo254	3.1	0.1	<i>Chloromonas rostafinskii</i> HQ404863.1	<i>Chloromonas rostafinskii</i> HQ404863.1	No blast hit (82%, 48% - denovo254 vs. <i>Chloromonas rostafinskii</i> : 88%, 84% - denovo254 vs. <i>Chloromonas miwae</i> LC012762.1, three

					CBCs [one out of in the most conserved part of the structure] when compared denovo254 and <i>Chloromonas miwae</i> , see Figs S12, S14)
denovo23	0.1	2.2	No blast hit	No blast hit	No blast hit (no significant similarity found)
denovo259	2.6	0.2	Uncultured Chlorophyta clone ALBC6 JX435348.1	Uncultured Chlorophyta clone ALBC6 JX435348.1	Uncultured Chlorophyta clone ALBC6 JX435348.1 (100%, 100%)
denovo76	0.1	1.9	<i>Chloromonas alpina</i> CCCryo032-99	<i>Chloromonas alpina</i> CCCryo032-99 HQ404864.1	<i>Chloromonas alpina</i> CCCryo032-99 HQ404864.1 (100%, 100%)
denovo219	1.8	0	No blast hit	No blast hit	No blast hit (no significant similarity found)
denovo85	1.5	<0.1	<i>Chloromonas pichincae</i> CCCryo 2616-06 HQ404889.1	<i>Chloromonas pichincae</i> CCCryo 2616-06 HQ404889.1	<i>Chloromonas pichincae</i> CCCryo 2616-06 HQ404889.1 (95%, 100%), see Figs S6, S7
denovo166	0.1	0.8	No blast hit	No blast hit	No blast hit (no significant similarity found)
denovo74	0.6	0.3	<i>Raphidonema nivale</i> AJ431676.1	<i>Raphidonema nivale</i> AJ431676.1	uncultured <i>Chlorella</i> sp. 5 AB903011.1 (100%, 100%)
denovo93	0.7	0	No blast hit	No blast hit	<i>Stichococcus</i> sp. SAG 2482 KX094848.1 (100%, 100%)
denovo35	<0.1	0.5	No blast hit	No blast hit	No blast hit (no significant similarity found)
denovo69	0.6	0	No blast hit	No blast hit	No blast hit (82%, 52%, <i>Prasiola delicata</i> MF801375.1, six CBCs in helix III, see Figs S21, S22)
denovo36	<0.1	0.5	No blast hit	No blast hit	No blast hit (no significant similarity found)
denovo127	0.3	0.1	<i>Chloromonas rostafinskii</i> HQ404863.1	<i>Chloromonas rostafinskii</i> HQ404863.1	No blast hit (85%, 48% - denovo127 vs. <i>Chloromonas rostafinskii</i> : 90%, 82% - denovo127 vs. <i>Chloromonas miwae</i> LC012762.1, two CBCs in helix III [one CBC out of it in the most conserved part of the structure] when compared denovo127 and <i>Chloromonas miwae</i> , see Figs S12, S14)
denovo13	0.3	0	No blast hit	No blast hit	No blast hit (84%, 85%, <i>Desmococcus endolithicus</i> KX094830.1; four CBCs in helix III, see Figs S19 and S20).
denovo44	0.2	0	Uncultured Chlorophyta clone ALBC6 JX435348.1	<i>Scotiella cryophila</i> K-1	<i>Scotiella cryophila</i> K-1 (96%, 100%, 4CBCs in helix III [outside the most conserved part] when compared denovo44 and <i>Scotiella cryophila</i> K-1, see Figs S15, S16)
denovo249	0.2	0	Uncultured Chlorophyta clone ALBC6 JX435348.1	<i>Chloromonas brevispina</i> K-2	<i>Chloromonas brevispina</i> K-2 (96%, 82%, one CBC in helix III [outside the most conserved part] when compared denovo249 and <i>Chloromonas brevispina</i> K-2, sequence-secondary structure alignment in Fig. S5)
denovo188	<0.1	0.1	No blast hit	No blast hit	No blast hit (no significant similarity found)
denovo101	0.2	<0.1	No blast hit	No blast hit	No blast hit (84%, 75%, <i>Chloromonas miwae</i> LC012762.1; three CBCs in helix III [two out of in the most conserved part of the

					structure] when compared denovo101 and <i>Chloromonas miwae</i> , see Fig. S13)
denovo168	0.2	0	No blast hit	No blast hit	No blast hit (no significant similarity found)
denovo143	0.1	0	No blast hit	No blast hit	<i>Stichococcus</i> sp. KX094857.1 (99%, 100%)
denovo109	0.1	0	No blast hit	No blast hit	<i>Stichococcus</i> sp. KX094848.1 (89%, 89%, four changes at both side of secondary structure found in less conserved part of the structure, likely no CBC, Figs S17, S18)
denovo28	0.1	0	No blast hit	No blast hit	<i>Lobosphaera</i> sp. K-1 KT119889.1 (94.0%, 100%), no CBC found when compared denovo28, <i>Lobosphaera</i> sp. K-1 KT119889.1 and <i>Lobosphaera incisa</i> KM020046.1, so denovo28 can be assigned to <i>Lobosphaera incisa</i> , sequence-structure alignment in Fig. S8
denovo124	0.1	0	No blast hit	No blast hit	<i>Lobosphaera incisa</i> KM020046.1 (94%, 100%), see Figs S8, S9
denovo45	0.1	0	No blast hit	No blast hit	No blast hit (no significant similarity found)
denovo72	<0.1	0.1	<i>Chlamydomonas nivalis</i> GU117577.1	<i>Chlamydomonas nivalis</i> GU117577.1	<i>Chlamydomonas nivalis</i> GU117577.1 (94%, 100%), no CBC when denovo72 compared to <i>Chlamydomonas nivalis</i> DL07; [interestingly, ITS2 of denovo72 has higher sequence similarity with Uncultured <i>Chlamydomonas</i> clone H14 KX063729.1 (98%, 100%) but there is one CBC in helix II between denovo72 and clone H14], see Fig. S10, S11.
denovo180	0.1	0	No blast hit	No blast hit	No blast hit (84%, 100%, <i>Chlorocloster engadinensis</i> FM946011.1; one CBC in basal part of helix I and one CBC in the basal part of helix II, see Figs S23, S24)
denovo212	<0.1	0.1	No blast hit	No blast hit	<i>Trebouxia</i> sp. MG098229 (100%, 100%)
denovo173	0.1	0	<i>Chloromonas</i> sp. CCCryo289-06 HQ404893.1	<i>Chloromonas brevispina</i> K-2	<i>Chloromonas brevispina</i> K-2 (100%, 75%, two CBCs in helix III [outside the most conserved part] when compared denovo173 and <i>Chloromonas brevispina</i> K-2, sequence structure alignment in Fig. S5)
denovo266	0.1	0	Uncultured Chlorophyta clone ALBC6 JX435348.1	<i>Chloromonas brevispina</i> K-2	<i>Chloromonas brevispina</i> K-2 (96%, 69%, 2 CBCs in basal part of helix II and 1 CBC in helix II when compared denovo266 and <i>Chloromonas brevispina</i> K-2, sequence structure alignment in Fig. S5)
denovo248	<0.1	<0.1	<i>Chloromonas</i> sp. CCCryo289-06 HQ404893.1	<i>Chloromonas brevispina</i> K-2	No blast hit (92%, 54%, 6 CBCs when compared denovo248 and <i>Chloromonas brevispina</i> K-2, one CBC out of it is located in the most conserved part of the structure, sequence structure alignment in Fig. S5)
Other	1.2	0.4			

Paper VIII

Temperature dependence of photosynthesis and thylakoid lipid composition in the red snow alga *Chlamydomonas cf. nivalis* (Chlorophyceae)

Lukeš M^{1,2*}, Procházková L^{3*}, Shmidt V¹, Nedbalová L³ & Kaftan D^{1,2}

FEMS Microbiology Ecology 89(2): 303–315, 2014

¹ Faculty of Science, University of South Bohemia in České Budějovice, České Budějovice, Czech Republic;

² Department of Phototrophic Microorganisms, Institute of Microbiology CAS, Opatovický mlýn, Třeboň, Czech Republic;

³ Department of Ecology, Faculty of Science, Charles University in Prague, Prague, Czech Republic

*ML and LP contributed equally to this work

Temperature dependence of photosynthesis and thylakoid lipid composition in the red snow alga *Chlamydomonas cf. nivalis* (*Chlorophyceae*)

Martin Lukeš^{1,2}, Lenka Procházková³, Volha Shmidt¹, Linda Nedbalová³ & David Kaftan^{1,2}

¹Faculty of Science, University of South Bohemia in České Budějovice, České Budějovice, Czech Republic; ²Department of Phototrophic Microorganisms, Institute of Microbiology CAS, Opatovický mlýn, Třeboň, Czech Republic; and ³Department of Ecology, Faculty of Science, Charles University in Prague, Prague, Czech Republic

Correspondence: David Kaftan, Department of Experimental Plant Biology, Faculty of Science, University of South Bohemia in České Budějovice, Branišovská 31, 37005 České Budějovice, Czech Republic. Tel.: +420 387772342; fax: +420 387772351; e-mail: david.kaftan@prf.jcu.cz

Received 5 September 2013; revised 4 February 2014; accepted 4 February 2014.
Final version published online 7 March 2014.

DOI: 10.1111/1574-6941.12299

Editor: Johanna Laybourn-Parry

Keywords

electron transfer; snow algae; *Chlamydomonas*; phosphatidylglycerol; photosystem II; temperature adaptation.

Introduction

Photosynthetic organisms inevitably become acclimated to seasonal, diel as well as rapid aperiodic changes in ambient conditions. Thermal fluctuations instantaneously influence rates of photosynthetic electron transfer, while longer exposure to supra- or super-optimal temperatures causes reversible or permanent changes in rates of synthesis and degradation of both primary and secondary metabolites. Prolonged thermal stress decreases the organism's fitness or even leads to its death unless remediated through the acclimation processes. The phenomenon of temperature dependence of photosynthesis attracted further attention in the past decade due to concerns over the stability of ecosystems in the predicted global climatic changes.

Snow algae comprise an ecologically distinct group of photosynthetic microorganisms. Most of the known species populating polar and mountain regions worldwide belong to the genera *Chloromonas* and *Chlamydomonas* (*Chlorophyta*). Their native environment is defined by

Abstract

Here, we report an effect of short acclimation to a wide span of temperatures on photosynthetic electron transfer, lipid and fatty acid composition in the snow alga *Chlamydomonas cf. nivalis*. The growth and oxygen evolution capacity were low at 2 °C yet progressively enhanced at 10 °C and were significantly higher at temperatures from 5 to 15 °C in comparison with the mesophilic control *Chlamydomonas reinhardtii*. In search of the molecular mechanisms responsible for the adaptation of photosynthesis to low temperatures, we have found unprecedented high rates of Q_A to Q_B electron transfer. The thermodynamics of the process revealed the existence of an increased structural flexibility that we explain with the amino acid changes in the D1 protein combined with the physico-chemical characteristics of the thylakoid membrane composed of > 80% negatively charged phosphatidylglycerol.

frigid temperatures interrupted by episodic freeze-thaw cycles while solar irradiation is high and variable (Hoham & Duval, 2001). Their physiological and biochemical processes must therefore be optimized to respond to the environmental extremes. To this end, studies performed on snow algae can provide a valuable insight into the diversity of various adaptation and acclimation mechanisms in microorganisms. The life histories and ecology of many species of snow algae were studied in detail for example by Hoham (1975a, b, c). Studies focusing on physiology and biochemistry of snow algae are relatively rare with their scope ranging from photoprotective effect of carotenoids in *Chlamydomonas nivalis* (Bidigare *et al.*, 1993) to the ability to survive freezing and thawing as a potential for effective cryoprotection (Morris *et al.*, 1979). Unfortunately, the majority of the studies were performed on field samples (Remias *et al.*, 2005, 2010a, b; Stibal *et al.*, 2007; Leya *et al.*, 2009).

The available data on temperature dependence of photosynthesis and growth are often controversial (Hoham,

1975a; Mosser *et al.*, 1977; Remias *et al.*, 2005; Hoham *et al.*, 2008), suggesting a broader range of ecophysiological strategies in snow algae than expected. Numerous studies reported that the occurrence of certain lipid characteristics coincided with the capacity to withstand low temperature stress. A high proportion of unsaturated fatty acids were observed in red cells of *C. nivalis* from Antarctica (Bidigare *et al.*, 1993), while unusual short- and medium-chain polyunsaturated fatty acids were isolated from the flagellated cells of the snow alga *Chloromonas brevispina* (Rezanka *et al.*, 2008). However, these reports were based on single measurements of field samples. Only limited evidence exists that documents the variability in fatty acid content of different strains under varying controlled conditions in the laboratory (Spijkerman *et al.*, 2012).

Here, we study the temperature dependence of photosynthesis and thylakoid lipid content in the red snow alga *C. cf. nivalis* (Bauer) Wille. We have investigated growth, electron transfer in photosystem II (PSII) and oxygen evolution rates in cells exposed to temperatures from 2 to 35 °C. PSII function at sub- and supra-optimal temperatures was studied within the context of the primary structure of the D1 protein and the content of thylakoid lipids and fatty acids. Our results indicate the snow alga ranks as a cryotolerant mesophile.

Materials and methods

Organisms and growth conditions

The snow alga *C. cf. nivalis* Nedbalova strain CCALA 970 was isolated from melting snow in the Tatra Mountains in northern Slovakia (Nedbalova *et al.*, 2006). The family *Chlamydomonadaceae* including the snow species undergoes rapid taxonomic changes. Using combined morphological and molecular data, Matsuzaki *et al.* (2012) revised the taxonomic position of two strains causing red snow that were originally identified as *C. nivalis* and reported under different names in culture collections. Since a taxonomic revision of the strain CCALA 970 is also necessary, we use the name *C. cf. nivalis* for the red snow alga investigated in this paper.

Cells were grown in BBM medium (2.94 mM NaNO₃, 0.30 mM MgSO₄, 0.42 mM NaCl, 0.33 mM K₂HPO₄, 1.28 mM KH₂PO₄, 0.17 mM CaCl₂, 30.68 μM ZnSO₄, 7.27 μM MnCl₂, 4.93 μM MoO₃, 6.29 μM CuSO₄, 1.68 μM Co(NO₃)₂, 0.18 mM H₃BO₃, 0.17 mM Na₂-EDTA, 0.552 mM KOH, 17.92 μM FeSO₄ and 18.71 μM H₂SO₄). Cultures on agar plates and starter cultures of *C. cf. nivalis* in liquid medium were therefore always grown at 2.5 °C. Cultures of *Chlamydomonas reinhardtii* P. A. Dangeard strain UTEX 2246 were maintained at 24 °C, close to its optimal growth temperature.

Air-bubbled liquid cultures of *C. cf. nivalis* and *C. reinhardtii* were grown at 2.5 and 24 °C, respectively, in 2-L bottles under 16/8 light/dark periodic illumination of 100 μmol photons m⁻² s⁻¹ provided by fluorescent light (Fluora; Osram). Our photosynthesis vs. irradiance measurements performed at light intensity of 100 μmol photons m⁻² s⁻¹ corresponded to 50–70% of a maximal photosynthetic activity in either of the strains at any of the examined temperatures. As such, it has been assumed the selected light intensity will not cause any significant photoinhibition. Cells reaching late exponential phase were diluted to 1 μg Chl mL⁻¹ and transferred to sub- and supra-optimal temperatures 5, 10, 15, 20, 25, 30 and 35 °C, respectively. Their growth was monitored for 10 days by measurements of total chlorophyll concentration in cells. Ten millilitre of cell culture was extracted into 100% dimethylsulphoxide, and absorption spectra were measured using a Shimadzu UV-2401PC spectrophotometer every 24 h. Chlorophyll concentration was calculated according to the method of Lichtenthaler & Wellburn (1983) with use of these equations:

$$\text{Chl } a = 12.19 \cdot A_{665.1} - 3.45 \cdot A_{649.1} \text{ [}\mu\text{g mL}^{-1}\text{]}$$

$$\text{Chl } b = 21.99 \cdot A_{649.1} - 5.32 \cdot A_{665.1} \text{ [}\mu\text{g mL}^{-1}\text{]}$$

The respective absorbances were corrected for turbidity at 730 nm.

Specific growth rates μ were determined as a slope of linear regression of semi-logarithmic plot of ln(Chl) vs. time during the exponential phase of the growth. The generation time (number of doublings per day) was calculated as $\mu/\ln 2$. All growth experiments were run in triplicates.

Fatty acid analysis carried out in cells grown for 3, 5 and 10 days at temperatures *c.* 10 °C higher and lower than the initial (2.5 and 24 °C in *C. cf. nivalis* and *C. reinhardtii* respectively) showed that no significant changes in the fatty acid content occurred within a time span longer than 3 days (Supporting Information, Fig. S1). All the acclimation experiments therefore consisted of 3 days exposure of cells to the particular temperature.

Oxygen evolution

Cells of *C. cf. nivalis* grown at 2.5 and 24 °C for 72 h, respectively, and of *C. reinhardtii* grown at 24 °C were diluted with fresh BBM medium to a suspension containing 5 μg Chl mL⁻¹. The oxygen evolution rate was measured with Clark-type concentration electrode in a thermostated, magnetically stirred cuvette (Hansatech Instruments Ltd, UK). Electrical current was monitored with a sampling frequency of 30 Hz with a polarization potential of 700 mV by Oxycorder (PSI Ltd, Czech

Republic). The 2.5 mL of cell suspension was homogeneously illuminated by high-intensity light-emitting diodes ($\lambda_{\text{red}} = 635 \text{ nm}$, $\lambda_{\text{blue}} = 480 \text{ nm}$). A manually adjustable power source provided light intensities from 0 to $6500 \mu\text{mol photons m}^{-2} \text{ s}^{-1}$ of incident light. The oxygen evolution was measured at $2 \text{ }^\circ\text{C}$ and at increments of $5 \text{ }^\circ\text{C}$ in the range from 5 to $35 \text{ }^\circ\text{C}$, at a saturating light intensity of $2000 \mu\text{mol photons m}^{-2} \text{ s}^{-1}$. Each cycle of oxygen evolution measurement at the chosen temperature comprised of 600 s of dark adaptation, 600 s of illumination followed by 600 s of dark relaxation. Calibration of the measured signals was carried out against a buffer equilibrated with the ambient air and then depleted of oxygen by the addition of sodium dithionide at all measured temperatures. Tabulated values of Henry's law constants for oxygen in water were used to convert measured signals into oxygen concentration [$\mu\text{mol O}_2$]. An oxygen evolution rate in $\mu\text{mol O}_2 \text{ mg Chl}^{-1} \text{ h}^{-1}$ was determined as a slope of linear regression of a plot of O_2 [μmol] vs. time during the light period of oxygen evolution cycle. All experiments were carried out in triplicates.

Electron transfer rate measurements

Cells of *C. cf. nivalis* and of *C. reinhardtii* grown at 2.5 and $24 \text{ }^\circ\text{C}$, respectively, were diluted with fresh BBM medium to yield $3 \mu\text{g Chl mL}^{-1}$. The cell suspension was dark-adapted for 1 h on ice prior to analysis to allow for re-oxidation of electron acceptors in and around PSII. Chlorophyll fluorescence measurements were conducted in a FL-3000 fluorometer equipped with a TR-2000 thermoregulator (PSI Ltd), and the sample cuvette contained 2.4 mL of dark-adapted sample. In the temperature-dependent Q_A reoxidation, fluorescence decay following single-turnover saturating pulse was measured as described (Dinamarca *et al.*, 2011) at increments of $2.5 \text{ }^\circ\text{C}$ in the range from 0 to $50 \text{ }^\circ\text{C}$. At least seven independent measurements were conducted at each temperature.

Fluorescence temperature curve

Cells grown for 72 h at a particular temperature were diluted with fresh BBM medium to yield $3 \mu\text{g Chl mL}^{-1}$. Critical temperature (T_C) was assessed in experiments that consisted of measuring chlorophyll fluorescence induced by weak measuring pulses in a linearly heated sample with a ramp of $1.5 \text{ }^\circ\text{C min}^{-1}$ from 0 to $60 \text{ }^\circ\text{C}$ essentially as described by Lazar & Ilik (1997). The T_C was estimated as the crossing of an extrapolation of the linear part of fluorescence rise to a point of maximum fluorescence (T_M) with constant fluorescence level before the fluorescence rise. M/F(30) ratio reflecting the inhibition or damage to PSII (Lazar & Ilik, 1997) is the ratio of

maximal fluorescence at temperature T_M and a steady-state minimal fluorescence F_0 at $30 \text{ }^\circ\text{C}$. All experiments were carried out in triplicates.

Isolation of thylakoid membranes

Thylakoid membranes were isolated using the method described by Chua & Bennoun (1975) with minor modifications. Cells grown for 72 h at the particular temperature were harvested by centrifugation at 2500 g for 15 min and washed twice in 0.3 M sucrose, 25 mM HEPES-KOH pH 7.5, 1 mM MgCl_2 . Cells were broken in a French-pressure cell at 4000 Psi. Broken cells were centrifuged at 2000 g for 10 min, and the pellet was resuspended in 0.3 M sucrose, 5 mM HEPES-KOH pH 7.5 and 10 mM EDTA (buffer B) and centrifuged at $50\,000 \text{ g}$ for 10 min. The pellet was resuspended to a total volume of 10 mL in 1.8 M sucrose in buffer B. Five millilitre of 2 M sucrose in buffer B was overlaid with 5 mL of sample in 1.8 M sucrose in buffer B, with 2 mL of 1.3 M sucrose in buffer B and 5 mL of 0.5 M sucrose in buffer B and centrifuged at $140\,000 \text{ g}$ for 1 h in Beckman Coulter Optima™ L-90K Ultracentrifuge. Thylakoid membranes were collected at the interlayer of 1.8 and 1.3 M sucrose. Collected membranes were washed with three volumes of 5 mM HEPES-KOH pH 7.5 and 10 mM EDTA and centrifuged at $50\,000 \text{ g}$ for 45 min.

Extraction of lipids

Lipids were extracted according to Wada *et al.* (1994). One millilitre of membranes was transferred to a teflon-lined screw-cap test tube with 3.75 mL of CHCl_3 : CH_3OH (1 : 2, v/v) and mixed by vortexing. The mixture was left to stand for 20 min at room temperature. Then, 1.25 mL of each CHCl_3 and H_2O was added, and the solution was vortexed, followed by centrifugation at 2500 g for 15 min. Then, the clear upper phase and fluff layer were carefully withdrawn and 2.5 mL of $\text{CH}_3\text{OH} : \text{H}_2\text{O}$ (10 : 9, v/v) was added. The solution was vortexed and centrifuged at 2500 g for 15 min at room temperature, and the lower phase was recovered and transferred to a new tube for evaporation. The sample was evaporated by either a rotary evaporator or a stream of nitrogen gas. The dry sample was dissolved in CHCl_3 : CH_3OH (2 : 1, v/v) and stored at $-80 \text{ }^\circ\text{C}$. BHT was added to a final concentration of 0.05% to avoid oxidation during long-time storage.

Lipid and fatty acid analysis

Lipid extracts were applied as 2.5-cm-wide streaks 1.5 cm from the bottom of 250- μm TLC plates (MERCK).

Developing solvent mixtures were either CHCl₃ : CH₃OH : acetic acid : water (80 : 9 : 12 : 2, v/v) or CHCl₃ : CH₃OH : NH₄OH (28%) (13 : 7 : 1, v/v). Separation was run to a height of 19 cm above the bottom. TLC plates were sprayed with primuline solution (0.01%, w/v in acetone : water 60 : 40, v/v) and visualized under UV light (365 nm). Major lipid constituents of thylakoid membranes, for example monogalactosyldiacylglycerol (MGDG), digalactosyldiacylglycerol (DGDG), sulfoquinovosyldiacylglycerol (SQDG) and phosphatidylglycerol (PG), were identified against known standards (Larodan, Malmo, Sweden).

Bands containing lipid classes were scraped and transferred to Teflon-lined screw-cap test tubes. Fifty microgram of pentadecanoic acid (C15:0) was added to each tube as an internal standard along with 0.5 mL of hexane and 1 mL of BF₃-CH₃OH (10% w/w), and the tube was flushed with nitrogen and incubated at 85 °C for 1 h. After cooling down to a room temperature, 0.5 mL of chloroform-extracted water was added and the solution was vortexed. Two millilitre of hexane was added, vortexed again and centrifuged at 2500 g for 5 min. Upper hexane layer was removed and placed in a new vial for evaporation. The remaining mixture was washed two times with 2 mL of hexane as described above. Collected hexane phases were pooled and concentrated under a stream of nitrogen to a final volume of 20 µL.

Quantitative and qualitative analysis was performed by means of GC-FID either on a Hewlett Packard HP6890 Series on sp2330 (30 m × 0.25 mm, df 0.20 µm; Supelco) or Carlo Erba HRGC 5300 megaserie on Omegawax 320 column (30 m × 0.32 mm, df 0.25 µm; Supelco). Hydrogen was used as a carrier gas at a pressure of 70 kPa. The temperature program in both cases was the following: start temperature of the oven was 140 °C, linear heating rate of 4.5 °C min⁻¹ was applied till 240 °C and held at this temperature for another 10 min. Injector temperature was 250 °C, and temperature of FID was 260 °C. Retention times of FAME were compared to known standards (Supelco® 37 Component FAME Mix and PUFA No.3 Supelco from menhaden oil).

DNA isolation

DNA was isolated from liquid culture of *C. cf. nivalis* Nedbalova strain CCALA 970 using DNeasy Plant Mini Kit (Qiagen). The protocol was slightly optimized: at the beginning of the procedure, the cells were mechanically disrupted by shaking for 5 min in the presence of glass beads (3 mm diameter; Sigma-Aldrich) in Mixer Mill MM 400 (Retsch, Haan, Germany). Subsequently, DNA was isolated in accordance with the manufacturer's recommended protocol. Quality and concentration of DNA

were measured on a NanoDrop® ND-1000 Spectrophotometer (NanoDrop Technologies, Inc.).

Amplification of gene coding D1 protein

The psbA gene region was amplified from the DNA isolate by PCR using primers psbA-F1 (ATGACTGCTACTT TAGAAAGACG) and psbA-R2 (TCATGCATWACTTC CATACCTA). The expected size of the PCR fragment was 1200 bp. The amplification reaction was performed using the following cycle parameters: 10 min hot start at 95 °C, followed by 35 cycles [1 min at 94 °C, 45 s at gradient of annealing temperature (57 and 59 °C), 2 : 50 min at 72 °C] and 10 min at 72 °C. Each 20 µL PCR reaction for this gene amplification contained 5 µL of DNA isolates (diluted to concentration of 10 ng µL⁻¹), 0.8 µL of each 10 µM primer, 1.6 µL of 25 mM MgCl₂, 1.5 µL of 2 mM dNTPs, 2 µL of 10× Taq buffer + KCl-MgCl₂, 7.8 µL sterile Milli-Q water and 0.5 µL of 1 U µL⁻¹ Taq DNA polymerase (Fermentas).

Alignment of gene coding D1 protein

Amino acid sequences of D1 protein were compared among *C. cf. nivalis* (this study, NCBI reference nucleotide sequence KF702330.1 and protein sequence AHB82278), *C. reinhardtii* (DAA00957.1), *Thermosynechococcus elongatus* (NP_682633.1), *Arabidopsis thaliana* (P83755.2), *Chlamydomonas raudensis* (AFU83031.1), *Dunaliella salina* (YP_005089831.1), *Acutodesmus obliquus* (ABD48259.1), *Chlorella vulgaris* (P56318.1), *Pyramimonas parkea* (ACJ71100.1), *Pycnococcus provasolii* (ACK36809.1), *Populus trichocarpa* (YP_001109480.1), *Cycas microcnesica* (ABU85314.1), *Magnolia grandiflora* (YP_007474516.1), *Oryza sativa* (AER12889.1), *Zea mays* (NP_043004.1), *Carica papaya* (YP_001671663.1), *Porphyridium purpureum* (BAO23682.1), *Cyanidium caldarium* (NP_045067.1), *Cyanophora paradoxa* (NP_043238.1), *Polarella glacialis* (BAC76007.1), *Kryptoperidinium foliaceum* (ADI40420.1), *Vaucheria litorea* (ACF70962.1), *Fucus vesiculosus* (CAX12449.1), *Nannochloropsis salina* (AGI99196.1), *Pinnularia cf. microstauron* (AER42084), *Ulnaria acus* (AEX37881.1), *Thalassiosira oceanica* (ADB27608.1), *Phaeocystis antarctica* (AEK26755.1), *Emiliana huxleyi* (AAX13814.1), *Geminigera cryophila* (ABL96289.1), *Rhodomonas salina* (ABO70840.1), *Eutreptiella gymnastica* (YP_006234198.1) and *Paulinella chromatophora* (ACB43269.1). Sequences were aligned with CLUSTALW (Higgins *et al.*, 1996) and BioEDIT (Ibis Biosciences, CA) software. Cluster analysis was based on the pairwise distance among amino acid sequences of D1 protein of species used in large alignment. Calculation of pairwise distances was carried out in MEGA 5.10 (Tamura *et al.*, 2011) with

following setting: method – number of differences, rates among sites – uniform, missing data treatment – complete deletion. Dendrogram was created in program PAST (Hammer *et al.*, 2001) with the settings: algorithm – Ward's method, similarity measure – Euclidean, number of bootstrap – 100.

Statistical analysis

We performed statistical comparisons with the two-sample *t*-test. A value of $P < 0.05$ was considered statistically significant. Error bars in all figures represent standard deviations of at least three independent measurements.

Results

Temperature dependence of growth

The growth of the snow alga *C. cf. nivalis* and the mesophilic *C. reinhardtii* was monitored under low light of $100 \mu\text{mol photons m}^{-2} \text{s}^{-1}$ at temperatures between 5 and 35 °C (Fig. 1). Surprisingly, the snow alga exhibits a rather slow growth at and below 5 °C (< 0.15 doubling per day) but keeps an invariant growth of 0.46 ± 0.06 doubling per day while grown above 10 °C (Fig. 1, open circles). The growth is suppressed only at temperatures > 30 °C falling by nearly 50% of the growth maximum at 35 °C. The mesophilic alga displayed almost no growth up to the temperature of 10 °C followed by a linear increase in its growth rate with raising temperature of incubation (Fig. 1, full circles). The growth rate peaked at 30 °C with 0.74 ± 0.05 doubling per day (1.6 times higher than the snow alga) and then dropped sharply. The mesophilic *C. reinhardtii* was outgrown by *C. cf. nivalis* in the whole range of temperatures from 5 °C up to 15 °C (*t*-test; $P < 0.05$), while both algae exhibited identical growth within the range of 20–25 °C.

Oxygen evolution rates

The photosynthetic oxygen-evolving activity from H_2O to CO_2 was measured at temperatures from 2 to 35 °C (Fig. 2). The snow alga *C. cf. nivalis* grown at 2.5 °C initially showed a drop in the activity below $100 \mu\text{mol O}_2 \text{ mg Chl}^{-1} \text{ h}^{-1}$ upon increasing the measurement temperature from 2 to 5 °C, followed by a linear increase in activity, peaking at 25–30 °C with $210 \pm 49 \mu\text{mol O}_2 \text{ mg Chl}^{-1} \text{ h}^{-1}$ (Fig. 2, open circles). A further increase in temperature leads to an abrupt decline of activity. No net oxygen evolution rate was observed at temperatures at and above 40 °C. Cells of the *C. cf. nivalis* grown for 72 h at 24 °C exhibit more stable temperature dependence of oxygen-evolving activity (Fig. 2, grey circles)

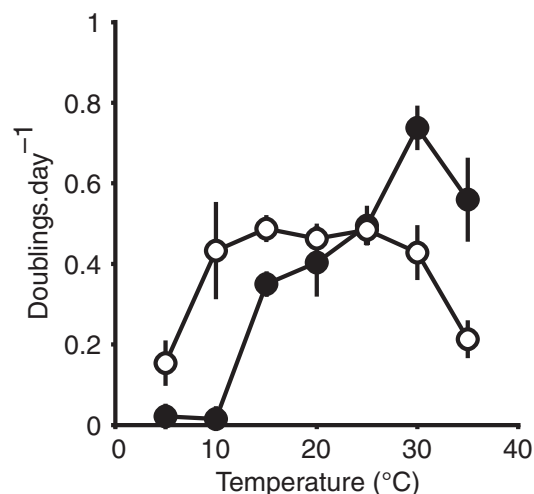


Fig. 1. Temperature dependence of autotrophic growth. Liquid cultures were incubated at the designated temperatures at illumination of $100 \mu\text{mol photons m}^{-2} \text{s}^{-1}$ and their growth was assayed by measurements of total chlorophyll content. The plot of temperature vs. the rate of doubling of the cell culture is shown in the snow alga *Chlamydomonas cf. nivalis* (open circles) and in the mesophilic *Chlamydomonas reinhardtii* (closed circles). Values represent mean of three independent measurements.

with significantly lower maximum activity than cells grown at 2.5 °C (*t*-test; $P < 0.03$ in the range of 25–35 °C). The control strain *C. reinhardtii* grown at 24 °C had significantly lower oxygen-evolving activity at temperatures from 2 up to 20 °C (Fig. 2, closed circles, *t*-test;

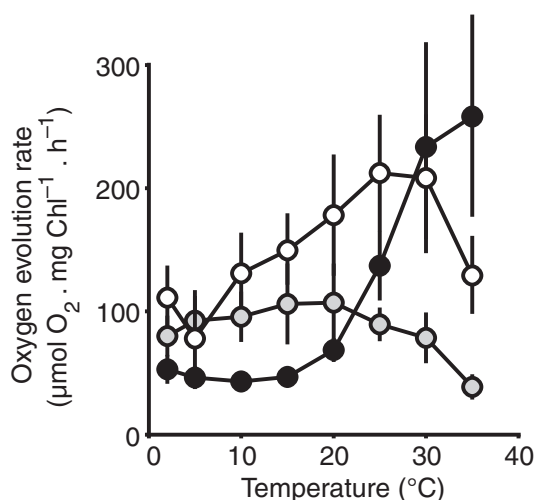


Fig. 2. Temperature dependence of oxygen evolution rate. The measurements were performed in the range from 2 to 35 °C at saturating light intensity of $2000 \mu\text{mol photons m}^{-2} \text{s}^{-1}$ with liquid cultures grown at 5 °C (*Chlamydomonas cf. nivalis*, open circles) and 24 °C (*Chlamydomonas reinhardtii*, closed circles; *C. cf. nivalis*, grey circles). Values represent mean of five independent measurements.

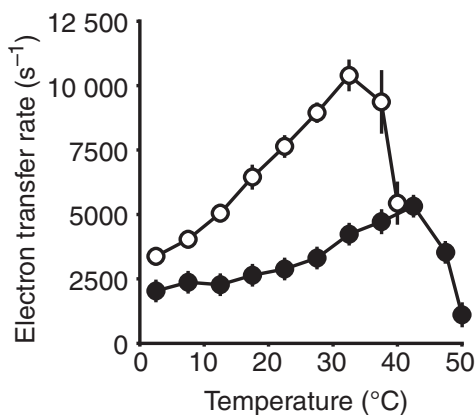


Fig. 3. Temperature dependence of electron transfer rate from Q_A^- to Q_B . Least squares numerical fitting of the chlorophyll fluorescence decay following single-turnover saturating flash yielded the rate constant for the electron transfer rate in the snow alga *Chlamydomonas cf. nivalis* (open circles) and in the mesophilic *Chlamydomonas reinhardtii* (closed circles). Values represent mean of seven independent measurements.

$P < 0.03$). The activity started to rise exponentially only at and above 20 °C while reaching $233 \pm 96 \mu\text{mol O}_2 \text{ mg Chl}^{-1} \text{ h}^{-1}$ at 30 °C. Additional temperature increase further stimulated the oxygen-evolving activity in contrast to the snow alga grown at 2.5 °C.

Q_A to Q_B electron transfer rates

Functional stability of PSII was assayed by measurements of electron transfer between the quinon Q_A bound in the D2 protein and Q_B (Fig. 3) that is transiently bound to the membrane accessible pocket of the D1 protein of the PSII reaction centre. In the mesophilic *C. reinhardtii*, the Q_A to Q_B electron transfer rate started at a value 2000 s^{-1} at 0 °C and was thermally accelerated up to $c. 5300 \text{ s}^{-1}$ at 42.5 °C (Fig. 3, closed circles). A further increase in temperature led to a decrease in the electron transfer rate with a loss of activity close to 50 °C (Fig. 3, closed circles). In contrast to the mesophilic strain, the snow alga *C. cf. nivalis* exhibits significantly higher Q_A to Q_B electron transfer rate at any measured temperature except at 40 °C (Fig. 3, open circles, t -test; $P < 0.001$). At 0 °C, the electron transfer rate reached $c. 3000 \text{ s}^{-1}$ and continued to rise exponentially up to $11\,000 \text{ s}^{-1}$ at 35 °C followed by a sudden drop to half of its maximal value at 40 °C (Fig. 3, open circles). The dissimilar trends in the rates' temperature dependence are shaped by the different activation parameters for the electron transfer rate in the two algae. The activation enthalpy ΔH^\ddagger in *C. cf. nivalis* had a value of $12.29 \text{ kJ mol}^{-1}$, while in *C. reinhardtii*, ΔH^\ddagger was lower by 4.78 kJ mol^{-1} . The activation entropy

$T\Delta S^\ddagger$ was 5.87 kJ mol^{-1} higher in the snow alga than in the mesophilic *C. reinhardtii*. In result, the Gibbs free energy of activation $\Delta G^\ddagger = \Delta H^\ddagger - T\Delta S^\ddagger$ was lower by 1.07 kJ mol^{-1} in *C. cf. nivalis* ($25.53 \text{ kJ mol}^{-1}$) in comparison with 26.6 kJ mol^{-1} in *C. reinhardtii*.

Fluorescence temperature curve

The critical temperature above which the PSII begins to denature, T_C and the maximal temperature of fluorescence rise, T_M parameters serve as indicators of PSII thermostability. Either of the parameters may also reflect on the change in thylakoid membrane fluidity during thermal acclimation. The T_C and T_M parameters were obtained by least squares numerical fitting of the fluorescence temperature curves measured in cell cultures acclimated for 3 days at the temperatures ranging from 5 to 25 °C (Fig. S2). Neither of the two parameters changed significantly in the *C. cf. nivalis* acclimated to temperatures from 5 to 25 °C (Fig. S2, open circles, Pearson's correlation; $R < 0.3$, $n = 14$). The value of $M/F(30)$ which reflects inhibition and/or damage to PSII decreased from 2.96 at 5 °C to 2.08 at 20 °C. The mesophilic *C. reinhardtii* showed a steady increase in both T_C and T_M by > 4 °C in response to the acclimation to a higher temperature (Fig. S2, closed circles). A similar trend was observed in $M/F(30)$ where a shift from 5 to 20 °C increased the $M/F(30)$ from 1.9 to 2.6.

Thylakoid lipid composition

The two *Chlamydomonas* species differed significantly in molar fractions of their thylakoid membrane lipid classes (Fig. 4, t -test; $P < 0.03$). PG was by far the most abundant lipid in the snow alga *C. cf. nivalis* regardless of the incubation temperature (Fig. 4a). Cells acclimated to temperatures from 10 to 35 °C contained at least 70 molar% of PG with the only exception of cells that

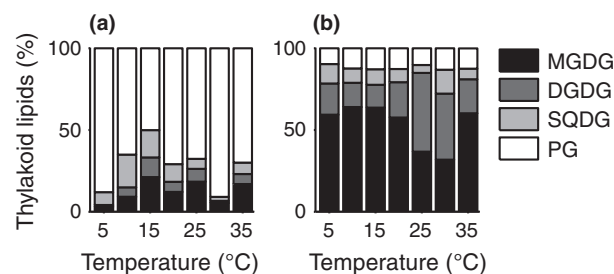


Fig. 4. Lipid composition of thylakoid membranes. Lipids were extracted from membranes of cells acclimated for 72 h to the designated temperatures in the range of 5–35 °C. (a) *Chlamydomonas cf. nivalis*, (b) *Chlamydomonas reinhardtii*. Values represent mean of three independent experiments.

were grown at 15 °C. Here, the molar ratio of PG dropped down to 50%. Interestingly, cells grown at 5 and 30 °C contained over 90 molar% of PG out of all lipids in the thylakoid membrane. The analysis of the mesophilic *C. reinhardtii* revealed a lipid content typically found in green algae and higher plants chloroplasts (Fig. 4b). Here, a dominant component of the thylakoid membrane of the mesophilic alga acclimated to the temperature range of 5–20 °C was MGDG representing *c.* 60% of all lipids. DGDG accounted for *c.* 20 molar% resulting in MGDG/DGDG ratios ranging from 2.6 at 20 °C, 2.9 at 35 °C and as high as 4.5 at 10 and 15 °C. This sharply contrasts with the lipid molar fractions in cells acclimated to temperatures that are considered optimal for the mesophilic strain. As molar fractions of DGDG in the membrane increased within the range of 25–30 °C, the MGDG/DGDG ratio decreased to 0.76–0.78. The molar fractions of the minor lipid constituents of the thylakoid membrane such as the PG and sulphoquinovosyldiacylglycerol (SQDG) were found nearly constant in a whole temperature scale both standing at or below the 10 molar %. The lowest amounts of SQDG were observed at 25 °C.

Fatty acid composition

Lipids isolated from the thylakoid membranes and separated by TLC were subjected to transmethylation, and the resulting fatty acid methyl esters corresponding to the four major lipid classes were analysed. The fatty acid content was normalized to their contributions in each lipid class summing up to 100%. The most dominant lipid species in the snow alga *C. cf. nivalis*, PG (Fig. S3), was predominantly palmitic (16:0), oleic (18:1) and α -linolenic (18:3) fatty acids. The palmitic acid of the PG was found constant (*c.* 10%) at all temperatures of acclimation, while its total amount was elevated in the range of 15–25 °C due to an increase in its content in the MGDG and SQDG. By far, the most dominant oleic acid in the PG decreased from 50% at 5 °C down to 15–20% at 15–25 °C and increased again to 55% at 30 °C. These changes were slightly compensated by an increase in the oleic acid content in the MGDG and SQDG in the range of 15–25 °C. The α -linolenic acid content shows a mirror image of its trends in PG vs. MGDG and SQDG. While its content is decreasing in PG from 20% at 5 °C down to 10% at 10–15 °C and increasing again up to *c.* 30% at 20–35 °C, the MGDG is enriched by the α -linolenic acid in the range 15–25 °C, resulting in the α -linolenic acid exceeding 40 molar% of all thylakoid fatty acids at 20–25 °C. The minor fatty acids namely the hexadecatetraenoic (16:4), hexadecatrienoic (16:3) and palmitoleic (16:1) acids remained under 10 molar% at all tempera-

tures of acclimation except for the linoleic acid (18:2) that increased to *c.* 15% at 25 °C.

A very different composition of fatty acids was observed in the mesophilic *C. reinhardtii* (Fig. S4). Palmitic acid (16:0) almost equally represented by PG, SQDG and DGDG was found always at total levels of 30% except for 30 °C where it accounted for 50% of all fatty acids in the thylakoid membranes. Similar trend was observed in the palmitoleic acid (16:1) although presented at significantly lower levels (10% throughout all the temperatures except for 25% at 30 °C). The remaining diversity of the fatty acid profiles was to the largest extent shaped by the MGDG. The hexadecatetraenoic acid (16:4) was present at levels of 30% in the temperature range of 5–15 °C, and then its content gradually decreased to 15% at 25–30 °C and then slightly increased to 20% at 35 °C. The α -linolenic fatty acid (18:3) followed a similar trend being present at amounts > 40% at temperatures 5–15 °C and then slowly decreasing to *c.* 20% at 35 °C.

The double bond index (DBI) that is indicative of relative fatty acid unsaturation reached in *C. cf. nivalis* its maximum value of 1.9 at 20 °C, while at both low and high temperatures, the values declined to 1.3–1.6. In *C. reinhardtii*, maximum values of DBI (2.6–2.7) were reached at temperatures 5–15 °C and then steadily decreased to 1.9 at 30 °C followed by an increase to 2.3 at 35 °C. The DBI was higher in *C. reinhardtii* than in *C. cf. nivalis* at any acclimation temperature due to the increased content of hexadecatetraenoic and α -linolenic fatty acids.

Sequence of D1 protein

The protein sequence alignment showed that the 323 amino acids of D1 protein of *C. cf. nivalis* differ in 33 amino acids from the *C. reinhardtii*, while only 29 amino acids were different from the higher plant sequence of *A. thaliana* (Fig. 5). The alignment containing all sequences of D1 protein is shown in Supporting Information (Fig. S5). The stromal N terminus of the snow alga's D1 protein contains six changes (N10S, S11I, A15E, E19S, I36L, C40T) in comparison with the control *C. reinhardtii* strain's D1 protein. Two changes are found at the luminal side of the A helix (V47C, F48Y), six small amino acids are exchanged for even smaller ones in the luminal AB loop (S68A, T79S, T85S, L91V, I96V, L102V), followed by four changes in the B helix (C117L, Y124A, C125S and F135Y) and two at the stromal edge of the C helix (A144F, Y147F). The CD helix carries a single change (I184L) just as the D helix (L200A). The stromal DE loop has five differences in sequence between the two *Chlamydomonas* strains: T228S, N230V, A233T, E235Y,



Fig. 5. D1 protein alignment. The psbA amino acid sequence of *Chlamydomonas cf. nivalis* was aligned against psbA sequences of *Chlamydomonas reinhardtii*, *Arabidopsis thaliana* and *Thermosynechococcus elongatus* (psbA1 gene sequence).

R238K. The DE helix has identical sequence in all four aligned sequences of D1 protein. The remaining differences were found within the E helix (S270A, I281V, F285L and L290V) and the C terminus of the D1 protein (L314I, N325D). Within the context of all aligned D1

sequences (Fig. S5), it becomes evident that the majority of the reported changes between the D1 protein sequence of snow alga and the control *C. reinhardtii* occur in extremophilic organisms other than green algae and higher plants (Fig. S6).

Discussion

Temperature is a fundamental factor that affects growth rate, physiological and metabolic processes in algae (Eppley, 1985; Raven & Geider, 1988; Beardall & Raven, 2004; Chu *et al.*, 2005; Staehr & Birkeland, 2006). It also appears to be one of the main factors that dictate the distribution of photosynthetic microorganisms (Pakker *et al.*, 1995; Hoffmann, 1996; Bischoff-Baermann *et al.*, 1997). It has been generally assumed that the photosynthetic organisms occupying habitats where temperatures fluctuate little, typically sites with extremely low or high temperatures, do not possess the ability to acclimate far outside of their optimum growth temperature. Representative examples of extremophiles that have not been observed to successfully colonize other habitats include the well-known cyanobacteria exclusively inhabiting hot springs (Miller & Castenholz, 2000) or green algae forming visible biomass within surface layers of melting snow (Hoham *et al.*, 2008). Questions still remain concerning the response of the photosynthesis and growth of the cryophiles to a significant shift in ambient temperatures and their capacity to grow outside their indigenous territory.

Snow algae from the genera *Chloromonas* and *Chlamydomonas* were considered to be obligate cryophiles with optimal growth below 10 °C (Hoham, 1975a). Low temperature growth optima were reported, for example for *Chloromonas pichinchae* (1 °C; Hoham, 1975a), *Chloromonas chenangoensis*, *Chloromonas tughillensis* (2.5–5 °C; Hoham *et al.*, 2008), *C. raudensis* (8 °C; Pocock *et al.*, 2011) and *Chlamydomonas* sp. (5 °C; Eddie *et al.*, 2008). Strains with higher temperature limits that can still be assumed as cryotolerants were described in isolates from Antarctic oases (Seaburg *et al.*, 1981). The optimal growth for *Chlamydomonas subcaudata* and *Chlamydomonas alpina* was reported in the range of 12.5–15 °C, while the one for *Chlamydomonas intermedia* is slightly higher (15–18 °C). Concerning the widely distributed *C. nivalis*, contrasting results were obtained due to the lack of laboratory cultures and taxonomic uncertainty (Hoham, 1975a; Komárek & Nedbalová, 2007). Great variability of *in situ* maximal photosynthetic activity was demonstrated among samples collected in the Beartooth Mountains on the Montana-Wyoming boundary (USA; Mosser *et al.*, 1977). No inhibition of photosynthesis at temperatures up to 20 °C was observed in short-term experiments with natural samples containing *C. nivalis* red cysts (Remias *et al.*, 2005, 2010b). The results of our comprehensive study including temperature dependence of growth, rate of photosynthesis including the electron transport within PSII and the whole electron transfer chain from H₂O to CO₂ are clearly indicating that our strain of red snow-forming *C. cf. nivalis* cannot be

regarded as cryophilic but rather a cryotolerant species with very good photosynthetic performance at low temperatures. Moreover, our analysis of control samples taken from cells grown for 3, 5 and 10 days showed that all the changes in the fatty acid content occurred within a time span shorter than 3 days. This fact documents cells' potential to quickly acclimate their fatty acid composition regardless of the temperature outside its growth optimum (Fig. S1).

What molecular mechanisms are employed to yield the snow alga this rather broad thermal tolerance? It is important to note that our strain of *C. nivalis* acclimated to 2.5 °C exhibits significantly faster growth (at 5–15 °C) and oxygen evolution rate (at 5–20 °C) in comparison with the mesophilic control. Oxygen evolution rates of the snow alga surpass the mesophilic control within the range of 5 to *c.* 20 °C even when the two strains were pregrown at identical temperature of 24 °C. The important role of lipids as mediators of thermal acclimation of membrane proteins (Domonkos *et al.*, 2008), particularly the degree of fatty acid unsaturation (Gombos *et al.*, 1994; Wada *et al.*, 1994), has been recognized for decades. Photosynthetic membranes of cyanobacteria, algae and plants are unique for their richness in glycolipids dominated by galactolipids MGDG and DGDG, followed by sulfolipid SQDG. PG carrying a negative charge makes up, as the only glycerophospholipid, for 9% of all thylakoid lipids in green alga *C. reinhardtii* (Janero & Barrnett, 1981). Numerous physiological functions were reported for the PG (reviewed in Sato, 2004; Loll *et al.*, 2007) that include mediation of the protein–lipid interface within the membrane (Szalontai *et al.*, 2003; Domonkos *et al.*, 2008; Guskov *et al.*, 2009), control of membrane's surface charge (Apostolova *et al.*, 2008), mediation of electron flow in and stabilization of photosystem I (PSI; Rawlyer & Siegenthaler, 1981; Yang *et al.*, 2005), stabilization of PSII and trimeric light-harvesting complex 2 (LHCII; El Maanni *et al.*, 1998; Dubertret *et al.*, 2002), mediation of PSII assembly in *C. reinhardtii* (Pineau *et al.*, 2004) and PSII activity (Sato *et al.*, 2000) in *Synechocystis* sp. PCC6803 (Laczko-Dobos *et al.*, 2008), particularly at the lumenal face of the thylakoid membrane of spinach chloroplasts (Duchene *et al.*, 2000), indispensable role in stabilization of the Q_B binding site in PSII of *Synechocystis* sp. PCC6803 (Gombos *et al.*, 2002) and development of thylakoid membranes in *A. thaliana* (Hagio *et al.*, 2002). So far, the investigation of the function of PG in photosynthesis has relied on targeted elimination of the PG molecules by either downregulation of enzymes responsible for PG synthesis in whole cells and/or by treatment of isolated thylakoid membranes with phospholipase *in vitro*. Upregulation of the PG synthesis was studied only in *C. reinhardtii* subjected to sulphur starvation (Sugimoto

et al., 2008). Here, we have adopted a reverse strategy by examining cells of the snow alga *C. cf. nivalis* that have thylakoid membranes in their chloroplasts dominated by over 80% PG. We have put particular emphasis on the detailed study of the temperature dependence of the electron transport at the acceptor side of PSII that is expected to be mostly affected by the absence of PG and hence might be also perturbed by its overabundance.

All strains of cyanobacteria, algae and higher plants examined to date showed the temperature dependence of the Q_A to Q_B electron transfer rate following an analogous trend (Shlyk-Kerner *et al.*, 2006; Dinamarca *et al.*, 2011). First, the rate of electron transfer gets accelerated, up to a temperature that corresponds to, and/or is close to the growth optimum. This activation phase is then followed by an activationless regime of a various widths spanning from not more than 5–10 °C up to as much as 20–25 °C. Here, electron transfer becomes rate limited by the coupled proton mobilization. The third phase corresponds with the onset of denaturation and is characterized by a steep decline both in rate as well as the amplitude of the electron transfer. Here, we report the temperature dependence of the Q_A to Q_B electron transfer rate in a snow alga *C. cf. nivalis* that completely lacks the activationless regime as the electron transfer rate ideally obeys the Arrhenius law. The rate at temperatures close to 0 °C equals the peak rates of cyanobacteria, algae and higher plants at their respective activationless regimes, while the peak rate at 35 °C exceeds any previously reported rate of Q_A to Q_B electron transfer by 4-fold to 10-fold. This trend differs from the typical temperature dependence due to the different thermodynamics of the electron transfer in the snow alga. The higher activation enthalpy in comparison with the mesophile is unfavourable as it decreases the reaction turnover at low temperatures representing the natural environment of *C. cf. nivalis*. This effect is sufficiently compensated by more positive activation entropy that is achieved by the increase in local flexibility of the transition state for the Q_A to Q_B electron transfer. As a consequence, this compensation leads to the acceleration of the reaction rate to nonphysiologically high values at 35 °C counterbalancing the negative effect of the activation enthalpy. The necessary flexibility can be made possible through a number of structural elements, including, but not limited to, the unique lipid composition of the thylakoid membrane and the D1 protein structure. Here, we propose to rule out a dominant role of fatty acids to gain the additional PSII flexibility. The lipids in the snow alga's thylakoid membrane had a lower DBI in all experimental treatments compared to the control. Based on the fatty acids themselves alone, *C. reinhardtii* always displayed a more flexible membrane. To add to the controversy, the role of PG,

particularly its high-melting point form, was disputed as a possible factor in modulating membrane flexibility and hence the chilling resistance in higher plant chloroplasts (Kaniuga *et al.*, 1998). Yet PG is an essential lipid that was found in close vicinity of the Q_B binding pocket in crystals of PSII of thermophilic cyanobacterium (reviewed in Mizusawa & Wada, 2012). We also cannot ignore the fact that membranes dominated by PG exhibit, at neutral pH, considerable negative surface charge density inducing a tilt of PG molecules of *c.* 30° relative to the membrane normal (Watts *et al.*, 1981). This can introduce a significant disorder to the membrane packing and hence increase membrane fluidity.

Most of the differences in the D1 protein of the snow alga are situated in the interhelical domains of both lumen (AB)- and stroma (DE)-exposed loops. Fifteen amino acids in the snow algal D1 protein (in comparison to the control *C. reinhardtii*) are smaller in size yet of a similar chemical nature, while four represent neutral changes. The most common exchange included three counts of L – I, V – L, S – T and Y – F, followed by two counts of V – I and A – S. Only six of 33 changes instituted amino acid residues with significantly larger volume and different chemical nature (e.g. A15E, A144F, A233T, E235Y). Two of the latter are part of the DE loop, while two changes within the same region bring about smaller amino acids (T228S, R238K). Interestingly, mutation at some of these sites in the DE loop and the sites that either surround or are close to the Q_B binding pocket were reported to have a lower binding affinity to the herbicide diuron (D1–228), ioxynil (D1–238; Kless *et al.*, 1994) or atrazine (D1–238) (Narusaka *et al.*, 1998) in mutants of cyanobacterium *Synechocystis* sp. PCC6803 while having minor effect on its saturated rate of O₂ evolution or yield of chlorophyll fluorescence. Similarly, change in the amino acid at the D1–184 site within the lumenal CD loop has been reported to alter the structure in the vicinity of the quinon binding site as seen in a metribuzin-resistant mutant of *Chenopodium rubrum* (Schwenger-Erger *et al.*, 1999). This evidence must, however, be regarded as circumstantial as most of the aforementioned cyanobacterial mutants carried in fact double or even triple mutations within the same region and sometimes also a different amino acid.

Here, we present a hypothesis that a combination of changes in protein structure and an unusually high abundance of charged lipids modulate the electron transfer rate in PSII allowing for fast transfer of electrons from Q_A to Q_B even at low or close to cryophilic temperatures. The structural flexibility that is the necessary prerequisite for the electron transfer at the acceptor side of PSII is probably made possible by the cumulative effect of the amino acid changes in the D1 protein combined with the physico-

chemical characteristics of the PG thylakoid membrane including possible substitution of MGDG, DGDG and SQDG lipids by the PG in places around and within the PSII (Loll *et al.*, 2007; Mizusawa & Wada, 2012). It seems, however, highly unlikely that the increased rate of terminal electron transfer in PSII that is even orders of magnitude faster than necessary for the capacity of plastoquinol pool to be reoxidized is the only factor responsible for the increased carbon fixation efficiency at low temperatures as inferred from our measurements of oxygen evolution capacity reporting on H₂O to CO₂ electron transfer in the snow alga. We assume that the handicap of the catalytic activity of Ribulose-1,5-bisphosphate carboxylase oxygenase and its activase being greatly lowered at low temperatures is alleviated by their increased expression and accumulation akin to the Antarctic *Chloromonas* species (Devos *et al.*, 1998). Despite the numerous uncertainties, we present here a host of novel information about the strategies employed by cold-tolerating green alga *C. cf. nivalis* including the outline of some of the molecular mechanisms that make this tolerance possible.

Acknowledgements

This work has been supported by Algatech (CZ.1.05/2.1.00/03.0110) and GAJU (143/2013/P) projects (ML, DK). The authors greatly acknowledge the methodical assistance of Jiří Kopecký in gas chromatography analyses and are grateful to Jason Dean for critical reading of the manuscript. The authors declare no competing financial interests.

Authors' contribution

M.L. and L.P. contributed equally to this work.

References

- Apostolova EL, Domonkos I, Dobrikova AG, Sallai A, Boqos B, Wada H, Gombos Z & Taneva SG (2008) Effect of phosphatidylglycerol depletion on the surface electric properties and the fluorescence emission of thylakoid membranes. *J Photochem Photobiol B* **91**: 51–57.
- Beardall J & Raven JA (2004) The potential effects of global climate change on microalgal photosynthesis, growth and ecology. *Phycologia* **43**: 26–40.
- Bidigare RR, Ondrusek ME, Kennicutt MC, Iturriaga R, Harvey HR, Hoham RW & Macko SA (1993) Evidence for a photoprotective function for secondary carotenoids of snow algae. *J Phycol* **29**: 427–434.
- Bischoff-Baermann B, Bartsch I, Xia B & Wiencke C (1997) Temperature responses of macroalgae from the tropical island Hainan (P.R. China). *Phycological Res* **45**: 91–104.
- Chu WL, Wong CY, Teoh ML & Phang SM (2005) Response and adaptation of algae to the changing global environment. *Algae Culture Collections and the Environment* (Kasai F, Kaya K & Watanabe MM, eds), pp. 177–195. Tokai University Press, Kanagawa.
- Chua NH & Bennoun P (1975) Thylakoid membrane polypeptides of *Chlamydomonas reinhardtii*: wild-type and mutant strains deficient in photosystem 2 reaction center. *P Natl Acad Sci USA* **72**: 2175–2179.
- Devos N, Ingouff M, Loppes R & Matagne RF (1998) Rubisco adaptation to low temperatures: a comparative study in psychrophilic and mesophilic unicellular algae. *J Phycol* **34**: 655–660.
- Dinamarca J, Shlyk O, Kaftan D, Goldberg E, Dulebo A, Gidekel M, Gutierrez A & Scherz A (2011) Double mutation in photosystem II reaction centers and elevated CO₂ grant thermotolerance to mesophilic cyanobacterium. *PLoS ONE* **6**: e28389.
- Domonkos I, Laczko-Dobos H & Gombos Z (2008) Lipid-assisted protein-protein interactions that support photosynthetic and other cellular activities. *Prog Lipid Res* **47**: 422–435.
- Dubertret G, Gerard-Hirne C & Tremolieres A (2002) Importance of trans-Delta(3)-hexadecenoic acid containing phosphatidylglycerol in the formation of the trimeric light-harvesting complex in *Chlamydomonas*. *Plant Physiol Biochem* **40**: 829–836.
- Duchene S, Smutny J & Siegenthaler PA (2000) The topology of phosphatidylglycerol populations is essential for sustaining photosynthetic electron flow activities in thylakoid membranes. *Biochim Biophys Acta* **1463**: 115–120.
- Eddie B, Krembs C & Neuer S (2008) Characterization and growth response to temperature and salinity of psychrophilic, halotolerant *Chlamydomonas* sp ARC isolated from Chukchi Sea ice. *Mar Ecol Prog Ser* **354**: 107–117.
- El Maanni A, Dubertret G, Delrieu MJ, Roche O & Tremolieres A (1998) Mutants of *Chlamydomonas reinhardtii* affected in phosphatidylglycerol metabolism and thylakoid biogenesis. *Plant Physiol Biochem* **36**: 609–619.
- Eppley RW (1985) Temperature and phytoplankton growth in the sea. *CC/Agr Biol Environ* **37**: 20.
- Gombos Z, Wada H, Hideg E & Murata N (1994) The unsaturation of membrane-lipids stabilizes photosynthesis against heat-stress. *Plant Physiol* **104**: 563–567.
- Gombos Z, Varkonyi Z, Hagio M, Iwaki M, Kovacs L, Masamoto K, Itoh S & Wada H (2002) Phosphatidylglycerol requirement for the function of electron acceptor plastoquinone Q(B) in the photosystem II reaction center. *Biochemistry* **41**: 3796–3802.
- Guskov A, Kern J, Gabdulkhakov A, Broser M, Zouni A & Saenger W (2009) Cyanobacterial photosystem II at 2.9-Å resolution and the role of quinones, lipids, channels and chloride. *Nat Struct Mol Biol* **16**: 334–342.
- Hagio M, Sakurai I, Sato S, Kato T, Tabata S & Wada H (2002) Phosphatidylglycerol is essential for the development

- of thylakoid membranes in *Arabidopsis thaliana*. *Plant Cell Physiol* **43**: 1456–1464.
- Hammer R, Harper DAT & Ryan PD (2001) PAST: paleontological statistics software package for education and data analysis. *Palaeontol Electronica* **4**: 9. Available at: <http://folk.uio.no/ohammer/past/>.
- Higgins DG, Thompson JD & Gibson TJ (1996) Using CLUSTAL for multiple sequence alignments. *Methods Enzymol* **266**: 383–402.
- Hoffmann L (1996) Geographic distribution of freshwater blue-green algae. *Hydrobiologia* **336**: 33–40.
- Hoham RW (1975a) Environmental factors pertaining to developmental stages in snow alga, *Chloromonas pichincae*. *J Phycol* **11**: 21.
- Hoham RW (1975b) The life history and ecology of the snow alga *Chloromonas pichincae* (Chlorophyta, Volvocales). *Phycologia* **14**: 213–226.
- Hoham RW (1975c) Optimum temperatures and temperature ranges for growth of snow algae. *Arct Antarct Alp Res* **7**: 13–24.
- Hoham RW & Duval B (2001) Microbial ecology of snow and freshwater ice with emphasis on snow algae. *Snow Ecology: An Interdisciplinary Examination of Snow Covered Ecosystem* (Jones HG, Pomeroy JW, Walker DA & Hoham RW, eds), pp. 166–226. Cambridge University Press, Cambridge, UK.
- Hoham RW, Frey FM, Mohn WW, Felio JH, Todd S, Duncan JE & Banghart JB (2008) Optimum growth temperatures of three species of green *Chloromonas* snow algae from Upstate New York and the White Mountains, Arizona. *Arct Antarct Alp Res* **40**: 355–363.
- Janero DR & Barnett RJ (1981) Cellular and thylakoid-membrane species of phosphatidylglycerol in *Chlamydomonas reinhardtii* 137+. *J Lipid Res* **22**: 1126–1130.
- Kaniuga Z, Saczynska V & Miskiewicz E (1998) Galactolipase activity but not the level of high-melting-point phosphatidylglycerol is related to chilling tolerance in differentially sensitive *Zea mays* inbred lines. *Plant Cell Rep* **17**: 897–901.
- Kless H, Oren-Shamir M, Malkin S, McIntosh L & Edelman M (1994) The D-E region of the D1 protein is involved in multiple quinone and herbicide interactions in photosystem II. *Biochemistry* **33**: 10501–10507.
- Komárek J & Nedbalová L (2007) Green cryosestic algae. *Algae and Cyanobacteria in Extreme Environments* (Seckbach J, ed.), pp. 321–342. Springer, Dordrecht.
- Laczko-Dobos H, Ughy B, Toth SZ, Komenda J, Zsiros O, Domonkos I, Parducz A, Bogos B, Komura M & Itoh S (2008) Role of phosphatidylglycerol in the function and assembly of photosystem II reaction center, studied in a *cdsA*-inactivated PAL mutant strain of *Synechocystis* sp. PCC6803 that lacks phycobilisomes. *Biochim Biophys Acta* **1777**: 1184–1194.
- Lazar D & Ilik P (1997) High-temperature induced chlorophyll fluorescence changes in barley leaves – comparison of the critical temperatures determined from fluorescence induction and from fluorescence temperature curve. *Plant Sci* **124**: 159–164.
- Leya T, Rahn A, Lutz C & Remias D (2009) Response of arctic snow and permafrost algae to high light and nitrogen stress by changes in pigment composition and applied aspects for biotechnology. *FEMS Microbiol Ecol* **67**: 432–443.
- Lichtenthaler H & Wellburn A (1983) Determinations of total carotenoids and chlorophylls *a* and *b* of leaf extracts in different solvents. *Biochem Soc T* **11**: 591–592.
- Loll B, Kern J, Saenger W, Zouni A & Biesiadka J (2007) Lipids in photosystem II: interactions with protein and cofactors. *Biochim Biophys Acta* **1767**: 509–519.
- Matsuzaki R, Hara Y & Nozaki H (2012) A taxonomic revision of *Chloromonas reticulata* (Volvocales, Chlorophyceae), the type species of the genus *Chloromonas*, based on multigene phylogeny and comparative light and electron microscopy. *Phycologia* **51**: 74–85.
- Miller SR & Castenholz RW (2000) Evolution of thermotolerance in hot spring cyanobacteria of the genus *Synechococcus*. *Appl Environ Microbiol* **66**: 4222–4229.
- Mizusawa N & Wada H (2012) The role of lipids in photosystem II. *Biochim Biophys Acta* **1817**: 194–208.
- Morris GJ, Coulson G & Clarke A (1979) Cryopreservation of *Chlamydomonas*. *Cryobiology* **16**: 401–410.
- Mosser JL, Mosser AG & Brock TD (1977) Photosynthesis in snow alga *Chlamydomonas nivalis* (Chlorophyceae). *J Phycol* **13**: 22–27.
- Narusaka Y, Narusaka M, Kobayashi H & Satoh K (1998) The herbicide-resistant species of the cyanobacterial D1 protein obtained by thorough and random *in vitro* mutagenesis. *Plant Cell Physiol* **39**: 620–626.
- Nedbalova L, Stuchlik E & Strunecky O (2006) Phytoplankton of a mountain lake (L'adove pleso, the Tatra Mountains, Slovakia): seasonal development and first indications of a response to decreased acid deposition. *Biologia* **61**: S91–S100.
- Pakker H, Breeman AM, Vanreine WFP & Vandenhoeck C (1995) A comparative study of temperature responses of Caribbean seaweeds from different biogeographic groups. *J Phycol* **31**: 499–507.
- Pineau B, Girard-Bascou J, Eberhard S, Choquet Y, Tremolieres A, Gerard-Hirne C, Bennardo-Connan A, Decottignies P, Gillet S & Wollman FA (2004) A single mutation that causes phosphatidylglycerol deficiency impairs synthesis of photosystem II cores in *Chlamydomonas reinhardtii*. *Eur J Biochem* **271**: 329–338.
- Pocock T, Vetterli A & Falk S (2011) Evidence for phenotypic plasticity in the Antarctic extremophile *Chlamydomonas raudensis* Ettl. UWO 241. *J Exp Bot* **62**: 1169–1177.
- Raven JA & Geider RJ (1988) Temperature and algal growth. *New Phytol* **110**: 441–461.
- Rawlyer A & Siegenthaler PA (1981) Regulation of photosystem-I electron flow activity by phosphatidylglycerol

- in thylakoid membranes as revealed by phospholipase treatment. *Biochim Biophys Acta* **638**: 30–39.
- Remias D, Lutz-Meindl U & Lutz C (2005) Photosynthesis, pigments and ultrastructure of the alpine snow alga *Chlamydomonas nivalis*. *Eur J Phycol* **40**: 259–268.
- Remias D, Albert A & Lutz C (2010a) Effects of realistically simulated, elevated UV irradiation on photosynthesis and pigment composition of the alpine snow alga *Chlamydomonas nivalis* and the arctic soil alga *Tetracystis* sp. (Chlorophyceae). *Photosynthetica* **48**: 269–277.
- Remias D, Karsten U, Lutz C & Leya T (2010b) Physiological and morphological processes in the Alpine snow alga *Chloromonas nivalis* (Chlorophyceae) during cyst formation. *Protoplasma* **243**: 73–86.
- Rezanka T, Nedbalova L & Sigler K (2008) Unusual medium-chain polyunsaturated fatty acids from the snow alga *Chloromonas brevispina*. *Microbiol Res* **163**: 373–379.
- Sato N (2004) Roles of the acidic lipids sulfoquinovosyl diacylglycerol and phosphatidylglycerol in photosynthesis: their specificity and evolution. *J Plant Res* **117**: 495–505.
- Sato N, Hagio M, Wada H & Tsuzuki M (2000) Requirement of phosphatidylglycerol for photosynthetic function in thylakoid membranes. *P Natl Acad Sci USA* **97**: 10655–10660.
- Schwenger-Erger C, Bohnisch N & Barz W (1999) A new psbA mutation yielding an amino-acid exchange at the lumen-exposed site of the D1 protein. *Z Naturforsch C* **54**: 909–914.
- Seaburg KG, Parker BC, Wharton RA & Simmons GM (1981) Temperature-growth responses of algal isolates from Antarctic oases. *J Phycol* **17**: 353–360.
- Shlyk-Kerner O, Samish I, Kaftan D, Holland N, Sai PS, Kless H & Scherz A (2006) Protein flexibility acclimatizes photosynthetic energy conversion to the ambient temperature. *Nature* **442**: 827–830.
- Spijkerman E, Wacker A, Weithoff E & Leya T (2008) Elemental and fatty acid composition of snow algae in Arctic habitats. *Front Microbiol* **3**: 380.
- Staehr PA & Birkeland MJ (2006) Temperature acclimation of growth, photosynthesis and respiration in two mesophilic phytoplankton species. *Phycologia* **45**: 648–656.
- Stibal M, Elster J, Sabacka M & Kastovska K (2007) Seasonal and diel changes in photosynthetic activity of the snow alga *Chlamydomonas nivalis* (Chlorophyceae) from Svalbard determined by pulse amplitude modulation fluorometry. *FEMS Microbiol Ecol* **59**: 265–273.
- Sugimoto K, Midorikawa T, Tsuzuki M & Sato N (2008) Upregulation of PG synthesis on sulfur-starvation for PSI in *Chlamydomonas*. *Biochem Biophys Res Commun* **369**: 660–665.
- Szalontai B, Kota Z, Nonaka H & Murata N (2003) Structural consequences of genetically engineered saturation of the fatty acids of phosphatidylglycerol in tobacco thylakoid membranes. An FTIR study. *Biochemistry* **42**: 4292–4299.
- Tamura K, Peterson D, Peterson N, Stecher G, Nei M & Kumar S (2011) MEGA5: molecular evolutionary genetics analysis using maximum likelihood, evolutionary distance, and maximum parsimony methods. *Mol Biol Evol* **28**: 2731–2739.
- Wada H, Gombos Z & Murata N (1994) Contribution of membrane lipids to the ability of the photosynthetic machinery to tolerate temperature stress. *P Natl Acad Sci USA* **91**: 4273–4277.
- Watts A, Harlos K & Marsh D (1981) Charge-induced tilt in ordered-phase phosphatidylglycerol bilayers – evidence from X-Ray-diffraction. *Biochim Biophys Acta* **645**: 91–96.
- Yang Z, Su X, Wu F, Gong Y & Kuang T (2005) Photochemical activities of plant photosystem I particles reconstituted into phosphatidylglycerol liposomes. *J Photochem Photobiol B* **78**: 125–134.

Supporting Information

Additional Supporting Information may be found in the online version of this article:

Fig. S1. Time course of fatty acid composition in thylakoid lipids extracted from *C. reinhardtii* and *C. cf. nivalis*.

Fig. S2. Temperature dependence of critical temperature (T_c) and maximal temperature of fluorescence rise (T_M) in the snow alga *C. cf. nivalis* and in the mesophilic *C. reinhardtii*.

Fig. S3. Fatty acid content in MGDG, DGDG, SQDG and PG isolated from thylakoid membranes of snow alga *C. cf. nivalis* in the temperature range from 5 to 35 °C.

Fig. S4. Fatty acid content MGDG, DGDG, SQDG and PG isolated from thylakoid membranes of control green alga *C. reinhardtii* in the temperature range from 5 to 35 °C.

Fig. S5. Multiple sequence alignment of amino acid sequence translated from psbA gene coding for D1 protein isolated from *C. cf. nivalis* with 33 corresponding sequences representing all major groups of oxygenic photosynthetic organisms.

Fig. S6. Dendrogram of amino acid sequences coding for D1 protein of *C. cf. nivalis* and species representing all major groups of oxygenic photosynthetic organisms, based on pairwise distances.

1 **Temperature dependence of photosynthesis and thylakoid lipid**
2 **composition in the red snow alga *Chlamydomonas cf. nivalis***
3 **(Chlorophyceae)**

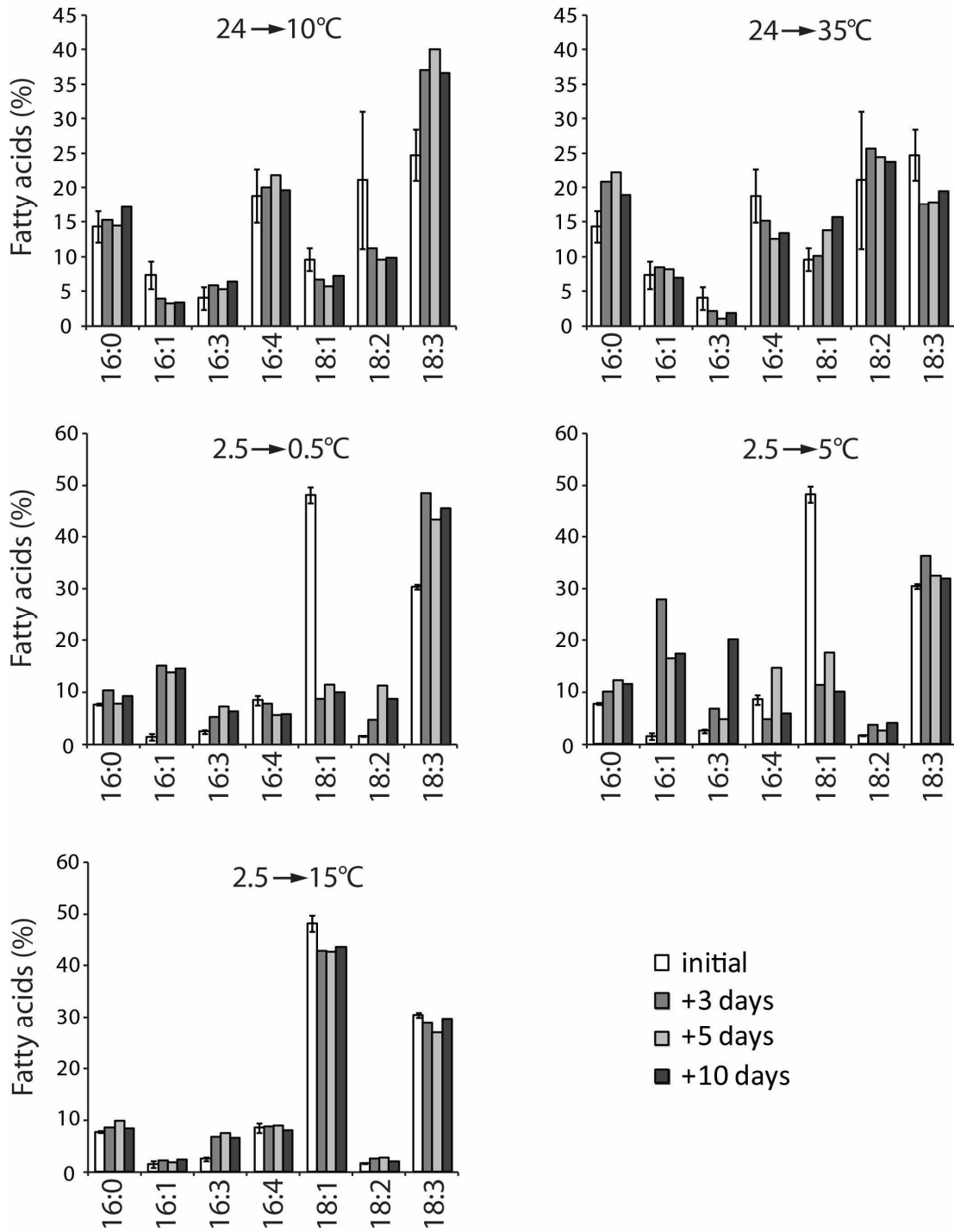
4
5 Martin Lukeš^{1,2,*}, Lenka Procházková^{3,*}, Volha Shmidt¹, Linda Nedbalová³ & David Kaftan^{1,2}
6
7

8 ¹University of South Bohemia in České Budějovice, Faculty of Science, Branišovská 31, 37005 České
9 Budějovice, Czech Republic; ²Institute of Microbiology CAS, Opatovický mlýn, 37981 Třeboň, Czech
10 Republic, ³Charles University in Prague, Faculty of Science, Department of Ecology, Viničná 7,
11 12844 Prague, Czech Republic
12
13

14 *These authors contributed equally to the study.
15
16
17
18

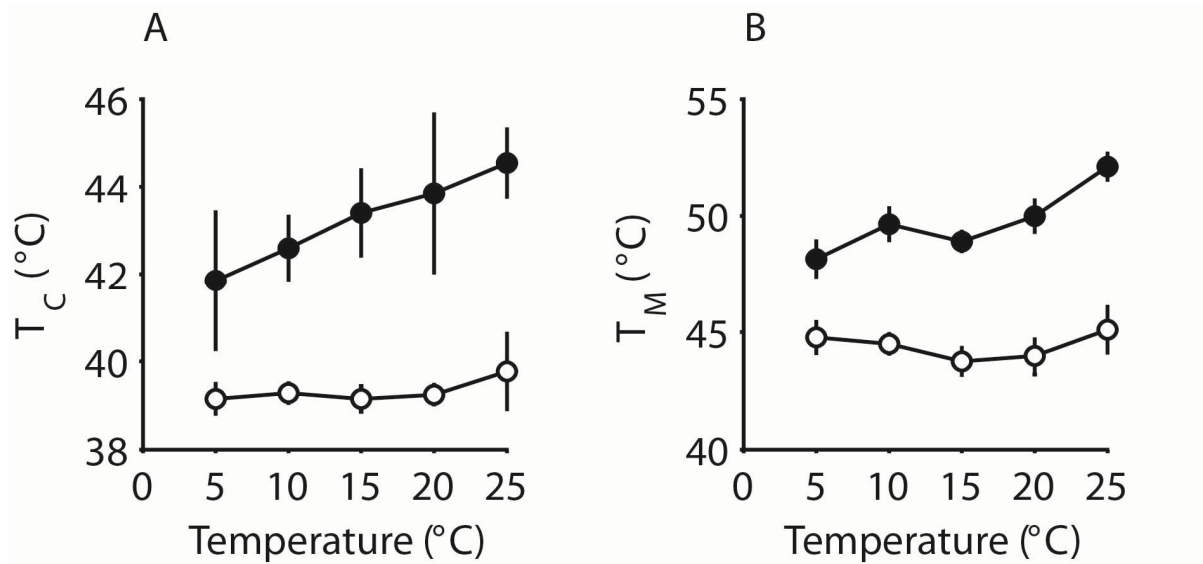
19 **Supplementary Material**

20
21 The following supplementary information includes Figures S1-S6
22
23
24
25
26
27
28
29
30
31
32
33
34
35



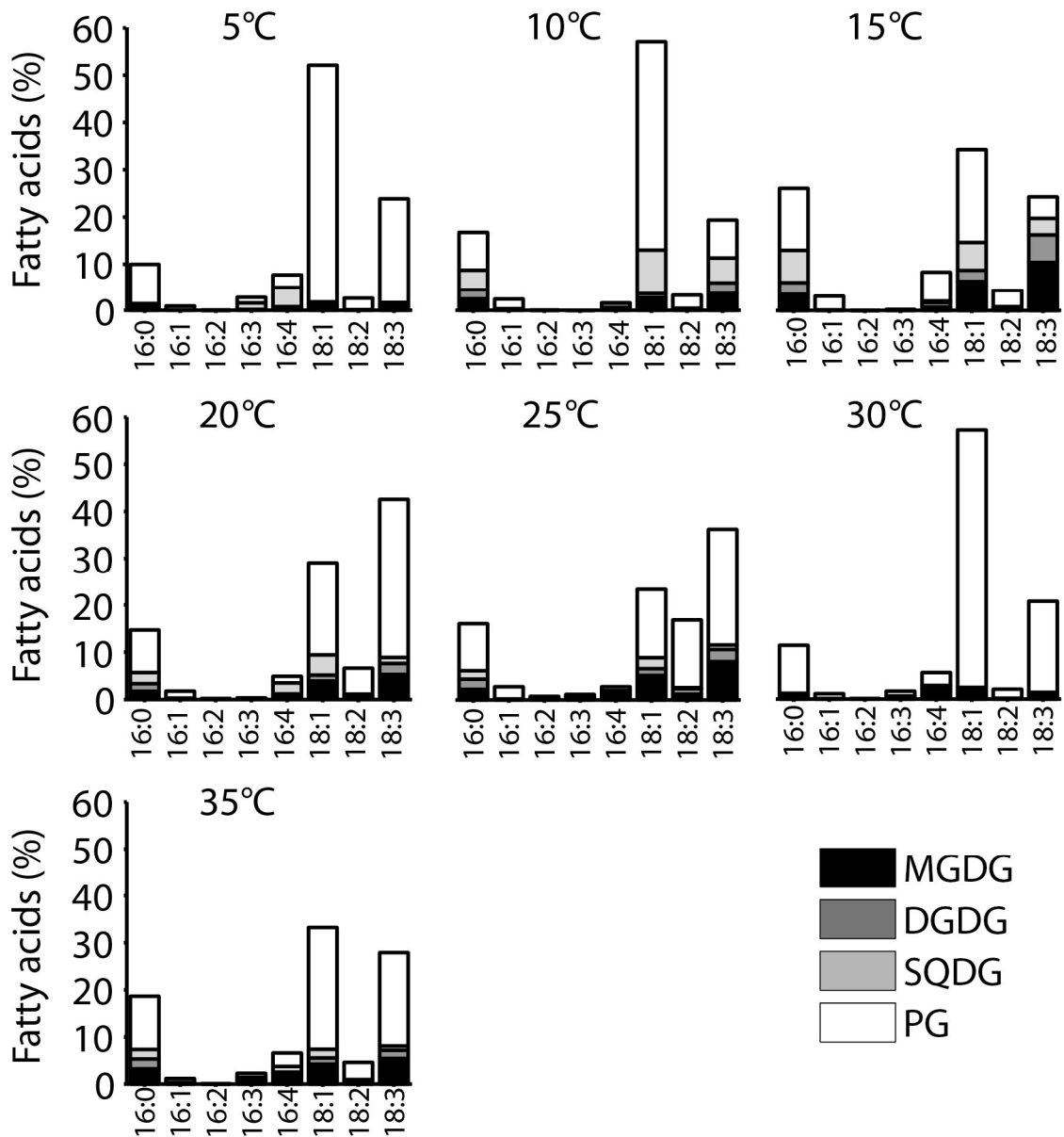
36
37

38 **Figure S1.** Time course of fatty acid composition in thylakoid lipids extracted from *C.*
39 *reinhardtii* (top panels) and *C. cf. nivalis* (middle and lower panels). Initial levels correspond
40 to cells in their mid exponential growth phase (24°C in *C. reinhardtii*; 2.5°C in *C. cf. nivalis*).
41 Following samples were taken after 3, 5, and 10 days after the cells were transferred to either
42 higher or lower temperature. Error bars in the initial level represent standard deviation of
43 three independent measurements.



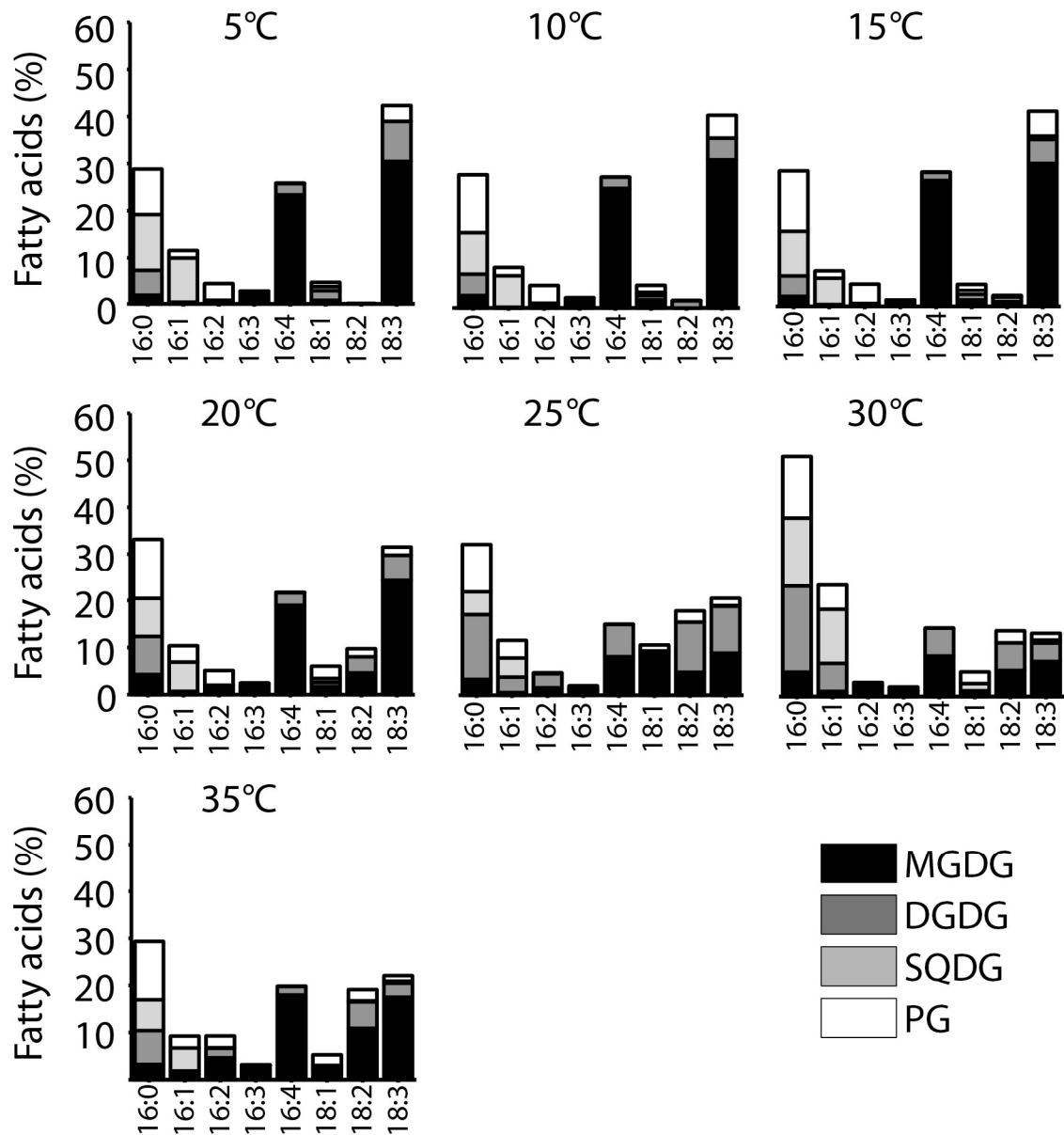
44
45
46
47
48
49
50
51
52
53
54
55
56
57
58
59
60
61
62
63
64
65
66
67

Figure S2. Temperature dependence of A: critical temperature (T_c) and B: maximal temperature of fluorescence rise (T_M) in the snow alga *Chlamydomonas cf. nivalis* (open circles) and in the mesophilic *Chlamydomonas reinhardtii* (closed circles). Values represent mean of three independent measurements.



68
69
70
71
72
73
74
75
76
77
78
79

Figure S3. Fatty acid content in monogalactosyldiacylglycerol (MGDG, black), digalactosyldiacylglycerol (DGDG, dark gray), sulphoquinovosyldiacylglycerol (SQDG, light gray) and phosphatidylglycerol (white) isolated from thylakoid membranes of snow alga *Chlamydomonas cf. nivalis* in the temperature range from 5 to 35°C. Values represent mean of three independent measurements.



80
81
82
83
84
85
86
87
88
89
90
91

Figure S4. Fatty acid content in monogalactosyldiacylglycerol (MGDG, black), digalactosyldiacylglycerol (DGDG, dark gray), sulphoquinovosyldiacylglycerol (SQDG, light gray) and phosphatidylglycerol (white) isolated from thylakoid membranes of control green alga *Chlamydomonas reinhardtii* in the temperature range from 5 to 35°C. Values represent mean of three independent measurements.

	10	20	30	40	50
<i>Chlam_cf_nivalis</i>	-	-	-	-	-
<i>Chlam_reinhardtii</i>	M	T	A	I	L
<i>Therm_elongatus</i>	M	T	T	T	L
<i>Arabid_thaliana</i>	M	T	A	I	L
<i>Chlam_raudensis</i>	M	T	A	I	L
<i>Dunaliel_salina</i>	M	T	A	I	L
<i>Acutodesmus_obl</i>	M	T	A	I	L
<i>Chlorella_vulg</i>	M	T	A	I	L
<i>Pyramimonas_par</i>	M	T	A	T	L
<i>Pycnococcus_pro</i>	M	T	A	I	L
<i>Populus_trichoc</i>	M	T	A	I	L
<i>Cycas_micronesi</i>	M	T	A	I	L
<i>Magnolia_grandi</i>	M	T	A	I	L
<i>Oryza_sativa</i>	M	T	A	I	L
<i>Zea_mays</i>	M	T	A	I	L
<i>Carica_papaya</i>	M	T	A	I	L
<i>Porphyridium_purp</i>	M	T	A	T	L
<i>Cyanidium_caldari</i>	M	T	V	T	L
<i>Cyanophora_parad</i>	M	T	A	T	L
<i>Polarella_glacial</i>	-	-	-	-	-
<i>Kryptoperid_folia</i>	M	T	A	T	L
<i>Vaucheria_litor</i>	M	T	A	T	L
<i>Fucus_vesiculosus</i>	M	V	A	T	L
<i>Nannochlorop_sal</i>	M	T	A	T	L
<i>Pinnularia_cf_mi</i>	-	-	-	-	-
<i>Ulnaria_acus</i>	M	T	A	T	L
<i>Thalassio_oceani</i>	M	I	A	T	L
<i>Phaeocyst_antarct</i>	M	T	T	T	L
<i>Emiliana_huxleyi</i>	M	T	T	T	L
<i>Geminig_cryophila</i>	-	-	-	-	-
<i>Rhodomonas_salina</i>	M	T	A	T	L
<i>Eutreptiella_gymn</i>	M	T	A	T	L
<i>Paulinella_chroma</i>	M	T	T	T	L

	60	70	80	90	100
<i>Chlam_cf_nivalis</i>	A	F	I	A	A
<i>Chlam_reinhardtii</i>	A	F	I	A	A
<i>Therm_elongatus</i>	A	F	I	A	A
<i>Arabid_thaliana</i>	A	F	I	A	A
<i>Chlam_raudensis</i>	A	F	I	A	A
<i>Dunaliel_salina</i>	A	F	I	A	A
<i>Acutodesmus_obl</i>	A	F	I	A	A
<i>Chlorella_vulg</i>	A	F	I	A	A
<i>Pyramimonas_par</i>	A	F	I	A	A
<i>Pycnococcus_pro</i>	A	F	I	A	A
<i>Populus_trichoc</i>	A	F	I	A	A
<i>Cycas_micronesi</i>	A	F	I	A	A
<i>Magnolia_grandi</i>	A	F	I	A	A
<i>Oryza_sativa</i>	A	F	I	A	A
<i>Zea_mays</i>	A	F	I	A	A
<i>Carica_papaya</i>	A	F	I	A	A
<i>Porphyridium_purp</i>	A	F	V	A	A
<i>Cyanidium_caldari</i>	A	F	I	A	A
<i>Cyanophora_parad</i>	A	F	V	A	A
<i>Polarella_glacial</i>	A	F	I	F	A
<i>Kryptoperid_folia</i>	A	F	I	A	A
<i>Vaucheria_litor</i>	A	F	I	A	A
<i>Fucus_vesiculosus</i>	A	F	I	A	A
<i>Nannochlorop_sal</i>	A	F	I	A	A
<i>Pinnularia_cf_mi</i>	A	F	I	A	A
<i>Ulnaria_acus</i>	A	F	I	A	A
<i>Thalassio_oceani</i>	A	F	I	A	A
<i>Phaeocyst_antarct</i>	A	F	I	A	A
<i>Emiliana_huxleyi</i>	A	F	I	A	A
<i>Geminig_cryophila</i>	-	-	-	-	-
<i>Rhodomonas_salina</i>	A	F	I	A	A
<i>Eutreptiella_gymn</i>	A	F	I	A	A
<i>Paulinella_chroma</i>	A	F	I	A	A

	110	120	130	140	150																																												
<i>Chlam_cf_nivalis</i>	S	V	D	E	W	L	N	G	G	P	Y	Q	L	I	V	L	H	F	L	L	G	V	A	S	M	G	R	E	W	E	L	S	Y	R	L	G	M	R	P	W	I	F	V	A	F	S	A	P	
<i>Chlam_reinhardtii</i>	S	L	D	E	W	L	N	G	G	P	Y	Q	L	I	V	C	H	F	L	L	G	V	Y	C	M	G	R	E	W	E	L	S	F	R	L	G	M	R	P	W	I	A	V	A	Y	S	A	P	
<i>Therm_elongatus</i>	S	L	D	E	W	L	N	G	G	P	Y	Q	L	I	I	F	H	F	L	L	G	A	S	C	M	G	R	Q	W	E	L	S	Y	R	L	G	M	R	P	W	I	C	V	A	Y	S	A	P	
<i>Arabid_thaliana</i>	S	V	D	E	W	L	N	G	G	P	Y	E	L	I	V	L	H	F	L	L	G	V	A	C	M	G	R	E	W	E	L	S	F	R	L	G	M	R	P	W	I	A	V	A	Y	S	A	P	
<i>Chlam_raudensis</i>	S	L	D	E	W	L	N	G	G	P	Y	Q	L	I	V	C	H	F	L	L	G	V	I	C	C	M	G	R	E	W	E	L	S	F	R	L	G	M	R	P	W	I	A	V	A	Y	S	A	P
<i>Dunaliel_salina</i>	S	L	D	E	W	L	N	G	G	P	Y	Q	L	V	V	C	H	F	L	L	G	V	C	C	M	G	R	E	W	E	L	S	Y	R	L	G	M	R	P	W	I	A	V	A	Y	S	A	P	
<i>Acutodesmus_obl</i>	S	L	D	E	W	L	N	G	G	P	Y	Q	L	I	V	C	H	F	L	L	G	I	C	C	M	G	R	E	W	E	L	S	Y	R	L	G	M	R	P	W	I	A	V	A	Y	S	A	P	
<i>Chlorella_vulg</i>	S	L	D	E	W	L	N	G	G	P	Y	Q	L	I	V	C	H	F	L	L	G	I	C	S	M	G	R	E	W	E	L	S	F	R	L	G	M	R	P	W	I	A	V	A	Y	S	A	P	
<i>Pyramimonas_par</i>	S	L	D	E	W	L	N	G	G	P	Y	Q	L	I	V	C	H	F	L	L	G	I	C	C	M	G	R	E	W	E	L	S	Y	R	L	G	M	R	P	W	I	A	V	A	Y	S	A	P	
<i>Pycnococcus_pro</i>	S	V	D	E	W	L	N	G	G	P	Y	L	M	V	V	C	H	F	L	L	G	V	C	C	M	G	R	E	W	E	L	S	F	R	L	G	M	R	P	W	I	A	V	A	Y	S	A	P	
<i>Populus_trichoc</i>	S	V	D	E	W	L	N	G	G	P	Y	E	L	I	V	L	H	F	L	L	G	V	A	C	M	G	R	E	W	E	L	S	F	R	L	G	M	R	P	W	I	A	V	A	Y	S	A	P	
<i>Cycas_micronesi</i>	S	V	D	E	W	L	N	G	G	P	Y	E	L	I	V	L	H	F	L	L	G	V	A	C	M	G	R	E	W	E	L	S	F	R	L	G	M	R	P	W	I	A	V	A	Y	S	A	P	
<i>Magnolia_grandi</i>	S	V	D	E	W	L	N	G	G	P	Y	E	L	I	V	L	H	F	L	L	G	V	A	C	M	G	R	E	W	E	L	S	F	R	L	G	M	R	P	W	I	A	V	A	Y	S	A	P	
<i>Oryza_sativa</i>	S	V	D	E	W	L	N	G	G	P	Y	E	L	I	V	L	H	F	L	L	G	V	A	C	M	G	R	E	W	E	L	S	F	R	L	G	M	R	P	W	I	A	V	A	Y	S	A	P	
<i>Zea_mays</i>	S	V	D	E	W	L	N	G	G	P	Y	E	L	I	V	L	H	F	L	L	G	V	A	C	M	G	R	E	W	E	L	S	F	R	L	G	M	R	P	W	I	A	V	A	Y	S	A	P	
<i>Carica_papaya</i>	S	V	D	E	W	L	N	G	G	P	Y	E	L	I	V	L	H	F	L	L	G	V	A	C	M	G	R	E	W	E	L	S	F	R	L	G	M	R	P	W	I	A	V	A	Y	S	A	P	
<i>Porphyridium_purp</i>	S	L	D	E	W	L	N	G	G	P	Y	G	L	I	V	L	H	F	L	L	G	V	A	C	M	G	R	E	W	E	L	S	Y	R	L	G	M	R	P	W	I	A	V	A	F	S	A	P	
<i>Cyanidium_caldari</i>	S	L	D	E	W	L	N	G	G	P	Y	Q	L	V	V	L	H	F	L	L	G	V	A	A	M	G	R	E	W	E	L	S	Y	R	L	G	M	R	P	W	I	C	V	A	F	S	A	P	
<i>Cyanophora_parad</i>	S	L	D	E	W	L	N	G	G	P	Y	Q	F	V	M	H	F	L	L	G	V	A	C	M	G	R	E	W	E	L	S	F	R	L	G	M	R	P	W	I	A	V	A	Y	S	A	P		
<i>Polarella_glacial</i>	G	F	D	E	W	L	N	G	G	T	Y	Q	F	V	V	L	H	F	L	L	G	V	C	W	M	G	R	E	W	E	L	S	F	R	L	G	M	R	P	W	I	F	V	A	F	S	A	P	
<i>Kryptoperid_folia</i>	S	I	D	E	W	L	N	G	G	P	Y	Q	L	I	V	L	H	F	L	L	G	V	A	A	M	G	R	E	W	E	L	S	Y	R	L	G	M	R	P	W	I	F	V	A	F	S	A	P	
<i>Vaucheria_litor</i>	S	V	D	E	W	L	N	G	G	P	Y	Q	L	I	V	L	H	F	L	L	G	V	A	S	M	G	R	E	W	E	L	S	Y	R	L	G	M	R	P	W	I	F	V	A	F	S	A	P	
<i>Fucus_vesiculosus</i>	S	I	E	E	W	L	N	G	G	P	Y	Q	L	V	V	F	H	F	L	L	G	V	A	C	W	M	G	R	E	W	E	L	S	Y	R	L	G	M	R	P	W	I	F	V	A	F	S	A	P
<i>Nannochlorop_sal</i>	S	V	D	E	W	L	N	G	G	P	Y	Q	L	V	V	L	H	F	L	L	G	V	A	C	M	G	R	E	W	E	L	S	Y	R	L	G	M	R	P	W	I	F	V	A	F	S	A	P	
<i>Pinnularia_cf_mi</i>	S	I	D	E	W	L	N	G	G	P	Y	Q	L	I	V	L	H	F	L	L	G	V	A	S	M	G	R	E	W	E	L	S	Y	R	L	G	M	R	P	W	I	F	V	A	F	S	A	P	
<i>Ulnaria_acus</i>	S	I	D	E	W	L	N	G	G	P	Y	Q	L	I	V	C	H	F	L	L	G	V	A	A	M	G	R	E	W	E	L	S	Y	R	L	G	M	R	P	W	I	F	V	A	F	S	A	P	
<i>Thalassio_oceani</i>	S	V	D	E	W	L	N	G	G	P	Y	Q	L	I	V	L	H	F	L	L	G	V	A	S	M	G	R	E	W	E	L	S	Y	R	L	G	M	R	P	W	I	F	V	A	F	S	A	P	
<i>Phaeocyst_antarct</i>	S	I	D	E	W	L	N	G	G	P	Y	Q	L	V	V	F	H	F	L	L	G	V	C	A	I	G	R	E	W	E	L	S	Y	R	L	G	M	R	P	W	I	C	V	A	F	S	A	P	
<i>Emiliana_huxleyi</i>	S	I	D	E	W	L	N	G	G	T	Y	Q	L	V	V	L	H	F	L	L	G	V	C	A	I	G	R	E	W	E	L	S	Y	R	L	G	M	R	P	W	I	C	V	A	F	S	A	P	
<i>Geminig_cryophila</i>	S	L	D	E	W	L	N	G	G	P	Y	Q	L	I	V	D	H	F	L	L	G	V	C	W	I	G	R	E	W	E	L	S	Y	R	L	G	M	R	P	W	I	F	V	A	F	T	A	P	
<i>Rhodomonas_salina</i>	S	L	D	E	W	L	N	G	G	P	Y	Q	L	I	V	D	H	F	L	L	G	V	C	W	I	G	R	E	W	E	L	S	Y	R	L	G	M	R	P	W	I	S	V	A	F	T	A	P	
<i>Eutreptiella_gymn</i>	S	L	D	E	W	L	N	G	G	P	Y	Q	L	I	V	C	H	F	L	L	G	V	C	S	M	G	R	E	W	E	L	S	F	R	L	G	M	R	P	W	I	A	V	A	Y	S	A	P	
<i>Paulinella_chroma</i>	S	L	D	E	W	L	N	G	G	P	Y	Q	L	V	V	F	H	F	L	L	G	I	F	C	M	G	R	E	W	E	L	S	Y	R	L	G	M	R	P	W	I	C	V	A	Y	S	A	P	

	160	170	180	190	200																																													
<i>Chlam_cf_nivalis</i>	V	A	A	S	A	V	F	L	V	Y	P	I	G	Q	G	S	F	S	D	G	M	P	L	G	I	S	G	T	F	N	F	M	L	V	F	Q	A	E	H	N	I	L	M	H	P	F	H	M	A	
<i>Chlam_reinhardtii</i>	V	A	A	S	A	V	F	L	V	Y	P	I	G	Q	G	S	F	S	D	G	M	P	L	G	I	S	G	T	F	N	F	M	I	V	F	Q	A	E	H	N	I	L	M	H	P	F	H	M	L	
<i>Therm_elongatus</i>	L	A	S	A	F	A	V	F	L	I	Y	P	I	G	Q	G	S	F	S	D	G	M	P	L	G	I	S	G	T	F	N	F	M	I	V	F	Q	A	E	H	N	I	L	M	H	P	F	H	Q	L
<i>Arabid_thaliana</i>	V	A	A	A	T	A	V	F	L	I	Y	P	I	G	Q	G	S	F	S	D	G	M	P	L	G	I	S	G	T	F	N	F	M	I	V	F	Q	A	E	H	N	I	L	M	H	P	F	H	M	L
<i>Chlam_raudensis</i>	V	A	A	A	T	A	V	F	L	I	Y	P	I	G	Q	G	S	F	S	D	G	M	P	L	G	I	S	G	T	F	N	F	M	I	V	F	Q	A	E	H	N	I	L	M	H	P	F	H	M	L
<i>Dunaliel_salina</i>	V	A	A	A	T	A	V	F	L	I	Y	P	I	G	Q	G	S	F	S	D	G	M	P	L	G	I	S	G	T	F	N	F	M	I	V	F	Q	A	E	H	N	I	L	M	H	P	F	H	M	F
<i>Acutodesmus_obl</i>	V	A	A	A	T	A	V	F	L	I	Y	P	I	G	Q	G	S	F	S	D	G	M	P	L	G	I	S	G	T	F	N	F	M	I	V	F	Q	A	E	H	N	I	L	M	H	P	F	H	M	L
<i>Chlorella_vulg</i>	V	A	A	A	T	A	V	F	L	I	Y	P	I	G	Q	G	S	F	S	D	G	M	P	L	G	I	S	G	T	F	N	F	M	I	V	F	Q	A	E	H	N	I	L	M	H	P	F	H	M	L
<i>Pyramimonas_par</i>	V	A	A	A	T	A	V	F	L	I	Y	P	I	G	Q	G	S	F	S	D	G	M	P	L	G	I	S	G	T	F	N	F	M	I	V	F	Q	A	E	H	N	I	L	M	H	P	F	H	M	L
<i>Pycnococcus_pro</i>	V	A	A	A	T	A	V	F	L	I	Y	P	I	G	Q	G	S	F	S	D	G	M	P	L	G	I	S	G	T	F	N	F	M	I	V	F	Q	A	E	H	N	I	L	M	H	P	F	H	M	L
<i>Populus_trichoc</i>	V	A	A	A	T	A	V	F	L	I	Y	P	I	G	Q	G	S	F	S	D	G	M	P	L	G	I	S	G	T	F	N	F	M	I	V	F	Q	A	E	H	N	I	L	M	H	P	F	H	M	L
<i>Cycas_micronesi</i>	V	A	A	A	T	A	V	F	L	I	Y	P	I	G	Q	G	S	F	S	D	G	M	P	L	G	I	S	G	T	F	N	F	M	I	V	F	Q	A	E	H	N	I	L	M	H	P	F	H	M	L
<i>Magnolia_grandi</i>	V	A	A	A	T	A	V	F	L	I	Y	P	I	G	Q	G	S	F	S	D	G	M	P	L	G	I	S																							

	210	220	230	240	250																																													
<i>Chlam_cf_nivalis</i>	G	V	A	G	V	F	G	G	S	L	F	S	A	M	H	G	S	L	V	T	S	S	L	I	R	E	T	S	E	V	E	S	T	N	Y	G	Y	K	F	G	Q	E	E	E	T	Y	N	I	V	A
<i>Chlam_reinhardtii</i>	G	V	A	G	V	F	G	G	S	L	F	S	A	M	H	G	S	L	V	T	S	S	L	I	R	E	T	T	E	N	E	S	A	N	E	G	Y	R	F	G	Q	E	E	E	T	Y	N	I	V	A
<i>Therm_elongatus</i>	G	V	A	G	V	F	G	G	A	L	F	G	A	M	H	G	S	L	V	T	S	S	L	I	R	E	T	T	E	T	E	S	A	N	Y	G	Y	K	F	G	Q	E	E	E	T	Y	N	I	V	A
<i>Arabid_thaliana</i>	G	V	A	G	V	F	G	G	S	L	F	S	A	M	H	G	S	L	V	T	S	S	L	I	R	E	T	T	E	N	E	S	A	N	E	G	Y	R	F	G	Q	E	E	E	T	Y	N	I	V	A
<i>Chlam_raudensis</i>	G	V	A	G	V	F	G	G	S	L	F	S	A	M	H	G	S	L	V	T	S	S	L	I	R	E	T	T	E	N	E	S	A	N	E	G	Y	R	F	G	Q	E	E	E	T	Y	N	I	V	A
<i>Dunaliel_salina</i>	G	V	A	G	V	F	G	G	S	L	F	S	A	M	H	G	S	L	V	T	S	S	L	I	R	E	T	T	E	N	E	S	A	N	E	G	Y	K	F	G	Q	E	E	E	T	Y	N	I	V	A
<i>Acutodesmus_obl</i>	G	V	A	G	V	F	G	G	S	L	F	S	A	M	H	G	S	L	V	T	S	S	L	I	R	E	T	T	E	N	E	S	A	N	E	G	Y	K	F	G	Q	E	E	E	T	Y	N	I	V	A
<i>Chlorella_vulg</i>	G	V	A	G	V	F	G	G	S	L	F	S	A	M	H	G	S	L	V	T	S	S	L	I	R	E	T	T	E	N	E	S	A	N	E	G	Y	K	F	G	Q	E	E	E	T	Y	N	I	V	A
<i>Pyramimonas_par</i>	G	V	A	G	V	F	G	G	S	L	F	S	A	M	H	G	S	L	V	T	S	S	L	I	R	E	T	T	E	N	E	S	A	N	E	G	Y	K	F	G	Q	E	E	E	T	Y	N	I	V	A
<i>Pycnococcus_pro</i>	G	V	A	G	V	F	G	G	S	L	F	S	A	M	H	G	S	L	V	T	S	S	L	I	R	E	T	T	E	N	E	S	A	N	E	G	Y	K	F	G	Q	E	E	E	T	Y	N	I	V	A
<i>Populus_trichoc</i>	G	V	A	G	V	F	G	G	S	L	F	S	A	M	H	G	S	L	V	T	S	S	L	I	R	E	T	T	E	N	E	S	A	N	E	G	Y	R	F	G	Q	E	E	E	T	Y	N	I	V	A
<i>Cycas_micronesi</i>	G	V	A	G	V	F	G	G	S	L	F	S	A	M	H	G	S	L	V	T	S	S	L	I	R	E	T	T	E	N	E	S	A	N	E	G	Y	K	F	G	Q	E	E	E	T	Y	N	I	V	A
<i>Magnolia_grandi</i>	G	V	A	G	V	F	G	G	S	L	F	S	A	M	H	G	S	L	V	T	S	S	L	I	R	E	T	T	E	N	E	S	A	N	E	G	Y	R	F	G	Q	E	E	E	T	Y	N	I	V	A
<i>Oryza_sativa</i>	G	V	A	G	V	F	G	G	S	L	F	S	A	M	H	G	S	L	V	T	S	S	L	I	R	E	T	T	E	N	E	S	A	N	E	G	Y	R	F	G	Q	E	E	E	T	Y	N	I	V	A
<i>Zea_mays</i>	G	V	A	G	V	F	G	G	S	L	F	S	A	M	H	G	S	L	V	T	S	S	L	I	R	E	T	T	E	N	E	S	A	N	E	G	Y	K	F	G	Q	E	E	E	T	Y	N	I	V	A
<i>Carica_papaya</i>	G	V	A	G	V	F	G	G	S	L	F	S	A	M	H	G	S	L	V	T	S	S	L	I	R	E	T	T	E	N	E	S	A	N	E	G	Y	R	F	G	Q	E	E	E	T	Y	N	I	V	A
<i>Porphyridium_purp</i>	G	V	A	G	V	F	G	G	S	L	F	S	A	M	H	G	S	L	V	T	S	S	L	I	R	E	T	T	E	N	E	S	A	N	E	G	Y	K	F	G	Q	E	E	E	T	Y	N	I	V	A
<i>Cyanidium_caldari</i>	G	V	A	G	V	F	G	G	A	L	F	S	A	M	H	G	S	L	V	T	S	S	L	I	R	E	T	T	E	N	E	S	P	N	Y	G	Y	K	L	G	Q	E	E	E	T	Y	N	I	V	A
<i>Cyanophora_parad</i>	G	V	A	G	V	F	G	G	S	L	F	S	A	M	H	G	S	L	V	T	S	S	L	I	R	E	T	T	E	N	E	S	A	N	E	G	Y	K	F	G	Q	E	E	E	T	Y	N	I	V	A
<i>Polarella_glacial</i>	G	V	A	G	V	F	G	G	S	L	F	S	A	M	H	G	S	L	V	T	S	S	L	L	A	E	T	G	G	D	V	S	L	N	V	G	Y	N	F	G	Q	E	D	E	T	Y	S	I	S	A
<i>Kryptoperid_folia</i>	G	V	A	G	V	F	G	G	S	L	F	S	A	M	H	G	S	L	V	T	S	S	L	I	R	E	T	T	E	N	E	S	T	N	Y	G	Y	K	F	G	Q	E	E	E	T	Y	N	I	V	A
<i>Vaucheria_litor</i>	G	V	A	G	V	F	G	G	S	L	F	S	A	M	H	G	S	L	V	T	S	S	L	I	R	E	T	S	E	V	E	S	T	N	Y	G	Y	K	F	G	Q	E	E	E	T	Y	N	I	V	A
<i>Fucus_vesiculosus</i>	G	V	A	G	V	F	G	G	S	L	F	S	A	M	H	G	S	L	V	T	S	S	L	I	R	E	T	S	E	V	E	S	V	N	Y	G	Y	K	F	G	Q	E	E	E	T	Y	N	I	V	A
<i>Nannochlorop_sal</i>	G	V	A	G	V	F	G	G	S	L	F	S	A	M	H	G	S	L	V	T	S	S	L	I	R	E	T	E	D	G	V	S	A	N	Y	G	Y	K	F	G	Q	E	E	E	T	Y	N	I	V	A
<i>Pinnularia_cf_mi</i>	G	V	A	G	V	F	G	G	S	L	F	S	A	M	H	G	S	L	V	T	S	S	L	I	R	E	T	T	E	N	E	S	V	N	Y	G	Y	K	F	G	Q	E	E	E	T	Y	N	I	V	A
<i>Ulnaria_acus</i>	G	V	A	G	V	F	G	G	S	L	F	S	A	M	H	G	S	L	V	T	S	S	L	I	R	E	T	T	E	N	E	S	T	N	Y	G	Y	K	F	G	Q	E	E	E	T	Y	N	I	V	A
<i>Thalassio_oceani</i>	G	V	A	G	V	F	G	G	S	L	F	S	A	M	H	G	S	L	V	T	S	S	L	I	R	E	T	T	E	N	E	S	T	N	Y	G	Y	K	F	G	Q	E	E	E	T	Y	N	I	V	A
<i>Phaeocyst_antarct</i>	G	V	A	G	V	F	G	G	S	L	F	S	A	M	H	G	S	L	V	T	S	S	L	I	R	E	T	T	E	N	E	S	A	N	E	G	Y	K	F	G	Q	E	E	E	T	Y	N	I	V	A
<i>Emiliana_huxleyi</i>	G	V	A	G	V	F	G	G	S	L	F	S	A	M	H	G	S	L	V	T	S	S	L	I	R	E	T	T	E	N	E	S	A	N	E	G	Y	K	F	G	Q	E	E	E	T	Y	N	I	V	A
<i>Geminig_cryophila</i>	G	V	A	G	V	F	G	G	S	L	F	S	A	M	H	G	S	L	V	T	S	S	L	I	R	E	T	T	E	N	E	S	A	N	E	G	Y	K	F	G	Q	E	E	E	T	Y	N	I	V	A
<i>Rhodomonas_salina</i>	G	V	A	G	V	F	G	G	S	L	F	S	A	M	H	G	S	L	V	T	S	S	L	I	R	E	T	T	E	N	E	S	A	N	E	G	Y	K	F	G	Q	E	E	E	T	Y	N	I	V	A
<i>Eutreptiella_gymn</i>	G	V	A	G	V	F	G	G	S	L	F	S	A	M	H	G	S	L	V	T	S	S	L	I	R	E	T	T	E	N	E	S	A	N	E	G	Y	K	F	G	Q	E	E	E	T	Y	N	I	V	A
<i>Paulinella_chroma</i>	G	V	A	G	V	F	G	G	S	L	F	S	A	M	H	G	S	L	V	T	S	S	L	V	R	E	T	T	E	S	E	S	Q	N	Y	G	Y	K	F	G	Q	E	E	E	T	Y	N	I	V	A

	260	270	280	290	300																																													
<i>Chlam_cf_nivalis</i>	A	H	G	Y	F	G	R	L	I	F	Q	Y	A	S	F	N	N	S	R	A	L	H	F	F	L	A	A	W	P	V	V	G	I	W	L	T	A	L	G	V	S	T	M	A	F	N	L	N	G	F
<i>Chlam_reinhardtii</i>	A	H	G	Y	F	G	R	L	I	F	Q	Y	A	S	F	N	N	S	R	S	L	H	F	F	L	A	A	W	P	V	V	G	I	W	F	T	A	L	G	L	S	T	M	A	F	N	L	N	G	F
<i>Therm_elongatus</i>	A	H	G	Y	F	G	R	L	I	F	Q	Y	A	S	F	N	N	S	R	S	L	H	F	F	L	A	A	W	P	V	V	G	I	W	F	T	A	L	G	I	S	T	M	A	F	N	L	N	G	F
<i>Arabid_thaliana</i>	A	H	G	Y	F	G	R	L	I	F	Q	Y	A	S	F	N	N	S	R	S	L	H	F	F	L	A	A	W	P	V	V	G	I	W	F	T	A	L	G	I	S	T	M	A	F	N	L	N	G	F
<i>Chlam_raudensis</i>	A	H	G	Y	F	G	R	L	I	F	Q	Y	A	S	F	N	N	S	R	S	L	H	F	F	L	A	A	W	P	V	V	G	I	W	F	T	A	L	G	L	S	T	M	A	F	N	L	N	G	F
<i>Dunaliel_salina</i>	A	H	G	Y	F	G	R	L	I	F	Q	Y	A	S	F	N	N	S	R	S	L	H	F	F	L	A	A	W	P	V	V	G	I	W	F	T	A	L	G	I	S	T	M	A	F	N	L	N	G	F
<i>Acutodesmus_obl</i>	A	H	G	Y	F	G	R	L	I	F	Q	Y	A	S	F	N	N	S	R	S	L	H	F	F	L	A	A	W	P	V	V	G	I	W	F	T	A	L	G	I	S	T	M	A	F	N	L	N	G	F
<i>Chlorella_vulg</i>	A	H	G	Y	F	G	R	L	I	F	Q	Y	A	S	F	N	N	S	R	S	L	H	F	F	L	A	A	W	P	V	V	G	I	W	F	T	A	L	G	I	S	T	M	A	F	N	L	N	G	F
<i>Pyramimonas_par</i>	A	H	G	Y	F	G	R	L	I	F	Q	Y	A	S	F	N	N	S	R	S	L	H	F	F	L	A	A	W	P	V	V	G	I	W	F	T	A	L	G	V	S	T	M	A	F	N	L	N	G	L
<i>Pycnococcus_pro</i>	A	H	G	Y	F	G	R	L	I	F	Q	Y	A	S	F	N	N	S	R	S	L	H	F	F	L	A	A	W	P	V	V	G	I	W	F	T	A	L	G	I	S	T	M	A	F	N	L	N	G	F
<i>Populus_trichoc</i>	A	H	G	Y	F	G	R	L	I	F	Q	Y	A	S	F	N	N	S	R	S	L	H	F	F	L	A	A	W	P	V	V	G	I	W	F	T	A	L	G	I	S	T	M	A	F	N	L	N	G	F
<i>Cycas_micronesi</i>	A	H	G	Y	F	G	R	L	I	F	Q	Y	A	S	F	N	N	S	R	S	L	H	F	F	L	A	A																							

	310	320	330	340	350																																												
<i>Chlam_cf_nivalis</i>	N	F	N	Q	S	V	V	D	S	Q	G	R	V	I	N	T	W	A	D	I	I	N	R	A	D	L	G	M	E	V	M	H	E	R	N	A	H	N	F	P	L	D	L	A	S	T	N	-	-
<i>Chlam_reinhardtii</i>	N	F	N	Q	S	V	V	D	S	Q	G	R	V	I	N	T	W	A	D	I	I	N	R	A	N	L	G	M	E	V	M	H	E	R	N	A	H	N	F	P	L	D	L	A	S	T	N	-	-
<i>Therm_elongatus</i>	N	F	N	Q	S	V	V	D	S	Q	G	R	V	I	N	T	W	A	D	I	I	N	R	A	N	L	G	M	E	V	M	H	E	R	N	A	H	N	F	P	L	D	L	A	S	T	N	-	-
<i>Arabid_thaliana</i>	N	F	N	Q	S	V	V	D	S	Q	G	R	V	I	N	T	W	A	D	I	I	N	R	A	N	L	G	M	E	V	M	H	E	R	N	A	H	N	F	P	L	D	L	A	S	T	N	-	-
<i>Chlam_raudensis</i>	N	F	N	Q	S	V	V	D	S	Q	G	R	V	I	N	T	W	A	D	I	I	N	R	A	N	L	G	M	E	V	M	H	E	R	N	A	H	N	F	P	L	D	L	A	S	T	N	-	-
<i>Dunaliel_salina</i>	N	F	N	Q	S	V	V	D	S	Q	G	R	V	I	N	T	W	A	D	I	I	N	R	A	N	L	G	M	E	V	M	H	E	R	N	A	H	N	F	P	L	D	L	A	S	T	N	-	-
<i>Acutodesmus_obl</i>	N	F	N	Q	S	V	V	D	S	Q	G	R	V	I	N	T	W	A	D	I	I	N	R	A	N	L	G	M	E	V	M	H	E	R	N	A	H	N	F	P	L	D	L	A	S	T	N	-	-
<i>Chlorella_vulg</i>	N	F	N	Q	S	V	V	D	S	Q	G	R	V	I	N	T	W	A	D	I	I	N	R	A	N	L	G	M	E	V	M	H	E	R	N	A	H	N	F	P	L	D	L	A	S	T	N	-	-
<i>Pyramimonas_par</i>	N	F	N	Q	S	V	V	D	S	Q	G	R	V	I	N	T	W	A	D	I	I	N	R	A	N	L	G	M	E	V	M	H	E	R	N	A	H	N	F	P	L	D	L	A	S	T	N	-	-
<i>Pycnococcus_pro</i>	N	F	N	Q	S	V	V	D	S	Q	G	R	V	I	N	T	W	A	D	I	I	N	R	A	N	L	G	M	E	V	M	H	E	R	N	A	H	N	F	P	L	D	L	A	S	T	N	-	-
<i>Populus_trichoc</i>	N	F	N	Q	S	V	V	D	S	Q	G	R	V	I	N	T	W	A	D	I	I	N	R	A	N	L	G	M	E	V	M	H	E	R	N	A	H	N	F	P	L	D	L	A	S	T	N	-	-
<i>Cycas_micronesi</i>	N	F	N	Q	S	V	V	D	S	Q	G	R	V	I	N	T	W	A	D	I	I	N	R	A	N	L	G	M	E	V	M	H	E	R	N	A	H	N	F	P	L	D	L	A	S	T	N	-	-
<i>Magnolia_grandi</i>	N	F	N	Q	S	V	V	D	S	Q	G	R	V	I	N	T	W	A	D	I	I	N	R	A	N	L	G	M	E	V	M	H	E	R	N	A	H	N	F	P	L	D	L	A	S	T	N	-	-
<i>Oryza_sativa</i>	N	F	N	Q	S	V	V	D	S	Q	G	R	V	I	N	T	W	A	D	I	I	N	R	A	N	L	G	M	E	V	M	H	E	R	N	A	H	N	F	P	L	D	L	A	S	T	N	-	-
<i>Zea_mays</i>	N	F	N	Q	S	V	V	D	S	Q	G	R	V	I	N	T	W	A	D	I	I	N	R	A	N	L	G	M	E	V	M	H	E	R	N	A	H	N	F	P	L	D	L	A	S	T	N	-	-
<i>Carica_papaya</i>	N	F	N	Q	S	V	V	D	S	Q	G	R	V	I	N	T	W	A	D	I	I	N	R	A	N	L	G	M	E	V	M	H	E	R	N	A	H	N	F	P	L	D	L	A	S	T	N	-	-
<i>Porphyridium_purp</i>	N	F	N	Q	S	V	V	D	S	Q	G	R	V	I	N	T	W	A	D	I	I	N	R	A	N	L	G	M	E	V	M	H	E	R	N	A	H	N	F	P	L	D	L	A	S	T	N	-	-
<i>Cyanidium_caldari</i>	N	F	N	Q	S	V	V	D	S	Q	G	R	V	I	N	T	W	A	D	I	I	N	R	A	N	L	G	M	E	V	M	H	E	R	N	A	H	N	F	P	L	D	L	A	S	T	N	-	-
<i>Cyanophora_parad</i>	N	F	N	Q	S	V	V	D	S	Q	G	R	V	I	N	T	W	A	D	I	I	N	R	A	N	L	G	M	E	V	M	H	E	R	N	A	H	N	F	P	L	D	L	A	S	T	N	-	-
<i>Polarella_glacial</i>	N	F	N	Q	S	V	V	D	S	Q	G	R	V	I	N	T	W	A	D	I	I	N	R	A	N	L	G	M	E	V	M	H	E	R	N	A	H	N	F	P	L	D	L	A	S	T	N	-	-
<i>Kryptoperid_folia</i>	N	F	N	Q	S	V	V	D	S	Q	G	R	V	I	N	T	W	A	D	I	I	N	R	A	N	L	G	M	E	V	M	H	E	R	N	A	H	N	F	P	L	D	L	A	S	T	N	-	-
<i>Vaucheria_litor</i>	N	F	N	Q	S	V	V	D	S	Q	G	R	V	I	N	T	W	A	D	I	I	N	R	A	N	L	G	M	E	V	M	H	E	R	N	A	H	N	F	P	L	D	L	A	S	T	N	-	-
<i>Fucus_vesiculosus</i>	N	F	N	Q	S	V	V	D	S	Q	G	R	V	I	N	T	W	A	D	I	I	N	R	A	N	L	G	M	E	V	M	H	E	R	N	A	H	N	F	P	L	D	L	A	S	T	N	-	-
<i>Nannochlorop_sal</i>	N	F	N	Q	S	V	V	D	S	Q	G	R	V	I	N	T	W	A	D	I	I	N	R	A	N	L	G	M	E	V	M	H	E	R	N	A	H	N	F	P	L	D	L	A	S	T	N	-	-
<i>Pinnularia_cf_mi</i>	N	F	N	Q	S	V	V	D	S	Q	G	R	V	I	N	T	W	A	D	I	I	N	R	A	N	L	G	M	E	V	M	H	E	R	N	A	H	N	F	P	L	D	L	A	S	T	N	-	-
<i>Ulnaria_acus</i>	N	F	N	Q	S	V	V	D	S	Q	G	R	V	I	N	T	W	A	D	I	I	N	R	A	N	L	G	M	E	V	M	H	E	R	N	A	H	N	F	P	L	D	L	A	S	T	N	-	-
<i>Thalassio_oceani</i>	N	F	N	Q	S	V	V	D	S	Q	G	R	V	I	N	T	W	A	D	I	I	N	R	A	N	L	G	M	E	V	M	H	E	R	N	A	H	N	F	P	L	D	L	A	S	T	N	-	-
<i>Phaeocyst_antarct</i>	N	F	N	Q	S	V	V	D	S	Q	G	R	V	I	N	T	W	A	D	I	I	N	R	A	N	L	G	M	E	V	M	H	E	R	N	A	H	N	F	P	L	D	L	A	S	T	N	-	-
<i>Emiliana_huxleyi</i>	N	F	N	Q	S	V	V	D	S	Q	G	R	V	I	N	T	W	A	D	I	I	N	R	A	N	L	G	M	E	V	M	H	E	R	N	A	H	N	F	P	L	D	L	A	S	T	N	-	-
<i>Geminig_cryophila</i>	N	F	N	Q	S	V	V	D	S	Q	G	R	V	I	N	T	W	A	D	I	I	N	R	A	N	L	G	M	E	V	M	H	E	R	N	A	H	N	F	P	L	D	L	A	S	T	N	-	-
<i>Rhodomonas_salina</i>	N	F	N	Q	S	V	V	D	S	Q	G	R	V	I	N	T	W	A	D	I	I	N	R	A	N	L	G	M	E	V	M	H	E	R	N	A	H	N	F	P	L	D	L	A	S	T	N	-	-
<i>Eutreptiella_gymn</i>	N	F	N	Q	S	V	V	D	S	Q	G	R	V	I	N	T	W	A	D	I	I	N	R	A	N	L	G	M	E	V	M	H	E	R	N	A	H	N	F	P	L	D	L	A	S	T	N	-	-
<i>Paulinella_chroma</i>	N	F	N	Q	S	V	V	D	S	Q	G	R	V	I	N	T	W	A	D	I	I	N	R	A	N	L	G	M	E	V	M	H	E	R	N	A	H	N	F	P	L	D	L	A	S	T	N	-	-

	360
<i>Chlam_cf_nivalis</i>	-
<i>Chlam_reinhardtii</i>	-
<i>Therm_elongatus</i>	V A M I A P S I N G
<i>Arabid_thaliana</i>	-
<i>Chlam_raudensis</i>	-
<i>Dunaliel_salina</i>	-
<i>Acutodesmus_obl</i>	-
<i>Chlorella_vulg</i>	-
<i>Pyramimonas_par</i>	-
<i>Pycnococcus_pro</i>	-
<i>Populus_trichoc</i>	-
<i>Cycas_micronesi</i>	-
<i>Magnolia_grandi</i>	-
<i>Oryza_sativa</i>	-
<i>Zea_mays</i>	-
<i>Carica_papaya</i>	-
<i>Porphyridium_purp</i>	V A L T A P A V N G
<i>Cyanidium_caldari</i>	V A S S S P S I N S
<i>Cyanophora_parad</i>	V A L T A P S I N A
<i>Polarella_glacial</i>	-
<i>Kryptoperid_folia</i>	V A L T A P A V N G
<i>Vaucheria_litor</i>	V A V T A P V I A G
<i>Fucus_vesiculosus</i>	V A V S A P S I I G
<i>Nannochlorop_sal</i>	V A L N A P A V N A
<i>Pinnularia_cf_mi</i>	-
<i>Ulnaria_acus</i>	V A L T A P A V N G
<i>Thalassio_oceani</i>	V A F T A P A V N A
<i>Phaeocyst_antarct</i>	V A L V A P A V A A
<i>Emiliana_huxleyi</i>	V A L V A P A V A A
<i>Geminig_cryophila</i>	-
<i>Rhodomonas_salina</i>	V A L T A P A V N G
<i>Eutreptiella_gymn</i>	-
<i>Paulinella_chroma</i>	V A L T A P A I G -

96
97

98 **Figure S5.** Multiple sequence alignment of amino acid sequence translated from psbA gene
99 coding for D1 protein isolated from *Chlamydomonas cf. nivalis* (this study, NCBI reference
100 nucleotide sequence **KF702330.1** and protein sequence **AHB82278**), *Chlamydomonas*
101 *reinhardtii* (**DAA00957.1**), *Thermosynechococcus elongatus* (**NP_682633.1**), *Arabidopsis*
102 *thaliana* (**P83755.2**), *Chlamydomonas raudensis* (**AFU83031.1**), *Dunaliella salina*
103 (**YP_005089831.1**), *Acutodesmus obliquus* (**ABD48259.1**), *Chlorella vulgaris* (**P56318.1**),
104 *Pyramimonas parkea* (**ACJ71100.1**), *Pycnococcus provasolii* (**ACK36809.1**), *Populus*
105 *trichocarpa* (**YP_001109480.1**), *Cycas micronesica* (**ABU85314.1**), *Magnolia grandiflora*
106 (**YP_007474516.1**), *Oryza sativa* (**AER12889.1**), *Zea mays* (**NP_043004.1**), *Carica papaya*
107 (**YP_001671663.1**), *Porphyridium purpureum* (**BAO23682.1**), *Cyanidium caldarium*
108 (**NP_045067.1**), *Cyanophora paradoxa* (**NP_043238.1**), *Polarella glacialis* (**BAC76007.1**),
109 *Kryptoperidinium foliaceum* (**ADI40420.1**), *Vaucheria litorea* (**ACF70962.1**), *Fucus*
110 *vesiculosus* (**CAX12449.1**), *Nannochloropsis salina* (**AGI99196.1**), *Pinnularia cf.*
111 *microstauron* (**AER42084**), *Ulnaria acus* (**AEX37881.1**), *Thalassiosira oceanica*
112 (**ADB27608.1**), *Phaeocystis antarctica* (**AEK26755.1**), *Emiliana huxleyi* (**AAX13814.1**),
113 *Geminigera cryophila* (**ABL96289.1**), *Rhodomonas salina* (**ABO70840.1**), *Eutreptiella*
114 *gymnastica* (**YP_006234198.1**), and *Paulinella chromatophora* (**ACB43269.1**).

115

Paper IX

Lipidomic profiling of snow algae by ESI-MS and silver-LC/APCI-MS

Řezanka T¹, Nedbalová L², Procházková L² & Sigler K¹

Phytochemistry 100: 34–42, 2014

¹ *Institute of Microbiology, Academy of Sciences of the Czech Republic, Videňská
1083, 142 20 Prague, Czech Republic*

² *Charles University in Prague, Faculty of Science, Department of Ecology, Viničná 7,
128 44 Prague 2, Czech Republic*



Lipidomic profiling of snow algae by ESI-MS and silver-LC/APCI-MS



Tomáš Řezanka^{a,*}, Linda Nedbalová^b, Lenka Procházková^b, Karel Sigler^a

^a Institute of Microbiology, Academy of Sciences of the Czech Republic, Vídeňská 1083, 142 20 Prague, Czech Republic

^b Charles University in Prague, Faculty of Science, Department of Ecology, Viničná 7, 128 44 Prague 2, Czech Republic

ARTICLE INFO

Article history:

Received 18 November 2013

Received in revised form 20 January 2014

Available online 15 February 2014

Keywords:

Snow alga

Chloromonas pichincae

Lipidomics

ESI

Triacylglycerols

Silver-LC/APCI-MS

NARP-LC/APCI-MS

ABSTRACT

The main analytical benefit of this study is the development of methods enabling a rapid determination of total lipids of algae by lipidomic analysis and detailed identification and quantification of a complex mixture of natural TAGs by silver-LC/APCI-MS and NARP-LC/APCI-MS. Both types of chromatography can readily identify, both qualitatively and semiquantitatively, triacylglycerols containing 16:3 and 16:4 acids in the molecule. We conclude that the genus *Chloromonas* is a major producer of C16 PUFAs mostly contained in TAGs. Since more detailed studies in this field have been stymied by the shortage of 16:3 and 16:4 FAs, we decided to study the alga *Chloromonas* as a potential biotechnological source of C16 PUFAs.

© 2014 Elsevier Ltd. All rights reserved.

Introduction

Snow algae grow in the alpine or polar regions worldwide. In addition to the biosynthesis of pigments, polyols, sugars and lipids generally performed by photosynthesizing organisms they developed a number of features such as mucilage sheaths, motile stages and spore formation, which enable them to adapt to the harsh snow environment (Hoham and Duval, 2001). At low temperatures, a major role in avoiding membrane rigidization is played by unsaturation of the fatty acids in membrane lipids (Morgan-Kiss et al., 2006). Moreover, the protective role of polyunsaturated fatty acids (PUFAs) against the damaging effect of high light intensity and UV radiation obviously helps the organism to survive and adapt in extreme environments (Whitelam and Codd, 1986).

The snow alga *Chloromonas pichincae* has a complex life cycle, which includes both asexual and sexual reproduction and formation of resting stages. The flagellates and immature zygotes are responsible for a green coloration of snow (Hoham, 1975). Studies of the optimum temperatures of snow algae of the genus *Chloromonas* showed that, regardless of whether acclimation experiments were made, the algae grew best at temperatures around 5 °C. However, the authors examined only growth (cells number) and the data on FAs or lipids in *Chloromonas* from snow are scarce (Hoham et al., 2008; Řezanka et al., 2008).

Snow algae had to develop a number of adaptive strategies to cope with cold environments. A major adaptation influencing their growth and photosynthesis is the maintenance of membrane fluidity at low temperatures. While the importance of changes in fatty acid content has been recognized, the role of lipids in the metabolism of cold-adapted microorganisms is largely unexplored (Morgan-Kiss et al., 2006).

A few studies have dealt with fatty acids in the genus *Chloromonas*. In our previous work, we analyzed the snow alga *C. brevispina* (Řezanka et al., 2008). By using GC-MS we have identified a relatively high amount of C16 unsaturated FAs, the major being 16:2 (7%), 16:3 (15.5%), and 16:4 (9.5% of total FAs). Spijkerman et al. (2012) identified C16 PUFAs, principally 16:4, in the strains of *Chloromonas nivalis* (CCCr005-99), and the tentatively designated *C. rostafinskii* (CCCr010-99). Extensive data were published in the study of Lang et al. (2011), which described the contents of individual FAs in 22 species of the genus *Chloromonas* (the comparison with our data is in Table 1). The highest content of 16:4, more than 30% of total FAs, was found in *C. rosae*. The taxonomy of the genera *Chloromonas* and *Chlamydomonas* is constantly evolving (Proschold et al., 2001) and brings about constant changes in the classification; we therefore also mention the lipids of *Chlamydomonas*.

One of the first papers describing the content of polar lipids in genus *Chlamydomonas* was the study of Giroud et al. (1988), who analyzed polar lipids (MGDG, DGDG, SQDG, DGTS, PG, PE, and PI) from *C. reinhardtii*. As the major acids in all studied lipids were identified trienoic and tetraenoic C16 and C18 FAs,

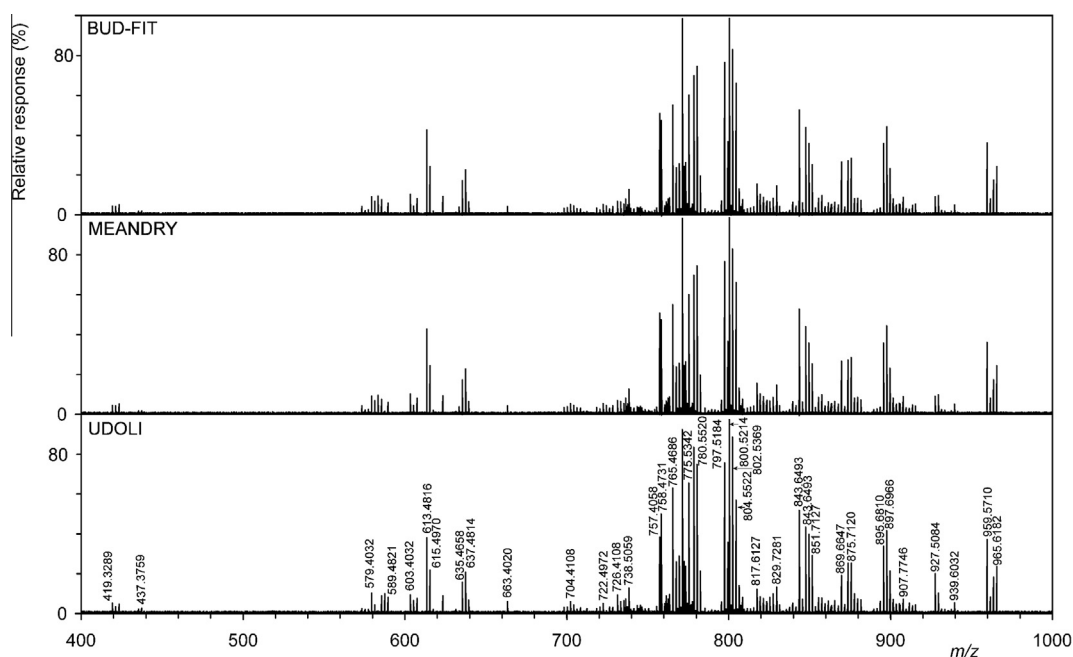
* Corresponding author. Tel.: +420 241 062 300; fax: +420 241 062 347.

E-mail address: rezanka@biomed.cas.cz (T. Řezanka).

Table 1

FA content in algal samples under study, identified by means of GC–MS of FAMES and its comparison with literature data.

Fatty acid	Abbreviation	Systematic name	BUD_FIT	MEANDRY	UDOLI	Lang et al. (2011) ^a
Myristic	M	14:0	0.8	1.3	0.7	0.4
Palmitic	P	16:0	12.5	11.2	14.9	13.0
Palmitoleic	Po	9–16:1	3.1	5.3	8.5	4.1
Palmitlinoleic	Pl	7,10–16:2	2.8	3.1	3.4	2.6
Palmitlinolenic	Pn	7,10,13–16:3	10.1	6.7	8.2	3.3
Hexadecatetraenoic	Pm ^b	4,7,10,13–16:4	18.7	16.2	15.6	15.3
Stearic	S	18:0	1.8	1.9	2.1	3.7
Oleic	O	9–18:1	11.3	17.1	13.3	9.4
Vaccenic	V	11–18:1	0.7	0.9	1.4	6.9
Linoleic	L	9,12–18:2	3.6	5.5	3.2	6.4
α -Linolenic	Ln	9,12,15–18:3	25.7	23.6	22.9	27.1
Stearidonic	St	6,9,12,15–18:4	8.9	7.2	5.8	7.6

^a Mean content of individual FAs in 22 *Chloromonas* species studied by Lang et al. (2011).^b According to Danielewicz et al. (2011).**Fig. 1.** Mass spectrum (positive ion mode) of total lipids from snow alga *C. pichincae*, acquired by high mass resolution ESI-MS. Numbers correspond to the accurate mass values.

i.e. 4,7,10,13–16:4 or 9,12,15–18:3, with lower amounts of 5,9,12,15–18:4 and 7,10,13–16:3. The authors demonstrated a high stereospecificity of MGDG having FAs bound in positions 1 and 2. For example, 96% of C18 acids was bound in position 1 of DGDG, whereas up to 97% of C16 FAs was bound in the 2-position.

Several tens of molecular species of lipids (MGDG, DGDG, SQDG, DGTS, PG, PE, and PI) from the snow alga *Chlamydomonas nivalis* cultivated under salt stress or in response to nitrate or phosphate deprivation were identified by ultra-high performance liquid chromatography–mass spectrometry (UHPLC/MS) e.g. (Lu et al., 2012a, 2013). Similar polar lipids were identified by UHPLC/MS in the exponential phase of growth of the snow alga *Chlamydomonas nivalis* cultivated under NaCl stress (Lu et al., 2012b).

UHPLC/MS was used to analyze TAGs in *Chlamydomonas reinhardtii* and *Nannochloropsis oceanica* grown in nitrogen (N)-replete or N-depleted medium. A total of 140 molecular species of TAGs were identified, but without any quantification and without the resolution of regioisomers (Liu et al., 2013).

The analysis of intact TAGs can be basically performed by using two methods, either direct sample inlet to the mass spectrometer

or a connection of liquid chromatograph with mass spectrometer (Vieler et al., 2007). The former method, called lipidomics (Han et al., 2012), is based on the identification of all lipids in cells and requires only an extraction of total lipids followed by identification and quantification of lipid molecular species (Bromke et al., 2013). High-resolution mass spectrometry is predominantly used for studies of lipidomic profiling of algae. ESI linear ion trap Orbitrap mass spectrometer with either a direct inlet (Danielewicz et al., 2011; Lee et al., 2013) or with UHPLC-MS (MacDougall et al., 2011) was used to analyze TAGs from miscellaneous algae including triacylglycerols containing C16 PUFAs by different collision energy (CID) using MSⁿ experiments, a combination of accurate mass and diagnostic fragment ions, or by MS² and MS³ analysis.

Nonaqueous reversed-phase high performance liquid chromatography (NARP-LC) represents one of the most common methods for the separation of natural TAGs. It was used to separate hundreds of TAGs (Christie, 1988; Laakso and Christie, 1991), which were then identified by MS. Silver-ion chromatography is another option for separating TAGs (Laakso and Christie, 1991).

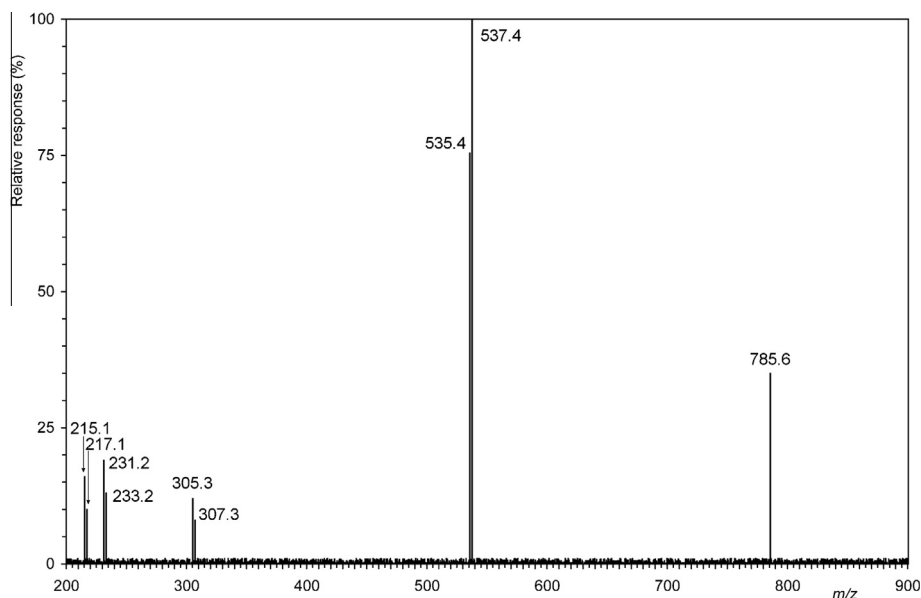


Fig. 4. Tandem mass spectrum of natural PnPmPm TAG.

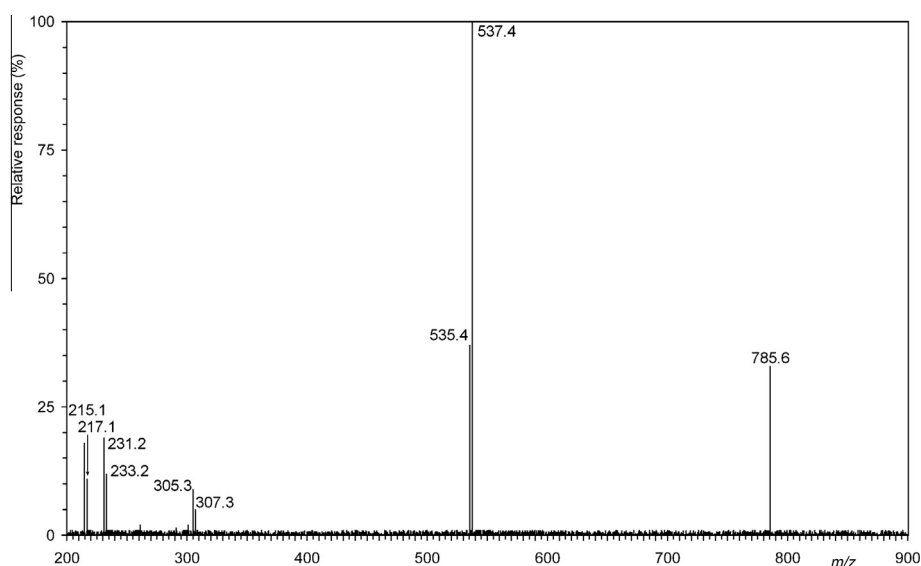


Fig. 5. Tandem mass spectrum of natural PmPnPm TAG.

ion $[M+Na]^+$ in the positive mode. It should be noted that hundreds, or even thousands, of other molecular species of lipids may be present. Indeed, as found by, e.g., Lu et al. (2012a), the snow alga *Chlamydomonas nivalis* was revealed to exhibit nearly 5000 peaks of ions in positive ESI; however, only a few tens of molecular species were identified.

Literature search (Danielewicz et al., 2011; Lee et al., 2013) and our own experience made us to choose ESI as the most effective ionization method for identification of lipid classes in snow algae. Since the focal point in our further analysis was to identify above all lipid classes that contain C16 PUFAs, i.e. both polar lipids (mostly phospholipids) and TAGs, we used the nearly universal ESI method in positive mode (see also Lee et al., 2013). Its advantage is in the possibility to use the presence of sodium ions directly in the extract; in their analyses Lee et al. (2013) supplied the extract with potassium acetate. HRMS thus allows a direct analysis of relevant lipids in the snow alga extract. One should however note that the ESI method has some limitations with regard to

highly nonpolar hydrocarbons (squalene), which are not efficiently ionized and thus also detected.

The use of HRMS offers considerable advantages mainly in the range of higher m/z values. An example concerns, e.g., the three molecular species at m/z 857, i.e. TAG 16:0/16:0/18:0 at m/z 857.7606, PI 16:0/18:2 at m/z 857.5163 and SQDG 18:4/18:4 at m/z 857.4501. However, it does not make it possible to distinguish structural isomers; some of them (e.g. regioisomers) can be identified by tandem MS, others (e.g. positional isomers of TAGs having oleic and/or vaccenic acids in the molecule) can be identified only by using chromatographic methods.

While Lee et al. (2013) characterized 48 lipid species, we succeeded in determining several hundreds of them. However, the method does not provide an exact quantitative determination of TAGs having a higher number of double bonds in the molecule. It is known that in ESI analysis the highest response in the MS spectrum is given by saturated TAGs, while in APCI analysis it is provided by unsaturated TAGs (Byrdwell and Neff, 2002).

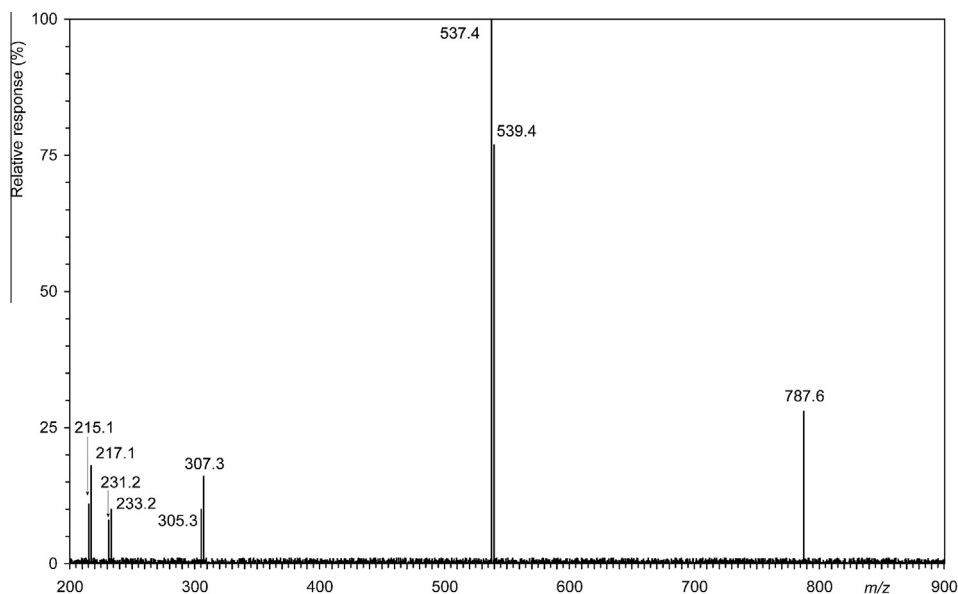


Fig. 6. Tandem mass spectrum of natural PnPm TAG.

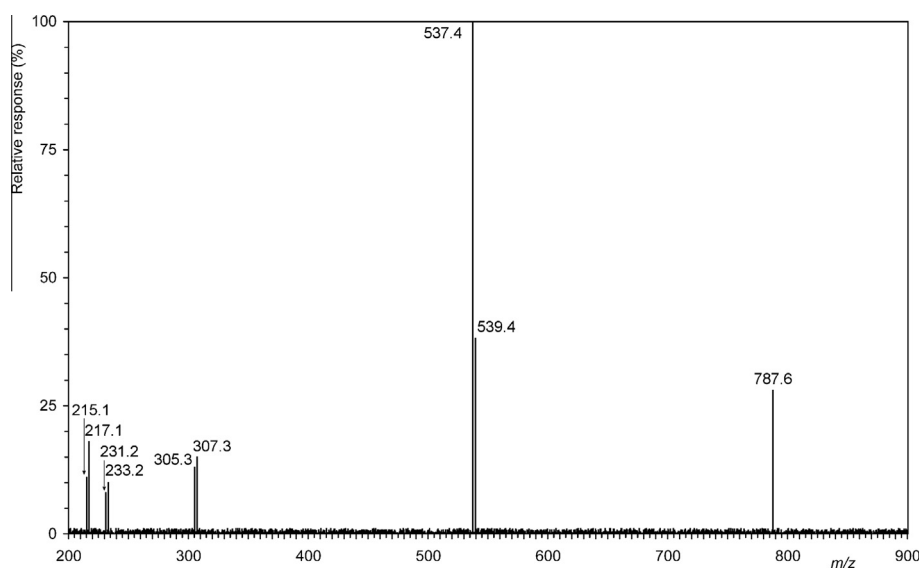


Fig. 7. Tandem mass spectrum of natural PnPmPn TAG.

Analysis by Orbitrap is very fast; when using autosampler with LC pump and without LC column (direct injection) and low sample injection (low solvent flow, about 1 $\mu\text{L/s}$), the whole analysis takes about half a minute. To exclude contamination, especially in very similar samples such as those we analyzed, each even-numbered analysis was performed by filling the vial up with pure solvent as a sort of washing run. About 60 samples per hour can be analyzed in this way.

Identification of triacylglycerols by silver-LC/MS and NARP-LC/MS

Since TAGs of all three samples of snow algae represented the most abundant lipid class (determined gravimetrically), they were separated on a Sep-Pak Cartridge with aminopropyl-silica based polar bonded phase, and non-polar lipids were eluted by chloroform–methanol mixture. We focused on their analysis using silver-LC with a gradient of a hexane/2-propanol/acetonitrile mobile phase and identification by APCI. Optimization of silver-

LC separation has been repeatedly discussed, in terms of selection of an appropriate column (laboratory-made silver-ion columns versus commercial cation exchange columns), the stability of the mobile phase (addition of low amounts of 2-propanol to a hexane–acetonitrile mixture), or the column temperature or length (Momchilova and Nikolova-Damyanova, 2012). The currently used combination of silver-LC/MS and NARP-LC/MS with tandem MS identification of structure was used not only for the analysis of a group of TAGs differing in the number of double bonds, but also for separation and identification of individual regioisomers of TAGs (Dugo et al., 2006).

Our TAGs were fractionated according to the number of double bonds; with increasing number of double bonds the interaction of TAGs with silver ions of the stationary phase is ever stronger, which leads to higher retention times. The total TAGs were separated into 13 fractions having from 0 to 12 double bonds, see Fig. 2, which were further analyzed by NARP-LC, see Fig 3. Saturated TAGs were eluted first while unsaturated TAGs were eluted

later according to the rising number of double bonds in the molecule. Retention times in silver-LC are affected above all by the number of double bonds, although, as evident from Fig. 2, TAGs having FAs of different chain length are partially separated; however, this was not sufficient to complete their identification, nor was it our aim. For example, Lisa et al. (2009) obtained a sufficient separation by three columns connected in series, but if the column length is extended 2- or 3-times, the retention time increases to reach more than two hours in TAGs having 10 double bonds. We therefore used the above-mentioned two-dimensional off-line separation. In the first dimension, the TAGs were separated only by the number of double bonds, while in the second dimension regioisomers of TAGs were analyzed by NARP-LC (Fig. 3) and identified by tandem MS, see Fig. 3. TAGs of snow algae are among the most complex mixtures so far analyzed in our laboratory (Rezanka and Sigler, 2007; Rezanka et al., 2008, 2011). Although they contain in principle only FAs with chain lengths C16 and C18 (the minor proportion of myristic acid, see Table 1, does not play any role in the fraction of TAGs), these TAGs contain 11 FAs, i.e. FAs with 0 to 4 double bonds, including positional isomers (oleic versus vaccenic acid). This is in contrast to the FA composition of another snow alga, *C. brevispina*, where 43 FAs were detected (Rezanka et al., 2008), which suggests a species-specific mechanism of maintaining membrane fluidity in cold environments.

If the TAGs contain 11 FAs, the number of all possible TAGs is very high, reaching 1000. When we neglect enantiomers, which can be separated only on a chiral column (Rezanka et al., 2013), the number of possible theoretical regioisomers is still 726 ($x = (n^3 + n^2)/2$).

Molecular species of TAGs are very often separated by using nonaqueous mobile phase with octadecylsilane columns, i.e. NARP-LC (Lisa et al., 2007; Rezanka and Sigler, 2007). In this separation mode the elution order depends on the length of the acyl chains and the number of double bonds. The method permits the identification of tens to hundreds of molecular species of TAGs from various plant and/or animal oils and fats.

TAGs having the same ECN value can be separated on a high-efficiency column such as a combination of two 25 cm columns in series (Rezanka et al., 2011), which provides an efficiency of about 52,000 theoretical plates. The combination effectively separated most of the TAGs and, in addition, also regioisomers of TAGs as illustrated in Fig. 3.

Positive ion APCI mass spectra of TAGs typically exhibited $[M+H]^+$ ion and fragment ions of type $[M+H-RCOOH]^+$ ($[DAG]^+$), resulting from the loss of an acyl chain from TAG. Monoacyl glycerol ($[MAG]^+$) is equivalent to $[RCO+74]^+$ ion. The positive ion APCI mass spectrum (PmPmPm, for abbreviations of FAs see Table 1), i.e. the peak at *t*_R 24.2 min represents $[M+H]^+$ ion at *m/z* 783.6 and the fragment ions $[M+H-RCOOH]^+$ at *m/z* 535.4 $[PmPm]^+$. Further ions at *m/z* 305.3 $[PI+74]^+$ and $[RCO]^+$ at *m/z* 231.2 were also present. These ions were observed with sufficient intensity to analyze the mass spectrum.

TAGs are often present as regioisomers, i.e. positional isomers on the glycerol backbone (Mottram et al., 2001). Symmetrical TAGs (e.g. the PEP type) are eluted before the corresponding asymmetrical TAGs such as PPE (Momchilova et al., 2006). The regioisomers are identified based on the fact that the loss of FA in the secondary hydroxyl is likely to be energetically less favorable than the loss of FA from the primary hydroxyls.

Here we examined two pairs of regioisomers of the most abundant TAGs having C16 PUFAs, i.e. *sn*-PnPmPm (Fig. 4) and *sn*-PmPnPm (Fig. 5), *sn*-PnPnPm (Fig. 6) and *sn*-PnPmPn (Fig. 7), see also Table 2. The least abundant $[M-RCOO]^+$ ion ($[DAG]^+$ ion of *sn*-PmPnPm, i.e. $[PmPm]^+$ at *m/z* 535.4), arises by loss of palmitolinolenate (16:3) from the *sn*-2 position. The more abundant $[DAG]^+$ ion is due to loss of 16:4 from *sn*-1 or *sn*-3 position giving

Table 2

NARP-LC/MS-APCI analysis of fraction having 8 to 12 double bonds of the TAGs mixture from snow alga *C. pichinchae*.

RT	TAG	Double bond	BUD_FIT	MEANDRY	UDOLI
24.2	PmPmPm	12	6.2	5.0	5.5
25.9	PmPmSt	12	3.3	3.5	3.4
26.4	PnPmPm	11	0.8	0.8	1.0
29.1	StStPm	12	1.6	1.7	1.8
29.5	PnPmSt	11	0.4	0.3	0.4
29.8	PmPmLn	11	6.2	6.4	6.3
30.0	PnPnPm	10	0.6	0.6	0.6
30.4	PIPmPm	10	0.7	0.7	0.6
33.0	StStSt	12	0.7	0.7	0.8
33.4	StStPn	11	0.2	0.2	0.4
33.8	LnStPm	11	3.1	3.0	4.3
34.0	PnPnSt	10	0.1	0.1	0.1
34.2	PIPmSt	10	0.2	0.2	0.2
34.5	PIStPm	10	0.2	0.2	0.2
34.8	LPmPm	10	0.9	0.9	0.9
35.1	PnPnPn	9	0.1	0.1	0.1
35.2	PIPnPm	9	0.2	0.2	0.2
35.6	PoPmPm	9	2.7	2.9	2.2
36.5	LnStSt	11	1.6	1.7	1.7
36.8	PIStSt	10	0.1	0.1	0.1
37.1	LPmSt	10	0.4	0.4	0.4
37.2	LnPmSt	10	1.8	1.9	1.9
37.4	LnLnPm	10	6.2	5.1	5.5
37.7	PIPnSt	9	0.1	0.1	0.1
37.9	PILnPm	9	0.4	0.4	0.4
38.1	LPnPm	9	0.6	0.6	0.6
38.2	PoPmSt	9	0.8	0.8	0.8
38.3	OPmPm	9	6.2	6.4	6.4
38.3	PIPIPm	8	0.2	0.2	0.2
38.4	PIPnPn	8	1.2	1.2	1.2
38.5	PoPnPm	8	0.1	0.1	0.1
38.6	PPmPm	8	0.3	0.3	0.3
39.4	PnPnLn	9	0.5	0.5	0.5
40.2	PosSt	9	0.4	0.4	0.4
40.4	PILnSt	9	0.9	0.9	0.9
40.5	OStPm	9	3.3	2.3	2.9
40.6	LStSt	10	0.2	0.2	0.2
40.7	LnLnSt	10	3.1	3.2	3.2
40.8	LnLnPn	9	3.9	4.1	3.9
40.9	LLnPm	9	4.2	5.3	4.8
40.9	PStPm	8	2.1	2.3	2.2
41.0	StPIPI	8	0.1	0.1	0.1
41.1	PoLnPm	8	2.6	2.9	3.2
41.2	LIPm	8	0.4	0.4	0.4
41.4	PILnPn	8	0.4	0.4	0.4
41.5	PoPmSt	8	0.7	0.7	0.7
41.6	SPmPm	8	1.2	1.3	1.2
41.8	LPnPn	8	0.1	0.1	0.1
44.1	OStSt	9	1.6	1.7	1.7
44.4	LnLnLn	9	3.6	4.6	3.4
45.2	LLnSt	9	2.1	2.2	2.2
46.0	PIStL	8	0.2	0.2	0.2
46.3	OPnSt	8	0.6	0.7	0.6
47.3	PILnLn	8	2.8	2.7	2.5
47.4	StPSt	8	0.7	0.7	0.7
47.5	PmLL	8	1.2	1.2	1.2
47.6	PoLnSt	8	0.8	0.9	0.8
47.7	SStPm	8	0.9	0.9	0.9
47.7	PStSt	8	1.1	1.1	1.1
47.8	LLnPn	8	0.6	0.6	0.6
48.7	LLnLn	8	6.2	7.3	7.7
48.9	SStSt	8	0.3	0.3	0.3
49.6	LLSt	8	0.4	0.4	0.4
50.3	OLnSt	8	4.6	2.6	1.9

$[PmPn]^+$ ion at *m/z* 537.4. The $[PmPm]^+:[PmPn]^+$ ratio observed for PmPnPm is 37:100. Consequently, the two enantiomers show mass spectra differing only in intensities of $[DAG]^+$ ions.

Another pair of regioisomers, *sn*-PnPnPm (Fig. 6) and *sn*-PnPmPn (Fig. 7), were similarly separated with respective elution times 29.95 and 30.05 min. The mass spectra also demonstrate the structure of separated TAGs. $[PnPm]^+$ and $[PmPm]^+$ ions were

again differently abundant, their ratio for PnPmPm being 75:100 and for PmPnPm 37:100.

Triacylglycerols of all three samples of snow algae consisted only of molecules with an even number of acyl carbons, i.e. from 48 to 54. TAGs with 46 acyl carbons or less were not determined. Since the fatty acids identified here (see Table 1) and by Lang et al. (2011) include myristic acid, this acid is obviously not present in TAGs. The most frequent were TAGs having 6–8 double bonds, and the most abundant TAGs were 50:7 (PPmLn), 54:8 (LLnLn) and 54:9 (LnLnLn), see Fig. 3. Only small differences in the abundance of TAGs were detected between the samples, which is understandable given their characteristics (the same species and life cycle stage) and similar environmental conditions of the three sampling sites.

Conclusion

HRMS in combination with ESI makes it possible to analyze a broad range of lipid classes in the crude algal extract (in our case snow algae) without preceding purification or separation by SPE or HPLC. The method allowed us to identify several hundreds of molecular species from many classes of both polar and nonpolar lipids including phospholipids and glycolipids, at the rate of up to 60 samples per hour. Apart from its merits the method has also some shortcomings; especially important is its inability to identify certain isomers, e.g. the TAGs triolein (OOO) versus trivaccenin (VVV), etc.

Detailed characterization of the three samples of snow algae by lipidomic analysis with HR MS, silver-LC/APCI-MS and NARP-LC/APCI-MS enabled us to identify more than 300 intact lipids and, after chromatography, also intact TAGs. Although the combination of all three methods is very time-consuming, it provides a maximum number of results that cannot be obtained by any of the methods alone.

The use of off-line two-dimensional silver-LC in the first dimension and NARP-LC in the second dimension, after a previous lipidomic analysis by HR MS with APCI-MS as detection, has made it possible to analyze complex samples of snow algae collected in nature.

We succeeded in separating TAGs having from 0 to 12 double bonds; these TAGs were found to contain only C16 and C18 fatty acids with 0 to 4 double bonds. This shows this alga as a unique biotechnological source of essential PUFAs.

Despite their obvious importance, metabolic adaptations of photoautotrophic extremophiles involving lipids are poorly known. The complex approach used in this study may represent a powerful tool enabling comprehensive studies of lipid content in microorganisms that are exposed to various environmental stresses both in the field and in laboratory experiments. This method can thus provide new insights into the adjustments of metabolic pathways in microorganisms living in cold environments.

Experimental

Plant material

Snow algae were aseptically collected in May 2012 from snow fields in the Krkonoše and Jizera Mountains (Czech Republic). All the three sampling sites were situated in a spruce forest, and the algae formed patchy green coloration of the surface layers of snow. Both sites in the Krkonoše Mountains were located in the Labský důl Valley, but they differed in altitude: The site Bud' Fit was located at an altitude of 810 m a.s.l. (50°44'35"N, 15°36'13"E), the site Meandry Labe at an altitude of 1060 m a.s.l. (50°45'42"N, 15°33'08"E). The sampling locality in the Jizera Mountains (Údolí

Jizery) was situated near the Jizera River at an altitude of 780 m a.s.l. (50°48'09"N, 15°21'53"E). The snow cover at all sites is seasonal. Snow samples were transported to the laboratory in a thermos bottle, identified under a light microscope, and the algal biomass was kept frozen until further analysis. The green blooms were formed entirely by vegetative stages of *C. pichincae* Wille, and no zygospores were observed in the samples.

Lipid extraction and isolation of TAGs

Acetonitrile, 2-propanol, hexane, chloroform and methanol were purchased from Sigma–Aldrich (Prague, CR). The extraction procedure was based on the method of Bligh and Dyer (1959), except that 2-propanol was substituted for methanol, since isopropanol does not serve as a substrate for phospholipases (Kates, 1986). The alcohol–water mixture of the frozen cells was cooled, one part chloroform was added and the lipids were extracted for 30 min. Insoluble material was sedimented by centrifugation and the supernatant was separated into two phases. The aqueous phase was aspirated off and the chloroform phase was washed three times with two parts 1 M KCl each. The resulting chloroform phase was evaporated to dryness under reduced pressure.

Total lipid extracts were applied to Sep-Pak Cartridge Vac 35 cc (Waters; with 10 grams of aminopropylsilica-based polar bonded phase), and from the cartridge were subsequently eluted neutral lipids with 40 mL of chloroform–methanol (7:3), and acidic lipids with 30 mL of chloroform–methanol–concentrated aqueous ammonia (70:30:2) containing 0.4% (w/v) ammonium acetate. The eluate of neutral lipids was reduced in volume, mixed with 1 mL of hexane and the mixture was stirred for 15 min. The solution was filtered, hexane was evaporated and the oil samples were dissolved in an acetonitrile–2-propanol–hexane mixture (1:1:1, v/v/v), which was injected on the HPLC column.

FAMES analysis

The total TAGs (~5 mg) were saponified overnight in 10% KOH–MeOH at room temperature. A fatty acid fraction obtained from the saponification was partitioned between alkali solution (pH 9) and diethyl-ether to remove basic and neutral components. The aqueous phase containing fatty acids was acidified to pH 2 and extracted with hexane. The fatty acid fraction was methylated using BF₃/MeOH (14% solution of BF₃ from Sigma–Aldrich).

Gas chromatography–mass spectrometry of FAME was done on a GC–MS system consisting of Varian 450-GC (Varian BV, Middelburg, The Netherlands), Varian 240-MS ion trap detector with electron ionization (EI), and CombiPal autosampler (CTC, USA) equipped with split/splitless injector. A DB-5MS column was used for separation (60 m, 0.25 mm ID, 0.25 μm film thickness). The temperature program started at 60 °C and was held for 1 min in splitless mode. Then the splitter was opened and the oven was heated to 160 °C at a rate of 25 °C min⁻¹. The second temperature ramp was up to 280 °C at a rate of 2.5 °C min⁻¹, this temperature being maintained for 10 min. The solvent delay time was set to 8 min. The transfer line temperature was set to 280 °C. Mass spectra were recorded at 3 scans s⁻¹ under electron ionization at 70 eV, mass range *m/z* 50–450. FAMES (fatty acid methyl esters) were identified according to their mass spectra [29, 30] and using a mixture of chemical standards obtained from Sigma–Aldrich.

Lipidomic analysis by HR ESI

The high-resolution hybrid mass spectrometer LTQ Orbitrap Velos (Thermo Scientific, FL, USA) was used. ESI–MS analysis was performed in the positive ion mode. MS spectra were obtained by the FT mode. MS spectra were acquired with target mass resolution of

$R = 30,000$ at m/z 400 (lock mass 413.6662 Da). The ion spray voltage was set at -2500 V and the scan range of the instruments was set at m/z 200–1500. Nitrogen was used as a nebulizer gas set at 18 arbitrary units (sheath gas) and 7 arbitrary units (aux gas). Helium was used as a collision gas for CID experiments. The CID normalization energy of 35% was used for the fragmentation of parent ions. The MS/MS product ions were detected by the low-resolution FT mode. Flow Injection Analysis (FIA) was used for sample introduction into the heated ESI (H-ESI) ion source. Acetonitrile/water (50/50 v/v) was used at the flow rate of 150 $\mu\text{L}/\text{min}$. The H-ESI temperature was set to 250 °C.

NARP-LC/APCI-MS

LC equipment consisted of a 1090 Win system, PV5 ternary pump and automatic injector (HP 1090 series, Agilent, USA) and two Hichrom columns HIRPB-250AM 250 \times 2.1 mm ID, 5 μm particle size, in series. This setup represented a high-efficiency column – approximately 26,000 plates/250 mm, a flow rate of 1 mL/min, an injection volume of 10 μL , and column temperature of 25 °C. The TAGs were separated using a gradient solvent program with acetonitrile (ACN) and 2-propanol (iPrOH) as follows: initial ACN/iPrOH (99:1, vol/vol); linear from 5 min to 110 min ACN/iPrOH 30:70 (vol/vol); held until 10 min; the composition was returned to the initial conditions over 10 min. The performance was measured by triheptadecenoin as an internal standard under the conditions given above.

The detector was an AB Sciex API 4000 mass spectrometer (AB Sciex, Ontario, Canada) using APCI mass spectra. The ionization mode was positive, using the following settings: source temperature 420 °C, nebulizer gas (GS1) 5, nebulizer current 3 μA , curtain gas 10, collision gas high and declustering potential 100 V. The optimal collision energy was dependent on the type of experiment and was set to +10 V (full scan mode) or +30 V (product ion mode). In all full scan runs spectra were obtained from m/z 200–1100. To identify the exact composition of high m/z value TAG species, an enhanced product ion spectrum (optimal CE +35 V) was made of all ions with an m/z value over 800.

CID ion mass spectra were acquired by colliding the Q1 selected precursor ions with Ar gas as a collision target gas and applying collision energy of 50 eV in Q2. Scanning range of Q3 was m/z 200–1100 with a step size of m/z 0.3 and a dwell time of 1 ms. A peak threshold of 0.3% intensity was applied to the mass spectra. The instrument was interfaced to a computer running Applied Biosystems Analyst version 1.4.2 software.

Silver-ion HPLC

The LC system used for separation in the silver-ion mode was the same as that used in the reversed-phase mode. TAGs (~ 1 $\mu\text{g}/\mu\text{L}$ in methanol) were chromatographed on two silver-ion columns Chrom-Spher Lipids (250 \times 4.6 mm, 5 μm , Varian, Palo Alto, CA, USA) connected in series. Mobile phase was a gradient from 100% of A and 0% of B at 0 min to 60% of A and 40% of B during 120 min, where A is hexane-2-propanol-acetonitrile (99.8:0.1:0.1, v/v/v) and B is mixture of hexane-2-propanol-acetonitrile (96:2:2, v/v/v). The flow rate, column temperature, and injection volume were 0.5 mL/min, 25 °C, and 10 μL , respectively. Columns were conditioned by mobile phase A at flow rate of 0.5 mL/min for one hour before the every analysis. Other separation conditions used were as in the RP-LC, see above.

Acknowledgments

The research was supported by the project GACR 14-00227S and by the Institutional Internal Project RVO61388971.

Appendix A. Supplementary data

Supplementary data associated with this article can be found, in the online version, at <http://dx.doi.org/10.1016/j.phytochem.2014.01.017>.

References

- Bligh, E.G., Dyer, W.J., 1959. A rapid method of total lipid extraction and purification. *Can. J. Biochem. Physiol.* 37, 911–917.
- Bromke, M.A., Giavalisco, P., Willmitzer, L., Hesse, H., 2013. Metabolic analysis of adaptation to short-term changes in culture conditions of the marine diatom *Thalassiosira pseudonana*. *PLoS One* 8 (6), art. no. e67340.
- Byrdwell, W.C., Neff, W.E., 2002. Dual parallel electrospray ionization and atmospheric pressure chemical ionization mass spectrometry (MS), MS/MS and MS/MS/MS for the analysis of triacylglycerols and triacylglycerol oxidation products. *Rapid Commun. Mass Spectrom.* 16, 300–319.
- Christie, W.W., 1988. Separation of molecular species of triacylglycerols by high-performance liquid chromatography with a silver ion column. *J. Chromatogr. A* 454, 273–284.
- Danielewicz, M.A., Anderson, L.A., Franz, A.K., 2011. Triacylglycerol profiling of marine microalgae by mass spectrometry. *J. Lipid Res.* 52, 2101–2108.
- Dugo, P., Kumm, T., Crupi, M.L., Cotroneo, A., Mondello, L., 2006. Comprehensive two-dimensional liquid chromatography combined with mass spectrometric detection in the analyses of triacylglycerols in natural lipidic matrices. *J. Chromatogr. A* 1112, 269–275.
- Fahy, E., Subramaniam, S., Murphy, R.C., Nishijima, M., Raetz, C.R.H., Shimizu, T., Spener, F., van Meer, G., Wakelam, M.J.O., Dennis, E.A., 2009. Update of the LIPID MAPS comprehensive classification system for lipids. *J. Lipid Res.* 50, S9–S14.
- Giroud, C., Gerber, A., Eichenberger, W., 1988. Lipids of *Chlamydomonas reinhardtii*. Analysis of molecular species and intracellular site(s) of biosynthesis. *Plant Cell Physiol.* 29, 587–595.
- Han, X., Yang, K., Gross, R.W., 2012. Multi-dimensional mass spectrometry-based shotgun lipidomics and novel strategies for lipidomic analyses. *Mass Spectrom. Rev.* 31, 134–178.
- Hoham, R.W., Duval, B., 2001. Microbial ecology of snow and freshwater ice with emphasis on snow algae. In: Jones, H.G., Pomeroy, J.W., Walker, D.A., Hoham, R.W. (Eds.), *Snow Ecology: An Interdisciplinary Examination of Snow-covered Ecosystems*. Cambridge University Press, Cambridge, pp. 168–228.
- Hoham, R.W., 1975. The life history and ecology of the snow alga *Chloromonas pichincha* (Chlorophyta, Volvocales). *Phycologia* 14, 213–226.
- Hoham, R.W., Frey, F.M., Mohn, W.W., Felio, J.H., Todd, S., Duncan, J.E., Banghart, J.B., 2008. Optimum growth temperatures of three species of green *Chloromonas* snow algae from Upstate New York and the White Mountains, Arizona. *Arct. Antarct. Alp. Res.* 40, 355–363.
- Kates, M., 1986. Techniques of lipidology: isolation, analysis and identification of lipids. In: Work, T.S., Work, E. (Eds.), *Laboratory Techniques in Biochemistry and Molecular Biology*, second ed. Elsevier, Amsterdam, pp. 220–223.
- Laakso, P., Christie, W.W., 1991. Combination of silver ion and reversed-phase high-performance liquid chromatography in the fractionation of herring oil triacylglycerols. *J. Am. Oil Chem. Soc.* 68, 213–223.
- Lang, I., Hodac, L., Friedl, T., Feussner, I., 2011. Fatty acid profiles and their distribution patterns in microalgae: a comprehensive analysis of more than 2000 strains from the SAG culture collection. *BMC Plant Biol.* 11, art. no. 124.
- Lee, Y.J., Leverage, R.C., Smith, E.A., Valenstein, J.S., Kandel, K., Trewyn, B.G., 2013. High-throughput analysis of algal crude oils using high resolution mass spectrometry. *Lipids* 48, 297–305.
- LIPID MAPS-Nature Gateway Web Site Page. Available from: <<http://www.lipidmaps.org/>> (accessed Nov 2013).
- Lisa, M., Holcapek, M., Řezanka, T., Kabatova, N., 2007. High-performance liquid chromatography-atmospheric pressure chemical ionization mass spectrometry and gas chromatography-flame ionization detection characterization of $\Delta 5$ -polyenoic fatty acids in triacylglycerols from conifer seed oils. *J. Chromatogr. A* 1146, 67–77.
- Lisa, M., Velínska, H., Holcapek, M., 2009. Regioisomeric characterization of triacylglycerols using silver-ion HPLC/MS and randomization synthesis of standards. *Anal. Chem.* 81, 3903–3910.
- Liu, B., Vieler, A., Li, C., Jones, A.D., Benning, C., 2013. Triacylglycerol profiling of microalgae *Chlamydomonas reinhardtii* and *Nannochloropsis oceanica*. *Bioresour. Technol.* 146, 310–316.
- Lu, N., Wei, D., Chen, F., Yang, S.T., 2012a. Lipidomic profiling and discovery of lipid biomarkers in snow alga *Chlamydomonas nivalis* under salt stress. *Eur. J. Lipid Sci. Technol.* 114, 253–265.
- Lu, N., Wei, D., Chen, F., Yang, S.-T., 2013. Lipidomic profiling reveals lipid regulation in the snow alga *Chlamydomonas nivalis* in response to nitrate or phosphate deprivation. *Process Biochem.* 48, 605–613.
- Lu, N., Wei, D., Jiang, X.-L., Chen, F., Yang, S.-T., 2012b. Regulation of lipid metabolism in the snow alga *Chlamydomonas nivalis* in response to NaCl stress: an integrated analysis by cytochrome and lipidomic approaches. *Process Biochem.* 47, 1163–1170.
- MacDougall, K.M., McNichol, J., McGinn, P.J., O'Leary, S.J.B., Melanson, J.E., 2011. Triacylglycerol profiling of microalgae strains for biofuel feedstock by liquid chromatography-high-resolution mass spectrometry. *Anal. Bioanal. Chem.* 401, 2609–2616.

- Momchilova, S., Itabashi, Y., Nikolova-Damyanova, B., Kuksis, A., 2006. Regioselective separation of isomeric triacylglycerols by reversed-phase high-performance liquid chromatography: stationary phase and mobile phase effects. *J. Sep. Sci.* 29, 2578–2583.
- Momchilova, S.M., Nikolova-Damyanova, B.M., 2012. Advances in silver ion chromatography for the analysis of fatty acids and triacylglycerols-2001 to 2011. *Anal. Sci.* 28, 837–844.
- Morgan-Kiss, R.M., Priscu, J.C., Pockock, T., Gudynaite-Savitch, L., Huner, N.P.A., 2006. Adaptation and acclimation of photosynthetic microorganisms to permanently cold environments. *Microbiol. Mol. Biol. Rev.* 70, 222–252.
- Mottram, H.R., Crossman, Z.M., Evershed, R.P., 2001. Regiospecific characterisation of the triacylglycerols in animal fats using high performance liquid chromatography-atmospheric pressure chemical ionisation mass spectrometry. *Analyst* 126, 1018–1024.
- Nikolova-Damyanova, B., 2009. Retention of lipids in silver ion high-performance liquid chromatography: facts and assumptions. *J. Chromatogr. A* 1216, 1815–1824.
- Proschold, T., Marin, B., Schlosser, U.G.T., Melkonian, M., 2001. Molecular phylogeny and taxonomic revision of *Chlamydomonas* (Chlorophyta). I. Emendation of *Chlamydomonas* Ehrenberg and *Chloromonas* Gobi, and description of *Oogamochlamys* gen. nov and *Lobochlamys* gen. nov. *Protist* 152, 265–300.
- Rezanka, T., Sigler, K., 2007. The use of atmospheric pressure chemical ionization mass spectrometry with high performance liquid chromatography and other separation techniques for identification of triacylglycerols. *Curr. Anal. Chem.* 3, 252–271.
- Rezanka, T., Nedbalová, L., Sigler, K., 2008. Unusual medium-chain polyunsaturated fatty acids from the snow alga *Chloromonas brevispina*. *Microbiol. Res.* 163, 373–379.
- Rezanka, T., Lukavský, J., Nedbalová, L., Sigler, K., 2011. Effect of nitrogen and phosphorus starvation on the polyunsaturated triacylglycerol composition, including positional isomer distribution, in the alga *Trachydiscus minutus*. *Phytochemistry* 72, 2342–2351.
- Rezanka, T., Kolouchová, I., Cejková, A., Cajthaml, T., Sigler, K., 2013. Identification of regioisomers and enantiomers of triacylglycerols in different yeasts using reversed- and chiral-phase LC–MS. *J. Sep. Sci.* 36, 3310–3320.
- Spijkerman, E., Wacker, A., Weithoff, G., Leya, T., 2012. Elemental and fatty acid composition of snow algae in Arctic habitats. *Front. Microbiol.* 3, art. no. 380.
- Vieler, A., Wilhelm, C., Goss, R., Süß, R., Schiller, J., 2007. The lipid composition of the unicellular green alga *Chlamydomonas reinhardtii* and the diatom *Cyclotella meneghiniana* investigated by MALDI-TOF MS and TLC. *Chem. Phys. Lipids* 150, 143–155.
- Whitelam, G.C., Codd, G.A., 1986. Damaging effects of light on microorganisms. In: Herbert, R.A., Codd, G.A. (Eds.), *Microbes in Extreme Environments*. Academic Press, London, pp. 129–169.

Supplements

Table 1S. List of total lipids from snow alga *C. pichincha* analyzed by high mass resolution ESI-MS in positive ion mode.

molecular species	HR MS	BUD_FIT	MEANDRY	UDOLI
ergosterol	419.3289	2934	2515	3832
ergosta-5,7-dienol 7	421.3439	1916	2401	1497
ergosta-7-enol	423.3602	2695	2874	1737
7-dehydroporiferasterol	433.3446	192	228	234
stigmasterol	435.3602	1198	1048	1144
stigmasta-7-enol	437.3759	1563	1012	1275
γ -tocopherol	439.3552	251	461	407
α -tocopherol	453.3708	389	581	287
lysoPE 16:4	468.2141	168	216	257
lysoPE 16:3	470.2298	365	317	353
lysoPE 16:2	472.2455	251	305	299
vitamin K1	473.3390	581	365	323
lysoPE 16:1	474.2612	222	198	269
lysoPE 16:0	476.2769	170	175	131
lysoPE 18:4	496.2455	317	174	246
lysoPE 18:3	498.2612	142	129	112
lysoPG 16:4	499.2066	48	18	42
lysoPE 18:2	500.2769	86	80	76
lysoPG 16:3	501.2223	12	42	12
lysoPE 18:1	502.2926	51	51	38
lysoPG 16:2	503.2380	24	24	54
lysoPG 16:1	505.2537	50	50	50
lysoPG 16:0	507.2693	62	61	54
lysoPC 16:4	510.2614	156	251	251
lysoPC 16:3	512.2771	365	210	305
lysoPC 16:2	514.2928	102	281	293
lysoPC 16:1	516.3085	126	174	210
lysoPC 16:0	518.3242	673	686	606
lysoPG 18:4	527.2380	156	222	186
lysoPG 18:3	529.2537	212	212	212
lysoPG 18:2	531.2694	62	63	62
lysoPG 18:1	533.2851	54	30	36
lysoPG 18:0	535.3008	30	24	6
lysoPC 18:4	538.2927	355	371	309
lysoPC 18:3	540.3084	344	344	300
lysoPC 18:2	542.3235	252	261	219
lysoPC 18:1	544.3399	44	36	34
lysoPC 18:0	546.3552	65	56	69
α + β -carotene	559.4279	305	335	473

echinenone	573.4066	1437	2365	4251
DAG 32:8	575.3718	1138	1198	1377
β-cryptoxanthin	575.4223	557	515	317
DAG 32:7	577.3875	1078	1437	1497
DAG 32:6	579.4032	5808	5150	5509
DAG 32:5	581.4188	2515	3892	3234
DAG 32:4	583.4343	719	5389	2635
DAG 32:3	585.4502	5090	4311	1976
canthaxanthin	587.3865	138	168	192
DAG 32:2	587.4656	5629	838	5389
DAG 32:1	589.4821	4671	3353	5269
zeaxanthin+lutein	591.4178	443	281	365
DAG 34:8	603.4032	5329	5868	5509
DAG 34:7	605.4189	3713	2515	2096
antheraxanthin	607.4121	335	299	263
DAG 34:6	607.4346	4270	4632	5012
DAG 34:5	609.4502	231	225	205
DAG 34:4	611.4657	322	355	418
DAG 34:3	613.4816	21663	24289	23571
pheophorbide a	615.2577	407	437	293
DAG 34:2	615.4970	12378	13827	14130
DAG 34:1	617.5135	1083	1107	983
astaxanthin	619.3757	90	114	126
violaxanthin	623.4094	5041	5273	5056
chl c2	631.1801	437	581	275
DAG 36:8	631.4344	1138	778	1257
chl c1	633.1964	371	305	108
DAG 36:7	633.4501	725	2156	3234
DAG 36:6	635.4658	8957	9812	10245
DAG 36:5	637.4814	11861	12855	12545
DAG 36:4	639.4974	3768	3717	3689
DAG 36:3	641.5135	586	581	581
DAG 36:2	643.5288	454	497	510
DAG 36:1	645.5457	112	104	122
fucoxanthin	663.4020	3353	2365	2395
PE 32:8	698.3794	1772	1868	1707
PE 32:7	700.3951	1898	2102	1910
PE 32:6	702.4108	3377	3006	2862
PE 32:5	704.4275	2467	2557	3042
PE 32:4	706.4432	1180	1743	1443
PE 32:3	708.4589	1575	1713	1838
PE 32:2	710.4745	1898	1862	1449
PE 32:1	712.4909	1443	904	1683
PS 32:8	718.3766	665	701	856
DGTS 32:8	718.4659	1431	1922	2467

PS 32:7	720.3923	629	683	587
DGTS 32:7	720.4815	1898	1461	1886
PS 32:6	722.4080	737	707	784
DGTS 32:6	722.4972	2904	3012	1868
PS 32:5	724.4237	587	569	557
DGTS 32:5	724.5128	808	2587	1862
PE 34:8	726.4108	1862	1707	4263
PS 32:4	726.4394	377	365	437
PE 34:7	728.4265	1772	2377	2341
PS 32:3	728.4551	222	563	401
PE 34:6	730.4422	203	163	140
PS 32:2	730.4698	335	234	353
PG 32:8	731.3912	5329	3892	4431
PE 34:5	732.4589	699	426	520
PG 32:7	733.4069	3413	3683	3000
PE 34:4	734.4746	322	16	430
PG 32:6	735.4226	3713	3060	3988
PE 34:3	736.4903	4182	4576	4984
MGDG 32:8	737.4239	784	766	737
PG 32:5	737.4383	1976	2874	2659
PE 34:2	738.5059	7256	7187	7617
MGDG 32:7	739.4396	713	844	826
PG 32:4	739.4540	1263	1868	1533
PC 32:8	740.4280	671	599	641
PE 34:1	740.5223	588	581	490
MGDG 32:6	741.4553	814	790	749
PG 32:3	741.4697	1437	1701	1796
PC 32:7	742.4437	563	563	713
MGDG 32:5	743.4720	1024	922	892
PG 32:1	743.4854	2234	2105	1921
PC 32:6	744.4594	509	509	581
DGTS 34:8	744.4815	1401	1952	2120
MGDG 32:4	745.4878	563	838	713
PG 32:0	745.5011	2357	2223	2124
PS 34:8	746.4080	222	335	371
PC 32:5	746.4778	1862	1778	1575
DGTS 34:7	746.4972	898	862	994
MGDG 32:3	747.5028	689	749	641
PS 34:7	748.4237	293	413	222
PC 32:4	748.4921	1287	1275	1683
DGTS 34:6	748.5128	982	946	850
MGDG 32:2	749.5194	509	563	635
PS 34:6	750.4394	341	222	329
PC 32:3	750.5054	1430	1091	1181
DGTS 34:5	750.5285	790	802	820

MGDG 32:1	751.5348	737	844	766
PS 34:5	752.4551	174	377	395
PC 32:2	752.5206	449	397	343
DGTS 34:4	752.5441	665	910	790
PE 36:8	754.4417	671	1260	673
PS 34:4	754.4708	216	198	263
PC 32:1	754.5373	535	555	474
PE 36:7	756.4574	2034	2013	1386
PS 34:3	756.4865	616	612	541
PC 32:0	756.5535	531	561	594
PG 34:8	757.4058	21916	28982	7216
PE 36:6	758.4731	28375	26976	22782
PS 34:2	758.5012	299	259	233
PG 34:7	759.4215	6108	8503	10479
PE 36:5	760.4888	2853	2628	2661
PG 34:6	761.4372	4995	3770	4952
PE 36:4	762.5062	4202	4567	4274
PG 34:5	763.4529	5482	4885	5467
PE 36:3	764.5219	345	370	395
MGDG 34:8	765.4553	1186	1263	1281
PG 34:4	765.4686	35791	31311	30064
PE 36:2	766.5382	565	512	558
MGDG 34:7	767.4710	1419	994	916
PG 34:3	767.4843	14786	13460	12099
PC 34:8	768.4594	1563	1707	1802
PE 36:1	768.5555	34	31	32
MGDG 34:6	769.4867	16108	14251	13772
PG 34:2	769.4973	9763	9412	8703
PC 34:7	770.4751	1898	1838	1443
MGDG 34:5	771.5034	52441	55929	53744
PG 34:1	771.5164	1592	1549	1339
plastoquinone	771.6065	2500	3123	3108
PC 34:6	772.4908	14858	13915	12519
MGDG 34:4	773.5192	13619	14956	13691
PG 34:0	773.5311	410	368	339
PS 36:8	774.4394	551	539	533
PC 34:5	774.5092	980	1137	1193
DGTS 36:8	774.5285	3012	3210	3389
MGDG 34:3	775.5342	37248	34208	35511
PS 36:7	776.4551	461	377	335
PC 34:4	776.5235	1054	1109	980
DGTS 36:7	776.5441	2587	1886	2485
MGDG 34:2	777.5508	3362	3104	2864
PS 36:6	778.4708	407	305	281
PC 34:3	778.5368	47442	39713	33898

DGTS 36:6	778.5587	1952	1994	1868
MGDG 34:1	779.5662	967	1026	1017
PS 36:5	780.4865	293	234	263
PC 34:2	780.5520	42621	42377	36337
DGTS 36:5	780.5737	1802	1659	1293
PS 36:4	782.5022	189	275	151
PC 34:1	782.5687	12124	11171	9415
DGTS 36:4	782.5894	1497	2162	1868
PS 36:3	784.5179	170	161	159
PG 36:8	785.4372	1533	1683	1443
PS 36:2	786.5326	305	341	293
PG 36:7	787.4529	766	976	1036
PS 36:1	788.5483	503	533	485
PG 36:6	789.4686	1036	1263	1174
PG 36:5	791.4843	904	1180	1275
PG 36:4	793.5000	820	1036	671
PG 36:3	795.5157	3234	3916	3629
PC 36:8	796.4901	714	716	1321
MGDG 36:6	797.5184	43013	43576	33476
PG 36:2	797.5287	2216	4257	3623
PC 36:7	798.5057	1352	1418	2017
SQDG 32:8	799.3638	533	665	599
MGDG 36:5	799.5347	20365	20833	21647
PG 36:1	799.5478	5509	2934	2216
PC 36:6	800.5214	55289	56064	54472
SQDG 32:7	801.3795	557	551	509
MGDG 36:4	801.5498	2442	2676	2922
PC 36:5	802.5365	50262	47140	44999
SQDG 32:6	803.3952	545	539	563
MGDG 36:3	803.5658	1138	1200	1192
PC 36:4	804.5522	32319	37628	31437
SQDG 32:5	805.4109	509	527	527
MGDG 36:2	805.5815	1305	964	563
PC 36:3	806.5686	7909	7350	6570
PC 36:3	806.5687	6917	5723	5518
SQDG 32:4	807.4266	287	323	281
TAG 48:12	807.5529	2337	2375	1831
MGDG 36:1	807.5972	689	1180	533
PC 36:2	808.5836	4583	4308	4170
TAG 48:11	809.5686	1230	1492	1669
PC 36:1	810.6009	371	307	343
SQDG 32:3	811.4652	323	401	461
TAG 48:10	811.5843	1455	1695	2341
SQDG 32:2	813.4812	377	395	329
TAG 48:9	813.6001	1377	1989	1796

SQDG 32:1	815.4969	581	551	527
TAG 48:7	815.6157	1651	2304	1826
CoQ9	817.6127	7024	8744	10318
TAG 48:6	817.6314	2365	2407	2413
PI 32:7	819.4071	4850	5874	503
TAG 48:5	819.6471	2147	2661	2696
PI 32:6	821.4228	4311	5006	4695
TAG 48:4	821.6628	2429	3326	3018
PI 32:5	823.4385	3353	3575	3898
TAG 48:3	823.6785	2954	3992	5570
PI 32:4	825.4542	4671	3772	3174
TAG 48:2	825.6942	1226	1588	1637
PI 32:3	827.4699	5629	4760	5611
TAG 48:1	827.7124	1879	2209	2448
SQDG 34:8	829.4109	581	545	509
PI 32:2	829.4849	2216	2461	3036
TAG 48:0	829.7281	7567	8235	8521
SQDG 34:7	831.4266	335	347	275
PI 32:1	831.5009	2515	2365	2413
SQDG 34:6	833.4423	203	181	179
TAG 50:12	833.5708	720	781	1378
SQDG 34:5	835.4580	200	212	187
TAG 50:11	835.5865	1139	840	1559
TAG 50:10	837.6022	1754	1251	1875
SQDG 34:3	839.4966	1140	1213	1261
TAG 50:9	839.6179	3018	3557	3296
SQDG 34:2	841.5126	856	783	768
TAG 50:8	841.6336	1811	2457	2456
SQDG 34:1	843.5283	4016	3875	3438
TAG 50:7	843.6493	29413	30014	27665
TAG 50:6	845.6650	4138	3490	3006
PI 34:7	847.4385	581	491	581
TAG 50:5	847.6807	24658	24981	24862
PI 34:6	849.4542	509	515	545
TAG 50:4	849.6972	22564	20330	21066
PI 34:5	851.4699	377	575	485
TAG 50:3	851.7127	16576	14342	15078
PI 34:4	853.4856	323	485	377
TAG 50:2	853.7282	1960	1925	2336
PI 34:3	855.5013	4538	4775	4903
TAG 50:1	855.7437	2260	2806	2957
SQDG 36:8	857.4501	4299	5491	4880
PI 34:2	857.5163	2499	2323	2847
TAG 50:0	857.7606	805	1006	1112
SQDG 36:7	859.4658	2731	2299	3754

PI 34:1	859.5323	1302	1330	113
SQDG 36:6	861.4815	3573	3479	3259
TAG 52:12	861.6046	1314	2647	1737
SQDG 36:5	863.4977	686	660	588
TAG 52:11	863.6203	2264	3001	1859
SQDG 36:4	865.5134	3648	3640	3123
TAG 52:10	865.6360	2881	3229	2941
SQDG 36:2	867.5291	115	112	98
TAG 52:9	867.6517	2131	2849	3069
SQDG 36:1	869.5448	63	50	46
TAG 52:8	869.6647	10869	15137	12716
TAG 52:7	871.6804	2608	2136	3672
PI 36:8	873.4550	1455	1383	1299
TAG 52:6	873.6961	14344	15449	16166
PI 36:7	875.4707	1024	587	988
TAG 52:5	875.7120	14324	16143	16350
PI 36:6	877.4864	1270	1184	1186
TAG 52:4	877.7284	5648	4613	5941
PI 36:5	879.5021	614	526	458
TAG 52:3	879.7432	4230	4786	5078
PI 36:4	881.5180	223	264	313
TAG 52:2	881.7595	3864	4082	4437
PI 36:3	883.5332	291	319	291
TAG 52:1	883.7676	655	604	630
PI 36:2	885.5491	545	412	412
CoQ10	885.6748	485	605	631
PI 36:1	887.5643	259	236	410
TAG 54:12	889.6339	1206	1244	1936
TAG 54:11	891.6496	1446	1557	1894
pheophytin a	893.5551	1461	1503	1263
pheophytin	893.5564	3473	1999	2018
TAG 54:10	893.6653	2583	1678	1888
TAG 54:9	895.6810	19199	20322	23264
TAG 54:8	897.6966	23601	25211	28018
DGDG 32:8	899.4770	4132	3234	3413
TAG 54:7	899.7118	12113	13161	14736
DGDG 32:7	901.4927	3102	3204	2515
TAG 54:6	901.7273	4008	4529	4969
DGDG 32:6	903.5084	2695	2545	1886
TAG 54:5	903.7425	2554	2845	3545
DGDG 32:5	905.5234	2814	3114	1766
TAG 54:4	905.7583	2357	2925	3790
DGDG 32:4	907.5391	1078	1856	2455
TAG 54:3	907.7746	4127	4980	7012
DGDG 32:3	909.5550	1257	1743	1976

DGDG 32:2	911.5718	2934	1611	1557
DV chl a	913.5088	2515	2275	3060
DGDG 32:1	913.5872	2096	2695	2521
chl a	915.5244	156	168	293
DV chl b	927.4881	4311	5030	4491
DGDG 34:8	927.5084	11377	5126	11976
chl b	929.5037	246	317	168
DGDG 34:7	929.5241	5868	5509	6048
DGDG 34:6	931.5398	1210	1240	1198
DGDG 34:5	933.5548	1132	1086	1078
DGDG 34:4	935.5705	792	653	683
DGDG 34:3	937.5864	1066	1018	1012
DGDG 34:2	939.6032	3125	2835	2960
DGDG 34:1	941.6186	778	727	658
DGDG 36:6	959.5710	21078	20539	21437
DGDG 36:5	961.5865	4712	4553	3866
DGDG 36:4	963.6043	10414	9860	9369
DGDG 36:3	965.6182	13465	13835	12074
DGDG 36:2	967.6339	83	93	88
DGDG 36:8	989.6218	299	420	350
DGDG 36:7	993.6494	113	120	108

Paper X

Analyzing carotenoids of snow algae by Raman microspectroscopy and high-performance liquid chromatography

Osterrothová K¹, Culka A¹, Němečková K¹, Kaftan D^{2,3},
Nedbalová L⁴, Procházková L⁴ & Jehlička J¹

Spectrochimica Acta Part A:

Molecular and Biomolecular Spectroscopy 212: 262–271, 2014

¹ *Institute of Geochemistry, Mineralogy and Mineral Resources, Faculty of Science, Charles University, Prague, 128 43, Czech Republic*

² *Center Algatech, Institute of Microbiology of the Czech Academy of Sciences, Třeboň, Czech Republic,*

³ *Faculty of Science, University of South Bohemia, České Budějovice, Czech Republic*

⁴ *Department of Ecology, Faculty of Science, Charles University, Viničná 7, Prague, 128 44, Czech Republic*



Analyzing carotenoids of snow algae by Raman microspectroscopy and high-performance liquid chromatography

Kateřina Osterrothová^{a,*}, Adam Culka^a, Kateřina Němečková^a, David Kaftan^{b,c}, Linda Nedbalová^d, Lenka Procházková^d, Jan Jehlička^a

^a Institute of Geochemistry, Mineralogy and Mineral Resources, Faculty of Science, Charles University, Albertov 6, Prague 128 43, Czech Republic

^b Center Algatech, Institute of Microbiology of the Czech Academy of Sciences, Třeboň, Czech Republic

^c Faculty of Science, University of South Bohemia, České Budějovice, Czech Republic

^d Department of Ecology, Faculty of Science, Charles University, Viničná 7, Prague 128 44, Czech Republic



ARTICLE INFO

Article history:

Received 12 September 2018

Received in revised form 4 January 2019

Accepted 5 January 2019

Available online 06 January 2019

Keywords:

Snow algae

Raman spectroscopy

HPLC

Carotenoids

Exobiology

Biomarker

ABSTRACT

We tested the potential of Raman microspectroscopy to determine carotenoid pigments – both primary (lutein, beta-carotene) and secondary (astaxanthin) carotenoids – in the different species and life-cycle stages of snow algae from the order Chlamydomonadales (Chlorophyta). We compared the performance of Raman spectrometry to a reference method of biological pigment analysis, high-performance liquid chromatography (HPLC). The three main carotenoid Raman bands of the astaxanthin-rich red cysts were located at 1520, 1156 and 1006 cm^{-1} . The shifts (orange aplanozygotes and green motile cells with flagella) in the position of the $\nu_1(\text{C}=\text{C})$ Raman band of the polyenic chain is consistent with the expected changes in the ratios of the various carotenoid pigments. Flagellated green cells commonly contain lutein as a major carotenoid, together with minor amounts of β -carotene and varying amounts of antheraxanthin, violaxanthin and neoxanthin. Aplanozygotes contain mixtures of both primary and secondary carotenoids. In most cases, the $\nu_1(\text{C}=\text{C})$ band is an overlapping set of bands, which is due to the signal of all carotenoid pigments in the sample, and a deconvolution along with the band position shifts (mainly ν_1) could be used to characterize the mixture of carotenoids. However, the ability of Raman spectroscopy to discriminate between structurally slightly differing carotenoid pigments or several carotenoids in an admixture in an unknown biological system remains limited.

© 2019 Elsevier B.V. All rights reserved.

1. Introduction

The only planet in our solar system thus far known to harbor life is our home planet, Earth. Lacking evidence of life elsewhere, exobiology research is generally focused on the origin and early evolution of life, the potential of life to adapt to different environments and the implications for life elsewhere. Organisms that inhabit extreme environments, known as extremophiles, thrive in habitats which are intolerably hostile or even fatal for other terrestrial life-forms [1]. The solar system contains several locations of exobiological interest. The subsurface oceans of Europa and Enceladus could host ecosystems like the ones found around hydrothermal vents on Earth. Considering the low Martian temperatures, abundant salt deposits and harsh UV-radiation (UVR), extremophiles such as halophiles (organisms that require NaCl for growth) and psychrophiles (organisms that grow best at low temperatures) represent the best model organisms for Mars [2].

Extremophiles include members of all three domains of life, i.e., bacteria, archaea and eukarya. Most extremophiles are microorganisms (of which a high proportion are archaea), but this group also includes eukaryotes such as protists (e.g., algae, fungi and protozoa) and multicellular organisms. The majority of extremophilic organisms are prokaryotes, some of which use pigments to cope with conditions in their natural habitats (mainly increased UVR), e.g., orange-pigmented *Planococcus antarcticus* and *P. psychrophilus* (from the McMurdo Dry Valleys in Antarctica) [3]. A similar strategy is also common for extremophilic eukaryotes, namely snow algae, which typically inhabit locations exposed to high UVR and low temperatures.

Photosynthetic pigments (chlorophylls and carotenoids) are organic molecules with conjugated double bonds that selectively absorb ultraviolet and visible light. The excited state of the molecules then provides energy for the subsequent catalytic steps collectively known as photosynthesis. In addition, carotenoid pigments serve a photoprotective role by intercepting chlorophyll triplet species and preventing the formation of singlet oxygen ($^1\text{O}_2$) [4]. Pigments absorbing UV-C and UV-B are widely distributed through all domains of life. For exobiological

* Corresponding author.

E-mail address: osterrot@natur.cuni.cz (K. Osterrothová).

Table 1

Investigated cryoflora with sample codes, species, collection dates, sampling sites, altitude, geographic positions (GPS) and basic description.

Sample	Species	Date	Location	Altitude (m)	GPS	Life cycle stages	Snow color
1	<i>Chlainomonas</i> sp.	02.07.2012	Ľadové pleso, High Tatras	2064	49°11'0.65"N, 20°9'41.26"E	Mature cysts	Red
2	<i>Chlamydomonas nivalis</i>	18.07.2015	Tiefenbachgletscher, Ötztal Alps	2810	46°55'23.8"N, 10°56'50.1"E	Mature cysts	Red
3	<i>Chlamydomonas nivalis</i>	18.07.2015	Rettenbachgletscher, Ötztal Alps	2807	46°56'34.5"N, 10°55'29.1"E	Mature cysts	Red
4	<i>Chloromonas</i> cf. <i>nivalis</i>	12.06.2015	Luční hora, Krkonoše Mountains	1515	50°43'46.1"N, 15°40'54.4"E	Dominant flagellates, minor aplanozygotes	Green
5	<i>Chloromonas</i> cf. <i>nivalis</i>	12.06.2015	Luční hora, Krkonoše Mountains	1515	50°43'46.1"N, 15°40'54.4"E	Dominant aplanozygotes	Orange
6	<i>Chlamydomonas nivalis</i>	04.07.2002	Zamrznuté pleso, High Tatras	2062	49°10'32.06"N, 20°8'16.79"E	Mature cysts	Red
7	<i>Chloromonas</i> cf. <i>nivalis</i> , <i>Scotiella cryophila</i>	10.05.2017	Meandry Labe, Krkonoše Mountains	1044	50°45'40.68"N, 15°33'8.4"E	Prevailing unidentified flagellates, cysts of <i>Scotiella cryophila</i> and aplanozygotes of <i>Chloromonas</i> cf. <i>nivalis</i>	Green
8	<i>Chloromonas</i> cf. <i>nivalis</i> , <i>Scotiella cryophila</i>	10.05.2017	Meandry Labe, Krkonoše Mountains	1045	50°45'42.18"N, 15°33'8.94"E	Dominant unidentified flagellates, minor cysts of <i>Scotiella cryophila</i> and aplanozygotes of <i>Chloromonas</i> cf. <i>nivalis</i>	Green
9	<i>Chloromonas</i> cf. <i>nivalis</i> , <i>Scotiella cryophila</i>	11.05.2017	Dlouhý důl, Krkonoše Mountains	1002	50°43'15.3"N, 15°39'26.52"E	Aplanozygotes of <i>Chloromonas</i> cf. <i>nivalis</i> and cysts of <i>Scotiella cryophila</i>	Orange
10	<i>Chloromonas</i> cf. <i>nivalis</i>	18.06.2017	Furkotská dolina, High Tatras	2061	49°9'32.58"N, 20°1'36.74"E	Aplanozygotes	Orange
11	<i>Chloromonas</i> sp.	14.6.2017	Dolina Za Mnichem, High Tatras	1871	49°11'39.24"N, 20°03'10.08"E	Aplanozygotes	Orange

purposes, it is important to note that the surface of Mars is still exposed to high radiation levels.

According to the thermodynamic dissipation theory [5], pigments could be fundamental molecules in the origin of life. Another similar theory assumes the geothermal origin of life on Earth (and possibly on Mars); it suggests that pigments may have originated as thermal sensors for detecting suitable thermal spots. During evolution, photosynthetic pigments and pigments protecting against UVR would have

been selected as an advantageous survival strategy. This has led to a proposal that pigments such as carotenoids and scytonemin are relicts of early life, since protection against UV-C and UV-B is not required today due to the existence of the ozone layer. Because pigments could be key biomarkers for the detection of extinct (or extant) life on Mars and other planets [6], Raman spectrometers will be on board two Mars rover missions, ExoMars and Mars 2020, to search for evidence of life and habitable geological niches on Mars [7,8].



Fig. 1. Sample locations at (1) the Krkonoše Mountains, Czech Republic, (2) the High Tatras, Slovakia, and (3) the Ötztal Alps, Austria.

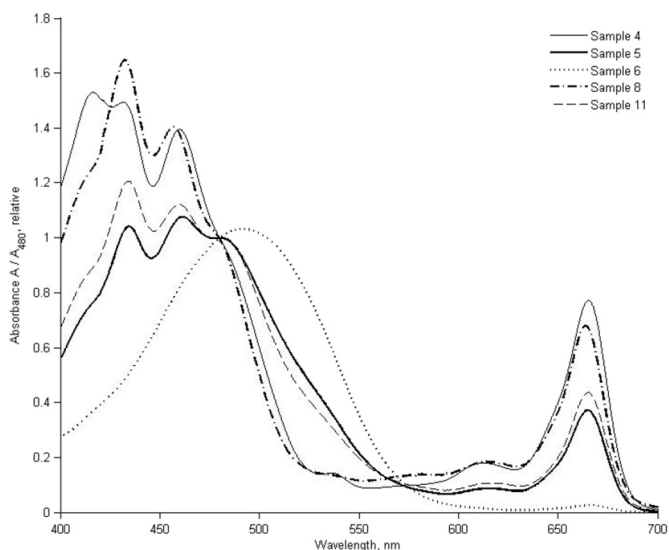


Fig. 2. Absorption spectra of extracted pigments. Absorbance of pigments from samples 4 (simple line), 5 (bold line), 6 (dotted line), 8 (dash-dot line) and 11 (dashed line) in a visible light range normalized to the absorbance at 480 nm.

Carotenoid pigments exhibit specific and strong signals in Raman spectroscopy [9,10]. By tuning the wavelength of the laser (for carotenoids, this phenomenon is related to green and blue lasers), a selective enhancement of the Raman signal can be achieved through the Resonance Raman Effect. This means that the energy of the scattered photon matches the energy of the electronic transition of the molecule, and the absorption and scattering of cross sections of the chromophore are strongly increased. This resonance effect may enhance the Raman spectrum by several orders of magnitude [11].

Large areas of our planet are covered with snow, which creates habitats for various psychrophilic microorganisms [12]. In 1819, the British polar explorer John Ross came across large patches of red snow in the area around Baffin Bay in the Arctic. Initially it was thought to be iron-nickel meteorite detritus, but in an appendix to Ross's mission report published that same year the Scottish botanist Robert Brown proposed – correctly, as was later proven – that the color came from an alga, a photosynthetic microbe. Several extreme physical/chemical factors (e.g., low temperatures, high levels of photosynthetically active radiation [PAR] and UV irradiation, repeating freeze-thaw cycles, nutrient depletion) characterize environments that are home to psychrophilic microorganisms. Snow algal communities dwell within liquid water retained among snow crystals and form the macroscopic phenomenon of green, orange and red snow in polar and alpine habitats. The phenomenon is commonly called watermelon, red or blood snow. Snow algae have developed multiple adaptations to life in extreme conditions, e.g., the synthesis of secondary carotenoids (mainly astaxanthin), which protects the cells against excessive light and UV radiation. In addition, the presence of both flagellates and immotile resting stages represents a successful life strategy adaptation to the snow habitat [12]. Colorful cryosestonic algal blooms have been reported from locations such as the European Alps [13–15], the High Tatras in Slovakia [16], Svalbard [17], the Krkonoše Mountains in the Czech Republic [18], the Andes in Ecuador [19], glaciers in Greenland [20] and Russia [21], Japanese alpine snowfields [22] and many others. Several studies have shown that the overproduction of pigments decreases the albedo of snow resulting in faster melting, which may contribute to a more rapid development of algal blooms [20,23].

Carotenoids of microalgae are categorized as primary and secondary. Primary carotenoids (e.g., β -carotene, lycopene, lutein) participate in photosynthesis, whereas secondary carotenoids (e.g. astaxanthin, canthaxanthin) are synthesized under stress conditions (increased salinity, high irradiance, etc.). Secondary carotenoids are usually accumulated in

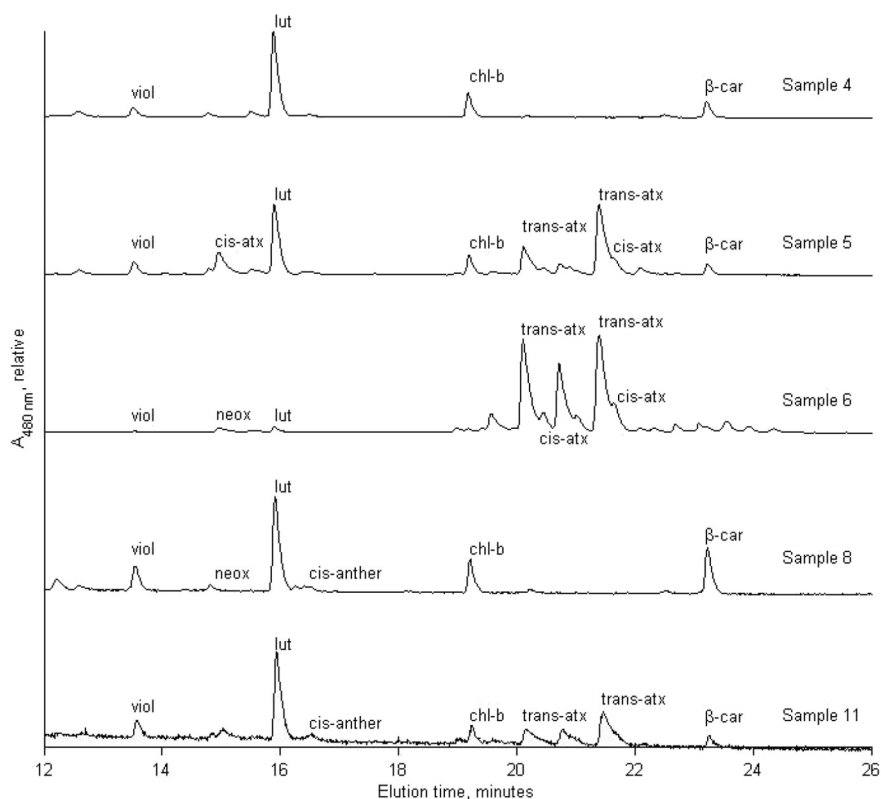


Fig. 3. Chromatograms of pigments extracted from representative samples of snow algae (detection wavelength was 480 nm). Maximum absorbances correspond to 0.56, 0.59, 0.81, 0.17 and 0.06 of relative units in the samples 4, 5, 6, 8 and 11, respectively.

Table 2

Relative content of pigments normalized to chlorophyll *a* in the samples determined by HPLC. Abbreviations: viol, violaxanthin; neox, neoxanthin; anther, antheraxanthin; lut, lutein; chl *b*, chlorophyll *b*; β -car, β -carotene; *cis*-atx, astaxanthin *cis*-isomers (mainly 13Z), *trans*-atx, astaxanthin (all-*trans*); total atx = *trans*-atx + *cis*-atx; n.d., not detected.

Sample	viol	neox	anther	lut	chl <i>b</i>	β -car	<i>cis</i> -atx	<i>trans</i> -atx	Total atx
1	n.d.	n.d.	n.d.	1.2307	0.2953	n.d.	39.3037	18.8672	58.1709
2	n.d.	n.d.	n.d.	0.1227	0.0367	n.d.	n.d.	57.9693	57.9693
3	0.0875	0.0578	n.d.	0.2089	0.0567	n.d.	0.0994	57.6259	57.7253
4	0.1348	n.d.	0.0789	1.1799	0.3365	0.2188	n.d.	0.0885	0.0885
5	0.1400	n.d.	0.0543	0.7505	0.1903	0.0961	n.d.	1.8203	1.8203
6	0.0497	0.0304	0.0336	0.3548	0.0689	n.d.	0.7409	25.1805	25.9214
7	0.2383	0.0423	0.0826	0.6681	0.1414	0.1339	n.d.	0.1799	0.1799
8	0.1272	0.0337	0.0500	0.4654	0.1616	0.2279	n.d.	n.d.	n.d.
9	0.1213	n.d.	0.1039	0.4144	0.0864	n.d.	n.d.	1.2629	1.2629
10	0.1452	0.0168	0.0317	0.5218	0.0972	0.0820	n.d.	1.2629	1.2629
11	0.3208	n.d.	0.1098	1.2898	0.1764	0.1546	n.d.	1.1840	1.1840

lipid globules, e.g., astaxanthin of *Haematococcus* [24,25] and the red snow alga *Chlamydomonas nivalis* [13]. Astaxanthin and its fatty acid ester derivatives are the main secondary carotenoids in snow algae (*Chlamydomonas nivalis*, *Chlainomonas* spp., etc.). The red snow phenomenon is related to the production of this carotenoid. Besides astaxanthin, other carotenoids such as echinenone, or pigments of xanthophyll cycle (violaxanthin, antheraxanthin, zeaxanthin), are produced [13]. The content of secondary carotenoids can be used for chemotaxonomy of sometimes morphologically similar species of snow algae. For example, adonixanthin has been detected only in *Chlorococcum* spp. and *Chlamydocapsa* spp. [26]. The amount of astaxanthin fatty acid derivatives also varies. *Chlainomonas* sp. favors astaxanthin fatty acid diester derivatives, while *Chlamydomonas nivalis* [14] and *Chloromonas nivalis* prefer monoesteric form [27].

Several analytical methods are used to analyze pigments, e.g., high-performance liquid chromatography (HPLC) [28], hyperspectral imaging [29], mass spectrometry [30] and GC–MS [31]. The easiest method is the measurement of absorption maxima of pigments dissolved in a solvent. Most of methods mentioned provide precise pigment identification, but they require chemical extraction from a complex matrix of biomolecules. This is very time consuming and is usually expensive. Besides, extracted pigments are very sensitive to light and oxygen, which may lead to the deterioration of samples [30]. For this reason, non-invasive techniques are being developed.

In the last decade, Raman spectroscopy has been applied in the determination of various microbial pigments, e.g., bacterioruberin and salinixanthin of halophiles [32–34]. Raman spectroscopy has been also used to analyze several extremophiles and their habitats, e.g., endolithic communities in halite [35] and halophilic microorganisms in the stratified gypsum crusts [36] or in powders of colonized gypsum crystals [9]. The first study that focused on snow blooms using this method was published

in 2004 [37]. In this study, a 1064-nm laser was used to analyze red and green snow located in the cold deserts of Antarctica. In green snow, Raman spectroscopy allowed the detection of several pigments including cyanobacterial scytonemin (1592 cm^{-1}) and chlorophylls (~1320 cm^{-1}). Algal communities of red snow showed strong Raman bands at 1524 cm^{-1} (C=C) and 1157 cm^{-1} (C–C). The observed band at 1524 cm^{-1} could be assigned to lutein.

Another advantage of Raman spectroscopy is the miniaturization of Raman spectrometer allowing in situ measurements [38,39].

Many studies have shown that individual carotenoids cannot be unambiguously distinguished in the mixture of structurally similar compounds (e.g., carotenoids with the same conjugated chain length). This phenomenon is well documented in the case of plant tissues [40], halophiles and selected algae [34] or in the case of nicotine-treated bacteria [41].

In this study, we used both Raman microspectroscopy and HPLC, for the sake of comparison, to identify the pigments of 11 field samples of snow algae from various locations in Europe. We tested the potential of Raman spectroscopy to determine the ratios of carotenoid pigments – both primary (lutein, beta-carotene) and secondary (astaxanthin) carotenoids – in the different life-cycle stages of snow algae and how these changes are reflected in the Raman spectra.

2. Materials and Methods

2.1. Sampling Sites

Samples of snow algae were collected over the years 2002–2017 at nine geographic locations in the Krkonoše Mountains, the Ötztal Alps and the High Tatras (Table 1, Fig. 1). Living samples of the cryoflora of red, green or orange snow fields were harvested into sterile plastic

Table 3

Raman band positions for major carotenoid bands of investigated snow algae. Abbreviations: (Ch.), *Chlainomonas* sp.; (Cd.), *Chlamydomonas nivalis*; (Cr.n.) *Chloromonas cf. nivalis*; (Sc.c.), *Scotiella cryophila*; (Cr.) *Chloromonas* sp.; fl, flagellates; az, aplanozygotes; cy, cysts; un, unidentified.

Samples	1	2	3	4	5	6
Snow color	Red	Red	Red	Green	Orange	Red
Species	Ch.	Cd.	Cd.	Cr.n.	Cr.n.	Cd.
Life cycle stage	cy	cy	cy	fl	az	cy
Band assignment						
ν_1 (C=C)	1519.7	1519.9	1520	1522.8	1519.6	1520.1
ν_2 (C–C)	1155.6	1156.6	1156.7	1154.8	1156.8	1156.7
ν_3 (C–CH ₃)	1005.5	1005.7	1005.8	1004.4	1005.5	1005.8
Samples	7	8	9	10	11	
Snow color	Green	Green	Orange	Orange	Orange	
Species	Sc.c.	Cr.n.	un.	Sc.c.	Cr.n.	
Life cycle stage	cy	az	fl	cy	az	
Band assignment						
ν_1 (C=C)	1521.6	1519.5	1522.7	1522.9	1519.7	
ν_2 (C–C)	1155.9	1156.6	1155.4	1155.8	1156.1	
ν_3 (C–CH ₃)	1004.9	1005.4	1004.5	1004.8	1005	

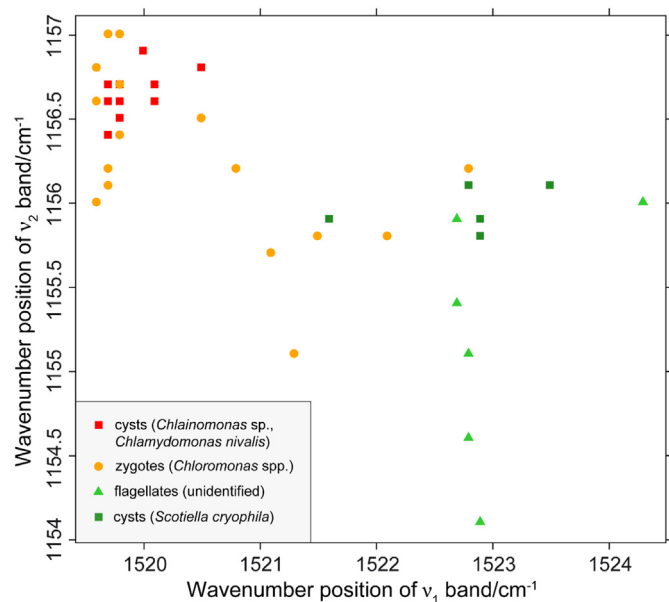


Fig. 4. Plot of C=C stretching frequency (ν_1) vs. C=C stretching frequency (ν_2) for different life stages of snow algae. Red cysts contain almost exclusively astaxanthin, while flagellates mostly lutein.

tubes and transported in a thermos bottle to the laboratory. The algal biomass was inspected under a light microscope for species and life-cycle stage identification and was kept frozen until further analysis.

2.2. Organisms

Light microscopy (LM) was conducted using an Olympus BX43 (Olympus Corporation, Japan) equipped with a digital camera DXM 1200F (Nikon, USA). Microphotographs were processed using the QuickPHOTO Camera 3.0 software (Promicra, Czech Republic). Based on light microscopy examination, colored snow was formed by the

following species: *Chlainomonas* (Ch.) sp., *Chlamydomonas* (Cd.) *nivalis*, *Chloromonas* (Cr.) cf. *nivalis*, *Scotiella* (Sc.) *cryophila* and *Chloromonas* (Cr.) sp.

2.3. HPLC Analyses

Samples were centrifuged for 2 min at 10,000 revolutions min^{-1} in Eppendorf miniSpin plus centrifuge (Eppendorf AG, Germany). Pigments were extracted from the pellet by the addition of a mixture of 50:50 methanol:acetone (v:v) in samples containing low amounts of astaxanthin, while a mixture of 10:50:40 methanol:acetone:DMSO (v:v:v) was used to extract pigments from samples dominated by astaxanthin.

Pigments were purified using a Waters HPLC system (Delta 600 Pump Controller, PDA 2996 detector) fitted with a manual injection system. Twenty microliters of extracted pigments were separated on a reverse-phase, non-end-capped Zorbax SB-C18 column (4.6 \times 150 mm, 5 μm , Agilent, USA) using a ternary gradient elution as in Wright et al. [42]: 0–4 min linear gradient from 100% solvent mixture A to 100% solvent mixture B, 4–18 min linear gradient from 100% solvent mixture B to 20% solvent mixture B and 80% of solvent C. Solvent mixture A: 80:20 methanol:0.5 M ammonium acetate (aq., pH 7.2, v:v); solvent mixture B: 90:10 acetonitrile: water (v:v); solvent C: ethyl acetate. The flow rate was 1 mL min^{-1} .

Chromatograms were aligned and baseline corrected using a chromatogram run with a blank solvent. Pigments were assigned to the peaks by comparing the measured chromatograms with a reference chromatogram of known pigment composition (acetone extract of *Chlamydomonas reinhardtii* cells grown at low light) and by transferring the HPLC fractions to standard solvents and comparing their respective absorption spectra with a reference spectra in Britton et al. [43]. Absorption spectra of the purified pigments were measured in a Lambda 35 spectrophotometer (Perkin Elmer, USA). The concentrations of chlorophyll *a*, chlorophyll *b* and total carotenoids in sample extracts were estimated spectroscopically by their absorption at 665.1, 649.1 and 480 nm normalized to a turbidity at 730 nm with the use of equations in Lichtenthaler and Wellburn [44]. Relative content of the individual

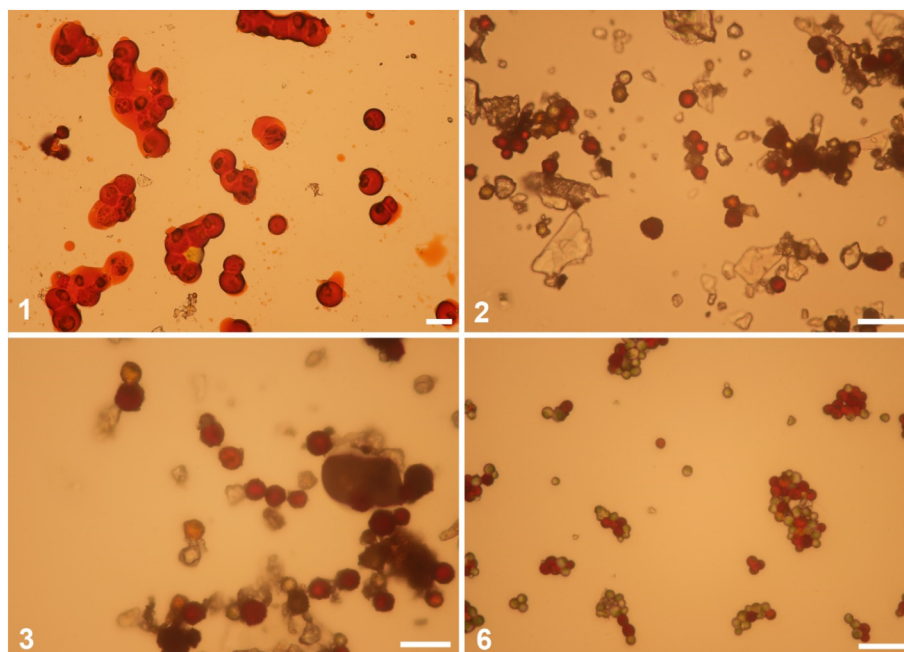


Fig. 5. Microphotographs of mature cysts of *Chlainomonas* sp. (sample 1) and *Chlamydomonas nivalis* (samples 2–3 and 6). Scale = 50 μm .

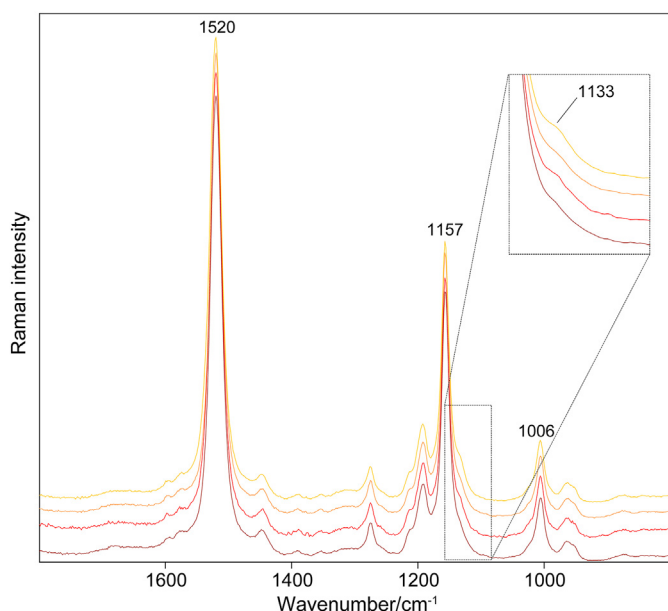


Fig. 6. Raman spectra of samples 1, 2, 3 and 6 (from the bottom). No shift in position of ν_1 (C=C) band is visible. Samples 2, 3 and 6 show a slight shoulder on the high-intensity ν_2 mode. This mode appears at $\sim 1133\text{ cm}^{-1}$.

pigments was determined by summing the area under the specific HPLC chromatographic peaks. The analysis of the spectroscopic and chromatographic data was carried out in MatLab™ (MathWorks Inc., Natick, MA) utilizing a custom-made script.

2.4. Raman Spectroscopy Analysis

Micro-Raman analyses of preserved samples was performed on a multichannel Renishaw In ViaReflex spectrometer coupled with a Peltier-cooled CCD detector. Excitation was provided by a 514.5 nm Ar laser (power $\sim 0.1\text{--}0.2\text{ mW}$). To improve signal-to-noise ratios, Raman signals from 10 scans were accumulated each of 10 s exposure. Spectra

were recorded at a resolution (FWHM) better than 1 cm^{-1} (CCD array detector/CCD chip with 576×400 pixels) between 100 and 2000 cm^{-1} . The laser spot size was $1.5\text{ }\mu\text{m}$ in diameter when focusing at the surface. By using a $50\times$ objective (NA 0.75), it was possible to analyze single algal cells. At least three spectra were recorded from different cells of snow algae in the sample. Benzonitrile was used for spectral wavenumber calibration. Raman spectra were exported into the Galactic *.SPC format. Spectra were compared using GRAMS AI (8.0, Thermo Electron Corp., Waltham, MA, USA). All of the spectra were baseline corrected. The position of the Raman bands was determined by the peak-fitting procedure of GRAMS/AI (8.0, Thermo Electron Corp., Waltham, MA, USA) program, which is based on the Levenberg-Marquardt nonlinear least-square method. A mixed Gaussian and Lorentzian peak shape was used. Peaks constituting the spectrum were manually selected to start the best-fit procedure. The best fit was then performed to determine convolution peaks with optimized intensity, position and width. Its performance was evaluated by means of the χ^2 parameter.

3. Results and Discussion

3.1. Analysis of Pigment Composition by HPLC

Absorbance spectra of the total extracted pigments demonstrate prominent differences in pigment content among the snow algae samples (Fig. 2). The concentration of chlorophyll *a*, chlorophyll *b* and total carotenoids in the extracted phase was analyzed spectroscopically. The samples 1–3 and 6 stand out among the other samples by containing only minor amounts of chlorophylls (absorbance peak at 665 nm) in respect to the total carotenoids (absorbing at the blue side of the spectrum). An illustrative example of sample 6 is shown in Fig. 2 (dotted line) exhibiting a value of carotenoid-to-chlorophyll weight ratio of 9.3.

Chlorophyll *a* and *b* and the primary carotenoids violaxanthin, neoxanthin, antheraxanthin, lutein and β -carotene were identified by means of HPLC (Fig. 3). The only prominent secondary carotenoid identified was astaxanthin and its fatty acid ester derivatives. Both *cis* and *trans* isoforms were particularly abundant in the samples 1, 2, 3 and 6. Elution chromatogram of sample 6 shown in Fig. 3 is practically devoid of any other pigments except for the all-*trans* astaxanthin, with slightly

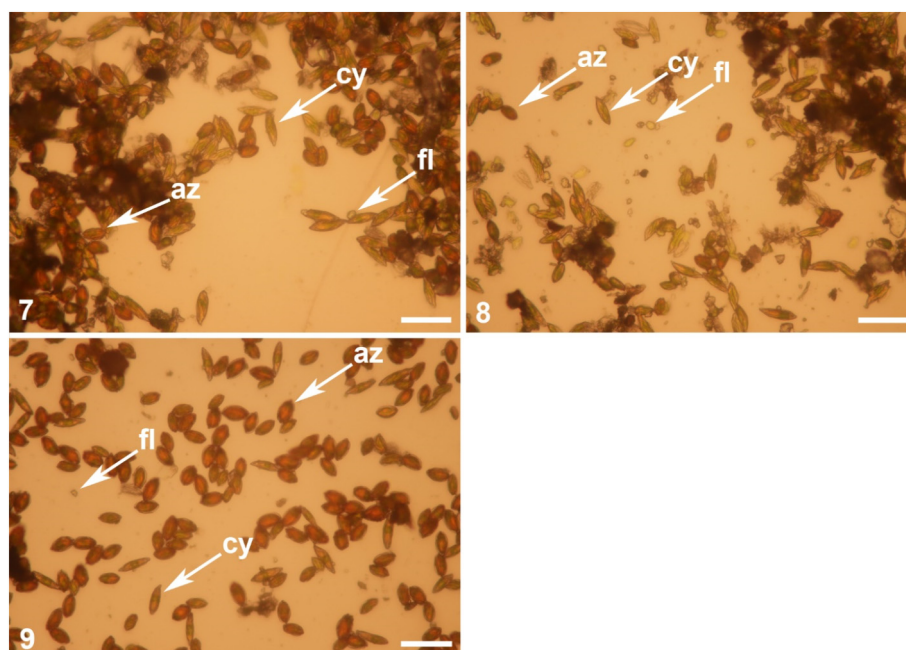


Fig. 7. Microphotographs of cysts (cy) of *Scotiella cryophila*, aplanozygotes (az) of *Chloromonas cf. nivalis* and unidentified flagellates (fl) (samples 7–9). Scale = $50\text{ }\mu\text{m}$.

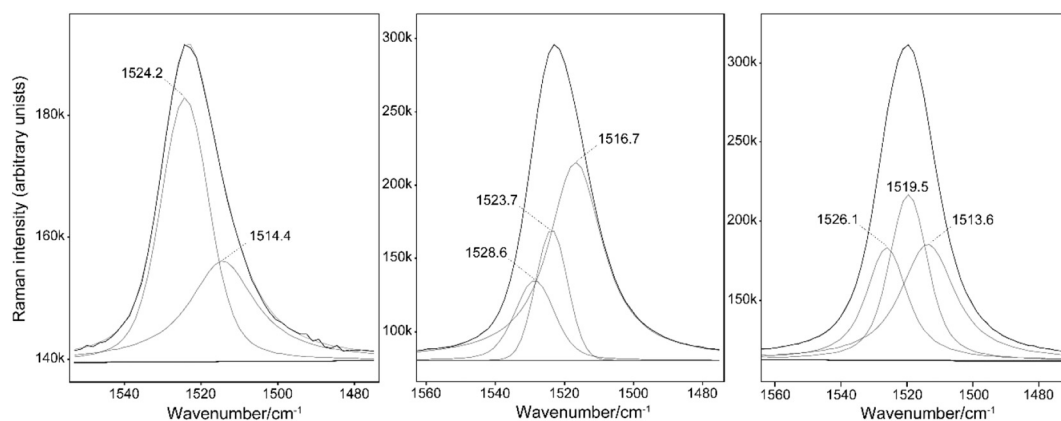


Fig. 8. Deconvolution in Gaussian/Lorentzian peaks of ν_1 region ($1460\text{--}1570\text{ cm}^{-1}$). A. flagellate (sample 4), B cyst of *Scotiella* (sample 9), C aplanozygote (sample 5). The fitted spectra matched the empirical data revealed by HPLC closely.

minor but still significant amount of *cis*-astaxanthin tailing behind the major peaks of *trans*-astaxanthin. Additionally, samples 5 and 11 contained sizeable amounts of the astaxanthin. The relative contents of individual primary and secondary carotenoids normalized to the chlorophyll *a* concentration determined spectroscopically are shown in Table 2. An overview of retention times and absorption maxima specific for the identified pigments are depicted in the Supplementary Table S1.

3.2. Analysis of Pigments by Raman Microspectroscopy

The cryoflora of green, orange and red snow fields was either homogenous, like mature cysts of *Chlainomonas* sp. (sample 1), or heterogenous, like mixture of flagellates and aplanozygotes of *Chloromonas* cf. *nivalis* (sample 4), which are different life stages in one species. The ability to analyze single cells for their carotenoid content is very important because the carotenoid composition of individual species and life stages has not been fully explored yet. Table 3 summarizes the positions of the major carotenoid bands in the samples. Reported values are characteristic for the most mature cells in the samples. In all samples, three distinctive bands were observed. The ν_1 band arises from stretching vibrations of C=C double bonds. Its frequency depends on the length of the π -electron conjugated chain and on the molecular configuration of the carotenoid. The ν_2 band is due to stretching vibrations of C—C single

bonds coupled with C—H in-plane bending modes, and this region is a fingerprint for the assignment of carotenoid configurations, i.e., isomerization states (*cis* and *trans*). The ν_3 band is due to in-plane rocking vibrations of the methyl groups attached to the conjugated chain, coupled with in-plane bending modes of the adjacent CHs [45].

Changes in pigment ratios of different maturation stages of cysts and aplanozygotes are presented as a plot of C=C stretching frequency (ν_1) vs. C—C stretching frequency (ν_2) in Fig. 4. Older cells contain more astaxanthin than younger cells, which contain more lutein [27], so there is a significant shift of the ν_1 (C=C) band position toward a higher wavenumber in the case of the younger cells.

Raman spectra of homogenous samples of mature cysts depicted in Fig. 5 (samples 1, 2, 3 and 6) show the three main carotenoid bands, which are located approximately at 1520, 1156–1157 and 1006 cm^{-1} . HPLC of sample extracts revealed that astaxanthin is the predominant carotenoid of *Chlainomonas* sp. (sample 1) and *Chlamydomonas nivalis* cysts (samples 2, 3 and 6). It is responsible for the red coloration of cells due to its high abundance. Observed ν_1 (C=C) band at approximately 1520 cm^{-1} in the Raman spectra can then be assigned to astaxanthin in its ester form [46,47]. We were not able to identify the *trans* and *cis* isomers of astaxanthin in the samples (Fig. 6), probably because they coexist in the sample. The ν_1 band in the Raman spectra undergoes no change in position. The ν_1 band appears at 1519.7 cm^{-1} in sample 1, where HPLC estimate 2:1 ratio *cis-trans* astaxanthin isomers.

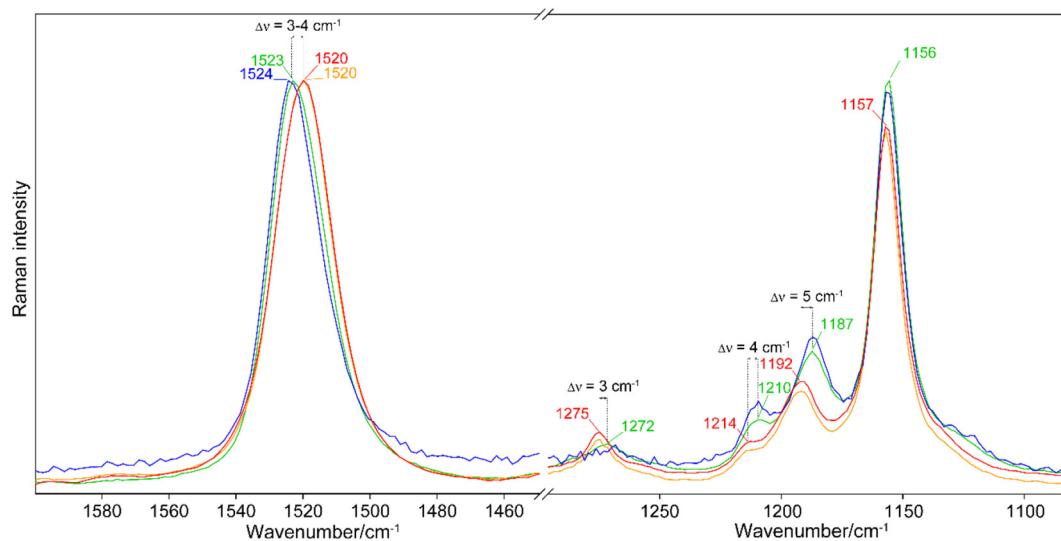


Fig. 9. Raman spectra of cyst of *Chlainomonas* sp. (sample 1) in red, aplanozygotes of *Chloromonas* cf. *nivalis* (sample 5) in orange, flagellates of *Chloromonas* cf. *nivalis* (sample 4) in blue, cyst of *Scotiella cryophila* (sample 8) in green.

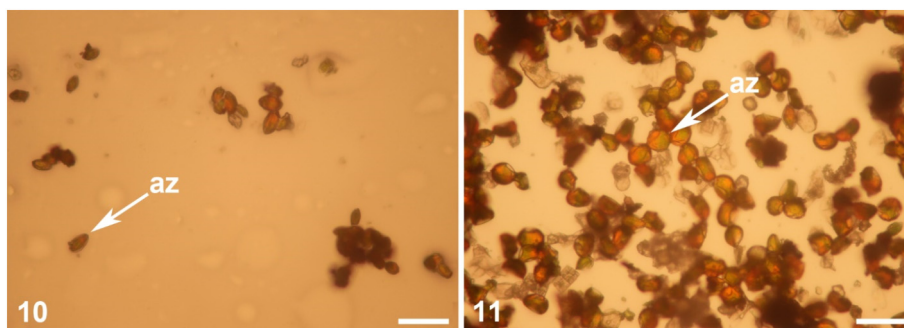


Fig. 10. Microphotographs of aplanozygotes (az) (samples 10 and 11). Scale = 50 μm .

According to Subramanian et al., who on the contrary were working with pure substances, *cis*-isomers of astaxanthin also show the new mode (ν_2') in addition to the high-intensity ν_2 mode. This mode appears at $\sim 1135\text{ cm}^{-1}$, whereas *trans*-AST isomers do not possess it [48]. We have observed a small shoulder located at around 1133 cm^{-1} in the Raman spectra of samples 2, 3 and most obviously 6. In contrast, in the spectra taken on sample 1, this feature was not detected. This variance in the spectra could be explained by the different ratios between *cis* and *trans* isomers, although we observe an opposite effect than Subramanian et al. Also, we have to note that free astaxanthin is rare in these species. Astaxanthin is present mostly in its esterified forms as diesters and monoesters (depending on the species). It has been shown that *Chlainomonas* sp. (sample 1) stores the majority of astaxanthin derivatives in the diester form, and on the contrary, *Chlamydomonas nivalis* (samples 2, 3 and 6) stores them in the less apolar monoester form [14]. We also cannot exclude the effect of the cellular environment. In any case, the reasons for this shoulder band at $\sim 1135\text{ cm}^{-1}$ are quite unclear and further investigation is required.

Heterogenous samples 7, 8 and 9 (Fig. 7) consist of immotile cells of two different species and green flagellates, probably of those two species. Green flagellates show an upshift of $\nu_1(\text{C}=\text{C})$ band to about 1523 cm^{-1} (in contrast to astaxanthin rich cysts, which have $\nu_1(\text{C}=\text{C})$ band in Raman spectra at 1520 cm^{-1}) because of their major pigment lutein. The observed asymmetry of the band at $\nu_1(\text{C}=\text{C})$ band is due to the superimposition of several bands with different line parameters. Peak fitting is optional in this situation. In the Raman spectra of carotenoids, the position of ν_1 varies according to the number of conjugated $\text{C}=\text{C}$ bonds of these molecules; there is an up-shift in the case of shorter conjugated polyenic chains [49]. Beta-carotene ($\text{C}_{40}\text{H}_{56}$) has both ends of the molecule cyclized into β -rings and has the system of 11 conjugated double bonds, two of which are in the β -rings. Lutein ($\text{C}_{40}\text{H}_{56}\text{O}_2$) is dihydroxy, dicyclic carotenoid, which derives from α -carotene and has 10 conjugated $\text{C}=\text{C}$ bonds, one of which is in the β -ring and the other of which is an isolated double bond in the ϵ -ring. Astaxanthin has nine conjugated double bonds in the polyene chain

extended by two double bonds in β -rings and two carbonyl groups double bonds. Epoxy carotenoids, antheraxanthin ($\text{C}_{40}\text{H}_{56}\text{O}_3$) has 10 conjugated double bonds, while violaxanthin ($\text{C}_{40}\text{H}_{56}\text{O}_4$) and neoxanthin ($\text{C}_{40}\text{H}_{56}\text{O}_4$) have only 9 conjugated double bonds. Thus, the frequency of ν_1 can be used to determine which carotenoids contribute to the Raman spectra. Fig. 8 reports an example of deconvolution in Gaussian/Lorentzian peaks of the ν_1 region ($1460\text{--}1570\text{ cm}^{-1}$). While deconvoluting, it is necessary to determine the number of bands to be included. In the absence of other information, initial fitting is carried out with the number of bands indicated by the topology of the Raman spectra. The Levenberg-Marquardt algorithm iteratively adjusts every variable for each peak to minimize the χ^2 . χ^2 is simply a weighted difference measure between the actual and measured data. We can assign some of the peaks in our known system to different carotenoids. In the case of flagellates, we can fit the ν_1 region into two bands as seen in Fig. 8A; the wavenumber value of pure lutein and beta-carotene (from our own measurements) are expected to be approximately at 1525 cm^{-1} and 1514 cm^{-1} , respectively (see [49]). This is in good agreement with HPLC results. Xanthophyll-cycle components: violaxanthin (1525 cm^{-1}) and antheraxanthin (1523 cm^{-1}) (from our measurements) may also contribute to the shift in $\nu_1(\text{C}=\text{C})$ band position. In the case of mature cysts of *Scotiella cryophila* (green cells containing reddish pigmented “droplets” close to the cell pole) and orange-colored aplanozygotes of *Chloromonas nivalis*, the $\nu_1(\text{C}=\text{C})$ band is also a compound band, which is due to the signal of all carotenoid pigments in the sample, and a deconvolution along with the band position could be used to tentatively characterize the mixture of carotenoids (Fig. 8B, C). On closer inspection, mature cysts of *Scotiella cryophila* had a $\nu_1(\text{C}=\text{C})$ band around 1523 cm^{-1} , similarly as was found for green flagellates (Table 3), whereas mature aplanozygotes of *Cr. nivalis* had similar position of the band in Raman spectra as mature red cysts of *Chlainomonas* sp. and *Cd. nivalis* (1520 cm^{-1}) (Fig. 9). The shift of the $\nu_1(\text{C}=\text{C})$ band position between lutein rich flagellates and astaxanthin rich cysts is about $3\text{--}4\text{ cm}^{-1}$. There is only slight shift considering $\nu_2(\text{C}=\text{C})$ vibration modes about 1 cm^{-1} . Significant shifts ($5, 4$

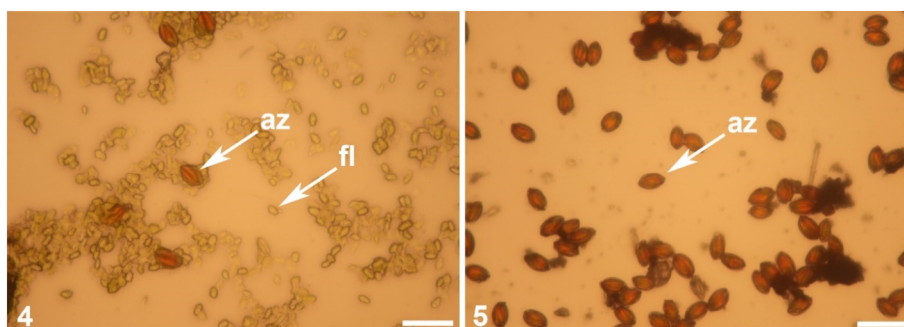


Fig. 11. Microphotographs of flagellates (fl) and aplanozygotes (az) of *Chloromonas* cf. *nivalis* (samples 4 and 5). Scale = 50 μm .

and 3 cm^{-1}) are seen considering C—H bending motions in C=C bonds, appearing at 1187 and 1192, at 1210 and 1214 cm^{-1} and 1272 and 1275 cm^{-1} , respectively.

In the case of homogenous samples, formed by aplanozygotes of *Chloromonas* cf. *nivalis* (sample 10) and *Chloromonas* sp. (sample 11) (Fig. 10), we expected several carotenoids in the admixture (as revealed by means of HPLC), and the observed band at $\nu_1(\text{C}=\text{C})$ is due to the superimposition of several bands with different line parameters.

3.3. Homogenous Samples Versus Heterogenous Samples

The efficiency of these two methods for pigment identification has been shown through the study of homogenous and heterogenous samples. Raman microspectroscopy allows us to obtain spectra from individual cells, while HPLC performs bulk analysis.

HPLC analysis (Table 2) showed that the heterogenous mixture of dominant flagellates and minor aplanozygotes of *Chloromonas* cf. *nivalis* (sample 4) contained lutein as the main carotenoid (69%), followed by betacarotene (13%), violaxanthin (8%), antheraxanthin (5%) and *trans*-astaxanthin (5%). On the contrary, only aplanozygotes of *Chloromonas* cf. *nivalis* (sample 5) contained as the main carotenoid *trans*-astaxanthin (64%) and lutein (26%) plus minor amounts of violaxanthin (5%), betacarotene (3%) and antheraxanthin (2%). Clearly, minor amounts of secondary carotenoid astaxanthin in sample 4 revealed by HPLC comes from minor aplanozygotes of *Chloromonas* cf. *nivalis*. Microphotographs of the samples are depicted in Fig. 11.

Single-cell analyses performed by means of Raman microspectroscopy on the heterogenous sample 4 (one species and two different life stages) detected that flagellates have an upshift toward higher wavenumbers in the position of the $\nu_1(\text{C}=\text{C})$ Raman band. Raman bands were observed at 1523, 1155 and 1004 cm^{-1} , caused by their major pigment lutein and xanthophyll-cycle pigments (violaxanthin and antheraxanthin), as discussed above. Aplanozygotes (samples 4 and 5) with 64% of astaxanthin and 26% of lutein according to HPLC have identical Raman spectra as expected, with compound bands at around 1520, 1157 and 1006 cm^{-1} .

It has been shown that structurally similar carotenoids exhibit in Raman spectra only slightly different wavenumbers. Moreover, in the cells, values of the ν_1 band of deinoxanthin has a narrow range (around 1510 cm^{-1}), while β -carotene can have values from 1513 to 1524 cm^{-1} , lutein from 1521 to 1526 cm^{-1} and astaxanthin from 1518 to 1524 cm^{-1} [34]. The ν_1 band of carotenoids in biological systems differs from the one of pure carotenoid standards, mainly because of various interactions within the biological matrix [50]. Besides, using various excitation wavelengths provides slightly different bands as well [51]. This complicates the precise discrimination of carotenoids using Raman spectroscopy.

4. Conclusions

Snow algae represent eukaryotic extremophiles that are mainly subject to increased PAR as well as UVR and low temperatures. They serve as model organisms to study adaptation to life at the limit of physiological possibilities. By producing carotenoids, they cope with their natural environments. As the content of carotenoids in snow algae varies among individual species and life-cycle stages, this group represents a suitable model for testing the possibilities of Raman spectrometry in pigment detection.

We have characterized snow algae carotenoids using a combination of resonance Raman spectroscopy and HPLC and built a spectral library for different life-cycle stages of snow algae. Analyzed samples were collected in European mountain ranges in a wide altitudinal gradient. Individual species and life stages of snow algae had unique pigment compositions. Stress-resistant cysts produced high amounts of astaxanthin. The three main carotenoid Raman bands of the astaxanthin-rich red cysts were located at 1520, 1156–1157 and

1006 cm^{-1} . While flagellated green cells commonly contained lutein as a major carotenoid, together with minor amounts of β -carotene and varying amounts of antheraxanthin, violaxanthin and neoxanthin, aplanozygotes contained mixtures of both primary and secondary carotenoids. Chlorophylls *a* and *b* were always present, but they were not analyzed in this study by means of Raman spectroscopy.

Detailed analysis of pigment contents in biomass can be provided by HPLC. However, this method requires the extraction of the pigments from the biomass, which may lead to a loss of information (e.g., protein/lipid interactions). On the other hand, Raman microspectroscopy permits fast pigment detection of individual cells, which could be another advantage especially when analyzing heterogenous mixtures of cells. We can easily monitor the maturing process of the cells. Hence still, the exact identification of carotenoids may remain problematic. However, the potential detection of Raman spectroscopic signatures of carotenoids *sensu lato* in Martian outcrops or subsurface rocks would be highly beneficial.

Supplementary data to this article can be found online at <https://doi.org/10.1016/j.saa.2019.01.013>.

Acknowledgements

The authors wish to thank the Czech Science Foundation Projects (17-04270S and 18-02634S), Center for Geosphere Dynamics (UNCE/SCI/006), the Czech Ministry of Education projects Algatech Plus (LO1416) and European Regional Development Fund-Project “Mechanisms and dynamics of macromolecular complexes: from single molecules to cells” (No. CZ.02.1.01/0.0/0.0/15_003/0000441).

References

- [1] E.V. Pikuta, R.B. Hoover, J. Tang, Microbial extremophiles at the limits of life, *Crit. Rev. Microbiol.* 33 (2007) 183–209.
- [2] L.J. Preston, L.R. Dartnell, Planetary habitability: lessons learned from terrestrial analogues, *Int. J. Astrobiol.* 13 (2014) 81–98.
- [3] G.S.N. Reddy, J.S.S. Prakash, M. Vairamani, S. Prabhakar, G.I. Matsumoto, S. Shivaji, *Planococcus antarcticus* and *Planococcus psychrophilus* spp. nov isolated from cyanobacterial mat samples collected from ponds in Antarctica, *Extremophiles* 6 (2002) 253–261.
- [4] T.A. Moore, D. Gust, A.L. Moore, The function of carotenoid pigments in photosynthesis and their possible involvement in the evolution of higher plants, in: N.I. Krinsky, M.M. Mathews-Roth, R.F. Taylor (Eds.), *Carotenoids: Chemistry and Biology*, Springer, US, Boston, MA 1989, pp. 223–228.
- [5] K. Michaelian, A. Simeonov, Fundamental molecules of life are pigments which arose and co-evolved as a response to the thermodynamic imperative of dissipating the prevailing solar spectrum, *Biogeosciences* 12 (2015) 4913–4937.
- [6] D.D. Wynn-Williams, H.G.M. Edwards, E.M. Newton, J.M. Holder, Pigmentation as a survival strategy for ancient and modern photosynthetic microbes under high ultraviolet stress on planetary surfaces, *Int. J. Astrobiol.* 1 (2002) 39–49.
- [7] F. Rull, S. Maurice, I. Hutchinson, A. Moral, C. Perez, C. Diaz, M. Colombo, T. Belenguer, G. Lopez-Reyes, A. Sansano, O. Forni, Y. Parot, N. Striebig, S. Woodward, C. Howe, N. Tarcea, P. Rodriguez, L. Seoane, A. Santiago, J.A. Rodriguez-Prieto, J. Medina, P. Gallego, R. Canchal, P. Santamaria, G. Ramos, J.L. Vago, R.L.S. Team, The Raman laser spectrometer for the ExoMars rover mission to Mars, *Astrobiology* 17 (2017) 627–654.
- [8] R.C. Wiens, S. Maurice, F.R. Perez, The SuperCam remote sensing instrument suite for the Mars 2020 rover: a preview, *Spectroscopy* 32 (2017) 50–55.
- [9] C. Malherbe, I.B. Hutchinson, M. McHugh, R. Ingley, J. Jehlička, H.G.M. Edwards, Accurate differentiation of carotenoid pigments using flight representative Raman spectrometers, *Astrobiology* 17 (2017) 351–362.
- [10] J.H. Hooijschuur, M.F.C. Verkaaik, G.R. Davies, F. Ariese, Will Raman meet bacteria on Mars? An overview of the optimal Raman spectroscopic techniques for carotenoid biomarkers detection on mineral backgrounds, *Netherlands, J. Geosci.* 95 (2016) 141–151 (*Geologie En Mijnbouw*).
- [11] M. Meinhardt-Wollweber, C. Suhr, A.K. Kniggendorf, B. Roth, Absorption and resonance Raman characteristics of beta-carotene in water-ethanol mixtures, emulsion and hydrogel, *AIP Adv.* 8 (2018) 14.
- [12] J. Komárek, L. Nedbalová, Green cryosestic algae, in: J. Seckbach (Ed.), *Algae and Cyanobacteria in Extreme Environments*, Springer, Netherlands, Dordrecht 2007, pp. 321–342.
- [13] D. Remias, U. Lütz-Meindl, C. Lütz, Photosynthesis, pigments and ultrastructure of the alpine snow alga *Chlamydomonas nivalis*, *Eur. J. Phycol.* 40 (2005) 259–268.
- [14] D. Remias, M. Pichrtová, M. Pangratz, C. Lütz, A. Holzinger, Ecophysiology, secondary pigments and ultrastructure of *Chlainomonas* sp. (Chlorophyta) from the European Alps compared with *Chlamydomonas nivalis* forming red snow, *FEMS Microbiol. Ecol.* 92 (2016), fiw030.

- [15] D. Remias, L. Procházková, A. Holzinger, L. Nedbalová, Ecology, cytology and phylogeny of the snow alga *Scotiella cryophila* K-1 (Chlamydomonadales, Chlorophyta) from the Austrian Alps, *Phycologia* 57 (2018) 581–592.
- [16] L. Procházková, D. Remias, A. Holzinger, T. Řezanka, L. Nedbalová, Ecophysiological and morphological comparison of two populations of *Chlainomonas* sp. (Chlorophyta) causing red snow on ice-covered lakes in the High Tatras and Austrian Alps, *Eur. J. Phycol.* 53 (2018) 230–243.
- [17] J. Kvíderová, Research on cryosestic communities in Svalbard: the snow algae of temporary snowfields in Petuniabukta, Central Svalbard, Czech Polar Rep. 2 (2012) 8–19.
- [18] L. Nedbalová, M. Kociánová, J. Lukavský, Ecology of snow algae in the Giant Mts./ Ekologie snežných ras Krkonos, Opera Corcontica 2008, pp. 59–68.
- [19] L. Nedbalová, P. Sklenár, New records of snow algae from the Andes of Ecuador, *Arnaldia* 15 (2008) 17–20.
- [20] S. Lütz, A.M. Anesio, S.E.J. Villar, L.G. Benning, Variations of algal communities cause darkening of a Greenland glacier, *FEMS Microbiol. Ecol.* 89 (2014) 402–414.
- [21] N. Takeuchi, J. Uetake, K. Fujita, V.B. Aizen, S.D. Nikitin, A snow algal community on Akkem glacier in the Russian Altai mountains, *Ann. Glaciol.* 43 (2006) 378–384.
- [22] M. Terashima, K. Umezawa, S. Mori, H. Kojima, M. Fukui, Microbial community analysis of colored snow from an alpine snowfield in northern Japan reveals the prevalence of betaproteobacteria with snow algae, *Front. Microbiol.* 8 (2017) 1481.
- [23] S. Lütz, A.M. Anesio, R. Raiswell, A. Edwards, R.J. Newton, F. Gill, L.G. Benning, The biogeography of red snow microbiomes and their role in melting arctic glaciers, *Nat. Commun.* 7 (2016) 11968.
- [24] V. Henríquez, C. Escobar, J. Galarza, J. Gimpel, Carotenoids in microalgae, *Carotenoids in Nature*, Springer 2016, pp. 219–237.
- [25] S. Takaichi, Distributions, biosyntheses and functions of carotenoids in algae, *Agro Food Ind Hi Tech* 24 (2013) 55–58.
- [26] T. Leya, A. Rahn, C. Lütz, D. Remias, Response of arctic snow and permafrost algae to high light and nitrogen stress by changes in pigment composition and applied aspects for biotechnology, *FEMS Microbiol. Ecol.* 67 (2009) 432–443.
- [27] D. Remias, U. Karsten, C. Lütz, T. Leya, Physiological and morphological processes in the Alpine snow alga *Chloromonas nivalis* (Chlorophyceae) during cyst formation, *Protoplasma* 243 (2010) 73–86.
- [28] Y. Aluc, G.B. Kankilic, I. Tuzun, Determination of carotenoids in two algae species from the saline water of Kapulukaya reservoir by HPLC, *J. Liq. Chromatogr. Relat. Technol.* 41 (2018) 93–100.
- [29] A. Holzinger, M.C. Allen, D.D. Deheyn, Hyperspectral imaging of snow algae and green algae from aeroterrestrial habitats, *J. Photochem. Photobiol. B Biol.* 162 (2016) 412–420.
- [30] B. Schoefs, Chlorophyll and carotenoid analysis in food products. Properties of the pigments and methods of analysis, *Trends Food Sci. Technol.* 13 (2002) 361–371.
- [31] K.L. French, D. Rocher, J.E. Zumberge, R.E. Summons, Assessing the distribution of sedimentary C–40 carotenoids through time, *Geobiology* 13 (2015) 139–151.
- [32] J. Jehlička, H.G.M. Edwards, A. Oren, Bacterioruberin and salinixanthin carotenoids of extremely halophilic Archaea and Bacteria: a Raman spectroscopic study, *Spectrochim. Acta A Mol. Biomol. Spectrosc.* 106 (2013) 99–103.
- [33] J. Jehlička, A. Oren, Raman spectroscopy in halophile research, *Front. Microbiol.* 4 (2013) 380.
- [34] J. Jehlička, H.G.M. Edwards, K. Osterrothová, J. Novotná, L. Nedbalová, J. Kopecký, I. Němec, A. Oren, Potential and limits of Raman spectroscopy for carotenoid detection in microorganisms: implications for astrobiology, *Phil. Trans. R. Soc. A* 372 (2014) 20140199.
- [35] P. Vítek, J. Jehlička, H.G.M. Edwards, I. Hutchinson, C. Ascaso, J. Wierzbos, The miniaturized Raman system and detection of traces of life in halite from the Atacama Desert: some considerations for the search for life signatures on Mars, *Astrobiology* 12 (2012) 1095–1099.
- [36] A. Culka, K. Osterrothová, I. Hutchinson, R. Ingley, M. McHugh, A. Oren, H.G.M. Edwards, J. Jehlička, Detection of pigments of halophilic endoliths from gypsum: Raman portable instrument and European Space Agency's prototype analysis, *Phil. Trans. R. Soc. A* 372 (2014) 20140203.
- [37] H.G.M. Edwards, L.F. De Oliveira, C.S. Cockell, J.C. Ellis-Evans, D.D. Wynn-Williams, Raman spectroscopy of senescing snow algae: pigmentation changes in an Antarctic cold desert extremophile, *Int. J. Astrobiol.* 3 (2004) 125–129.
- [38] J. Jehlička, A. Culka, L. Nedbalová, Colonization of snow by microorganisms as revealed using miniature Raman spectrometers—possibilities for detecting carotenoids of psychrophiles on Mars? *Astrobiology* 16 (2016) 913–924.
- [39] J. Jehlička, A. Oren, Use of a handheld Raman spectrometer for fast screening of microbial pigments in cultures of halophilic microorganisms and in microbial communities in hypersaline environments in nature, *J. Raman Spectrosc.* 44 (2013) 1285–1291.
- [40] V.E. de Oliveira, H.V. Castro, H.G.M. Edwards, L.F.C. de Oliveira, Carotenoids and carotenoids in natural biological samples: a Raman spectroscopic analysis, *J. Raman Spectrosc.* 41 (2010) 642–650.
- [41] A. Oren, J. Hirschberg, V. Mann, J. Jehlička, Effects of nicotine on the biosynthesis of carotenoids in halophilic Archaea (class Halobacteria): an HPLC and Raman spectroscopy study, *Extremophiles* 22 (2018) 359–366.
- [42] S.W. Wright, S.W. Jeffrey, R. Mantoura, C. Llewellyn, T. Bjørnland, D. Repeta, N. Welschmeyer, Improved HPLC method for the analysis of chlorophylls and carotenoids from marine phytoplankton, *Mar. Ecol. Prog. Ser.* 77 (1991) 183–196.
- [43] George Britton, Synnove Liaaen-Jensen, Hanspeter Pfander (Eds.), *Carotenoids Handbook*, Birkhäuser, Basel, 2004 <https://doi.org/10.1007/978-3-0348-7836-4>, (647 pp.).
- [44] H.K. Lichtenthaler, A.R. Wellburn, Determinations of total carotenoids and chlorophylls a and b of leaf extracts in different solvents, *Biochem. Soc. Trans.* 11 (1983) 591–592.
- [45] M.M. Mendes-Pinto, D. Galzerano, A. Telfer, A.A. Pascal, B. Robert, C. Ilioaia, Mechanisms underlying carotenoid absorption in oxygenic photosynthetic proteins, *J. Biol. Chem.* 288 (2013) 18758–18765.
- [46] A. Kaczor, M. Baranska, Structural changes of carotenoid astaxanthin in a single algal cell monitored in situ by Raman spectroscopy, *Anal. Chem.* 83 (2011) 7763–7770.
- [47] J. Jehlička, H.G.M. Edwards, A. Oren, Raman spectroscopy of microbial pigments, *Appl. Environ. Microbiol.* 80 (2014) 3286–3295.
- [48] B. Subramanian, N. Tchoukanova, Y. Djaoued, C. Pelletier, M. Ferron, J. Robichaud, Investigations on the geometrical isomers of astaxanthin: Raman spectroscopy of conjugated polyene chain with electronic and mechanical confinement, *J. Raman Spectrosc.* 45 (2014) 299–304.
- [49] A.V. Ruban, A.A. Pascal, B. Robert, Xanthophylls of the major photosynthetic light-harvesting complex of plants: identification, conformation and dynamics, *FEBS Lett.* 477 (2000) 181–185.
- [50] H. Schulz, M. Baranska, R. Baranski, Potential of NIR-FT-Raman spectroscopy in natural carotenoid analysis, *Biopolymers* 77 (2005) 212–221.
- [51] C.P. Marshall, S. Leuko, C.M. Coyle, M.R. Walter, B.P. Burns, B.A. Neilan, Carotenoid analysis of halophilic archaea by resonance Raman spectroscopy, *Astrobiology* 7 (2007) 631–643.

Supplementary Data

Tab. S1 Overview of retention times and absorption maxima specific for identified pigments

Retention time [min]	Pigment	Abbreviation	Absorption maxima [λ]	
			in acetone	in eluent
13	chlorophyllide a	chl a	430; 577; 617; 663	410; 466; 537; 610; 663
13.5	violaxanthin	viol	419; 443; 472	416; 440; 470
14	neochrome	neoch	400; 424; 450	400; 422; 450
14.5	neoxanthin	neox	416; 438; 466	416; 438; 464
14.9	antheraxanthin	anther	424; 448; 476	423; 446; 476
15	trans astaxanthin	trans-atx	480	474
15.6	cis astaxanthin	cis-atx	374; 480	373; 474
16	lutein	lut	425; 448; 476	422; 446; 476
16.5	cis antheraxanthin	cis-anther	331; 424; 448; 476	331; 423; 446; 476
19	chlorophyll b	chl b	453; 598; 645	457; 599; 646
20	chlorophyll a	chl a	412; 431; 581; 616; 663	410; 431; 581; 616; 663
22	phaeophytin a	pheo a	410; 505; 535; 609; 666	408; 504; 534; 608; 666
22.2	γ carotene	γ -car	380; 402; 426	(433); 462; 490
23	β carotene	β -car	453; 480	(425); 452; 480

